september 1960
the
institute
of
radio
engineers

Proceedings of the IRE

in this issue

TV TRANSMISSION BY BINARY PULSES: PAGE 1546

PULSE TRANSFORMERS

FROM STOCK

MINIATURE STABLE WOUND CORE — HERMETIC MIL-T-27A TYPE TF5SX36ZZ

UTC miniature, wound core, pulse transformers are precision (individually adjusted under test conditions), high reliability units, hermetically sealed by vacuum molding and suited for service from —70° C. to +130° C. Wound core structure provides excellent temperature stability (unlike ferrite). Designs are high inductance type to provide minimum of droop and assure true pulse width, as indicated on chart below. If used for coupling circuit where minimum rise time is important, use next lowest type number. Rise time will be that listed for this lower type number . . . droop will be that listed multiplied by ratio of actual pulse width to value listed for this type number. Blocking oscillator data listed is obtained in standard test circuits shown. Coupling data was obtained with H. P. 212A generator (correlated where necessary) and source/load impedance shown. 1:1:1 ratio.

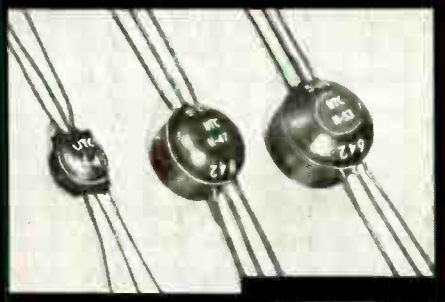

DEFINITIONS

Amplitude: Intersection of leading pulse edge with smooth curve approximating top of pulse.
Pulse width: Microseconds between 50% amplitude points on leading and trailing pulse edges.
Rise Time: Microseconds required to increase from 10% to 90% amplitude.
Overshoot: Percentage by which first excursion of pulse exceeds 100% amplitude.
Droop: Percentage reduction from 100% amplitude a specified time after 100% amplitude point.
Backswing: Negative swing after trailing edge as percentage of 100% amplitude.

Type No.	APPROX. DCR, OHMS 1-2	3-4	5-6	BLOCKING OSCILLATOR PULSE Width μ Sec.	Rise Time	% Over Shoot	Droop %	% Back Swing	P Width μ Sec.	COUPLING CIRCUIT CHARACTERISTICS Volts Out	Rise Time	% Over Shoot	Droop %	% Back Swing	Imp. in, out, ohms
H-45	3	3.5	4	.05	.022	0	20	10	.05	17	.01	20	0	35	250
H-46	5.5	6.5	7	.10	.024	0	25	10	.10	19	.01	30	10	50	250
H-47	3.7	4.0	4	.20	.026	0	25	8	.20	18	.01	30	15	65	500
H-48	5.5	5.8	6	.50	.03	0	20	5	.50	20	.01	30	20	65	500
H-49	8	8.5	9	1	.04	0	20	10	1	24	.02	15	15	65	500
H-50	20	21	22	2	.05	0	20	10	2	27	.05	10	15	35	500
H-51	28	31	33	3	.10	1	20	8	3	26	.07	10	10	35	500
H-52	36	41	44	5	.13	1	25	8	5	23	.15	10	10	45	1000
H-53	37	44	49	7	.28	0	25	8	7	24	.20	10	10	50	1000
H-54	50	58	67	10	.30	0	20	8	10	24	.25	10	10	50	1000
H-55	78	96	112	16	.75	0	20	10	16	23	.40	5	15	20	1000
H-56	93	116	138	20	1.25	0	25	10	20	23	.6	5	10	10	1000
H-57	104	135	165	25	2.0	0	30	10	25	24	1.5	5	10	10	1000
H-60	.124	.14	.05	.05	.016	0	0	30	.05	9.3	.012	0	0	20	50
H-61	.41	.48	.19	.1	.016	0	0	30	.1	8.2	.021	0	0	15	50
H-62	.78	.94	.33	.2	.022	0	0	18	.2	7.4	.034	0	5	12	100
H-63	1.86	2.26	.70	.5	.027	2	10	20	.5	7.5	.045	0	20	25	100
H-64	3.73	4.4	1.33	1	.033	0	12	25	1	7	.078	0	15	23	100
H-65	6.2	7.3	2.22	2	.066	0	15	25	2	6.6	.14	0	10	20	100
H-66	10.2	12	3.6	3	.087	0	18	30	3	6.8	.17	0	10	20	100
H-67	14.5	17.5	5.14	5	.097	0	23	28	5	7.9	.2	0	18	28	200
H-68	42.3	52.1	14.8	10	.14	0	15	28	10	6.5	.4	0	15	30	200

Note: 0 = Negligible

Vacuum Tube Type Ratio 1:1:1

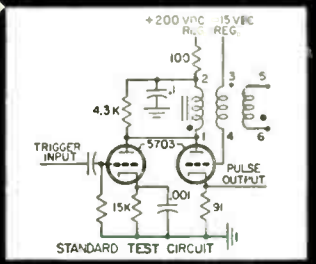

Transistor Type Ratio 4:4:1

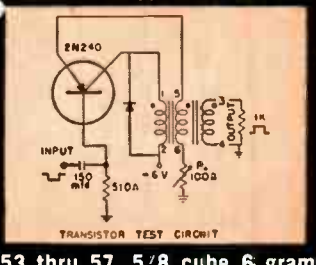

H-45 46, 60 thru 68 are 3/8 cube, 1 gram — **H-47 thru 52, 9/16 cube 4 grams** — **H-53 thru 57, 5/8 cube 6 grams**

AND SPECIAL UNITS TO YOUR SPECS

While stock items cover low level uses only, most of UTC's production is on special units to customers' needs, ranging from low levels to 10 megawatts.

Write for Catalog for full details on these and 1000 other stock items

UNITED TRANSFORMER CORPORATION
150 Varick Street, New York 13, N. Y.
PACIFIC MFG. DIVISION: 4008 W. JEFFERSON BLVD., LOS ANGELES 16, CALIF.
EXPORT DIVISION 13 EAST 40th STREET, NEW YORK 16, N. Y. CABLES: "ARLAB"

VOLUME 48, NUMBER 9

September, 1960

published monthly by The Institute of Radio Engineers, Inc.

Proceedings of the IRE®

contents

COVER

An experimental seven-digit pulse-code-modulation system has been developed by Bell Telephone Laboratories for the transmission of television signals, as described on p. 1546. The sequence of photographs, taken from a TV monitor, shows the effect of adding one digit at a time.

SEPTEMBER

published monthly by The Institute of Radio Engineers, Inc.

Proceedings of the IRE®

continued

SEPTEMBER

PROCEEDINGS OF THE IRE, published monthly by The Institute of Radio Engineers, Inc. at 1 East 79 Street, New York 21, N. Y. Manuscripts should be submitted in triplicate to the Editorial Department. Responsibility for contents of papers published rests upon the authors, and not the IRE or its members. All republication rights, including translations, are reserved by the IRE and granted only on request. Abstracting is permitted with mention of source.

Thirty days advance notice is required for change of address. Price per copy: members of the Institute of Radio Engineers, one additional copy $1.25; non-members $2.25. Yearly subscription price: to members $9.00, one additional subscription $13.50; to non-members in United States, Canada, and U. S. Possessions $18.00; to non-members in foreign countries $19.00. Second-class postage paid at Menasha, Wisconsin under the act of March 3, 1879. Acceptance for mailing at a special rate of postage is provided for in the act of February 28, 1925, embodied in Paragraph 4, Section 412, P. L. and R., authorized October 26, 1927. Printed in U.S.A.

September, 1960
Vol. 48 No. 9

Proceedings of the IRE

Poles and Zeros

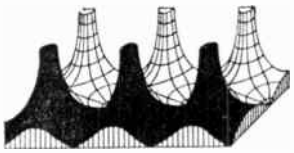

Information for Authors. The readability of any journal or periodical is enhanced by the use of a uniform format and style in the preparation of the manuscripts which it publishes. To assure this adequate uniformity, it is customary to provide a guide for authors of a specific journal to assist them in the preparation of their manuscripts. Such guides may vary from the elaborate approach represented by the Style Manual of of the AIP (see P & Z, March, 1960) to instructions comprising only general information. IRE has taken an intermediate course in the form of its "Information for IRE Authors." This document was published in the PROCEEDINGS in November, 1954 and has now been revised and brought up-to-date by the Editorial Board. It is included in this issue of the PROCEEDINGS.

All prospective authors for IRE publications are urged to study the Editorial Board's new "Information" when preparing material for publication. The adoption of revised abbreviations should be particularly noted. The adopted system calls for the use of lower case letters for the abbreviation of units of measure (exceptions being Angstrom (A) and °C, °F, and °K). Capital letters are used for all other abbreviations (the exceptions being ac, dc, cgs, mks, rms, rss, and certain metric symbols listed in the complete document). The new guide emphasizes the preference of the Editorial Board for the metric prefixes and symbols. It should be observed that, for example, gigacycle, nanosecond, and picofarad become the preferred terms.

In P & Z in May, 1960, the Editor discussed, in an item titled "Feedback," the question of abbreviations and the desirability of the use of the metric system. This discussion provoked a most satisfactory response from readers in the form of letters expressing points of view in both matters. To those who responded, the Editorial Board expresses thanks; the comments were extremely helpful in formulating the new "Information for IRE Authors."

Career Brochure. Have you ever asked yourself how young people become interested in electronics? The Cedar Rapids Section has not only asked itself this question but also, it has done something about it. Cedar Rapids realized that IRE has always demonstrated its interest in the college student but has not participated in activities at the high school level as extensively as might be desirable. They conceived the idea of preparing material that would be useful to high school counselors and students as a guide to a career in electronics.

Thus the brochure "Electronics—Career for the Future" was born. It has survived its birth pains and is being published this month. They have completed a truly monumental task and in the excellent fashion that is characteristic of all their undertakings. The brochure, in color, features the outstanding artwork of Ted Papajohn. It is directed to answering the questions and doubts that may occur to a youngster considering a career in electronics. It features sections defining electronics, discussing the applications of electronics, communication electronics, instrumentation and control electronics, computer electronics, solid state electronics, the future of electronics, careers in electronics, and planning an electronics education. Despite this array of topics, the brochure has been so skillfully assembled that it comprises only twenty-three pages of inviting reading.

IRE has supported the project by financing the printing and distribution of a trial run of 10,000 copies. This first printing will be used to assess the acceptance and value of the brochure. Approximately one-half of the print run will be distributed by the Cedar Rapids Section. They plan to distribute copies to all the high schools in Iowa and to conduct an intensive distribution to the students in the high schools of the Cedar Rapids area. It is hoped to thus obtain a direct feedback from students and counselors to evaluate the usefulness of the brochure.

The other half of the print order will be available for distribution to interested IRE members through Headquarters. Those members who wish copies of the booklet for introduction to high schools in their area may obtain copies upon request. It is hoped that many individuals will consider this an opportunity and a challenge and will report the reactions that the brochure encounters. If the effort of the Cedar Rapids Section is as successful as the product deserves, the next printing may have to be in megacopies.

Meetings, Meetings, Meetings. Most IRE members belong to more than one professional organization. Even if they are not members they are frequently interested in meetings and symposia of other societies and institutes. The time seems to have come when some consideration should be given to the establishment of an agency to be known as OFCDCTAC, an abbreviation as difficult to pronounce as it is difficult to achieve its aims. The Organization for Convention Date Correlation to Avoid Conflicts should be equipped with the latest available communications and computing equipment and should be adequately staffed. If all these qualifications are met, and it therefore operates successfully, perhaps AIEE will not be meeting in Atlantic City while ASEE is meeting in Lafayette, and the Conference on Standards and Electronic Measurements is meeting in Boulder, the Spring Conference on Broadcast and Television Receivers is meeting in Chicago, and the Workshop on Solid State Electronics is meeting at Purdue.—F. H., Jr.

C. F. Horne

Director, 1960–1961

Charles F. Horne, Jr. (A'35–SM'53–F'58), Rear Admiral, U. S. Navy (Retired), electronics engineer and former Civil Aeronautics Administrator, has been Manager of Convair/Pomona, Convair Division of General Dynamics Corporation, Pomona, Calif., since July 15, 1953. In February, 1957, Mr. Horne was elected a Vice President of the Convair organization.

He was born in New York City on January 3, 1906, and attended public, elementary, and high schools there. He was graduated from the United States Naval Academy at Annapolis, Md., in 1926. He attended the Navy's postgraduate school in communications and electronics. In 1935 he received the master of science degree in communications and electronics from Harvard University, Cambridge, Mass.

Admiral Horne was one of the pioneers in the application of electronic concepts in the United States Navy. During World War II he was Communications and Radar Officer, Battleships, Pacific Fleet; Communications Officer, South Pacific Area; Communications and Radar Officer, Amphibious Forces, Pacific. He received several combat citations and campaign ribbons. From 1946–1948 he was Deputy Chief, Naval Communications.

In 1949–1950 he was on loan from the Navy to the Civil Aeronautics Administration, where he was Acting Director of the Federal Airways Division. Upon his retirement from the Navy in 1951, he was appointed by the President of the United States as Civil Aeronautics Administrator and served in that capacity until 1953. In 1952 he also was a member of the Presidential Airport Commission. He is a recipient of the CAA International Region Medal.

Admiral Horne is a member of the Electronic Industries Association's Military Products Division Policy Committee and Executive Committee, and Chairman of the Association's Military Systems Management Committee. He is West Coast adviser to the Radio Technical Commission for Aeronautics. He is a member of the Board of Directors of the Armed Forces Communications and Electronics Association, President of the Aero Club of Southern California, and Vice President of the Los Angeles Chamber of Commerce. He is a member of the Board of Directors of Pomona Valley Community Hospital Association, and of the Los Angeles Post, American Ordnance Association. He is also a member of the Aircraft Owners and Pilots Association.

He has served on the Administrative Committee of the IRE Professional Group on Engineering Management in 1956–1957.

One of his chief interests is closer cooperation between industry and education. In this area he serves as President of the Southern California Industry Education Council.

Scanning the Issue

Information for IRE Authors (p. 1536)—Six years have passed since the IRE last published a guide for authors on preparing papers for the PROCEEDINGS. The Editorial Board has now revised these instructions in order to make them applicable to the TRANSACTIONS as well as the PROCEEDINGS, and to spell out in greater detail present IRE practices with regard to matters of style. Authors will note in particular the addition of a section on Units, Abbreviations and Symbols which includes examples of commonly misused graphical symbols and, in an Appendix, a list of abbreviations used by the IRE Editorial Department. With regard to the latter, a most important change is the adoption this summer by the IRE Editorial Board of the expanded list of metric prefixes recently set forth by the International Committee on Weights and Measures. The list now includes giga and tera for 10^9 and 10^{12}, nano and pico for 10^{-9} and 10^{-12}, and calls for using the capital letter M as the abbreviation for mega in the future to differentiate it from m for milli. Reprints of Information for IRE Authors are available from the Editorial Department on request.

Theory of a Monolithic Null Device and Some Novel Circuits (Kaufman, p. 1540)—A sizable effort is being made by many organizations to construct semiconductor blocks that will perform the functions of a multiplicity of conventional components. One such development is reported here. A semiconductor distributed bridged-T structure has been developed which, when placed in a feedback path around an amplifier, provides a way of tuning the amplifier, even though no inductance is obtainable with semiconductor materials. This novel concept will be of especial interest in tuned circuit applications where small size is of primary importance.

Video Transmission Over Telephone Cable Pairs by Pulse Code Modulation (Carbrey, p. 1546)—This paper describes an interesting experiment in which monochrome and color television signals of broadcast quality were encoded into a seven digit binary code and transmitted over seven pairs of regular telephone cable. The results point to two important possibilities: first, the use of binary pulse transmission on transcontinental coaxial and microwave circuits, which would greatly simplify the repeater design requirements because the signal would be regenerated at each repeater, thus avoiding troublesome cumulative effects; and second, the use of telephone cables for providing, more economically, additional short-haul television circuits in metropolitan areas.

Thin-Film Cryotrons (Smallman, *et al.*, p. 1562)—For the third successive month, the PROCEEDINGS reports on important progress in the use of thin superconducting films to produce a new generation of computer components that are extremely compact, very reliable, and readily fabricated in large quantities. This paper, which is three papers in one, provides an excellent and complete description of the theory and applications of thin-film cryotrons. Part 1 discusses the properties of thin superconducting films; Part 2, cryotron characteristics and applications; and Part 3, cryotron ring oscillators.

Optimum Noise and Gain-Bandwidth Performance for a Practical One-Port Parametric Amplifier (Greene and Sard, p. 1583)—The analysis presented here provides an important step in completing the theoretical picture of junction diode parametric amplifier performance. The authors determine the conditions under which minimum effective noise temperature and maximum gain-bandwidth product can be obtained, and develop universal curves for designing optimum amplifiers. The analysis reveals that parametric amplifiers operated at room temperature are not yet a serious challenge to masers with respect to low noise at microwave frequencies.

Fractional Millimicrosecond Electrical Stroboscope (Goodall and Dietrich, p. 1591)—This paper describes a novel device for displaying extremely high-speed short-term electrical waves on an oscilloscope. It operates like a stroboscope for light in that it slows down a rapidly recurring phenomenon to a speed where it can be observed by sampling the phenomenon at a regular rate. Waveforms with rise times as fast as 2×10^{-10} seconds can be displayed with this device, making it a valuable tool for millimicrosecond pulse work.

Symmetrical Matrix Analysis of Parametric Amplifiers and Converters (Deutsch, p. 1595)—Although parametric devices have been dealt with at considerable length in the literature, the expressions for analyzing their characteristics have generally proved to be unwieldy. The analysis presented here proceeds from a set of four equations which have the virtue of being readily manipulated by matrix methods. These equations and the matrix analysis of them provide a new and simpler way of describing the gain, bandwidth, and noise figure performance of this important family of devices.

An Analog Solution for the Static London Equations of Superconductivity (Meyers, p. 1603)—The static London equations referred to in the title have been found to provide a good qualitative description of the behavior of fields and currents in superconductors. Unfortunately, they are presently soluble only in simple one- and two-dimensional problems, even with a computer. This paper presents a novel analog method of obtaining solutions in more complicated geometries which takes advantage of the similarity between skin-effect and London equations. This technique will be of considerable value to the growing number of cryogenic device designers who need practical solutions to problems of this type.

IRE Standards on Circuits: Definitions of Terms for Linear Passive Reciprocal Time Invariant Networks, 1960 (p. 1608)—In much of the technical literature on networks, the properties of physical networks are described in terms of idealized mathematical models for convenience of analysis. This Standard deals with the small but important group of terms by which these mathematical concepts are expressed.

IRE Standards on Circuits: Definitions of Terms for Linear Signal Flow Graphs, 1960 (p. 1611)—The appearance of this Standard reflects the fact that in the last 7 years the signal flow graph has become an increasingly useful analytic tool, requiring a language of its own.

Error Probabilities for Telegraph Signals Transmitted on a Fading FM Carrier (Barrow, p. 1613)—The author has made a comprehensive study of telegraphy multiplexed by frequency modulation onto an RF carrier. This form of point-to-point communication seems the most practical way to utilize the communication channels afforded by tropospheric scattering. Thus, the study will be of interest to many engineers engaged in this modern form of radio signaling. A few of the results are also pertinent to other types of digital modulation on ionospheric, tropospheric, or moon-relay circuits.

Forward Scattering by Coated Objects Illuminated by Short Wavelength Radar (Hiatt, *et al.*, p. 1630)—A theoretical and confirming experimental study has been made of the effects of covering highly conducting objects with radar absorbing material. The results show that when the wavelength is small compared to the dimensions of the object, absorbing materials are ineffective in reducing forward scattering, and in fact, increase it.

The Ineffectiveness of Absorbing Coatings on Conducting Objects Illuminated by Long Wavelength Radar (Hiatt, *et al.*, p. 1636)—Complementing the preceding paper, this study dispells the notion that objects can be covered by absorbing material in order to make them invisible radar targets, even at low frequencies.

Scanning the Transactions appears on page 1670.

Information for IRE Authors

Reprints of these instructions are available on request from the Editorial Department, Institute of Radio Engineers, 1 East 79 Street, New York 21, N. Y.

THESE instructions are for the guidance of authors in preparing papers for the following IRE publications:

1) PROCEEDINGS OF THE IRE, the monthly journal of the IRE, devoted primarily to papers of long-range importance and general interest.
2) IRE TRANSACTIONS, published by each of the Professional Groups of the IRE at frequencies ranging from two to six times a year, and devoted principally to papers of specialized interest within the field of one Professional Group.

The instructions that follow have been divided into three sections: Organization, Style and Format, and Submitting the Paper. Unless otherwise indicated, they apply equally well to PROCEEDINGS papers and TRANSACTIONS papers.

PROCEEDINGS authors should bear in mind that the PROCEEDINGS serves to keep a wide audience of engineers generally informed on progress in various branches of communications and electronics. It is therefore essential that PROCEEDINGS papers be written in a manner intelligible to engineers working in other fields.

ORGANIZATION

To be well written, a paper must be well organized. IRE papers should ordinarily consist of a Title, Summary, Introduction, Body of the Paper, and Conclusions. Suggestions for preparing each of these parts of the paper are offered below.

The Title

The title should be short if possible but not so short that the subject will not be indicated clearly. Remember that a paper is indexed by significant words in the title and that many readers select the papers they read from the table of contents. The title, therefore, should be carefully chosen. Eight words is the usual maximum length.

The Summary

A well-written summary not only helps the reader to determine whether he should read the paper in full, but also makes the paper much more suitable for abstracting by the major abstract services of the world.

The summary should state concisely, in less than 200 words:

1) What the author has done.
2) How it was done (if that is important).
3) The principal results (numerically, when possible).
4) The significance of the results.

The summary should *not* be merely a list of general topics covered in the paper.

The Introduction

The introduction serves the vital function of orienting the reader with respect to the problem. The fact that it need not be long does not diminish its importance. The introduction should briefly tell the reader the following:

1) The nature of the problem.
2) The background of previous work on the problem, including published work.
3) The purpose of the paper.

Where applicable, the following points may also be included.

4) The method by which the problem will be attacked.
5) The organization of the material in the paper.

The Body of the Paper

Here, the writer should avoid following a stereotyped form and should bear in mind constantly that his object is to communicate information effectively to the reader. Even workers in the same field appreciate clear indications of the line of thought that is being followed. Moreover, when writing for the PROCEEDINGS, frequent guideposts are essential for nonspecialists who want to understand the general nature of the work and its significance but do not want to go into the mathematical details.

In work that is essentially mathematical, it is most helpful to the reader to carry along with the mathematics a physical picture of the successive stages through which the work is being carried. It is frequently advantageous to put long, purely mathematical derivations in appendices to avoid interrupting the main train of thought.

Figures, tables, curves, etc., should be labelled so that they are self-explanatory and can be used with a minimum of reference to the text.

The Conclusions

Failure to state the conclusions clearly is perhaps the most common fault in writing a scientific paper. It is of the greatest importance that the author evaluate what he has done. The concluding discussion should cover the following points where applicable:

1) What is shown by this work.
2) The significance of the results.
3) Limitations and advantages.

Where applicable, the following points should be included.

4) Applications of the results.
5) Recommendations for further work.

Style and Format

The review and publication of papers may be seriously delayed if manuscripts and illustrations are not submitted in proper and complete form. This section provides information on the form and style in which the paper should be prepared.

First Page

The first page should include the title of the paper, author, summary, and a footnote giving the author's affiliation.

Text

Manuscripts must be typed double spaced on one side of the sheet only. Allow ample margins, at least one inch on a side. Number all pages, illustrations, footnotes and tables. All illustrations must be referred to in the text.

References

References should be typed as footnotes at the bottom of the pages on which they are cited. For extended bibliographies, however, references may be placed at the end of the paper. References must be complete and should be in the form shown below. Please note that the title of the article must be included.

For a periodical: R. N. Hall, "Power rectifiers and transistors," Proc. IRE, vol. 40, pp. 1512–1518; November, 1952.

For a book: W. A. Edson, "Vacuum Tube Oscillators," John Wiley and Sons, Inc., New York, N. Y., pp. 170–171; 1948.

Illustrations

Drawings for printing must be in black ink on white paper or tracing cloth. Photographs must be glossy prints. The size should not exceed $8\frac{1}{2}\times 11$ inches. Identify each illustration by figure number and author's name.

It should be borne in mind that most illustrations will be reduced in size to a $3\frac{1}{2}$-inch column width when printed. It is particularly important, therefore, that all letters, numbers, and lines be drawn large enough and heavy enough to remain legible after reduction. Letters and numbers should be at least $\frac{1}{16}$ inch high *after* reduction.

Drawings with typewriting on them are not acceptable. All information to be reproduced must be lettered in ink.

Graphs should be drawn with only the major coordinate lines showing. A chart containing a large number of closely spaced lines will not reproduce legibly.

Captions, if they are included on the drawing itself, should not appear within the area to be reproduced. They should be placed under the illustration.

Captions

A list of all captions, with figure numbers, should be provided on a separate sheet. The captions should be self-explanatory.

Units, Abbreviations and Symbols

Authors are requested to use the rationalized mksa system of units, which has been officially adopted by the IRE as the preferred system.

Abbreviations should be in accordance with IRE editorial practice. A list of abbreviations used in IRE publications is given in the Appendix.

Graphical symbols must be drawn in accordance with IRE Standards.[1] Authors should be especially careful to employ the proper form of the symbols shown below.

CAPACITOR: one plate *must* be curved.

INDUCTOR: Use scallops instead of loops.

RESISTOR: Symbol has only 3 peaks.

SEMICONDUCTOR DEVICES: P emitter arrowhead should not touch line.

Mathematical Notation

Although the printer is familiar with mathematical material, reasonable care should be used to ensure that subscripts, superscripts, and Greek letters are readily recognizable as such. Bold face symbols should be underscored with a wavy line. Be particularly certain

[1] A compilation of all IRE standard graphical symbols, as of 1959, is contained in "IRE Dictionary of Electronic Terms and Symbols," which is available from the Institute of Radio Engineers at $5.20 per copy to IRE members, and $10.40 per copy to nonmembers.

that there is a clear distinction between the following (by means of a note in the margin, if necessary):

1) Capital and small letters, when used as symbols.
2) Small letter "l" (el) and the number "one."
3) Zero and the letter "o."

Submitting the Paper

Proceedings of the IRE

Proceedings papers should be submitted to the Managing Editor, Proceedings of the IRE, Institute of Radio Engineers, 1 East 79 Street, New York 21, N. Y. The following material is required:

1) Three copies of the paper for review purposes, each copy to include illustrations, a separate list of captions, and a summary of less than 200 words.
2) The original illustrations in a form suitable for reproduction.
3) A photograph and biography (125 words) of each author.

IRE Transactions

Items 1 and 2 above are required by all Transactions. Item 3 is required only by some. Transactions papers should be submitted directly to the Editor of the appropriate Professional Group Transactions rather than to IRE headquarters. A list of Professional Groups, their Editors and addresses is published every odd-numbered month in the IRE News and Notes section of the Proceedings of the IRE.

The instructions given under "Submitting the Paper" apply also to submitting a letter to the Editor, except that the summary and author's photograph and biography are not required.

Further information on any of the foregoing may be obtained from the Transactions Editors, or from the IRE Editorial Department at 1 East 79 Street, New York 21, N. Y.

—*The IRE Editorial Board*

Appendix

Abbreviations Used in IRE Publications

In general, all abbreviations for units of measure are lower case (the exceptions being Angstrom (A) and °C, °F, and °K) and all others are capitalized (the exceptions being ac, dc, cgs, mks, rms, rss, and certain metric symbols shown immediately below).

Metric Symbols

In 1958, the International Committee on Weights and Measures adopted an expanded list of metric prefixes and symbols. This list is regarded by the IRE Editorial Board as preferred, and has been so identified below. Thus, for example, gigacycle, nanosecond, and picofarad become the preferred terms.

Metric Prefixes and Symbols

Multiplier	Preferred Prefix	Preferred Symbol	Alternate Prefix	Alternate Symbol
10^{12}	tera	T	megamega	MM
10^{9}	giga	G	kilomega	kM
10^{6}	mega	M		
10^{3}	kilo	k		
10^{2}	hecto	h		
10^{1}	deca	dk		
10^{-1}	deci	d		
10^{-2}	centi	c		
10^{-3}	milli	m		
10^{-6}	micro	μ		
10^{-9}	nano	n	millimicro	mμ
10^{-12}	pico	p	micromicro	$\mu\mu$

Abbreviation	*Term*
AEW	airborne early warning
API	air-position indicator
ac	alternating current
AWG	American wire gauge
a	ampere
ah	ampere-hour
AM	amplitude modulation
A	Angstrom
ATR	anti-transmit-receive
AF	audio frequency
ADF	automatic direction finder
AFC	automatic frequency control
AGC	automatic gain control
AVC	automatic volume control
Bev	billion electron-volt
cp	candle power
CRO	cathode-ray oscilloscope
CRT	cathode-ray tube
°C	degree Centigrade
cm	centimeter
cgs	centimeter-gram-second
CW	continuous wave
c	cycle
cps	cycle per second
db	decibel
dbm	decibel referred to 1 milliwatt
dbv	decibel referred to 1 volt
dbw	decibel referred to 1 watt
°	degree
dc	direct current
DF	direction finder
DME	distance-measuring equipment
DSB	double sideband
emu	electromagnetic unit
EMF	electromotive force
ev	electron-volt
esu	electrostatic unit
EHF	extremely-high frequency
ELF	extremely-low frequency
f	farad
°F	degree Fahrenheit
ft	foot
fc	foot-candle
fl	foot-lambert
FM	frequency modulation
FSK	frequency-shift keying
Gc	gigacycle per second
GCA	ground-controlled approach
h	henry
HF	high frequency
hr	hour
IFF	identification friend or foe
in	inch
LC	inductance-capacitance
ID	inside diameter
ILS	instrument landing system
IF	intermediate frequency
ICW	interrupted continuous wave
°K	degree Kelvin
kc	kilocycle per second
kev	kiloelectron-volt

Abbreviation	*Term*
kMc	kilomegacycle per second
km	kilometer
kv	kilovolt
kva	kilovolt-ampere
kw	kilowatt
kwh	kilowatt-hour
l	lambert
LC	inductance-capacitance
LF	low frequency
lm	lumen
MUF	maximum usable frequency
MF	medium frequency
Mc	megacycle
Mw	megawatt
m	meter
mks	meter-kilogram-second
μa	microampere
μf	microfarad
μh	microhenery
μμf	micromicrofarad
μmho	micromho
μsec	microsecond
μv	microvolt
μw	microwatt
MEW	microwave early warning
mph	mile per hour
ma	milliampere
mf	millifarad
mh	millihenry
ml	millilambert
mm	millimeter
mμsec	millimicrosecond
Mev	million electron-volt
msec	millisecond
mv	millivolt
mw	milliwatt
MCW	modulated continuous wave
MTI	moving-target indicator
nsec	nanosecond
Ω	ohm
OD	outside diameter
ppm	part per million
PP	peak to peak
PM	phase modulation
pf	picofarad
PPI	plan-position indicator

Abbreviation	*Term*
psi	pound per square inch
PF	powerfactor
PAM	pulse-amplitude modulation
PCM	pulse-code modulation
PCM	pulse-count modulation
PDM	pulse-duration modulation
PPM	pulse-position modulation
PRF	pulse-repetition frequency
PRR	pulse-repetition rate
PTM	pulse-time modulation
PWM	pulse-width modulation
pps	pulse per second
RDF	radio direction finder
RF	radio frequency
RFI	radio frequency interference
RC	resistance-capacitance
rpm	revolution per minute
rms	root-mean-square
rss	root-sum-square
sec	second
SW	short wave
SNR	signal-to-noise ratio
SSB	single sideband
SWR	standing-wave ratio
SHF	super-high frequency
TV	television
TVI	television interference
Tc	teracycle per second
TR	transmit-receive
TE	transverse electric
TEM	transverse electromagnetic
TM	transverse maguetic
TWT	traveling-wave tube
UHF	ultra-high frequency
VTVM	vacuum-tube voltmeter
VHF	very-high frequency
VLF	very-low frequency
VOR	VHF omnirange
VSB	vestigial sideband
v	volt
VR	voltage regulator
VSWR	voltage standing-wave ratio
va	volt-ampere
vpm	volt per meter
vu	volume unit
w	watt
wh	watt-hour

Theory of a Monolithic Null Device and Some Novel Circuits*

W. M. KAUFMAN†, MEMBER, IRE

Summary—An important trend in modern electronics is toward decreased size and increased reliability of electronic systems. This paper discusses a new simple structure which performs the function of a twin-T network, *i.e.*, a null output is produced at a single frequency. This new structure has the advantage of being very small, simple to fabricate, and easy to use in conjunction with transistorized circuits. The theory of operation of the device, experimental verification of the theory, and some circuits containing the device is also discussed. The structure has been found useful to create a high-Q tuned amplifier, an oscillator, and a threshold transducer. The physical simplicity of the structure should result in a high degree of reliability and uniformity of response. It should be noted that the structure can be fabricated from semiconductor materials and is thus suited to "molecularized" or "integrated" solid state systems.

Introduction

An important trend in modern electronics is toward decreased size and increased reliability of electronic systems. One manifestation of this trend is the very sizable effort exerted by many organizations to construct semiconductor blocks or monoliths that will perform electronic functions that presently require a multiplicity of components. The development of a monolithic null device to replace a twin-T network was a direct result of the desire to create a tuned amplifier in the form of a semiconductor monolith. The normal inductance-capacitance tuned amplifier could not be used because, with the present state of the art, significant inductance is not obtainable in semiconductor structures. However, various references demonstrate that frequency selectivity is obtainable by means of a narrow band rejection filter (sometimes called a notch filter or null circuit) used in a degenerative feedback loop around a high gain amplifier.[1–3] If a null circuit such as a twin-T or a Wien-bridge is used, then the frequency selective system (tuned amplifier) would not contain any inductance. For this reason, the first step was the design of a monolithic device which would act as a notch filter.

Physical Structure

The monolithic structure that was found to possess the desired notch filter characteristics has been given the name "distributed bridged-T." An idealized distributed bridged-T structure is shown in Fig. 1. It consists of a capacitor-like sandwich of a dielectric layer between a resistive layer and a good conducting layer. Two terminals are connected, one at either end, to the resistive strip. A resistor, R, is connected between the good conducting layer and ground. (This resistor, R, could be "built in," for example, as a fourth layer of resistive material.) Employing the symbolic notation used by Hager, the electrical schematic symbol for this structure is also shown in Fig. 1.[4] An analog to the distributed structure is shown in Fig. 2. It consists of a multisection r-c ladder network (series r, shunt c), with all the capacitors connected together to one terminal of a resistor, R; the other terminal of R is at ground.

The idealized structure can also be approximated with semiconductor materials. Semiconductor materials are of interest for two reasons. One reason is that a semiconductor distributed bridged-T is more readily

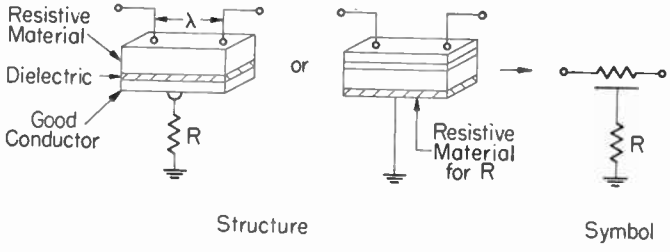

Fig. 1—An idealized distributed bridged-T filter.

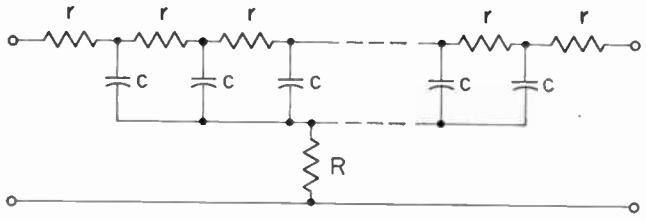

Fig. 2—A lumped circuit analog of the distributed bridged-T.

* Received by the IRE, August, 1960; revised manuscript received, November 6, 1959.

† Westinghouse Electric Corp., Research Laboratory, Churchill Borough, Pa.

[1] H. H. Scott, "A new type of selective circuit and some applications," PROC. IRE, vol. 26, pp. 226–235; February, 1938.

[2] G. E. Valley, Jr., and H. Wallman, "Vacuum Tube Amplifiers," Mass. Inst. Tech., Cambridge, Mass., Rad. Lab. Ser., vol. 18, McGraw-Hill Book Co., Inc., New York, N. Y.; 1948.

[3] S. Seely, "Radio Electronics," McGraw-Hill Book Co., Inc., New York, N. Y.; 1956

[4] C. K. Hager, "Distributed Parameter Networks for Circuit Miniaturization," AIEE-IRE-EIA-WCEMA Joint Electronic Components Conference, Philadelphia, Pa.; May, 1959.

employed in monolithic structures with other semiconductor devices such as diodes and transistors. Another reason is that the properties of semiconductor junctions permit electrical adjustment of the bridge parameters. A typical semiconductor structure is shown in Fig. 3. The distributed resistance is obtained by means of a lightly doped layer (shown as p-type in Fig. 3). The good conducting layer is obtained by means of a heavily doped region (shown as n-type). Distributed capacitance is obtained at the p-n junction when a reverse bias potential is applied. The resistor, R, can be connected externally or may be included as a resistive region connected to the highly doped region on the same block of semiconductor. Reverse bias can be applied to the junction in several ways. For simplicity of the sketch, it is shown connected between R and ground. It should be noted that the p- and n-impurity types can be interchanged; this would merely require a change in polarity of the bias supply.

Electrical Characteristics

Gain and phase characteristics can be calculated readily by employing the lumped circuit analog shown in Fig. 2, and then by allowing the number of lumped elements to become infinite. A portion of the network is shown in Fig. 4. Circuit equations can be written for this portion of the system:

$$i(x) = i(x + \Delta x) + c\Delta x \frac{\partial e_c(x)}{\partial t}, \tag{1}$$

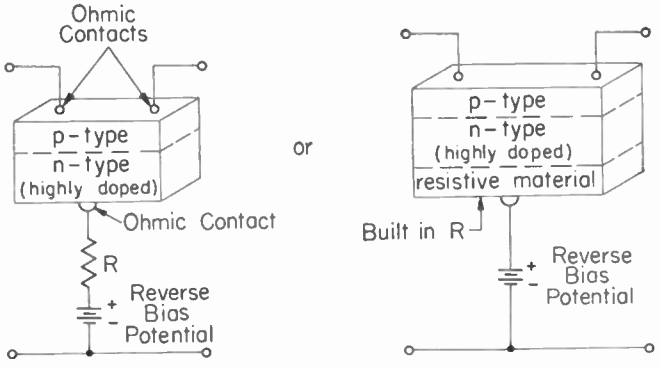

Fig. 3—Semiconductor structure for a distributed bridged-T.

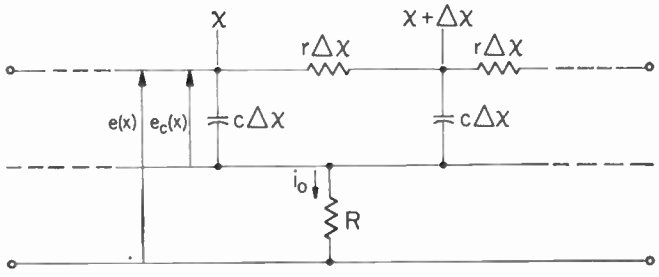

Fig. 4—One portion of the lumped analog network.

$$e_c(x) = i(x + \Delta x)r\Delta x + e_c(x + \Delta x), \tag{2}$$

$$e(x) = e_c(x) + Ri_0, \tag{3}$$

$$i_0 = \sum_{s=0}^{n} c\Delta x \frac{\partial}{\partial t}\left[e_c(s\Delta x)\right] \tag{4}$$

with $n\Delta x = \lambda$, a constant length. These equations can be reduced to partial differential equations in space and time by letting $\Delta x \to 0$. If all time variation is assumed sinusoidal (steady-state ac analysis), then the equations become ordinary second order differential equations in the space variable, x. The equations can then be solved for the rms voltage with respect to ground, $E(x)$, at any point $(0 \leq x \leq \lambda)$ along the structure for any given boundary conditions.

Of particular interest is the expression for complex gain as a function of ω, the angular frequency of the input signal. The gain of the device is defined as the ratio of output to input potential,

$$G(\omega) = \frac{E(\lambda)}{E(0)}. \tag{5}$$

Under no-load conditions, this becomes

$$G(\omega) = \operatorname{sech} u + \frac{1 - \operatorname{sech} u}{1 + \dfrac{\alpha}{u}\coth u} \tag{6}$$

or

$$G(\omega) = \frac{\alpha + u \sinh u}{\alpha \cosh u + u \sinh u} \tag{7}$$

where

$$u = (1 + j)\left(\frac{\omega}{\omega_1}\right)^{1/2}$$

$$\alpha = \frac{r\lambda}{R}$$

$$\omega_1 = \frac{2}{rc\lambda^2}.$$

Eqs. (6) and (7) are two different ways of expressing the same thing. Eq. (6) is useful in investigating the gain as frequency approaches infinity, and (7) is useful in determining gain at zero frequency.

From (6)

$$\lim_{u \to \infty} G\left(\frac{\omega}{\omega_1}\right) = 1$$

and

$$G(0) = 1.$$

The notch filter effect is obtained if the numerator of (7) can contain a zero as a function of frequency. Investigation has shown that there is an infinite set of

values for α which will allow a zero in the numerator of (7) for some frequency. The numbers of the set will be denoted $\alpha_{0,n}$, where n can take on any odd integer. The integer values of n correspond to the odd numbered intersections of the $-\tanh(\omega/\omega_1)^{1/2}$ curve with the family of curves $\tan(\omega/\omega_1)^{1/2}$ (see Fig. 5). The values of ω/ω_1 at which an intersection occurs will be denoted by $\omega_{0,n}/\omega_1$. The value of α corresponding to a given intersection is

$$\alpha_{0,n} = 2\left(\frac{\omega_{0,n}}{\omega_1}\right)^{1/2} \cosh\left(\frac{\omega_{0,n}}{\omega_1}\right)^{1/2} \sin\left(\frac{\omega_{0,n}}{\omega_1}\right)^{1/2}. \tag{8}$$

The first intersection occurs at

$$\frac{\omega}{\omega_1} = \frac{\omega_{0,1}}{\omega_1} = 5.5951 \cdots.$$

and the corresponding α is

$$\alpha_{0,1} = 17.786 \cdots.$$

The third intersection and all higher ordered intersections very nearly occur at

$$\frac{\omega_{0,n}}{\omega_1} = \left(n\pi - \frac{\pi}{4}\right)^2.$$

Further investigation of the gain function has shown that there are no zeros of the denominator for real frequency.

The behavior of the gain function for α near $\alpha_{0,1}$ and $\alpha_{0,3}$ was investigated thoroughly. What has been learned can best be presented in the form of a polar plot of $G(\omega)$. The polar plot is created by expressing the complex gain in the form of an amplitude, A, and a phase angle, ϕ. On a polar coordinate system, the radial distance corresponds to A and the angular position corresponds to ϕ. Thus, the polar plot of the gain function is the locus of points (A, ϕ) for all frequencies, ω. Fig. 6 contains polar plots of $G(\omega)$ for α in the vicinity of $\alpha_{0,1}$. Fig. 7 contains a polar plot of $G(\omega|\alpha=\alpha_{0,3})$. Of particular interest is the fact that for $\alpha<\alpha_{0,1}$ the plot does not encircle the origin; therefore ϕ is restricted to $-\pi<\phi<\pi$. However, for $\alpha>\alpha_{0,1}$ the plot does encircle the origin, and ϕ goes from 0 to 2π. Therefore, there is a discontinuity in ϕ for $\alpha=\alpha_{0,1}$ at $\omega=\omega_{0,1}$. Furthermore, for $\alpha_{0,1}<\alpha<\alpha_{0,3}$, then $0\leq\phi\leq 2\pi$. But for $\alpha_{0,3}<\alpha<\alpha_{0,5}$, ϕ goes from 0 to 4π, and there is another discontinuity in ϕ for $\alpha=\alpha_{0,3}$ at $\omega=\omega_{0,3}$. Although it has not been verified it is expected that for $\alpha_{0,5}<\alpha<\alpha_{0,7}$, ϕ will go from 0 to 6π, etc. Corresponding to the polar plot, both amplitude and phase could be plotted as functions of frequency. These curves are shown in Fig. 8(a), Fig. 8(b), and Fig. 9. For the purpose of comparison, the amplitude response curves for the distributed bridged-T ($\alpha=\alpha_{0,1}$) and for the classical twin-T are plotted in Fig. 12. The close similarity is apparent from the graphs.

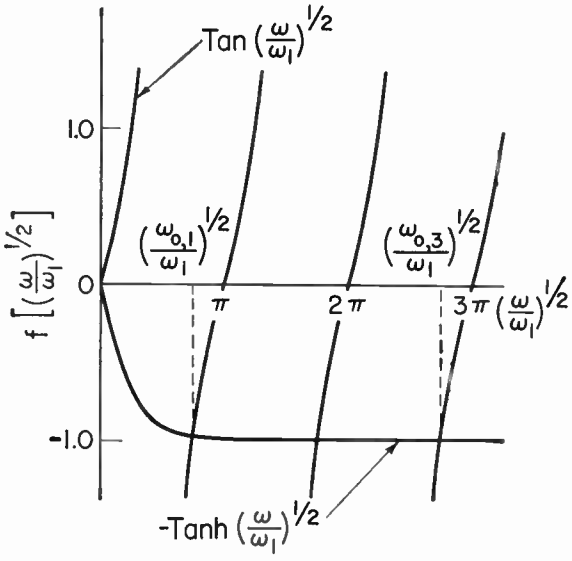

Fig. 5—Tanh $(\omega/\omega_1)^{1/2}$ and ton $(\omega/\omega_1)^{1/2}$.

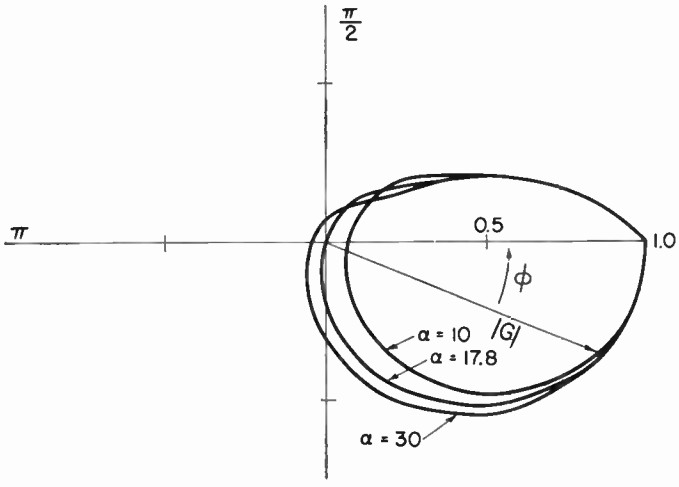

Fig. 6—Polar plots of the complex gain for α in the vicinity of $\alpha_{0,1}$.

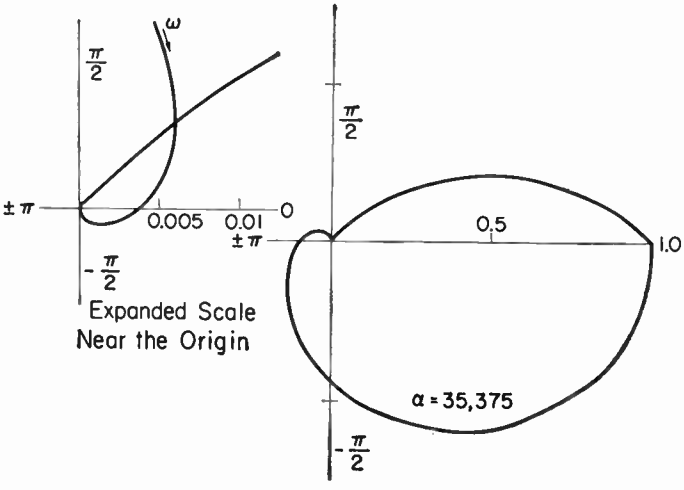

Fig. 7—Polar plot of the complex gain $\alpha=\alpha_{0,3}$.

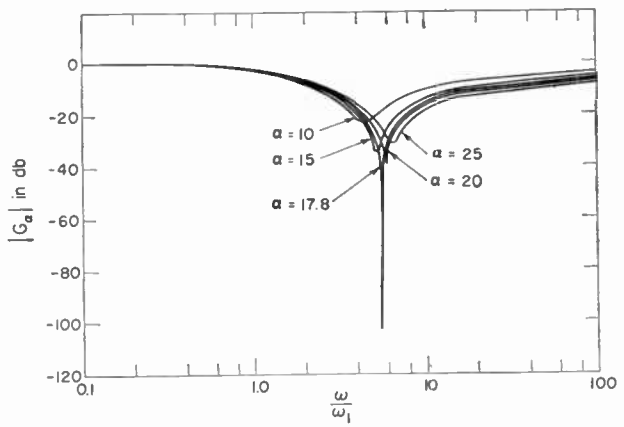

(a)

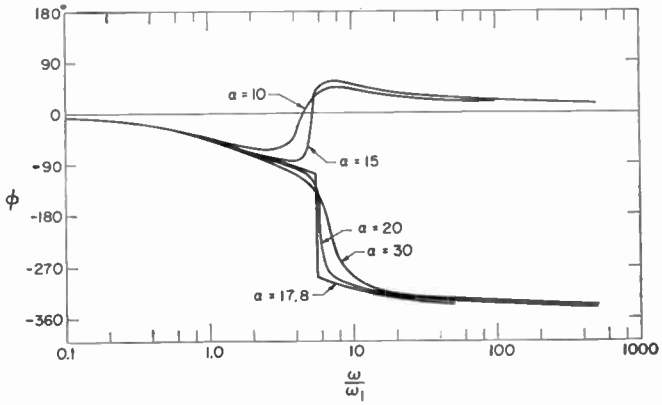

(b)

Fig. 8—(a) Amplitude response vs frequency for α in the vicinity of $\alpha_{0,1}$. (b) Phase vs frequency for α in the vicinity of $\alpha_{0,1}$.

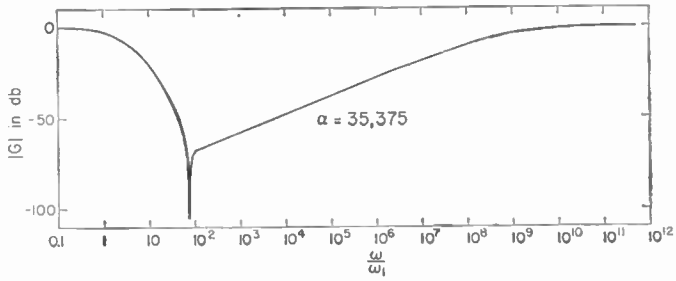

Fig. 9—Amplitude response vs frequency for $\alpha=\alpha_{0,3}$.

Tunability of the Semiconductor Structure

As was shown above, there is a definite relationship between the null frequency and the system parameters. The null frequency depends on α and on ω_1. The null frequency for $\alpha_{0,n}$ will be $\omega_{0,n}$. As was defined above, each number $\omega_{0,n}/\omega_1$ is an intersection of the negative hyperbolic tangent curve with the trigonometric tangent curves. Therefore, for given $\alpha_{0,n}$

$$\omega_{0,n} = \left(\frac{\omega_{0,n}}{\omega_1}\right)\omega_1$$

or

$$\omega_{0,n} = \left(\frac{\omega_{0,n}}{\omega_1}\right)\frac{2}{rc\lambda^2}. \tag{9}$$

For an abrupt p-n junction, the width of the depletion layer, and thus the capacitance per unit area, varies inversely with the square root of the reverse bias potential. For a given device geometry, the capacitance per unit length is

$$c = c_0 V^{-1/2}. \tag{10}$$

The resistance per unit length is

$$r = \frac{\rho}{WT}, \tag{11}$$

where

ρ = resistivity of material,
W = width of the device,
T = thickness of the resistive layer.

For a particular material and geometry,

$$T = T_0 - T_1 V^{1/2}, \tag{12}$$

where

T_0 = original thickness of the resistive layer,
T_1 = the rate of increase of the depletion layer with respect to the square root of bias potential.

Using (10), (11), and (12) in (9), and combining constants

$$\omega_{0,n} = \left(\frac{\omega_{0,n}}{\omega_1}\right)(AV^{1/2} - BV). \tag{13}$$

Eq. (13) describes a parabola in $V^{1/2}$ with zeroes at $V^{1/2}=0$ and at $V^{1/2}=A/B$, and a maximum for $\omega_{0,n}$ of $A^2/4B$ occurring at $V^{1/2}=A/2B$. This parabola is an idealized tuning curve for the distributed bridged-T if it is fabricated from a semiconductor with an abrupt p-n junction.

Novel Circuits Employing the Distributed Bridged-T

The distributed bridged-T is suitable as a substitute for the twin-T null network in essentially all circuits. However, the electrical tunability of the semiconductor structure and the abrupt change in phase shift characteristics from $\alpha<\alpha_{0,1}$ to $\alpha>\alpha_{0,1}$ provide certain advantages over the lumped parameter twin-T network.

An important circuit employs the distributed bridged-T in conjunction with a high gain amplifier to form a narrow band tuned amplifier. This is accomplished by connecting the filter in a degenerative feedback loop around the amplifier (see Fig. 10). For a high gain amplifier, the response will then approach the reciprocal of the filter characteristics. The Q obtainable is theoretically unlimited depending only on the gain of the amplifier if the filter is properly adjusted to $\alpha_{0,1}$. An

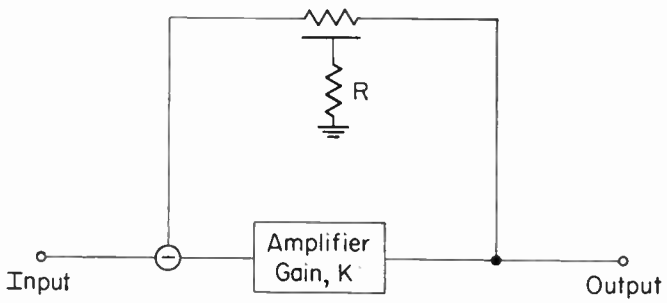

Fig. 10—A high-Q tuned amplifier.

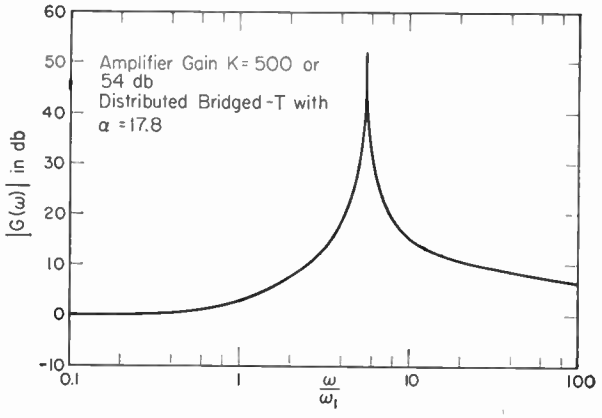

Fig. 11—Response of an amplifier employing selective degenerative feedback through a distributed bridged-T.

example of tuned amplifier characteristics is given in Fig. 11. This is a theoretical curve based on an amplifier with 54-db voltage gain and negligible phase shift in the frequency range of interest.

This circuit of Fig. 10 can also be used as an oscillator with adjustable frequency of oscillation by maintaining $\alpha > \alpha_{0,1}$. Under these conditions, as can be seen from the polar plots of Fig. 6, the distributed bridged-T will contribute exactly 180 degrees phase shift at some frequency, ω_{osc}. If α is just slightly greater than $\alpha_{0,1}$, then ω_{osc} will be nearly equal to $\omega_{0,1}$. In fact,

$$\lim_{\alpha \to \alpha_{1,0}} \omega_{osc} = \omega_{0,1}.$$

However, since $\alpha > \alpha_{0,1}$ must hold, $\omega_{osc} < \omega_{0,1}$. With α fixed, the frequency of oscillation can be varied by varying $\omega_{0,1}$. As was described above, when using semiconductor materials, $\omega_{0,1}$ can be changed electrically by varying junction bias potential.

The extreme sensitivity of phase shift to changes in α in the vicinity of $\alpha_{0,1}$, makes it possible to create a bistable device operating on this principle. Such a system would also use the basic circuit of Fig. 10, but the lumped resistor, R, is now variable. If the resistance is greater than some critical value the system will not oscillate. If the resistance is equal to or less than the critical value the system will go into oscillation. The critical resistance, R_c, satisfies the equation

$$KG\left(\omega \mid \frac{r\lambda}{R_c}\right) = -1. \tag{47}$$

For large K, R_c will be slightly less than $r\lambda/\alpha_{0,1}$.

$$\lim_{K \to \infty} R_c = \frac{r\lambda}{\alpha_{0,1}}. \tag{48}$$

This bistable system can be used as a threshold transducer that would switch to an oscillating condition whenever R goes below R_c. The transducer could then be used with any physical quantity that can be transformed into an electrical resistance. Some examples are temperature, strain, light intensity, atomic radiation, and electrical potential.

Experimental Results

Certain experiments were performed to verify the theoretical conclusions concerning the distributed bridged-T. The forward transfer characteristics were measured for a distributed bridged-T device, made at the Youngwood plant.[5] The device was fabricated from a p-n junction in silicon. Lumped resistor R was applied externally. The optimum value of R was found to be 190 ohms when 1 volt reverse bias was applied. The value of $r\lambda$ measured with no bias at dc was found to be approximately 3200 ohms. The experimental α is then approximately 16.8. The 6 per cent discrepancy here from theoretical 17.8 is probably due to the combination of reverse bias of 1 volt and device operation in the megacycle range. Further experimental results agree more closely with theory. The measured amplitude response is plotted in Fig. 12 along with the theoretical bridged-T and the theoretical twin-T response curves. Since only the output was measured, the point measured at lowest frequency (0.075 mc) was chosen as a reference and was assumed to lie on the theoretical curve. All the other points were determined with respect to the reference point (in db) and were then plotted. It is clear that the experimental results agree almost exactly with the theoretical curve. The only area of disagreement is the depth of the measured null. This is shown in the inset of Fig. 12. The theoretical null drops to $-\infty$ but the measured null was finite. It was found that the wave shape from the signal generator used at the input had very high harmonic content, and that the harmonics were being passed when the fundamental was being rejected at the null frequency. This certainly accounts for the discrepancy at the null. To further check this, the transfer characteristic of a 10-section lumped approximation to the distributed system was measured with the same equipment. Normalizing the data to the same null frequency (actually, the nulls were very close, 1.78 mc for the distributed circuit, 1.88 mc for the lumped circuit), it can be seen in Fig. 13 that the distributed system and the 10-section approximation act almost identically in the same test setup. The difference here between the depths of the nulls is about 4 db and is probably due to the fact, as can be seen in Fig. 13, that the lumped approximation attenuates harmonics of the input to a somewhat greater degree than the distributed

[5] Westinghouse Electric Corp.

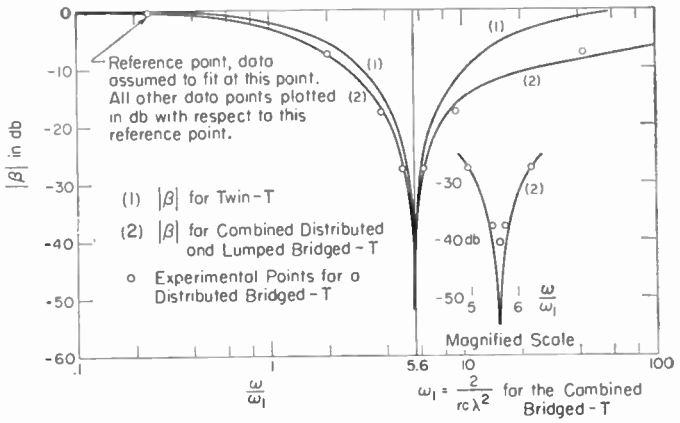

Fig. 12—Theoretical curves for t, twin-T and distributed bridged-T, and experimental points for the distributed bridged-T.

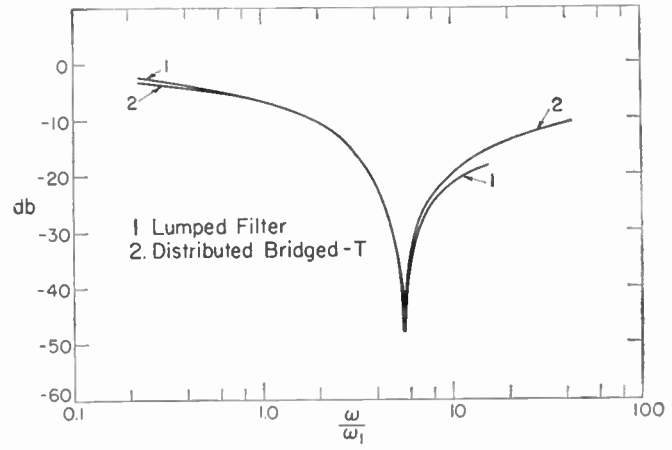

Fig. 13—Experimental comparison between a distributed bridged-T and a lumped parameter approximation to it.

system. Data was also obtained on the variation of null frequency with bias voltage. As explained above, the theoretical tuning curve is parabolic in the half power of the bias potential. This parabolic shape could not be fully tested because the junction breakdown voltage prevented a wide enough range of test voltages. However, the curve has been compared with a parabola merely to show that some parabola does give a reasonable fit. This is shown in Fig. 14. The experimental curve does not go to dc at $V=0$, because junctions have a depletion layer even with zero externally applied bias, and, furthermore, any input signal would cause self-biasing because of the rectifying action of the junction.

Experiments were also performed using the distributed bridged-T device in the circuit of Fig. 10. Operation was possible as a frequency controllable oscillator, but the inherent additional 75° phase shift of the amplifier caused the oscillation frequency to be quite different (and lower) than the null frequency $\omega_{0,1}$. Instead of 180° the distributed bridged-T network had to contribute only 105°, which occurs at a frequency somewhat lower than $\omega_{0,1}$. This oscillator frequency was still controllable by varying the bias potential, for the phase shift contribution of the filter at any frequency is related to $\omega_{0,1}$.

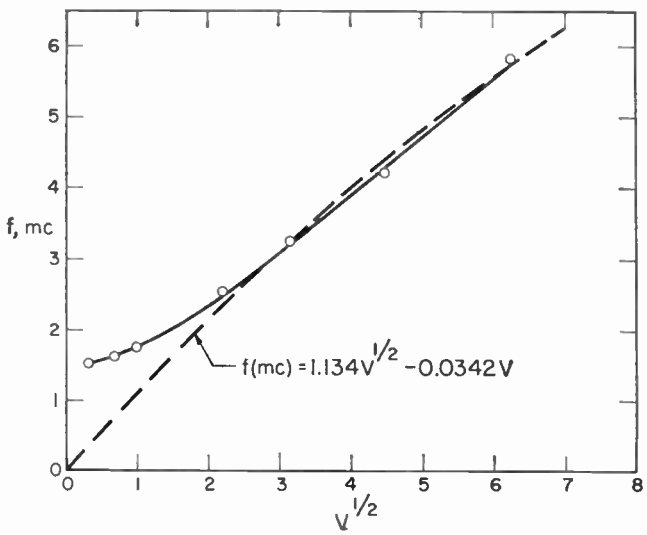

Fig. 14—Tuning curve for a distributed bridged-T filter.

Conclusions

The primary goal of providing a tuned amplifier without inductance in a monolithic structure has been accomplished as described above, and the adjustability of the selected frequency by electrical means is a useful by-product of the semiconductor embodiment of the structure. There is no reason to place all emphasis on the semiconductor embodiment of the distributed bridged-T. Because of the simplicity of the structure, fabrication of the device by means of material deposits on a dielectric slab resulting in a configuration similar to Fig. 1 should be very inexpensive and should, therefore, provide significant competition to the tuned IF transformer in those tuned circuit applications where small size is of primary importance. An example of the small size obtainable is the fact that sample devices have been constructed with nulls at approximately 1 mc, with dimensions 0.09 inch by 0.04 inch and 0.003 inch. The great similarity between the response of the distributed filter and the twin-T network as shown in Fig. 12 indicates that the distributed bridged-T can be used virtually interchangeably with the twin-T circuit. The fact that a similar characteristic to that of a twin-T is obtainable in a physically simpler structure indicates that there may be much value in investigating general analytic and synthetic techniques for combined parameter systems.

Acknowledgment

The author wishes to thank Dr. G. C. Sziklai of the Westinghouse Electric Corporation for suggesting this problem, and John Stelmak and John Husher of the Westinghouse Semiconductor Department and Dr. H. C. Lin, C. Benjamin, J. Philips, and P. Smith of the Westinghouse Materials Engineering Department, for the preparation of distributed bridged-T structures and the measurement of filter characteristics. The author is grateful to the Westinghouse Electric Corporation and the United States Air Force for permission to publish this paper.

Video Transmission Over Telephone Cable Pairs by Pulse Code Modulation*

R. L. CARBREY†, MEMBER, IRE

Summary—An experimental seven digit pulse code modulation (PCM) system has been built for the transmission of monochrome and color television signals over seven pairs of 22-gauge exchange area telephone cable, installed in the laboratory. A beam coding tube converts the signal to seven parallel digits of a binary Gray code at a 10 mc rate. All circuits except the coding tube deflection amplifier are transistorized. The coded digits are sent over the cable in parallel form with alternate groups converted to complements of the coded signal, thus substantially removing the low frequency component. This makes it possible to use simple repeaters without special compensation for duty factor variation. A repeater group is used after every 3000 foot section of cable. One ten megabit repeater, consisting of an amplifier and blocking oscillator, is required for each digit. All seven digit repeaters are retimed with a common timing wave. At the decoding terminal, transmitted complements are restored to Gray code before translation to natural binary. A binary weighted resistance network decoder converts the signals to a quantized reproduction of the video signal. Good quality composite color and monochrome pictures are obtained with six digits. Seven digits are believed to be necessary for broadcast quality with some margins. Waveform photographs illustrate the various functions, and photographs of decoded pictures are shown.

Introduction

THIS PAPER describes an experiment whose primary objective was to encode standard broadcast television signals into seven digit PCM, and to transmit the digits in parallel over seven pairs of type CSA 22-gauge paper-pulp insulated exchange area telephone cable. Transistors are used in the repeaters as well as at the coding and decoding terminals, but they are not used for the beam tube coder and its associated deflection amplifier.

In order to add a single television cable circuit using present analog signal transmission techniques, it would be necessary to bury or pull into cable ducts either a coaxial cable, such as that shown at the bottom of Fig. 1, or a double-shielded balanced 19-gauge pair video cable. In large metropolitan areas this is a very expensive operation. However, a signal which has been converted to binary pulse code modulation at the point of origin can be transmitted over existing telephone cable either directly to the destination, or to a backbone transmission system.[1] This should permit circuits to be added more economically with all of the advantages of digital transmission provided, of course, that the repeaters and terminals have adequate reliability, and that their installation and manufacturing costs are kept within reasonable limits.

The type of cable which was used for the experiments to be described is shown at the top of Fig. 1. It is a 51-pair cable of the type normally used to connect the subscriber's telephone to the central office. It was intended to be used only for short haul voice frequency work. The cable attenuation characteristics are shown in Fig. 2. The ten mc loss is 116.6 db per mile, the five mc loss, which is the major one of interest, is 77.5 db. Loading coils are spaced 6000 feet apart in this cable. It would be desirable to replace the loading coils with repeaters; so one would like to space the repeaters 6000 feet apart. This requires more gain than should be handled in a single repeater. Therefore, the repeaters, one per digit, are spaced only 3000 feet apart. The lower loss-curve shows the 3000 foot attenuation. At five mc, the loss is 44 db. Crosstalk characteristics have been measured on the laboratory cable installation and several others. The worst far-end crosstalk for ten megabit pulses was found to be 45 db below the signal. The 51-pair cable could be used to transmit seven TV programs

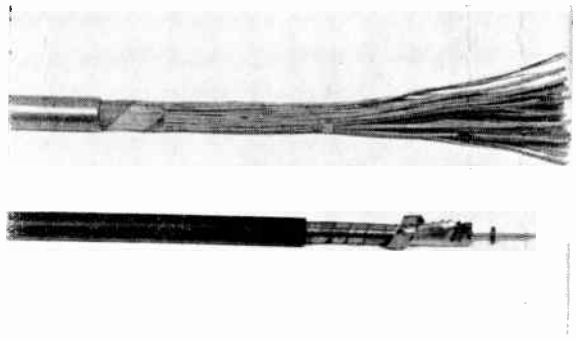

Fig. 1—$\frac{3}{8}$-inch coaxial cable, and 51-pair exchange area cable.

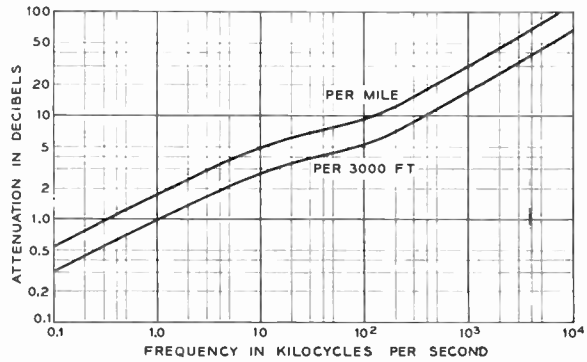

Fig. 2—Attenuation characteristic of 22-gauge cable pairs.

* Received by the IRE, January 29, 1960; revised manuscript received May 30, 1960.

† Bell Telephone Labs. Inc., Murray Hill, N. J.

[1] S. E. Miller, "Waveguide as a communication medium," *Bell Sys. Tech. J.*, vol. 33, pp. 1209–1266; November, 1954.

in one direction with two pairs left over for spares.[2] Incidentally, each pair could be used for 178 seven-digit voice frequency channels. Most exchange area cables are made up of a number of such 50- or 51-pair bundles inside a common sheath.

In an analog system such as that used for transcontinental TV transmission, it is necessary to design and maintain the repeaters to a very high degree of precision.[3] Coaxial repeaters are spaced about four miles apart, so it is necessary to use almost a thousand repeaters in some of the long circuits. Any noise, crosstalk, or distortion which occurs will be passed along to the rest of the repeaters in the chain. Because the effects are cumulative, each repeater must meet requirements which are appreciably better than the over-all requirements. It is a tribute to the analog transmission art that such excellent quality is achieved over circuits of this length. In order to do so, however, it is necessary to measure some of the coaxial amplifier components to a thousandth of a db, and the gains and equalization characteristics are frequently held to a hundredth of a db. The repeaters must be both expensive and complex, and they cannot eliminate unwanted disturbances which do occur.

Although ordinary voice frequency telephone cable pairs are capable of passing a wide enough frequency band to handle standard broadcast television signals, they are subject to so much interpair crosstalk at video frequencies, the loss equalization problem is so severe, and the total loss is so high, that transmission over exchange cable pairs of a broadcast type television signal by present conventional analog methods is impractical except for very short distances.

With binary pulse transmission, on the other hand, the signal is regenerated at each repeater, so it is necessary only to design the repeaters to be able to handle a single span from one repeater to the next. It is theoretically possible to tolerate a zero-to-peak interference of half the amplitude of the peak-to-peak signal. This six db limit must usually be reduced to about nine db by practical circuit limitations, but even so, considerable distortion and interference can be handled without error as will be shown later. It is also theoretically possible to transmit a TV signal over any distance by the use of regenerative repeaters without increasing the noise or getting any more distortion of the signal than would be present in transmitting the signal directly from the PCM coder to the decoder. The noise which does exist is quantizing noise caused by the transmission of a finite number of signal levels. With seven digits, 128 levels can be transmitted.

Transmission of a broad-band signal in pulse form permits separating the signal into as many parallel paths as desired, so that transmission facilities can be used which would be inadequate for transmission of the entire signal over a single path. Conversely, the pulse signals from more than one signal source can be interlaced for transmission over a common path of adequate capacity.

Coding Terminal

The basic system and sampling frequency is set by a 10-mc crystal oscillator, so, in accordance with the Nyquist theorem,[4] the maximum frequency which can be transmitted is just under 5 mc. The 10-mc sampling rate was selected somewhat arbitrarily because it was a nice round number, and because it would permit a gradual roll-off in the video output filter. This is more than adequate for the standard NTSC television signal which cuts off to permit the sound carrier to be inserted at 4.5 mc. The precise frequency to use in a system application must take into account a number of complex factors.

Fig. 3 is a pictorial diagram of a coder in which only five digits are shown for simplicity. A 10-mc pulse is used to operate the balanced transistor sample and hold gate represented in Fig. 3 as a switch. The switch is closed once every 100 nanosecond (nsec) for 50 nsec.[5] During this time, the capacitor is charged to the value of the video signal. During the 50-nsec interval when the switch is open, the signal level is stored as a flat sample. (See Fig. 4.) This is done in order to prevent the beam from moving up or down the aperture code plate while a decision is being made. A 10-mc sine wave is applied to the grid of the beam coder which turns the beam off during the sampling interval, and turns it on during the holding interval.

The coding tube, Fig. 5, is an improved version of the one which was used in some earlier work by W. M. Goodall.[6] It was developed by the Electron Tube Development Dept.[7] The rectangular gun structure forms a ribbon beam instead of the more conventional string beam. Referring again to Fig. 3, the held signal sample is first amplified by a broad-band deflection amplifier, so that a total deflection voltage of about 90 volts is available. This is the only place in the system where vacuum tubes are used. When the ribbon beam is turned on by the 10-mc blanking circuit, it will hit the aperture plate at a position corresponding to the analog amplitude. Where the beam hits the solid metal of the coding plate, the electrons are blocked, and a space, or zero condition, will appear at the output. Where the beam hits an

[2] Both far-end crosstalk and near-end interaction crosstalk must be studied in field installed cable before any definite estimate of the possible number of one-way transmission circuits can be made. Near-end crosstalk would probably limit two-way transmission to carefully selected pairs in separate bundles.

[3] See issue on "The L3 coaxial system," *Bell Sys. Tech. J.*, vol. 32, pp. 779–1005; July, 1953.

[4] H. Nyquist, "Certain topics in telegraph transmission theory," *Trans. AIEE*, vol. 47, pp. 617–644; April, 1928.

[5] One nsec = 10^{-9} seconds.

[6] W. M. Goodall, "Television by pulse code modulation," *Bell Sys. Tech. J.*, vol. 30, no. 1, pp. 33–49; January, 1951.

[7] R. W. Sears, "Flash coding tube," presented at the IRE WESCON Convention, Los Angeles, Calif.; August 21, 1956.

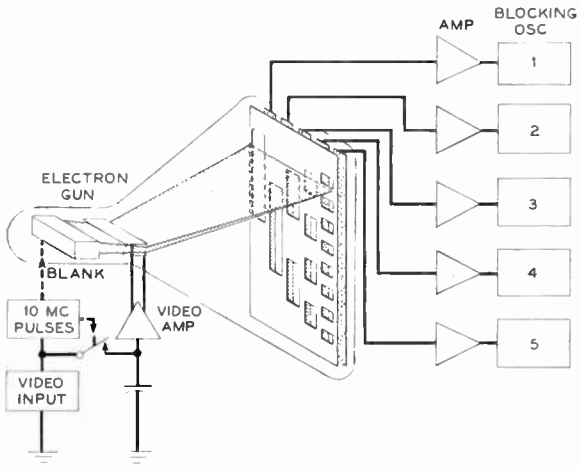

Fig. 3—Pictorial diagram of five digit coder.

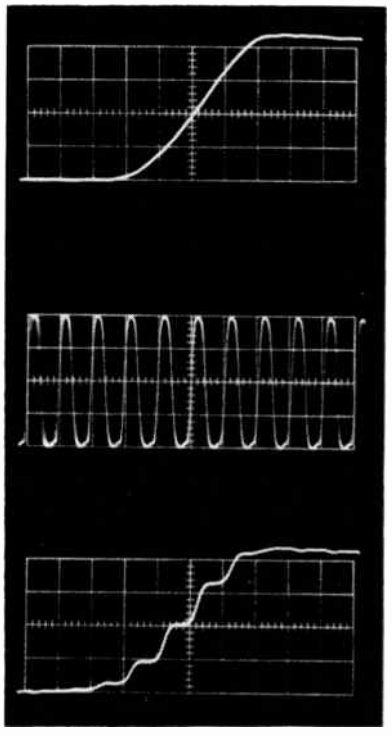

Fig. 4—Sample and hold circuit waveforms. (a) Video input to sample and hold circuit. (b) 10-mc control wave. (c) Sampled and held output of coder deflection amplifier. Time scale: 100 msec per major division.

opening in the plate, it "passes" through to the collector electrode. Individual collector electrodes are positioned behind each of the seven digit columns.

The output currents for a beam passing cleanly through the holes are of the order of 35 microamperes, depending upon the beam intensity and focus. An output pulse will result from this current burst. Because the beam has a finite height, it does not always fall in a position where it either passes cleanly through the hole or is completely stopped. When it hits an edge of a hole only partial current appears at the output, and a "maybe" condition exists instead of a clean-cut yes or no.

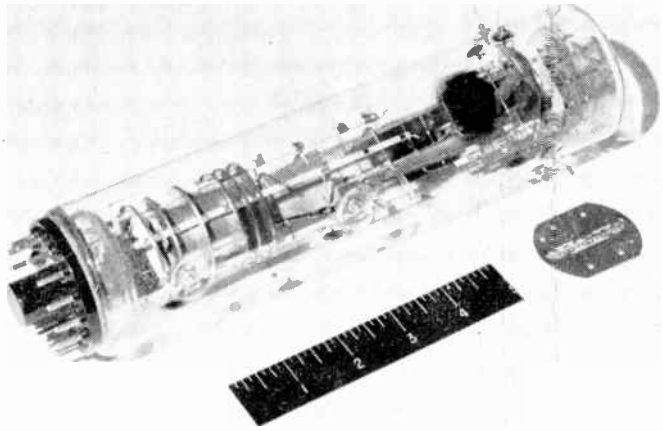

Fig. 5—Beam coder tube and aperture plate.

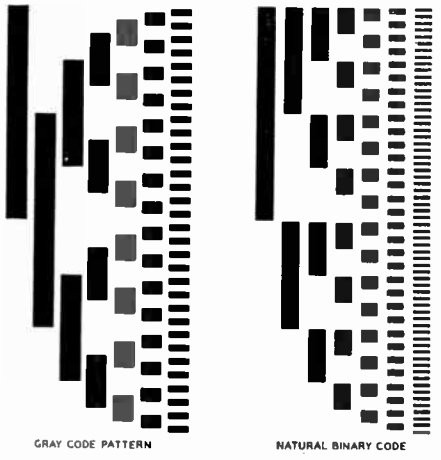

Fig. 6—Gray and natural binary code patterns.

If we were to use an aperture plate cut out in accordance with the natural binary code, as shown in Fig. 6(b), from one to seven separate decisions would have to be made when the beam was positioned across the edge of an aperture. The stability and precision of simple decision circuits are such that they all might not make a consistent decision. When a "Gray code" pattern[8] of the type shown in Fig. 6(a) is used, only a single decision has to be made at any transition from one level to the next.

The output beam current which appears on each of the individual collector wires is first amplified, and then the amplified output is applied to a blocking oscillator which uses a small ferrite core cup-type feedback transformer and a diffused base transistor. It is in this decision circuit that the quantizing operation really takes place. The amplitude of the one input signal which is in a "maybe" state is a measure of the quantizing error. When it is midway between the pulse and space condition, the quantizing error is a half step.

[8] F. Gray, "Pulse code communication," U. S. Patent No. 2,632,058; March 17, 1953.

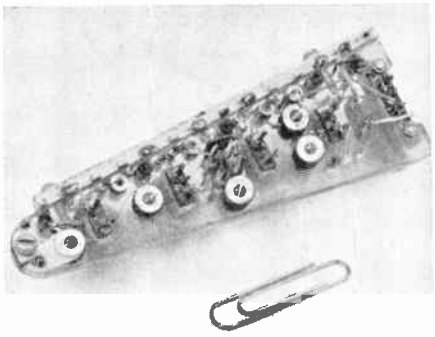

Fig. 7—Coder output regenerator package.

Fig. 7 is a photograph of one of the coder output regenerator units. This is a three stage transformer coupled amplifier with diode clipping of the center and peak levels. A differentiating type transformer is used in the input circuit in order to remove the dc component from the signal train. The resulting output caused by the blanked beam current has the general appearance of a 10-mc sine wave whose amplitude is modulated by the signal position. Fig. 8(a) shows the output when a sawtooth wave with some noise present sweeps the beam slowly across the edge of an aperture plate hole in one of the digit 5 positions. The blocking oscillator is triggered whenever the negative pulses swing below the nominal slicing level which is the second graticule line from the bottom. Waveform *b* shows the resulting output pulses. Observe that good clean decisions are made by the transistor blocking oscillator. The slight "fuzzing" at the leading edge of the pulses is caused by the variation in trigger time between triggering at the $-45°$ and $-90°$ points on the "sine wave" as well as by the finite decision time required. Regating the input with a narrow timing pulse could be used to reduce this variation further, if desired. The pulses are, of course, 100 nsec apart. Note that each pulse of about 50 nsec duration is followed by a blank interval of about the same length in order to give the circuit sufficient time to recover to a stable rest point before the next decision has to be made. Waveform *c* shows the amplified output wave from the coder tube as the beam sweeps completely across a digit 5 hole. The sweep speed is 2 μsec per major division. Fig. 8(d) shows the resulting long group of regenerated pulses. Note that the amplitude regeneration is not perfect, and that the height does vary slightly with triggering magnitude.

Alternate Interchange

The regenerated pulses from the coder output regenerator could be coupled directly to the balanced 22 gauge cable pair through an unbalance-to-balance coupling transformer. It is necessary to use a transformer at the input and output of the line, because an unbalanced regenerator is used and the transmission line must be operated balanced in order to maintain the good crosstalk margins. The pulses which are to be

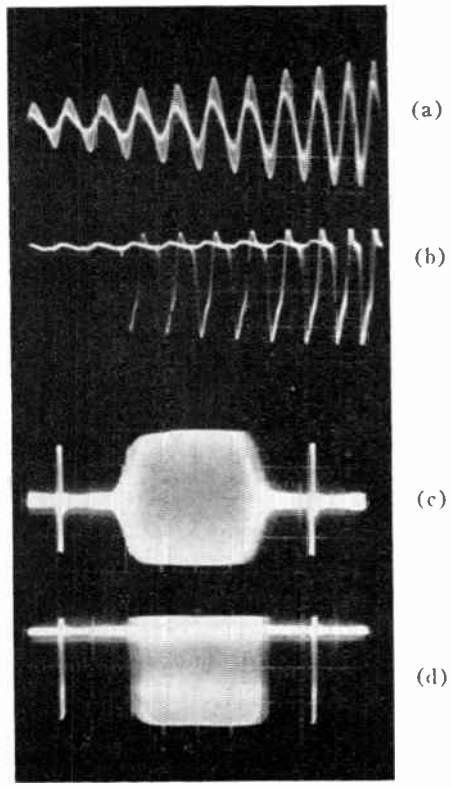

Fig. 8—Coder output regenerator waveforms. (a) Amplified output with coder beam sweeping across the aperture edge. (b) Blocking oscillator output pulses showing decision (0.1 μsec/division). (c) Output with beam sweeping across digit 5 aperture (2 μsec/division). (d) Blocking oscillator output pulses for input *c*.

transmitted are subject to two major forms of distortion. One of these is the spreading out of the pulses caused by the marked increase in attenuation with frequency as noted in Fig. 2. This can be taken care of by equalization as discussed later. The other distortion is caused by the low frequency cutoff of the transformers which are used. This changes the effective decision level of the regenerator as the signal duty factor changes.

Fig. 9 shows what the low frequency cutoff of the transformers does to the signal. Fig. 9(a) shows a train of about 500 pulses at the primary side of the line driving transformer. Fig. 9(b) shows the resulting wave train after passing through a balance-to-unbalance transformer at the output of 3000 feet of cable. Both the input and output transformers have, naturally, a low frequency cutoff which attenuates the step function. (The transmission time is about 3.5 μsec.) Fig. 9(c) shows the same wave at the output of the equalized repeater amplifier which includes an additional transformer. This waveform would be a flat-top-and-bottom square wave if the transformers could pass very low frequencies. If the second graticule line from the bottom represents the slicing level, only about 60 pulses would get through correctly in the absence of any interference. Everything following would be classified as a space. This is a problem that arises in ac coupled variable-duty-cycle single polarity circuits, even though the runs are not long. Designing better transformers, lowering the impedance,

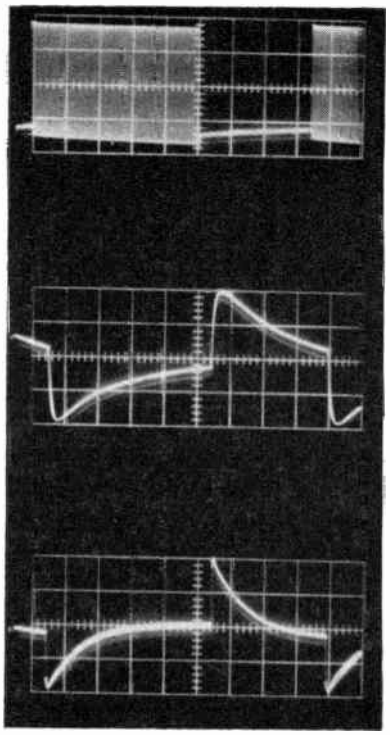

Fig. 9—Response of transformers and line to long pulse train. (a) 500-Pulse group at primary of input transformer to 22-gauge cable (10 μsec/division). (b) Transformer coupled unequalized output of 3000 feet of cable. (c) Equalized output of repeater amplifier showing low frequency cutoff of transformers.

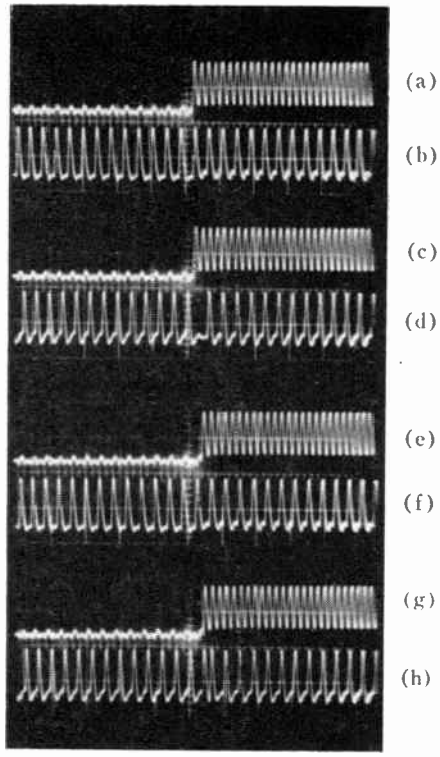

Fig. 10—Alternate interchange at start of pulse train, with pulse train shifted to show double space and double pulse transition conditions. (a) Coded signal input (0.5 μsec/division). (b) 5-mc control wave (c) Repeat of (a). (d) Alternate interchanged output. (e) Pulses period later. (f) 5-mc control wave. (g) Repeat of (e). (h) Alternate interchanged output.

and equalizing to high frequency would extend the pulse handling capacity, but practical limits do exist. L. R. Wrathall used quantized feedback to handle pulse trains of several seconds duration at 672 kc.[9] Unfortunately, quantized feedback around the whole repeater turned out to be difficult at 10 mc. Local quantized feedback around the blocking oscillator only could be used effectively, but the adjustment must be very precise. Quantized feedback should always be sufficiently less than ideally required, in order to prevent the circuit from breaking into spurious operation if the input signal level drops or the feedback increases slightly.

An effective method of virtually eliminating the problem is to modify the signal statistics by a method called alternate interchange (AI). Video signals lend themselves very well to this process, and most other types of ordinary signals are benefited also. First consider the statistics as coded. Runs of pulses such as those shown in Fig. 9 are not at all uncommon. Indeed, a single line of a TV signal between the back porch and the following front porch is 52.1 μsec, so a single line at constant level would produce 521 pulses or spaces in a row for each of the digits. Digit 1, the most significant, is a pulse in the grey-to-blacker-than-black region, so it might appear as a run of pulses from one commercial to the next for a night scene program. The most probable next binary signal is a repeat of the one being transmitted.

Fig. 10 shows how changing the pulses to spaces and the spaces to pulses in every even numbered time slot converts unfavorable runs of spaces or pulses to essentially a 5-mc wave. At the top, the start of a coded group of pulses is shown; a 5-mc pulse train is shown just below this. If these two waveforms are fed into a logic circuit which is essentially a half adder, waveform *d* will result. A half adder operates on the logic combinations $0+0=0$, $1+0=1$, $0+1=1$, and $1+1=0$. Therefore, when the two inputs are alike, a space output is produced. When they are different, a pulse output is produced. This changes every other group to its complement. During the time the input shown at *a* is a space, the output is a 5-mc pulse train in phase with the reference wave. A double space is produced at the transition from spaces to pulses because the first pulse is in phase with the 5-mc control wave. During the pulse run, a 5-mc wave 180° out of phase with the control wave is sent out. Had the pulse run started 0.1 μsec later (or earlier) as shown in waveform *e*, a double pulse would have occurred at the transition as shown in *h*.

Similarly, at the trailing edge transition, as shown in the waveforms of Fig. 11, a double space or a double pulse could occur. At every transition from pulse to space or from space to pulse, two spaces or two pulses will be sent out. If by chance the code should be generated as a long run of alternate pulses and spaces, this

[9] L. R. Wrathall, "Transistorized binary pulse regenerator," *Bell Sys. Tech. J.*, vol. 35, pp. 1059–1084; September, 1956.

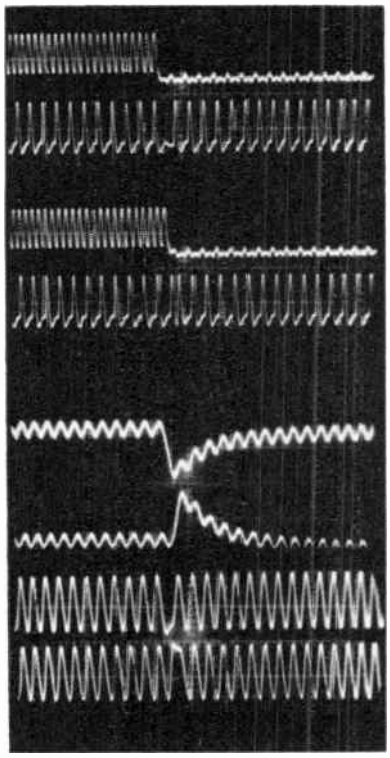

Fig. 11—Alternate interchange and repeater waveforms at end of pulse train. (a) End of coded pulses (0.5 μsec/division). (b) Interchange showing double space. (c) Pulses period later. (d) Interchange showing double pulse. (e) Unequalized output of 3000 feet of pair for double space. (f) Unequalized output for double pulse. (g) Equalized output of amplifier—double space. (h) Equalized output of amplifier—double pulse.

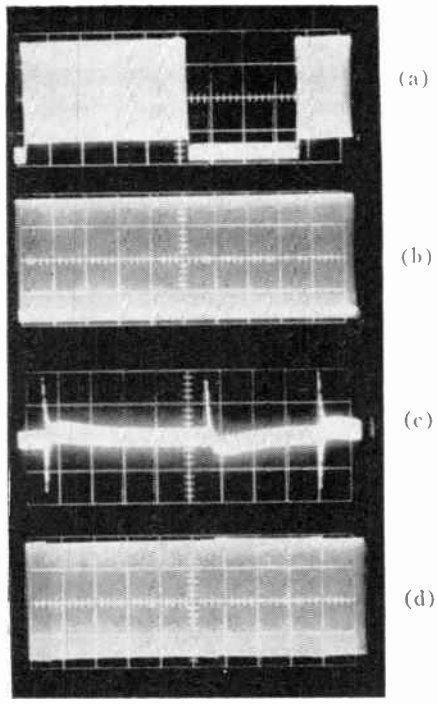

Fig. 12—Effect of alternate interchange on long pulse groups. (a) 500-pulse group from regenerated coder output (10 μsec/division). (b) Same signal after interchange at line input. (c) Unequalized output of 3000-foot line (note the two leading edge states). (d) Equalized output of repeater amplifier showing no low frequency component

would be converted to all pulses or all spaces, depending upon the particular phase. Fortunately, long sequences of this type are very unlikely. Any repeated pattern which is an odd number of bit intervals long will be converted to a sequence which has an equal number of pulses and spaces for every pair of patterns. Repeated patterns which are an even number of bit intervals long will either be improved, or their duty factor variation will remain the same as in the original signal, except for the previously mentioned alternate space and pulse pattern.

Waveforms *e* and *f* show the unequalized output of a 3000-foot line for a double space and a double pulse transition, respectively. The bottom pair of waveforms shows the corresponding output of the equalized amplifier. This is obviously a far easier signal to regenerate than the one of Fig. 9. Fig. 12 shows the original train of 500 pulses, the AI sequence as it is transmitted on the line, the unequalized output, and finally the amplified output which is applied to the blocking oscillator. The dc shift is negligible. Homogenizing the signal in this manner is advantageous not only from the standpoint of reducing the duty factor variation, but it also insures that a steady predominance of transitions between pulses and spaces will be present at each repeater in order to greatly simplify the timing recovery problem. Because the duty factor is 50 per cent, the ac coupling to the trigger circuit can automatically adjust the trigger level as the signal magnitude varies. In addition, the problem of power supply regulation at the repeaters is eased appreciably because the load stays practically constant all along the transmission line. Elimination of the low frequency components reduces the possibility of crosstalk into low frequency transmission systems which might use the same cable.

How often and how long a predominance of one condition or the other occurs is of interest in designing the repeater and the timing recovery circuits. Statistical measurements of off-the-air program material have not as yet been made, but some indication of what to expect can be obtained by simple oscillographic methods. These show that even for the least significant seventh digit, there is so much correlation in the signal as originally coded, that runs equivalent to twenty pulses in a row after interchange are very rare.

If the number of digits is increased to the point where pulses are coded almost at random for the smallest order digit, then the correlation will disappear and interchange will be of no help. When this situation exists there is almost no information in that digit anyway so falsification or complete elimination of it will have a negligible effect on the picture.

With alternate interchange, it is not necessary to use quantized feedback for either color or monochrome transmission. We will use some local quantized feedback, however, in order to provide an additional margin of safety, and to increase the variety of possible signals which can be handled.

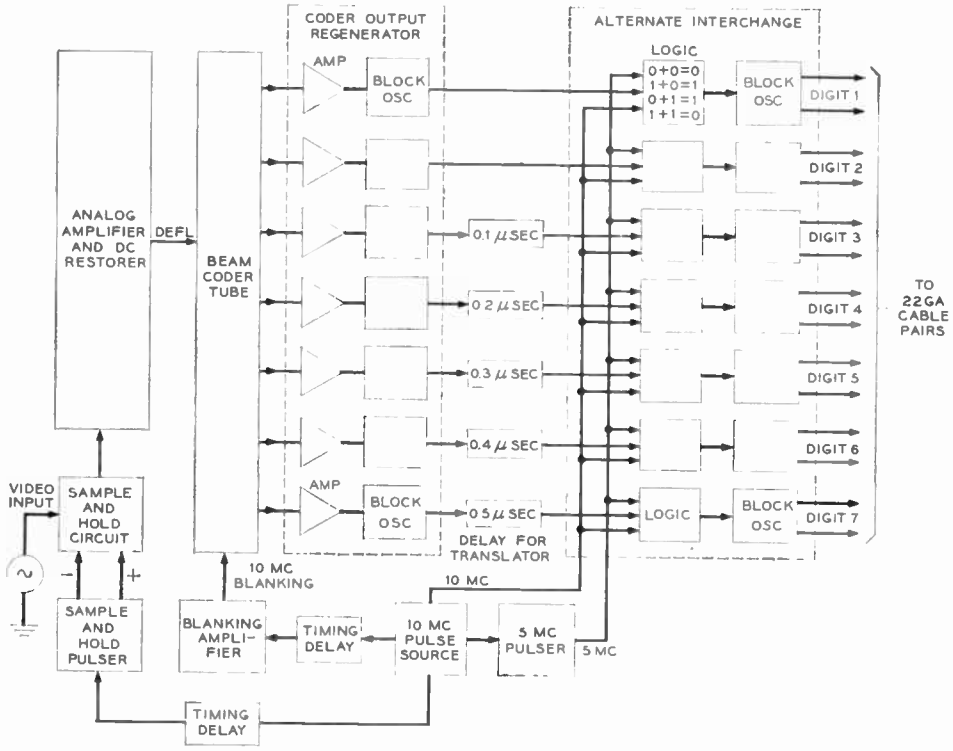

Fig. 13—PCM-TV transmitting coder terminal block diagram.

The transmitting terminal block diagram with AI added is shown in Fig. 13. A photograph of the actual transmitting terminal is shown in Fig. 14. The coding tube is inside the nu-metal shield projecting up from the front panel. The output regenerators are connected directly to the top of the tube. The deflection amplifier is inside the upper part of the cabinet. The alternate interchange circuitry appears at the top, and the regulated rectifier supplies and control circuits are mounted in the bottom.

Fig. 14—Complete coder terminal.

Cable Equalization

The foregoing has been concerned with the methods of overcoming the low frequency shortcomings of the coupling transformers. Now let us take a brief look at the effect of the high frequency shortcomings of the 22-gauge transmission pairs.

Because of the more than 40-db spread between the low and high frequency attenuation of the cable pair, the low frequency component of a pulse comes through at a much greater magnitude than the high frequency component, with the result that the pulses are "smeared out" on the time axis. Fig. 15(a) shows a repeated 1010100000000000 sequence at the input to the line. The unequalized output of the line is as shown in *b*. This pattern repeats at about 625 kc, so the low frequency cutoff of the transformers contributes only slightly to the distortion. The slicing level should be set at about the second graticule line from the top, in order to correctly regenerate the first pulse. With this setting, the next ten positions would also be classified as pulses, so this signal obviously cannot be used as received. The solution is to insert sufficient low frequency loss in some form of simple equalizer to bring the low frequency loss

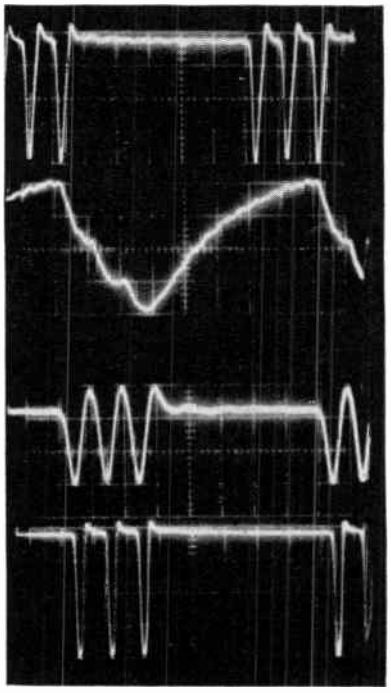

Fig. 15—Waveforms showing need for simple line equalization. (a) 10101 input to cable pair. (b) Unequalized output of 3000-foot pair showing effect of line distortion. (c) Equalized output of repeater amplifier. (d) Regenerated output pulses.

up to that of the high frequency. Fig. 15(c) shows the resulting waveform after equalization. This is an easy signal to regenerate.

Regenerative Repeaters

A single digit repeater section block diagram is shown in Fig. 16 together with the over-all characteristic of amplifier, transformers, and line. Each of the seven digits is sent over a pair of wires, so a total of seven regenerators is required at each 3000-foot repeater section. The block diagram of Fig. 17 shows such a repeater group. Each of the individual repeaters could be timed separately, but this would create a realignment problem at the decoding terminal. Because the delay per repeater span is 3.5 μsec, a dispersion of a few per cent at each span might result in a substantial spread of the positions of the seven digits after many repeaters. By retiming the entire group at each span, the dispersion problem is reduced to a minimum, and the output of all of the repeaters can be used to excite the common timing recovery filter.

In the simplest case, this filter is just a quartz crystal filter. A part of the output energy of each of the blocking oscillators is coupled to this common filter through an individual series tuned filter which serves as a buffer between the various digits. Although the blocking oscillators are triggered at essentially a 5-mc rate, the pulses are rich in second harmonic energy, so the output of the common filter is a 10-mc sine wave of nearly constant magnitude which is used for retiming the regenerative repeater. A narrow timing pulse gives better cleanup and stiffer timing control, but generating such a pulse in a common transistor circuit puts a premium on the reliability of the transistors in the common circuit. Normally, a failure of a transistor in any one of the digit circuits would just cut down the transmission capacity by a single digit,[10] but failure of the common timing circuit would wipe out all of the digits. In addition, backward acting timing such as we are using depends upon having a finite slope for both the signal and timing wave edges.

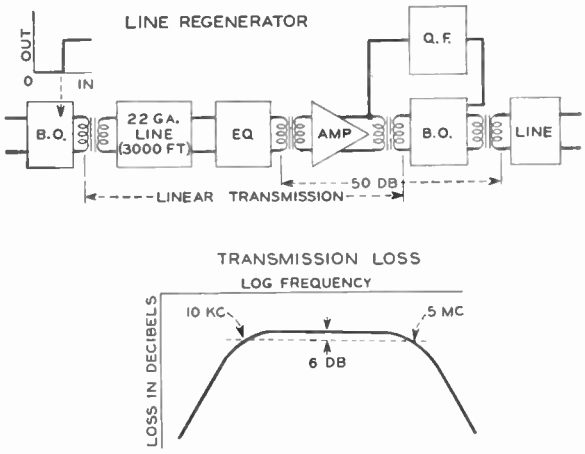

Fig. 16—Single digit regenerative repeater block diagram.

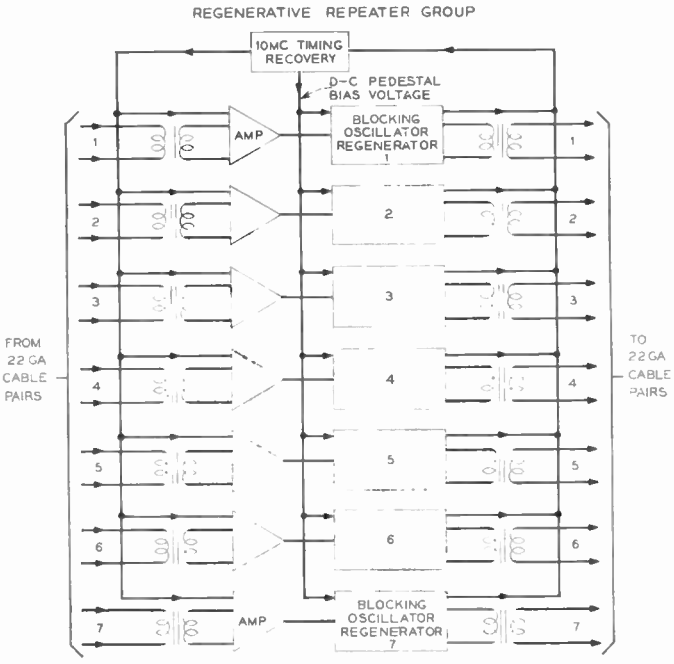

Fig. 17—Repeater block diagram for seven digits transmitted in parallel.

The waveforms of Fig. 18 show the input signal, the recovered 10-mc timing wave, and the sum of the two as they appear at the output of the amplifier of the repeater. The regenerated output pulses are shown at the bottom. One interesting problem arises with backward acting timing of this sort. The normal operating level for the blocking oscillator is set halfway between the peak of the input signal and the peak of the sum of the timing wave and the pulses. Unless a timing wave is

[10] The least significant digit should be the one eliminated by appropriate switching at the terminals.

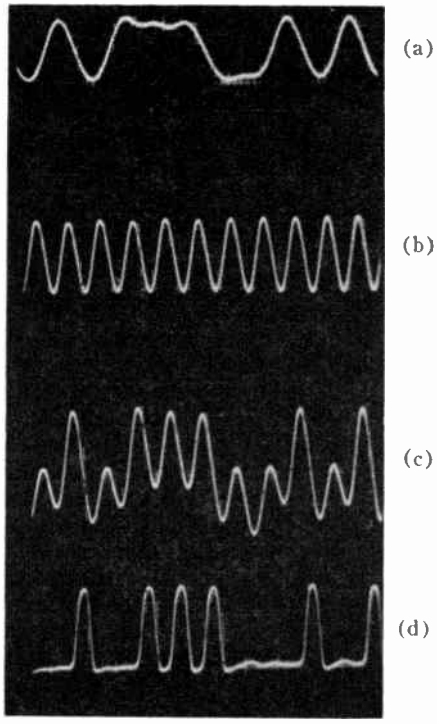

Fig. 18—Repeater waveforms with additive timing. (a) Equalized signal. (b) 10-mc timing wave. (c) Sum of signal and timing wave. (d) Regenerated output.

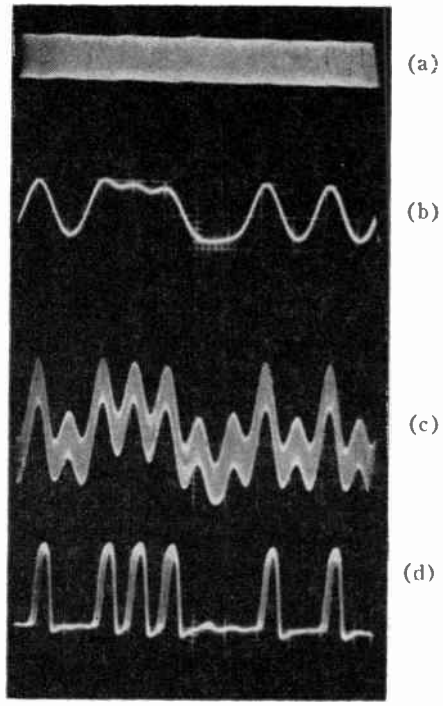

Fig. 19—Repeater waveforms with high level 3.0-mc sinusoidal interference added. (a) 3-mc sine wave interference (1 db below signal). (b) Signal with trigger level set at second line. (c) Sum of signal, timing wave, and noise—trigger level set at second line. (d) Regenerated output.

present, the blocking oscillator would never fire. But, there can be no timing pulse unless the blocking oscillators are producing pulses to shock excite the timing recovery filter circuit. Thus the system would never start into operation. This impasse is resolved by providing some form of pedestal bias. When the timing wave is absent, the dc bias drops to zero, so the blocking oscillators are biased to operate at the midlevel of the incoming raw signals. As the timing wave magnitude builds up, the bias builds up to set the bias at the correct operating point for signal plus timing wave. The net result is a system which can be made to operate correctly with or without timing wave. In the event of timing circuit failure, the signals would be regenerated reasonably well for transmission to the next span whose timing wave could clean up the variation permitted by the untimed section. The waveforms of Fig. 19 give some indication of the effectiveness of the regenerative repeater. At the top of the figure, the envelope of an interfering 3-mc sine wave as it appears at the output of the repeater amplifier when the signal and timing waves are removed is shown. Fig. 19(b) shows an equalized signal wave at the same point, with the timing and noise removed. Fig. 19(c) shows the sum of signal, timing, and noise. Note that the peak-to-peak sine wave interference level was adjusted to about one db below the peak-to-peak signal. The resulting regenerated output is shown in Fig. 19(d). The timing cleanup is not perfect, but the signals are adequate for transmission to the following span, provided it is not also subject to a high level interfering signal. The one db signal-to-noise ratio is not a violation of the theoretical limit of six db, because that

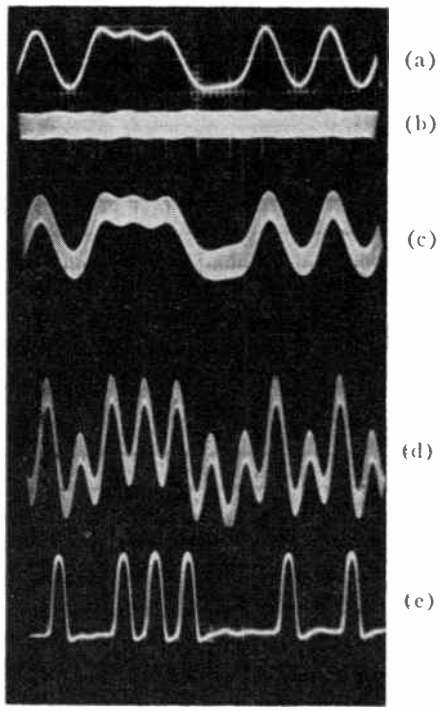

Fig. 20—Repeater waveforms with interference 6 db below signal. (a) Signal alone. (b) Sine wave "noise" 6 db below signal. (c) Signal plus noise. (d) Sum of signal, noise, and timing. (e) Regenerated output.

limit is based on zero-to-peak impulse noise not on peak-to-peak sinusoidal interference. It is interesting to note, however, that many forms of crosstalk exposure are of an ac nature, so that the zero db limit against peak-to-peak interference is frequently the limiting one.

It may be of interest to see how rapidly the regener-

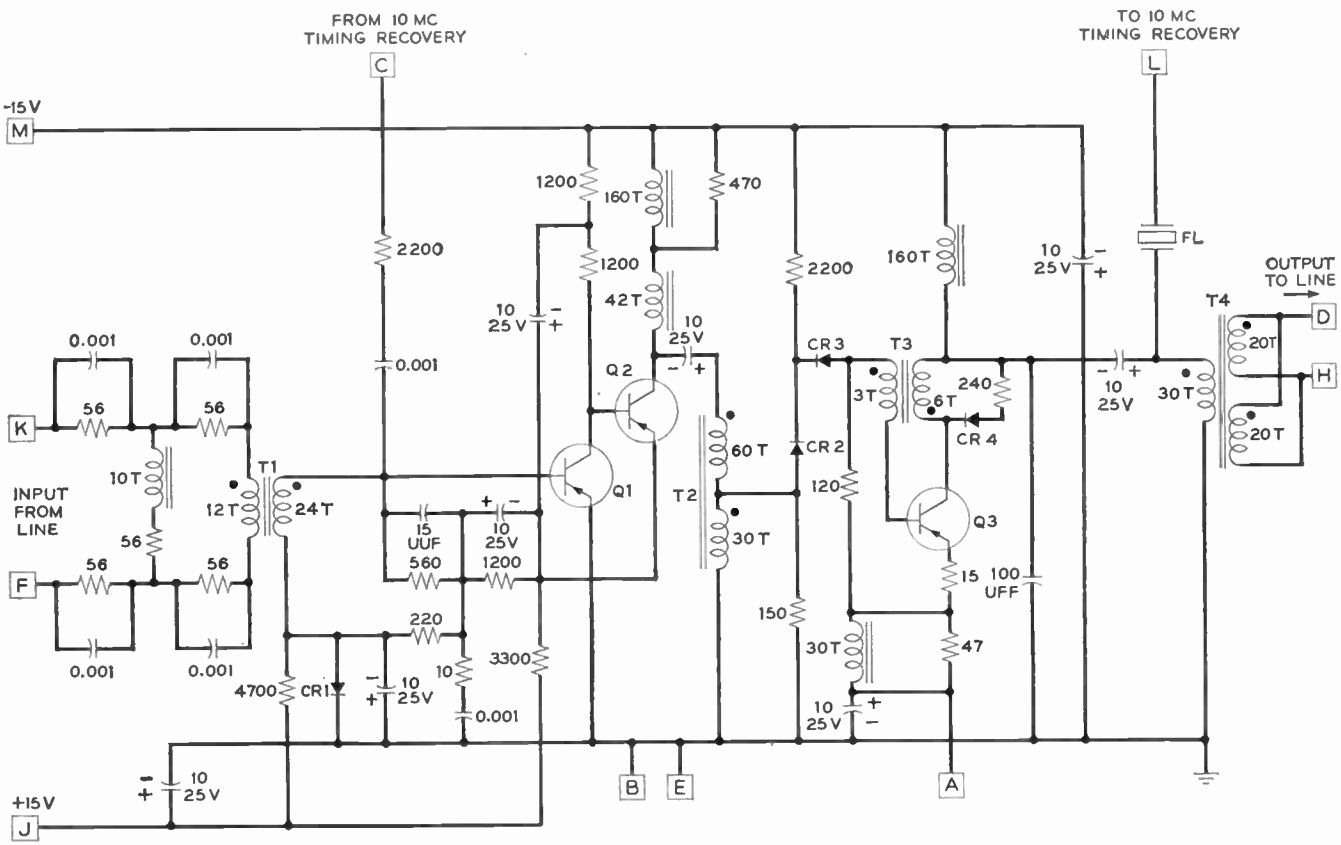

Fig. 21—Regenerative repeater schematic diagram.

ated signal improves as the interference is reduced. Fig. 20 shows the same input signal, but the interfering wave amplitude is set to just half of the signal magnitude. The sum of signal and noise is shown in *c*, and the sum of signal, noise, and timing is shown in *d*. The regenerated output at the bottom varies only a small amount. Note also that in this, as in the previous picture, the trailing edges of the regenerated pulses are subject to much less timing variation than the leading edges.

Several types of experimental repeater circuits have been used, ranging from a single stage tetrode transistor amplifier followed by a tetrode transistor blocking oscillator, to a unit using five transistors including a transistor to operate a timing pulse gate. The one used for these pictures, and for most of our experiments, is shown schematically in Fig. 21, and a photograph of a repeater package is shown in Fig. 22. It consists of a two stage amplifier followed by a diffused base transistor blocking oscillator triggered through a pair of diodes acting as an isolation gate. Peak output powers can be set from 90 milliwatts to about 500 milliwatts. Typical repeater amplifier gains are held at 30 db. The balance of the gain is in the blocking oscillator. Additional gain could be effected in the blocking oscillator by triggering with a lower level signal, but this would put a more severe requirement on bias threshold and trigger stability.

The waveforms of Fig. 20 illustrate the real reason for going through all of the trouble to convert what was a somewhat less than 5-mc analog signal to a combination of 70 million bits per second. At each repeater the noise, crosstalk, distortion, and phase variation of the previous span can be wiped out by complete regeneration, or very substantially reduced by almost complete regeneration. Thus, the repeaters have to be designed only to handle the signal from one span to the next, and not for the complete full length system. If the signals can be handled for a single span, it is theoretically possible to transmit them through hundreds of spans without any additional difficulty. The only limitation appears to be one of accumulated timing variation,[11–13]

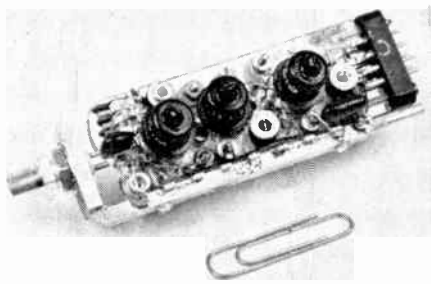

Fig. 22—Experimental regenerative repeater package.

[11] O. E. De Lange, "The timing of high speed regenerative repeaters," *Bell Sys. Tech. J.*, vol. 37, pp. 1455–1486; November, 1958.
[12] O. E. De Lange and M. Pustelynick, "Experiments on the timing of regenerative repeaters," *Bell Sys. Tech. J.*, vol. 37, pp. 1487–1500; November, 1958.
[13] H. E. Rowe, "Timing in a long chain of regenerative binary repeaters," *Bell Sys. Tech. J.*, vol. 37, pp. 1543–1598; November, 1958.

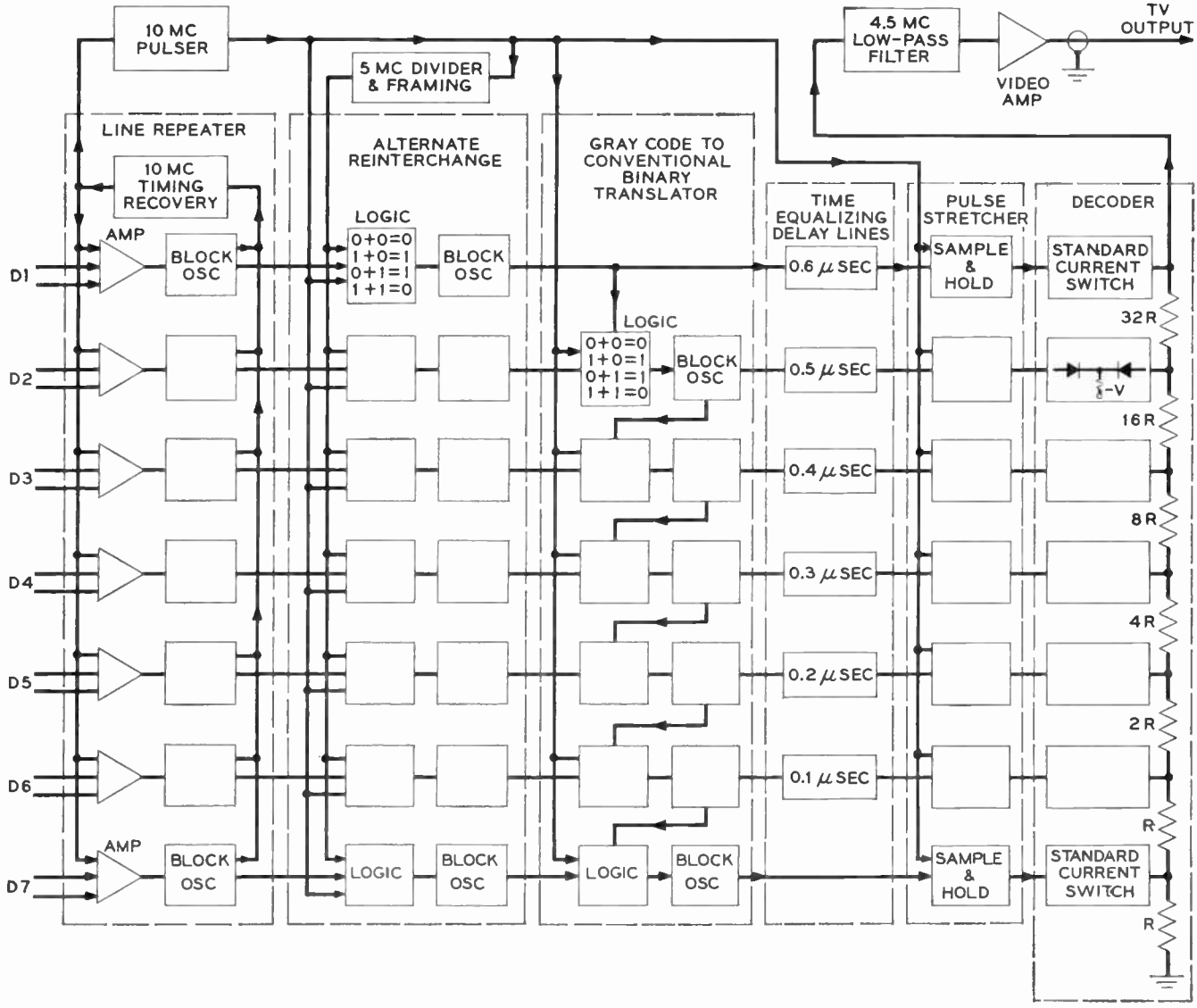

Fig. 23—Decoder terminal block diagram.

which is a problem subject unto itself. Use of an interchanged signal simplifies this problem materially, because pulse pattern variations are reduced. Additive backward acting timing is only one of the possible methods of operating. This and several other methods are being studied.

Decoder Terminal

Ultimately, the signal arrives at the decoder terminal for conversion to a quantized analog signal. Fig. 23 shows a block diagram of the decoding terminal. A conventional seven digit line repeater is first used to regenerate the signals as they arrive over the transmission pairs. The recovered 10-mc signal is used not only for operation of the regenerative repeater, but it will also be used to control all of the operations in the decoder. The 10-mc pulser shown at the upper left generates the clock pulses for the decoder. It also drives a 2:1 divider blocking oscillator, so a 5-mc control pulse is present at the receiver to do the alternate reinterchange operation. This 5-mc wave must be synchronized with that at the transmitter.

Alternate reinterchange is used to restore the signal back to the original Gray Code. The operation should be performed before translation. The circuit operation is identical to that at the transmitter. Fig. 24 shows the waveforms associated with this operation. At the top is the control 5-mc wave. Fig. 24(b) shows a short section of alternate interchanged digit 3 signal. Where pulses or spaces are present simultaneously on these two inputs, a space output condition will result. Where the two inputs are different, a pulse output will result. Fig. 24(c) shows an overlay of the upper two waveforms, and 24(d) shows the resulting output waveform restored back to the original Gray Code. A similar operation takes place for all of the other digits. When the 5-mc framing is incorrect, pulses will replace the spaces, and spaces will replace the pulses. The output of the logic circuits is regenerated as a matter of course in order to mop up any slight variations.

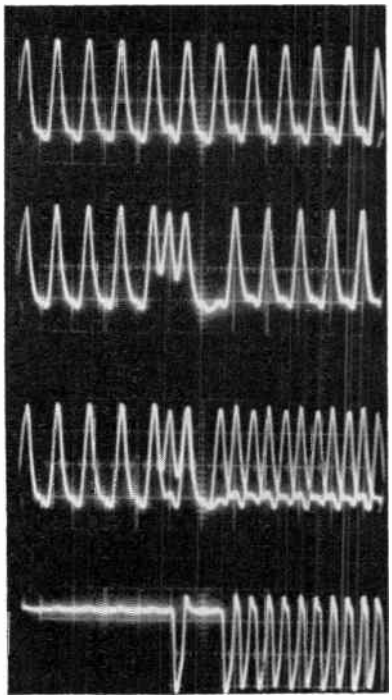

Fig. 24—Alternate reinterchange waveforms. (a) 5-mc control wave for alternate reinterchange (0.2 μsec/division). (b) Received digit 3 signal after regeneration (150 μμf shunt load). (c) Overlay of *a* and *b*. (d) Digit 3 restored to original Gray code at alternate reinterchange output.

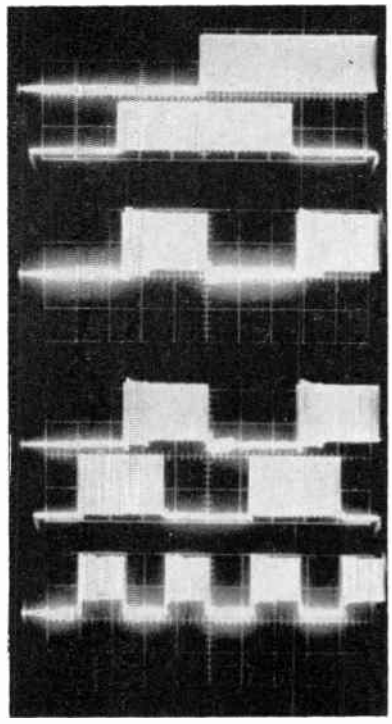

Fig. 25—Gray-to-natural binary code translator waveforms. (a) Digit 1, Gray and conventional code into translator. (b) Digit 2, Gray code into translator. (c) Translated output—conventional code to decoder and digit 3 translator. (d) Translated digit 2 into translator digit 3. (e) Digit 3—Gray code into translator. (f) Translated digit 3 output—conventional code to decoder and digit 4 translator.

Gray-to-Binary Code Translation

Referring again to the block diagram of Fig. 23, the Gray Code to conventional binary code translator appears next. This translator uses the same kind of logic operation as the alternate interchange and reinterchange circuits.[14] In this case, however, the 5-mc control wave is replaced with the translated output of the next higher order digit. Fortunately, the most significant digit, number 1, is the same in both the Gray and conventional code patterns; therefore, this digit does not have to be translated, and a starting point is available.

The output of the alternate reinterchange blocking oscillator can be used as the input to the logic circuit of the digit 2 translator. Reinterchanged digits 1 and 2 are compared in this circuit. Where they are alike, a space is produced, and where they are different, a pulse is produced as the translated digit 2. This is shown in Fig. 25. Waveform *a* represents digit 1 with a sawtooth sweep as an input signal. Digit 2 in Gray Code is shown as 25(b). The translated output is that shown in 25(c). This translated signal is passed on to the decoder, and it is also used as one of the inputs for the translation of digit 3. Time is "used up" in translating and regenerating digit 2, so the digit 2 output appears later in time than its input. This amount of decision time delay has been deliberately increased to be a full 100 nsec. Therefore, the translated output appears one bit interval late. If digit number 3 had not been delayed one interval at the transmitter, it would arrive in the wrong slot for translation, and an error would occur. As a result of the deliberately inserted delay at the transmitter, however, this digit arrives at the correct time, and digit 3 is translated as shown in the lower three waveforms of Fig. 25.

Once the third digit has been translated, the resulting output can be used for comparison with an incoming digit 4 pulse which was delayed two intervals at the transmitter, thus bringing it to the correct time for translation of digit 4. This process is carried on with each digit in order until the translation is complete. The translation operation is the only one which could not be readily carried out independently by parallel transmission of the digits. A form of pseudo serial operation is necessary for translation. The staggered outputs from the translator must be realigned in a common time slot before the decoding operation. This is accomplished by delaying each of the digits inversely to the amount already inserted. Hence, no delay is inserted in the digit 7 path, while 0.6 μsec delay is inserted in the digit 1 path to the pulse stretcher.

Pulse Stretching and Decoding

The blocking oscillator output pulses are "on" only for a nominal 50 nsec out of each 100 nsec interval. In addition, the duration of the pulses and the trigger instants are subject to a slight variation. Both of these situations

[14] R. L. Carbrey, U. S. Patents, No. 2,571,680, October 16, 1951, and No. 2,755,459, July 17, 1956.

add to the problem of correctly decoding and filtering the output signal. Therefore, the pulses are first stretched out by a balanced diode gate type of sample-and-hold circuit. An input digit sequence might appear as shown in Fig. 26. Short sampling pulses are used to gate the pulse or space condition into a storage capacitor which holds the 1 or 0 state until the following sample. The output of the storage capacitor is then applied to a transistor amplifier which is driven to saturation during the pulse, and is cut off during the space intervals. The resulting stretched output pulse sequence is as shown in 26(b). This is the control voltage which is applied to the standard current switch of the decoder proper. The bottom two waveforms of Fig. 26 show the corresponding input and output conditions when a TV signal is used as a signal source instead of a sawtooth wave. This is digit 4 with a one second photographic exposure. It is important that the crossovers between pulse and space or between a space and a pulse of this and the other digits all occur at the same time to a high degree of precision. If this is not done, short spikes may be introduced at transitions from one code group to an adjacent code group. Even though these spikes are as short as one nsec, they will have a low frequency energy component which can get through the output filter to appear as a slight discontinuity in the picture. This is most apparent in flat fields where the signal level is switching from the code 10000000 to 01111111, or where it is switching in the reverse direction. The energy of the short spike gives the appearance of increasing the quantizing noise slightly, without adding to the contour amplitude difference.

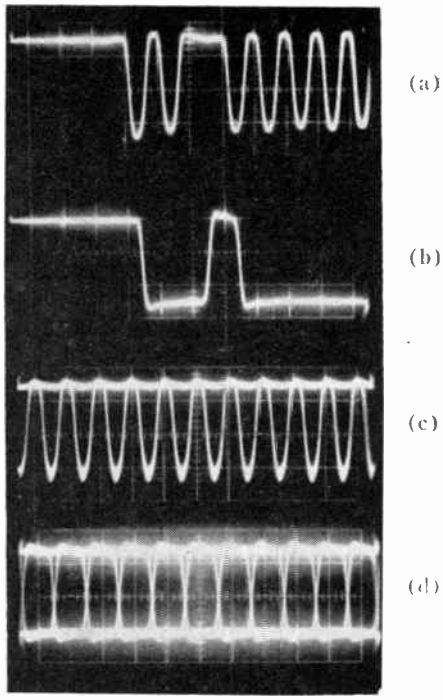

Fig. 26—Decoder pulse stretcher waveforms. (a) Blocking oscillator pulses from emitter of translator. (b) Stretched output to standard current switch of decoder. (c) Same as *a*, with TV signal source (1 sec exposure). (d) Same as *b*, with TV signal source (1 sec exposure).

Decoder Network

The decoder is a simple binary weighted voltage addition network type of decoder,[15] as shown in the block diagram of Fig. 23. When a space condition is present at each of the input diodes to the standard current switch, the standard current flows through this diode to the high negative reference voltage V, and no current flows in the network. If a pulse is present on digit 1, for example, the stretcher output voltage will be more negative than any decoder output voltage, so the input diode is open circuited, and all of the current flows from ground through the binary weighted resistance network, through the output diode of the standard current switch, and then through the standard current resistor to the reference battery V. Suppose this current is 1 ma, and that R is one ohm, then

$$32R+16R+8R+4R+2R+R+R=64 \text{ ohms},$$

and the total voltage drop will be 64 mv. This produces the most significant digit voltage step. When the second digit only is a pulse, the current will flow through a total of 32 ohms to produce a 32-mv step. If both the first and second are present, the output drop would equal the sum of the two, so that the total would be 96 mv. The other digits act similarly with the effective resistance being cut in half for each lower order of digit, with the result that digit 7 can contribute only a 1-mv step. The possible combinations of pulses and spaces range from all zeros where no voltage is developed, to all ones where 127 mv would be developed.

In actual practice, R was set at four ohms and the standard current was set at five ma. The total network resistance is then 254 ohms, which is matched by the same impedance in the output filter network which is connected directly across the "high end" of the resistance network. The maximum voltage swing is, therefore, limited to 1.27 volts. The waveforms of Fig. 27 show a buildup of a sawtooth wave across the binary resistance network when one digit at a time is added, starting with the most significant digit. The bottom wave is the filtered output for the input shown just above. The output low-pass filter removes the sampling frequency components, leaving a quantized analog voltage reproduction of the input signal which is amplified to the standard voltage and impedance. Fig. 28 is a photograph of the decoder terminal with power supplies and video switching gear in the base cabinet. Fig. 29 is a photograph of the decoder chassis.

[15] R. L. Carbrey, U. S. Patents, No. 2,610,295, September 9, 1952, and No. 2,636,159, October 30, 1947.

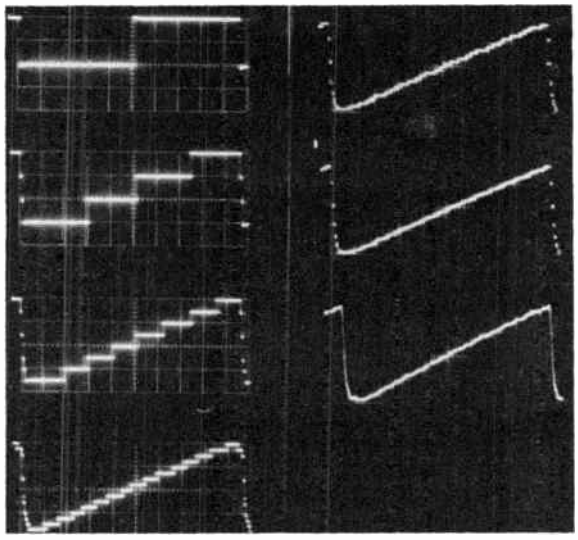

Fig. 27—Quantized approximation of coded sawtooth signal by addition of one digit at a time. (Shown before filter, except for lower right which is filter output with six digits.)

Fig. 28—Complete decoder terminal.

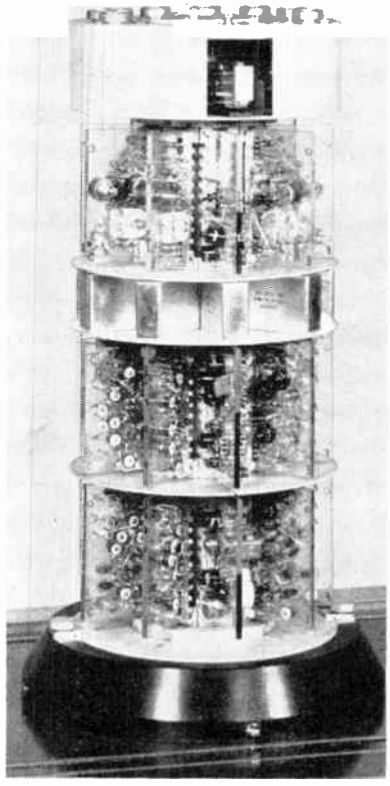

Fig. 29—Decoder terminal chassis.

Photographs of Output Pictures

Still photographs are not a completely accurate way of illustrating the subjective effects of any TV modulation process, but they will have to suffice here. Fig. 30 was taken from the TV monitor, with the signal applied directly instead of by way of the PCM system. Fig. 31 shows the same picture as it appears after being coded in a seven digit system, and transmitted through exchange area cable. Fig. 32 shows the same picture transmitted with two, three, four, five, six, and seven digits. The synchronizing signal is included in the transmission in its standard set-up value, 25 per cent, which means

Fig. 30—Direct display of TV picture.

Fig. 31—TV picture after transmission as seven digit PCM.

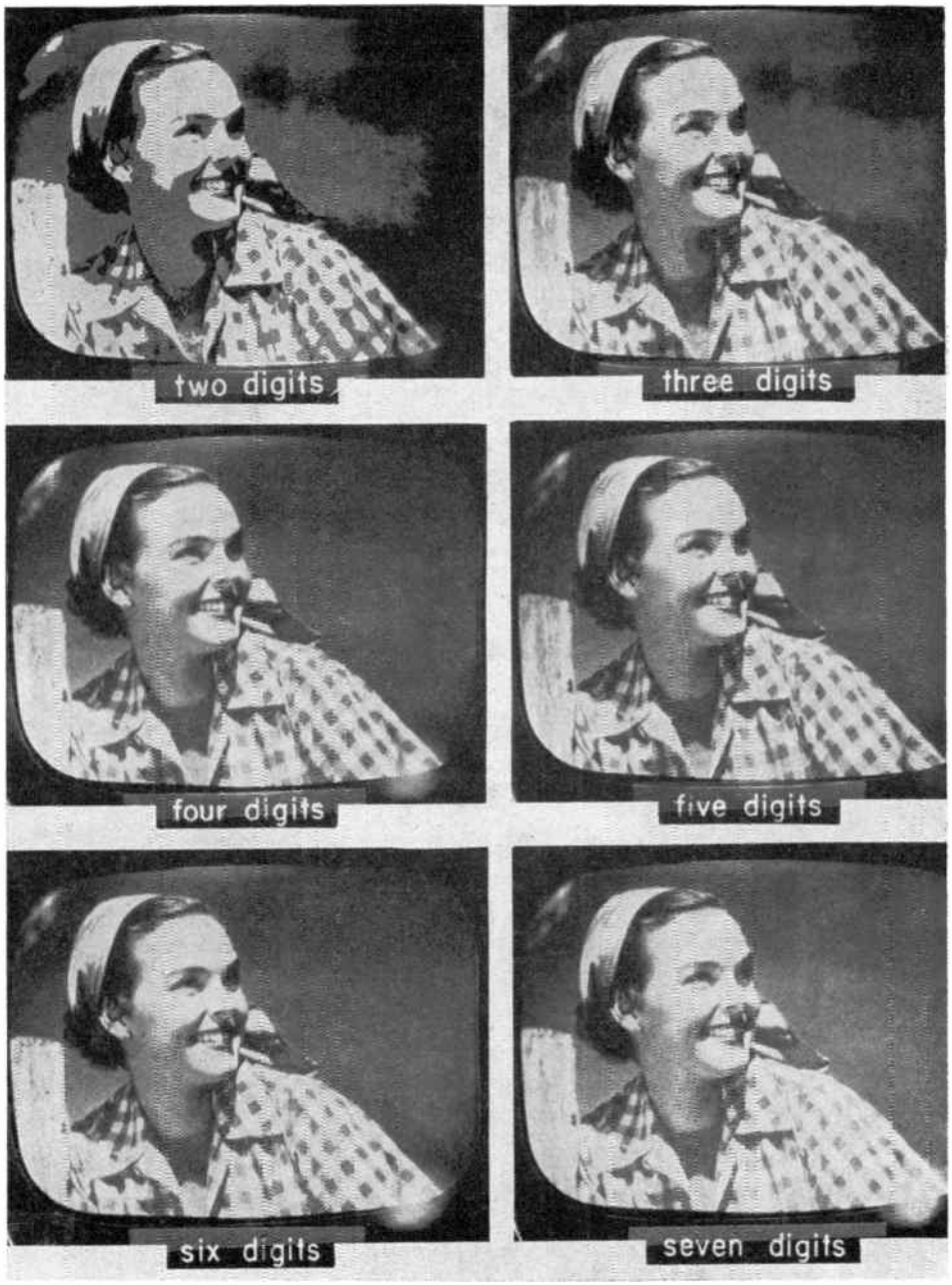

Fig. 32—TV picture showing the effect of adding one digit at a time, starting with two digits and ending at seven digits.

Fig. 33—Monochrome display of color picture after transmission as seven digit PCM.

that one-fourth of the possible combinations is used for the transmission of this information. (Thus, only three levels are visible for the two digit signal. Six levels out of the possible eight are visible with the three digit signal.)

This is wasteful of transmission capacity, when composite monochrome signals are transmitted. Color carrier signals extend almost to the top of the blacker-than-black level, so the full range is utilized more effectively with color transmission.

A monochrome display of a decoded color signal is shown in Fig. 33. Incidentally, getting a good monochrome reproduction of a coded color signal turned out to be more difficult than getting a good color display. All of these pictures are subject to the limitations of photographic integration and printing reproduction.

Conclusions

A. What Has Been Shown

It has been demonstrated that a beam coder tube and transistorized circuitry can be used to encode and decode both monochrome and color television signals. When seven digit PCM is used, the decoded signals are of a quality suitable for broadcast transmission. Subjective tests with six digits indicate that this number is adequate for many types of programs. This digital system is being used only in an experimental study of a possible alternate to coaxial cable or microwave radio transmission of the analog signal. It could be adapted to transmission over coaxial cable, microwave radio, or waveguide, but for these tests exchange area telephone cable was used.

The PCM signals can be transmitted over 22-gauge cable by using one pair for each of the digits, and a repeater spacing of the order of 3000 feet. Ten million bits per second were transmitted over each pair in this test. The repeater spacing or gain can be adjusted to accommodate other gauge cables. The problem of variation of the duty factor can be reduced appreciably by changing the pulses to spaces and the spaces to pulses in every other time slot, before the signals are applied to the transmission circuit. This alternate interchange operation is effective with both color and monochrome signals.

B. What Has Not Been Shown

The subjective effect of coding and decoding the same signal several times has not been determined. One or more additional digits may be required if this is done. The transmission tests were carried out on a cable installed in the laboratory, so it was not subject to the impulse noise or cable discontinuities which might appear on an in-service telephone cable. The effect of cumulative noise on the recovered timing wave has not been adequately determined, so the number of repeaters which can be connected in tandem is not known. Several methods of timing recovery are still being studied. Which one is best has not been determined. The problem of supplying the dc power over the transmission line has been ignored. Before any system of this type could be used, it would have to be subjected to both temperature and long term reliability studies.

Acknowledgment

A system of this type is the result of the efforts of many people, and it is impossible to properly extend thanks to all of them for their efforts and help. Much of the preliminary work was done in the Transmission Research Dept. under the direction of R. L. Wallace. Most of the early work was done with tetrode and diffused base transistors made in that department by E. Dickten and R. P. Riesz. The work was completed under E. B. Ferrell and M. Karnaugh in the Communications Techniques Research Dept.

The members of the staff working directly on the project for a substantial part of the time contributed in many ways and, in particular: F. W. Kammerer was responsible for the mechanical design of the transmitting terminal, as well as many of the features of the coding tube and associated circuits. A. C. Norwine is designing timing recovery circuits and making theoretical and experimental studies of their behavior. A. J. Rack contributed heavily to the design of several types of repeaters, the deflection amplifier, and the translator. P. A. Reiling designed the transistor sample and hold circuits, and video dc restorers, as well as designing test gear, one version of a decoder, and repeater experiments.

Senior and technical aides contributed much in the layout, wiring, and testing of the terminals and packages, and in the process made well over a thousand pulse transformers of various types starting with a raw blank of ferrite. Among those who worked on the project are M. R. Biazzo, J. Magelnicki, J. J. Poklemba, R. W. Proudfoot, and J. H. Whitten. The apparatus would never have been built without the able help of the mechanical and wiring branch shops.

R. W. Sears, J. A. McCarthy, and M. H. Crowell are among those responsible for the design and development of the beam coding tubes.

Thin-Film Cryotrons*

C. R. SMALLMAN†, A. E. SLADE†, AND M. L. COHEN†, MEMBER, IRE

Part I—Properties of Thin Superconducting Films

C. R. SMALLMAN

Summary—**This paper, consisting of three parts, describes the thin-film cryotron. This device, constructed by vacuum deposition of layers of lead, tin and silicon monoxide, is considerably smaller and faster than its wire-wound predecessor.**

Part I describes the characteristics of evaporated superconductive films as they apply to cryotrons. Their current-carrying capacity has been found to be proportional to width and proportional to thickness when the film is thinner than twice the penetration depth. Thermal effects caused by poor heat transfer to the bath distort the data, and the use of quartz substrates and low duty cycle pulse measurements help to reduce this distortion. The function of a superconductive reflector or ground plane under a film is discussed. The current-carrying capacity of such a film is increased because of effective cancellation of the normal component of magnetic field.

INTRODUCTION

IN 1954, D. A. Buck demonstrated the feasibility of using the phenomenon of superconductivity to construct an active computer component.[1] Since that time several papers have described the characteristics of the cryoton[2–4] and other superconductive devices.[5–7]

Limitations in speed, size, and fabrication of wire-wound cryotron circuits have suggested another geometry in the form of an evaporated film structure wherein entire circuits can be fabricated by vacuum deposition of successive layers of superconductive metals and insulation.

The first part of this paper describes the electrical and physical properties of superconducting films. Vacuum-evaporated superconducting films have been of interest to a number of investigators since 1938, when Shalnikov[8] studied the variation in critical external magnetic fields with the size of tin and lead films, and Appleyard *et al.*[8] made a detailed study of critical field variation with the size and temperature of mercury films. Alekseyevsky[8] made similar studies of tin films in 1941. In 1951, Lock[8] completed measurements of the magnetization curves of tin, indium, and lead films on mica.

Very few experimental data that pertain to the critical currents in thin, flat specimens have been published, however, and the data provided by Shalnikov are not comprehensive enough to be useful in cryotron design work. Theoretical treatment of the current-carrying properties of thin films is problematical because, except for two limiting cases (which do not correspond to films having dimensions and shapes that would be of interest in cryotron development work), it is difficult to find a solution for the current distribution in a thin, rectangular strip according to London's equations.

Because of the nature of most cryotron circuits, current passing through the control element of a cryotron must produce a magnetic field of sufficient strength to switch the gate element, and that same current must be borne by a gate somewhere else in the circuit. The amount of current a thin, flat superconducting film can carry without quenching[9] and the magnetic field effects associated with that current in both the control and gate elements are, therefore, of vital interest in thin-film cryotron work.

CURRENT-CARRYING CAPACITY OF SUPERCONDUCTING FILMS

As is true of any superconductor below its critical temperature (*e.g.*, a wire), there is a maximum (critical) current that a thin superconducting film can carry before the magnetic field associated with that current causes restoration of resistance in the film.

Restoration of resistance in a round wire occurs at the same value of the tangential magnetic field, regardless of whether the field is internally generated by current flow or externally applied. This phenomenon, known as Silsbee's Hypothesis, can be derived from

* Received by the IRE, January 28, 1960. The work reported here is supported by the U. S. Army Signal Corps under Contract No. DA-18-119-SC-45. The contributions of Dr. John Miles are gratefully acknowledged.

† Arthur D. Little, Inc., Acorn Park, Cambridge, Mass.

[1] D. A. Buck, "The cryotron—a superconductive computer component," PROC. IRE, vol. 44, pp. 482–493; April, 1956.

[2] A. E. Slade and H. O. McMahon, "A cryotron catalog memory system," *Proc. Eastern Joint Computer Conf.*, pp. 115–120; December, 1956.

[3] A. E. Slade, "The woven cryotron memory," *Proc. Internatl. Symp. on the Theory of Switching*, Part 11, Cambridge, Mass., Harvard University Press, Cambridge, Mass., vol. XXX, pp. 326–333; 1959.

[4] A. E. Slade and H. O. McMahon, "A review of superconductive switching circuits," *1957 Proc. National Electronics Conf.*, Chicago, Ill., vol. 13, p. 574; 1958.

[5] E. C. Crittenden, Jr., "A Computer Memory Element Employing Super-conducting Persistent Currents," presented at the Fifth International Conference on Low Temperature Physics and Chemistry Session 22-3, Madison, Wis.; August, 1957.

[6] M. J. Buckingham, "The Persistatron: A Superconducting Memory and Switching Element for Computers," presented at the Fifth International Conference on Low Temperature Physics and Chemistry, Session 22-5, Madison, Wis.; August, 1957.

[7] J. W. Crowe, "Trapped-flux superconducting memory," *IBM J. Res. Dev.*, vol. 1, p. 295; October, 1957.

[8] D. Schoenberg, "Superconductivity," Cambridge University Press, Cambridge, Eng., pp. 166–168; 1952.

[9] Quenching means switching from the super-conducting (zero resistance) state to the resistive or normal state.

London's equations and has been experimentally verified with the use of pure materials.[10]

To predict how much current a thin film can carry, we may assume that Silsbee's rule applies and consider two simple choices of current distribution in the film. We may assume either that the current distribution will be able to maintain $B=0$ in the film, or that the current will be distributed uniformly across the width of the film.

Under the first assumption, the current is concentrated at the edges of the film where the curvature is greatest. By using an elliptical cross section to approximate the rectangular cross section of the film, it can be shown that the exterior magnetic field is greatest at the ends of the major axes (edges of the film), and that the critical current where destruction of superconductivity occurs is *independent* of the film width. Experimental values of critical current are much greater than those predicted by this assumption and are not independent of width; it must therefore be assumed that the supercurrent is more uniformly distributed over the width of the film.

Under the second assumption (uniform current distribution), the width of the film is assumed to be infinite so that edge effects do not have to be considered. This leads to the following equation, which can be derived from London's equations:[11]

$$J'_{\text{crit}} = \frac{10H_c}{2\pi} \tan h\left(\frac{t}{2\lambda}\right) \qquad (1)$$

where

J'_{crit} = the critical current per unit width of film (a/cm),
H_c = the critical magnetic field for the bulk specimen,
λ = the penetration depth, and
t = the thickness of the film.

For small limiting values of $t/2\lambda$ as $t/2\lambda$ approaches zero, we see from (1) that J'_{crit} approaches the value $10\ H_c t/4\pi\lambda$; as $t/2\lambda$ becomes very large, J'_{crit} approaches the value $10\ H_c/2\pi$. The critical current for a film should therefore be proportional to the critical magnetic field, the width of the film, and (for thin films) the thickness of the film.

For thick films, the critical current should be independent of thickness, and the crossover between thick and thin films should be in the region of thickness equal to twice the penetration depth, or about 3000 Å for a tin film at a temperature of 0.25°K below T_c.

The assumption of uniform current distribution leads to calculated values of critical current per unit width of film that are about five times greater than experimentally observed values.

The discrepancy between the theory and the experimental results indicates that there is no obvious model for detailed theoretical treatment involving edge effects, surface-energy terms, and imperfect metallic homogeneity of the film. The *shape* of the film is such that Silsbee's rule probably does not apply, because of the extreme distortion of the magnetic field at the edge of the film when the film is carrying current. Furthermore, the metallic perfection of the film is to be questioned because of the method by which the film is made. Evaporated metal films are indeed not homogeneous, nor are they likely to be strain-free.[12] Fig. 1, an electron micrograph of a typical evaporated tin film, 1620 Å thick deposited on a glass substrate, reveals a rough surface and numerous holes that penetrate the film almost completely. These imperfections undoubtedly lower the true critical-current values, since such behavior is known to occur in bulk specimens that have been locally strained or made nonhomogeneous.

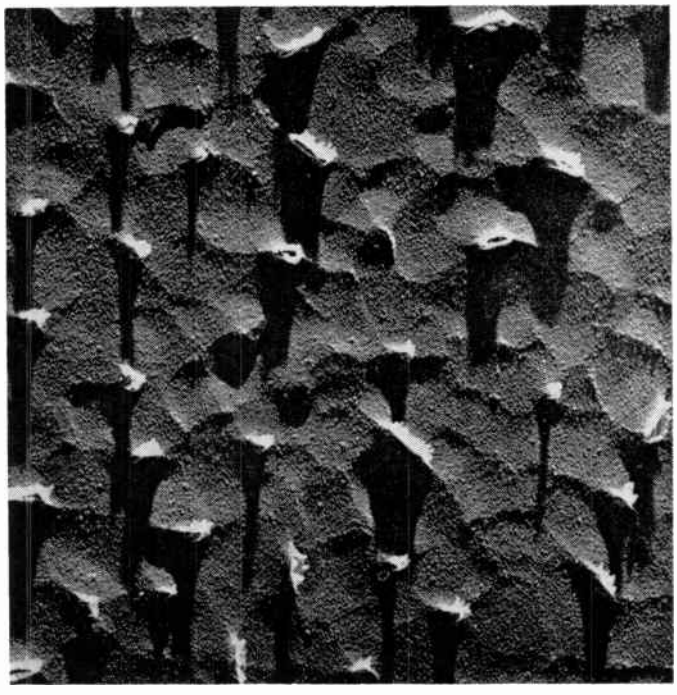

Fig. 1—Electron micrograph, 16,000×, of a replica of a 1620 Å thick evaporated tin film showing an irregular surface and numerous holes.

Experimental Results

In the present work, we have been primarily concerned with the current-carrying capacity of thin tin films, because tin is a potential gate material for thin-film cryotrons. The films were prepared by conventional vacuum-evaporation techniques. Pure tin was evapo-

[10] R. B. Scott, "Destruction of superconductivity by current," *NBS J. Res.*, vol. 41, p. 581; December, 1948.
[11] J. Daunt, private communication.
[12] L. Holland, "Vacuum Deposition of Thin Films," J. Wiley & Sons, Inc., New York, N. Y., pp. 212–215; 1956.

rated from a heated molybdenum boat in a vacuum of the order of 10^{-6} mm Hg and deposited on a glass or quartz substrate after passing through a mask that governed the shape of the deposited film. The majority of the specimens were deposited onto substrates at room temperature. Thickness was measured by a multiple-beam interferometer, and later experimentation revealed that the evaporation of weighed amounts from a suitably shaped boat was sufficient to establish reproducible film thicknesses. Fig. 2 is a photograph of some typical test specimens.

The helium cryostat used to test the films was arranged so that the pressure on the helium bath could be lowered with a vacuum pump; a mercury manometer was used to measure the temperature of the bath.

The four-wire method of resistance measurement was used where current was passed through the specimen longitudinally, and voltage drop across the specimen was sensed by two taps placed at the sides of the film. Fig. 3 shows the results of an experiment where voltage drop across the film is measured as a function of current through the film.

As current is increased from zero, the specimen is superconducting in the region A–B, and there is no voltage drop across it; at B, resistance begins to appear in the specimen; and, from B to C, the resistance increases nonlinearly with applied current as the transition from superconducting to completely normal takes place. At C, resistance is completely restored; and from C to D, the voltage is a linear function of the current. Since current flowing through the restored resistance produces Joule heat, there is a limit to the amount of current that can be passed through the sample before the sample becomes almost completely thermally isolated from the bath. If too much current is passed through the sample, a gas film forms on the surface of the specimen. At this point, D, the sample may burn out if a constant current source is used. The curve from point B and beyond is distorted because resistive heating changes the specimen's temperature, which, in turn, increases the resistance. Thus, the resistive heating produces a positive feedback effect.

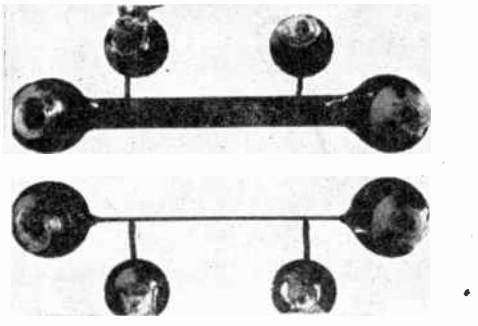

(a)

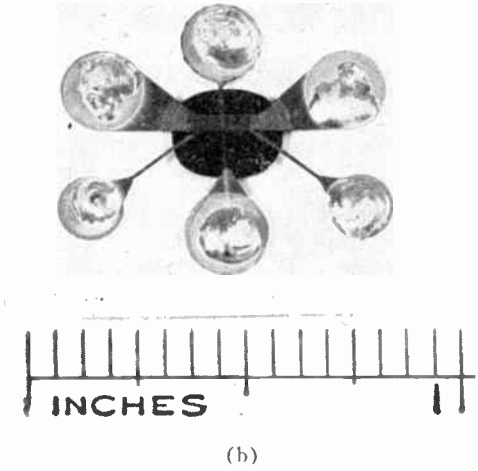

(b)

Fig. 2—Test specimens. (a) Tin film for current carrying-capacity measurements. (b) Single cryotron.

A. Thermal Effects

Mitigating factors in the phenomenon of Joule heating are the heat transfer to both the bath and the substrate and the heat capacity and thermal conductivity of the substrate.

We can change the equilibrium temperature of the film somewhat by choosing a suitable substrate material and by working at bath temperatures above and below the lambda point (a temperature where the thermal conductivity of the bath changes markedly). However, the thermal conductivity of the substrate and the heat transfer coefficient cannot be made infinite; and when fairly wide tin films are being tested, the critical current becomes inconveniently high below the lambda temperature.

Fig. 4 compares the voltage drop-current characteristics of two tin films deposited on different substrates.

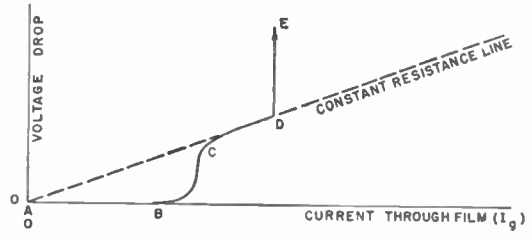

Fig. 3—Schematic behavior of a superconductive film carrying current showing the transition from superconducting to normal states and the effect of Joule heating.

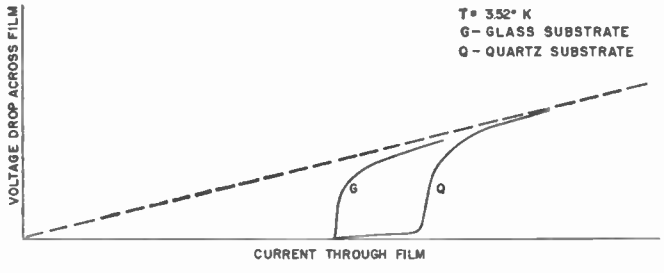

Fig. 4—Effect of thermal conductivity of the substrate upon the transition from superconducting to normal states of a tin film.

The temperature and dimensions of the films were constant so that the effect of thermal conductivity of the substrate on the current-carrying capacity could be compared directly. These curves show that at a critical value of current some resistance appears in the film and that the film undergoes a more rapid transition at a higher value of current. The rapid transition of the film on glass at the lower value of current indicates that the film starts to heat with the appearance of the first trace of resistance, whereas the film on quartz apparently dissipates its heat to the bath more effectively because of the higher thermal conductivity of quartz at low temperatures.[13] The rapid transition is not a "thermal runaway," but the shape of the whole transition curve is distorted by heating. The effect of heating can be further minimized if the heat input to the specimen is limited by the use of pulsed current rather than direct current. By using triangular-shaped pulses of adjustable current amplitude, duration, and repetition rate, it is possible to sweep through the current range of interest in both directions; information on restored resistance vs current was displayed on an oscilloscope. This method is used primarily for measuring the current-carrying capacity of tin films. Because of the difficulty of isolating the high input-current signal from the low-voltage output signal, we found it virtually impossible to test cryotrons by pulsing the control.

The rate of rise of the current pulse has been made as high as possible without introducing excessive errors that would be caused by film inductance or phase shift in the oscilloscope. A short pulse duration also minimized the amount of energy introduced into the film, and a slow repetition rate was used to prevent cumulative heating effects.

Fig. 5 is an example of the kind of information available from pulse measurements. Fig. 5(a) is an oscillogram of a 100-μsec pulse input having a peak current of 2 amperes and a repetition rate of 100 pulses/sec. Fig. 5(b) is a voltage-vs-current trace of a film on glass in the normal state at 3.9°K. Fig. 5(c) is a voltage-current trace of a film at 3.65°K and 3.56°K. According to the slope of the voltage-current curve in Fig. 5(b), the resistance of the film between voltage taps is 0.075 ohm. From Fig. 5(c), we know that the critical currents at the half-resistance points are 0.86 ampere at 3.65°K and 1.20 amperes at 3.56°K. A sufficient number of measurements on this film yields data that can be reduced to give a critical temperature of 3.84°K and a current-carrying capacity of 4.3 a/degree K (the slope of the I_{g-crit} vs temperature curve).

Fig. 5(c) also shows a hysteresis effect, in which the return to the superconducting state is not coincident with the critical current of the super-to-normal transition. We can estimate the temperature rise of the film by dividing this ΔI by the current-carrying capacity of the film in a/degree. The temperature rises obtained in this way are approximately 0.15°K and 0.20°K. Since the repetition rate of the pulses was low enough to prevent cumulative heating, the temperature rise of the film was caused by the energy of a single pulse. We can determine the energy of this pulse by integrating I^2RdT or $(E^2/R)dT$ for a single pulse. Pulse energies used in this experiment were of the order of 10 μwatt-sec.

[13] R. L. Powell and W. A. Blampied, "Thermal Conductivity of Metals and Alloys at Low Temperatures," Nat'l. Bur. Stand., Washington, D. C., Circ. 556, 59, 63; 1954.

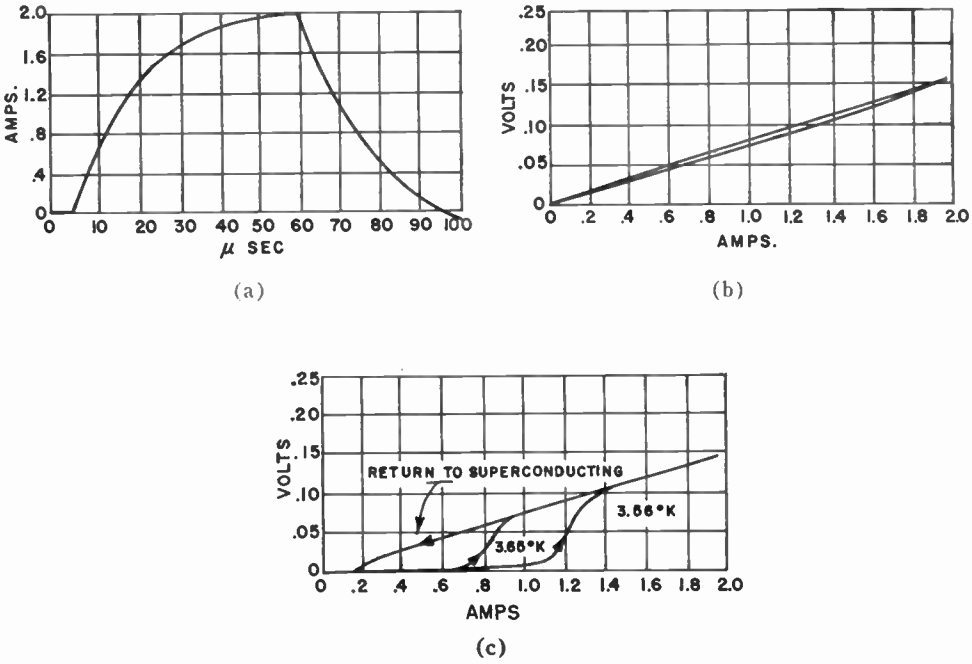

Fig. 5—Pulse test oscillograms. (a) Input-current wave shape. (b) Voltage drop—current trace of a tin film in the normal state. (c) Voltage drop—current trace of a film at 3.65°K and 3.56°K.

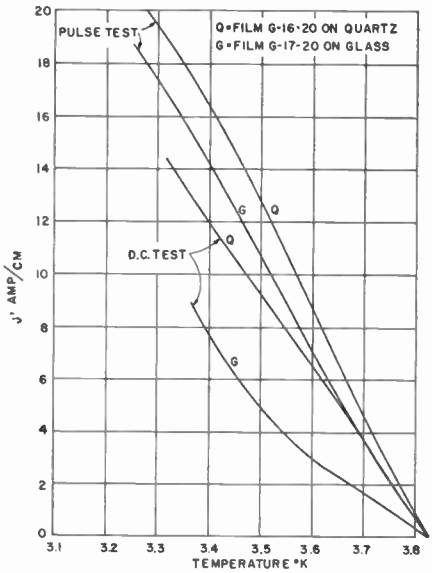

Fig. 6—Comparison of dc and pulse tests of films on glass and on quartz substrates.

Fig. 6 is a plot of J' (a/cm width) vs temperature for two films of comparable thickness. One film was deposited on glass; the other, on quartz. Both dc and pulse measurements were made on these films, and the plot effectively summarizes the thermal problem. The dc tests yield lower values of critical current than pulse tests, and quartz increases the current-carrying capacity of the films, regardless of the method of measurement.

A comparison of critical-current information obtained by the pulse technique with that obtained by the dc method indicates the magnitude of error caused by Joule heating. However, because of limitations imposed by oscilloscopes, which must be used in pulse tests, the pulse test data are not as numerically accurate as the dc test data.

B. Films Under DC Test

Several film sets were measured, each of which consisted of four different widths of film prepared by one evaporation so that the thicknesses would be identical. Figs. 7 and 8 show typical curves of critical current (taken at the half-resistance point) vs temperature for widths of 0.2, 0.1, 0.05, and 0.025 cm. Fig. 7 shows a thin film of 3000 Å, and Fig. 8 represents a thick film of 16,300 Å. The curves show a linear dependence on width that is plotted in Fig. 9. Appraisal of data from many specimens indicates a slight increase in J' as width decreases. However, the concept of $J'_{crit}(I_{g-crit}/\text{width})$ appears to be reasonable.

According to Silsbee's rule, the critical current should show a parabolic dependence upon temperature of opposite curvature from that shown in Fig. 7; however, the curvature would not be conspicuous over the limited temperature range under consideration. The critical temperature for bulk tin given in the literature is 3.73°K. The critical temperature is higher for both of these samples, the T_c of the thinner film more nearly approaching the bulk value of $T_c°$.

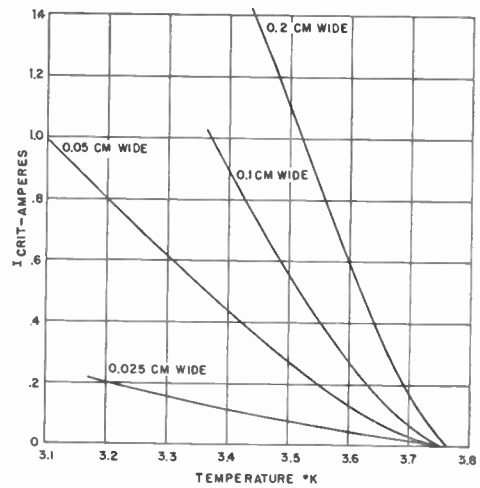

Fig. 7—Critical current vs temperature for various widths of 3500 Å thick tin films of glass.

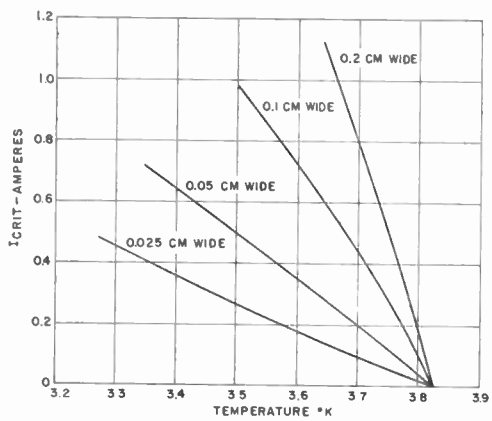

Fig. 8—Critical current vs temperature for various widths of 16,300 Å thick tin films on glass.

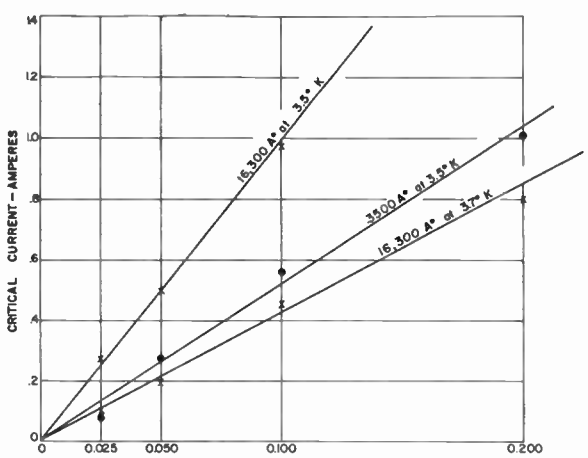

Fig. 9—Critical current vs width of tin films showing linear correspondence of current-carrying capacity with width of film.

Data from 17 specimens of different thicknesses are presented as a curve of J'_{crit} vs thickness at a constant reduced temperature in Fig. 10. There is a great deal of scatter; but the curve [see (1)] drawn through the points indicates that there is some tendency for J'_{crit} to be independent of thickness for thick films; it also

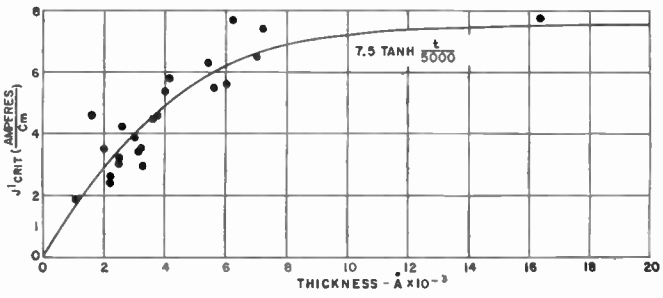

Fig. 10—Linear current density (a/cm-width) of several tin films vs thickness.

shows a crossover between thick and thin films in the region of 5000 Å. Neither of these characteristics is so prominent as the theoretical treatment indicates, but the general behavior does not disagree with the theory. It was not possible to prepare films much thinner than 1000 Å on a 300°K substrate, since the film's agglomeration destroys conduction.

C. Resistivity of Tin Films

The measured low-temperature resistivity of tin films is presented as a function of film thickness in Fig. 11. A typical value of resistivity for pure pulk tin at 4.2°K is 13/28,000 μohm cm, whereas our thick films approach a value of 0.1 μohm cm, indicating that all the factors which influence bulk resistivity, such as strain, impurity and metallic inhomogeneity, are probably present to a high degree in these films. High resistivity in these films is a desirable feature, however, if they are being considered as a gate material in film cryotrons.

D. Magnetic Field Effects

Our measurements of the critical, tangential, externally applied magnetic field are presented in Fig. 12 as initial slope of the critical field curve vs thickness. The curve drawn through the scattered points was derived from the following empirical equation given in Shoenberg[14]

$$h_c/H_c = 1 + \frac{b}{2a} \tag{2}$$

where

$$\left(\frac{dh_c}{dT}\right)_{T_c} = \left(\frac{dH_c}{dT}\right)_{T_c}\left(1 + \frac{1500}{l}\right) \tag{3}$$

$$= 150\left(1 + \frac{1500}{l}\right)$$

for tin films where t is thickness in Angstrom Units.

The magnetic fields associated with current flow in a thin film can be derived from Ampere's law.[15] If we assume an infinitely long film of rectangular cross section, uniform current distribution, and negligibly small thick-

[14] Shoenberg, *op. cit.*, p. 17.
[15] L. Page, "Introduction to Theoretical Physics," D. Van Nostrand Co., Inc., New York, N. Y., p. 370; 1928.

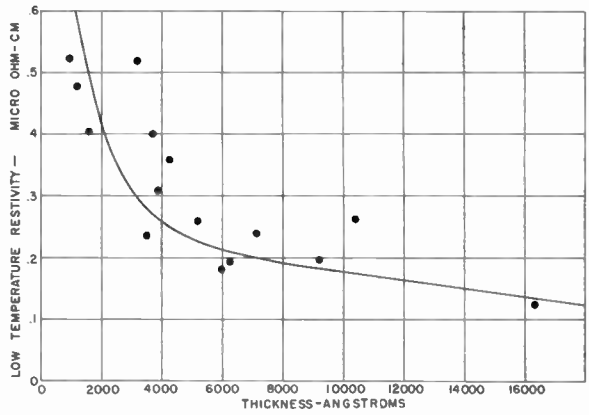

Fig. 11—Low-temperature resistivity of tin films vs thickness.

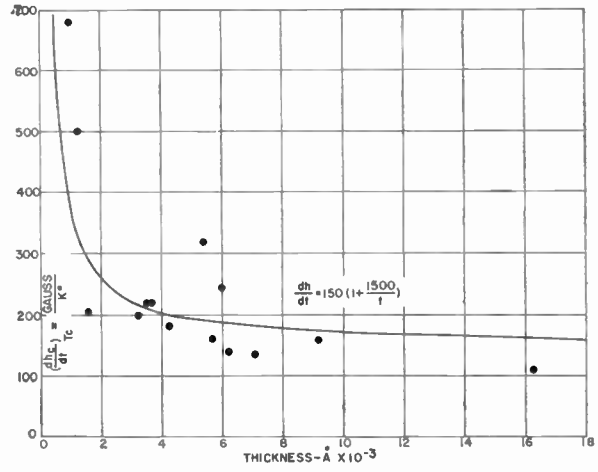

Fig. 12—Initial slope of the critical magnetic field curves for several tin films vs thickness of the film.

ness, the tangential (H_T) and normal (H_n) components of the field at a point, p, outside the film are given by

$$H_T = \frac{I}{5w}\phi \tag{4}$$

and

$$H_n = \frac{I}{5w}\ln\frac{r_1}{r_2} \tag{5}$$

where I is the total current, w is the width, r_1 and r_2 the distances from the point, p, to the edges of the film, and ϕ is the angle formed by lines projected from the edge of the film to point, p. Therefore, at the surface of the film, the tangential field has the constant value of $I/5w$; and the normal field varies logarithmically across the width. If we integrate Ampere's law without neglecting thickness, we find that the normal component at the edge of the film has a maximum value of

$$\frac{I}{5w\left(1 + \ln\frac{w}{l}\right)}$$

and does not become infinite as shown in (5).

For a typical film, w/t is 10^3–10^5, the logarithmic term is 8–12.5, and the maximum normal field is therefore

2.5–4 times the tangential field. Since its shape gives the film a high demagnetization coefficient when it is subjected to a normal field, and since the normal component is 2.5–4 times the tangential component, we must conclude that the normal field associated with the edge of the film is important in the quenching process.

Interestingly enough, when the film was deposited in the shape of a cylinder so that no normal component existed, the increase in critical-current density, J'_{crit}, was about equal to the ratio of the maximum normal field to the tangential field.

E. The Ground Plane

Early work with superconductive tantalum foils at this laboratory verified our prediction that the critical current of the foil could be increased by placing it close to a parallel lead foil. Similarly, when a tin film is deposited upon an insulated lead film, we find that the critical current of the tin film is higher than it is if the lead is not present. At the critical temperature of tin, the lead remains superconducting. Thus the lead resists penetration of a magnetic field normal to its surface by a mechanism, whereby induced circulating currents flowing on the surface of the lead create a magnetic field which effectively cancels the imposed normal magnetic field.

The sensitivity of the edges of a tin film to a magnetic field normal to the plane of the film has been previously discussed, and we have seen an increase in critical current when the tin film is deposited in a cylindrical shape where no normal component can exist. By the use of the lead ground plane, we now have another method of eliminating the normal component of magnetic field while preserving the planar nature of the film. The magnitude of the increase in critical current of a tin film on a ground plane agrees with that of a comparable film in the shape of a cylinder and amounts to a factor of about $2\frac{1}{2}$.

In experiments with persistent current loops of tin films with and without a ground plane, we have found that for equal film and loop dimensions it was possible to induce and maintain a *persistent* current equal to the critical current of the tin film on a ground plane, whereas the induced current in the tin loop without a ground plane rapidly fell off to a very low value in a fraction of a second. This experiment clearly shows that 1) a tin film is very susceptible to normal field, 2) the normal field is effectively canceled by the ground plane and 3) the use of a ground plane makes possible circuitry which depends upon storage of a persistent current (*e.g.*, flip-flops which remember the state they were in when the supply current has been shut off and restored again).

The ground plane also serves as a means of reducing circuit inductance to a low value.[16]

[16] A. E. Slade, "Thin film cryotrons; Part II—Cryotron characteristics and circuit applications," PROC. IRE, this issue, p. 1569.

Discussion

Although there is qualitative agreement between theory and experimental results in that critical current of a thick tin film is substantially independent of thickness and that the critical current of a thin film is proportional to the width and thickness, experimentally measured films will carry only one-fifth of the current indicated by (1). Electron micrographs of evaporated films indicate that the evaporated film is metallographically poor and that we are working with a system which is so far from perfect that the experimental approach seems to be the only reasonable one. There is little doubt that some improvement in films can be realized by evaporation of pure material in extremely good vacuum but operable cryotrons have been made with the materials and conditions at hand and we have studied these films in order to gain some knowledge of their behavior.

The comparison of the transition behavior of a film on glass with that of a film on quartz illustrates a heating effect which must be considered in circuit design. Because quartz is unavailable in large sheets and is expensive, most circuits will be made on glass although a substrate with a higher thermal conductivity may replace glass in the future. The heating effect also depends upon the duty cycle of the operating circuit. The dc characteristics of a circuit will differ from the ac characteristics and this should be considered in the design of a circuit.

The high resistivity of these films at 4.2°K is a desirable feature in that the higher the value of restored resistance, the lower the L/R time constant of the cryotron, hence the higher the speed of the cryotron circuit.

The resistivity of bulk specimens can be increased by alloying with another metal. However, high resistivity of films is primarily due to surface scattering of the electrons and the contribution to resistivity of impurity scattering, as in the case of an alloy, is relatively small. Also, alloying cannot be done indiscriminately because of an effect whereby the critical external magnetic field becomes larger than the critical internal (due to current flow) magnetic field. This effect is a disadvantage in cryotron design.

The use of the ground plane under a tin film produces a significant increase in the critical current of the tin film. The ground plane, however, increases the probability of short-circuiting the circuitry placed upon it, because the entire area covered by the circuit must be insulated from the ground plane by a silicon monoxide layer of the order of 3000 Å thick. The cause of short circuits is presently being studied, but dust on the substrate prior to deposition and spatter of metal from the sources during deposition of the circuit appear to be the principal causes of shorts. The advantages of the ground plane in reducing inductance and increasing critical current of films placed upon it assure its use in almost all cryotron circuitry.

Part II—Cryotron Characteristics and Circuit Applications

A. E. SLADE

Summary—**Part II describes the characteristics of the thin-film cryotron. The superconducting to normal transition in a tin gate 0.125 inch wide and 3×10^{-5} cm thick is controlled by current in a single lead control, 0.006 inch wide, which crosses the gate. Silicon monoxide is used for insulation. The switching time of a cryotron circuit is dependent upon the inductance and resistance of the circuit. Therefore, it is important to reduce the inductance by using a superconductive ground plane and by reducing the length of all interconnecting leads. Nonlocking flip-flops have been constructed, and a ring of five flip-flops have operated with a delay per stage of $\frac{1}{2}$ μsec.**

Introduction

THE purpose of this paper is to describe the characteristics of thin-film cryotrons and their application to computer circuits.

Thin-film cryotrons have many advantages over their wire-wound predecessors.[1] They are easier to construct and assemble into circuits and they are 1000 times faster than wire-wound cryotrons. A typical configuration for a test cryotron is shown in Fig. 1. The control is 0.006 inch wide, the gate is 0.125 inch wide, and the lead, tin, and silicon monoxide are all 3000 Å thick.

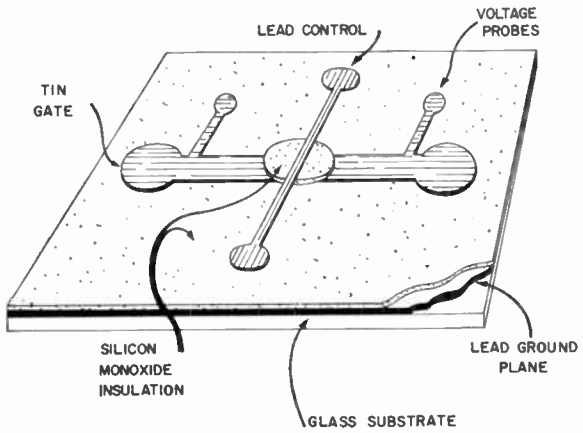

Fig. 1—Thin-film-cryotron configuration used for testing a single cryotron.

The cryotrons and the circuit interconnections are constructed at the same time by the evaporation of superconductive metals in a vacuum bell jar and the deposition of their vapors through suitable metal masks onto a glass substrate. Simultaneous deposition of the devices and their interconnections greatly simplifies the construction of circuits and challenges the engineer to design circuit configurations that utilize the advantages of their small dimensions.

Current Gain

Cryotrons are interconnected in circuits in much the same way as relay circuits. It is not necessary to use any component but the cryotron in designing a circuit. The low impedance of the cryotron dictates the use of a current source, and this current flows in series through the gates and controls of the circuit.

The concept of current gain follows directly from the necessity of having the same current flowing in both gate and control. Current gain (G) is defined as the maximum current the gate can carry without quenching, divided by the minimum current in the control necessary to quench the gate.

$$G = \frac{\text{Critical gate current}}{\text{Critical controlling current}} . \tag{1}$$

The current gain must be at least unity, and in practice it is made equal to 2 or 3 to provide a margin of safety against variations in cryotrons.

In thin-film cryotrons, the current gain is governed by the relative widths of the gate and control conductors. In the previous paper, it was shown that the critical gate current is proportional to the width of the gate, and experiments have shown that the critical controlling current is proportional to the width of the control. A typical cryotron with a gate width of 0.125 inch and control width of 0.006 inch has a current gain of unity at about 3.7°K.

Gate Current vs Control-Current Characteristics

Fig. 2 shows the gate-current-vs-control-current curves for a typical cryotron. These curves represent the threshold between the superconductive and resistive regions at various temperatures. One can determine the current gain from the graph by dividing the x intercept by the y intercept. Another design parameter, the incremental current gain, is defined as the slope of the curves at a specified operating point. The incremental current gain (μ) is important in small signal applications such as current amplifiers, and it is also important in many switching circuits where the current does not swing from zero to critical.[2]

Both the current gain and the incremental current gain increase with lower temperature. For example, in Fig. 2 the current gain is $\frac{1}{3}$ at 3.73°K, and it increases to 1.6 at 3.55°K; by the same token, the incremental current gain at $I_c = I_g$ is 0.14 at 3.73°K, and it increases

[1] D. A. Buck, "The cryotron—a superconductive computer component," Proc. IRE, vol. 44, pp. 482–493; April, 1956.

[2] M. L. Cohen, "Thin film cryotrons. Part III—An analysis of cryotron ring oscillators," Proc. IRE, this issue, p. 1576.

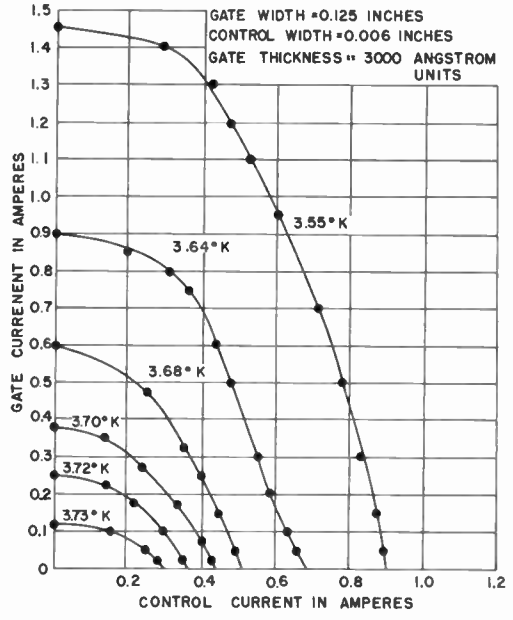

Fig. 2—Gate current vs control current of a thin-film cryotron for various temperatures.

to 2.4 at 3.55°K. Operating at lower temperatures has the advantage of higher current gain and the disadvantage of higher current. A lower limit in operating temperature is reached when the current becomes large enough to self-quench the control.

The Superconductive Ground Plane

The use of a ground plane is well known to those working with very high frequencies. The ground plane has added significance, however, when it is superconducting. A superconductive ground plane is a thin film of lead deposited directly under the gate of the cryotron and as close to the gate as insulation will allow. Because of its high transition temperature, the lead is always superconducting during the operation of the circuit.

Since flux cannot penetrate a superconducting material, the normal components of field at the surface of the ground plane must be zero.[3] Presumably, the ground plane satisfies this requirement by generating eddy currents that produce a field which exactly opposes the applied field. In a superconductor, of course, an eddy current does not decay with time.

The ground plane affects both the inductance and the resistance of a cryotron in the following ways.

A. Inductance

In cryotron circuits, the impedance levels are so small that capacitance can be ignored. The switching speed of a circuit is dependent upon the L/R time constant. Therefore, one of the most important effects of a ground plane is that it reduces the inductance of the cryotron and the interconnecting leads. The inductance of a superconducting film without a ground plane can be approximated by

$$L = 2\left(\ln\frac{2d}{w} - 1\right) \times 10^{-9} \text{ henry/cm}, \tag{2}$$

where d is the distance between the conductor and the return path and w is the width of the conductor.[4]

The inductance of a superconducting film with a ground plane can be calculated from

$$L = \frac{2W}{I^2}. \tag{3}$$

The energy W is

$$W = \frac{1}{8}\int_v BH dv \times 10^{-7} \text{ watt seconds}. \tag{4}$$

If we assume that the energy is nearly all confined to the volume between the conductor and the ground plane and that the current is uniformly distributed in the film, then the magnetic field is constant in that volume and equal to

$$B = H = \frac{4\pi I}{10w}. \tag{5}$$

The volume is $d \times w \times l$; thus, the inductance per unit length is

$$L = 4\pi\frac{d}{w} \times 10^{-9} \text{ henry/cm}. \tag{6}$$

From an examination of (2) and (6) it can be seen that the inductance is reduced by several orders of magnitude through the use of a ground plane. The inductance with a ground plane is proportional to the distance between the conductor and the ground plane, whereas the inductance without a ground plane is proportional to the distance between the conductor and its return path. This conclusion is important when the design of cryotron circuits is discussed, since one can calculate the inductance of any path in a circuit simply by knowing the dimensions of the conductor. It is not necessary to consider the return path, since the ground plane is the return path as far as calculations of inductance are concerned.

Typical values of inductance for conductors 0.02 cm wide with and without a superconductive ground plane are 10^{-11} henrys/cm and 10^{-8} henrys/cm, respectively (assuming that in the no-ground-plane case the return path is 1 cm from the conductor).

[3] C. R. Smallman, "Thin film cryotrons. Part I—Properties of thin superconducting films," Proc. IRE, this issue, p. 1562.

[4] The usual formula for round wires (K-Henny, "Radio Engineering Handbook," McGraw-Hill, New York, N. Y., 3rd Ed., pp. 70–100 is

$$2\left(\ln\frac{d}{r} - 1\right) \times 10^{-9} \text{ henry/cm}.$$

The assumption has been made that $w/2$ may be substituted for r for a first approximation.

B. Resistance

The resistance restored in a gate as a function of control current is plotted in Fig. 3. When no ground plane is used, the field around the control is not restricted, and the amount of gate that is quenched is proportional to the control current. When a ground plane is used, however, the normal component of field is cancelled and resistance is restored because of the tangential component of field in that portion of the gate which is directly under the control.

One can measure the effect of the addition of a ground plane on the characteristics of a cryotron by testing a cryotron that has been constructed with the gate on top of the control. After this test, a ground plane may be added and the test repeated. The results of this procedure are shown in Fig. 3.

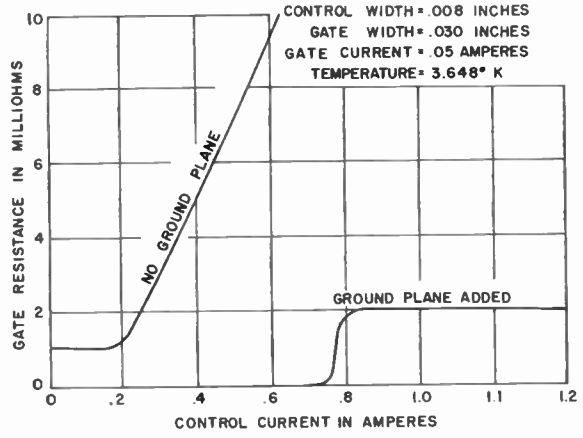

Fig. 3—Restoration of gate resistance vs control current for a cryotron with and without a ground plane.

The no-ground-plane curve shows the presence of gate resistance even when there is no control current. This residual resistance is present in many no-ground-plane cryotrons, and it is significant that the addition of a ground plane completely eliminates it—presumably by cancellation of the normal fields.

"Under and Over" Cryotron

In the previous section, the difference in the characteristics of a cryotron with and without a ground plane was attributed to the effects of normal and tangential fields. So that these effects could be investigated more carefully, a cryotron was constructed with one control under the gate and another control over the gate.

The "under and over" control provides a simple means of generating a field that is either normal to the gate or tangential. If current flows in the same direction in both controls, the tangential component of field at the surface of the gate will be cancelled and only normal field will be present. The normal field is greatest at the edge of the control, diminishing with distance away from the control.

On the other hand, if current flows in opposite directions in the controls, the normal component of field at the surface of the gate will be cancelled and only tangential field will be present. The magnitude of the tangential field is constant between the controls; it becomes negligible at a distance from the edge that is equal to the separation between the controls. Since the controls are about 200 times wider than the distance between them, the tangential field can be considered to exist only between the controls.

Fig. 4 is a plot of gate resistance vs control current for the under and over cryotron. The restoration of resistance resulting from the normal field (control currents in the same direction) begins at a low value of control current and increases with increasing control current; the restoration of resistance caused by the tangential field (control currents in opposite directions) starts at higher values of control current and reaches a value that is independent of control current.

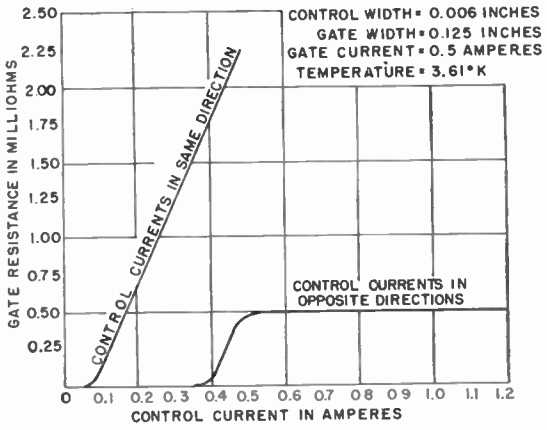

Fig. 4—Restoration of gate resistance vs control current for "under and over" cryotron.

The curves show that less normal field than tangential field is required to quench the gate. The curves of Fig. 4 also bear a close resemblance to the curves of Fig. 3; this similarity indicates that the ground plane does cancel the normal field just as effectively as a second control does.

Calculation of Switching Times for Cryotron Circuits

The calculation of switching times of cryotron circuits is considerably different than the same calculations for transistor circuits. The resistances involved are so low that capacitance can be ignored, but all circuit inductances must be considered. The time required for current to switch from one path to another is given by the inductance of the cryotrons and their interconnecting leads divided by the resistance that is causing the change to occur. Very often, the interconnecting leads have more inductance than the cryotrons.

It becomes a matter of considerable importance, then, to construct compact, minimum-time-constant circuits. In fact, the time constant of a circuit cannot be discussed before a layout is decided upon.

Fortunately, as was pointed out in the section on ground planes, the inductance of a loop in which the current is changing does not depend upon the area enclosed by that loop, but only upon the length and width of the leads involved. Clearly, then, the object of the circuit designer should be to make all leads as short and as wide as possible.

Time Constant of a Cryotron

The time constant of a single device is, of course, meaningless. Nevertheless, it is useful to calculate the inductance of a control and the resistance of a gate and to call the ratio of L_c/R_g the time constant of a cryotron. This time constant is useful in calculating circuit time constants, and it can also be used to compare the merits of different cryotron designs.

To discuss time constants, one must be more specific about the definition of a control and a gate. The control of a cryotron is only that length of conductor which is directly on top of the gate; conversely, the gate of a cryotron is only that portion which is directly under the control. The rest of the conductors are considered to be interconnecting leads.

The inductance of a control (for a cryotron with a control 0.006 inch wide and a gate 0.125 inch wide) can be calculated from (6).

$$L_c = 4\pi \frac{dl_c}{w_c} \times 10^{-9} \text{ henry}, \tag{6}$$

where

$$w_c = 1.5 \times 10^{-2} \text{ cm}$$

and

$$l_c = 31 \times 10^{-2} \text{ cm}.$$

The distance between the control and ground plane is

$$d = 10^{-4} \text{ cm};$$

therefore,

$$L_c \approx 3 \times 10^{-11} \text{ henrys}.$$

The inductance of a gate by the same calculation is only 2×10^{-14} henrys and can therefore be neglected.

The gate resistance is given by

$$R_g = \frac{\rho l_g}{t w_g}, \tag{7}$$

where

l_g, the length of the gate, $= 1.5 \times 10^{-2}$ cm,
w_g, the width of the gate, $= 31 \times 10^{-2}$ cm,
t, the thickness of the gate, $= 3 \times 10^{-5}$ cm,

and

ρ, the resistivity of the gate, $= 3 \times 10^{-7}$ ohm-cm.

Therefore, the resistance of the quenched area is

$$R_g = 5 \times 10^{-4} \text{ ohm},$$

and the calculated L/R time constant of a single cryotron is

$$L/R = 6 \times 10^{-8} \text{ second}$$

Time Constant of a Cryotron Flip-Flop

Fig. 5 is a circuit diagram of a cryotron flip-flop. This circuit differs from the usual flip-flop in that it is nonlatching; there is no feedback coupled from one branch of the flip-flop to the other. Operation of the circuit is as follows.

The supply current is initially divided equally between the ONE and the ZERO branches, which, at this time, have zero resistance. When sufficient current is applied to the ZERO IN control, the gate of that cryotron becomes resistive and the supply current redistributes to the ONE branch of the circuit. When the current in the ZERO IN control is removed, the current remains in the ONE branch indefinitely, since there is no resistance to cause the current to redistribute. Similarly, a pulse of current in the ONE IN control causes the current to redistribute to the ZERO branch of the flip-flop.

The time constant for the current redistribution is two to five times the L/R of a single cryotron, depending upon the amount of inductance in the interconnecting leads. Fig. 6 shows the actual circuit layout of a flip-flop designed for minimum inductance in which the time constant is approximately three times that of a single cryotron.

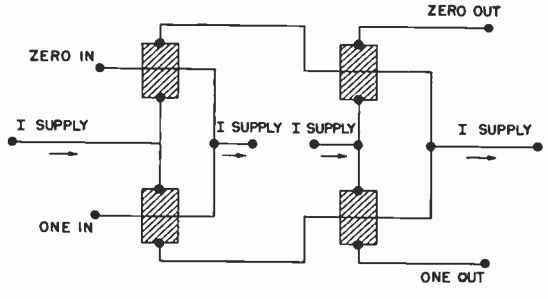

Fig. 5—Circuit diagram of nonlocking cryotron flip-flop.

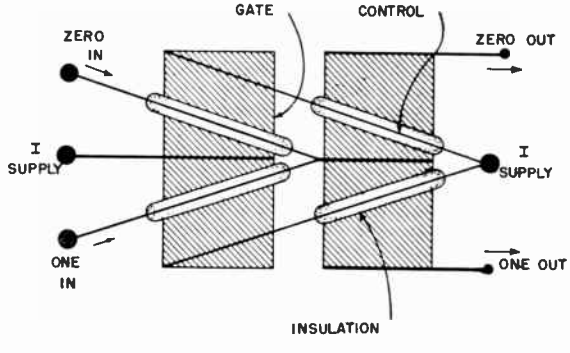

Fig. 6—Nonlocking cryotron flip-flop: actual layout of deposited circuit.

The output of the flip-flop is in the form of current in either the ZERO or ONE output lead. If a ZERO is stored in the flip-flop, current is flowing in the ZERO output lead.

One can calculate the L/R time constant for the redistribution of current from the ZERO path to the ONE path by adding the inductance of the interconnecting leads to the inductance of the cryotrons and dividing by the resistance of one gate. Usually, the interconnecting leads can be made quite short. For instance, Fig. 6 shows the actual circuit layout of a flip-flop in which the inductance of the interconnecting leads is about twice the inductance of a single cryotron. The time constant for this circuit is therefore

$$4\frac{L_c}{R_c} = 2.4 \times 10^{-7} \text{ second.}$$

The Complement Time of a Flip-Flop

The time constant of a flip-flop defines the rate at which current redistributes from one branch to the other. The actual time required to complement the flip-flop depends upon the amount of current that must be switched.

By definition, the flip-flop is completely complemented when the current in the output control has reached the critical value necessary to quench the output gate. The amount of current which must be switched so that it will be possible to reach this critical value depends upon the magnitude of the supply current. For instance, if the supply current is 1 ampere and is divided so that a critical current of 0.8 ampere flows in the ZERO path and 0.2 ampere flows in the ONE path, then to complement the flip-flop it is necessary to switch 0.6 ampere. If the supply current is 1.4 amperes, however, and it is divided so that a critical current of 0.8 ampere flows in the ZERO path and 0.6 ampere flows in the ONE path, then to complement the flip-flop it is necessary to switch only 0.2 ampere.

The flip-flop supply current acts as a self-bias; it biases the controls closer to critical. The dependence of complement time on supply current can be expressed as

$$t_{\text{complement}} = \frac{4L}{R}\left(\ln\frac{a}{a-1}\right), \tag{8}$$

where $4L$ is the inductance of the flip-flop loop,

R is the resistance of one gate,

and

a is the ratio of supply current to critical control current,

$$\frac{I_s}{I_{c\,\text{crit}}}.$$

Applying (8), we find that

when $I_s = 1I_{c\,\text{crit}}$, $t_{\text{complement}} = \infty$;

when $I_s = 1.1I_{c\,\text{crit}}$, $t_{\text{complement}} = 9.6\frac{L}{R}$;

and

when $I_s = 2I_{c\,\text{crit}}$, $t_{\text{complement}} = 2.8\frac{L}{R}$.

In an experiment, a flip-flop was complemented in 20 μsec with a supply current 1.1 times $I_{c\,\text{crit}}$. If we use (8), the time constant of this flip-flop can be calculated; it is about 2×10^{-6} second.

This time constant, derived from a measurement of the complement time, is not in agreement with the calculated time constant. The reason for this is not fully understood. Part of the discrepancy results from the fact that at the same time the input control current is increasing (causing the gate resistance to increase) the gate current is decreasing. The decreasing gate current reduces the magnetic field and tends to reduce the gate resistance. This has the effect of negative feedback, which increases the switching time. The magnitude of the negative feedback is proportional to the incremental current gain.[2] Similar time constants have been measured in a circuit composed of a ring of flip-flops; a circuit of this kind is discussed in the last section of this paper.

Relationship Between Switching Time and Size

It is interesting to note that the switching time of cryotron circuits does not decrease with miniaturization of the circuit. This seems to be contrary to general notions about size and speed relationships.

The usual conclusions are based upon a reduction of volume. In cryotron circuits, however, the thickness is already minimum, and size reduction may be considered in only two dimensions.

The relationship between size and the time constant is apparent when the expression for the time constant is arranged as follows:

$$\frac{L}{R} = \frac{dl}{\rho} \times \frac{l_c}{w_c} \times \frac{w_g}{l_g} \times 10^{-8} \text{ second.} \tag{9}$$

If the length and width of the cryotron are changed by the same amount, the ratio of l_c/w_c and w_g/l_g will not change, and the value of the expression will be invariant with size (assuming a constant thickness).

The critical current is directly proportional to the width of the control; thus, the current does decrease directly with size. The total power dissipated decreases as the square of the size reduction, and therefore the power dissipated per square centimeter of circuit, is not affected by miniaturization.

Time Constants of Externally Driven Cryotrons

When cryotrons are used in circuits such as tree switches or translators, their controls may be driven from an external pulse source; in these cases, it is not necessary to have a current gain greater than unity. The time constant of externally driven cryotrons can be considerably shorter than that of cryotrons which are required to have current gain for the following reasons:

1) If all controls are driven from current sources external to the cryotron circuit, then the only inductances in the cryotron switching network must result from the gates and their interconnecting leads. Gate inductance is, of course, much lower than control inductance.
2) The externally driven controls can be made wider than controls for cryotrons that must have current gain; therefore, more of the gate is made resistive.
3) The gate resistance can be restored in a shorter time, since the rise time of the control current can be extremely short when the controls are driven by external pulse generators.

The time constant of a cryotron is defined as the inductance of the control divided by the resistance of the gate. The time constant of an externally driven cryotron, however, is defined as the inductance of the gate divided by the resistance of the gate. From (9)

$$\frac{L_g}{R_g} = \frac{dt}{\rho} \times \frac{l_g}{w_g} \times \frac{w_g}{l_g} 10^{-8} = \frac{dt}{\rho} \times 10^{-8} \text{ second.}$$

and

$$\frac{L_g}{R_g} = \frac{2 \times 10^{-5} \times 2 \times 10^{-5}}{3 \times 10^{-7}} \times 10^{-8} \approx 10^{-11} \text{ second.}$$

The Cryotron Catalog Memory[5] is an excellent example of the application of externally driven cryotrons. The Catalog Memory is a recognition circuit that simultaneously compares a binary word with a large store of words. The output of the memory can be either a "yes" or "no" answer as to the comparison, or, in a more complicated circuit, the answer can be information about the stored word. The recognition time for a simple yes-no comparison in a memory containing 4000 twenty-five-bit words is calculated to be 10^{-8} second for thin-film cryotrons. Other similar applications such as translators or function tables have equally interesting calculated time constants. It should be emphasized that inductive coupling between input and output or heating effects may increase the time constants beyond the calculated value.

A Cryotron Ring Oscillator

So that the feasibility of thin-film cryotron circuits could be demonstrated and the switching characteristics of cryotron flip-flops could be studied, a ring of five flip-flops was constructed. Each stage of the ring is the same as the flip-flop shown schematically in Fig. 5.

A circuit diagram of the ring is shown in Fig. 7. The flip-flops are arranged so that the output of one stage complements the next stage and the output of the last stage is fed back to the input of the first stage 180 degrees out of phase. The circuit oscillates at a frequency

[5] A. E. Slade and H. O. McMahon, "A cryotron catalog memory system," *Proc. Eastern Joint Computer Conf.*, pp. 115–120; December, 1956.

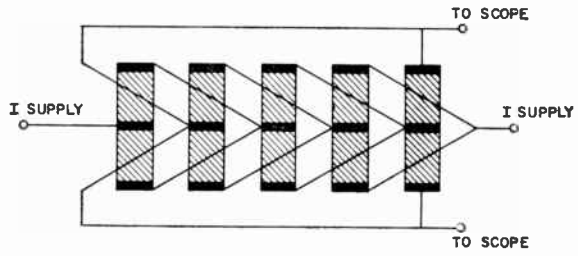

Fig. 7—Circuit diagram of five-stage flip-flop ring.

determined by the switching times of the flip-flops.

One can obtain an approximate prediction of the behavior of a flip-flop ring as a function of supply current and temperature by rearranging (8).

$$f_{osc} = K \frac{1}{\ln\left(\frac{a}{a-1}\right)}, \tag{10}$$

where

$$a = \frac{I_s}{I_{c\,crit}}$$

and

$$K = \frac{R}{4L}.$$

As the supply current increases, the value of a increases and therefore the frequency of oscillation increases. If the temperature is reduced, the value of a will be smaller and the frequency of oscillation will be reduced, since a reduction in temperature is equivalent to increasing $I_{c\,crit}$. (See Fig. 2.) The use of a ground plane, of course, reduces L/R and thus increases the maximum frequency of oscillation.

A complete analysis of the circuit is discussed in the next paper.[2]

Fig. 8 shows the measured characteristics of a typical flip-flop ring. The measured characteristics agree with the above predictions. This ring was constructed upside-down so that it could first be tested without a ground plane and then be retested after the addition of a ground plane.

The highest frequency that has been observed for a five-stage ring is 200 kc. During the time of one period (5×10^{-6} second), each flip-flop is complemented twice; the delay per stage is therefore approximately $\frac{1}{2}$ μsec. From the characteristics shown in Fig. 8, L/R can be computed to be about 10^{-6} second.

So that inductance in the actual circuit layout could be minimized, the interconnecting leads were reduced to a minimum. As a result, the input gates are pushed together, the output controls are only slightly longer than one gate width, and the feedback line from output

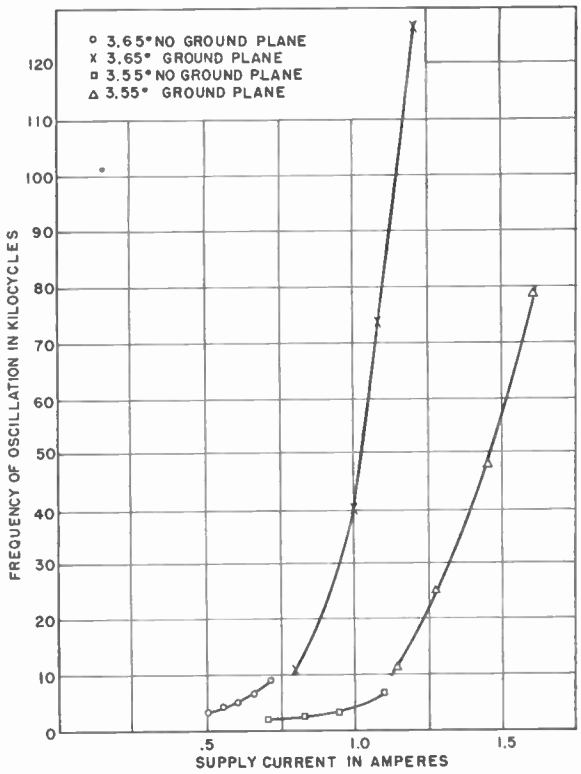

Fig. 8—Oscillating frequency vs supply current at two temperatures for five-stage flip-flop ring.

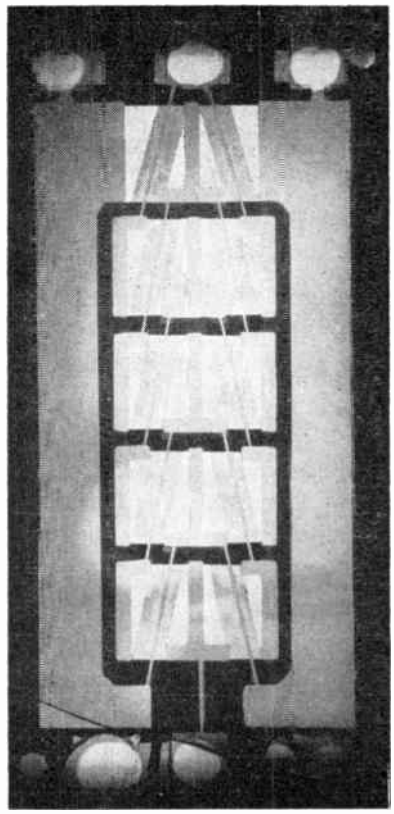

Fig. 9—A five-stage flip-flop ring circuit.

to input is as wide as possible. The completed circuit is shown in Fig. 9.

The size of this circuit containing 10 cryotrons is 1 inch by 2 inches. The lead controls are 0.008 inch wide, and the tin gates are 0.250 inch wide. Identical circuits were also constructed that were one half this size. Further size reductions are possible; however, the construction of masks limits the minimum line width to about 0.003 inch at present. The present state of the art makes possible packing densities ranging from 200 cryotrons per cubic inch for the ring oscillators to 4000 cryotrons per cubic inch for some memory circuits.

Discussion

The feasibility of constructing switching circuits from thin-film cryotrons has been demonstrated. Thin-film-cryotron circuits are microminiature, solid-state circuits. They have an equivalent parts density of 2×10^{-6} parts per cubic foot at the present time, and further reduction in size is feasible.

The anticipated advantages of cryotron circuitry are high packing density and reliability; it should also be possible to construct this circuitry automatically and at a low cost. At present, however, it is too early to know to what extent these advantages will be realized.

One disadvantage of cryotron circuitry is the requirement of a low-temperature refrigerator. Present-day cryostats do not meet the requirement of reliability, which is necessary for computer applications. Research is in progress in this area, however, and a small, reliable refrigerator will be available when cryotrons are beyond the research stage and ready for applications.[6]

There are a number of temporary disadvantages that should not be overlooked.

1) Short circuits do, at times, occur between layers of metal. Shorting is caused by a flaw (dust or splattered metal) in the insulation layer. The probability of a short is, of course, dependent upon how extensive the circuitry is. A single cryotron is very seldom shorted; however, about 10 per cent of the ring oscillator circuits were found to have shorts. The reduction of short circuits is only a matter of refining our present techniques.
2) The requirements on device reproducibility are severe when a large number of devices are simultaneously manufactured and interconnected in a circuit. At present, cryotrons made at the same time are similar, but they differ somewhat from cryotrons made at a later time. Critical temperatures will vary by as little as $3.85\pm0.01°K$ for one series of cryotrons and by as much as $\pm0.07°K$ for another. A typical operating point for our work to date has been 0.25 degree below critical, and therefore a variation of ±0.07 degree would not

[6] H. O. McMahon and W. E. Gifford, "A New Low Temperature Gas Expansion Cycle," presented at the Cryogenic Engineering Conference, Berkeley, Calif.; September 2–4, 1959.

be acceptable. Improvements are being made in reproducibility, and the causes of variations are being investigated.

3) Although the frequency response of externally driven cryotrons is quite adequate, the response time of cryotrons that must have current gain is not acceptable for many applications. It may be possible to increase frequency response by the use of superconductive alloys. It is difficult, however, to deposit an alloy having a higher resistance that at the same time retains a sharp superconductive-to-normal transition and a high current gain.

None of the problems enumerated above will prevent the cryotron from becoming a useful and versatile computer component. The general acceptance of the cryotron by computer designers will depend upon the cryotron's ability to solve problems at a lower cost, at a higher speed, or with more reliability than other solid-state, microminiature concepts.

The cost of cryotron circuits, even including the cost of the refrigerator, will probably be competitive with that of other solid-state circuits and be considerably less than that of circuits constructed by present-day techniques. Reliability is hard to predict; however, superconductors have the advantage of operating at a constant temperature near absolute zero, where chemical-activity and diffusion processes have essentially stopped. Because of their unique property of zero resistance, cryotrons can be used in circuits that are impractical to consider with any other component. Therefore, many problems such as storage and retrieval of information can be solved at a higher speed with less complex circuitry.

Part III—An Analysis of Cryotron Ring Oscillators

M. L. COHEN

Summary—**Part III is a circuit analysis of cryotron ring oscillators. Ring oscillators have been constructed so that the dynamic behavior of film cryotrons in circuits could be studied. The analysis is concerned with the frequency-L/R time constant and circuit resistance-gate resistance relationships so that the results of measurements on oscillators can be properly interpreted. Two analyses, based on different ideal characteristics, are made. The first treats each stage as a linear amplifier, and the second treats each stage as a switching circuit. Although the two analyses start with rather different assumed ideal characteristics, the results agree in many respects.**

Introduction

IN THE course of film cryotron development, ring oscillators[1] were made so that the dynamic behavior of film cryotrons in circuits could be studied. Of particular interest are the L/R time constants of cryotron circuits. A typical oscillator (shown in Fig. 1) is a

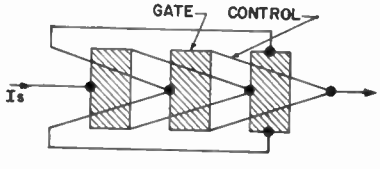

Fig. 1—Cryotron ring oscillator.

closed ring of identical amplifier stages. Suitable analyses of these circuits are necessary if the results of measurements on these oscillators are to be properly interpreted. Since the characteristics of real cryotrons are highly nonlinear, linear or ideal characteristics must be assumed for the purpose of circuit analysis. In this paper two analyses, based on different ideal characteristics, will be made in an attempt to bracket the behavior of real cryotron oscillators. The first analysis will treat each stage as a linear amplifier. Expressions for stage gain and phase shift will be derived, and the operating range and frequency of the oscillators thus determined. The second analysis will treat each stage of the oscillator as a switching circuit and, assuming oscillation, will determine the frequency of oscillation. Both analyses also consider the relation between the resistance of a single gate and the resistance the whole oscillator presents to the supply current. If this relationship is known, the gate resistance while the circuit is in oscillation may be computed, since the resistance of the whole circuit is readily measured.

Linear Amplifier Analysis

Consider a single stage, push-pull cryotron amplifier. (See Fig. 2.) The dc supply current, I_s, is assumed to divide equally. The ac input current, i_{in}, modulates the resistances of the cryotron gates, R_1 and R_2, so as to produce an ac output current, i_0. In the linear small signal analysis, we assume first that the gate resistance, R_g, is a linear function of current, I, above some critical value.

$$R_g = m(I - I_{crit}). \quad (1)$$

[1] A. E. Slade, "Thin film cryotrons. Part II—Cryotron characteristics and circuit applications," PROC. IRE, this issue, p. 1569.

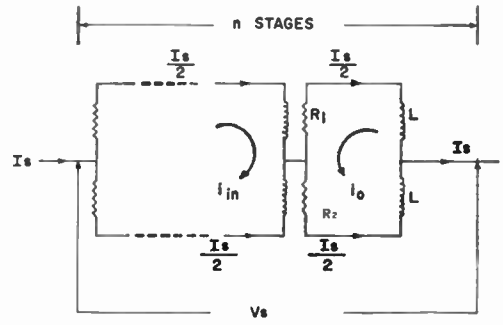

Fig. 2—Single-stage equivalent circuit.

We also assume that the current I is a linear combination of control and gate currents.

$$I = I_c + \frac{I_g}{\mu} \tag{2}$$

where μ is the incremental current gain, $\partial I_g/\partial I_c$. Combination of (1) and (2) give

$$R_g = m\left(I_c + \frac{I_g}{\mu} - I_{\text{crit}}\right). \tag{3}$$

These assumptions are shown graphically in Figs. 3(a) and 3(b).

The loop equation for Fig. 2 is

$$0 = i_0(R_1 + R_2 + 2j\omega L) + \frac{I_s}{2}(R_2 - R_1) \tag{4}$$

and, since the operating point is $I_c = I_g = I_s/2$, we have from (3)

$$R_1 = m\left[\frac{I_s}{2} + i_{\text{in}} + \frac{1}{\mu}\left(\frac{I_s}{2} - i_0\right) - I_{\text{crit}}\right]$$

$$R_2 = m\left[\frac{I_s}{2} - i_{\text{in}} + \frac{1}{\mu}\left(\frac{I_s}{2} + i_0\right) - I_{\text{crit}}\right]. \tag{5}$$

Substituting (5) in (4) and solving for gain, we obtain

$$A = \frac{i_0}{i_{\text{in}}} = \frac{1}{1 + \frac{2}{\mu} - \frac{2}{a} + \frac{2j\omega L}{mI_s}}. \tag{6}$$

where

$$a = \frac{I_s}{I_{\text{crit}}}$$

There is a less rigorous approach which gives more insight into the operation of the circuit. Consider the incremental current gain to be infinite; that is, gate current has no effect on gate resistance. The alternating component of resistance in each gate is then

$$r = mi_{\text{in}}. \tag{7}$$

The two alternating resistance components are out of phase; that is, as the resistance of one gate increases, the resistance of the other decreases. The currents through

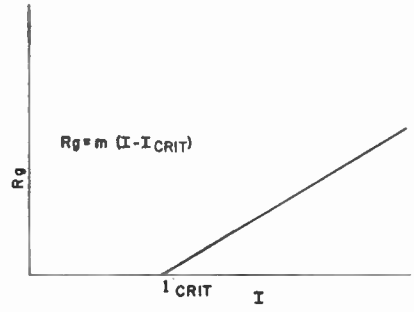

(a)

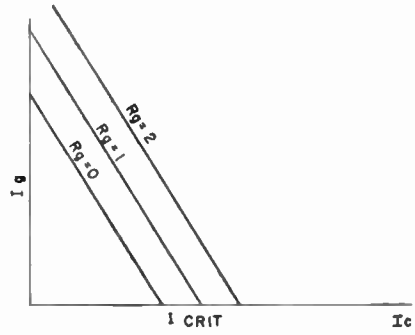

(b)

Fig. 3—Assumed ideal characteristics. (a) Quenching characteristic; (b) Control characteristic.

these gates are in opposite directions also; thus, the total ac voltage in the loop is

$$V = 2mi_{\text{in}}\frac{I_s}{2} \tag{8}$$

and the output current is

$$i_0 = \frac{V}{Z} = \frac{mI_s i_{\text{in}}}{2(R_g + j\omega L)}. \tag{9}$$

The stage gain is therefore

$$A_\infty = \frac{i_0}{i_{\text{in}}} = \frac{mI_s}{2(R_g + j\omega L)}. \tag{10}$$

Finite incremental current gain is, in effect, internal negative feedback. As control current increases, gate resistance increases, and gate current decreases. The decrease in gate current tends to decrease gate resistance. Since the dc values of gate and control current are equal, the feedback is $1/\mu$. The gain is therefore

$$A = \frac{mI_s}{2(R_g + j\omega L) + \frac{mI_s}{\mu}}, \tag{11}$$

and by substituting (3) for an operating point, $I_c = I_g = I_s/2$, we obtain (6).

A necessary requirement for oscillation is that the loop gain of the oscillator be $1 + j0$. If there are n stages in the cryotron ring oscillator connected with 180 degree

phase shift, the required phase shift per stage at the frequency of oscillation is $180°/n$. Eq. (11) shows that the phase shift per stage is $\tan^{-1} \omega L/R_{eq}$ where R_{eq}, the equivalent resistance, is

$$\frac{mI_s}{2}\left(1+\frac{2}{\mu}-\frac{2}{a}\right).$$

Therefore, the frequency of oscillation is given by

$$f_{osc} = \frac{1}{2\pi}\frac{R_{eq}}{L}\tan\frac{180°}{n}. \tag{12}$$

At low frequencies, ωL is small compared with R_{eq}, and the gain is

$$A_{LF} = \frac{1}{1+\frac{2}{\mu}-\frac{2}{a}}. \tag{13}$$

The gain at the frequency of oscillation is less than the low-frequency gain by a factor equal to the cosine of the phase shift per stage. Thus, the minimum low-frequency gain,

$$A_{LF_{min}} = \sec\frac{180°}{n}, \tag{14}$$

determines the upper current limit of operation. If we assume that no oscillation can occur until some resistance is restored, then the lower current limit of oscillation is

$$a_{min} = \frac{2\mu}{\mu+1} \tag{15}$$

since this current, equally divided, will cause both gates to be on the verge of resistance.

These results are shown graphically in Fig. 4, a plot of operating range vs incremental current gain, and Fig. 5, frequency vs current for various values of μ. Plotted in Fig. 4 are the contours of constant low-frequency gain which form the upper current limit of operation for three-, four-, and five-stage oscillators. Contours of constant ratio, R_{eq}/R, are also shown.

A. Resistance Relationship in the Linear Analysis

The power dissipated in a ring oscillator is

$$P = V_s I_s = I_s^2 R_0 \tag{16}$$

where I_s is the supply current, V_s is the supply voltage and R_0 is the effective resistance of the oscillator (Fig. 2). However, from a consideration of the currents and resistances in a single stage of the oscillator, we have

$$P = n\left[\left(\frac{I_s}{2}\right)^2 + i_0^2\right](R_1+R_2) \tag{17}$$

where n is the number of stages, i_0 is the rms value of the ac output current, and R_1 and R_2 are the gate resistances. But

$$R_1 + R_2 = 2R_g \text{ a constant} \tag{18}$$

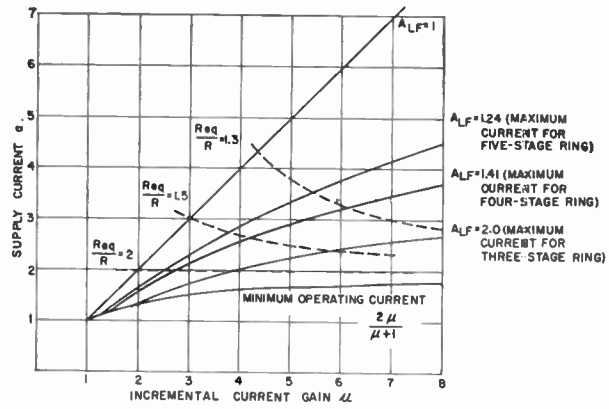

Fig. 4—Operating range vs incremental current gain, linear analysis.

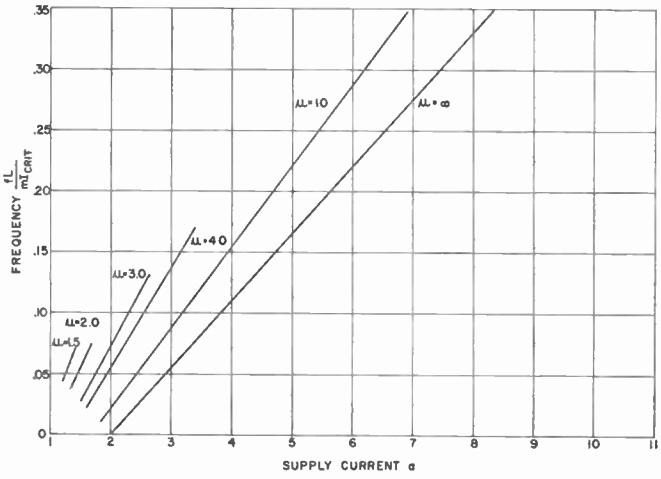

Fig. 5—Frequency vs supply current, linear analysis.

hence

$$\frac{R_g}{R_0} = \frac{2}{n}\frac{1}{1+\left(\frac{2i_0}{I_s}\right)^2}. \tag{19}$$

For very weak oscillations, i_0 is negligible, compared with I_s, and for $n=5$,

$$\frac{R_g}{R_0} = \frac{2}{n} = 0.4. \tag{20}$$

The maximum value i_0 may have without any clipping occurring is $0.707\ I_s/2$. In this case (a moderately strong oscillation),

$$\frac{R_g}{R_0} = \frac{4}{3n} = 0.27 \tag{21}$$

for $n=5$.

Thus, R_g/R_0 may be expected to range from about 0.2 to 0.4, and a good estimate of this ratio may be made by observing the wave shape and amplitude of the oscillator output.

B. Extension of the Linear Analysis

The usefulness of the second, less rigorous approach will be demonstrated by two examples. First, let us consider a more general resistance-current function of the form

$$R_g = K(I - I_{crit})^p \tag{22}$$

where as before $I = I_c + I_g/\mu$.

We now replace m in (11) by $\partial R_g/\partial I_c$, with the result

$$A = \frac{\frac{\partial R_g}{\partial I_c} I_s}{2(R_g + j\omega L) + \frac{\partial R_g}{\partial I_c}\frac{I_s}{\mu}} \tag{23}$$

and

$$A_{LF} = \frac{1}{\frac{2R_g}{\frac{\partial R_g}{\partial I_c} I_s} + \frac{1}{\mu}} . \tag{24}$$

But

$$R_g = K\left(I_c + \frac{I_g}{\mu} - I_{crit}\right)^p \tag{25}$$

and

$$\frac{\partial R_g}{\partial I_c} = pK\left(I_c + \frac{I_g}{\mu} - I_{crit}\right)^{p-1} . \tag{26}$$

Substituting these above expressions in (24), at the operating point $I_c = I_g = I_s/2$, we have

$$A_{LF} = \frac{p}{1 + \frac{p+1}{\mu} - \frac{2}{a}} . \tag{27}$$

The maximum operating current is still determined by the minimum stage gain (sec $180°/n$). Curvature of the resistance characteristic increases the gain and, consequently, the operating range. Fig. 6 shows this effect for $n = 5$ and several values of the exponent p. Note that slight nonlinearity greatly increases the range of operation.

As a second example, let us consider a more complicated circuit, the flip-flop ring oscillator shown in Fig. 7.

Again, assume the linear characteristics used for the amplifier ring.

This circuit differs from the amplifier ring only in that there is unit positive feedback and twice the impedance. Therefore,

$$A_\infty = \frac{mI_s}{4(R_g + j\omega L) - mI_s} . \tag{28}$$

A negative feedback effect of finite current gain is now $2/\mu$, since there are two gates in each circuit branch. Hence,

$$A = \frac{mI_s}{4(R_g + j\omega L) + mI_s\left(\frac{2}{\mu} - 1\right)} . \tag{29}$$

The equivalent resistance is now

$$R_{eq} = R_g + \frac{mI_s}{4}\left(\frac{2}{\mu} - 1\right) \tag{30}$$

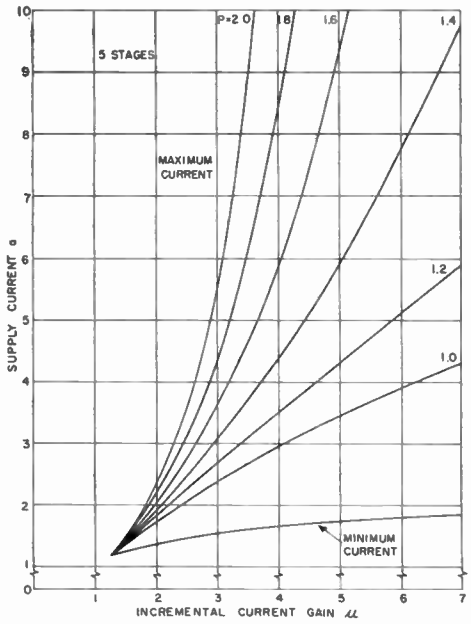

Fig. 6—Effect of nonlinearity on operating range.

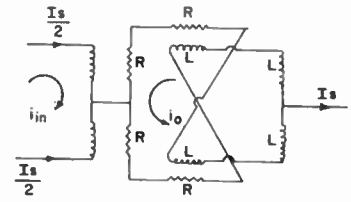

Fig. 7—Single-stage equivalent circuit for a flip-flop ring.

and the low-frequency gain is

$$A_{LF} = \frac{mI_s}{4R_g + mI_s\left(\frac{2}{\mu} - 1\right)} = \frac{mI_s}{4R_{eq}} . \tag{31}$$

Substituting for R_g

$$R_g = \frac{mI_s}{2}\left(1 + \frac{1}{\mu} - \frac{2}{a}\right) \tag{32}$$

$$R_{eq} = \frac{mI_s}{2}\left(\frac{1}{2} + \frac{2}{\mu} - \frac{2}{a}\right). \tag{33}$$

And

$$A_{LF} = \frac{1}{1 + \frac{4}{\mu} - \frac{4}{a}} . \tag{34}$$

The results of the above analysis are summarized in Fig. 8, a graph of operating range similar to Fig. 4. There is an additional restriction on minimum operating current. R_{eq} may not be negative; therefore,

$$a > \frac{4\mu}{\mu + 4} . \tag{35}$$

Note that the operation of a flip-flop ring is rather similar to that of an amplifier ring, except that since the ratio of R_{eq} to R is smaller, the frequency will be lower for the same L/R time constant.

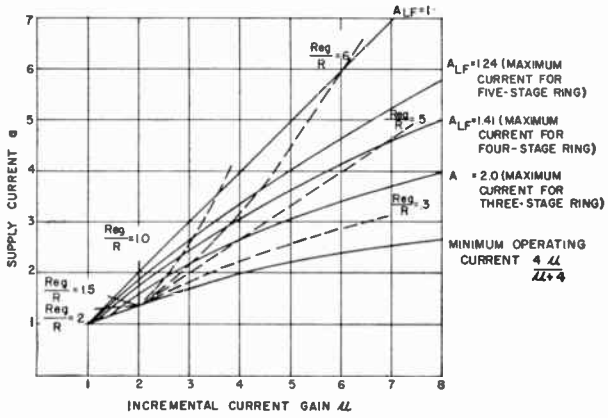

Fig. 8—Operating range vs incremental current gain for flip-flop ring oscillators.

Switching Analysis

For the switching analysis, we assume that the gate resistance, R_g, is a discontinuous function of current, I, as shown in Fig. 9.

$$I < I_{crit} \qquad R_g = 0$$
$$I > I_{crit} \qquad R_g = R. \tag{36}$$

As assumed in the linear analysis, I is a linear combination of gate and control currents.

$$I = I_c + \frac{I_g}{\mu}. \tag{37}$$

We will now assume that the circuit is in oscillation and examine the nature of the transients in each stage of the oscillator. Note that there are two modes of operation. For small values of supply current, I_s, there will be some time interval when neither gate in a stage is resistive. For large values of supply current, there will be a time interval when both gates are resistive. We will call these the first and second modes of operation, respectively. These transients are shown in Figs. 10 and 11. All currents have been normalized with respect to the critical current, I_{crit}; a is the ratio of supply current to critical current, and x is the ratio of the transient current to critical current.

Consider the first mode of operation (Fig. 10). During the time interval t_3–t_4, neither gate is resistive and the currents are constant. At time t_2, the rising control current, $x = s_2$, switches a gate to the resistive state. This corresponds to time t_4 for that gate; that is, the current in that gate is $a-b$. Therefore, from (36) and (37),

$$s_2 + \frac{a-b}{\mu} = 1. \tag{38}$$

At time t_1, the falling control current, $a-x=a-s_1$, switches a resistive gate to the superconducting state. This corresponds to time t_3 for current in the opposite gate, or time 0 for that gate; the current in the gate being switched is b. Therefore, from (36) and (37).

$$a - s_1 + \frac{b}{\mu} = 1. \tag{39}$$

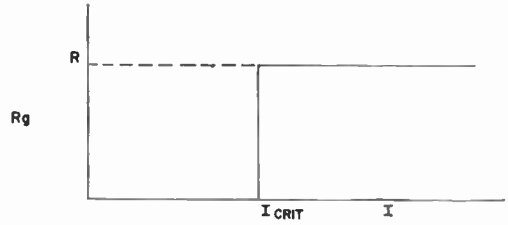

Fig. 9—Ideal quenching characteristic assumed in the switching analysis.

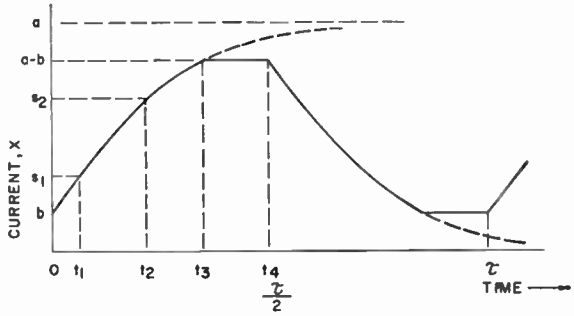

Fig. 10—First mode transients.

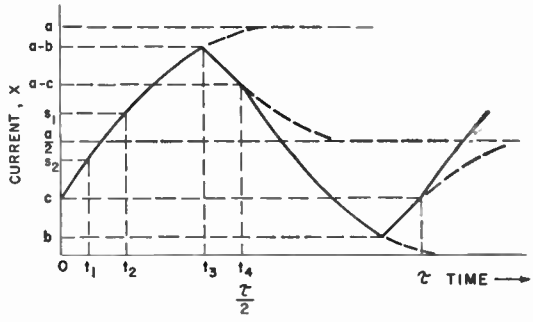

Fig. 11—Second mode transients.

We also recognize that during the time interval t_1–t_2 for the control current, neither gate associated with these controls is resistive. Therefore,

$$t_2 - t_1 = t_4 - t_3. \tag{40}$$

The delay time of a stage is t_2, for this is the time from the start of a transient in one stage to the start of a transient in the next stage. Therefore,

$$\tau = 2t_4 = 2nt_2 \tag{41}$$

where τ is the period of the oscillator and n is the number of stages.

Finally, time and current are related by the following:

$$t_1 = \frac{2L}{R} \ln \frac{a-b}{a-s_1}$$
$$= \frac{2L}{R} \ln \frac{a-b}{a-s_2}$$
$$t_3 = \frac{2L}{R} \ln \frac{a-b}{b}. \tag{42}$$

Substituting (41) and (42) in (40), we obtain

$$\ln\frac{a-b}{a-s_2}-\ln\frac{a-b}{a-s_1}=n\ln\frac{a-b}{a-s_1}-\ln\frac{a-b}{b} \tag{43}$$

or

$$\left(\frac{a-b}{a-s_2}\right)^{n-1}=\frac{a-s_1}{b}, \tag{44}$$

and substituting the values of s_1 and s_2 obtained from (38) and (39) yields

$$b=\frac{\mu-b}{\mu^n}\left(\frac{a(\mu+1)-\mu-b}{a-b}\right)^{n-1}. \tag{45}$$

For desired values of a and μ, b may be computed through the use of this last equation in a first-order iterative process. The frequency of oscillation in terms of R/L may then be found from the values of a, b and μ using

$$f=\frac{1}{\tau}=\frac{1}{2nt_2}=\left[\frac{4nL}{R}\ln\frac{(a-b)\mu}{a(\mu+1)-\mu-b}\right]^{-1}. \tag{46}$$

A similar solution may be made for the second mode of operation. Consider Fig. 11. During the time interval t_3–t_4, both gates are resistive and the currents tend toward an equal division. At time t_1, the rising control current, $x=s_2$, switches a gate resistive. As before, this corresponds to time t_3 for that gate, and the current in that gate is $a-b$. At time t_2, the falling control current, $a-x=a-s_1$, switches a resistive gate to the superconducting state. This corresponds to time 0 for that gate, or time t_4 for the opposite gate, and the current in the switched gate is c. Therefore, corresponding to (38) and (39) for the first mode, the following equations are derived:

$$s_2+\frac{a-b}{\mu}=1 \tag{47}$$

and

$$a-s_1+\frac{c}{\mu}=1. \tag{48}$$

As before

$$t_2-t_1=t_4-t_3 \tag{40}$$

and

$$\tau=2t_4=2nt_2. \tag{41}$$

Replacing (42) we have

$$t_1=\frac{2L}{R}\ln\frac{a-c}{a-s_2}$$

$$t_2=\frac{2L}{R}\ln\frac{a-c}{a-s_1}$$

$$t_3=\frac{2L}{R}\ln\frac{a-c}{b}$$

$$t_4-t_3=\frac{L}{R}\ln\frac{a/2-b}{a/2-c}, \tag{49}$$

and by substitution, we obtain

$$b=\frac{a(\mu+1)-\mu-b}{\mu n}\left(\frac{\mu-c}{a-c}\right)^{n-1} \tag{50}$$

and

$$c=\frac{a}{2}-\left(\frac{a}{2}-b\right)\left[\frac{\mu-c}{a(\mu+1)-\mu-b}\right]^2. \tag{51}$$

As before, these last equations may be solved by iterative methods, and the values of c thus obtained may be used to find the frequency of oscillation by use of

$$f=\frac{1}{\tau}=\frac{1}{2nt_2}=\left[\frac{4nL}{R}\ln\frac{\mu(a-c)}{\mu-c}\right]^{-1}. \tag{52}$$

These calculations have been made for $n=5$ and values of μ of 1.5, 2, 3, 4, 10, and ∞, for both the first and second modes. The crossover between modes occurs when $s_1=s_2$. The value of a at crossover, a_x, is

$$a_x=\frac{2\mu}{\mu+1}. \tag{53}$$

Note that this is the minimum current assumed in the linear analysis.

The range of a for which the calculations were made was that for which the equations applied. The minimum value of a was that which made $s_1=b$; the maximum value of a was that which made $s_2=c$.

The results are shown in Fig. 12, a graph of frequency vs current for the several values of μ.

A. Resistance Relationship for the Switching Analysis

The energy, W, dissipated per stage per cycle may be computed by integrating Joule's law for the instantaneous power in the gates over one cycle. For the first mode,

$$W=2I_c^2R\int_0^{t_3}(a-x)^2dt. \tag{54}$$

The power input to the oscillator must equal the power dissipated; thus,

$$P=I_s^2R_0=2nfI_c^2R\int_0^{t_3}(a-x)^2dt \tag{55}$$

and

$$\frac{R}{R_0}=\frac{a^2}{2nf\int_0^{t_3}(a-x)^2dt}. \tag{56}$$

The transient current, $a-x$, is

$$a-x=(a-b)e^{-Rt/2L}; \tag{57}$$

f is given by (17) and t_3 by (13). Performing the indicated substitutions and integration we have

$$\frac{R}{R_0}=\frac{2a}{a-2b}\ln\frac{a-b}{a-s_2}. \tag{58}$$

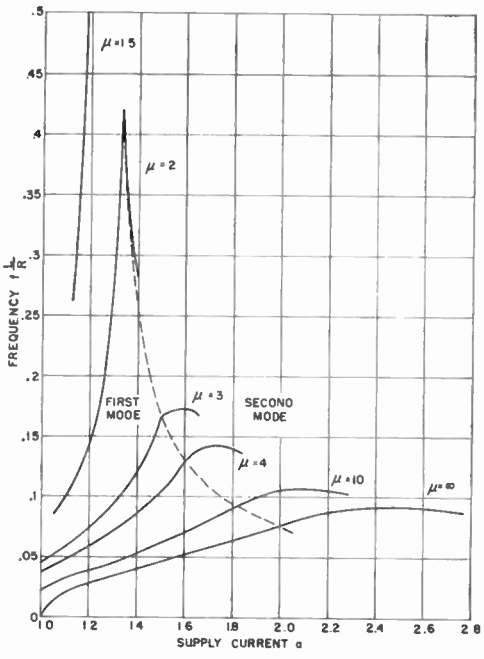

Fig. 12—Frequency vs supply current, switching analysis.

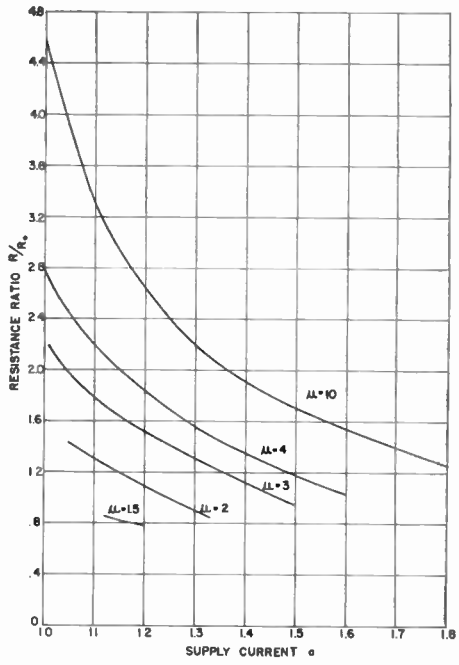

Fig. 13—Resistance ratio vs supply current, switching analysis.

This ratio has been computed for $n=5$ and $\mu=1.5$, 2, 3, 4 and 10, and the results are shown graphically in Fig. 13 as a function of a.

Discussion

Although the two above analyses start with rather different assumptions, the results agree in many respects. The current range of oscillation increases with increasing incremental current gain. Frequency increases with increasing current. Frequency is approximately one tenth R/L or mI_s/L, and R is of the order of 0.2 to 2 times R_0. Thus, if we measure the frequency of a real oscillator and its resistance to the supply current, we may readily estimate L/R, R, and L for the circuit.

The characteristics of a cryotron without a ground plane[1] fit the model used in the linear analysis quite well, except that μ is a function of current. DC measurements on ground-plane cryotrons give a resistance-current characteristic similar to that shown in Fig. 14.[1] This is not very different from that assumed in the switching analysis, except that there is some small resistance for currents below critical. It is believed that these oscillators operate mostly in the first mode, and that this resistance "toe" provides the starting mechanism for oscillation.

Measurements made on five-stage ring oscillators and treated as described above result in the following approximate values: No ground plane:

$$f \approx 100 \text{ cps to } 10 \text{ kc}$$

$$\frac{L}{R} \approx 2 \times 10^{-3} \text{ to } 2 \times 10^{-5} \text{ seconds}$$

$$R \approx 5 \times 10^{-6} \text{ to } 5 \times 10^{-4} \text{ ohm}$$

$$L \approx 10^{-8} \text{ henry.}$$

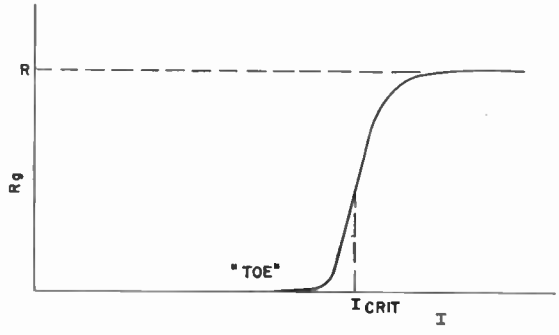

Fig. 14—Typical quenching characteristic of a ground plane cryotron.

These values are in good agreement with those expected from the dimensions of the cryotrons involved. Furthermore, contours of constant resistance and contours of constant frequency coincide in a current-temperature plane with surprising accuracy and thus confirm the analysis. Ground plane:

$$f \approx 10 \text{ kc to } 200 \text{ kc}$$

$$\frac{L}{R} \approx 10^{-6} \text{ seconds}$$

$$R \approx 10^{-4} \text{ ohm}$$

$$L \approx 10^{-10} \text{ henry.}$$

The expected values[2] are 5×10^{-4} ohm and 3×10^{-11} henry for R and L, respectively. Here the agreement is not good, the discrepancy being about an order of magnitude for both L and R. Further investigations, now in progress, should clarify this matter.

[2] *Ibid.*, see for the calculation of expected values.

Optimum Noise and Gain-Bandwidth Performance for a Practical One-Port Parametric Amplifier*

J. C. GREENE† AND E. W. SARD†, MEMBER, IRE

Summary—A practical one-port parametric amplifier is analyzed to determine the conditions under which minimum effective noise temperature and maximum gain-bandwidth product can be obtained. The analysis considers the effects of resistive loss and stray parasitic reactance in the junction-diode that provides the essential nonlinear reactance. It is shown that the conditions necessary for minimum noise temperature are compatible with those necessary for maximum gain-bandwidth product only if the diode has a high self-resonant frequency (the frequency at which the average diode capacitance resonates with the diode lead inductance). It is also shown that minimum noise temperature is always achieved when the diode loss alone is used as the idler circuit loading (regardless of the temperature of any additional idler loading), that there is a characteristic figure of merit for the diode, and that there is an optimum pump frequency.

Based on the equations derived, universal curves have been drawn that enable the design of an optimum amplifier when the signal frequency and diode characteristics are specified. In conclusion, it is shown that if junction-diode parametric amplifiers operated at room temperature are to seriously challenge the low-noise performance of the maser at microwave frequencies, a substantial improvement in the diode figure of merit is required.

I. Introduction

INTENSE interest has been aroused by the low-noise potential of junction-diode parametric amplifiers, resulting in considerable efforts at many laboratories directed toward developing such devices. The most useful amplifier of this type for microwave frequencies has an inherent negative conductance characteristic, and provides an amplified output signal at the same frequency as the input signal. Because of its negative-conductance characteristic, the amplifier has a nearly constant gain-bandwidth product, and stable amplification is obtained only when the net loading from the signal source conductance and post-receiver input conductance counterbalances the amplifier negative conductance.

For large amplifier gains, the negative and net positive conductances are nearly equal. Consequently, small changes in the loading admittances, when these admittances are connected directly to the amplifier terminals, can produce large gain fluctuations or even sustained oscillation. The use of nonreciprocal devices, such as circulators and isolators, minimizes the effective change in loading admittance seen by the amplifier, resulting in a gain characteristic that is stable and reliable. In turn, the stable gain characteristic allows the low-noise potential of these amplifiers to be realized in practice by keeping the gain fluctuation noise level below the internally generated noise level (a serious problem without the use of nonreciprocal devices, since the antenna and post-receiver admittances usually vary significantly in practical systems).

The performance of this amplifier will be related in detail to junction-diode characteristics, the limitations imposed by diode resistive loss and stray parasitic reactances, and the pump frequency. This analysis is subject to the restrictions that the amplifier is operated in conjunction with an ideal circulator and that the diode is only moderately lossy at the frequencies involved. As already described, the circulator is necessary for practical reasons; in addition, the presence of the circulator 1) allows achievement of the maximum possible gain-bandwidth product for the amplifier, 2) if ideal, will not degrade the minimum achievable noise figure when the amplifier gain is large, and 3) permits a straightforward derivation of effective noise temperature and gain-bandwidth product for the negative-conductance amplifier, since the resulting input and output conductances are positive.

In particular, expressions are derived for the minimum effective noise temperature and the maximum gain-bandwidth product of the amplifier in terms of diode characteristics and an optimum pump frequency. It is shown that the conditions necessary for minimum noise temperature are compatible with those necessary for maximum gain-bandwidth product only if the diode has a high self-resonant frequency (the frequency at which the average diode capacitance resonates with the diode lead inductance). Furthermore, it is shown that minimum noise temperature is always achieved when the diode loss alone is used as the idler circuit loading, regardless of the temperature of any additional idler loading. The analysis also indicates that there is a characteristic figure of merit for the junction diode.

Based on the equations derived, universal curves have been drawn that enable the design of an optimum amplifier when the signal frequency and diode characteristics are specified. By inserting typical values for presently available diodes into these curves, performance results to be expected at the present state of the art are set forth. In conclusion, it is shown that if junction-diode parametric amplifiers operated at room temperature are to seriously challenge the low-noise performance of the maser at microwave frequencies, a substantial improvement in the diode figure of merit is required.

II. Effective Input Noise Temperature

We shall first derive a general expression for the effective input noise temperature of a one-port parametric amplifier operated in conjunction with an ideal circu-

* Received by the IRE, December 28, 1959. The work reported here was performed under Air Force Contract AF 30(602)-1854.

† Airborne Instruments Lab., Melville, N. Y.

lator, but using a moderately lossy junction-diode. In this derivation, it is assumed that the signal and idler terminals are each shunted by a single loss conductance, G_1 and G_2 respectively, that includes the effects of diode loss, circuit loss, and any intentional loading. The resulting expression will then be analyzed to determine the conditions under which the minimum effective noise temperature is obtainable.

Fig. 1 is a small-signal equivalent circuit of the assumed amplifier-circulator combination. It is similar to that proposed by Rowe[1] and includes conductance components G_1 and G_2 in the admittances (Y_1 and Y_2) of the signal and idler tuning circuits, respectively, and an ideal transformer preceding the network representing the nonlinear capacitance. The ideal transformer permits the choice of any effective generator conductance, $G_G = G_0/n^2$, despite the fixed characteristic conductance (G_0) of the ideal circulator.

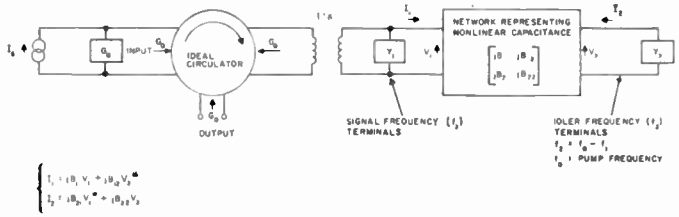

Fig. 1—Small-signal circuit of one-port parametric amplifier operated with an ideal circulator.

The available power gain from the input to the output port of the circulator is merely the square of the reflection coefficient at the terminals of the ideal transformer and will be required in the subsequent noise temperature derivation. From Fig. 1, and adapting (18) of footnote 1, this reflection coefficient is

$$\Gamma = \frac{G_G - (Y_1 + Y_{1in})}{G_G + (Y_1 + Y_{1in})} = \frac{G_G - Y_1 - \left[jB_{11} - \dfrac{B_{12}B_{21}}{Y_2^* - jB_{22}}\right]}{G_G + Y_1 + \left[jB_{11} - \dfrac{B_{12}B_{21}}{Y_2^* - jB_{22}}\right]}, \quad (1)$$

where

$$Y_1 = G_1 + jB_1$$
$$Y_2 = G_2 + jB_2,$$
$$G_G = G_0/n^2,$$

and

$$Y_{1in} = I_1/V_1.$$

(In contrast to footnote 1, B_{21} and B_{22} are positive, since the idler current rather than its conjugate is used here.)

[1] H. E. Rowe, "Some general properties of nonlinear elements." "II. Small signal theory," PROC. IRE, vol. 46, pp. 850–860; May, 1958.

Considering midband conditions only ($B_{11}+B_1=B_{22}+B_2=0$), the midband value of Y_1+Y_{1in} is

$$[Y_1 + Y_{1in}]_0 = (G_G + G_1)(1 - a) - G_G, \quad (2)$$

and the midband available power gain is thus

$$K_0 = \Gamma_0^2 = \left[\frac{\dfrac{1+a}{1-a} - \dfrac{G_1}{G_G}}{1 + \dfrac{G_1}{G_G}}\right]^2, \quad (3)$$

where

$$a = \frac{B_{12}B_{21}}{G_2(G_G + G_1)} \quad (4)$$

(same as α of [1]).

Next consider Fig. 2, which is an equivalent circuit

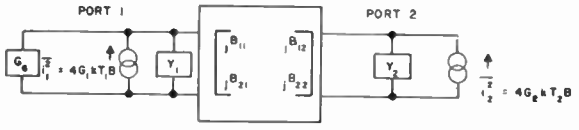

Fig. 2—Equivalent circuit (including noise sources) of one-port parametric amplifier operated with ideal circulator.

of the amplifier-circulator combination including noise sources corresponding to conductances G_1 and G_2 at temperatures T_1 and T_2. It is desired to calculate the available output noise power of the circuit of Fig. 1, exclusive of noise contributed by the generator at the input port of the circulator. Referring to Fig. 2, and because of the presence of the circulator, this is equivalent to calculating the power from noise sources $\overline{i_1^2}$ and $\overline{i_2^2}$ developed in equivalent generator conductance G_G. Thus, the available output noise power, exclusive of the generator contribution, is

$$N_0' = \frac{\overline{i_1^2}G_G}{|G_G + Y_1 + Y_{1in}|^2} + \overline{i_2^2}\left|\frac{V_1}{I_{G2}}\right|^2 G_G, \quad (5)$$

where V_1/I_{G2} is the ratio of voltage developed at port 1 in response to a current generator connected to port 2. Substitution of the terminal conditions, $I_2 = I_{G2} - Y_2V_2$ and $I_1 = -(G_G+Y_1)V_1$, into the network equations of Fig. 1 gives the value of the ratio

$$\frac{V_1}{I_{G2}} = -\frac{jB_{12}}{(G_G + Y_1 + jB_{11})(Y_2^* - jB_{22}) - B_{12}B_{21}}. \quad (6)$$

After again substituting the midband conditions ($B_{11}+B_1=B_{22}+B_2=0$), (5) reduces to

$$\left[\frac{V_1}{I_{G2}}\right]_0 = -\frac{jB_{12}}{G_2(G_G + G_1)(1 - a)}. \quad (7)$$

Effective input noise temperature is defined as

$$T_e = \frac{N_0'}{KkB}, \tag{8}$$

where K = available power gain, k = Boltzmann's constant, and B = bandwidth. Substitution of (5), (2), (7), (3), and the relations for $\overline{i_1^2}$ and $\overline{i_2^2}$ in Fig. 2 into (8) gives the midband effective input noise temperature

$$[T_e]_0 = \left[\frac{2}{1 + a - \frac{G_1}{G_G}(1-a)}\right]^2 \cdot \left[\frac{G_1}{G_G}T_1 + a\frac{f_{10}}{f_{20}}\left(1 + \frac{G_1}{G_G}\right)T_2\right], \tag{9}$$

where the relation $B_{12}/B_{21} = f_{10}/f_{20}$ has been used, with f_{10} and f_{20} being the center values of f_1 and f_2, the signal and idler frequencies respectively. Only the high gain condition ($a \approx 1$) is normally of interest, and thus the midband effective input noise temperature reduces to

$$[T_e]_0 \approx \frac{G_1}{G_G}T_1 + \frac{f_{10}}{f_{20}}\left(1 + \frac{G_1}{G_G}\right)T_2. \tag{10}$$

It is of interest to note that under low gain conditions, (9) predicts that the presence of the ideal circulator degrades the noise temperature of the one-port parametric amplifier by the factor

$$\left[\frac{2}{1 + a - \frac{G_1}{G_G}(1-a)}\right]^2,$$

since it can be shown that T_e for the amplifier without a circulator is just

$$\left[\frac{G_1}{G_G}T_1 + a\frac{f_{10}}{f_{20}}\left(1 + \frac{G_1}{G_G}\right)T_2\right].$$

III. Minimum Effective Noise Temperature

It is evident that to obtain minimum effective noise temperature, the incidental losses associated with the signal and idler resonant circuits, as well as the losses associated with the diode linear parasitic reactances, should be negligible. It is not evident whether the presence of an intentionally controlled idler load that is refrigerated will or will not degrade the minimum achievable noise temperature. In the following analysis it is therefore assumed that conductance G_1 in the signal circuit is due only to the loss associated with the nonlinear diode capacitance, and that conductance G_2 in the idler circuit is due to both the loss in the nonlinear diode capacitance and that of an intentionally added load conductance.

If the nonlinear capacitance has moderately high Q ($Q = 1/2\pi f C_0 R_s$, where C_0 is the average pumped capacitance defined in [1], and the only losses are in the form of series resistance R_s) at both f_1 and f_2, the non-ideal nonlinear capacitor can be approximated by an ideal capacitor of the same capacitance shunted by loss conductances G_{D1} and G_{D2} at center signal and idler frequencies f_{10} and f_{20}

$$G_{D1} \approx 4\pi^2 f_{10}^2 C_0^2 R_s = \frac{2\pi f_{10}^2 C_0}{f_c}, \tag{11a}$$

$$G_{D2} \approx 4\pi^2 f_{20}^2 C_0^2 R_s = \frac{2\pi f_{20}^2 C_0}{f_c}, \tag{11b}$$

where the cutoff frequency is $f_c = 1/2\pi C_0 R_s$.[2]

The other loss conductance to be considered is the deliberate loading of G_i having a temperature T_i at the idler frequency. The quantities G_1, G_2, T_1, and T_2 in (10) can now be identified as

$$G_1 = G_{D1}, \tag{12a}$$

$$G_2 = G_{D2} + G_i, \tag{12b}$$

$$T_1 = T_D, \tag{12c}$$

$$T_2 = \frac{G_{D2}T_D + G_iT_i}{G_{D2} + G_i}, \tag{12d}$$

where T_D is the temperature of the nonlinear capacitor (diode). Substitution of (12) and (11) into (10) then gives

$$\frac{[T_e]_0}{T_D} \approx \left[\frac{x}{x-1}\right]\left[1 + \frac{1}{y}\left(t + \frac{1-t}{z}\right)\right] - 1, \tag{13a}$$

subject to the high gain condition

$$a = rxyz \approx 1, \tag{13b}$$

where

$$x = 1 + \frac{G_G}{G_{D1}}, \tag{13c}$$

$$y = \frac{f_{20}}{f_{10}}, \tag{13d}$$

$$z = 1 + \frac{G_i}{G_{D2}}, \tag{13e}$$

$$r = \left(\frac{f_{10}}{f_c}\right)^2\left(\frac{C_0}{C_1}\right)^2 \tag{13f}$$

$$t = \frac{T_i}{T_D}. \tag{13g}$$

(*Note:* (4) and the values of $B_{12} = 2\pi f_1 C_1$ and $B_{21} = 2\pi f_2 C_1$ from footnote 1 have been used in (13b).)

The merits of additional idler loading ($z > 1$) can be investigated by eliminating y from (13a) and (13b).

[2] Just how high a value of Q is required to make this a good approximation is not known. A more exact analysis of the effect of series resistance would have to consider signal voltages at frequencies other than f_1 and f_2, and thus could not be based on [1].

There results

$$\frac{[T_e]_0}{T_D} \approx \left[\frac{x}{x-1}\right][1 + rx + rxt(z-1)] - 1. \quad (14)$$

Examination of (14) shows that the effect of additional idler loading is to increase the effective input noise temperature through the presence of the term $(rxt)(z-1)$. This term will be absent only if there is no extra idler loading ($z=1$), or if the temperature of the additional idler loading equals 0°K ($t=0$). Thus, additional refrigerated idler loading can never improve the optimum noise performance and, in general, will degrade noise performance. Qualitatively this happens because additional idler loading necessitates a less favorable impedance transformation at the signal frequency to maintain a high gain condition. In the remainder of this section, therefore, no additional idler loading or $z=1$ will be assumed.

Optimum values of x and y can now be derived. Substituting $z=1$ into (14), differentiating, and equating to zero, gives the condition for optimum generator conductance,

$$x_{opt} = 1 + \sqrt{1 + \frac{1}{r}}. \quad (15a)$$

From (13b) (with $z=1$) the corresponding optimum value of y is

$$y_{opt} = \sqrt{1 + \frac{1}{r}} - 1. \quad (15b)$$

An alternative form of (15b) is

$$\left[\frac{f_0}{f_{10}}\right]_{opt} = \sqrt{1 + \frac{1}{r}}, \quad (15c)$$

where $f_0 = f_{10} + f_{20}$ is the pump frequency.

Finally, from (14) (with $z=1$) and (15a), the minimum effective input noise temperature is

$$\frac{[T_e]_{0,min}}{T_D} \approx 2r\left[1 + \sqrt{1 + \frac{1}{r}}\right]. \quad (15d)$$

Eqs. (15) can be further simplified if $r \ll 1$. There results [using (13f)],

$$x_{opt} \approx 1 + \left(\frac{f_c}{f_{10}}\right)\left(\frac{C_1}{C_0}\right), \quad (16a)$$

$$y_{opt} \approx \left(\frac{f_c}{f_{10}}\right)\left(\frac{C_1}{C_0}\right) - 1, \quad (16b)$$

$$[f_0]_{opt} \approx f_c\left(\frac{C_1}{C_0}\right), \quad (16c)$$

$$\frac{[T_e]_{0,min}}{T_D} \approx 2\left(\frac{f_{10}}{f_c}\right)\left(\frac{C_0}{C_1}\right)\left[1 + \left(\frac{f_{10}}{f_c}\right)\left(\frac{C_0}{C_1}\right)\right]. \quad (16d)$$

Eqs. (15) and (16) suggest the importance of a figure of merit, $f_c(C_1/C_0)$, that determines the optimum noise performance at a given signal frequency. Eq. (16c) is also of interest, because it predicts a constant optimum pump frequency (equal to the figure of merit) for any signal frequency. Eqs. (15c) and (15d) are plotted versus $(r)^{1/2}$ as the solid curves in Figs. 3 and 4 (opposite).

IV. Maximum Gain-Bandwidth Product

We next consider the conditions under which maximum gain-bandwidth product can be achieved with the amplifier-circulator combination. The following analysis assumes that, 1) singly resonant networks are used in the signal and idler circuits, 2) the nonlinear capacitance diode has a series resistance and a parasitic lead inductance (in general a function of the diode mount), 3) the diode parasitic shunt capacitance has a negligible effect on the external circuits (since it can usually be made very small by proper mounting, for example by using coaxial structures), 4) incidental circuit losses are negligible, and 5) a controllable conductance can be added in the idler circuit (if needed) to broaden the bandwidth. The use of multiply resonant networks in the signal and idler circuits will, of course, yield larger bandwidths than those obtainable with singly resonant networks, but for the sake of simplicity they are not considered.[3,4] The analysis presented here is, however, applicable to the use of more complex resonant structures.

The voltage gain-fractional bandwidth[5] product for the amplifier-circulator combination, based on an expression previously derived [(20a) of footnote 6], can be written as

$$[K_0]^{1/2}\cdot\left[\frac{\beta}{f_{10}}\right] \approx \left[\frac{1 - \dfrac{G_1}{G_G}}{1 + \dfrac{G_1}{G_G}} + a\right]\left[\frac{1}{f_{10}\left(\dfrac{1}{\beta_1} + \dfrac{1}{\beta_2}\right)}\right], \quad (17a)$$

where β, β_1, and β_2 are, respectively, the bandwidths of the overall amplifier, the signal circuit, and the idler circuit.

Again, the high gain condition ($a \approx 1$) is usually the only one of interest, and (17a) reduces to

$$[K_0]^{1/2}\cdot\left[\frac{\beta}{f_{10}}\right] \approx \left[\frac{2}{1 + \dfrac{G_1}{G_G}}\right]\left[\frac{1}{f_{10}\left(\dfrac{1}{\beta_1} + \dfrac{1}{\beta_2}\right)}\right]. \quad (17b)$$

[3] H. Seidel and G. F. Herrmann, "Circuit aspects of parametric amplifiers," 1959 IRE WESCON Convention Record, pt. 2, pp. 83–90.

[4] E. W. Sard, "Tunnel (Esaki) diode amplifiers with unusually large bandwidths," Proc. IRE, vol. 48, pp. 357–358; March, 1960.

[5] Fractional bandwidth is the amplification bandwidth divided by the signal frequency.

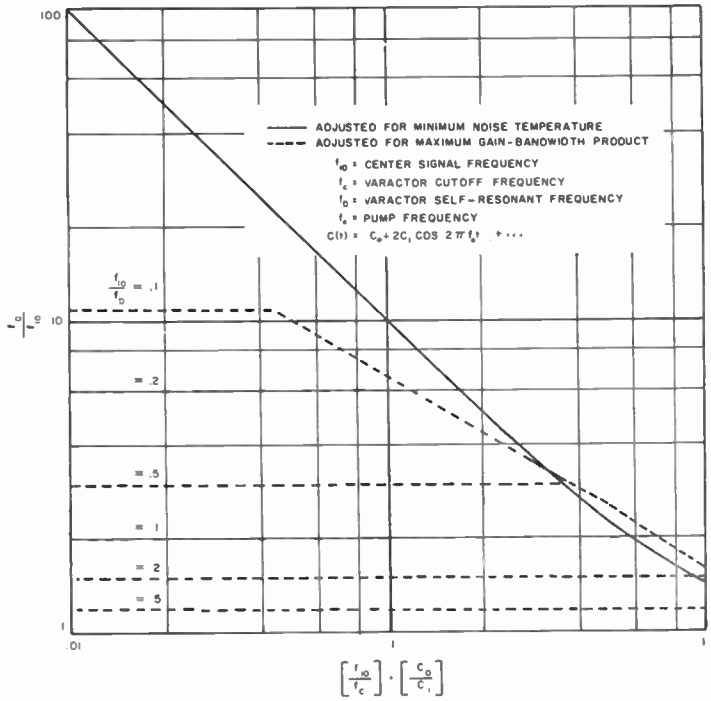

Fig. 3—Range of pump frequency for one-port parametric amplifier with ideal circulator.

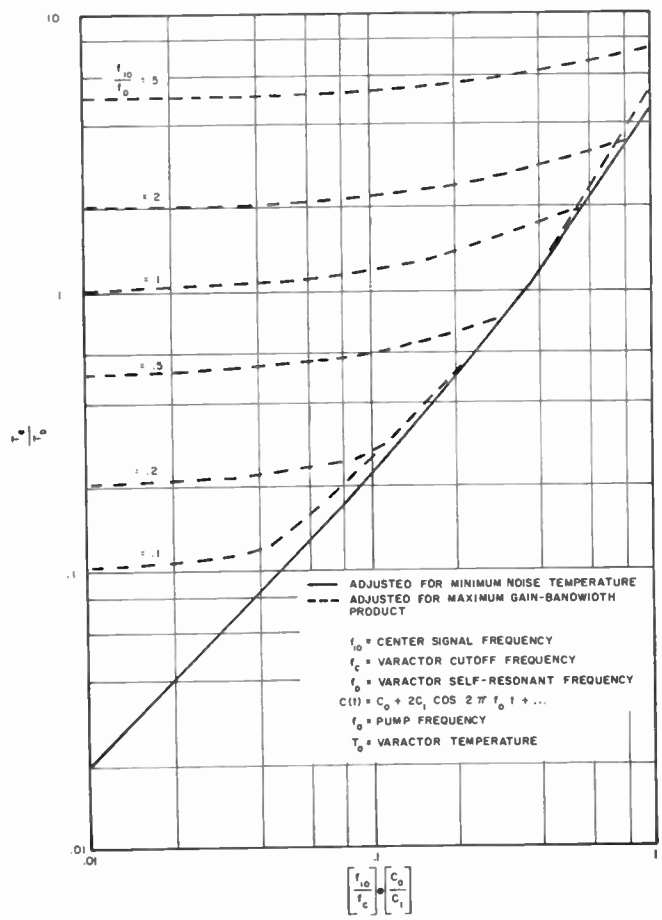

Fig. 4—Range of effective input noise temperatures for one-port parametric amplifier with ideal circulator.

Next, expressions that consider four possibilities are required for β_1 and β_2. These are case 1a), $f_{10} \leq f_D$ and $f_{20} \leq f_D$; case 1b), $f_{10} \leq f_D$ and $f_{20} \geq f_D$; case 2a), $f_{10} \geq f_D$ and $f_{20} \leq f_D$; and case 2b), $f_{10} \geq f_D$ and $f_{20} \geq f_D$, where f_D is the self-resonant frequency of a nonlinear capacitor having series inductance, as given in the article by Lombardo and Sard.[6] By extension of (29) and (37) of footnote 6, the values of β_1 and β_2 to be used are

$$\beta_1 \approx \frac{G_G + G_1}{2\pi C_0}, \qquad f_{10} \leq f_D, \tag{18a}$$

$$\beta_1 \approx \left[\frac{G_G + G_1}{2\pi C_0}\right]\left[\frac{f_D}{f_{10}}\right]^2, \qquad f_{10} \geq f_D, \tag{18b}$$

$$\beta_2 \approx \frac{G_2}{2\pi C_0}, \qquad f_{20} \leq f_D, \tag{18c}$$

$$\beta_2 \approx \left[\frac{G_2}{2\pi C_0}\right]\left[\frac{f_D}{f_{20}}\right]^2, \qquad f_{20} \geq f_D, \tag{18d}$$

where conductances G_G, G_1, and G_2 are effective values as transformed to the terminals of the ideal nonlinear capacitance in Fig. 1.

Eqs. (11a), (11b), (12a), and (12b) still apply, and thus (18) reduce to

$$\beta_1 \approx x\frac{f_{10}^2}{f_c}, \qquad f_{10} \leq f_D, \tag{19a}$$

$$\beta_1 \approx x\frac{f_D^2}{f_c}, \qquad f_{10} \geq f_D, \tag{19b}$$

$$\beta_2 \approx z\frac{f_{20}^2}{f_c}, \qquad f_{20} \leq f_D, \tag{19c}$$

$$\beta_2 \approx z\frac{f_D^2}{f_c}, \qquad f_{20} \geq f_D, \tag{19d}$$

where x and z are defined by (13c) and (13e). From (17b), (19), (12a), (13b), and (13c), the gain-bandwidth products for the four cases are

$$\text{Case 1a, } [K_0]^{1/2} \cdot \left[\frac{\beta}{f_{10}}\right] \approx \left[\frac{2f_{10}}{f_c}\right]\left[\frac{x-1}{1+\dfrac{rx^2}{y}}\right], \tag{20a}$$

$$\text{Case 1b, } [K_0]^{1/2} \cdot \left[\frac{\beta}{f_{10}}\right] \approx \left[\frac{2f_{10}}{f_c}\right]\left[\frac{x-1}{1+\left(\dfrac{f_{10}}{f_D}\right)^2 rx^2 y}\right], \tag{20b}$$

[6] P. P. Lombardo and E. W. Sard, "Low-noise microwave reactance amplifiers with large gain-bandwidth products," 1959 IRE WESCON Convention Record, pt. 1, pp. 83–98.

Case 2a, $[K_0]^{1/2}\cdot\left[\frac{\beta}{f_{10}}\right]$

$$\approx\left[\frac{2f_{10}}{f_c}\right]\left[\frac{f_D}{f_{10}}\right]^2\left[\frac{x-1}{1+\left(\frac{f_D}{f_{10}}\right)^2\frac{rx^2}{y}}\right], \quad (20c)$$

Case 2b, $[K_0]^{1/2}\cdot\left[\frac{\beta}{f_{10}}\right]$

$$\approx\left[\frac{2f_{10}}{f_c}\right]\left[\frac{f_D}{f_{10}}\right]^2\left[\frac{x-1}{1+rx^2y}\right]. \quad (20d)$$

Optimum values of x, y, and z can now be derived, keeping in mind the transitions from one case to another.

First, consider $f_{10}\leq f_D$, cases 1a) and 1b). For a particular value of $f_{10}/f_D\leq 1$, assume that the conditions for maximum gain-bandwidth product are such that $f_{20}\leq f_D$, subject to later verification. This is case 1a), and (20a) applies. Examination of (20a) shows that it is maximized for a given value of y when x is given by

$$x_{opt}=1+\sqrt{1+\frac{y}{r}}. \quad (21a)$$

The corresponding optimum value of z is

$$z_{opt}=\frac{1}{rx_{opt}y}=\frac{\sqrt{1+\frac{y}{r}}-1}{y^2}. \quad (21b)$$

Furthermore, the corresponding maximum value of gain-bandwidth product is

$$\left([K_0]^{1/2}\cdot\left[\frac{\beta}{f_{10}}\right]\right)_{max}\approx\left[\frac{f_{10}}{f_c}\right]\left[\sqrt{1+\frac{y}{r}}-1\right]. \quad (21c)$$

From (21c), it is seen that the largest possible value of y should be used. The largest possible value of y is determined either from the assumption that this is case 1a) (then $y_{opt}=f_D/f_{10}$) or by (21b), calling for a value of $z_{opt}<1$. Investigating (21b) further, $z_{opt}\geq 1$ requires

$$r\leq\frac{1}{y^3+2y}. \quad (22)$$

As the nonlinear capacitance becomes more and more ideal with respect to losses, $r\to 0$, and inequality (22) will ultimately be satisfied for the maximum value of y in case 1a), or $y_{opt}=f_D/f_{10}$. Thus for $r\leq r_1$, (21) for case 1a) reduce to

$$x_{opt}=1+\sqrt{1+\frac{1}{r\left(\frac{f_{10}}{f_D}\right)}}, \quad (23a)$$

$$y_{opt}=\frac{1}{\left(\frac{f_{10}}{f_D}\right)}, \quad (23b)$$

$$z_{opt}=\left[\frac{f_{10}}{f_D}\right]^2\left[\sqrt{1+\frac{1}{r\left(\frac{f_{10}}{f_D}\right)}}-1\right] \quad (23c)$$

$$\left([K_0]^{1/2}\cdot\left[\frac{\beta}{f_{10}}\right]\right)_{max}\approx\left[\frac{f_{10}}{f_c}\right]\left[\sqrt{1+\frac{1}{r\left(\frac{f_{10}}{f_D}\right)}}-1\right], \quad (23d)$$

where

$$r_1=\frac{\left(\frac{f_{10}}{f_D}\right)^3}{1+2\left(\frac{f_{10}}{f_D}\right)^2}. \quad (23e)$$

For $r\geq r_1$, it is seen from the above reasoning that $z_{opt}=1$. To determine the corresponding optimum values of x and y requires going back to (20a) and substituting (13b) with $z=1$. The result is

$$[K_0]^{1/2}\cdot\left[\frac{\beta}{f_{10}}\right]\approx\left[\frac{2f_{10}}{f_c}\right]\left[\frac{x-1}{1+r^2x^3}\right]. \quad (24)$$

Examination of (24) shows that it is maximized for x_{opt} a root of

$$2x_{opt}^3-3x_{opt}^2-\frac{1}{r^2}=0. \quad (25a)$$

The corresponding values of y and z are

$$y_{opt}=\frac{1}{rx_{opt}z_{opt}}=\sqrt{2x_{opt}-3}, \quad (25b)$$

$$z_{opt}=1. \quad (25c)$$

Furthermore, the corresponding maximum value of gain-bandwidth product is

$$\left([K_0]^{1/2}\cdot\left[\frac{\beta}{f_{10}}\right]\right)_{max}\approx\left[\frac{f_{10}}{f_c}\right]\left[\frac{2(2x_{opt}-3)}{3}\right]. \quad (25d)$$

Recalling that this is assumed to be case 1a), it still must be true that $y_{opt}\leq f_D/f_{10}$. Then, from (25a) and (25b), there results

$$r\geq r_2=\frac{2\left(\frac{f_{10}}{f_D}\right)^3}{1+3\left(\frac{f_{10}}{f_D}\right)^2}. \quad (25e)$$

Eqs. (25e) and (23e) are used to plot $(r_1)^{1/2}$ and $(r_2)^{1/2}$ vs f_{10}/f_D in Fig. 5, and it is seen that for $f_{10}/f_D \leq 1$, $r_2 > r_1$. Thus, still assuming case 1a), optimum conditions for $r \leq r_1$ are given by (23a) through (23d), whereas optimum conditions for $r \geq r_2$ are given by (25a) through (25d). The optimum conditions for the small region in between, $r_1 \leq r \leq r_2$, must then be

$$x_{\text{opt}} = \frac{1}{r y_{\text{opt}} z_{\text{opt}}} = \frac{1}{r}\left(\frac{f_{10}}{f_D}\right), \tag{26a}$$

$$y_{\text{opt}} = \frac{1}{\left(\frac{f_{10}}{f_D}\right)}, \tag{26b}$$

$$z_{\text{opt}} = 1, \tag{26c}$$

$$\left([K_0]^{1/2}\cdot\left[\frac{\beta}{f_{10}}\right]\right)_{\max} \approx \left[\frac{2f_{10}}{f_c}\right]\left[\frac{\frac{1}{r}\left(\frac{f_{10}}{f_D}\right) - 1}{1 + \frac{1}{r}\left(\frac{f_{10}}{f_D}\right)^3}\right]. \tag{26d}$$

All that remains is to show that the assumption of case 1b) gives no larger gain-bandwidth products than does the previous assumption of case 1a). Therefore, assume now that for a particular value of $f_{10}/f_D \leq 1$, the conditions for maximum gain-bandwidth product are such that $f_{20} \geq f_D$. This is case 1b), and (20b) applies. Reasoning similar to the foregoing then gives the same results as previously for $r \leq r_1$ and for $r_1 \leq r \leq r_2$. Furthermore, for $r > r_2$, case 1b) no longer is possible, and the previous results also hold. This completes the case of $f_{10} \leq f_D$.

In a similar manner, if $f_{10} \geq f_D$, cases 2a) and 2b), there result the following conditions for maximum gain-bandwidth product. If $r \leq r_3$,

$$x_{\text{opt}} = 1 + \sqrt{1 + \frac{1}{r}\left(\frac{f_{10}}{f_D}\right)}, \tag{27a}$$

$$y_{\text{opt}} = \frac{1}{\left(\frac{f_{10}}{f_D}\right)}, \tag{27b}$$

$$z_{\text{opt}} = \sqrt{1 + \frac{1}{r}\left(\frac{f_{10}}{f_D}\right)} - 1, \tag{27c}$$

$$\left([K_0]^{1/2}\cdot\left[\frac{\beta}{f_{10}}\right]\right)_{\max} \approx \left[\frac{f_{10}}{f_c}\right]\left[\frac{\sqrt{1 + \frac{1}{r}\left(\frac{f_{10}}{f_D}\right)} - 1}{\left(\frac{f_{10}}{f_D}\right)^2}\right], \tag{27d}$$

where

$$r_3 = \frac{1}{3}\left(\frac{f_{10}}{f_D}\right). \tag{27e}$$

If $r \geq r_4$,

$$2x_{\text{opt}}^3 + 3x_{\text{opt}}^2 - \frac{\left(\frac{f_{10}}{f_D}\right)^2}{r^2} = 0, \tag{28a}$$

$$y_{\text{opt}} = \frac{\sqrt{2x_{\text{opt}} - 3}}{\left(\frac{f_{10}}{f_D}\right)}, \tag{28b}$$

$$z_{\text{opt}} = 1, \tag{28c}$$

$$\left([K_0]^{1/2}\cdot\left[\frac{\beta}{f_{10}}\right]\right)_{\max} \approx \left[\frac{f_{10}}{f_c}\right]\left[\frac{2(2x_{\text{opt}} - 3)}{3\left(\frac{f_{10}}{f_D}\right)^2}\right], \tag{28d}$$

where

$$r_4 = \frac{1}{2}\left(\frac{f_{10}}{f_D}\right). \tag{28e}$$

If $r_3 \leq r \leq r_4$,

$$x_{\text{opt}} = \frac{1}{r}\left(\frac{f_{10}}{f_D}\right), \tag{29a}$$

$$y_{\text{opt}} = \frac{1}{\left(\frac{f_{10}}{f_D}\right)}, \tag{29b}$$

$$z_{\text{opt}} = 1, \tag{29c}$$

$$\left([K_0]^{1/2}\cdot\left[\frac{\beta}{f_{10}}\right]\right)_{\max} \approx \left[\frac{2\left(\frac{f_{10}}{f_c}\right)}{\left(\frac{f_{10}}{f_D}\right)^2}\right]\left[\frac{\frac{1}{r}\left(\frac{f_{10}}{f_D}\right) - 1}{\frac{1}{r}\left(\frac{f_{10}}{f_D}\right) + 1}\right]. \tag{29d}$$

The quantities $(r_3)^{1/2}$ and $(r_4)^{1/2}$ are also plotted in Fig. 5 with the quantities $(r_1)^{1/2}$ and $(r_2)^{1/2}$, the dividing line being $f_{10}/f_D = 1$.

The appropriate expressions for maximum gain-bandwidth product [(23d), (25d), (26d), (27d), (28d), or (29d)] are plotted for several values of f_{10}/f_D as dashed lines in Fig. 6. For comparison, solid lines show the (generally lower) gain-bandwidth products under conditions of minimum effective input noise temperature, obtained by substituting (15a) and (15b) into the appropriate expression for gain-bandwidth product, (20a), (20b), (20c), or (20d). Furthermore, for comparison in

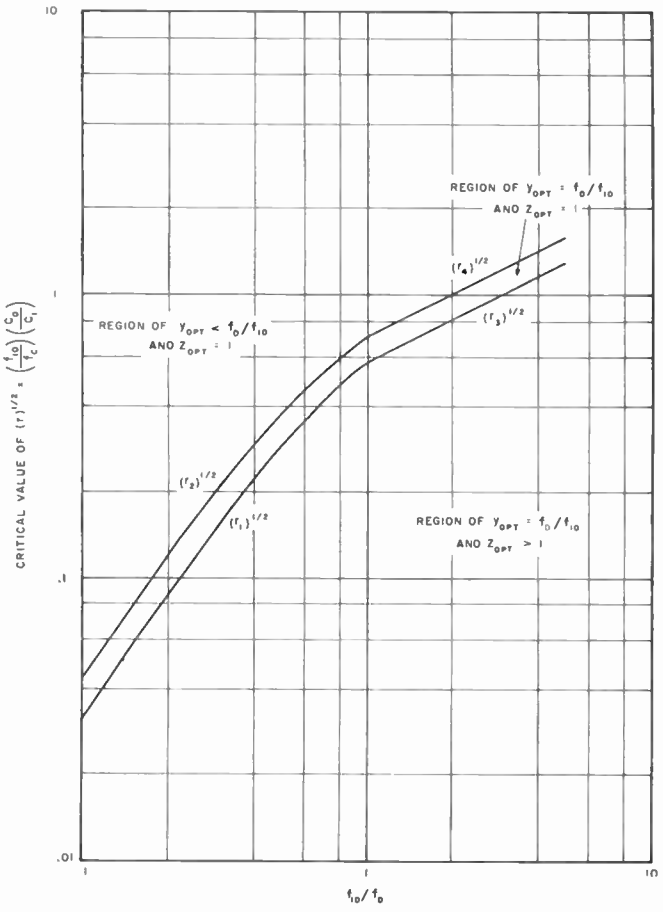

Fig. 5—Transition regions in adjusting for maximum gain-bandwidth product of one-port parametric amplifier with ideal circulator.

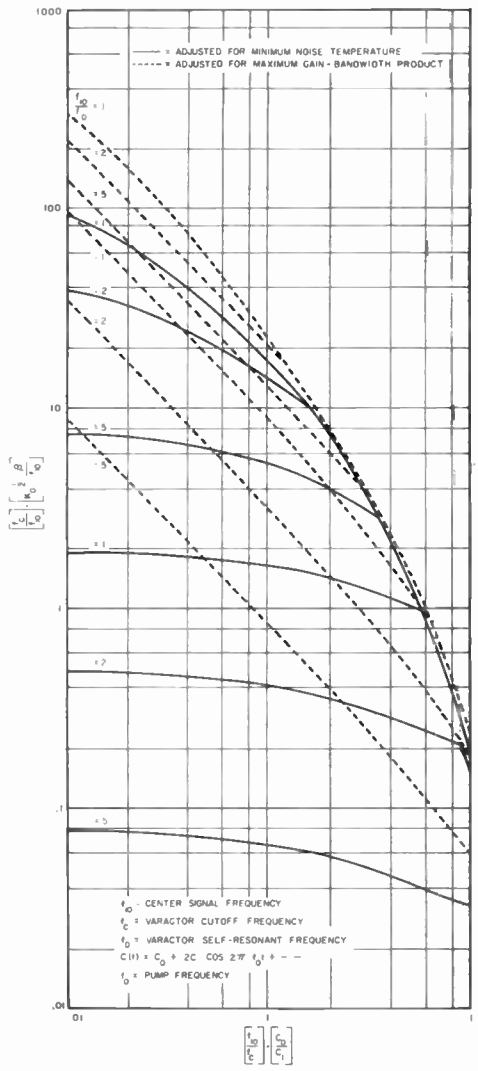

Fig. 6—Range of gain-bandwidth products for one-port parametric amplifier with ideal circulator.

Fig. 4, the (generally higher) values of effective input noise temperature corresponding to the conditions for maximum gain-bandwidth product are plotted as dashed lines by substituting x_{opt} and y_{opt} from the appropriate equations [(23a), (25a), (26a), (27a), (28a), or (29a) and (23b), (25b), (26b), (27b), (28b), or (29b)] and $t=1$ into (13a). Finally, for comparison in Fig. 3, the (generally different) values of $(1+y_{opt})$ corresponding to the conditions for maximum gain-bandwidth product [(23b), (25b), (26b), (27b), (28b), or (29b)] are plotted as dashed lines. Figs. 3, 4 and 6 show that minimum noise temperature and maximum gain-bandwidth product are generally compatible when the diode self-resonant frequency is high compared with the signal frequency.

V. Discussion of Universal Curves

For the best commercially available silicon varactor diodes, the cutoff frequency under operating conditions will typically be 50 kmc, C_1/C_0 will be about 0.16, and the diode self-resonant frequency will be about 5000 mc. Inserting these values into Figs. 4 and 6, the following results are predicted for a one-port amplifier operated at room temperature (290°K):

Signal Frequency (mc)	Minimum Effective Noise Temperature (degrees K)	Approximate Maximum Gain-Bandwidth Product (mc) Compatible with Minimum Effective Noise Temperature
400	30	112
1000	82	260
2800	290	392
5000	650	500

It is interesting to note that this performance is obtained for a relatively constant optimum pump frequency of about 8000 mc (see Fig. 3).

These data show that if the one-port parametric amplifier operated at room temperature is to seriously challenge the maser at microwave frequencies, an improvement of at least 10 in diode figure of merit is required. If such improvements cannot be obtained, the varactor diode (like the maser) will have to be cooled. This implies that the diode must be designed to maintain its figure of merit at reduced temperatures, or still better, that the figure of merit is improved as the temperature is lowered.

Fractional Millimicrosecond Electrical Stroboscope*

W. M. GOODALL†, FELLOW, IRE, AND A. F. DIETRICH†

Summary—**A simple electrical stroboscope having a rise time of 6×10^{-11} seconds and a 6-db bandwidth of 5.5 kmc is described. Oscillograms showing 160-mc square waves and 640 million pulses per second are shown. These waveforms display rise times as fast as 2×10^{-10} seconds. Instrumentation includes a strobe-pulse generator, a coaxial gate using a gallium-arsenide point-contact crystal, suitable wide-band coaxial attenuators, a low-pass integrating filter and a low-frequency oscilloscope.**

Introduction

In high-frequency work an oscilloscope has come to be a commonplace instrument. Nowhere is this more true than for high-speed short-pulse studies. In communication applications the pulse patterns may change in a random or in a regular manner. For study purposes, much can be learned by using an oscilloscope with suitable sweep circuits to observe repetitive pulse patterns. Improvements in short-pulse techniques go hand in hand with improved oscilloscopes.

For high-speed pulses the two most important oscilloscope characteristics are the rise time and the sensitivity. In conventional oscilloscopes, where broad-band electrical amplifiers are used, fast rise time is obtained at the expense of reduced amplifier gain and, conversely, high sensitivity is obtained at the expense of fast rise time.

The traveling-wave-deflection oscilloscope[1] improves the sensitivity of the oscilloscope tube. With optical or electron-optical magnification, conventional electrical amplifiers can be avoided. The resulting device, while very useful, still has a relatively poor sensitivity.

For repetitive patterns another technique can be used in which fast rise time and high sensitivity are not mutually exclusive, as they are for conventional amplifiers. In an electrical stroboscope or sampling oscilloscope the rise time depends primarily upon the bandwidth of the sampling circuits and the effective duration of the strobe pulse, while the sensitivity depends upon the gain of the electrical amplifier used in the low-frequency part of the oscilloscope. The penalty paid for these advantages is the time required for integration.

Electrical Stroboscope

A stroboscope for light consists of a suitable light source which emits short pulses of light. When these pulses occur at a regular rate, the stroboscope produces the optical effect of slowing down or stopping the motion of the recurrent phenomena. An electrical stroboscope can be made which does the same thing for recurrent electrical waves. In a simple form it consists of a gate, a strobe-pulse generator, a low-pass integrating filter, and a low-frequency oscilloscope. When the repetition rates of the signal and the strobe pulse are the same, the stroboscope continues to observe the same part of the signal. When the repetition rate of the strobe pulse is less than that of the signal by a constant amount, the signal interval is scanned repetitively and the output of the gate reproduces the signal on a slowed-down basis. If the difference between the recurrence frequencies of the signal and pulse is δ cps, the recurrence frequency of the gate output will be δ cps.

This paper describes a simple electrical stroboscope which has a 10 to 90 per cent rise time of 6×10^{-11} seconds, and an over-all sensitivity of 2 mv/cm. It is being used in studies of binary pulses in the range of 1000 megabits. As will be seen, the simple instrumentation described above is especially suitable for work with synchronous communication pulses.

Early electrical stroboscopes, or sampling oscilloscopes, used synchronous or quasi-synchronous operation.[2,3] Recently more sophisticated devices[4,5] have been made which can display pulse shapes for similar pulses that repeat in a nonsynchronous as well as a synchronous manner. As this paper is being written, commercial versions of these latter oscilloscopes have been announced by several companies.

A block diagram of a simple electrical stroboscope is shown in Fig. 1. The gate blocks the input signal except when it is opened by the strobe pulse. When the strobe-pulse frequency is identical with the recurrence frequency of the signal, the output of the filter will be a constant dc representing the amplitude of the signal at the time the gate is opened. Suppose we had a variable delay in the line between the gate and the strobe pulse generator. If we changed this delay in small steps, and observed the output for each step, we could trace the waveform of the recurrent signal. Our instrumentation is similar to this. However, instead of changing the delay we use a strobe frequency that is lower than the recurrent frequency of the signal by a small constant amount, δ. After one cycle of the δ frequency, we have scanned one interval of the complete high-frequency signal wave. Thus, we have slowed down the wave in the ratio of δ/f where f is the recurrent frequency of the signal wave.

* Received by the IRE, January 16, 1960; revised manuscript received, April 15, 1960.

† Bell Telephone Labs., Inc., Holmdel, N. J.

[1] J. R. Pierce, "Traveling wave oscilloscope," *Electronics*, vol. 22, pp. 97–99; November, 1949.

[2] J. M. L. Jansen, "An experimental 'stroboscopic' oscilloscope for frequencies up to about 50 mc/s—I. Fundamentals," *Philips Tech. Rev.*, vol. 12, pp. 52–57; August, 1950.

[3] J. G. McQueen, "The monitoring of high speed waveforms," *Electronic Engrg.*, vol. 24, pp. 436–441; October, 1952.

[4] R. Sugarman, "Sampling oscilloscope for statistically varying pulses," *Rev. Sci. Instr.*, vol. 28, p. 933; November, 1957.

[5] G. B. B. Chaplin, "Avalanche Circuits with Application to a Sensitive Transistor Oscilloscope," presented at Transistor and Solid-State Conference, Philadelphia, Pa.; February, 1958.

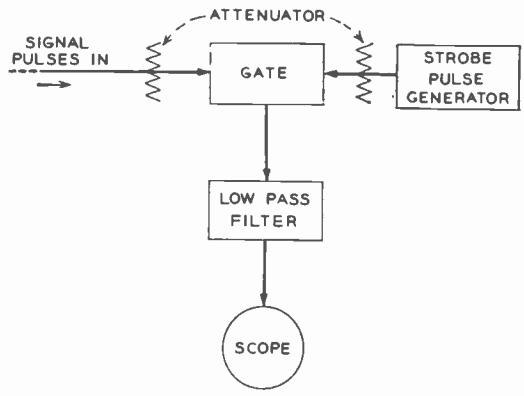

Fig. 1—Electrical stroboscope—block diagram.

As in other time-division systems, the sampling theorem applies and the theoretical cutoff frequency for the low-pass filter would be $f/2$ where f is the signal recurrence frequency. The value $f/2$ is an upper bound. If the high-frequency signal requires a band of nf where n is the number of harmonics of the recurrence frequency, f, then

$$n\delta < f/2,$$

which insures that the number of harmonics required to represent the slowed down signal will be transmitted by the low-pass filter.

Fractional Millimicrosecond Stroboscope

In working with ultra-wide-band components and systems we have frequently found that the best results are obtained by simplifying the experimental gear and by reducing the size and number of components to a bare minimum. Not only does this improve the operation of broad-band systems, but it also tends to improve reliability since, in general, fewer components give less trouble. For these reasons we have chosen the simple instrumentation represented by the block diagram of Fig. 1 for our electrical stroboscope.

In our experimental work on a 640-megabit microwave regenerative repeater we have need for an oscilloscope that will adequately display timing pulses having durations in the order of 3×10^{-10} seconds. We know that the signal pulses will repeat at a regular rate, and that our pulse groups will be repeated at a 10-mc rate, determined by a quartz-crystal oscillator. To simplify our stroboscope, we have taken advantage of this and have generated our strobe pulse from a second quartz-crystal oscillator. The difference frequency, δ, remains sufficiently constant for our purposes and no control or lock between our signal and strobe frequency is required.

Although it is not critical, we have chosen the δ frequency to be 100 cycles when f is 10 mc. In Fig. 1 the low-frequency oscilloscope shown is one with a 300-kc band. Because this oscilloscope has negligible transmission at 10 mc, only a nominal low-pass filter is required. The two critical broad-band elements are the strobe-pulse generator and the gate.

Strobe-Pulse Generator[6]

The technique of clipping high-amplitude sine waves has provided a means of generating short timing pulses at rates of 160, 320, and 640 million pulses per second, for use in our microwave regenerative repeater studies. In our arrangement a 10-mc control frequency is harmonically multiplied to 160 mc. A high-amplitude 160-mc sine wave is applied to the grid of a 6AK5 tube with a broad-band output circuit. By applying proper negative bias on the grid, conduction takes place for only a small part of the 160-mc sine wave. A short pulse with half amplitude duration of less than 10^{-9} seconds is produced in the plate circuit output.

In the present strobe application, the crystal-controlled 10-mc strobe frequency is multiplied in a series of harmonic generators to 320 mc. A sine wave of this frequency is applied to the grid of a special ceramic tetrode.[7] A short negative pulse having a half-amplitude duration of 3×10^{-9} seconds and a 10-mc repetition frequency is simultaneously applied to the cathode of the same tetrode. This pulse repetition frequency is determined by the crystal-controlled, strobe-frequency oscillator. Delays are adjusted so that each 10-mc pulse occurs in coincidence with the positive maximum of one of the sine wave cycles. With proper negative bias on the grid of the tetrode it acts as an AND gate, because it conducts plate current only when the pulse and a positive maximum occur simultaneously. In this way only one out of every 32 sine wave cycles produces an output. Conduction takes place during only a small part of a cycle. The final result, at the plate of the tube, is a train of pulses occurring at a 10-mc rate and having a half-amplitude duration of less than 3×10^{-10} seconds.

Short pulses of this same duration have also been obtained from another pulse-generator circuit, in which a WE 416B planar triode has been used as the output clipper. In this generator the triode is used in a grounded-grid circuit and both the 320-mc sine wave, a short 10-mc pulse, and dc bias are applied to the cathode.

Gate

A cross section of the gate is shown in Fig. 2 and a block schematic of a gate test circuit is shown in Fig. 3. The gate uses a special gallium-arsenide point-contact rectifier,[8] which is mounted between the inner and outer conductors of a 50-ohm coaxial line. A small by-pass capacitor C between the ground side of the crystal and the outer conductor presents a low impedance to the strobe and signal-frequency harmonics and a high impedance to the gate output. This capacitor and the shunt resistance in the gate output form a simple low-pass integrating filter.

[6] An alternate method of generating strobe pulses is given in A. F. Dietrich and W. M. Goodall, "Solid state generator for 2×10^{-10} second pulses," PROC. IRE, vol. 48, pp. 791–792; April, 1960.

[7] This experimental tube, A1983, designed by L. H. Von Ohlsen, has been supplied to the authors by R. E. Caffrey, both of the Bell Telephone Laboratories.

[8] W. M. Sharpless, "High-frequency gallium arsenide point-contract rectifiers," *Bell Sys. Tech. J.*, vol. 38, pp. 259–270; January, 1959.

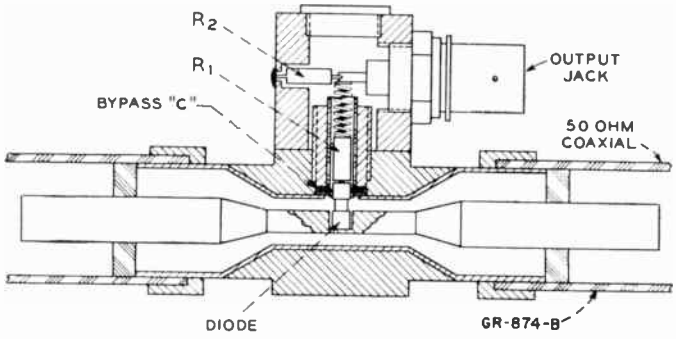

Fig. 2—Cross section of gate assembly.

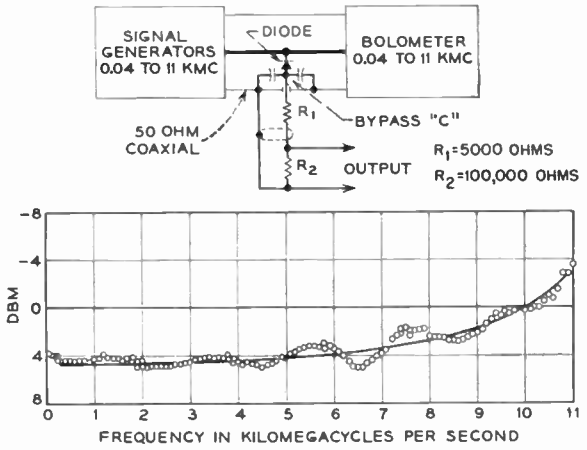

Fig. 3—Block schematic of gate test circuit and curve of CW power required for constant output vs frequency.

In our stroboscope the gate functions as a peak detector and the output of the gate, after the low-pass filter, is the envelope of the product of the strobe and signal pulses. The gate was tested as shown in Fig. 3. The points show the signal power in dbm as a function of frequency, as measured by the bolometer, required to produce a constant dc voltage in the output. This dc voltage was measured by means of a high sensitivity dc voltmeter. Good agreement was obtained between the bolometer and signal generator power readings, which showed that little power was required by the detector crystal.

It is believed that the smooth curve would represent the response of the gate as a peak voltmeter, except for standing waves produced by the terminating load circuit. The rising characteristic is believed to be due to series resonance of the diode capacity and the inductance of the leads including the "cat whisker."

It should be noted that the curve on Fig. 3 gives the frequency response of the gate to CW test signals and does not represent the over-all response of the electrical stroboscope.

Over-All Response

The over-all response of the electrical stroboscope (Fig. 1) can be given in terms of its impulse response, or in terms of its frequency response. When the gate, attenuators, and other coaxial circuits are sufficiently broad-band, the impulse response of the electrical stroboscope is given by the duration of the effective strobe pulse. The frequency response of the stroboscope to CW test signals is similar to that of a comb filter, with a series of responses centered about harmonics of the base strobe frequency; 10 mc in the present example. For the case where the broad-band circuits are not limiting the performance, the frequency response of the stroboscope would be given by the frequency transform of the time function. The time function is specified by the shape, *i.e.*, the duration and amplitude, of the effective strobe pulses.

The measured frequency response taken with respect to multiples of 25 harmonics of 10 mc, *i.e.*, taken every 250 mc, is given by the points shown on Fig. 4. These data were obtained with a gallium arsenide point-contact crystal[8] in a gate of the type shown in Fig. 2, using a solid-state strobe-pulse generator.[6] For later reference the strobe pulse amplitude of the crystal was approximately as shown in Fig. 5(b), with a base duration, T_2, of 6×10^{-10} seconds.

The solid curve of Fig. 4 is a theoretical curve which gives the envelope of the harmonics of the 10-mc strobe frequency for cosine-squared pulses. The curve shown on Fig. 4 is 6 db down at 5.5 kmc, which gives a good fit for the data for frequencies up to 7 kmc and a satisfactory fit over the whole frequency spectrum up to 10 kmc.

It should be noted that impulse response corresponding to the curve on Fig. 4, 1.8×10^{-10} seconds, is appreciably shorter than the duration of the pulse from the strobe generator, 6×10^{-10} seconds. An explanation of this apparent discrepancy is given by the curves on Fig. 5.

Because of the wide-band performance of the gallium-arsenide crystal in the gate circuit, additional clipping of the strobe pulse occurs in the gate and the effective strobe pulse is even shorter than that provided by the strobe-pulse generator.

The curves on Fig. 5 indicate in a general way how this clipping action occurs. Fig. 5(a) gives the dc voltage-current characteristic for a typical diode.[9] Fig. 5(b) shows the voltage waveform of a strobe pulse applied to the diode. Fig. 5(c) gives the resulting current waveform. The average value of this current pulse for a 10-mc repetition rate is approximately 6.0×10^{-6} amperes, which is the value of current required to develop 0.6 volt in a 100,000-ohm resistor. Note that the base duration of the current pulse T_1 is about 0.3 of T_2, the base duration of the voltage pulse. The 0.3 factor also applies to the half-amplitude durations of these pulses. These curves assume no frequency limitation in the operation of the diode. It is possible that with voltage pulses having a half-amplitude duration as short as 3×10^{-10} seconds, some frequency limitation is present. However, experimental results show that appreciable clipping action must be realized in order to obtain the observed resolution of the oscilloscope.

[9] See Fig. 1, curve B of Sharpless, *ibid.*

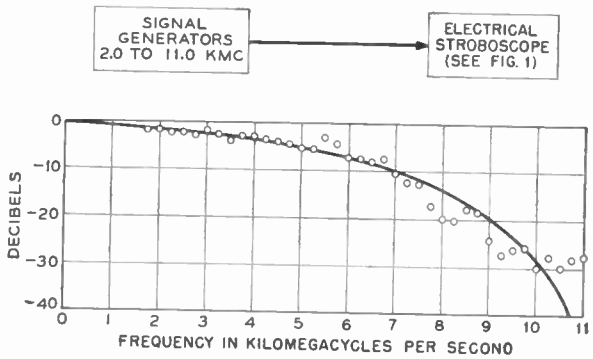

Fig. 4—Over-all frequency response.
Circles: measured data.
Curve: frequency transform for 1.8×10^{-10} seconds base duration cosine-squared pulse. 6 db down at 5.5 kmc.
Conclusion: Impulse response of stroboscope 1.8×10^{-10} seconds.

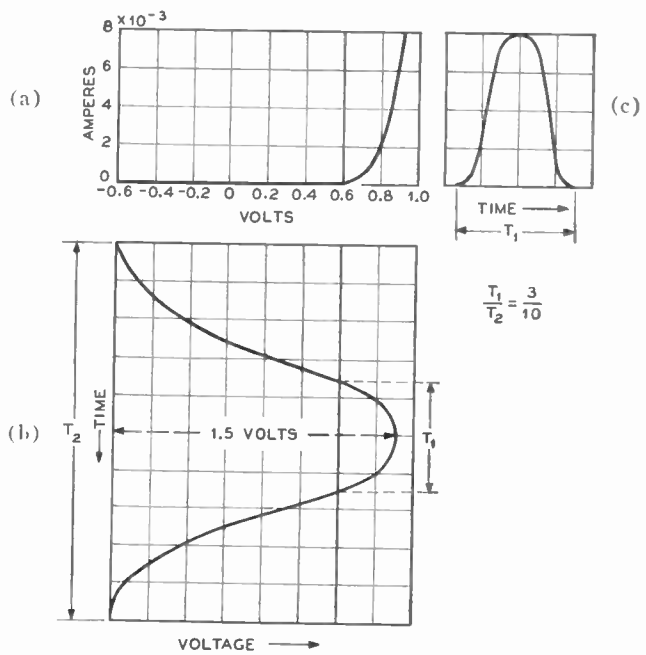

Fig. 5—(a) Diode characteristic. (b) Strobe pulse voltage waveform. (c) Strobe pulse diode current waveform.

To the extent that the clipping action represented by Fig. 4 is present for pulses this short,

$$T_1 = T_2 \times 0.3 = 1.8 \times 10^{-10} \text{ seconds},$$

based on the measured value of $T_2 = 6\times10^{-10}$ seconds.

In review, we now have two values for T_1: one based on the frequency response of the stroboscope, and the other based on the measured value of the strope pulse duration and the clipping action of the gallium-arsenide diode. Both values of T_1 are 1.8×10^{-10} seconds. This agreement is much better than could be expected, due to uncertainties in the 6-db bandwidth of the frequency curve and in the ratio of T_1 to T_2.

One additional point can be mentioned. The observed 2×10^{-10} second base duration pulses[6] are the shortest pulses we have been able to generate. Because the impulse response of our stroboscope is 1.8×10^{-10} seconds

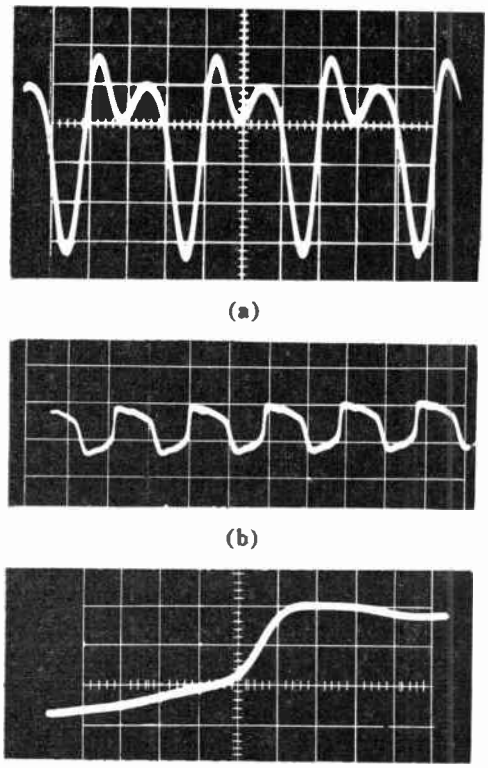

Fig. 6—Oscillograms. (a) 0.5-volt, 640-mc, negative pulses, half-amplitude duration 4×10^{-10} seconds. Horizontal sensitivity 5×10^{-10} seconds per large division. (b) 0.3-volt, 160-mc square wave. (c) 2×10^{-10} second rise time for 160-mc square wave. Horizontal sensitivity 2×10^{-10} seconds per large division.

it is likely that it was limiting the resolution and that these test pulses were appreciably shorter than 2×10^{-10} seconds, and in fact may have been as short as 0.9×10^{-10} seconds base duration.

In summary, we have shown that our electrical stroboscope has a 6-db bandwidth of 5.5 kmc, with a corresponding impulse response of 1.8×10^{-10} seconds base duration or of 9×10^{-11} seconds half-amplitude duration. The corresponding 10 to 90 per cent rise time would be 6×10^{-11} seconds.

Oscillograms

Oscillograms of 640-mc pulses and a 160-mc square wave are shown on Fig. 6. The 160-mc square wave was generated using a special Esaki tunnel diode.[10] The oscillogram in the center of Fig. 6 shows the 160-mc square wave, while the bottom oscillogram shows the rise time for this same square wave. The time scale for the rise time is 2×10^{-10} seconds for one large division. It will be noted that these waveforms do not fully test the expected rise time. Other tests not reported in this paper indicate that a rise time of at least as short as 1×10^{-10} seconds can be displayed satisfactorily by our stroboscope.[6]

[10] R. L. Batdorf, G. C. Dacey, R. L. Wallace, and D. J. Walsh, "An Esaki diode in InSb," *J. Appl. Phys.*, vol. 31, pp. 613–614; March, 1960.

Symmetrical Matrix Analysis of Parametric Amplifiers and Converters*

SID DEUTSCH†, MEMBER, IRE

Summary—**It is shown that the parametric amplifier and frequency converter can be described by four equations whose coefficients form a matrix that is symmetrical. Because of this symmetry, the calculations for gain, bandwidth, and noise figure yield simple and manageable results. By regarding the matrix as a nodal admittance array, an equivalent conductance circuit is constructed.**

The derived expressions show that, for low noise figure, the idle-frequency should be much higher than the signal-frequency. This is also the requirement for wide bandwidth. Numerical examples of amplifier and converter design are given.

Introduction

THE parametric (variable reactance) amplifier and frequency converter have been thoroughly analyzed in regard to gain, bandwidth, and noise figure.[1–9] Unfortunately, these analyses have employed unwieldy equations; this has undoubtedly hindered the full exploitation of this important new field.

In this paper it is shown that the parametric device can be described by four equations whose coefficients form a determinant or matrix that is symmetrical. Because of this symmetry, the calculations for gain, bandwidth, and noise figure yield simple and manageable results.

The circuit of Fig. 1 is used as the model for further discussion. Here the "signal" branch, in combination with C_v, is series-resonant at the nominal signal-frequency, ω_S. The signal to be amplified is the antenna voltage, V_{ins}. Power is supplied by the relatively large-amplitude "local oscillator" or pump at the frequency $\omega_P = \omega_S + \omega_I$. The "idle" branch, in combination with C_v, is series-resonant at the nominal beat or idle-frequency, ω_I. The dotted V_{inI} generator in the idle-branch will subsequently be used in the calculation for noise figure, but it is not normally present as an idle-signal source.

The capacitance of the shunt element, C_v, is a function of its voltage, v_v. An idealized plot of C_v vs v_v is shown in Fig. 2(a). The capacitor voltage usually includes a dc bias component, but this contributes nothing to the ac analysis and is therefore omitted. As defined in Fig. 2(a), C_v has the nominal value C_0 when v_v is zero, and $dC_v/dv_v = -m$.

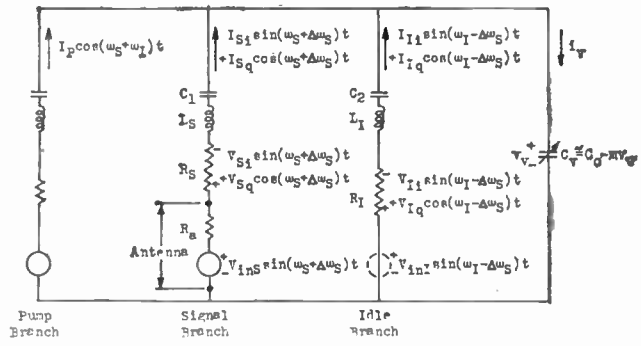

Fig. 1—Parametric amplifier and frequency converter circuit.

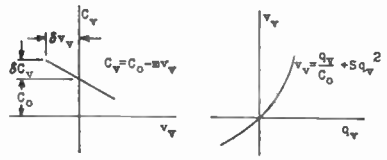

Fig. 2—Idealized variable-capacitor curves. (a) Capacitance as a function of voltage. (b) Voltage as a function of charge.

For our purposes, it is more convenient to give v_v as a function of its charge, q_v. For a fixed capacitor, $v = q/C$. The nonlinearities of a "varactor" can be represented by q_v^2, q_v^3, etc., terms. For a first approximation, we can omit cubic and higher power terms, as in Fig. 2(b), retaining

$$v_v = \frac{q_v}{C_0} + Sq_v^2. \tag{1}$$

The constant S is given as a function of C_0 and m in Appendix I.

In Fig. 1, outputs can either be taken at the signal-frequency across R_S or at the idle-frequency across R_I.

* Received by the IRE, July 31, 1959; revised manuscript received March 30, 1960. This work was supported in part by the AF Cambridge Research Center under Contract AF-19(604)-4143.

† Microwave Research Inst., Polytechnic Institute of Brooklyn, Brooklyn, N. Y.

[1] J. M. Manley and H. E. Rowe, "Some general properties of nonlinear elements," "Part I. General energy relations," PROC. IRE, vol. 44, pp. 904–913; July, 1956.

[2] B. Salzberg, "Masers and reactance amplifiers—basic power relations," PROC. IRE, vol. 45, pp. 1544–1545; November, 1957.

[3] S. Bloom and K. K. N. Chang, "Theory of parametric amplification using nonlinear reactances," *RCA Rev.*, vol. 18, pp. 578–593; December, 1957.

[4] H. Heffner and G. Wade, "Gain, bandwidth and noise characteristics of the variable-parameter amplifier," *J. Appl. Phys.*, vol. 29, pp. 1321–1331; September, 1958.

[5] P. A. Clavier, "The Manley-Rowe relations," PROC. IRE, vol. 47, pp. 1781–1782; October, 1959.

[6] J. M. Manley and H. E. Rowe, "General energy relations in nonlinear reactances," PROC. IRE, vol. 47, pp. 2115–2116; December, 1959.

[7] H. E. Rowe, "Some general properties of nonlinear elements." "II. Small signal theory," PROC. IRE, vol. 46, pp. 850–860; May, 1958.

[8] K. L. Kotzebue, "A Semiconductor-Diode Parametric Amplifier at Microwave Frequencies," Electronics Lab., Stanford University, Stanford, Calif., Rept. No. 49; November, 1958.

[9] M. Uenohara, "Noise considerations of the variable capacitance parametric amplifier," PROC. IRE, vol. 48, pp. 169–179; February, 1960.

It is assumed that the impedance of each branch is infinite at frequencies removed from the vicinity of resonance. It is also assumed that the variable capacitor is lossless. This is adequate for a first approximation; in practice, the losses that are associated with C_v can significantly increase the noise figure.[9–15]

No loss of generality is incurred by assuming that the signal source is a sine function while the pump current is a cosine function, as in Fig. 1, because ω_S and ω_P are usually incommensurate. The phase shift between input and output voltages can be handled by means of in-phase and quadrature components. It is the use of these components, rather than phase angles, that leads to the symmetrical matrix formulation.

Derivation of Symmetrical Matrix

The circuit behavior can be completely described in terms of the 12 quantities of Table I.

TABLE I

C_0	Nominal value of variable capacitance.
C_S	Nominal capacitance tuning the signal loop, $C_S = C_0C_1/(C_0+C_1)$.
C_I	Nominal capacitance tuning the idle loop, $C_I = C_0C_2/(C_0+C_2)$.
R_a	Antenna resistance.
R_S	Signal-branch load resistance.
R_I	Idle branch load resistance.
V_{inS}	Antenna peak signal voltage.
t	Time.
ω_S	Nominal signal frequency.
Δ	Relative deviation from the nominal signal frequency.
ω_I	Nominal idle frequency.
γ	A gain factor, $1-\gamma = (\delta C_v)^2/[4C_0^4\omega_S\omega_I R_I(R_a+R_S)]$.

Although the symbols in Table I will be used when the design equations are presented in final form, the interim derivations will be carried out with more convenient symbols. Some of these are defined in Fig. 1.

As shown in Fig. 1, the current in the variable capacitor is given by

$$\begin{aligned} i_v = {} & I_{Si}\sin(\omega_S+\Delta\omega_S)t + I_{Sq}\cos(\omega_S+\Delta\omega_S)t \\ & + I_{Ii}\sin(\omega_I-\Delta\omega_S)t + I_{Iq}\cos(\omega_I-\Delta\omega_S)t \\ & + I_P\cos(\omega_S+\omega_I)t. \end{aligned} \tag{2}$$

The instantaneous charge is, therefore,

$$\begin{aligned} q_v = \int i_v dt = {} & -\frac{I_{Si}}{\omega_S(1+\Delta)}\cos\omega_S(1+\Delta)t \\ & + \frac{I_{Sq}}{\omega_S(1+\Delta)}\sin\omega_S(1+\Delta)t + \cdots. \end{aligned} \tag{3}$$

[In (3) to (5), only the signal-frequency components are given since the idle- and pump-frequency components have a similar form.] We next find q_v^2 by squaring the right-hand side of (3). This is the heart of the amplification process, for the idle- and pump-frequency components beat to produce signal-frequency components, etc. We get

$$\begin{aligned} q_v^2 = {} & -\frac{I_PI_{Ii}}{(\omega_S+\omega_I)(\omega_I-\Delta\omega_S)}\sin\omega_S(1+\Delta)t \\ & + \frac{I_PI_{Iq}}{(\omega_S+\omega_I)(\omega_I-\Delta\omega_S)}\cos\omega_S(1+\Delta)t + \cdots. \end{aligned} \tag{4}$$

When (3) and (4) are substituted into (1), we obtain

$$\begin{aligned} v_v = {} & \left[\frac{I_{Sq}}{\omega_SC_0(1+\Delta)} - \frac{SI_PI_{Ii}}{(\omega_S+\omega_I)(\omega_I-\Delta\omega_S)}\right] \\ & \cdot\sin\omega_S(1+\Delta)t \\ & + \left[-\frac{I_{Si}}{\omega_SC_0(1+\Delta)} + \frac{SI_PI_{Iq}}{(\omega_S+\omega_I)(\omega_I-\Delta\omega_S)}\right] \\ & \cdot\cos\omega_S(1+\Delta)t + \cdots, \end{aligned} \tag{5}$$

The product of i_v and v_v in (2) and (5) will show that the Manley-Rowe power relations are satisfied; that is, pump-frequency power enters C_v and is converted into signal-frequency power (P_S) and idle-frequency power (P_I) in accordance with

$$\frac{P_S}{\omega_S(1+\Delta)} = \frac{P_I}{\omega_I-\Delta\omega_S}. \tag{6}$$

This is incidental, however, to what follows.

The summation of voltage drops along the "signal" branch of Fig. 1 is now set equal to the signal-frequency components of v_v, as shown in Appendix II. When v_S and v_I (the voltages across R_S and R_I, respectively) are employed in place of i_SR_S and i_IR_I, the sin $\omega_S(1+\Delta)t$ coefficients yield

$$\psi D_S V_{Si} - 2\psi\Delta V_{Sq} - MV_{Ii} = \omega_I R_I\sqrt{C_SC_I}V_{inS} \tag{7}$$

while the cos $\omega_S(1+\Delta)t$ coefficients yield

$$-2\psi\Delta V_{Si} - \psi D_S V_{Sq} - MV_{Iq} = 0, \tag{8}$$

where

$$\psi = \frac{\omega_I R_I}{\omega_S R_S}\sqrt{\frac{C_I}{C_S}} \tag{9}$$

$$M = \frac{SI_P\sqrt{C_SC_I}}{\omega_S+\omega_I} \tag{10}$$

[9] G. F. Herrmann, M. Uenohara, and A. Uhlir, Jr., "Noise figure measurements on two types of variable reactance amplifiers using semiconductor diodes," PROC. IRE, vol. 46, pp. 1301–1303; June, 1958.

[11] R. C. Knechtli and R. D. Weglein, "Low noise parametric amplifier," PROC. IRE, vol. 47, pp. 584–585; April, 1959.

[12] N. Houlding, "Low-noise parametric amplifier," PROC. IRE, vol. 47, p. 2025; November, 1959.

[13] M. Uenohara and A. E. Bakanowski, "Low-noise parametric amplifier using germanium p-n junction diode at 6 kmc," PROC. IRE, vol. 47, pp. 2113–2114; December, 1959.

[14] M. Uenohara and W. M. Sharpless, "An extremely low-noise 6-kmc parametric amplifier using gallium arsenide point-contact diodes," PROC. IRE, vol. 47, pp. 2114–2115; December, 1959.

[15] B. C. DeLoach and W. M. Sharpless, "X-band parametric amplifier noise figure," PROC. IRE, vol. 47, p. 2115; December, 1959.

and D_S is the reciprocal of the signal-frequency loop Q; *i.e.*,

$$D_S = \omega_S C_S (R_a + R_S). \tag{11}$$

In an analogous manner, the summation of voltage drops along the "idle" branch of Fig. 1 is set equal to the idle-frequency components of v_p. The sin $(\omega_I - \Delta\omega_S)t$ coefficients then give

$$-MV_{Si} + \frac{D_I}{\psi} V_{Ii} + \frac{2\rho\Delta}{\psi} V_{Iq} = \omega_S R_S \sqrt{C_S C_I} V_{inI} \tag{12}$$

while the cos $(\omega_I - \Delta\omega_S)t$ coefficients result in

$$-MV_{Sq} + \frac{2\rho\Delta}{\psi} V_{Ii} - \frac{D_I}{\psi} V_{Iq} = 0, \tag{13}$$

where

$$\rho = \frac{\omega_S}{\omega_I} \tag{14}$$

and D_I is the reciprocal of the idle-frequency loop Q, or

$$D_I = \omega_I R_I C_I. \tag{15}$$

Eqs. (7), (8), (12), and (13) form a set of 4 equations with the 4 unknowns V_{Si}, V_{Sq}, V_{Ii}, and V_{Iq}. In matrix form the set appears as

$$\begin{bmatrix} \psi D_S & -2\psi\Delta & -M & 0 \\ -2\psi\Delta & -\psi D_S & 0 & -M \\ -M & 0 & D_I/\psi & 2\rho\Delta/\psi \\ 0 & -M & 2\rho\Delta/\psi & -D_I/\psi \end{bmatrix} \begin{bmatrix} V_{Si} \\ V_{Sq} \\ V_{Ii} \\ V_{Iq} \end{bmatrix} = \begin{bmatrix} \omega_I R_I \sqrt{C_S C_I} V_{inS} \\ 0 \\ \omega_S R_S \sqrt{C_S C_I} V_{inI} \\ 0 \end{bmatrix}. \tag{16}$$

Notice that the square array in (16) is a symmetrical matrix.

Equivalent Circuit

If the square array in (16) is regarded as a nodal admittance matrix, we can construct the network of Fig. 3 as an equivalent circuit representation of the parametric device. The current and conductance values are normalized, but the node voltages have the units of volts. The dotted V_{inI} generator of Fig. 1 has been omitted, as it normally would be.

The circuit of Fig. 3 is not particularly useful because it is only equivalent in a mathematical but not physical sense. The circuit does show at a glance, however, that if the input signal is at band center ($\Delta = 0$), then V_{Sq} and V_{Iq} vanish. If the pump is removed ($M = 0$), then V_{Ii} and V_{Iq} vanish.

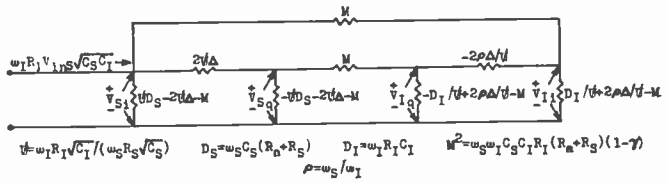

Fig. 3—The equivalent conductance circuit.

Gain as an Amplifier

If the input signal is at band center and V_{inI} is zero, (16) simplifies to

$$\begin{bmatrix} \psi D_S & -M \\ -M & D_I/\psi \end{bmatrix} \begin{bmatrix} V_{Si} \\ V_{Ii} \end{bmatrix} = \begin{bmatrix} \omega_I R_I \sqrt{C_S C_I} V_{inS} \\ 0 \end{bmatrix}. \tag{17}$$

The signal-frequency voltage gain is then, since $|v_S| = V_{Si}$,

$$\frac{|v_S|}{V_{inS}} = \frac{\omega_S R_S C_S}{D_S\left(1 - \dfrac{M^2}{D_S D_I}\right)}. \tag{18}$$

The characteristics of the amplifier are critically dependent on the $1 - M^2/D_S D_I$ term. In order to obtain reasonable gain, the capacitance modulation ratio, M, must be chosen so that the term is much less than unity. A slight decrease in M then results in a large loss of gain; a slight increase in M results in infinite gain or oscillations. The $1 - M^2/D_S D_I$ term is one of the important design quantities of a parametric device, and is listed in Table I in the form of the gain factor, γ:

$$\gamma = 1 - \frac{M^2}{D_S D_I}. \tag{19}$$

As γ decreases, the amplifier becomes unstable and may break into oscillations; as γ increases, the amplifier gain becomes too low to overcome second-stage noise. The value $\gamma = 0.2$ is a reasonable compromise between these two extremes.

As shown later, the input resistance to a parametric amplifier is negative. It is, therefore, meaningless to define the power gain as the output power divided by the input power. Instead, we can define the *insertion power gain* as the output power with the parametric device inserted divided by the output power across a matched load, R_a, when the device is removed. As a function of Table I quantities, (18) shows that the insertion power gain is

$$(IPG) = \frac{4R_a R_S}{\gamma^2 (R_a + R_S)^2}. \tag{20}$$

For given values of R_a and γ, R_S should be chosen so as to maximize the insertion power gain. This occurs when $R_S = R_a$. We then have simply

$$(IPG)_{max} = \frac{1}{\gamma^2}. \tag{21}$$

Input Resistance

At band center, the signal-branch current is given by (18) as

$$|i_S| = \frac{|v_S|}{R_S} = \frac{V_{inS}}{\gamma(R_a + R_S)} . \quad (22)$$

The resistance seen by the V_{inS} generator is, therefore, $\gamma(R_a+R_S)$ ohms. The resistance seen from the antenna terminals of Fig. 1 is this value less R_a ohms, or

$$R_{input} = -[R_a - \gamma(R_a + R_S)]. \quad (23)$$

For example, if $R_a = R_S = 50$ ohms and $\gamma = 0.2$, then the antenna sees -30 ohms. If this is the case, it is ordinarily impossible to match a 50-ohm antenna transmission line to the input resistance of the amplifier. To avoid standing waves, it is necessary to mount the parametric amplifier at the antenna. The load resistor R_S can then take the form of a 50-ohm transmission line feeding a conventional receiver.

At microwave frequencies, it becomes feasible to employ nonreciprocal devices such as gyrators, isolators, and circulators. These make it possible to match a transmission line or waveguide to the input resistance of the amplifier. The literature describes many practical applications of nonreciprocal devices to parametric amplifiers.[7-10,16-19]

Bandwidth as an Amplifier

Returning to (16) and solving for the in-phase signal-frequency gain, we get

$$\frac{V_{Si}}{V_{inS}} = \frac{\omega_S R_S C_S D_S(\gamma D_I^2 + 4\rho^2\Delta^2)}{\text{Denom}}, \quad (24)$$

while the quadrature gain is

$$\frac{V_{Sq}}{V_{inS}} = \frac{-2\omega_S R_S C_S \Delta(D_I^2 + \rho M^2 + 4\rho^2\Delta^2)}{\text{Denom}} \quad (25)$$

where

$$\text{Denom} = 16\rho^2\Delta^4 + 4\Delta^2(\rho^2 D_S^2 + D_I^2 + 2\rho M^2) + (\gamma D_S D_I)^2. \quad (26)$$

The total gain, $\sqrt{V_{Si}^2 + V_{Sq}^2}/V_{inS}$, appears after simplification as

$$\frac{|v_S|}{V_{inS}} = \omega_S R_S C_S \sqrt{\frac{D_I^2 + 4\rho^2\Delta^2}{\text{Denom}}} . \quad (27)$$

Note that at band center, where $\Delta = 0$, (18) and (27) become identical.

We define the relative bandwidth as $2\Delta_B$, where Δ_B is the relative deviation from ω_S at which a 3-db loss in gain is experienced. From (18) and (27), the following quadratic form is obtained:

$$16\rho^2\Delta_B^4 + 4\Delta_B^2[\rho^2 D_S^2(1 - 2\gamma^2) + D_I^2 + 2\rho M^2] - (\gamma D_S D_I)^2 = 0. \quad (28)$$

The exact solution for $2\Delta_B$ in (28) is quite complicated. Fortunately, for typical numerical values, the solution can be simplified. If D_S and D_I are replaced by their reciprocals Q_S and Q_I, respectively, the relative bandwidth is given, with negligible error, by

$$2\Delta_B = \frac{\gamma}{Q_S + Q_I \dfrac{\omega_S}{\omega_I}} . \quad (29)$$

This is illustrated by the following: Suppose that $\gamma = 0.2$, $D_S = 0.2$, $D_I = 0.25$, $\rho = 0.5$, and $M = 0.2$ (these values are used later in a numerical example). Then (28) yields $2\Delta_B = 0.02989$ while (29) yields $2\Delta_B = 0.02857$.

For design purposes, (29) can be rewritten using Table I symbols. If in addition $R_S = R_a$,

$$2\Delta_B\Big|_{\text{max power out}} = \frac{2\gamma\omega_S R_a C_S}{1 + \dfrac{2\omega_S^2 R_a C_S}{\omega_I^2 R_I C_I}} . \quad (30)$$

For wide bandwidth, ω_I should be much greater than ω_S and R_I should be large (*i.e.*, the Q of the idle loop should be low). When ω_I and R_I are increased, however, it becomes difficult to obtain the desired value of γ because the capacitance modulation ratio, M, must then be increased (*i.e.*, a greater pumping amplitude is required).

The gain-bandwidth product of an amplifier is useful information when gain can be traded for bandwidth. A limited degree of "trading" is possible with a parametric amplifier, where gain must be selected so that second-stage noise is overcome while good stability is maintained. We can multiply the square-root of the insertion power gain in (21) by the actual bandwidth to get the gain-bandwidth product:

$$2\Delta_B\omega_S\sqrt{IPG}\Big|_{\text{max power out}} = \frac{2\omega_S^2 R_a C_S}{1 + \dfrac{2\omega_S^2 R_a C_S}{\omega_I^2 R_I C_I}} . \quad (31)$$

Noise Figure as an Amplifier

As usually defined, noise figure is the available signal-to-noise power ratio at the receiver input divided by the signal-to-noise power ratio at the output (before demodulation). It is more convenient to express the noise figure in terms of voltages, as per the model of Fig. 4. Here the antenna is not necessarily matched to the receiver input impedance. As shown in Appendix III, the definition of noise figure becomes

[16] F. A. Brand, W. G. Matthei, and T. Saad, "The reactatron—a low-noise, semiconductor diode, microwave amplifier," PROC. IRE, vol. 47, pp. 42–44; January, 1959.
[17] L. U. Kibler, "Directional bridge parametric amplifier," PROC. IRE, vol. 47, pp. 583–584; April, 1959.
[18] B. B. Bossard, "Superregenerative reactance amplifier," PROC. IRE, vol. 47, pp. 1269–1271; July, 1959.
[19] C. B. DeLoach, and W. M. Sharpless, "An X-band parametric amplifier," PROC. IRE, vol. 47, pp. 1664–1665; September, 1959.

$$F = \frac{v_{nout}^2}{4kR_aT_aB(VG)^2}, \tag{32}$$

where

v_{nout} is the output noise voltage,
k is Boltzmann's constant,
T_a is the absolute temperature of R_a,
B is the noise bandwidth, (VG) is the voltage gain from the antenna source to the output.

In using (32), it is assumed that the IF bandwidth of the receiver is much less than that of the parametric amplifier. In other words, the gain of the latter is approximately constant from $\omega_S-(B/2)$ to $\omega_S+(B/2)$ and is equal to the gain at band center (*i.e.*, at $\Delta=0$).

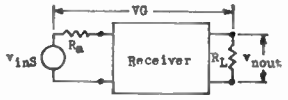

Fig. 4—The model used to derive a simplified expression for noise figure.

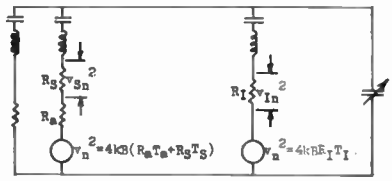

Fig. 5—The assumed noise sources and voltages of the parametric device.

Noise that is generated in R_a, R_S, and R_I can be represented by v_n^2 sources, as in Fig. 5. Eq. (18) gives the output voltage across R_S caused by a voltage source in the signal-frequency branch. From (18), the output noise voltage squared because of R_a and R_S, is given by

$$v_{Sn}^2\Big|_{\text{due to } R_a,\ R_S} = \frac{4kBR_S^2(R_aT_a + R_ST_S)}{\gamma^2(R_a + R_S)^2}. \tag{33}$$

To find the contribution caused by R_I, we set Δ and V_{inS} equal to zero in (16) to get

$$\frac{|v_S|}{V_{inI}} = \frac{M\omega_SR_S\sqrt{C_SC_I}}{\gamma D_SD_I}. \tag{34}$$

When V_{inI} is replaced by the noise voltage source of Fig. 5, the contribution caused by R_I is given by

$$v_{Sn}^2\Big|_{\text{due to } R_I} = \frac{4kB\omega_ST_IR_S^2(1-\gamma)}{\omega_I\gamma^2(R_a + R_S)}. \tag{35}$$

From (33) and (35), the total output noise voltage squared is

$$v_{Sn}^2 = \frac{4kBR_S^2}{\gamma^2(R_a + R_S)^2} \cdot \left[R_aT_a + R_ST_S + \frac{\omega_ST_I(R_a+R_S)(1-\gamma)}{\omega_I}\right]. \tag{36}$$

In (32), we can now substitute (36) for the numerator and (18) for the (VG) term to get

$$F = 1 + \frac{R_ST_S}{R_aT_a} + \frac{\omega_ST_I(R_a + R_S)(1-\gamma)}{\omega_IR_aT_a}. \tag{37}$$

Under the condition of maximum signal power output, where $R_S=R_a$,

$$F\Big|_{\text{max power out}} = 1 + \frac{T_S}{T_a} + \frac{2\omega_ST_I(1-\gamma)}{\omega_IT_a}. \tag{38}$$

A brief discussion of the various quantities in (38) follows:

T_S: In a typical application, R_S will be the input resistance of a conventional receiver and, in the absence of refrigeration, T_S will be 293 degrees or more. The antenna temperature, on the other hand, may be much less than 293 degrees. The T_S/T_a term in (38) can therefore cause a large deterioration in noise figure.

T_I: The idle-branch resistor should be at a low effective temperature. One ingenious way of accomplishing this is to use an antenna in place of R_I. The antenna is then directed toward a low-noise region of the sky.

ω_I: For low noise figure, ω_I should be much greater than ω_S. This is also the requirement for wide bandwidth.

Note that the measurement of noise figure for a parametric amplifier requires special techniques because the input resistance is negative. If a 30-db attenuator is inserted between the parametric device and the noise source, the latter will be properly matched, but 30 db must be subtracted from the noise figure reading. It is obvious that a slight error in the attenuator calibration will result in a large error in measured noise figure.

Eq. (37) and the subsequent discussion become modified when nonreciprocal devices are employed. The reader should refer to the aforementioned literature.

Numerical Example of an Amplifier Design

As a numerical example, suppose that the following Table I values are employed:

$C_0=2$ $\mu\mu$f
$C_S=1$ $\mu\mu$f
$C_I=1$ $\mu\mu$f
$R_a=10$ ohms
$R_S=10$ ohms
$R_I=12.5$ ohms
$\omega_S=10^{10}$ radians/sec (1592 mc)
$\omega_I=2\times10^{10}$ radians/sec (3183 mc)
$\gamma=0.2$.

The resistance values that are listed above are the equivalent values seen in combination with matching transformers and 50-ohm lines.

The numerical values cannot be chosen arbitrarily. Capacitors C_S and C_I must be smaller than C_0. The gain factor, γ, and the peak capacitance swing (δC_v), are related as shown in Appendix I. For the above set of values,

$$(\delta C_v) = 2C_0^2\sqrt{\omega_S\omega_I R_I(R_a + R_S)(1 - \gamma)} = 1.6\ \mu\mu f$$

which is physically possible in view of the fact that $C_0 = 2\mu\mu$f.

The Q's are given by

$$Q_S = 1/[\omega_S C_S(R_a + R_S)] = 5$$

and

$$Q_I = 1/(\omega_I R_I C_I) = 4.$$

Since $R_S = R_a$, the gain, bandwidth, and noise figure appear as

(21): (IPG) $= 1/\gamma^2 = 25 = 13.98$ db,

(29): $2\Delta_B = \gamma\omega_I/(\omega_I Q_S + \omega_S Q_I) = 0.02857$,

$$2\Delta_B f_S = 45.48 \text{ mc},$$

(38): $F = 1 + \dfrac{T_S}{T_a} + \dfrac{2\omega_S T_I(1 - \gamma)}{\omega_I T_a} = 2.8 = 4.47$ db,

$(T_a = T_S = T_I)$.

Gain as a Converter

The remaining sections of this paper consider the parametric device as a frequency converter. The output is taken across R_I at the idle-frequency.

If the input signal is at band center, (17) gives the conversion voltage gain as

$$\frac{|v_I|}{V_{inS}} = \frac{M\omega_I R_I\sqrt{C_S C_I}}{\gamma D_S D_I}. \tag{39}$$

As a function of Table I quantities, (39) shows that the insertion power gain is

$$(\text{IPG}) = \frac{4\omega_I R_a(1 - \gamma)}{\gamma^2\omega_S(R_a + R_S)}. \tag{40}$$

Notice that the power output is independent of R_I. For given values of R_a, ω_S, and γ, the insertion power gain is maximum when R_S is zero and ω_I is large. For $R_S = 0$ we get

$$(\text{IPG})_{\max} = \frac{4\omega_I(1 - \gamma)}{\gamma^2\omega_S}. \tag{41}$$

Bandwidth as a Converter

Solving for the in-phase idle-frequency gain in (16), we get

$$\frac{V_{Ii}}{V_{inS}} = \frac{M\omega_I R_I\sqrt{C_S C_I}(\gamma D_S D_I - 4\rho\Delta^2)}{\text{Denom}}, \tag{42}$$

while the quadrature gain is

$$\frac{V_{Iq}}{V_{inS}} = \frac{2M\Delta\omega_I R_I\sqrt{C_S C_I}(\rho D_S + D_I)}{\text{Denom}} \tag{43}$$

where "Denom" is given by (26). The total gain, $\sqrt{V_{Ii}^2 + V_{Iq}^2}/V_{inS}$, appears after simplification as

$$\frac{|v_I|}{V_{inS}} = M\omega_I R_I\sqrt{\frac{C_S C_I}{\text{Denom}}}. \tag{44}$$

At band center, where $\Delta = 0$, (39) and (44) become identical.

From (39) and (44), the following quadratic form for the relative bandwidth $2\Delta_B$ is obtained:

$$16\rho^2\Delta_B^4 + 4\Delta_B^2(\rho^2 D_S^2 + D_I^2 + 2\rho M^2) - (\gamma D_S D_I)^2 = 0. \tag{45}$$

Notice that (45) and (28) are identical except for a $1 - 2\gamma^2$ term. In practice, $1 - 2\gamma^2 \cong 1$, so that (29) also expresses the bandwidth of the converter, relative to ω_S, with negligible error.

For design purposes, (29) can be rewritten using Table I symbols. If in addition $R_S = 0$,

$$2\Delta_B\Big|_{\text{max power out}} = \frac{\gamma\omega_S R_a C_S}{1 + \dfrac{\omega_S^2 R_a C_S}{\omega_I^2 R_I C_I}}. \tag{46}$$

The discussion relating to the bandwidth as an amplifier again applies: For wide bandwidth, the device should be used as an up-converter and the Q of the idle-branch should be low.

Noise Figure as a Converter

Eq. (39) gives the output voltage across R_I caused by a voltage source in the signal-frequency branch. From this, the output noise voltage squared, because of R_a and R_S, is given by

$$v_{In}^2\Big|_{\text{due to } R_a,\ R_S} = \frac{4kB\omega_I R_I(1 - \gamma)(R_a T_a + R_S T_S)}{\gamma^2\omega_S(R_a + R_S)}. \tag{47}$$

To find the contribution caused by R_I, we set Δ and V_{inS} equal to zero in (16) to get

$$\frac{|v_I|}{V_{inI}} = \frac{1}{\gamma}. \tag{48}$$

When V_{inI} is replaced by the noise voltage source of Fig. 5, the contribution caused by R_I is given by

$$v_{In}^2\Big|_{\text{due to } R_I} = \frac{4kBR_I T_I}{\gamma^2}. \tag{49}$$

From (47) and (49), the total output noise voltage squared is

$$v_{In}^2 = \frac{4kB\omega_I R_I(I - \gamma)}{\gamma^2\omega_S(R_a + R_S)} \cdot \left[R_a T_a + R_S T_S + \frac{\omega_S T_I(R_a + R_S)}{\omega_I(1 - \gamma)}\right]. \tag{50}$$

In (32), we can now substitute (50) for the numerator and (39) for the (VG) term to get

$$F = 1 + \frac{R_S T_S}{R_a T_a} + \frac{\omega_S T_I (R_a + R_S)}{\omega_I R_a T_a (1 - \gamma)} . \tag{51}$$

Notice that the noise figure depends on the temperature of R_I but not on its resistance value. Under the condition of maximum signal power output, where $R_S = 0$,

$$F\Big|_{\text{max power out}} = 1 + \frac{\omega_S T_I}{\omega_I T_a (1 - \gamma)} . \tag{52}$$

In a typical application, R_I will be the input resistance of a conventional receiver and, in the absence of refrigeration, T_I will be 293 degrees or more. The ratio T_I/T_a can therefore cause a large deterioration in noise figure.

For low noise figure, the device should be used as an up-converter. This is also the requirement for wide bandwidth.

Eq. (51) and the subsequent discussion become modified when nonreciprocal devices are employed.

Numerical Example of a Converter Design

Suppose that the previous numerical amplifier example is modified so that the output is taken across R_I rather than R_S. The following Table I values are employed:

$C_0 = 2\ \mu\mu f$
$C_S = 1\ \mu\mu f$
$C_I = 1\ \mu\mu f$
$R_a = 10$ ohms
$R_S = 0$
$R_I = 25$ ohms
$\omega_S = 10^{10}$ radians/sec (1592 mc)
$\omega_I = 2 \times 10^{10}$ radians/sec (3183 mc)
$\gamma = 0.2$.

In choosing $R_I = 25$ ohms, it is assumed that the previous peak capacitance swing of $(\delta C_v) = 1.6\ \mu\mu f$ is retained (see Appendix I).

The Q's are now given by

$$Q_S = 1/[\omega_S C_S (R_a + R_S)] = 10$$

and

$$Q_I = 1/(\omega_I R_I C_I) = 2.$$

Since $R_S = 0$, the gain, bandwidth, and noise figure appear as

(41): (IPG) $= 4\omega_I(1 - \gamma)/(\gamma^2 \omega_S) = 160 = 22.04$ db.

(29): $2\Delta_B = \gamma\omega_I/(\omega_I Q_S + \omega_S Q_I) = 0.01818$,

$2\Delta_B f_S = 28.94$ mc/sec.

(52): $F = 1 + \dfrac{\omega_S T_I}{\omega_I T_a (1 - \gamma)} = 1.625 = 2.109$ db,

$(T_a = T_I)$.

Comparing the amplifier with the converter, we see that the latter is much better in regard to gain and noise figure. This is partly because ω_I is greater than ω_S and partly because R_S has been allowed to vanish in the above numerical example, whereas R_I must be finite when the device is employed as an amplifier.

Appendix I

Variable Capacitor Relationships

The following expression is assumed for the variable capacitor:

$$v_v = \frac{q_v}{C_0} + S q_v^2 . \tag{53}$$

Solving for q_v, we get

$$q_v = \frac{\sqrt{1 + 4SC_0^2 v_v} - 1}{2SC_0} . \tag{54}$$

This can be expanded into

$$q_v = C_0 v_v - SC_0^3 v_v^2 + 2S^2 C_0^5 v_v^3 - \cdots \tag{55}$$

so that the instantaneous capacitance, dq_v/dv_v, becomes

$$C_v = C_0 - 2SC_0^3 v_v + 6S^2 C_0^5 v_v^2 - \cdots . \tag{56}$$

Comparing (56) with the form assumed in Fig. 2(a), where

$$C_v = C_0 - m v_v \tag{57}$$

we see that

$$S \cong \frac{m}{2C_0^3} \quad \text{if} \quad \frac{(\delta C_v)}{C_0} \ll 1. \tag{58}$$

It is useful to relate the variable capacitance modulation ratio, M, to the peak capacitance swing, (δC_v). As defined in (10),

$$M = \frac{S I_P \sqrt{C_S C_I}}{\omega_P} . \tag{59}$$

But the peak pump current, I_P, is accompanied by a peak voltage swing

$$(\delta v_v) = \frac{I_P}{\omega_P C_0} = \frac{(\delta C_v)}{m} . \tag{60}$$

Substituting for S and I_P from (58) and (60), we get

$$M = \frac{(\delta C_v)\sqrt{C_S C_I}}{2C_0^2} . \tag{61}$$

Furthermore, since $1 - \gamma = M^2/(D_S D_I)$ from (19), we have

$$1 - \gamma = \frac{(\delta C_v)^2}{4C_0^4 \omega_S \omega_I R_I (R_a + R_S)} . \tag{62}$$

Appendix II

Derivation of the Output Voltage Equations

The signal-frequency components of v_v are given by (5). These must equal the summation of voltage drops along the "signal" branch of Fig. 1. Using Ldi/dt for coil voltage and $C^{-1}\int idt$ for capacitor voltage, the sin $\omega_S(1+\Delta)t$ coefficients around the signal loop yield

$$I_{Si}(R_a + R_S) - \omega_S L_S(1+\Delta)I_{Sq} + \frac{I_{Sq}}{\omega_S C_1(1+\Delta)} + \frac{I_{Sq}}{\omega_S C_0(1+\Delta)} - \frac{SI_PI_{Ii}}{(\omega_S+\omega_I)(\omega_I-\Delta\omega_S)} = V_{inS}, \quad (63)$$

while the cos $\omega_S(1+\Delta)t$ coefficients give

$$I_{Sq}(R_a + R_S) + \omega_S L_S(1+\Delta)I_{Si} - \frac{I_{Si}}{\omega_S C_1(1+\Delta)} - \frac{I_{Si}}{\omega_S C_0(1+\Delta)} + \frac{SI_PI_{Iq}}{(\omega_S+\omega_I)(\omega_I-\Delta\omega_S)} = 0. \quad (64)$$

The signal loop is series-resonant at ω_S. This permits L_S and C_1 to be replaced by

$$L_S = \frac{1}{\omega_S^2 C_S} \quad (65)$$

and

$$\frac{1}{C_1} = \frac{1}{C_S} - \frac{1}{C_0}. \quad (66)$$

For convenience, R_a+R_S can be expressed as a function of the reciprocal Q, D_S:

$$R_a + R_S = \frac{D_S}{\omega_S C_S}. \quad (67)$$

Also, it is assumed that the relative deviation from the nominal signal-frequency, Δ, will be small. In that event,

$$\frac{1}{1+\Delta} \cong 1 - \Delta \quad \text{and} \quad \omega_I - \Delta\omega_S \cong \omega_I. \quad (68)$$

These approximations are subsequently justified when it turns out that the bandwidth of the device is relatively narrow, so that Δ will be of the order of 1 per cent or less.

When (65) to (68) are applied to (63), the latter becomes

$$\frac{D_S I_{Si}}{\omega_S C_S} - \frac{2\Delta I_{Sq}}{\omega_S C_S} - \frac{SI_PI_{Ii}}{\omega_I(\omega_S+\omega_I)} = V_{inS}. \quad (69)$$

The substitution of V_{Si}/R_S for I_{Si} and V_{Sq}/R_S for I_{Sq}, and multiplication by $\omega_I R_I\sqrt{C_S C_I}$, then yields (7). The remaining output voltage equations—(8), (12), and(13)—are derived by a similar process.

Appendix III

Derivation of Noise Figure Equation

For Fig. 4, we have

Available signal power at receiver input $= v_{inS}^2/(4R_a)$ (70)

Available noise power at receiver input $= kT_aB$ (71)

Signal power at receiver output $= v_{inS}^2(VG)^2/R_L$ (72)

Noise power at receiver output $= v_{nout}^2/R_L$. (73)

Substituting the above in the definition for noise figure,

$$F = \frac{(70)(73)}{(71)(72)} = \frac{v_{nout}^2}{4kR_aT_aB(VG)^2}. \quad (74)$$

Acknowledgment

The many useful comments of Lowell I. Smilen and Dante C. Youla of the Microwave Research Institute are gratefully acknowledged.

An Analog Solution for the Static London Equations of Superconductivity*

NORMAN H. MEYERS†, SENIOR MEMBER, IRE

Summary—**Growing interest in the theoretical as well as applied aspects of superconductivity has focused considerable attention upon the static London equations. These macroscopic relationships describe the spatial distribution of magnetic fields and currents in superconductors. In this paper a novel analog method of obtaining solutions in complicated geometries is discussed. The method makes use of the similarity in form of the static London equations and the dynamic skin-effect equations of normal conduction under exponentially-growing steady-state conditions. Conveniently scaled copper models of superconducting geometries of interest can be constructed and excited from a growing-exponential function generator. Field distributions measured in the space around the normal conductors of the model correspond with the desired distributions in the analogous superconductor geometry. Fields within conductors themselves cannot be determined directly by this method, but the surface fields are generally most important. The method is particularly useful in studying thin films which are appreciably penetrated by magnetic fields.**

The experimental setup and the measurement technique are discussed. Illustrative results from a copper model of a long rectangular superconducting strip, 1830 penetration depths wide and 3.81 penetration depths thick are presented.

Introduction

EXPERIMENTAL evidence indicates that the static London equations[1,2] provide a good qualitative description of the behavior of fields and currents in superconductors over a frequency range extending all the way from dc to about 1 kmc and for temperatures ranging from absolute zero to about 99 per cent of the critical temperature. At present they are the only simple formulation of the macroscopic behavior of currents in superconductors. To aid in evaluation of various theories as well as in cryogenic device design, it would be advantageous to have a fairly flexible method for obtaining solutions of these equations in three-dimensional configurations of interest.

Analytically, the solutions can be obtained in only a few very simple geometries. Generally, such solutions are one-dimensional in nature. Digital-computer techniques can be employed to solve the static London equations in two-dimensional problems. However, such problems severely tax the capabilities of present computers. Three-dimensional solutions are possible in principle but are beyond present-day machines.

The very small size of practical superconducting circuitry makes direct measurement of field patterns a formidable problem. Methods using niobium powder patterns, the Faraday effect, a bismuth Hall-effect probe,[3] and the magneto-resistive effect[4] have all been employed with limited success. None of these field-measuring techniques has yet proven satisfactory for use by cryogenic-circuit designers. Thus, at present, components and circuits can be evaluated only by means of terminal measurements. The design of such devices would be facilitated if quantitative information on the fields to be expected were available.

An analog method has been devised which permits solution of the static London equations in complicated geometries. The method should be a valuable aid to the cryogenic-circuit design effort, enabling one to investigate the effects of changes in geometry, lead-in wire arrangement, and shielding by means of measurements made upon the fields in the vicinity of large-size properly-scaled copper models of the structures.

The method makes use of the analogy between the static London equations in a superconductor and the dynamic skin-effect equations[5] in a normal conductor under exponentially-growing steady-state conditions.

The Analogy with Skin Effect

To understand fully the analogy, consider the superconducting wire whose cross section is shown in Fig. 1(a) and the normal conducting wire of similar shape whose cross section is shown in Fig. 1(b). Inside the superconducting wire, the magnetic field intensity $\overline{H}$ is assumed to satisfy the static London equation

$$\nabla^2\overline{H} = \beta^2\overline{H}. \tag{1}$$

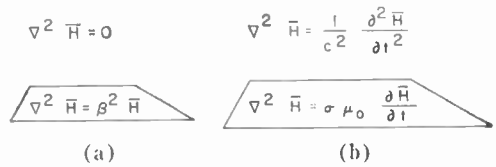

Fig. 1—(a) A superconducting wire under essentially static conditions, and (b) a similar normal-conducting wire under dynamic conditions.

* Received by the IRE, November 9, 1959; revised manuscript received, March 18, 1960.

† IBM Research Laboratory, Poughkeepsie, N. Y.

[1] F. London, "The electrodynamics of the pure superconducting state," in "Superfluids," John Wiley and Sons, Inc., New York, N. Y., ch. B, p. 27; 1950.

[2] M. Von Laue, "Fundamental Equations of the Maxwell-London Theory," in "Theory of Superconductivity," Academic Press, New York, N. Y., ch. 3, p. 13; 1952.

[3] H. E. Kronick, "Magnetic field plotter for superconducting film," *IBM J. Res. and Dev.*, vol. 2, p. 252; July, 1958.

[4] D. Shoenberg, "Superconductivity," University Press, p. 53; 1952.

[5] S. Ramo and J. R. Whinnery, "Fields and Waves in Modern Radio," John Wiley and Sons, Inc., p. 235; 1953.

Outside the wire under essentially static conditions the field satisfies Laplace's equation

$$\nabla^2 \overline{\Pi} = 0. \tag{2}$$

At the boundary between the two regions, the field must be continuous. The quantity β is a constant of the material, independent of position, and is the reciprocal of the "penetration depth." Rationalized mks units are assumed throughout this discussion.

Eqs. (1) and (2), together with the boundary conditions, may be regarded as a general representation of the problem for which a solution is sought. Compare this problem with that represented in Fig. 1(b). Within the normal wire, under dynamic conditions, the field satisfies the skin-effect equation

$$\nabla^2 \overline{\Pi} = \sigma\mu_0 \frac{\partial \overline{\Pi}}{\partial t}. \tag{3}$$

The quantity σ is the conductivity of the wire, while μ_0 is the permeability of free space. Outside the normal wire, also under dynamic conditions, the field satisfies the wave equation

$$\nabla^2 \overline{\Pi} = \frac{1}{c^2} \frac{\partial^2 \overline{\Pi}}{\partial t^2}. \tag{4}$$

The quantity c is the velocity of light in free space. Again, just as in the superconducting case, the magnetic field must be continuous at the boundary of the wire.

At this point it is necessary to note the possible existence of an exponentially-growing steady state in the physical situation of Fig. 1(b). That is, assume that the field everywhere may be written as the product of a real function of position $\overline{\Pi}_s(x, y, z)$ and an exponentially-growing time factor $e^{\alpha t}$ which is position independent.

$$\overline{\Pi}(x, y, z, t) = \overline{\Pi}_s(x, y, z)e^{\alpha t} \tag{5}$$

If (5) is substituted into (3) and (4), we have

$$\nabla^2 \overline{\Pi}_s = \sigma\mu_0\alpha \overline{\Pi}_s \tag{6}$$

inside the normal wire and

$$\nabla^2 \overline{\Pi}_s = \frac{\alpha^2}{c^2} \overline{\Pi}_s \tag{7}$$

in the surrounding space. The justification for the assumption of an exponentially-growing steady state is the fact that time does not appear in either (6) or (7). This is identical with the situation which arises when one assumes the existence of a sinusoidal steady state.

The right-hand side of (7) is nonzero, so it is not of the same form as Laplace's equation. However, the right-hand side arises from the displacement current-density term which appears in Maxwell's equations. That is, the difference between the simultaneous solution of (6) and (7) and the simultaneous solution of (6) and Laplace's equation is a distortion resulting from the capacitive displacement current in the space around the conductors. If the rise rate (α) is not too great, this effect is negligible.

Fortunately, one can generally determine experimentally when it is permissible to ignore the effect of displacement currents. Consider, for example, the geometry shown in Fig. 2. Two very long normal conducting wires of essentially-arbitrary cross-sectional shape carry equal and opposite currents. The component of the resultant magnetic field caused by conduction current must be directed perpendicularly to the axis of the wires, as shown. However, the field contribution resulting from displacement current is directed along the wires. If a field pickup coil gave a nearly null indication at every position when its axis was aligned with that of the wires, the effect of displacement current on the magnetic field pattern would be clearly negligible. Under such circumstances, it would be legitimate to write (7) as

$$\nabla^2 \overline{\Pi}_s \approx 0. \tag{8}$$

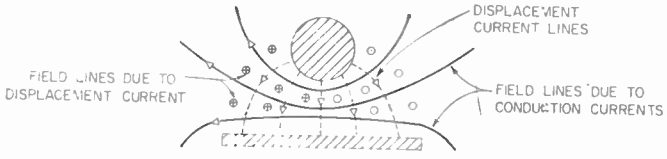

Fig. 2—Infinitely long normal conductors carrying equal and opposite currents.

Eqs. (6) and (8) are identical in form with (1) and (2). This is the basis of the analogy. One may build a scaled copper model of the superconducting geometry of interest, excite it with an exponentially-growing field or set of currents, wait for the steady state to be reached, measure the field distribution in space by means of a pickup coil, and thus obtain a solution to the corresponding superconductor problem.

The quantity in the normal conductor problem which is analogous to the penetration depth[6] in the superconductor is determined by comparison of (1) and (6).

$$\lambda = \frac{1}{\beta} \text{ is analogous to } \frac{1}{\sqrt{\sigma\mu_0\alpha}}$$

superconductor — normal conductor

The quantities σ and α may be chosen so as to make the normal model the same number of penetration depths in every dimension as the original superconductor. This is the only restriction in scaling the model. The field patterns about the model and the superconductor will then be identical in shape.

The field and current distributions inside superconductors cannot be determined directly by the method of this paper. However, the field patterns in the spaces between conductors provide much useful information. Furthermore, the surface fields are generally the most im-

[6] D. Shoenberg, *op. cit.*, ch. 5, p. 138.

portant ones. Knowledge of the surface fields provides some information as to internal field and current distributions.

Exponentially-Growing Excitation

It has been shown that a stable spatial-field distribution will result in and around a copper model if an exponentially-growing excitation is applied for a sufficiently long time. Such an excitation cannot be applied indefinitely, so it is necessary to determine just how long it must continue.

Consider the true exponentially-growing function shown by the dotted curve of Fig. 3. If such an excitation could actually be applied to a linear system, that system would be in the exponentially-growing steady state at each instant of time including all finite negative times. On the other hand, if the excitation shown by the solid curve of Fig. 3 were applied to the same physical system, several time constants of the system would have to elapse after the instant $t=0$ before the steady state was reached. The difference between the response of a linear system to the solid-curve excitation of Fig. 3 and the response to a true exponential would simply be the transient resulting from the difference between the two excitations. That is, the undesired transient would be that caused by the excitation of Fig. 4.

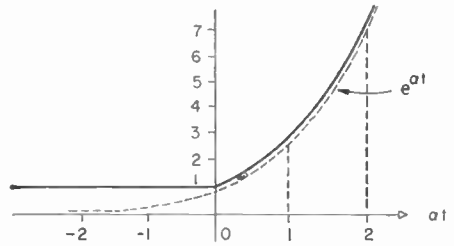

Fig. 3—A true growing exponential (dotted) and an appproximation to it (solid).

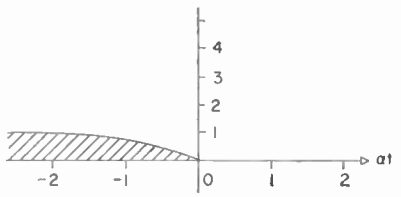

Fig. 4—Excitation which produces the transient response.

At no time does the excitation of the transient exceed unity on the arbitrary amplitude scale of Figs. 3 and 4. Therefore, even though the transient in the physical system might die out very slowly, it would never be very large. In fact, the transient response becomes negligible compared with the exponentially-growing steady-state response as soon as the exponentially-growing excitation becomes large compared with the maximum value of the transient excitation of Fig. 4. Thus, it is not necessary to wait for the model to reach the steady state before measuring the field distribution, since the transient response can be swamped out by the steady-state response merely by permitting the excitation to grow to a value which is large compared with its starting value at $t=0$.[7] Since e^7 is approximately 1100, an interval of seven time constants of the excitation brings about essentially steady-state conditions in any linear model regardless of the time constants of the model itself.

The Experimental Setup

A schematic diagram of a practical arrangement for exploiting the analogy of this paper is shown in Fig. 5. An exponential function generator drives a power amplifier which in turn feeds the model of interest through a matching transformer. A pickup coil near the model develops a voltage proportional to the field component along the coil axis. This signal is amplified and displayed on an output scope.

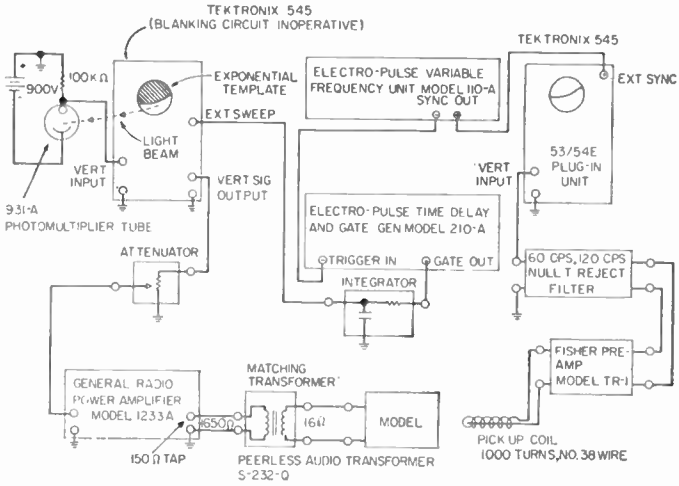

Fig. 5—Complete system for analog solution of the static London equations.

The rising exponential excitation cannot be continued indefinitely. Interruption of the excitation produces a severe transient in the system which must be allowed to die out completely before the excitation can be reapplied. This is accomplished by triggering the function generator and output scope from an external, low repetition-rate sync source, as shown.

We can obtain the desired field distribution by moving the coil about the model and noting relative output amplitudes at a fixed instant of time during the exponential cycle. The instant chosen for comparison purposes should be well toward the end of the exponential rise, when the transient is negligible, but prior to the termination of the exponential, when a second, much larger transient beings.

The range of time constants of excitation successfully used thus far is from about 0.2 millisecond to about 0.16 microsecond. In general, much shorter time constants cannot be used, because capacitive displacement currents begin to distort the field patterns. Better ampli-

[7] The author is indebted to Dr. Richard L. Garwin for pointing this out.

fying and filtering schemes would, however, permit longer time constants to be used. At present, a copper sheet 0.050 inches thick can be used to simulate a superconducting film of anywhere from about 0.78 penetration depth thick to about 27.5 penetration depths, a very interesting range.

Typical Results for an Open Field Strip

As a typical example of the sort of field distribution which can be evaluated using the analogy of this paper, consider the open field strip model shown in Fig. 6. A flat copper strip 2 feet wide, 5 feet long, and 0.050 inch thick is fed at one end from the center conductor of a co-

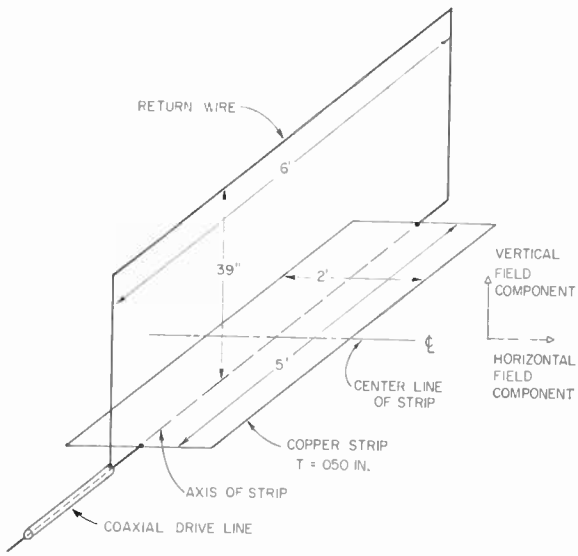

Fig. 6—Open field strip model.

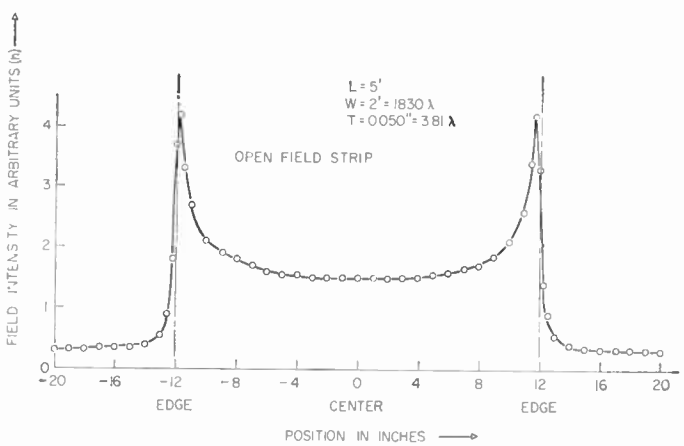

Fig. 7—Tangential field component inside loop.

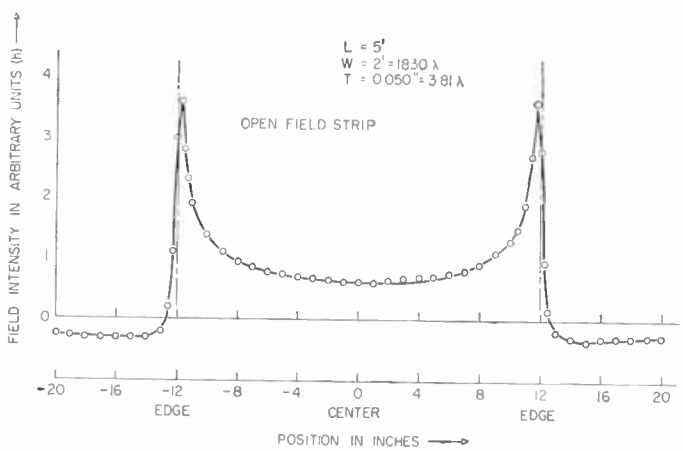

Fig. 8—Tangential field component outside loop.

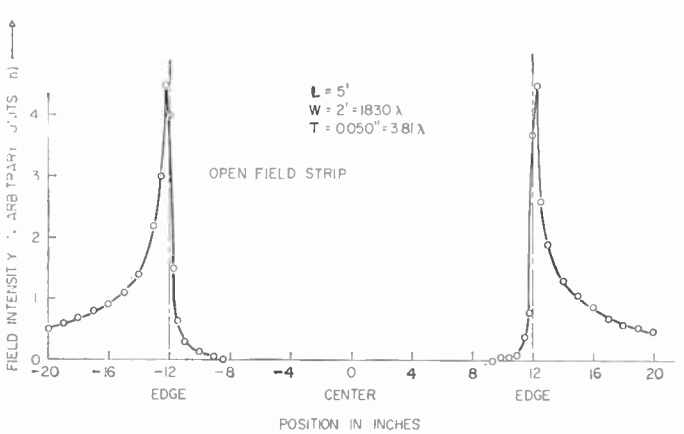

Fig. 9—Magnitude of normal field component inside loop.

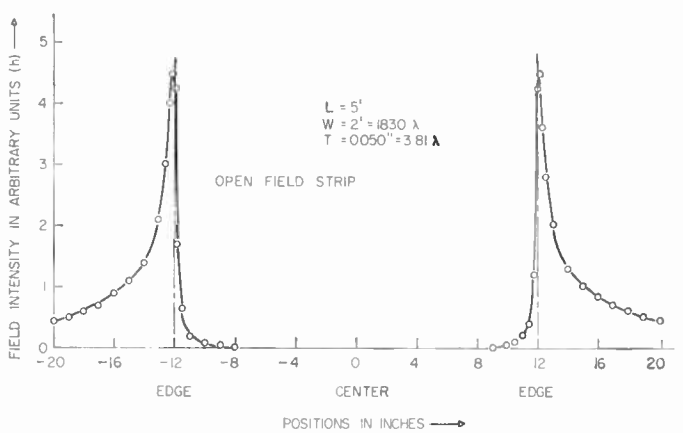

Fig. 10—Magnitude of normal field component outside loop.

axial cable. The exciting current passes through the strip and returns to the shield of the cable through an open wire as shown. The return wire is close enough to the strip to cause an appreciable difference between the field on the top and bottom surfaces of the strip. Furthermore, the model is not sufficiently long to permit one to regard the field distribution as truly two-dimensional.

The rise rate of the driving exponential was set so as to make the model 3.81 penetration depths thick and 1830 penetration depths wide. The pickup coil was passed along the center line, shown in Fig. 6, and the horizontal and vertical field components were separately determined. Such data were taken on both the top and bottom surfaces of the model. The results are shown in Figs. 7–10. The vertical scales are in arbitrary units. Only the shapes of the curves have meaning as they stand. However, the vertical scales could be related to the actual field intensities per ampere by excitation of the analogous superconducting strip by application of Ampere's Law.

The pick-up coil used in this work occupied a volume roughly 3/16 inch on a side. The voltage induced in it was thus a measure of the average field intensity over the volume of the coil. The coil was small compared with the width and length of the model but was not small compared with the thickness. Consequently, one should have some reservations in interpreting the results of Figs. 7–10 as the fields of the surfaces of the model. Better results could be obtained by use of a smaller coil and a larger model. A smaller coil than that currently in use is possible but would require additional amplification and filtering. Narrow-band amplifiers and filters can be used to pass a rising exponential.[8] The chief effect of the finite size of the pickup coil is to round the peaks of the field distributions. This is due to the fact that the field varies appreciably over one coil length only in the vicinity of the peaks.

Appendix

The Narrow-Band Filtering of Pure Exponentials

The purpose of this Appendix is to make clear the fact that pure exponential time functions may be passed through narrow-band amplifiers and filters.

If a passive linear system has a transfer function $T(p)$, where p denotes complex frequency, one may determine the sinusoidal steady-state frequency response, *i.e.*, the response to an excitation characterized by e^{jwt}, simply by replacing p in $T(p)$ by jw, where $j=\sqrt{-1}$. Similarly, the steady-state response of this same system to a growing exponential excitation characterized by $e^{\alpha t}$ may be obtained by replacing p in $T(p)$ by α. Since α is real, $T(\alpha)$ is also real in contrast with $T(jw)$, which is complex. Thus, the system does not have a separate magnitude and phase response when subjected to exponential excitation.

As an example, consider the simple band pass filter of Fig. 11. The voltage transfer function is given by

$$T(p) = E_0(p)/E_i(p) = \frac{(R/L)p}{p^2 + (R/L)p + (1/LC)}. \quad (9)$$

The magnitude of the sinusoidal steady-state frequency response passes through a maximum of unity at a radian frequency of $w=1/\sqrt{LC}$. The exponential steady-state response $T(\alpha)$ has maxima at $\alpha=\pm 1/\sqrt{LC}$. The response is not symmetrical about $\alpha=0$, however. Fig. 12 is a sketch of $T(\alpha)$ as it would appear for $R=\sqrt{L/C}$. For different values of damping, $T(\alpha)$ changes quite drastically. At critical damping, $R=2\sqrt{L/C}$, the positive maximum is $\frac{1}{2}$ while the negative maximum blows up. This just means that an output is temporarily possible at such a negative real frequency with no input.

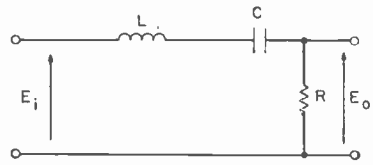

Fig. 11—Simple band-pass filter.

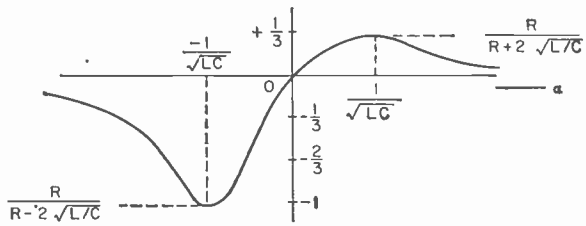

Fig. 12—Exponential response of a band-pass filter.

The important point, in so far as the present paper is concerned, is that growing exponentials can be passed through narrow-band filters and amplifiers without distortion of the waveform or alteration of the rate of rise. To pass an exponential waveform characterized by a certain value of α, one simply uses an amplifier or filter with a passband centered about $w=\alpha$.

Acknowledgment

The work described in this paper was done under the IBM Lightning Program, Task 3, Contract NObsr 77508 and was supported by the Bureau of Ships, U. S. Navy.

The author is indebted to Drs. R. L. Garwin and J. J. Lentz for their valuable suggestions. J. F. O'Hanlon and C. E. Newman were of great assistance in setting up the system and carrying out the measurements.

[8] This is discussed in more detail in the Appendix.

IRE Standards on Circuits: Definitions of Terms for Linear Passive Reciprocal Time Invariant Networks, 1960*

COMMITTEE PERSONNEL

60 IRE 4. S2

Subcommittee on Linear Lumped-Constant Passive Circuits

1956–1960

L. WEINBERG, *Chairman*
J. A. Aseltine
R. Kahal
G. L. Matthaei
J. G. Truxal

Committee on Circuits

1956–1960

J. T. BANGERT, *Chairman* 1958–1960
W. A. LYNCH, *Chairman* 1956–1958
S. J. MASON, *Vice-Chairman* 1958–1960
J. T. BANGERT, *Vice-Chairman* 1956–1958

W. R. Bennett
J. G. Brainerd
A. R. D'Heedene
T. R. Finch
R. M. Foster
W. H. Huggins
R. Kahal
B. K. Kinariwala
H. L. Krauss
J. G. Linvill
J. C. Logue
S. J. Mason
C. H. Page
E. H. Perkins
E. J. Robb
J. J. Suran
A. P. Stern
W. N. Tuttle

Standards Committee

1959–1960

R. F. SHEA, *Chairman*

J. G. KREER, JR., *Vice-Chairman* C. H. PAGE, *Vice-Chairman* L. G. CUMMING, *Vice-Charman*

J. Avins
W. F. Bailey
M. W. Baldwin, Jr.
J. T. Bangert
W. R. Bennett
J. G. Brainerd
P. S. Carter
A. G. Clavier
S. Doba, Jr.
R. D. Elbourn
G. A. Espersen
R. J. Farber
D. G. Fink
G. L. Fredendall
E. A. Gerber
A. B. Glenn
V. M. Graham
R. A. Hackbusch
R. T. Haviland
A. G. Jensen
R. W. Johnston
I. Kerney
A. E. Kerwien
E. R. Kretzmer
G. S. Ley
Wayne Mason
D. E. Maxwell
P. Mertz
H. I. Metz
H. R. Mimno
E. Mittelmann
L. H. Montgomery, Jr.
G. A. Morton
R. C. Moyer
J. H. Mulligan, Jr.
A. A. Oliner
M. L. Phillips
R. L. Pritchard
P. A. Redhead
R. Serrell
W. A. Shipman
H. R. Terhune
E. Weber
R. B. Wilcox
W. T. Wintringham

Definitions Coordinator

C. H. Page

* Approved by the IRE Standards Committee, January 14, 1960. Reprints of IRE Standard 60 IRE 4.S2, may be purchased while available from the Institute of Radio Engineers, 1 East 79th Street, New York, N. Y. at $0.50 per copy. A 20 per cent discount will be allowed for 100 or more copies mailed to one address.

INTRODUCTION

All of the terms in this Standard apply to mathematical concepts which represent idealizations of physical phenomena. Thus the definitions apply to idealized models which are useful in describing properties of physical networks. However, the question of whether or not a certain term is applicable to a particular physical situation must be answered by the user.

Accordingly, the terms *impedance* and *admittance* are more properly thought of as *impedance function* and *admittance function*. Similarly, where the term *network* is used, reference is to an idealized model. Because of well-established usage, however, the shortened forms are preferred and are used in this set of definitions.

The functions to which the definitions apply are functions of the complex frequency, $s=\sigma+j\omega$, and are formed by taking specified ratios of the Laplace transforms (or other appropriate transforms) of the excitation and response. For signals which are simple exponential functions of time the ratios of the complex signal amplitudes can be used.

Wherever possible, the definitions apply to both lumped-parameter and distributed-parameter networks. The additional restrictions that apply when the networks are of the lumped-parameter type, are specified in a note associated with the particular definition.

The concept of realizability is used in some of the definitions, but no attempt has been made to include detailed properties of realizable functions.

DEFINITIONS

All-Pass Function. A *transmittance* which provides only phase shift, its *magnitude characteristic* being constant.

Note 1: For lumped-parameter networks, this is equivalent to specifying that the zeros of the function are the negatives of the poles.

Note 2: A realizable *all-pass function* exhibits nondecreasing phase lag with increasing frequency.

Note 3: A trivial *all-pass function* has zero phase at all frequencies.

Complementary Functions. Two *driving-point functions* whose sum is a positive constant.

Constant-Resistance (Conductance) Network. A network having at least one *driving-point impedance* (*admittance*) that is a positive constant.

Driving-Point Admittance. A *driving-point function* for which the excitation is a voltage and the response is a current.

Driving-Point Function. A *response function* for which the variables are measured at the same port (terminal pair).

Driving-Point Impedance. A *driving-point function* for which the excitation is a current and the response is a voltage.

Immittance. A *response function* for which one variable is a voltage and the other a current.

Note: Immittance is a general term for both impedance and admittance, used where the distinction is irrelevant.

Magnitude Characteristic. The absolute value of a *response function* evaluated on the imaginary axis of the complex-frequency plane.

Minimum Conductance Function. See *Minimum Resistance* (*Conductance*) *Function.*

Minimum-Driving-Point Function. A *driving-point function* that is a *minimum-resistance, minimum-conductance, minimum-reactance* and *minimum-susceptance function.*

Minimum-Phase Function. A *transmittance* from which a nontrivial realizable *all-pass function* cannot be factored without leaving a nonrealizable remainder.

Note: For lumped-parameter networks, this is equivalent to specifying that the function has no zeros in the interior of the right half of the complex-frequency plane.

Minimum-Reactance Function. A *driving-point impedance* from which a *reactance function* cannot be subtracted without leaving a nonrealizable remainder.

Note 1: For lumped-parameter networks, this is equivalent to specifying that the impedance function has no poles on the imaginary axis of the complex-frequency plane, including the point at infinity.

Note 2: A *driving-point impedance* (*admittance*) having neither poles nor zeros on the imaginary axis is both a *minimum-reactance* and a *minimum-susceptance function.*

Minimum-Resistance (Conductance) Function. A *driving-point impedance* (*admittance*) from which a positive constant cannot be subtracted without leaving a nonrealizable remainder.

Minimum-Susceptance Function. A *driving-point admittance* from which a *susceptance function* cannot be subtracted without leaving a nonrealizable remainder.

Note 1: For lumped-parameter networks, this is equivalent to specifying that the admittance function has no poles on the imaginary axis of the complex-frequency plane, including the point at infinity.

Note 2: A driving-point *immittance* having neither poles nor zeros on the imaginary axis is both a *minimum-susceptance* and a *minimum-reactance function.*

Phase Characteristic. The angle of a *response function* evaluated on the imaginary axis of the complex-frequency plane.

Reactance Function. The *driving-point impedance* of a lossless network.

Note: This is an odd function of the complex frequency.

Realizable Function. A response function which can be realized by a network containing only positive resistance, inductance, capacitance, and ideal transformers.

Note: This is the sense of realizability in the theory of linear, passive, reciprocal, time-invariant networks.

Response Function. The ratio of response to excitation, both expressed as functions of the complex frequency, $s=\sigma+j\omega$.

Note: The response function is the Laplace transform of the response due to unit impulse excitation.

Susceptance Function. The *driving-point admittance* of a lossless network.

Note: This is an odd function of the complex frequency.

Transfer Admittance. A *transmittance* for which the excitation is a voltage and the response is a current.

(Transfer) Current Ratio. A *transmittance* for which the variables are currents.

Note: The word "transfer" is frequently dropped in current usage.

Transfer Function. A relationship between one system variable and another that enables the second variable to be determined from the first. See also *Transmittance.*

Transfer Immittance. See *Transmittance.*

Transfer Impedance. A *transmittance* for which the excitation is a current and the response is a voltage.

(Transfer) Voltage Ratio. A *transmittance* for which the variables are voltages.

Note: The word "transfer" is frequently dropped in current usage.

Transmittance (Transfer Function). A *response function* for which the variables are measured at different ports (terminal pairs).

IRE Standards on Circuits: Definitions of Terms for Linear Signal Flow Graphs, 1960*

COMMITTEE PERSONNEL

60 IRE 4. S1

Committee on Circuits

J. T. BANGERT, *Chairman* 1958–1960
W. A. LYNCH, *Chairman* 1956–1958

S. J. MASON, *Vice-Chairman* 1958–1960 J. T. BANGERT, *Vice-Chairman* 1956–1958

W. R. Bennett	R. Kahal	C. H. Page
J. G. Brainerd	B. N. Kinariwala	E. H. Perkins
A. R. D'Heedene	H. L. Krauss	E. J. Robb
T. R. Finch	J. G. Linvill	J. J. Suran
R. M. Foster	J. C. Logue	A. P. Stern
W. H. Huggins	S. J. Mason	W. N. Tuttle

Standards Committee

1959–1960

R. F. SHEA, *Chairman*

J. G. KREER, JR., *Vice-Chairman* C. H. PAGE, *Vice-Chairman* L. G. CUMMING, *Vice-Chairman*

J. Avins	R. J. Farber	A. E. Kerwien	R. C. Moyer
W. F. Bailey	D. G. Fink	E. R. Kretzmer	J. H. Mulligan, Jr.
M. W. Baldwin, Jr.	G. L. Fredendall	G. S. Ley	A. A. Oliner
J. T. Bangert	E. A. Gerber	Wayne Mason	M. L. Phillips
W. R. Bennett	A. B. Glenn	D. E. Maxwell	R. L. Pritchard
J. G. Brainerd	V. M. Graham	P. Mertz	P. A. Redhead
P. S. Carter	R. A. Hackbusch	H. I. Metz	R. Serrell
A. G. Clavier	R. T. Haviland	H. R. Mimno	W. A. Shipman
S. Doba, Jr.	A. G. Jensen	E. Mittelmann	H. R. Terhune
R. D. Elbourn	R. W. Johnston	L. H. Montgomery, Jr.	E. Weber
G. A. Espersen	I. Kerney	G. A. Morton	R. B. Wilcox

W. T. Wintringham

Definitions Coordinator

C. H. Page

Branch. A line segment joining two *nodes*, or joining one *node* to itself.

Note: See also *Directed Branch.*

Branch Input Signal. The signal, x_j, at the input end of branch jk.

Branch Output Signal (of branch jk). The component of signal x_k contributed to node k via branch jk.

Branch Transmittance. The ratio of *branch output signal* to *branch input signal.*

Cascade Node (Branch). A *node* (*branch*) not contained in a *loop.*

Cofactor (or Path Cofactor). See *Path* (*Loop*) *Factor.*

Dependent Node. A *node* having one or more incoming *branches.*

* Approved by the IRE Standards Committee, January 14, 1960. Reprints of this Standard 60 IRE 4.S1, may be purchased while available from the Institute of Radio Engineers, 1 East 79th Street, New York, N. Y., at $0.25 per copy. A 20 per cent discount will be allowed for 100 or more copies mailed to one address.

Directed Branch. A *branch* having an assigned direction.

Note: In identifying the branch direction, the branch, *jk*, may be thought of as outgoing from node *j* and incoming at node *k*. Alternatively, branch *jk* may be thought of as originating or having its input at node *j*, and terminating or having its output at node *k*. The assigned direction is conveniently indicated by an arrow pointing from node *j* toward node *k*.

Feedback Node (Branch). A *node* (*branch*) contained in a *loop*.

Graph Determinant. One plus the sum of the *loop-set transmittances* of all *non-touching loop sets* contained in the graph.

Note 1: The graph determinant is conveniently expressed in the form:

$$\Delta = (1 - \sum L_i + \sum L_i L_j - \sum L_i L_j L_k + \cdots)$$

where L_i is the loop transmittance of the ith loop of the graph, and the first summation is over all of the different loops of the graph, the second is over all of the different pairs of non-touching loops, and the third is over all the different triplets of non-touching loops, etc.

Note 2: The graph determinant may be written alternatively as

$$\Delta = [(1 - L_1)(1 - L_2) \cdots (1 - L_n)]\dagger$$

where $L_1, L_2, \cdots, L_n$, are the loop transmittances of the n different loops in the graph, and where the dagger indicates that, after carrying out the multiplications within the brackets, a term will be dropped if it contains the transmittance product of two touching loops.

Note 3: The graph determinant reduces to the *return difference* for a graph having only one *loop*.

Note 4: The graph determinant is equal to the determinant of the coefficient equations.

Graph Transmittance. The ratio of signal at some specified *dependent node*, to the signal applied at some specified *source node*.

Note: The graph transmittance is the weighted sum of the path transmittances of the different *open paths* from the designated *source node* to the designated *dependent node*, where the weight for each path is the *path factor* divided by the *graph determinant*.

Loop (Feedback Loop). A simple closed *path*.

Loop Factor. See *Path Factor*.

Loop Graph. A *signal flow graph* each of whose branches is contained in at least one *loop*.

Note: Any *loop* graph embedded in a general graph can be found by removing the *cascade branches*.

Loop-Set Transmittance. The product of the negatives of the *loop transmittances* of the *loops* in a set.

Loop Transmittance. The product of the *branch transmittances* in a *loop*.

Loop Transmittance of a Branch. The *loop transmittance* of an interior node inserted in that branch.

Note: A branch may always be replaced by an equivalent sequence of *branches*, thereby creating interior *nodes*.

Loop Transmittance of a Node. The *graph transmittance* from the *source node* to the *sink node* created by splitting the designated *node*.

Node. One of the set of discrete points in a flow graph.

Node Absorption. A flow-graph transformation whereby one or more *dependent nodes* disappear and the resulting graph is equivalent with respect to the remaining *node signals*.

Note: For example, a circuit analog of *node absorption* is the Star-Delta transformation.

Node Signal. A variable, x_k, associated with node *k*.

Non-Touching Loop Set. A set of *loops* no two of which have a common *node*.

Open Path. A *path* along which no *node* appears more than once.

Path. Any continuous succession of *branches*, traversed in the indicated branch directions.

Path (Loop) Factor. The *graph determinant* of that part of the graph not touching the specified *path* (*loop*).

Note 1: A *path* (*loop*) *factor* is obtainable from the *graph determinant* by striking out all terms containing transmittance products of *loops* which touch that *path* (*loop*).

Note 2: For loop L_k, the *loop factor* is

$$-\partial\Delta/\partial L_k.$$

Path Transmittance. The product of the *branch transmittances* in that *path*.

Return Difference. One minus the *loop transmittance*.

Signal Flow Graph. A network of *directed branches* in which each dependent *node signal* is the algebraic sum of the incoming *branch* signals at that *node*.

Note: Thus, $x_1 t_{1k} + x_2 t_{2k} + \cdots + x_n t_{nk} = x_k$, at each dependent node *k*, where t_{jk} is the *branch transmittance* of branch *jk*.

Sink Node. A *node* having only incoming *branches*.

Source Node. A *node* having only outgoing *branches*.

Split Node. A *node* that has been separated into a *source node* and a *sink node*.

Note 1: Splitting a *node* interrupts all signal transmission through that *node*.

Note 2: In splitting a *node*, all incoming *branches* are associated with the resulting *sink node*, and all outgoing branches with the resulting *source node*.

Error Probabilities for Telegraph Signals Transmitted on a Fading FM Carrier*

BRUCE B. BARROW†, SENIOR MEMBER, IRE

Summary—This paper presents an analysis of error probabilities for multiplexed binary telegraph signals that are used to frequency-modulate an RF carrier that is subsequently corrupted by fading and noise. Frequency-shift keying, amplitude keying, and phase-shift keying are considered. It is shown that most telegraph errors occur when the carrier fades below threshold, and the principal results of the study therefore concern the effects of the FM threshold on error rate.

Various methods of diversity reception are considered. For a maximal-ratio baseband combiner and certain types of telegraph receiver, a method is given for extending the results obtained for a single receiver to *n*th-order diversity. This makes it possible to use experimental data to describe either the threshold or the fading of the carrier. Study of threshold models indicates a serious conflict between the requirements of telephone channels and those of telegraph channels. Furthermore, good telegraph performance demands great care in the design of diversity combiners to work *below* threshold. The analysis pertains most directly to troposcatter systems, but the general conclusions regarding the effect of FM threshold should be relevant also for fading transmission paths such as those met in line-of-sight and telemetry.

I. Introduction

A. The Problem

THIS paper presents an analysis of error probabilities for binary telegraph signals transmitted on an FM system disturbed by fading and noise. In such transmission the telegraph signal, multiplexed with other signals to be transmitted, becomes the baseband signal used to frequency-modulate an RF carrier. If the received RF carrier fades below the threshold of the FM receiver, the signal delivered to the telegraph equipment deteriorates markedly. Even if deep fades are rare (Rayleigh fading with diversity reception, for example), most telegraph errors will occur below threshold. The principal problem examined here is the effect of the FM threshold on telegraph error rate.

The analysis that follows is based on theoretical models (details given in Section I-B), though particular care is taken to discuss the results in terms of the design of practical systems. Only the error probabilities for elements (marks or spaces) are calculated in this paper. No attempt is made to consider character-error probabilities, or the effect that the clustering of element errors will have on various telegraph codes. It is assumed that the fading affects the amplitude of the received waveform but does not distort it; the noise is taken to be additive, with a flat spectrum and a Gaussian amplitude distribution. The analysis is first carried through for frequency-shift keyed (FSK) telegraph signals, and the results are then extended to apply to phase-shift-keyed (PSK) and amplitude-keyed (AK) signals. The extension is simple and direct, and results for all three systems are qualitatively similar. Unless otherwise stated, however, equations and figures apply only to the FSK/FM system.

In Section II a general result is given that relates the error probability of a system with a single FM receiver to one with *n*th-order diversity. This result applies for maximal-ratio baseband combining and either noncoherent FSK or differentially-coherent PSK telegraph receivers, and it holds for any FM threshold and for any fading distribution. Therefore experimental data for a threshold characteristic or for fading can easily be used in an analysis. The Section contains calculated results for Rayleigh fading of the RF carrier and for two different threshold characteristics, which represent extremes.

Section III gives distribution curves for the telegraph-receiver signal-to-noise ratio for each of the threshold models and for either baseband or IF combining. These results are used in Section IV, where various diversity receiving systems are compared. Section IV also compares FSK/FM, PSK/FM, and AK/FM. These comparisons lead to a discussion of the importance to telegraph performance of good combiner operation below threshold, of the difficulties involved in building a combiner to work below threshold, of the basic conflicts between telephone and telegraph requirements, and of possible practical solutions.

Section V is a summary of the conclusions, and the reader who likes to know where he is going may wish to read it before beginning with Section II. Appendix I contains the mathematical derivations, and Appendix II is a short study based on parameter values found in a particular tropospheric scatter system designed to use FSK/FM.

Many of the conclusions of this paper will apply quite generally to systems that involve data transmission over a fading carrier into a receiver with a threshold. Whether the telegraph signal produces changes in frequency, phase, or amplitude, most telegraph errors may be expected when the RF carrier falls below threshold and therefore the below-threshold performance of the combiner and the FM receiver will critically affect the error probability. Likewise, if the errors occur below threshold, increasing the FM bandwidth will not in

* Received by the IRE, October 26, 1959; revised manuscript received, March 28, 1960.

† SHAPE Air Defense Technical Center, The Hague, Netherlands.

general reduce the error probability, whether the carrier fades on a troposcatter path, a microwave relay, or a telemetry link.

B. The Model Studied

Transmitted Signals: The telegraph message is assumed to be coded into binary form. The elementary signals of the binary code, called mark and space, are assigned separate waveforms, which are of finite duration. During transmission of a message one and only one waveform is present at a time. In FSK telegraphy the two waveforms occupy separate frequency bands, are uncorrelated, and have equal energy.[1] In AK telegraphy the telegraph carrier is keyed on and off, so that one of the waveforms is identically zero. In binary PSK (phase-reversal telegraphy) the two waveforms are identical except for a change in sign.

Fading Medium: The fading medium is assumed to be frequency nonselective, so that the entire band occupied by the modulated carrier is uniformly affected. Changes in RF carrier amplitude are assumed to occur slowly with respect to the interval of time occupied by a single element. Wherever a specific distribution function is required, the received RF carrier is assumed to be Rayleigh distributed. All of these assumptions are appropriate to describe fading on troposcatter links that occurs within intervals of a few minutes.

Diversity Branches: The communication path between a single transmitter and a single receiving antenna and associated receiver is here called a *diversity branch.* The receiving equipment associated with a single diversity branch is called an *elementary receiver.* Diversity receiving systems take advantage of the fact that, under certain conditions, fading occurs more or less independently in different diversity branches. We assume that fading on the various diversity branches is entirely independent and that the mean carrier strength is the same for each branch.

Where these conditions are not met, the effect is similar to that produced by a decrease in the order of diversity. Precise calculations for a system with no threshold, using maximal-ratio combination (see below), may be made following the Pierce-Stein method.[2] The effects of introducing a threshold may subsequently be estimated from the results presented in this paper, and superposed on the Pierce-Stein result. This somewhat rough procedure should not lead to gross errors, especially since the important effects of introducing a threshold are shown below to be independent of the order of diversity (or nearly so).

FM Receiver: The model FM receiver, whose function it is to recover the baseband from the received RF carrier plus noise, produces in the telegraph receiver a signal-to-noise ratio that above some threshold is proportional to the carrier-to-noise ratio at the input to the limiter-discriminator. In what follows the two ratios are called the *telegraph-receiver SNR* and *IF SNR*, respectively. Where a model is needed, telegraph-receiver SNR is assumed to behave in one of the following ways below threshold: a) for the smooth-threshold model it is assumed to decrease two db for every one db decrease in IF SNR; b) for the abrupt-threshold model it is assumed to drop to zero below threshold. In practice there is no precisely definable threshold, and Appendix II shows the complex relationship to be expected in a particular practical case. The idealized models represent extremes, however, in the sense that the threshold curve for a real receiver must be less steep than that of the abrupt-threshold model and will ordinarily be steeper than that of the smooth-threshold model. Therefore the models make it possible to predict some of the general effects of a practical threshold.

Noise: The restrictions on the interfering noise are discussed below, in connection with the combiner and telegraph-receiver models.

Combiner: Most of the results derived in what follows assume maximal-ratio combination of the several signals derived from the different diversity branches. The word "maximal-ratio" applies to a particular technique of combination first analyzed by Brennan in 1955.[3] This technique produces the highest SNR obtainable from the linear addition of signals from various diversity branches, but it requires knowledge of the signal and noise powers in each diversity branch. Maximal-ratio combination of either IF or baseband signals is possible, though in either case the signals to be combined must be in phase with each other or must be brought into phase. The practical difficulties that arise, especially for below-threshold combining, are discussed in Section IV, where the equal-gain combiner, a simpler device, is introduced for comparison.

Theory requires, for both maximal-ratio combination and equal-gain combination, that the noise in each diversity branch be additive, independent of the signal, and have zero mean, and that the noise waveforms in different diversity branches be uncorrelated. For the equal-gain combiner we require also that the noise powers in the different diversity branches be equal. The noise in the RF and IF sections of the receiver will ordinarily satisfy these requirements, but if the noise is externally produced (such as jamming or cosmic noise), it may not. Even if noise at IF meets the stated requirements, and therefore presents no obstacle to IF combination, noise at baseband frequencies will generally not behave so well. This is especially true when the RF carrier fades below threshold, the case of greatest interest for telegraph reception. During such fades one may

[1] The "energy" of a waveform is the integral of its square value. To say that two waveforms are uncorrelated implies that the integral of their product is very small compared with the energy of each of them.

[2] J. N. Pierce and S. Stein, "Multiple diversity with nonindependent fading," PROC. IRE, vol. 48, pp. 89–104; January, 1960.

[3] D. G. Brennan, "Linear diversity combining techniques," PROC. IRE, vol. 47, pp. 1075–1102; June, 1959.

expect nonadditive noise and noise that is not independent of the signal. If these components are not small, compared with the additive, independent noise, there will be some degradation of the theoretical performance of the maximal-ratio baseband combiner. The point requires a careful experimental study; very rough experimental checks do not indicate the presence of such abnormalities as would cause the theory of maximal-ratio combination to be useless. There is, of course, no question of any ordinary equal-gain combination at baseband frequencies, because of the unequal noise powers in the different diversity branches.

Telegraph Receiver: Synchronous, matched-filter telegraph receivers are postulated to detect the telegraph signal in the appropriate portion of the demodulated baseband, after combination. "Synchronous" reception implies that the time base of the telegraph message is known at the receiver. In other words, the receiver knows when the expect an element (mark or space). "Matched-filter" implies that the receiver has built into it precise knowledge of the form of the possible transmitted signals (the mark and space elements), so that at the end of each element interval the receiver can indicate "mark" or "space" on the basis of which transmitted signal appears to be the more likely cause of the received signal. Such a receiver is the realization of the probability-computing receiver discussed by Woodward.[4]

Both "coherent" and "noncoherent" FSK receivers are considered. A coherent receiver is assumed to know *a priori* the phase of the elementary waveform; a noncoherent receiver does not, and must therefore operate with an envelope detector. For amplitude-keyed telegraph reception only a coherent receiver is discussed, while for PSK both coherent and "differentially-coherent" receivers are examined. The differentially-coherent receiver does not work with a fixed phase base, but compares the last element received with the next-to-last, deciding whether the phase difference between the two indicates a phase reversal at the transmitter.

The error relationships used below require that the interfering noise be additive, Gaussian, and flat over the bandwidth occupied by mark and space waveforms. The question of additivity was discussed in connection with the combiner, and flatness of spectrum can be assumed since the telegraph signal will in general occupy only a small portion of the baseband. For below-threshold carriers, baseband noise will not be strictly Gaussian, but the narrow-band multiplex filter that precedes the telegraph receiver will ensure that the noise at telegraph-receiver input is very nearly Gaussian. Note that a wide-band telegraph signal, such as would be used on a troposcatter link designed only for very high speed data transmission, must be examined somewhat differently. Much of the argument below would apply, but one would have to consider a nonflat noise spectrum, threshold behavior that depends on baseband frequency, and non-Gaussian noise. The last two appear difficult.

[4] P. M. Woodward, "Probability and Information Theory with Applications to Radar," Pergamon Press, Ltd., London, Eng., ch. 4; 1955.

II. Element-Error Probability in FSK/FM Systems

A. A Theorem for the Maximal-Ratio Baseband Combiner

For a matched-filter FSK telegraph receiver using noncoherent (envelope) detection, the probability of element error is[5]

$$P(R) = \tfrac{1}{2}e^{-R/2}, \tag{1}$$

where R is the telegraph-receiver SNR, defined as the quotient of the energy received in the element divided by the power density of the additive Gaussian noise, in watts/cps (single-ended spectrum). Consider an elementary receiver with a fading carrier, so that R is a random variable with probability density function f. Then the average probability of element error is

$$P_1 = \int_0^\infty \tfrac{1}{2}e^{-r/2}f(r)dr. \tag{2}$$

If we have n such elementary receivers used in a diversity system with maximal-ratio baseband combining, then, from a theorem proved in Appendix I, the average probability of element error is

$$P_n = \tfrac{1}{2}(2P_1)^n. \tag{3}$$

This result enables us to proceed easily from an elementary receiver to nth-order diversity. Note that no assumptions have restricted the form of the probability density function f. This means that (3) holds for any fading distribution and for any type of FM threshold in the elementary receivers. It is easy to integrate (2) numerically if f is derived from experimental measurements. Thus one can consider non-Rayleigh fading, or the effects of changing a parameter in the FM receiver, for example, and base the analysis on measured fading statistics or on experimentally observed threshold characteristics.

Eq. (3) holds for a much broader class of communication links than the FSK/FM links that form the principal subject of this investigation. It holds, for example, if a phase-reversal (binary PSK) signal modulates the RF carrier, if differentially-coherent reception is used. It holds also if the RF transmission is suppressed-carrier AM, whether SSB or DSB.

[5] S. Reiger, "Error probabilities of binary data transmission systems in the presence of random noise," 1953 IRE Convention Record, pt. 9, pp. 72–79, (22). This equation also holds true with nonmatched filters under certain assumptions, if R is suitably defined. A simple example may be adduced where the filter is matched to a central portion of the element and is zero elsewhere. Such design might intentionally be introduced to avoid interelement interference when synchronism is imperfect.

B. Application to Special Cases with Rayleigh Fading

The No-Threshold Receiver: Let the IF SNR be X. Then for Rayleigh fading the probability density function of X is given by[6]

$$w_1(x) = \langle X\rangle^{-1} e^{-x/\langle X\rangle}, \tag{4}$$

where $\langle X\rangle$ is the mean value of X, and x is a dummy variable. In the no-threshold receiver, the telegraph-receiver SNR is proportional to X,

$$R = bX \tag{5}$$

and the probability density function of R is

$$g(r) = A^{-1} e^{-r/A}, \tag{6}$$

where

$$A \equiv b\langle X\rangle. \tag{7}$$

The constant of proportionality b may be obtained experimentally. For some purposes it may be useful to calculate b theoretically in terms of IF bandwidth, per-channel deviation of the RF carrier, and the like. Some indications of the method of calculation are given in Appendix II.

To write of a "no-threshold" receiver implies either that the FM threshold affects only such low values of R that it may be neglected (something that does not appear to happen in practical systems), or that the results apply to something other than FM (SSB-AM, for example). Even for FM the results are interesting, however, as limiting cases. When g is substituted for f, (2) and (3) give, for the average probability of element error in an nth-order-diversity no-threshold receiver with Rayleigh fading,

$$p_n(A) = \tfrac{1}{2}(\tfrac{1}{2}A + 1)^{-n}. \tag{8}$$

The Abrupt-Threshold Model: Here we postulate an FM receiver for which R, below threshold, drops abruptly to zero. Thus

$$R = 0 \qquad X < x_t \tag{9a}$$

$$= bX \qquad X \geq x_t, \tag{9b}$$

where x_t is the IF SNR at threshold. If the distribution of X is given by (4), the probability density function of R for the abrupt-threshold model will be

$$g_a(r) = cu_0(r) + A^{-1} e^{-r/A} u_1(r - r_t), \tag{10}$$

where

$$c \equiv 1 - \exp\left[-r_t/A\right], \tag{11}$$

$$r_t \equiv bx_t \tag{12}$$

$$u_1(t) = 0 \qquad t < 0 \tag{13a}$$

$$= 1 \qquad t \geq 0 \tag{13b}$$

and u_0 is that function (the impulse function) which when integrated gives u_1. The function u_0 is needed here to express the fact that there is a finite probability, equal to c, that R is equal to zero.

When g_a is substituted for f in (2), integration gives

$$p_{a1}(A, r_t) = \tfrac{1}{2}c + \frac{\exp\left[-r_t/A - r_t/2\right]}{A + 2} \tag{14}$$

and (3) allows this to be extended to nth-order diversity. Fig. 1 shows $p_{an}(A, r_t)$ plotted vs A for several different values of r_t. For large r_t all errors will occur below threshold [i.e., the second term in (14) will drop out], and the error rate will depend only upon c, which is a function of the ratio r_t/A. The physical implication is that raising r_t by one db will have the same effect as decreasing A by one db, regardless of the order of diversity.

The Smooth-Threshold Model: Here we postulate an FM receiver that operates so that

$$R = bX^2/x_t \qquad X \leq x_t \tag{15a}$$

$$= bX \qquad X \geq x_t. \tag{15b}$$

Calculation of the probability of element error follows the same steps as for the abrupt-threshold model, and Appendix I contains the details. Fig. 2 shows the results graphically. Again the family of curves is roughly parallel, though the spacing is closer than in Fig. 1. It turns out, in fact, that for large r_t the error probability depends only upon the parameter r_t/A^2, in contrast to the abrupt-threshold case, where the parameter was r_t/A.

C. Implications for System Design

Summary of Error-Probability Analysis: There are several conclusions to be emphasized at this point in the analysis:

a) Since 10 would be a very low level for r_t in a practical system, virtually all element errors occur while the receiver is operating below threshold. (See the example of Appendix II for typical parameter values.)

b) The curves for error probability vs average power, drawn for different values of r_t, are nearly parallel. Therefore the degradation that r_t causes in comparison with a no-threshold system, expressed in decibels, depends neither upon the order of diversity nor upon the average signal-to-noise ratio.

The first of these holds only for fading conditions, of course, but it holds even when deep fades are rare. For example, with quadruple-diversity combination, deep fades occur only when four diversity branches simultaneously have deep fades. Even so, with Rayleigh fading on the individual branches, the errors still occur below threshold. The second conclusion holds for the

[6] Throughout this paper distribution functions are assumed to be zero for negative values of the random variable. Note that (4) does not give the Rayleigh distribution, which pertains to envelope *amplitude*. The variable X is a *power* ratio.

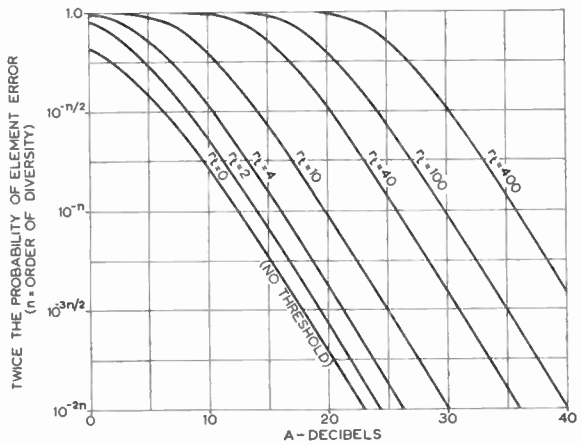

Fig. 1—Probability of element error with Rayleigh fading: maximal-ratio baseband combiner with abrupt-threshold model.

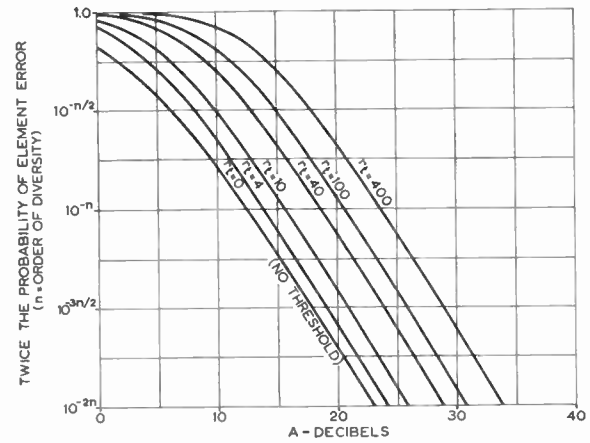

Fig. 2—Probability of element error with Rayleigh fading: maximal-ratio baseband combiner with smooth-threshold model.

models studied, and it presumably holds for usual cases that might be expected in practice. It is not as general a rule as that expressed by (3), however, and follows from it only under some restrictions.

Note that for large values of r_t, which are common in practice, there will be a considerable difference in performance between the two threshold models. Since an improperly designed combiner may cause a smooth-threshold receiver to act, in effect, like an abrupt-threshold one, combiner design becomes critical. This is discussed at length in Section IV.

Effect of Increasing Link Strength: By an increase in link strength is meant an increase in the parameter A. This may be obtained by increasing transmitter power or antenna gain, or by decreasing receiver noise figure, etc. The effect may be seen in Figs. 1 and 2. The decrease in probability of element error does not appear to depend upon whether or not there is a threshold, or upon the model used to describe the threshold. It does, of course, depend upon the order of diversity.

Effect of Increasing Level of Telegraph Carrier: The level at which the telegraph signals are to be inserted in the baseband may be chosen with some freedom. The designer must ask whether interchannel interference would remain below an acceptable level, and whether an unreasonable frequency deviation of the RF carrier would result, before he can increase the level of the telegraph carriers.[7] He must also ask whether anything would be gained.

Increasing the level of a telegraph carrier in the baseband increases both A and r_t by the same amount. By contrast, increasing transmitter power increases A alone. Since the probability of error with the smooth-threshold model depends on r_t/A^2, increasing telegraph-carrier level by one db will achieve the same result as an increase in transmitter power of 0.5 db. With the abrupt threshold model, on the other hand, there would be no change since the error probability depends on r_t/A.

Effect of Changing Position in Baseband: If the FM receiver operates without pre-emphasis, the high-frequency portion will be noisier than the low when operating above threshold. Below threshold, however, the power spectrum of baseband noise becomes nearly flat. Since the errors in a properly designed system will occur well below threshold, no portion of the baseband will be markedly superior for telegraph traffic. This conclusion is supported by the example worked out in Appendix II. If pre-emphasis is introduced into the system, the effect is to increase the level of those telegraph carriers that fall into the higher baseband frequencies, with the results noted above. The higher-frequency telegraph carriers will become somewhat superior, but at a cost of some degradation of the lower-frequency carriers (since the rms value of the baseband signal must be held constant if a fair comparison is to be made). Certainly the use of pre-emphasis cannot be justified by considerations of telegraph traffic.

Effect of Increasing Deviation of RF Carrier: If RF-carrier deviation is increased without increasing the IF bandwidth of the receiver, this in effect increases the level of the telegraph carrier. As pointed out above, however, increasing the level of the telegraph carrier by one db is generally less effective in reducing error probability than increasing transmitter power by one-half db. Furthermore, one cannot increase carrier deviation by very much unless the bandwidth of the receiver is also broadened. If IF bandwidth is increased, the threshold level of the carrier will be similarly increased, and the receiver will have to operate below threshold for a larger portion of the time. In addition, below-threshold performance for the same carrier power will in general so degenerate that the telegraph-receiver SNR will be lower, even though the carrier deviation has been increased. Thus there will be a net loss. This is shown with an example in Appendix II.

[7] In a system that carries both telephone and telegraph traffic, the interchannel interference will not ordinarily be high enough to cause telegraph errors, even with so-called busy-hour loading. Interchannel interference does, however, introduce telegraph tones into the telephone channels, and these annoying and undesired components must be held at a very low level.

The conclusion is that, from the point of view of FSK telegraph signals, the "FM improvement" is of questionable value, and increasing the deviation and bandwidth together is in general undesirable. In other words, improving above-threshold performance is no help for FSK telegraph, since the errors occur below threshold anyway, and the steps taken to improve FM performance above threshold tend to degrade performance below threshold.

III. Probability Distributions of Telegraph-Receiver SNR

A. Introduction

This section concerns the distribution functions of R and R_n, the telegraph-receiver SNR's for an elementary receiver and for an nth-order-diversity receiver, respectively. The preceding section demonstrated that a knowledge of the distribution function of R was sufficient to calculate error probability for any order of diversity, assuming maximal-ratio baseband combining and noncoherent matched-filter detection. Section IV treats other methods of combination and detection, and other types of telegraph signals, as well as problems related to the design of improved equipment. These topics require much more information about the distribution functions of the signal-to-noise ratios. Such distribution functions are calculated below for Rayeligh fading and the already familiar threshold models.

B. Distribution Functions for Maximal-Ratio Baseband Combining

No-Threshold System: With no threshold and maximal-ratio combining, the probability density function of R_n will be[8]

$$g_n(r) = [r^{n-1}/A^n(n-1)!]e^{-r/A}. \tag{16}$$

The distribution function, obtained by integrating g_n, is

$$G_n(r) = 1 - e^{-r/A}\sum_{m=0}^{n-1}\frac{r^m}{m!A^m} = e^{-r/A}\sum_{m=n}^{\infty}\frac{r^m}{m!A^m}. \tag{17}$$

Abrupt-Threshold Model: For nth-order diversity the telegraph-receiver SNR will be the sum of n random variables distributed according to the probability density function given in (10). The distribution function of R_n may therefore be obtained using standard methods, and Appendix I contains the derivation. Fig. 3 shows curves calculated for dual and quadruple diversity, for selected values of r_t/A. The figure shows clearly the degradation produced by a threshold, even for SNR's above r_t.

[8] F. J. Altman and W. Sichak, "A simplified diversity communication system for beyond-the-horizon links," IRE Trans. on Communications Systems, vol. CS-4, pp. 50–55; March, 1956. The result is also given by Brennan, *op. cit.*, see (29).

Smooth-Threshold Model: Integration of (4) gives, for the distribution function of X,

$$W_1(x) = 1 - e^{-x/(X)}. \tag{18}$$

Since (15), the expression characterizing the smooth-threshold model, indicates a one-to-one relation between R and X, simple substitution of this relation in (18) will give the distribution function of R

$$G_{s1}(r) = 1 - \exp\left[-(r_t r)^{1/2}/A\right] \qquad r \le r_t \tag{19a}$$

$$= 1 - \exp\left[-r/A\right] \qquad r \ge r_t. \tag{19b}$$

It is rather difficult to operate with this function to obtain the distribution functions for higher orders of diversity, but the method of calculation followed for dual and quadruple diversity is sketched in Appendix I. Fig. 4 shows curves calculated for several values of r_t/A.

It is interesting to observe in Fig. 4 that the dual-diversity curves below threshold run more or less parallel to the curve for G_1 (elementary receiver, no threshold). Similarly, the quadruple-diversity curves below threshold approach the same slope as the curve for G_2 (dual diversity, no threshold). This is no coincidence, for in Appendix I it is shown that G_1 and G_{s2} both decrease as r when r approaches zero, while G_2 and G_{s4} both decrease as r^2.

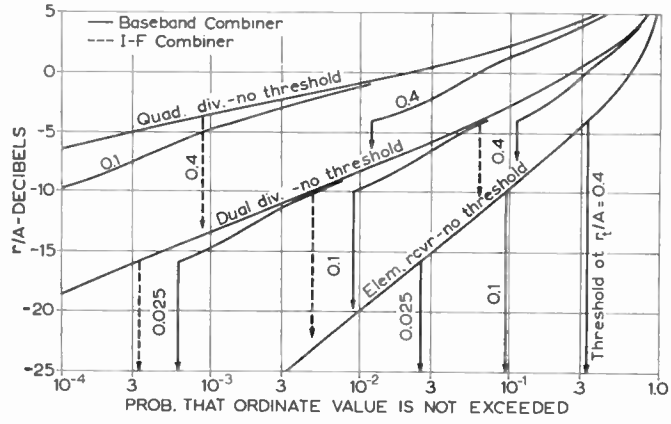

Fig. 3—Distribution functions for telegraph-receiver SNR: maximal-ratio combiners with abrupt-threshold model.

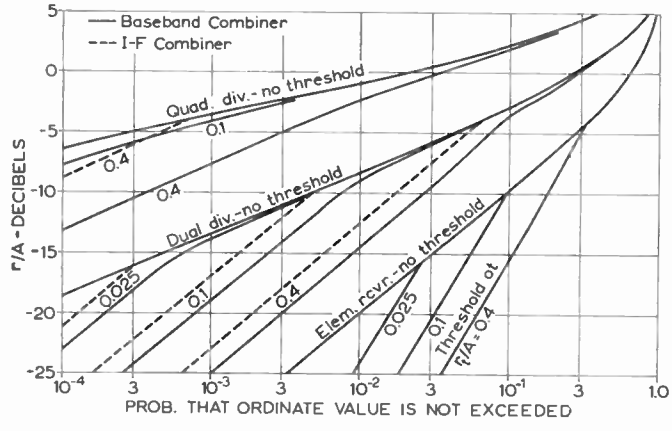

Fig. 4—Distribution functions for telegraph-receiver SNR: maximal-ratio combiners with smooth-threshold model.

C. Distribution Functions for Maximal-Ratio IF Combining

The IF Signal-to-Noise Ratio: It is much easier to perform calculations for the maximal ratio IF combiner than for the baseband combiner, because the random variables are added before the nonlinear threshold function must be introduced. The distribution function of X_n, the IF SNR after maximal ratio combining of n independent Rayleigh fading signals is

$$W_n(x) = 1 - e^{-x/\langle X\rangle} \sum_{m=0}^{n-1} \frac{x^m}{m!\langle X\rangle^m}$$

$$= e^{-x/\langle X\rangle} \sum_{m=n}^{\infty} \frac{x^m}{m!\langle X\rangle^m} . \qquad (20)$$

This is, of course, the same type of distribution as that given in (17) for R_n in a system without threshold.

Abrupt-Threshold Model: The dashed arrows in Fig. 3 show the result of passing the random variable X_n through a receiver with abrupt threshold. The distribution of the telegraph-receiver SNR, R_n, remains the same as it would be in a no-threshold system for all values of SNR above threshold, *i.e.*, greater than r_t. The probability that R_n will be below threshold, which is for this model the same as the probability that R_n will fall to zero, is simply $G_n(r_t)$. The complete distribution function for R_n is

$$G_{an}(r)^{\mathrm{IF}} = G_n(r) \qquad r \geq r_t \qquad (21a)$$

$$= G_n(r_t) \qquad r \leq r_t. \qquad (21b)$$

So far as telegraph reception is concerned, the advantage of IF combining over baseband combining is that the probability that R_n will fall to zero is less with the IF combiner. Fig. 3 clearly shows the difference.

Smooth-Threshold Model: Substitution of (7) and (15), in (20) gives the distribution function for R_n when X_n is passed through the smooth-threshold model.

$$G_{sn}(r)^{\mathrm{IF}} = G_n(r) \qquad r \geq r_t \qquad (22a)$$

$$= G_n([r_t r]^{1/2}) \qquad r \leq r_t. \qquad (22b)$$

A simple geometric interpretation of (22) is easily seen in the dashed curves in Fig. 4—below threshold the curves for the smooth-threshold model drop two db for every one db drop in the no-threshold curves. Fig. 4 also shows clearly the difference between baseband combining and IF combining for this threshold model.

D. Distributions under Condition Error has Occurred

At what SNR's are telegraph errors likely to occur? This question bears directly on questions of equipment design and system planning, and to answer it requires calculation of some conditional probability distribution functions of R_n. It is not sufficient to observe, from (1), that error probability increases as R decreases, because deep fades are less likely than shallow fades.

If the integral of (2) is taken only over the range between 0 and r, we obtain the probability that an element error occurs at some value of R less than r. Dividing by the total probability of error gives an expression for the fraction of errors that occur at SNR less than r. In other words, it gives the probability distribution of R (or R_n) under the condition that an error has occurred.

No-Threshold System: Fig. 5 shows conditional distribution functions of SNR given that an error has occurred. These functions, denoted by $V_n(r|\text{error})$, have the same form as the G_n (17), and are derived in Appendix I. From Fig. 5 it appears that, for large A, the conditional distribution functions depend very little upon A. Since A must be greater than 10 if the element error rate is not to be unreasonably large, we may conclude that the critical range of SNR values at which errors occur depends very little upon the mean signal strength.

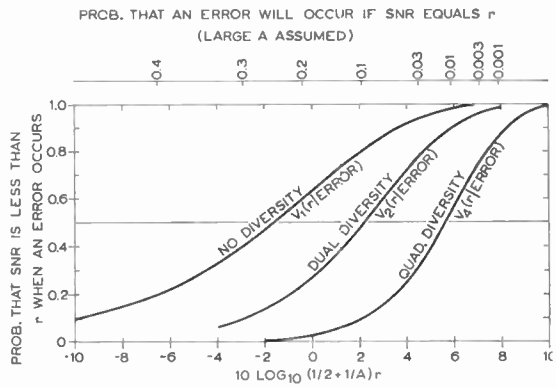

Fig. 5—Distribution functions for telegraph-receiver SNR under the condition that an element error has occurred (noncoherent FSK case).

Fig. 5 shows further that V_n depends very much on the order of diversity. With no diversity the element errors occur at much lower signal levels than with quadruple diversity. The percentage figures shown across the top of Fig. 5 give the element-error probabilities [from (1)] for various signal levels, assuming that A is large. They show, for example, that with no diversity 80 per cent of the element errors occur at levels where the probability of error in any particular element is greater than 10 per cent, while with quadruple diversity only 10 per cent of the element errors occur at such levels. During time intervals when the probability of element error is greater than 10 per cent, the clustering of element errors will be sufficient to affect even short-block codes.

There is thus a clear indication that increasing the order of diversity will tend to decrease the tendency of element errors to cluster, even when operating at the same average probability of error. This deduction does not follow from any assumptions about rate of fading, however defined, except for the quite realistic assumption that most fading, whether before or after combination, is slow compared with the duration of an element. The extent to which element errors cluster affects the relation between element-error probability and char-

acter-error probability, and it is an important consideration in choosing codes for error correction or error detection.[9]

Systems with Threshold: Comparison of Figs. 4 and 5 shows that increasing the steepness of the distribution curve for R (or R_n) moves the conditional distribution toward smaller values of R. In other words, if deep fades are nearly as probable as shallow fades, then nearly all of the errors will occur during deep fades. For the abrupt threshold model nearly all errors occur when the telegraph-receiver SNR is zero, whatever the order of diversity (for reasonable values of system parameters). For the smooth-threshold model the conditional distribution for dual diversity is very nearly V_1 of Fig. 5, and for quadruple diversity it is very nearly the same as V_2. This arises because of the similarity, noted above, between G_1 and G_{s2} and between G_2 and G_{s4} in Fig. 4. These remarks hold for both IF and baseband combining if r_t is large enough (≥ 10) so that nearly all errors occur below threshold.

IV. Systems Compared and the Design of Receiving Equipment

A. Error Probability for Other FSK/FM Models

The element-error probabilities calculated in Section II, as well as the simple theory relating various orders of diversity [see (3)], apply only for the maximal-ratio baseband combiner and the noncoherent matched-filter telegraph receiver. The results of Section III make possible some comparisons of performance with other types of receiving equipment.

Maximal-Ratio IF Combiner: When r_t is large enough so that nearly all errors occur below threshold, the element-error equations for Rayleigh fading approach the following expressions as A increases:

Abrupt-threshold model:

$$p_{an} \rightarrow \tfrac{1}{2}(r_t/A)^n \tag{23}$$

$$p_{an}{}^{\mathrm{IF}} \rightarrow \tfrac{1}{2}(r_t/A)^n/n!. \tag{24}$$

Smooth-threshold model:

$$p_{sn} \rightarrow \tfrac{1}{2}(\pi r_t/2A^2)^{n/2} \tag{25}$$

$$p_{sn}{}^{\mathrm{IF}} \rightarrow \frac{\tfrac{1}{2}\pi^{1/2}(r_t/2A^2)^{n/2}}{\Gamma(\tfrac{1}{2}n+\tfrac{1}{2})}. \tag{26}$$

Table I is based on these equations, which are derived in Appendix I. It gives the number of decibels by which A must be increased to make the error probability with maximal-ratio baseband combining equal to that with maximal-ratio IF combining. It is clear that the steeper the threshold, the greater the theoretical advantage of IF combining.

[9] H. B. Law has published curves from which the same conclusions may be drawn for the coherent telegraph receiver. See Figs. 4–6 in H. B. Law, "The detectability of fading radiotelegraph signals in noise," *Proc. IEE*, vol. 104, pt. B, pp. 130–140; March, 1957.

TABLE I

Relative Transmitter Powers Required to Produce Same Error Probability with Baseband Combining as with IF

Order of Diversity	Abrupt-Threshold		Smooth-Threshold	
	IF (db)	Baseband (db)	IF (db)	Baseband (db)
1	0	0	0	0
2	0	1.5	0	1.0
3	0	2.6	0	1.7
4	0	3.5	0	2.2
8	0	5.8	0	3.5
large	0	$10\log_{10}(n+1)/e$	0	$5\log_{10}[\pi(n+1)]/2e$

The numbers in Table I, which assume r_t large and A larger, give the maximum differences that may be expected between the two types of combiner. For smaller values of r_t or A the differences will not be as great, because (23) through (26) are based on the straight-line asymptotes approached by the distribution curves of Figs. 3 and 4. These asymptotes exhibit the maximum differences between the distributions for IF and for baseband combining. The results given in Table I can also be derived from the expressions for the asymptotes alone, for they do not depend upon the type of telegraph receiver used.

Equal-Gain IF Combiner: A simple alternative to the maximal-ratio combiner is the equal-gain combiner, in which the signals on the various diversity branches are added together (in phase) with equal gain in each diversity branch. The equal-gain combiner works well only when the noise power remains approximately the same in each diversity branch, and it is not appropriate for baseband combining with ordinary FM receivers.[10] Equal-gain combination of the IF signals is appropriate under conditions frequently met in practical systems, and under these conditions will in theory perform nearly as well as maximal-ratio combining. The difficulty lies in bringing the IF signals into phase with each other before combining them, but special receiving equipment built to do this has had considerable success.[2] Table II, which compares equal-gain IF combining with maximal-ratio IF combining, is based on Brennan's work.[11] It applies, roughtly, for all types of telegraph receiver.

Comparison of Table II with Table I shows that, in theory at least, the equal-gain IF combiner ought to be superior to the maximal-ratio baseband combiner, and of course the maximal-ratio IF combiner ought to be best of all. Designers of diversity receivers have not

[10] A special FM receiver, designed for equal-gain baseband combining, has been reported by R. T. Adams, "Simplified base-band diversity combiner (abstract)," 1959 IRE National Convention Record, pt. 8, p. 153.

[11] Brennan, *op. cit.*, Table II is based on the 99 per cent points in Brennan's Figs. 9 through 13. It therefore differs slightly from Brennan's Table I, which is based on average SNR's. For telegraph work, separation of the distribution curves at low levels affords a better comparison than average separation. Brennan gives a thorough discussion of the "appropriate conditions" for equal-gain combining, collects the earlier material on the subject, and presents much that is new.

and difficulties is so nice. Maximal-ratio combining requires knowledge, at the receiver, of signal power and noise power averaged over recent time. This knowledge must then be used to control gain in each diversity branch. IF combining requires knowledge of the IF phase, which must then be used to bring into phase the IF carriers in the various diversity branches. The problems involved in above-threshold combining are at least recognized, if not completely solved.[20] The problems met below threshold, though more severe, have as yet received little attention.

The most obvious of the special problems met below threshold is the increased difficulty in measuring either phase or amplitude of a weak signal. In theory, either or both could be measured to any desired accuracy if it were not for the fact that neither stays constant for very long. The receiver therefore has to estimate, in the statistical sense, the quantity that in combiner theory it is assumed to "know." Since the estimate must be made in a finite time, limited by the speed of fading, the errors in estimation will be finite, and will increase as the SNR decreases. But if the "knowledge" assumed in the combining process is in error, we cannot realize the advantage of theoretically ideal combination.

Let us examine these remarks first in the context of IF combining. The essential step in IF combining is to bring the different carriers into phase with each other. Precise synchronism is not necessary, and Stein[21] has given an upper bound for the degradation caused by imperfect phase control. Keeping the phase differences less than 45 degrees, a value large enough to cause significant degradation, may not be easy, especially since the phase of a fading carrier is most likely to change rapidly at precisely those moments when the amplitude is low. On the other hand, fading is slow enough so that a sizable fraction of a second is available for the observation. It therefore ought to be possible to make a suitably accurate estimate of the RF phase, even at IF SNR's of three db and below. Note that the IF SNR is referred to the very large IF bandwidth, which has nothing to do with the speed of fading.

The phase-control problem exists for both equal-gain IF combiners and maximal-ratio IF combiners. The latter also require knowledge of the carrier level, which must likewise be measured during deep fades. It is doubtful whether the small theoretical improvements indicated in Table II justify the increased complexity of equipment required for maximal-ratio combining at IF.

The maximal ratio baseband combiner avoids the problem of measuring IF phase. If it is to be used below threshold, however, both signal amplitude and noise power must be estimated, since neither remains constant as IF carrier fades below threshold. This complication does not arise above threshold, where signal amplitude remains constant and measurement of above-baseband noise gives the information needed for combining; nor does it arise with the maximal-ratio IF combiner, where noise power may be assumed equal in the different diversity branches. The situation is further confounded by the fact that the shape of the baseband noise spectrum changes. In theory, therefore, the baseband cannot be handled as a unit for maximal-ratio combining.

Baseband combining is not hopeless, however, because for telegraph reception the critical range of SNR's in which errors occur is only a few decibels wide. A working range of ten db in the baseband, or five db at IF, is sufficient. When the signal fades below the critical range it is too weak to be useful, and when it is above it, it is strong enough to be handled without much regard to theoretically optimum procedures. In the example treated in Appendix II, it happens that the critical range corresponds to IF SNR's between $+2$ and -3 db. Above-baseband noise is nearly inversely proportional to IF SNR, even over this range, so an effort toward weighted baseband combining using it to estimate SNR might have limited success. Below IF SNR's of five db or so, the noise spectrum over the baseband is flat (assuming no preemphasis), and it is there again possible to combine using the baseband as a whole.

Toward a Practical Solution: Tables I and II indicate that the equal-gain IF combiner ought to have an advantage of roughly two db over the maximal-ratio baseband combiner so far as telegraph over FM is concerned. The former requires phase control, however, and the latter presents the difficulties noted previously, including the difficulty that baseband noise may not fully satisfy all of the assumptions required to achieve the full theoretical diversity advantage. The important thing is to make an intelligent attempt at combining below threshold, and a choice between the two methods mentioned can hardly be made until some well conceived designs have been carefully compared in the field.

An IF equal-gain combiner to be used for telegraph traffic should be designed so that the phase control works at the lowest possible carrier levels. Furthermore, there should be no "squelch" to quiet the baseband when the carrier drops below the FM threshold.

A reasonable solution for baseband combination would be to design a conventional maximal-ratio baseband combiner that at very low SNR's became in effect an equal-gain combiner. Such a combiner would weight the various signals on the basis of measured noise power above the baseband, as is now conventional. Below threshold it would simply continue this type of operation until above-baseband noise approached its maximum. When this condition was approached in all diversity branches, the baseband signals would be added, without preference, and fed at a usable level into the telegraph receiver. The two ways in which such a combiner differs from standard practice for baseband com-

[20] Brennan, *op. cit.*, discusses these in fine detail. He defines clearly the interval of "recent time" over which signal power and noise power must be averaged. He states cogently the important advantage of the equal-gain combiner—its independence of "what one chooses to think of as a SNR."

[21] *Ibid.*, sec. XII.

bination are its emphasis on an attempt at weighted combining as far as possible below threshold, and its equal-gain operation *at a usable level* when weighted combining is impractical.

V. Conclusions

The results of this paper may be collected under four somewhat overlapping headings as follows:

1) A method for calculating error rates for FSK/FM receivers for all orders of diversity.
2) The study of model systems with different types of threshold behavior.
3) The comparison of performance with various combiners and telegraphy systems, and the practical difficulties met in building a combiner for telegraphy over FM.
4) The conflict between the requirements of telegraph channels and those of telephone channels.

The method of extending error-rate calculations from an elementary receiver to one for nth-order diversity applies, strictly, only for FSK and differentially-coherent PSK systems using noncoherent matched-filter telegraph receivers and maximal-ratio baseband combiners. However, the theory places no restrictions on either the shape of the FM threshold curve or the probability distribution of the fading carrier. Therefore experimental data for either or both can easily be included in an analysis.

A theoretical analysis was carried out, using two different models to describe the FM threshold, and assuming Rayleigh fading. The two models represent extremes so that the results of the analysis bound the performance that might be expected with a real receiver. It appears that, for a typical system, nearly all telegraph errors will occur when the carriers are below threshold. Furthermore, the behavior of the receiver below threshold determines the probability of telegraph error, and it therefore becomes important to design combiners that work reasonably well below threshold. It also appears that the error probability depends very little upon the position of the telegraph carrier in the multichannel baseband if the baseband is transmitted without preemphasis. Other results show that increasing the deviation of the RF carrier (or increasing the level of the telegraph carrier in the baseband) by one db is much less effective than increasing transmitter power by one db in reducing the probability of error, even if the receiver bandwidth is held constant. If the receiver bandwidth is increased so that deviation may be increased, the net effect in most practical cases will be to degrade telegraph performance.

Various receiving systems have also been compared. The best FSK/FM system (*i.e.*, the one with the lowest error rate) would use maximal-ratio combining at IF together with *coherent* matched-filter telegraph detection. The same combiner, working with a noncoherent matched-filter telegraph receiver would be worse by less than one db, in terms of the decrease in transmitter power that would produce the same increase in error probability. An equal-gain IF combiner would be approximately one db weaker still, and a maximal-ratio baseband combiner would lose yet another decibel or two. These numbers are theoretical values, and practical difficulties make it likely that the maximal-ratio IF combiner cannot yield the small improvement indicated in theory. On the other hand, both the equal-gain IF combiner and the maximal-ratio baseband combiner, suitably modified to operate below threshold, will greatly surpass the performance of a combiner that does not operate below threshold. Comparison with different systems of telegraph keying shows AK/FM to be about one db inferior to FSK/FM, and binary PSK/FM to be about one db superior. The exact difference depends upon the threshold characteristic of the FM receiver.

There is a serious conflict between the qualities desired for good telephone transmission and those that make for few telegraph errors. Short interruptions (of a fraction of a second) in a telephone channel cause little disturbance, but the average SNR should be high. For telegraph channels interruptions of only 0.1 second cause characters to be mutilated, while raising the SNR to a level considered good for telephone use is superfluous. This conflict in requirements makes itself felt in two ways. First, a combiner used for telephone traffic ought to block signals that fall below threshold, thereby keeping out noise bursts, whereas one used for telegraph channels ought to continue to pass the best available signals, no matter how noisy, to the telegraph receiver. Second, the FM bandwidth and deviation selected as optimum in some sense for telephone channels are almost sure to be much greater than those that would minimize the telegraph error probability. One can imagine ways to avoid the first difficulty—by modifying the channeling equipment, for example. The second is, however, a fundamental consequence of the FM process, which can be used to improve performance above threshold only at the cost of degrading performance when the carrier is weak.

Appendix I

Mathematical Derivations

A. A Theorem for the Maximal-Ratio Baseband Combiner

Consider an nth-order diversity system, with independent fading (not necessarily with the same probability distribution) on each diversity branch. Suppose that the average element-error probability for the mth branch alone, when operated with a noncoherent matched-filter telegraph receiver, is π_m. Then, if the outputs from the diversity branches are combined in a maximal-ratio baseband combiner, the average element-error probability for a noncoherent matched-filter telegraph receiver operating on the combined output is

$$\pi_e = \tfrac{1}{2}(2\pi_1 \cdot 2\pi_2 \cdot 2\pi_3 \cdot \cdots 2\pi_n). \tag{32}$$

Proof: Let the probability density function of β_m, the telegraph-receiver SNR on the mth branch, be $\Theta_m(r)$, and let its Laplace transform be

$$\phi_m(s) \equiv \int_0^\infty e^{-sr}\Theta_m(r)dr. \tag{33}$$

Then, by comparison with (2),

$$\phi_m(\tfrac{1}{2}) = 2\pi_m. \tag{34}$$

If the mth and kth diversity branches are combined in a maximal-ratio combiner, the resultant SNR will be $\beta_m+\beta_k$.[22] The probability density function of $\beta_m+\beta_k$ is formed by the convolution of Θ_m and Θ_k.[23] But one of the fundamental properties of the Laplace transformation is that convolution of the Θ's corresponds to multiplication of the ϕ's, and hence for this dual-diversity combiner,

$$\phi_c(\tfrac{1}{2}) = \phi_m(\tfrac{1}{2})\phi_k(\tfrac{1}{2}) = (2\pi_m)(2\pi_k) = 2\pi_c. \tag{35}$$

By the same argument, the extension step-by-step to nth-order diversity follows, proving (32). Eq. (3) represents a special case of the theorem, with the same fading distribution for all diversity branches (*i.e.* all Θ_m the same). A similar proof holds for PSK/FM with differentially coherent reception.

These proofs hold regardless of the distribution functions of the β_m, because all probability distribution functions that are zero for negative r are Laplace transformable.

B. Probability of Element Error with Smooth-Threshold Model

The probability density function of R, the telegraph-receiver SNR, obtained by differentiating (19), is

$$g_{s1}(r) = (1/2A)(r_t/r)^{1/2}\exp\left[-(r_t r)^{1/2}/A\right] \qquad r < r_t \tag{36a}$$

$$= A^{-1}e^{-r/A} \qquad r \geq r_t. \tag{36b}$$

When g_{s1} is substituted for f in (2), the resulting integral can be solved after completing the square in the exponent, giving

$$p_{s1}(A, r_t) = \left\{\frac{\pi r_t}{8A^2}\right\}^{1/2}\exp(r_t/2A^2)\left\{\operatorname{Erf}\left[1+\frac{1}{A}\right]\cdot\sqrt{\frac{r_t}{2}} - \operatorname{Erf}\frac{1}{A}\sqrt{\frac{r_t}{2}}\right\} + \frac{\exp\left[-r_t/A - r_t/2\right]}{A+2}. \tag{37}$$

The first term in (37) gives the probability of error below threshold, and the second, above threshold. The expression simplifies for large r_t to give

$$p_{s1}(A, r_t) \simeq (\pi r_t/8A^2)^{1/2}\exp(r_t/2A^2)\operatorname{Erfc}(r_t/2A^2)^{1/2} \qquad r_t > 10. \tag{38}$$

If, in addition, A is large,

$$p_{s1}(A, r_t) \simeq (\pi r_t/8A^2)^{1/2} \qquad A > r_t > 10. \tag{39}$$

The error probability for nth-order diversity, p_{sn}, may be found by substituting p_{s1} in (3).

C. Distribution of R_n for the Abrupt-Threshold Model

The probability density function of R is given by (10), and the Laplace transform of this function, obtained by substituting g_a for Θ_m in (33) is

$$\phi(s) = c + \frac{e^{-(s+1/A)r_t}}{As+1}. \tag{40}$$

If n random variables with density functions all given by g_a are added together, the probability density function of the sum will have the Laplace transform $\phi^n(s)$, and by the binomial theorem,

$$\phi^n(s) = \sum_{m=0}^{n}\binom{n}{m}c^{n-m}\frac{e^{-mr_t/A}e^{-mr_t s}}{(As+1)^m}. \tag{41}$$

Here

$$\binom{n}{m} = n!/m!(n-m)!. \tag{42}$$

We want the distribution function G_{an}, which is the integral of g_{an}, and which therefore has as its Laplace transform $\phi^n(s)/s$. In (38) the exponent $mr_t s$ produces a shift of magnitude mr_t in the inverse transform, and we write[24]

$$G_{an}(r) = \sum_{m=0}^{n}\binom{n}{m}c^{n-m}e^{-mr_t/A}G_m(r-mr_t)u_1(r-mr_t) \tag{43}$$

where G_n is the function defined in (17) and G_0 is unity. Curves of G_{a2} and G_{a4} are given in Fig. 3.

D. Distribution of R_n for the Smooth-Threshold Model

Dual Diversity: The probability density function for dual diversity, g_{s2}, may be obtained by convolving g_{s1}, as given in (36), with itself. For R_2 below threshold, only the expressions in (36a) enter the convolution integral, which may be written

$$g_{s2}(r) = \int_0^r (1/4A^2)(r_t/t)^{1/2}\cdot\exp\left[-(r_t/A^2)^{1/2}\right]\left[r_t/(r-t)\right]^{1/2}\cdot\exp\left[-(r_t\{r-t\}/A^2)\right]^{1/2}dt \qquad r \leq r_t. \tag{44}$$

[22] Brennan, *op. cit.*, (13). Note also the assumptions required for this relation to exist.

[23] W. R. Bennett, "Methods of solving noise problems," PROC. IRE, vol. 44, pp. 609–638, (41); May, 1956.

[24] Bateman Manuscript Project, "Tables of Integral Transforms," McGraw-Hill Book Co., Inc., New York, N. Y., vol. 1, Transforms 4.1(9), 4.1(4), and 5.2(18); 1954. Subsequent references to this work will be indicated simply by "I.T."

If the exponential functions are expressed in power series and the two series are multiplied, the integration may be carried out term by term.[25] Some manipulation then yields

$$g_{s2}(r) = \frac{\pi r_t}{4A^2}\sum_{n=0}^{\infty}\frac{(-\frac{1}{2})^n(r_t r/A^2)^{n/2+1}}{\Gamma(\frac{1}{2}b+1)} \cdot \sum_{m=0}^{n}\frac{1}{\Gamma(\frac{1}{2}m+1)\Gamma(\frac{1}{2}n-\frac{1}{2}m+1)}$$
$$= (r_t/A^2)\sum_{n=0}^{\infty}(-1)^n a_n (r_t r/A^2)^{n/2} \qquad r \le r_t. \quad (45)$$

This expression serves to define a_n. Integrating it gives G_{s2}.

For telegraph-receiver SNR above twice the threshold value, the convolution integral for g_{s2} can be solved to yield

$$g_{s2}(r) = \frac{e^{-r/A}}{A}(r/A - k) \qquad r \ge 2r_t \quad (46)$$

where

$$k = \frac{r_t^2}{3A^2} - \frac{r_t^3}{30A^3} + \frac{r_t^4}{420A^4} - \cdots + \cdots. \quad (47)$$

The integral of (46) from r to infinity, when subtracted from unity, gives

$$G_{s2}(r) = 1 - (1 - k + r/A)e^{-r/A}$$
$$= G_2(r) + ke^{-r/A} \qquad r \ge 2r_t. \quad (48)$$

The values of k required to compute the cases plotted in Fig. 4 are given in Table IV.

TABLE IV
VALUES OF k, k_1, AND k_2

r_t/A	k	k_1	k_2
0.4	0.05126	0.01690	0.00508
0.1	0.003300	0.000225	0.000019
0.025	0.000208		

Eqs. (45) and (48) leave G_{s2} undefined over the interval $(r_t, 2r_t)$. So far as the curves of Fig. 4 are concerned, G_{s2} can be easily interpolated by eye to cover this gap. For the calculation of G_{s4}, however, some analytical expression was needed, and it was found suitably accurate to simply continue the expression of (48). At r_t, the error in G_{s2} involved in using this approximation is only about 6 per cent of the true value.

Quadruple Diversity: The steps in the calculation for quadruple diversity follow precisely the calculation for dual diversity. The power series expansion for g_{s2} given in (45) is convolved with itself, and multiplication and reordering of terms yield an expression that may be integrated as before to give

$$g_{s4}(r) = \frac{r_t}{A^2}\sum_{n=0}^{\infty}\sum_{m=0}^{n}a_m a_{n-m}(-1)^n(r_t r/A^2)^{n/2+1} \cdot \frac{\Gamma(\frac{1}{2}m+1)\Gamma(\frac{1}{2}n-\frac{1}{2}m+1)}{\Gamma(\frac{1}{2}n+2)} \qquad r \ge r_t. \quad (49)$$

The convolution above twice threshold can be reduced with some difficulty to give an expression of the form

$$G_{s4}(r) \simeq G_4(r) + e^{-r/A}\left[k\frac{r^2}{A^2} - k_1\frac{r}{A} + k_2\right] \quad r \ge 2r_t. \quad (50)$$

The expressions for k_1 and k_2 are complicated, and Table IV gives the values for the special cases plotted in Fig. 4. In those curves the gap between r_t and $2r_t$ was interpolated by eye.

E. Conditional Distribution of R_n

The probability that R_n is less than r, given that an element error has occurred, is (see Section III-D),

$$V_n(r \mid \text{error}) = \frac{\int_0^r \tfrac{1}{2}e^{-t/2}[t^{n-1}/A^n(n-1)!]e^{-t/A}dt}{p_n(A)}$$
$$= G_n(r + \tfrac{1}{2}Ar), \quad (51)$$

where G_n is the function defined in (17). This relationship assumes Rayleigh fading, a no-threshold system, and nth-order maximal-ratio combining. The conditional distribution functions V_1, V_2, and V_4 are plotted in Fig. 5.

F. The Maximal-Ratio IF Combiner

The comparison in Section IV-A of the IF combiner with the baseband combiner assumes r_t large and A still larger, because these conditions give the maximum difference between the two combiners. Eq. (14) thus becomes

$$p_{a1}(A, r_t) \simeq \tfrac{1}{2}c \simeq \tfrac{1}{2}r_t/A. \quad (52)$$

Application of (3) leads to (23).

With the IF combiner the probability that the receiver will drop below threshold is, from (21b) and the right-hand sum of (17),

$$G_n(r_t) \simeq (r_t/A)^n/n!. \quad (53)$$

Since for the abrupt-threshold model the receiver will yield 50 per cent errors while below threshold, this gives (24).

Eq. (25), for the smooth-threshold model with baseband combining, follows from substituting (39) in (3). To derive (26), for IF combining, first note that from (22b) and (17),

$$G_{sn}(r)^{\mathrm{IF}} \simeq (r_t r)^{n/2}/n!A^n \qquad A > r_t > 10. \quad (54)$$

[25] I.T., 13.1(7).

This relation holds for the small values of r at which errors occur. Differentiating gives

$$g_{sn}(r)^{IF} \simeq \tfrac{1}{2} r_t^{n/2} r^{n/2-1}/A^n(n-1)! \qquad A > r_t > 10. \quad (55)$$

When this expression is substituted for $f(r)$ in (2), the integral takes the form of a gamma function, whence

$$p_{sn}^{IF} \simeq \frac{2^{n/2-2} r_t^{n/2}}{(n-1)!A^n}\Gamma(\tfrac{1}{2}n), \quad (56)$$

which may be reduced to the form given in (26) by use of Legendre's duplication formula.[26]

The expressions in Table I for "large" orders of diversity may be obtained by using Stirling's approximation[27] in (24) and (26).

G. The Coherent Telegraph Receiver

If the telegraph-receiver SNR fades with probability density function g, then from (1) and (27) the ratio between error probability with noncoherent and with coherent FSK telegraph reception is

$$\frac{p}{q} = \frac{\int_0^\infty \tfrac{1}{2} e^{-r/2} g(r)\,dr}{\int_0^\infty \tfrac{1}{2}\,\mathrm{Erfc}\sqrt{\frac{r}{2}}\; g(r)\,dr}, \quad (57)$$

where p, as before, denotes noncoherent reception and q denotes coherent reception.

For the no-threshold receiver, nth-order diversity, the probability density function is proportional to $r^{n-1}A^{-n}$. This is true for the small values of r where errors occur, as long as A is large, and it holds for maximal-ratio IF combination, equal-gain IF combination, and maximal-ratio baseband combination. Eq. (57) thus becomes, when common factors are divided out,[28]

$$\frac{p_n}{q_n} = \frac{\int_0^\infty r^{n-1} e^{-r/2}\,dr}{\int_0^\infty r^{n-1}\,\mathrm{Erfc}\sqrt{\frac{r}{2}}\,dr} = \frac{\Gamma(n)}{\frac{\Gamma(n+\frac{1}{2})}{n\sqrt{\pi}}}$$

$$= \frac{2^{2n-1}}{\binom{2n-1}{n}}. \quad (58)$$

Both p_n and q_n are proportional to A^{-n}, and A is proportional to transmitted power. Therefore the superiority of coherent reception, expressed in terms equivalent to decibels of transmitted power, is

$$10n^{-1}[\log_{10}(p_n/q_n)].$$

[26] Bateman Manuscript Project, "Higher Transcendental Functions," McGraw-Hill Book Co., Inc., New York, N. Y., vol. 1, eq. 1.3(15); 1954. Subsequent references to this work will be indicated simply by "H.T.F."

[27] H.T.F., 1.18(2).

[28] The denominator may be integrated by applying H.T.F., 9.9(2) and 9.3(8). Note that the definition of Erfc used in H.T.F. differs by a factor of $2/\sqrt{\pi}$ from that of (28). The last expression in (58) is obtained with Legendre's duplication formula.

This expression may be used to obtain the "No Threshold" column in Table III.

For the smooth-threshold receiver, the probability density function of SNR is proportional to $r^{n/2-1}A^{-n}$, no matter which of the three combiners is used. The ratio of error probabilities, which may be obtained by substituting $\frac{1}{2}n$ where n appears in (58), is thus

$$\frac{p_{sn}}{q_{sn}} = \frac{\Gamma(\frac{1}{2}n)}{\frac{\Gamma(\frac{1}{2}n+\frac{1}{2})}{\frac{1}{2}n\sqrt{\pi}}} = \frac{\pi^{1/2}\Gamma(\frac{1}{2}n+1)}{\Gamma(\frac{1}{2}n+\frac{1}{2})}. \quad (59)$$

The expression in terms of decibels, used to obtain the "Smooth Threshold" column of Table III, is

$$10n^{-1}[\log_{10}(p_{sn}/q_{sn})].$$

For the abrupt-threshold receiver there is no advantage to coherent telegraph reception except for r_t small enough so that a significant portion of the errors occur above threshold. This case appears to have little practical interest.

Appendix II

Examination of a Specific System

A. Method of Calculation

The results presented in this paper are most useful as a guide in system planning. When the design engineer compares two similar systems to determine the effect of changing a single parameter, he is on reasonable ground because errors in the many assumptions will usually similarly affect both systems compared. Nevertheless it may be helpful sometimes to calculate numerical results based on the theory given above.

A No-Threshold Receiver: Consider first an FSK/SSB-AM system, which may be treated as a no-threshold case, following the discussion in Section II-B. With SSB and a complex baseband consisting of multiplexed signals, some of them voice signals, the carrier power varies. Superposition of baseband signals produces superposition of RF carrier waves with SSB, however, and therefore we need consider only the case in which the single telegraph subcarrier of interest is transmitted alone. If we know the instantaneous path loss, and the transmitter power given to the single subcarrier, we can calculate the carrier power at receiver input, and we denote it by S. The IF SNR will be given by

$$X = S/kTFB \quad (60)$$

where kT is the thermal noise power at receiver input in a bandwidth of 1 cps, F is the over-all noise factor of the receiver, and B is the noise bandwidth at the IF stage. The receiver gain between RF and IF appears in both numerator and denominator and is canceled out.

Following the definition of R in Section II-A we can set

$$R = S\tau/kTF \quad (61)$$

assuming that the telegraph element is of constant amplitude and duration τ and canceling out gain between IF and telegraph receiver. Then from (5) and (7) we get

$$b = B\tau \tag{62}$$

$$A = \langle S\rangle\tau/kTF. \tag{63}$$

A is the parameter needed in (8) to calculate error probability. Note that with Rayleigh fading the mean carrier power $\langle S\rangle$ is 1.6 db above the median, which is the quantity commonly measured.

Receivers with Threshold: With FM, the quantity S denotes the power in the RF carrier, which must be treated as a whole. Then X is again given by (60). There is no loss in generality if we express the amplitude of telegraph signal and noise in terms of the frequency deviation of the IF carrier at the input to the limiter-discriminator.

Let the peak deviation caused by the telegraph subcarrier be ω_t. Then the energy of the received telegraph element will be[29]

$$E = \tfrac{1}{2}\omega_t^2(1 - e^{-X})^2\tau. \tag{64}$$

This expression holds for all values of X; it was derived assuming a single sinusoid as modulation signal, but it will be assumed to be valid also for the complex baseband signals considered here. We have the two asymptotic expressions

$$E \simeq \tfrac{1}{2}\omega_t^2\tau \qquad \text{for } X \text{ large,} \tag{65a}$$

$$\simeq \tfrac{1}{2}\omega_t^2X^2\tau \qquad \text{for } X \text{ small.} \tag{65b}$$

To determine R we must also know the noise power density per cps after frequency demodulation. Above threshold it will be, assuming flat IF filters,[30]

$$\omega^2kTF/S = \omega^2/BX, \tag{66}$$

where ω is the baseband frequency, in rad/sec, and where B is taken in cps. Thus we have, for an FM receiver operating above threshold

$$R = \tfrac{1}{2}\omega_t^2\tau BX/\omega^2 \tag{67}$$

where ω is the frequency of the telegraph subcarrier *in the baseband*. This equation defines b of (9) and (15).

To determine baseband noise below threshold we turn to Rice's results.[31] Admittedly his calculations assumed an unmodulated RF carrier, but they should nevertheless give a satisfactory first estimate. Rice gives curves for various IF SNR's. He shows a maximum noise power density, occurring at small baseband frequencies and with negligible carrier power, of

$$0.74(4\pi^2\sigma) = 11.5B \qquad \text{(in rad}^2\text{/sec}^2\text{ per cps).} \tag{68}$$

Combining this with (65b) gives an asymptotic expression for R when X approaches zero,

$$R \simeq \omega_t^2\tau X^2/23B. \tag{69}$$

This is exactly the below-threshold behavior assumed for the smooth-threshold model, and gives a means of calculating b/x_t for (15a). Actually, as noted in Section II-B, the error probabilities for this model [see (38) and (39)] will ordinarily depend only upon

$$r_t/A^2 = x_t/b\langle X\rangle^2 = 23B/\omega_t^2\tau\langle X\rangle^2. \tag{70}$$

Let us now see how these results may be applied to the analysis of a specific FSK/FM system.

B. The System Parameters

The ACE High network, now under construction for SHAPE, includes the largest troposcatter net yet planned. The FM receivers will operate in quadruple diversity, with maximal-ratio baseband combining, at least above threshold. Typical operating values for a link designed to carry 36 telephone channels, some of which will carry FSK telegraph, are as follows:

RMS test-tone deviation of RF carrier = 60 kc ≡ 0 dbm0.
Level of telegraph subcarrier = −15 to −20 dbm0.
Noise bandwidth of receiver = 1.1 mc.
Signaling speed = 50 baud (τ = 0.02 sec).

These data suffice for a simple calculation of the curve relating X and R, both above and below threshold, for one of the elementary receivers.

C. The Theoretical Curves

Fig. 6 gives curves for signal power and noise power, expressed in rad²/sec². The curve for signal power is based on a signal of −20 dbm0, *i.e.* on an rms deviation per subcarrier of 6 kc. Thus the maximum approached by this curve is $(2\pi)^2(6000)^2$ rad²/sec² [cf. (65a)].

Three curves are given for noise power in 50-cps bands near 154 kc, 88 kc, and 22 kc. These correspond to high, middle, and low portions of the baseband, which extends from 12 to 156 kc, and are taken from the family of curves calculated by Rice.[32] The dashed lines indicate the asymptotes approached above threshold [cf. (66)]. The asymptote for very low IF SNR, given by (69), is for this system

$$R = 2.2X^2, \tag{71}$$

and it can be seen to lie only a fraction of a decibel below the curves of R vs X given in the lower left corner of Fig. 6. This asymptotic expression for the SNR apparently holds for much larger X than might have been expected, because the errors in (65b) and (68) tend to cancel out when the ratio is taken.

[29] F. L. H. M. Stumpers, "Theory of frequency-modulation noise," PROC. IRE, vol. 36, pp. 1081–1092; September, 1948. See p. 1090.

[30] Bennett, *op. cit.*, (269).

[31] *Ibid.*, etc. Fig. 7(b) and 7(c). Rice's ρ is the same as X. His bandwidth parameter $\sigma = B/(2\pi)^{1/2}$.

[32] For a receiver noise bandwidth of 1.1 mc, Rice's bandwidth parameter (see footnote 31) is 440 kc. Therefore, for the three sample channels in the baseband, f/σ = 0.35, 0.2, and 0.05.

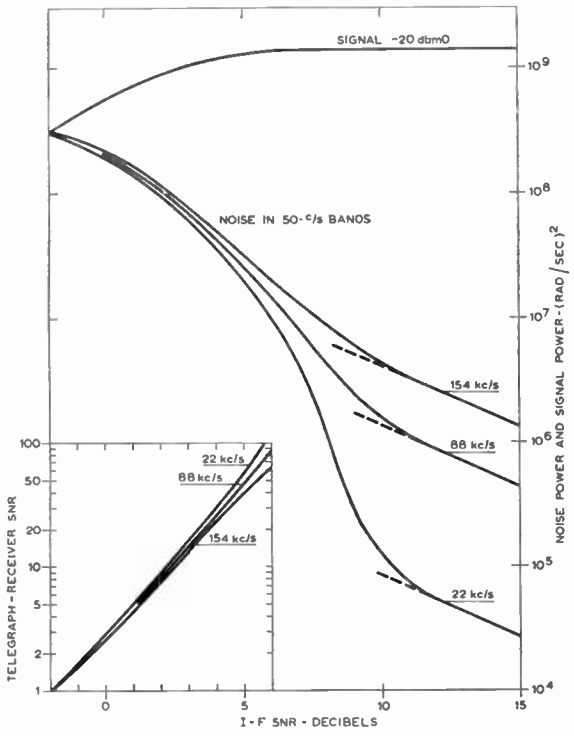

Fig. 6—Telegraph-receiver signal power and noise power vs IF SNR, for various baseband frequencies. Inset shows telegraph-receiver SNR.

Frequently it will appear, when the above formulas are used to calculate x_t and b for a smooth-threshold model to approximate a real system, that x_t turns out to be unreasonably large. (In a real receiver x_t should be about 12 db.) This means only that the curve of R vs X is S-shaped (see the 22-kc noise curve in Fig. 6 for example) and that the two asymptotes do not intersect near the real threshold. The point is of no importance unless the critical range of telegraph-receiver SNR lies near the real threshold, in which case the smooth-threshold model is not a good representation.

D. Notes on System Design

The plots of the telegraph receiver SNR in the lower left corner of Fig. 6 cover the "critical" region. Since the slope here is only slightly greater than that for the smooth-threshold model, we conclude from Fig. 5 that the curve for V_2 will apply for the quadruple-diversity receiver with threshold. Therefore at least 90 per cent of the telegraph errors should occur when R_4 is less than 8, which implies that all four of the elementary receivers are operating with IF SNR's of less than two db. For such low SNR's the noise spectrum is flat over the baseband, and it therefore appears that, for telegraph work, all portions of the baseband are equally good.

For this example, increasing the telegraph-signal level to -15 dbm0 would move the critical region to IF SNR about two db smaller. The improvement, in terms of effective added transmitter power, would probably be less than two db, because the combining operation would become less efficient.

It is interesting to consider the effect of increasing the IF bandwidth. Suppose that the noise bandwidth of the FM receiver is doubled, and that this makes it possible to increase carrier deviation by a factor of 2.5 (more than double, since the receiver bandwidth contains fixed allowances for stability and the like). Above threshold, the telegraph-receiver noise power for the same carrier power remains unchanged. The improvement realized above threshold is eight db, which is gained at the cost of having the FM receiver below threshold for a somewhat greater portion of the time. Below threshold, however, the telegraph-receiver noise power for the same RF carrier power at receiver input may be estimated from (69). The bandwidth B is doubled, the deviation ω_t is multiplied by 2.5, and the IF SNR X is halved as a consequence of the wider IF bandwidth. The net result is a 20 per cent decrease in R, *i.e.* a *loss* of one db in telegraph-receiver SNR. In this way the improvement above threshold is paid for below threshold.

Author's Note

After submitting his final manuscript for publication, the author discovered the related work of du Castel and Magnen. In their interesting paper[33] they consider FSK/FM with selection diversity, and carry through an analysis for a particular threshold characteristic by means of numerical integration. Their conclusions agree qualitatively with those in the relevant portions of this present paper.

Acknowledgment

The author would like to thank John N. Pierce, of the Air Force Cambridge Research Center, and the IRE Reviewers for their carefully considered and very helpful comments on the early draft of this paper.

[33] F. du Castel and J.-P. Magnen, "Etude de la qualité télégraphique dans les faisceaux hertziens transhorizon," *Ann. Télécommun.*, vol. 14, pp. 93–103; March–April, 1959.

Forward Scattering by Coated Objects Illuminated by Short Wavelength Radar*

R. E. HIATT†, SENIOR MEMBER, IRE, K. M. SIEGEL†, SENIOR MEMBER, IRE, AND H. WEIL†

Summary—**Theoretical and experimental results are presented concerning the ineffectiveness for forward scattering of radar absorbing coatings applied to highly conducting objects which are large with respect to the wavelength of the incident energy. It is shown that such coatings can only increase the energy in the forward lobe of the scattering pattern. A rather simple accurate theoretical estimate is obtained of the width of this lobe for a sphere and verified experimentally.**

By using absorbing coatings, experimental verification is obtained of theoretical predictions of the energy focussing and reflecting effects at the rear of thin prolate spheroids.

Finally a section is devoted to the experimental procedures and equipment used to obtain the forward scattering data.

Introduction

THIS paper will discuss scattering of an incident plane electromagnetic wave by an object large with respect to the wavelength, particularly where the object has been all or partly covered with absorbing material. The scattering pattern for such an object exhibits a large lobe in the forward direction. The purpose of the first two sections of this paper is to illustrate by a heuristic argument backed by experimental results that any coating applied to the object can only serve to increase the amount of energy scattered into this lobe. This is true even for coatings which are radar absorbers. The angular width of the forward-scattered lobe (over which this effect may be expected) is consequently of interest. It is shown that the solid angle must be proportional to λ^2 and an accurate estimate of the angle is obtained theoretically for a sphere and experimentally verified.

Finally use is made of forward scattering theoretical results to analyze the surface wave behavior on a thin prolate spheroid irradiated nose-on by a plane wave. The correctness of various points of the analysis is confirmed by experimental results obtained by measuring backscattering and forward scattering from thin prolate spheroids partly covered with absorbing coatings.

Short Wavelength Forward Scattering

In this section scattering in the forward direction by convex obstacles whose dimensions are large relative to the incident wavelength λ will be considered. In particular our interest lies in the effect of covering all or parts of perfectly conducting scatterers with radar absorbing material. The point to be made is that, for sufficiently short wavelengths, the forward-scattered energy is not affected by coating the scatterer except that it is increased proportional to the square of any increase in the cross-sectional area, A, which is blocked out of the incident plane wave by the scatterer. This result is made evident by the fact that the leading term in an asymptotic expansion in inverse powers of $k=2\pi/\lambda$ of the forward-scattered field is not dependent on the material of which the scatterer is composed, nor on the shape of the scatterer except as it affects the above cross-sectional area. Moreover, this dominant contribution is a pure imaginary given simply by

$$f(\pi) \sim iA/\lambda \tag{1}$$

when the forward-scattered field is written in the form $f(\pi)^{ik(r-ct)}/r$, with r the distance from the scatterer, c the velocity of light and t the time. The resulting forward scattering radar cross section is

$$\sigma(\pi) \equiv 4\pi \left| f(\pi) \right|^2 \sim \frac{4\pi A^2}{\lambda^2} . \tag{2}$$

That one would expect the leading term in an expansion of $f(\pi)$ in powers of k^{-1} to be independent of the material composing the scatterer is a consequence of the conservation of energy and of the manner in which the shadow behind a scatterer is formed by interference between the incident and scattered waves. The energy removed from the beam by the scatterer may be measured by the total cross section σ_T. This energy is either scattered or absorbed (transmitted energy being included with scattered energy) and for a given shape and size of scatterer the material of which the scatterer is composed can, to the first order, affect only the relative proportions of scattered and absorbed energy but cannot affect σ_T itself.

The dominant part of the interference between the incident and scattered waves in the forward direction at any fixed distance from the scatterer and for any wavelength is found to be due to the imaginary part of $f(\pi)$. A direct consequence of this fact combined with conservation of energy is the well-known theorem

$$\sigma_T = \frac{4\pi}{k} \operatorname{Im} f(\pi), \tag{3}$$

which has been derived many times in optics, acoustics, electromagnetic theory and quantum mechanics.[1–3] The

* Received by the IRE, September 14, 1959; revised manuscript received February 29, 1960.

† University of Michigan Radiation Lab., Ann Arbor, Mich.

[1] H. C. Van de Hulst, "Light Scattering by Small Particles," John Wiley and Sons, Inc., New York, N. Y.; 1957.

[2] N. F. Mott and H. S. W. Massey, "The Theory of Atomic Collisions," Clarendon Press, London, Eng.; 1950.

[3] L. I. Schiff, "On an expression for the total cross section," *Prog. of Theor. Phys.*, vol. 11, pp. 288–290; March, 1954.

above theorems are special cases of theorems given by Saxon.[4]

Since σ_T is invariant to changes in composition of the scatterer, combining (3) with the asymptotic statement $f(\pi) \sim \mathrm{Im}\ |f(\pi)|$ leads to the conclusion that, for sufficiently short wavelengths, $f(\pi)$ is independent of the material composing the scatterer. A consequence of this is that the effect of absorbing coatings must be vitiated in forward scattering.

Eq. (2) is compared in Fig. 1 with computations made by Air Force Cambridge Research Center[5] using the exact sphere solution of Maxwell's equations (the Mie series) and with experimental results obtained in our laboratory. The results in Fig. 1 are for uncoated spheres.

The result on the ineffectiveness of coating in forward scattering is expected to be valid for values of k for which $k\sqrt{A} > 10$. This ineffectiveness has been verified in our laboratory experimentally for coated and uncoated spheres at a wavelength corresponding to $kr = 9.8$ (r = sphere radius). Backscattering measurement results are presented to show that the coating indeed acted as an absorber for backscattering. The results are presented in Table I. Further experimental results are given in Figs. 2 and 3. In Fig. 2 forward scattering from a coated cone is compared with forward scattering from an uncoated cone. The cone's base radius was equal to the radius of the calibrating sphere. The coating was made according to a formula for absorbing material developed by R. W. Wright and W. H. Emerson of the Naval Research Laboratory. As expected, the forward-

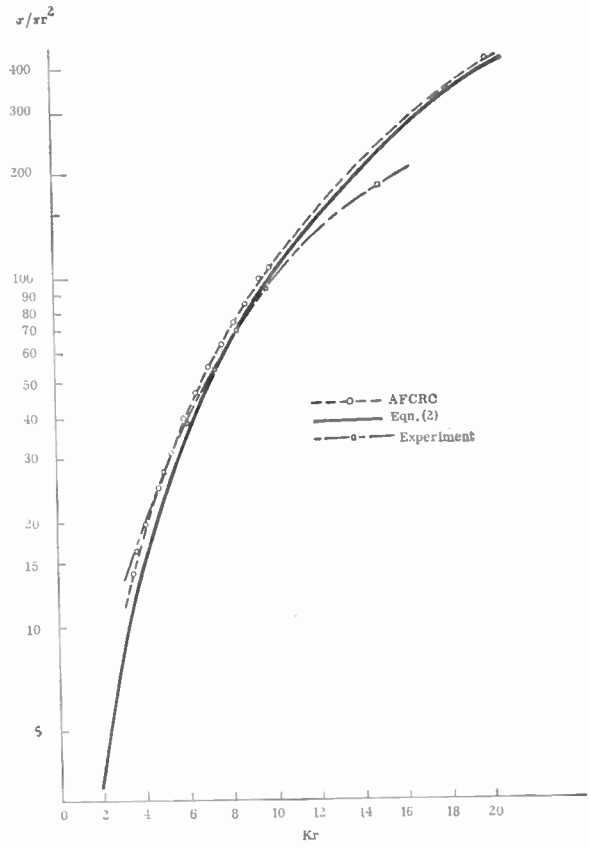

Fig. 1—Forward scattering from spheres.

TABLE I

SCATTERING FROM STANDARD VS COATED SPHERE

kr (uncoated sphere) = 9.8

	Backscatter db relative to m²	Forward Scatter db relative to m²
Standard sphere	−20.7	−1.5
Covered with absorbing material	−37.7	+0.1

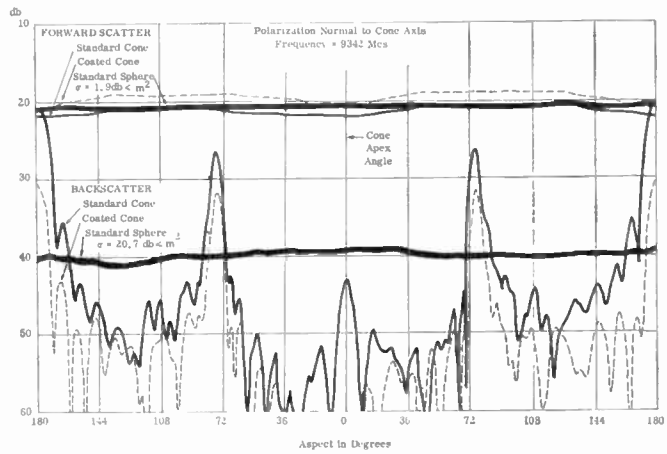

Fig. 2—60° cone $kr = 9.8$ backscatter and 180° forward scatter showing also a standard sphere $kr = 9.8$. r = cone base radius or radius of sphere.

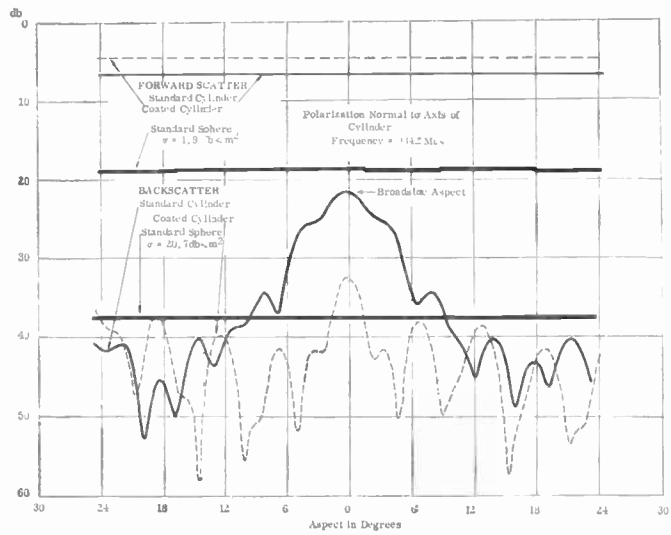

Fig. 3—Cylinder 8.7 λ long and 3.4 λ diameter backscatter and 180° forward scatter showing also a standard sphere $kr = 9.8$.

[4] D. S. Saxon, "Tensor scattering matrix for the electromagnetic field," *Phys. Rev.*, vol. 2, pp. 1771–1775; December, 1955.

[5] These computations were initiated by N. A. Logan at the AF Cambridge Research Center, Bedford, Mass. The results are now published in the Appendix of R. W. P. King and T. T. Wu, "Scattering and Diffraction of Radio Waves," Harvard University Press, Cambridge, Mass.; 1959.

scattering cross section for the coated cone was in fact larger than for the uncoated, and the uncoated cone results are very close indeed to the sphere return. Since the cones chosen do not have a great variation in projected area as a function of aspect, one would not expect the forward-scattering cross section to change much from that of the sphere as the aspect is changed. Hence this result is in agreement with the theory. In Fig. 2 the backscattering cross section is also given and shows that the absorbing material does in fact work well for backscattering. Fig. 2 also supports the statement that the forward-scattering cross section will always be equal to or greater than the backscattering cross section for a convex body.

This theory has also been tested for finite cylinders (Fig. 3). The forward-scattering cross section of the cylinder as well as the backscattering cross section were then measured up to $\pm 24°$ from broadside aspect. The trends are as predicted and the agreement between theory and experiment approaches ± 1 db. The forward-scattering cross section is not reduced by the addition of absorbing material and with or without absorbing material remains larger than the backscattering cross section with or without absorbing material.

Beamwidth in Forward Scattering

The bistatic pattern of a convex object for short wavelengths is fairly uniform except for a narrow lobe in the forward direction, whose peak amplitude is given by (1). Within this lobe the above considerations on the insensitivity of the scattered amplitude to the material composing the scatterer apply. Hence it is of interest to estimate the beamwidth of this narrow lobe.

The beamwidth discussion will be confined to perfectly conducting objects. To begin with, with the help of (1) and (3) one can determine that the angular beamwidth must be proportional to k^{-2}. If $\sigma(\theta, \phi)$ represents the bistatic scattering cross section, then combining (1) and (3) with the definition of total scattering cross section yields

$$\sigma_T = \sigma_T{}^S = \frac{1}{4\pi}\int_S \sigma(\theta, \phi)d\Omega \sim mA \qquad (4)$$

where S is the unit sphere, θ and ϕ are spherical polar-coordinates about an origin in the scatterer, $d\Omega$ is an element of solid angle. The integration may be split into two parts, the first part covering all of the unit sphere except a small angular region δ about the forward direction, $\theta = \pi$, the second part being an integration over δ. Our interest is in the geometric optics limit where $\sigma(\theta, \phi)$ is wavelength independent over $S-\delta$ and hence, so is the integral over $S-\delta$. Using (2), the integral over δ may be approximated by

$$\frac{A^2}{\lambda^2}\delta.$$

Since σ_T is wavelength independent, δ must be proportional to λ^2 or k^{-2}. The proportionality factor is, however, a function of the shape of the scatterer.

The integral expression for σ_T has been utilized by Siegel[6] to obtain the beamwidth of the forward-scattering beam for a sphere. Using a uniform beam approximation for the forward-scattered lobe for simplicity led Siegel to a forward-scattering beamwidth estimate of $4/kr$ where r is the radius of the sphere. This result is improved below by using a $(\sin x/x)^2$ beam pattern which leads to the beamwidth between half-power points for a sphere being $3.2/kr$. This improved estimate may be compared in the following table with the half-power beamwidth $\Delta\theta$ obtained by numerical evaluation of the Mie series for $kr = 10$, 20 at AFCRC[5] and with our experimental measurements. The experimental measurements used in Table II are reproduced in Fig. 4.

TABLE II
Beamwidth

kr	AFCRC Computation $kr\Delta\theta$		Univ. of Mich. Radiation Lab. Experiment $kr\Delta\theta$
	E Plane	H Plane	H Plane
20	3.3	3.2	
14.94			3.42
10	3.7	3.2	
9.8			3.45
8.4			3.47
7.33			3.28

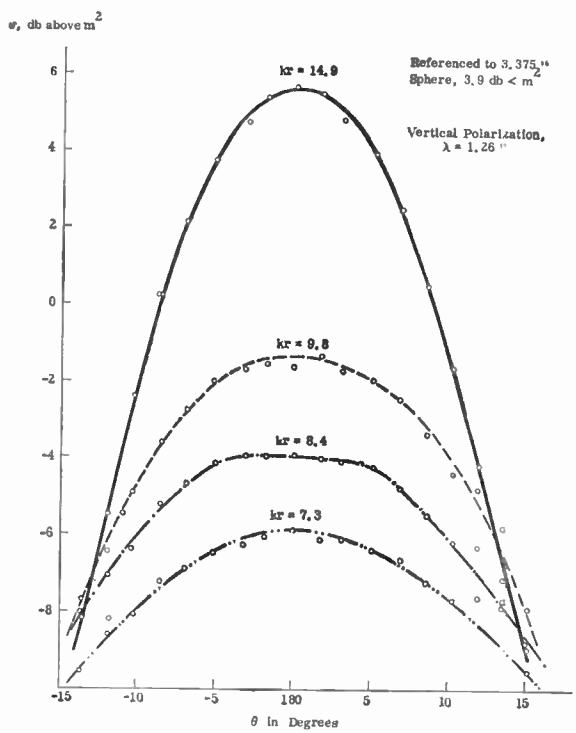

Fig. 4—Forward scattering from metal spheres.

[6] K. M. Siegel, "Bistatic Radars and Forward Scattering," *Aero Electronics 1958 Nat. Conf. Proc.*, Dayton, Ohio, pp. 286–290; 1958.

The refined version of the method to estimate the forward-scattering beamwidth for a sphere for large kr begins with the fact that for a perfectly conducting sphere the asymptotic value of σ_T is $\sigma_T \sim 2\pi r^2$.

The procedure also uses the fact that

$$\sigma(\theta, \phi) \sim \pi r^2$$

for all bistatic angles except those in a small cone in the region of the forward direction, $\theta = \pi$. In this region $\sigma(\theta, \phi)$ is given by

$$\sigma = \sigma_F = 4\pi \frac{(\pi r^2)^2}{\lambda^2} g(\theta) \quad \text{(no } \phi \text{ dependence in this case)} \quad (5)$$

where $g(\pi) = 1$. It is assumed that σ_F holds for

$$\pi - \frac{\Lambda}{kr} \leq |\theta| \leq \pi, \qquad \text{where } \Lambda \text{ is a numerical constant,}$$

so that the solid angle in which σ_F holds is proportional to k^{-2}. Using the approximations for $\sigma(\theta, \phi)$ in the integral in (4) yields a result for σ_T which is equated to $\sigma_T = 2\pi r^2$. The beamwidth is then determined from the resulting equality.

In Siegel[6] $g(\theta)$ was taken as

$$\begin{aligned} g(\theta) &= 1 \qquad \pi - \frac{l}{kr} \leq |\theta| \leq \pi \\ &= 0 \qquad |\theta| < \pi - \frac{l}{kr} \end{aligned} \quad (6)$$

so that $l = \Lambda$ and the procedure led to $l = 2$. (In this case one can speak of a beamwidth, but not half-power points.)

The present refinement consists of choosing

$$g(\theta) \equiv S(\theta) = \left(\frac{\sin \alpha(\pi - \theta)}{\alpha(\pi - \theta)}\right)^2 \quad (7)$$

and requiring that the half-power points will occur for $\pi - \theta = l/kr$. Since $g(\theta) = \frac{1}{2}$ when $\alpha(\pi - \theta) \sim 1.4$ this requirement fixes α to be

$$\alpha = 1.4(kr/l).$$

The cross section σ_F is now assumed to be

$$\sigma = 4\pi \frac{(\pi r^2)^2}{\lambda^2} S(\theta) \quad \text{for} \quad \pi - \frac{\Lambda}{kr} \leq \theta \leq \pi$$

where Λ will be chosen to correspond to the angle θ_0 for which

$$4\pi \frac{(\pi r^2)^2}{\lambda^2} S(\theta) = \pi r^2.$$

This means that

$$\theta_0 \sim \pi - \frac{\pi}{\alpha} = \pi - \frac{\pi}{1.4} \frac{l}{kr}.$$

Thus

$$\Lambda \sim \frac{\pi}{1.4} l.$$

We now evaluate σ_T as

$$\sigma_T = \int_0^{2\pi} \int_0^{\pi - (\pi/1.4)(l/kr)} \frac{\pi r^2}{4\pi} \sin \theta d\theta d\varphi + \int_0^{2\pi} \int_{\pi - (\pi/1.4)(l/kr)}^{\pi} \left(\frac{\pi r^2}{\lambda}\right)^2 g(\theta) \sin \theta d\theta d\phi. \quad (8)$$

The first integral is $\sim \pi r^2$ for $kr \gg 1$. The second integral can now be rewritten as

$$\begin{aligned} I &= 2\pi(\pi r^2/\lambda)^2 \frac{l}{1.4kr} \int_0^{\pi} (\sin u/u)^2 \sin\left(\pi - \frac{ul}{1.4kr}\right) du \\ &\sim \pi(\pi r^2/\lambda)^2 (l/1.4kr)^2 \int_0^{\pi} \frac{1 - \cos 2u}{u} du, \qquad (kr \gg 1) \\ &\sim \pi(\pi r^2/\lambda)^2 (l/1.4kr)^2 (3.2). \end{aligned} \quad (9)$$

Thus

$$\sigma_T = \pi r^2 (1 + 0.41 l^2). \quad (10)$$

Equating σ_T to $2\pi r^2$ then yields $l = 1.6$, the result quoted above.

Backscattering from Thin Prolate Spheroids

The backscattering cross section of a thin body (either a prolate spheroid or an ogive), in the nose-on direction, fits the following physical picture. The amount of scattering by the "point" (by points we mean the small regions at the front or rear wherein the radius of curvature is small with respect to the wavelength) at the front of the thin body is negligible. Much of the incident energy then creeps or travels along the surface of the body while part of it radiates tangentially. Most of the energy which is not radiated reaches the rear point. This may be considered either the point behind the ogive or the rear of the thin prolate spheroid. Then much of this energy is reflected back along the body and again much of it is forward scattered. However, forward scattering after the reflection from the rear point is now backscattering toward the transmitter. It is thus expected that the major returns in backscattering come from the rear point and this has been supported by Ohio State University experiments.[7] Further support has been given to this physical picture by using it to obtain a rough theoretical estimate of the expected backscattering from a thin prolate spheroid irradiated nose-on; then verifying the results in the laboratory using an uncoated metal prolate spheroid, and spheroids coated with absorbing material at the tips.

The experiments were carried out by measuring forward and backscattering from a spheroid of 10:1 ratio

[7] L. Peters, Jr., "End-fire echo area of long-thin bodies," IRE Trans. on Antennas and Propagation, vol. AP-6, pp. 133–139; January, 1958.

of major axis (2a) to minor axis (2b). With respect to the incident wavelength λ, (3.2 cm) $a=4.75\ \lambda$ and $b=0.475\ \lambda$. Hence the theory of the section on short wavelength forward scattering would give, for the forward-scattering aross section in square meters,

$$\frac{4\pi A^2}{\lambda^2} = \frac{4\pi}{\lambda^2}\left[\pi(0.475\lambda)^2\right]^2 = 6.6\times 10^{-3}m^2 = 22\ \text{db} < m^2. \quad (11)$$

The backscattered energy is primarily energy which is "reflected" from the rear since the direct backscattering from the nose is small. From the geometric optics formula for the cross section of this tip scattering, $\sigma=\pi b^4/a^2$, one finds this σ is less than 50 db $<$m^2. To estimate the contribution to the backscattering amplitude of the field that creeps toward the rear past the penumbra region one uses the fact that in the formula $\sigma_T=2.1$, one A is known to be due to large-angle scattering and one A to small-angle scattering. Thus the electric field amplitude on the spheroid just past the penumbra region would correspond to one A and not two. Thus f at the penumbra would correspond to half the forward-scattered field or $A/2\lambda$. It is then assumed on the basis of Belkina's[8] exact solution at smaller values of kr that the amplitude reflection coefficient at the rear tip is $\frac{1}{2}$, and that again only half of this would be forward scattered toward the transmitter. As a result the contribution to the scattering amplitude is of order

$$|f| \sim A/8\lambda \quad (12)$$

corresponding to a cross section in db relative to a square meter of

$$-22 - 10\log 64 \sim -40\ \text{db}. \quad (13)$$

These considerations neglect the small amount of radiation expected as the energy travels in from tip to penumbra region in two directions. The result given by (13) is slightly too high because of this neglect.

In the experiments absorbing material has been added to the front tip of the spheroid in one experiment and to the rear tip in a second experiment, as shown in the sketches in Table III. The material has been applied both symmetrically and asymmetrically with respect to the plane of the incident E vector. Arguments, such as those of the section on short wavelength forward scattering based on the conservation of energy and forward scattering theorems lead one to expect that the added coatings would increase the forward scattering above the 22 db $<m^2$ of (11), for when absorbing material is placed on the front, an increased forward scattering due to the increased area is expected to occur. This in turn will increase the amount of energy reaching the rear to be reflected and thus an increased backscattered cross section is to be expected. When absorbing material is placed on the rear tip, reflection from the rear is of course affected. If the material is placed symmetrically with respect to the plane of the E vector little change in radar cross section is to be expected, since the relative phase relations of the various rays are not affected. However, if this symmetry is destroyed, a marked decrease in cross section is to be expected. The experimental results, given in Table III and Fig. 5, are in accord with this theory.

[8] M. G. Belkina, "Radiation Characteristics of an Elongated Rotary Ellipsoid," appearing in "Diffraction of Electromagnetic Waves on Certain Bodies of Revolution," Sovetskoye Radio, Moscow, USSR; 1957.

Experimental Procedures

The experimental results presented in this paper were obtained on an indoor radar cross section measuring range housed in a room lined with radar absorbing material. The system used is the conventional type of continuous wave backscattering equipment with modifications to permit forward-scattering measurements. In backscattering measurements, a common transmitting and receiving antenna is used and the transmitted signal is separated from the received signal by a balanced hybrid tee. For the oscillator, a cavity stabilized system operating at X-band was used. The Scientific Atlanta "Wide Range Receiver" Model 402 was used as a receiver. This combination made it possible to obtain an isolation of about 100 db between the transmitter and receiver in backscattering measurements.

The forward-scattering measurements on the cone and cylinder were made with an angular separation of 180° between the transmitter and receiver antennas and with each pointing toward the target which was on the transmitter-receiver axis, half-way between the two antennas. The target was supported on a polyfoam column, which in turn rested on a turntable, making it possible to rotate the target 360° in azimuth. The turntable rotation was linked to the chart movement in the recorder.

To distinguish between the direct radiation and the forward-scattered signal at the receiving horn, the direct radiation was balanced out before the target was placed on the polyfoam support. The waveguide circuitry shown in Fig. 6 was used. The amplitude and phase of a balancing signal from the directional coupler was adjusted to cancel the directly radiated signal as the two signals entered the mixer via the symmetric arms of the hybrid tee. It was found possible to keep the level of the resultant signal 30 or 40 db below the forward-scattered signal for several minutes.

In measuring the width of the beam scattered in the forward direction by spheres (Fig. 4), the receiving horn was mounted on a trolley, and the received signal was recorded when the receiving horn was positioned at 180° and at several other positions within ±15° of the 180° position. For each new position, the directly radiated signal was balanced out before the target was placed in the beam.

Conclusions

One can conclude from the results given above that radar absorbing materials applied to conducting objects

TABLE III

SCATTERING BY A 10:1 PROLATE SPHEROID

$a = 4.75\ \lambda$ $b = 0.475\ \lambda$ $f = 9342$ Mcs

Target	Aspect	Backscatter db relative to m^2	Forward Scatter db relative to m^2
Standard Prolate Spheroid	Incident Energy ⟶ 	−42.9	−22.5
Modified Prolate Spheroid	Plane of Symmetry Parallel to E Vector 	−42.9	−19.5
	Plane of Symmetry Parallel to E Vector 	−36.9	−19.5
	Plane of Symmetry Normal to E Vector 	−48.4	−19.1
	Plane of Symmetry Normal to E Vector 	−40.4	−19.1

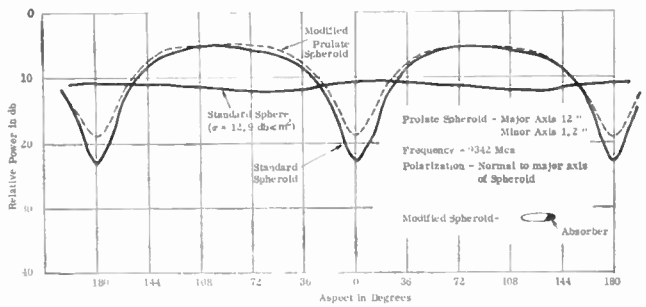

Fig. 5—Comparison of forward scatter (180°) cross section of standard spheroid and modified spheroid, showing also forward scatter cross section of standard sphere $kr = 4.9$.

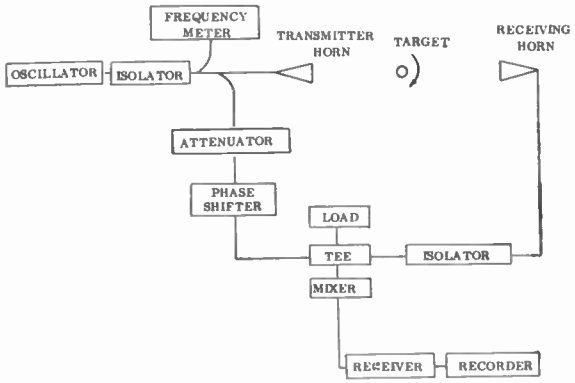

Fig. 6.

are ineffective in reducing the forward-scattering cross section; in fact, the coating increases the forward-scattering cross section. These conclusions are applicable when the wavelength is small compared to the dimensions of the object and within a narrow angular region about the forward direction. The beamwidth of this region is proportional to wavelength and, for a sphere of radius r, the beamwidth is given very well by $3.2/kr$.

A physical picture is presented showing how one could expect changes in the nose-on cross section of long thin shapes as a function of the use of absorbing materials in the rear of such objects. It is clear that the results are polarization dependent.

ACKNOWLEDGMENT

We should like to acknowledge the support given this program by Rome Air Development Center, Griffiss AFB, N. Y., and Air Force Cambridge Research Center, Bedford, Mass., under contracts AF-30(602)-1853 (RADC), AF-30(602)-1808 (RADC), and AF-19(604)-4993 (AFCRC).

We also wish to acknowledge the assistance of members of the Radiation Laboratory of The University of Michigan, Ann Arbor; A. Olte, D. L. Pepper, T. E. Hon, E. F. Knott, and R. L. Wolford for assistance in the experimental work.

The Ineffectiveness of Absorbing Coatings on Conducting Objects Illuminated by Long Wavelength Radar*

R. E. HIATT†, SENIOR MEMBER, IRE, K. M. SIEGEL†, SENIOR MEMBER, IRE, AND H. WEIL†

Summary—Theoretical and experimental electromagnetic scattering results are presented concerning the effects of applying thin coatings to perfectly conducting scatterers. Most of the paper is concerned explicitly with spheres and cones.

It is shown that thin coatings can have little effect on the Rayleigh scattering cross sections. It is also pointed out how the effect of conductivity is enhanced at low frequencies and how, as a consequence, a thin slightly lossy spherical shell scatters like a perfectly conducting sphere in the Rayleigh region.

Rayleigh Scattering by Coated Conducting Objects

This section considers the effect of a coating on perfectly conducting objects when the wavelength in the coating considerably exceeds the maximum diameter of the scatterer so that the scattering is Rayleigh scattering.

In this situation range the effect of any finite conductivity in the scatterer is almost the same as having infinite conductivity. That this is to be expected can be seen from the expression

$$k^2 = \omega^2\mu\epsilon\left(1 + \frac{is}{\epsilon\omega}\right)$$

for propagation constant k. Here ϵ and μ are respectively real permittivity and permeability, s is conductivity, ω is circular frequency, $i=\sqrt{-1}$. As $\omega\rightarrow 0$ the conductivity term dominates for any nonzero s. As a result the finite conductivity in a coating makes the coating act like a perfect conductor at sufficiently long wavelengths; energy cannot enter the coating to be absorbed. The effect of the finiteness of the conductivity enters the scattered field expressions to a higher order in an expansion in powers of k, the so-called Rayleigh series.

A fruitful alternate way to consider long-wavelength scattering is to note that an exact solution to Maxwell's equations and the boundary conditions, in the limit of long wavelengths, becomes the solution of the corresponding electrostatic ($k=0$) problem; then to use the fact pointed out by Rayleigh that an expansion of the field in powers of k must, in the near field (within a wavelength of the scatterer), coincide with the electrostatic solution. The constant coefficient of the leading term may then be determined by equating the static solution to the near-field solution. As a result in the near field the leading term of this expansion for the field is independent of the wavelength and is then, of course, independent of the magnitude of the conductivity. Thus, when the wavelength is large with respect to the dimensions of the scatterer, no coating material that is conducting can produce conduction current losses at the body of a magnitude to affect the leading term in the expansion of the far field in powers of k.

However, the far-field (electromagnetic as distinguished from electrostatic) backscattering consists of two components; the electric field corresponding to an electric dipole set up in the body and the electric field corresponding to a magnetic dipole set up in the body, and it is possible to have the effects of these two dipoles occur in such a manner that they tend to cancel. We shall illustrate these remarks by considering scattering by a coated perfectly conducting sphere since this case can be readily handled analytically. It turns out that with a coating material of large enough permeability the cross section of the sphere for backscattering could be significantly reduced. However, if one considers permeabilities achievable with real materials at microwave frequencies of interest one finds for thin layers that there are no materials available to accomplish this. The method of analysis used is based on specializing an exact solution of Maxwell's equations to the Rayleigh wavelength region. An alternate method based on extending the solution of the near-field static problem to the far field as described above yields identical results.

Coated Sphere

An exact solution for scattering of an incident plane wave by two concentric spheres of arbitrary material imbedded in an arbitrary medium has been given by Aden and Kerker.[1] The field and cross-section expressions have the forms of the well-known Mie series of spherical harmonics for scattering from a homogeneous sphere, but of course with different expressions for the coefficients a_n and b_n of the successive terms in the series. The series can be interpreted as giving the field as a superposition of multipole fields with a_n giving the strength of the magnetic multipole terms, b_n of the electric multipoles. We specialize Aden and Kerker's a_n and b_n to the case where the inner sphere is perfectly con-

* Received by the IRE, September 14, 1959; revised manuscript received, February 29, 1960.

† University of Michigan Radiation Lab., Ann Arbor, Mich.

[1] A. L. Aden and M. Kerker, "Scattering of electromagnetic waves from two concentric spheres," *J. Appl. Phys.*, 22, pp. 1242–1246; October, 1951.

ducting, or nearly so.[2] For wavelengths in the coating large with respect to the radii the dominant terms are the a_1 and b_1 terms. In this case the scattering is termed Rayleigh scattering. The coating, *i.e.*, the region between the concentric spheres, will be left arbitrary, *i.e.*, with general complex permittivity ϵ_2 and permeability μ_2, and will have thickness d. No extra work is involved in leaving the embedding medium arbitrary so its parameters ϵ_3 and μ_3 will also be left arbitrary and complex.

The resulting coefficients are, for an inner sphere of radius $a>0$, outer sphere of radius b:

$$a_1 = \frac{i(k_3b)^3}{3}\left[\frac{2+\rho-2M(1-\rho)}{2+\rho+M(1-\rho)}\right], \qquad \begin{matrix} a>0 \\ b\geq a \end{matrix}$$

$$b_1 = \frac{i(k_3b)^3}{3}\left[\frac{2(1-\rho)-2E(2\rho+1)}{2(1-\rho)+E(2\rho+1)}\right] \qquad \begin{matrix} a>0 \\ b\geq a \end{matrix}$$

where $M=\mu_2/\mu_3$, $E=\epsilon_2/\epsilon_3$ and $\rho=a^3/b^3$. When there is no coating; *i.e.*, when $b=a$, or $\mu_2=\mu_3$, $\epsilon_2=\epsilon_3$,

$$a_1 = \tfrac{1}{3}i(k_3a)^3$$

$$b_1 = -\tfrac{2}{3}i(k_3a)^3,$$

which are the usual results for a perfectly conducting sphere of radius a.

Let us consider the factors in square brackets in a_1 and b_1. Denote these factors by α and β respectively. For α, the terms involving the properties of the coating, *i.e.*, those with the M factor, become comparable to the other terms when

$$|M| \sim \frac{2+\rho}{2(1-\rho)} = M_\mu.$$

For thin layers M_μ is extremely large. As M varies from 1 to M_μ and greater, α decreases monotonically from ρ to -2.

From β, terms involving the coating material properties (*i.e.*, terms in E) come into play for

$$|E| \sim \frac{1-\rho}{2\rho+1} = E_\epsilon.$$

For thin coatings, $E_\epsilon<1$, hence all possible E values affect the results. However, the variation in β as E varies from 1 to very large values is relatively small, going only from -2ρ to -2.

In considering these very large values of M or E it should be borne in mind that k_2 can get very large; unless ω is sufficiently small the requirement $|k_2b|\ll 1$, will be violated. When $|k_2b|\sim 1$, the above expressions for a_1 and b_1 are not valid even though $|k_3b|\ll 1$ and in addition, the higher order a_n and b_n terms must be included. The situation, of course, simplifies if $|k_2b|\gg 1$ while $|k_3b|\ll 1$, for then the effect is essentially the same as Rayleigh scattering from an enlarged conducting sphere of radius b.

When the above a_1 and b_1 terms give an adequate description of the field (a very important restriction) the effect of a coating on radar backscattering cross section σ is found from the expression

$$\sigma \sim \frac{9\pi}{k_3^2}\,|a_1-b_1|^2 = \pi k^4\frac{a^6}{\rho^2}\,|\alpha-\beta|^2 \qquad (1)$$

and the preceding analysis.

For the no-coating case ($\rho=1$)

$$|\alpha-\beta|^2 = 9\rho^2 \qquad \sigma = (\pi k^4)(9a^6) = (\pi k^4)(9b^6). \qquad (2)$$

Particular special cases for coatings are of interest: For

$$|E|\gg 1, \quad |M|=1 \qquad |\alpha-\beta|^2 = \rho^2\left|1+\frac{2}{\rho}\right|^2.$$

Hence, any nonmagnetic coating at all placed on a perfectly conducting sphere will tend to increase the radar cross section for Rayleigh scattering.

Next consider magnetic coatings. For

$$|E|\gg E_\epsilon \text{ and } |M|\gg M_\mu; \qquad |\alpha-\beta|^2\sim 0.$$

Thus magnetic coatings can reduce the Rayleigh backscattering cross section appreciably. For thin coatings M_μ is extremely large. For a given reduction, *i.e.*, a specified value of $|\alpha-\beta|<3\rho^2$ and $b-a$ small, the dependence on thickness is approximated by

$$|M_\mu| = \left|\frac{[(\alpha-\beta)-3](2+\rho)(2\rho+1)E}{-6(1-\rho)^2+(\alpha-\beta)(2\rho+1)(1-\rho)E}\right|$$

which of course leads to very large M. However, with such large M, in order for $|k_2b|\ll 1$ to be satisfied, b must be so extremely small compared to the free space wavelength that the return would be negligible even if the spheres were not coated. Thus in no practical case could one expect to camouflage a sphere in Rayleigh scattering. This result is emphasized by a study of the ferrite materials listed in von Hippel's tables[3] which shows that large $|M|$'s are accompanied by large $|E|$'s. In addition, very large $|M|$'s are not available at all for frequencies above about 500 mc.

Pertinent examples using data from von Hippel are given in Table 1. The values of $b_{\max}$ were computed using $|k_2b|<0.1$ as an approximation to $|k_2b|\ll 1$. These values are to be compared with the wavelength of 30 meters.

The above expression for b_1 in terms of the complex quantity $E=\epsilon_2/\epsilon_3$ can be written out explicitly in terms of the conductivity s and real dielectric constant ϵ of the coating. When the resulting expression is expanded in

[2] The same procedure was used by H. Scharfman, "Scattering from dielectric coated spheres in the region of first resonance," *J. Appl. Phys.*, vol. 25, pp. 1352–1356, November, 1954, although Scharfman used $\mu_3=\mu_2$ and ϵ_2 real.

[3] A. R. von Hippel, Ed., "Dielectric Materials and Applications," Technology Press of Massachusetts Institute of Technology, Cambridge, Mass., and John Wiley and Sons, Inc., New York, N. Y.; 1954.

TABLE I

RELATIVE PERMITTIVITY E AND PERMEABILITY M FOR FERRITES, $f=10$ MC, TEMPERATURE $=25°C$

Material	$\|E\|$	$\|M\|$	$\|N\|$	$b_{\max}(m)$
Crowloy 20	26.5	93.2	49.9	0.01
Crowloy 70	28200	94.4	1640	0.0003
Ferramic A	8.86	24.7	14.8	0.036
Ferramic B	3250	114	60.6	0.008
Ferramic C	6280	256	1270	0.0004
Ferramic D	8069	214	1320	0.0004

powers of k the conductivity does not appear in the lowest order term; the expression for b_1 is that of a perfectly conducting sphere of the size of the coated sphere, the effect of finite conductivity entering only as a higher order correction.

In the following medium 3 will be assumed to be lossless. Then

$$E = \frac{\epsilon}{\epsilon_3} + \frac{is}{k_3\epsilon_3 c} = \frac{\epsilon}{\epsilon_3} + \frac{i\sum}{k_3} \tag{3}$$

where c is the velocity of light and $\sum = s/\epsilon_3 c$. The conductivity s will in general have a dc part $\bar{s}$ caused by migrating charge carriers and also a frequency dependent part s_D, due to rotation of polar molecules so that $s=\bar{s}+s_D$. The latter part, s_D, is described approximately by the Debye equation as

$$s_D = \epsilon_3 c K \frac{k_3^2\tau}{1 + k_3^2\tau}$$

where K and τ are constants for a given material. If k_3 is small enough $s\sim\bar{s}$, a constant. Likewise, if k_3 is large enough that $k_2^2\tau\gg 1$, s is again independent of frequency. To obtain the first terms in the expansion when s is independent of frequency, let b_1 be written as

$$b_1 = 2\frac{i(k_3b)^3}{3}\frac{Ak_3 - 1}{Bk_3 + 1}$$

where

$$A = \frac{b^3 - a^3 - (2a^3 + b^3)\epsilon/\epsilon_3}{(2a^3 + b^3)\, i\sum}$$

$$B = \frac{2(b^3 - a^3) + (2a^3 + b^3)\epsilon/\epsilon_3}{(2a^3 + b^3)\, i\sum}.$$

Thus for small k_3B

$$b_1 \sim \frac{-2i(k_3b)^3}{3}\left[1 - k_3(A + B)\right].$$

We shall assume $b-a=d$ is small so that $k_3B\ll 1$ implies $(k_3/\sum) = (\epsilon_3/\epsilon)$ which, of course, rules out letting $\sum\to 0$ unless $\epsilon\to 0$ also. Then using

$$b^3 - a^3 \sim 3b^2 d,$$

$$b_1 \sim \frac{-2i(k_3b)^3}{3}\left(1 + k_3\frac{3d\epsilon_3 ci}{b\bar{s}}\right).$$

Depending on the magnitude of the constants K, τ and $\bar{s}$ and the values of k_3 of interest s_D may dominate the expression for s in a dielectric. If this is the case, and also $k_3^2\tau\ll 1$, one can take

$$s \sim s_D \sim \epsilon_3 c K \tau k_3^2$$

and also use the dc value of ϵ/ϵ_3. The corresponding expansion is

$$b_1 \sim \frac{-2i(k_3b)^3}{3}\left[1 - \frac{3d}{b}\frac{\epsilon_3}{\epsilon} + ik_3\left(5K\tau\frac{d\epsilon_3}{b\epsilon}\right)\right]$$

so that the effect of finite conductivity again appears as a higher order effect.

EXPERIMENTAL RESULTS AND PROCEDURES

To check these theoretical results backscattering measurements were made of coated and uncoated spheres and cones.

The experimental results were obtained on an indoor radar backscattering range in a measurement room lined with microwave absorbing material. The system used was the conventional continuous wave type where a common transmitter and receiver antenna is used and the transmitted signal is separated from the received signal by a balanced hybrid tee. The oscillator was frequency controlled by the use of a crystal exciter and frequency multiplying circuits. The operating frequency was S band (2870 mc). The Scientific Atlanta Wide Range Receiver was used. This combination made it possible to obtain an isolation between the transmitted and received signal of about 100 db. The targets were supported on a polyfoam column. All measurements were made at a range of $2D^2/\lambda$ or greater where D is the maximum dimension of the horn aperture or of the target, whichever is greater.

Measurements procedures were as follows: with no target, the return from the background and from the polyfoam support was balanced out with waveguide tuners. The return was then recorded from the calibration sphere, from the test targets and then again from the calibration sphere. The points that appear on the curves represent the average of several measurements. Results before averaging usually agreed to within $\pm\frac{1}{2}$ db.

The material used for the coating layer on the test spheres and cones was a mixture of iron powder dispersed in a plastic binder. The proportions used and the layer thickness would form a good absorbing layer if applied to flat plates or other objects whose radius of

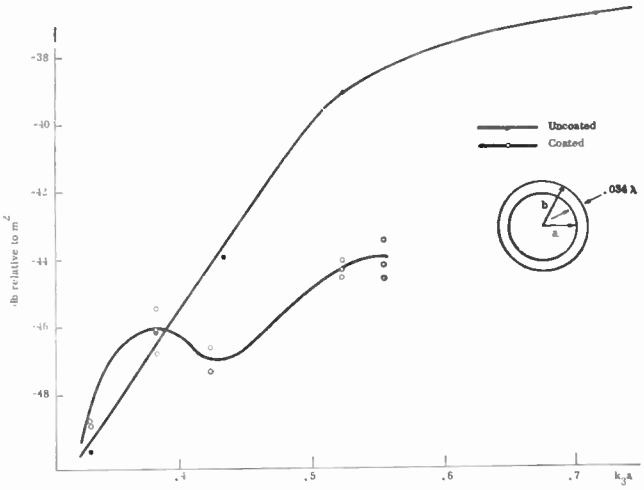

Fig. 1—Backscattering from spheres (referenced to uncoated 0.500 inch sphere).

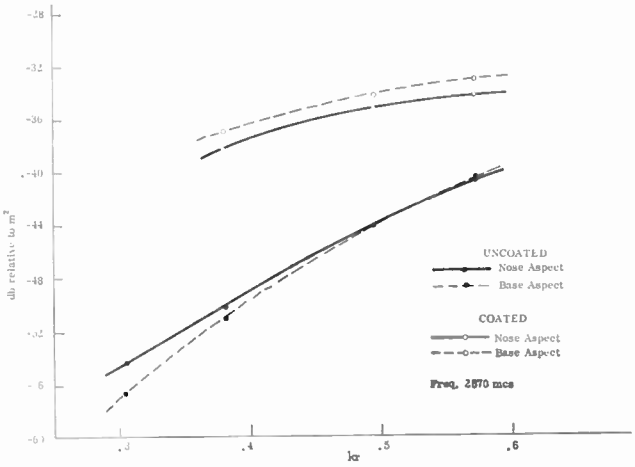

Fig. 2—60° cones backscattering.

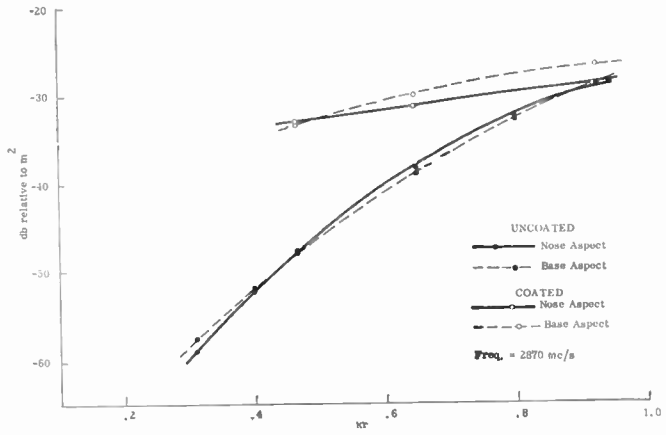

Fig. 3—90° cones backscattering.

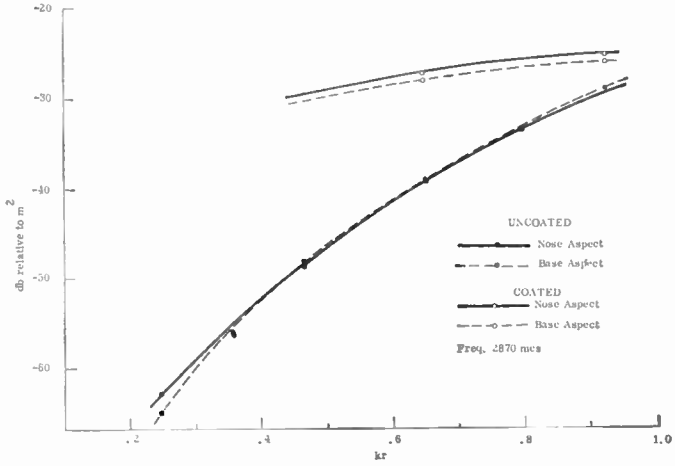

Fig. 4—120° cones backscattering.

curvature is not small compared to wavelength.[4]

The experimental results for spheres are shown in Fig. 1. As expected, in the resonance region the radar absorbing material works as an absorber and as one goes into the Rayleigh region one finds that this effect disappears. The return in the Rayleigh region is slightly higher than the inner sphere alone would give. Additional experimental work is needed to show more clearly the behavior of the curve for smaller values of kr.

Figs. 2, 3, and 4 show the Rayleigh-resonant effect quite well for cones of base radius r.

Similar results were predicted by Siegel.[5] It was found by Brysk, *et al.*,[6] that as one goes from the resonance region into the Rayleigh region and throughout the Rayleigh region there will be little difference between nose-on and base-on scattering for finite cones. However, with coated cones one would expect the cross section of the cone to increase. If it increases nose-on one would expect it also to increase base-on. The effect of μ and s is to increase the effect of length of the body and as a result the effective dipole moments increase. Hence one would expect a significant increase of the coated body over the uncoated body as one goes from the resonance region into the Rayleigh region. Of course, the increase in volume increases the cross section as the square of the volume.

Rayleigh Scattering by Hollow Shells

The property that, when the wavelength is sufficiently large with respect to the dimensions of the scatterer, a small amount of conductivity makes the body scatter very much like a perfect conductor, can be exploited in designing an object made of a thin slightly conducting (essentially nonmetallic) shell which will give a return

[4] The formula for this absorber was supplied by R. W. Wright and W. H. Emerson of the U. S. Naval Research Laboratory. The formula is not necessarily optimum for the frequency and target sizes involved in these measurements. Precise values of the refractive index of the material as a function of frequency were not measured.

[5] K. M. Siegel, "Far-field scattering from bodies of revolution," *Appl. Sci. Res.*, vol. 7, no. 4, pp. 293–328; 1958.

[6] H. Brysk, R. E. Hiatt, K. M. Siegel, and V. H. Weston, "The nose-on radar cross section of finite cones," *Can. J. Phys.*, vol. 37, pp. 675–679; May, 1959.

as though it were a perfect conductor. To make this idea more precise in an explicit case, Aden and Kerker's solution for concentric spheres will be used to obtain a relation between shell thickness and conductivity which will enable a spherical shell to simulate an infinitely conducting sphere in Rayleigh scattering.

Specifically, we specialize the Aden and Kerker results to the case of Rayleigh scattering from a spherical shell with large $s/\epsilon\omega$ ratio. The medium inside the shell is considered to have a small index of refraction and the outer medium will be considered to be lossless. The outer medium will be considered to be free space, the enclosed medium (2) will be arbitrary to the extent of having no very large magnitudes of ϵ, real permittivity, μ, real permeability or s, conductivity. The inner and outer radii are a and b and the media will be numbered 1, 2, and 3 as shown in Fig. 5.

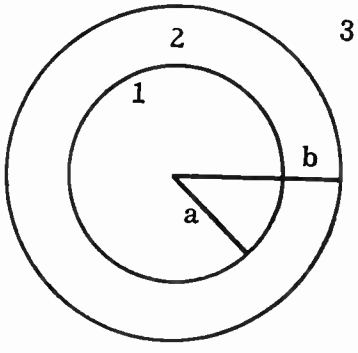

Fig. 5.

The Rayleigh field is given by two dipole terms, one magnetic, one electric , of respective strengths a_1 and b_1. Aden and Kerker express the general a_n and b_n in terms of complex indices of refraction N_1 and N_2 (propagation constants of media 1 and 2 relative to the propagation constant of medium 3) and characteristic admittances Y_1, Y_2 and Y_3.

In terms of ϵ, μ and s

$$N_2 = \sqrt{\frac{\mu_2\epsilon_2}{2\mu_3\epsilon_3}}\left\{\left[\sqrt{1+\frac{s_2^2}{\epsilon_2^2\omega^2}}+1\right]^{1/2} + i\left[\sqrt{1+\frac{s_2^2}{\epsilon_2^2\omega^2}}-1\right]^{1/2}\right\}$$

and

$$Y_2 = \frac{N_2 k}{\omega\mu_2}, \qquad \text{where } k = 2\pi/\lambda.$$

When $s_2^2/(\epsilon_2^2\omega^2) \gg 1$,

$$N_2 \sim \sqrt{\frac{\mu_2 s_2}{2\mu_3\epsilon_3\omega}}(1+i); \qquad |N_2| \gg 1.$$

The multipole strengths as given by Aden and Kerker, but for $e^{-i\omega t}$ time dependence, are

$$a_n = a_n^s \frac{1+\dfrac{[\nu j_n(\nu)]'}{\nu j_n(\nu)}\dfrac{A_{4n}}{A_{3n}}}{1+\dfrac{[\nu h_n(\nu)]'}{\nu h_n^{(1)}(\nu)}\dfrac{A_{4n}}{A_{3n}}} \tag{4}$$

$$b_n = b_n^s \frac{1+\dfrac{\nu j_n(\nu)}{[\nu j_n(\nu)]'}\dfrac{A_{2n}}{A_{1n}}}{1+\dfrac{\nu h_n(\nu)}{[\nu h_n(\nu)]'}\dfrac{A_{2n}}{A_{1n}}}. \tag{5}$$

Here $\nu = kb$, the coefficients $A_{1n} \cdots A_{4n}$, which will be discussed below, are functionals of Y_1, Y_2, Y_3 and spherical cylinder functions of arguments $N_2\nu$, $N_2\alpha$ and $N_1\alpha$, $(\alpha = ka)$ and

$$a_n^s = -\frac{j_n(\nu)}{h_n(\nu)}, \qquad b_n^s = -\frac{[\nu j_n(\nu)]'}{[h_n^{(1)}(\nu)]'}.$$

The a_n^s and b_n^s are the coefficients which apply for a solid sphere of very large s or ϵ. They may be obtained by replacing the cylinder functions of $N_1\alpha$ by the asymptotic expansions

$$h_n^{(1)}(\rho) \sim \frac{-1}{\rho}e^{i\rho}, \qquad j_n(\rho) \sim \frac{1}{\rho}\cos\left(\rho - \frac{n+1}{2}\pi\right),$$

valid for[7] $|\rho| \gg n^2$; and setting $\alpha = \nu$ in Aden and Kerker's general formulas for a_n and b_n. For $\nu \ll 1$, substitution of the power series expansions for $j_n(\nu)$ and $h_n(\nu)$ shows that a_1^s and b_1^s are lower of order than the terms of greater index n and the scattering for the solid sphere in this case is called Rayleigh scattering.

Using the power series in the factors multiplying a_n^s and b_n^s in (4) and (5) yields

$$a_n \sim a_n^s \frac{1+\dfrac{(n+1)}{\nu}\dfrac{A_{4n}}{A_{3n}}}{1-\dfrac{n}{\nu}\dfrac{A_{4n}}{A_{3n}}}$$

$$b_n \sim b_n^s \frac{1+\dfrac{\nu}{(n+1)}\dfrac{A_{2n}}{A_{1n}}}{1-\dfrac{\nu}{n}\dfrac{A_{2n}}{A_{1n}}}.$$

[7] Terms of high index n for which this inequality does not hold must be considered separately using the appropriate asymptotic forms. See H. Weil, "On the convergence of the Mie series for scattering spheres," *Bull. Am. Math. Soc.*, vol. 63, pp. 133–134; March, 1957, and H. Weil, M. L. Barasch and T. A. Kaplan, "Scattering of Electromagnetic Waves by Spheres," University of Michigan, Ann Arbor, Rept. No. 2255-20-T; July, 1956.

As stated, we shall assume the shell in the present problem has a large $|N_2|$. For $\nu \ll 1$ and $N_1\alpha \ll 1$ we shall then obtain an inequality relating N_2 and shell thickness such that, when the inequality is satisfied, the factors multiplying a_n^s and b_n^s are approximately unity, *i.e.*,

$$\frac{n+1}{\nu}\frac{A_{4n}}{A_{3n}} \ll 1, \qquad \frac{\nu}{n}\frac{A_{2n}}{A_{1n}} \ll 1.$$

By replacing the cylinder functions of $N_2\nu$ and $N_2\alpha$ by the above asymptotic expansions, one obtains

$$\frac{A_{2n}}{A_{1n}} = \frac{Y_3}{Y_2}\frac{Y_2T_2(\nu,\alpha) - iY_1\dfrac{N_1\alpha}{n+1}T_3(\alpha,\nu)}{Y_2T_1(\alpha,\nu) - Y_1\dfrac{N_1\alpha}{n+1}T_2(\alpha,\nu)}$$

$$\frac{A_{4n}}{A_{3n}} = \frac{Y_3}{Y_2}\frac{-Y_2T_2(\alpha,\nu) + Y_1\dfrac{n+1}{N_1\alpha}T_1(\alpha,\nu)}{-iY_2T_3(\alpha,\nu) + Y_1\dfrac{n+1}{N_1\alpha}T_2(\nu,\alpha)}$$

where $T_2 \equiv T_{jn}$ and

$$T_{1n}(\alpha,\nu) = \cos\left(N_2\nu - \frac{n+1}{2}\pi\right)e^{iN_2\alpha} - \cos\left(N_2\alpha - \frac{n+1}{2}\pi\right)e^{iN_2\nu}$$

$$T_{2n}(\alpha,\nu) = i\cos\left(N_2\nu - \frac{n+1}{2}\pi\right)e^{iN_2\alpha} + \sin\left(N_2\alpha - \frac{n+1}{2}\pi\right)e^{iN_2\nu}$$

$$T_{3n}(\alpha,\nu) = \sin\left(N_2\nu - \frac{n+1}{2}\pi\right)e^{iN_2\alpha} - \sin\left(N_2\alpha - \frac{n+1}{2}\pi\right)e^{iN_2\nu}.$$

Now write $N_2 = N' + iN''$ and make use of the fact that $|N''\nu| \gg 1$ and $|N''\alpha| \gg 1$. Then in exponential form

$$T_{1n}(\alpha,\nu) \sim \frac{1}{2}\left[e^{-iN'(\nu-\alpha)}e^{N''(\nu-\alpha)} - e^{iN'(\nu-\alpha)}e^{-N''(\nu-\alpha)}\right]e^{i\pi(n+1)/2}$$

$$T_{2n}(\alpha,\nu) \sim T_{2n}(\nu,\alpha) \sim \frac{i}{2}\left[e^{-iN'(\nu-\alpha)}e^{N''(\nu-\alpha)} + e^{iN'(\nu-\alpha)}e^{-N''(\nu-\alpha)}\right]e^{i\pi(n+1/2)}$$

$$T_{3n}(\alpha,\nu) \sim iT_{1n}(\alpha,\nu).$$

In general, interest is in small $\nu - a = k(b-a)$. If, nonetheless, N'' is so large that $N''(\nu-\alpha) \geq 1$ then

$$|T_{1n}| \sim |T_{2n}| \sim |T_{3n}|.$$

In this case, using the inequalities $|N_2| \gg 1$, $|N_2\nu| \gg n^2$, $|N_2\alpha| \gg n^2$ one finds

$$\left|\frac{A_{2n}}{A_{1n}}\right| \sim \left|\frac{A_{4n}}{A_{3n}}\right| \sim \frac{Y_3}{Y_2}$$

$a_n \sim a_n^s$, $b_n \sim b_n^s$. Thus there is no problem in this case; the criterion we are after, giving the minimum conductivity for a given thickness, or minimum thickness for a given conductivity, must stem from the situation where $N''(\nu-\alpha) \ll 1$. In this case, since $N' \sim N''$

$$T_{1n} \sim N'(\nu-\alpha)(1-i)$$
$$T_{2n} \sim i$$
$$T_{3n} \sim N'(\nu-\alpha)(1+i).$$

Then

$$a_n \sim a_n^s\frac{1 + \dfrac{n+1}{\nu}\overline{A}_n}{1 - \dfrac{n}{\nu}\overline{A}_n}, \qquad b_n \sim b_n^s\frac{1 + \dfrac{\nu}{n+1}B_n}{1 - \dfrac{\nu}{n}B_n}$$

where

$$\overline{A}_n = Y_3\frac{-1 - \dfrac{n+1}{N_2\alpha}\dfrac{\mu_2}{\mu_1}(1+i)N'(\nu-\alpha)}{(1+i)Y_2N'(\nu-\alpha) + Y_1(n+1)/N_1\alpha}$$

$$B_n \sim Y_3\frac{-1}{(1+i)Y_2N'(\nu-\alpha) + Y_1N_1\alpha/(n+1)}.$$

Now we assume μ_2/μ_1 small enough that the numerator of $\overline{A}_3 = -1$. This will rule out only extremely magnetic materials at very low frequencies since $N_2\alpha \gg (n+1)^2$ and $N'(\nu-\alpha) \ll 1$. Then we can be assured that $a_n \sim a_n^s$ if

$$\frac{n+1}{\nu}|A_n| \ll 1.$$

This will be true for all n if[8]

$$\frac{n+1}{\nu}\left|\frac{N_1Y_3}{Y_1}\right|\frac{1}{\left|2iN'^2(\nu-\alpha)\dfrac{\mu_1}{\mu_2} + \dfrac{n+1}{\alpha}\right|} \ll 1.$$

A more severe criterion on N' than is furnished by this inequality comes about by setting $(n+1)/\alpha = 0$. Then the resulting requirement on N' is

$$N'^2 \gg \frac{1}{2}\left|\frac{n+1}{\nu}\frac{N_1Y_3}{Y_1}\frac{1}{\nu-\alpha}\frac{\mu_2}{\mu_1}\right|$$

i.e.,

$$N'^2 \gg \frac{1}{2}\frac{n+1}{\nu}\frac{\mu_2}{\mu_3}\frac{1}{\nu-\alpha}.$$

[8] The authors are grateful to a reviewer for pointing out an error at about this stage (in an earlier version of this paper) which led to an incorrect criterion.

The analogous condition under which $b_n \sim b_n^s$ leads to a less severe criterion on N'; that is a smaller N' for a given thickness and wavelength. Finally we use the fact that the greatest value of n for which these expressions were derived is subject to the inequality $(n+1)^2 \ll |N_2\nu|$. Hence $(n+1)/\nu$ can be replaced by $\frac{1}{2}|N_2| = N'/\sqrt{2}$ on the right side to obtain a criterion independent of n. This leads to

$$N' > \frac{1}{2\sqrt{2}} \frac{\mu_2}{\mu_3} \frac{1}{(\nu - \alpha)}$$

or in terms of conductivity s_2

$$s_2 > \left(\frac{\mu_2}{\mu_3}\right)^2 \frac{1}{4\mu_2\omega} \frac{1}{(b-a)^2}.$$

By solving for $b-a$ this criterion can also be interpreted to say that if $b-a$ exceeds

$$\frac{1}{2\sqrt{2}} \frac{\mu_2}{\mu_3}$$

times the skin depth the Rayleigh return will be like that of a solid perfectly conducting sphere.

For an illustrative numerical example we assume $\mu_1 = \mu_2 = \mu_3 = 4\pi \times 10^{-7}$ henry/meter, the value for free space. Then for s_2 in mhos/m, $(b-a)$ in meters and f in cycles/second

$$s_2 > \frac{10^7}{4\pi(b-a)^2\omega} \sim \frac{1.3 \times 10^5}{(b-a)^2 f}.$$

Let us consider a 0.5-mm thick shell. Then

$$s_2 > \frac{10^{11}}{f}$$

is required. For 3-cm waves, $f = 10^{10}$ and the requirement is $s_2 > 10$ mhos/m, while for 3-meter waves, $f = 10^8$ and the requirement is $s_2 > 1000$ mhos/m. s_2 is very frequency sensitive for dielectrics and $s_2 = 10$ is just about the greatest value of s_2 reached for 3-cm waves by unloaded dielectrics listed in von Hippel's tables. It is greater than the values reached for $f = 10^8$ so that for 3-meter waves and a 0.5-mm thickness some loading of the dielectrics would be needed.

ACKNOWLEDGMENT

We should like to acknowledge the support given this program by Air Force Cambridge Research Center, Bedford, Mass., and Rome Air Development Center, Griffiss AFB, N. Y., under contracts AF19(602)-4993, AF30(602)-1853 and AF30(602)-1808.

We also wish to acknowledge the assistance of members of the Radiation Laboratory of The University of Michigan, Ann Arbor; T. B. A. Senior for aid on theoretical parts of this investigation, and A. Olte, D. L. Pepper, T. E. Hon, E. F. Knott and R. L. Wolford for assistance in the experimental work. We wish to thank our reviewers for many useful and stimulating criticisms of the original manuscript.

Correspondence

Epitaxial Diffused Transistors*

This letter describes diffused base transistors, the structures of which incorporate thin semiconductor layers epitaxially deposited on low-resistivity substrates of the same semiconductor. Collector series resistance and excess stored charge in the saturated switching condition are substantially lower than for diffused base transistors made by more conventional techniques. This makes possible significant increases in switching speed and high-frequency gain. The technique promises comparable improvements in diode speeds and opens possibilities of new complex structures.

The bulk resistivity of the semiconductor wafer used in conventional diffused base mesa transistors gives rise to an internal resistance in series with the collector. In small signal transmission applications of the transistor, this resistance reduces the high-frequency gain by absorbing power which might otherwise be coupled to the load. In switching or other large signal use, it causes excessive "on" voltage drop. In addition, the high-resistivity bulk region slows the recovery of the transistor from a saturated switching condition by providing a long-lifetime medium for stored charge. It is ordinarily not possible to suppress these effects by use of low-resistivity wafers because this also lowers the collector breakdown voltage and raises the collector capacitance.

A more ideal transistor structure is shown in Fig. 1. Here, the junction characteristics are controlled by diffusing the base and emitter layers into a thin, high-resistivity layer. The main body of the collector is a very-low-resistivity material. Such a structure possesses all the advantages of conventional diffused base mesa transistors and eliminates many of the disadvantages.

A technique for making such structures is now available. The thin high-resistivity layer can be produced by thermal decomposition of silicon tetrachloride or germanium tetrachloride on a low-resistivity

* Received by the IRE, July 5, 1960.

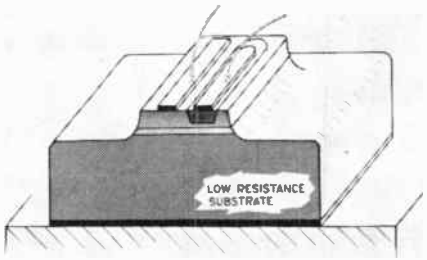

Fig. 1—Mesa transistor structure with thin high-resistivity layer between diffused collector junction and low-resistance collector body.

TABLE I

MEDIUM-POWER SILICON MESA TRANSISTORS
T_s (STORAGE TIME CONSTANT) FROM STORAGE TIME RELATION

$$t_s = T_s \ln\left(\frac{\beta I_{B1}}{I_c}\right) \text{ WITH } I_{B2} = 0$$

	Conventional Structure	Epitaxial Film Structure
Substrate Resistivity	—	0.002 Ω cm
Epitaxial Film Resistivity	—	1.5 Ω cm
Emitter Size	4×35	2×20 mil²
BV_{CBO}	80	90 volts
$C_c(V_{CB}=5V)$	30	10 μμf
$V_{CE}(I_C=500$ ma $I_B=50$ ma)	1.9	0.6 volts
T_s	1350	100 mμsec

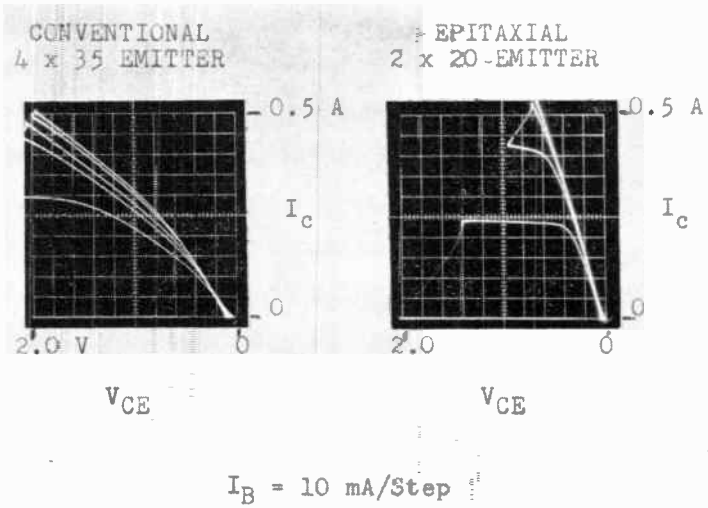

Fig. 2—Low voltage common emitter output characteristics of conventional and epitaxial silicon (medium-power, n-p-n) mesa transistors.

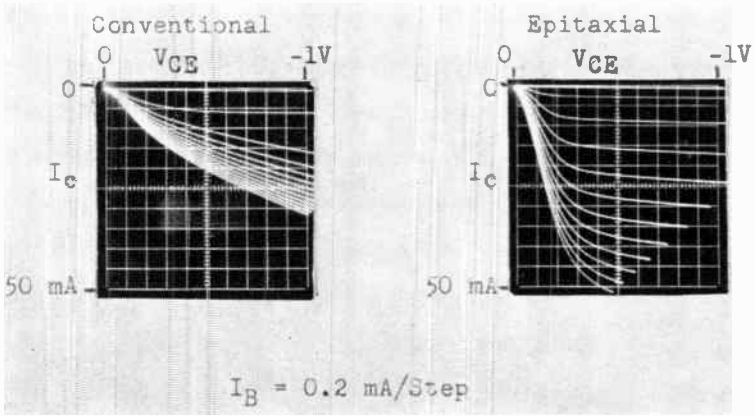

Fig. 3—Low-voltage common emitter output characteristics of conventional and epitaxial germanium mesa transistors. (Emitter 4×2 mil².)

substrate of the same material. When carried out under the proper conditions, the layers grow epitaxially; *i.e.*, the single crystal structure of the substrate is propagated into the thin film. Conventional diffused base technology can then be used to make transistors on this material.

Rough approximations to the structure of Fig. 1 have previously been obtained by diffusing or alloying a low-resistivity region into the wafer from the collector contact side. Because the critical thickness of the high-resistivity region is the difference between total wafer thickness and the depth of alloying or diffusion, these procedures have been difficult to control and therefore expensive.

Transistors of both germanium and silicon have been made on epitaxial material. In the case of silicon, a low-resistivity (0.002 ohm-cm) n-type crystal was used as a substrate. Epitaxial n-type layers several microns thick were produced by the decomposition of $SiCl_4$. The base and emitter layers were then diffused using conventional boron and phosphorus processes. The transistors have all the desirable features of conventional diffused base transistors. For example, they have high alpha, high gain and sharp junctions. None of the electrical parameters were degraded, while some parameters have been improved. Comparison data for two medium power silicon transistors with about equal power ratings are given in Table I, and their collector characteristics are shown in Fig. 2. One is a conventional 0.5-ampere switching transistor. The other is an epitaxial diffused transistor with a much smaller emitter area. As anticipated, the collector series resistance, switching speed and collector capacitance of the epitaxial transistor are significantly better than for the conventional transistor. Comparable and extended results have been obtained for low-level silicon switching transistors by A. E. Blakeslee and H. J. Patterson.

Similar improvements have been made in germanium transistors. In this case the epitaxial layer was again formed on a low-resistivity substrate by decomposition of the tetrachloride. The base and emitter layers were formed by diffusing antimony and alloying aluminum, respectively. The collector characteristics of a typical unit as compared with a conventional structure are shown in Fig. 3.

In addition to the improvements in electrical performance, many fabrication problems are eased by use of epitaxially grown material. For example, the problem of making noninjecting ohmic contacts to the collector body of a germanium transistor is eliminated. Also, in fabricating the epitaxial transistor structures, there is no need to lap or polish the wafer prior to diffusion. By the elimination of these processes, mechanical damage in the material is reduced. In addition, the epitaxial layer provides close control of the high-resistivity region of the collector body.

Although we have emphasized the compatibility of epitaxial films with conventional diffusion and alloying processes, the use of the material is by no means restricted to these techniques. For example, the need for a diffused base layer may be eliminated by doping the epitaxially grown film to an appropriate resistivity.

The same techniques obviously apply to diodes, p-n-p-n devices and similar junction elements. Comparable improvements are expected in these devices.

The use of epitaxial material, however, is not restricted to conventional devices. Complex structures, which are difficult to fabricate or not possible with conventional device technology now become feasible. These techniques will open many new horizons in the semiconductor device area.

The authors gratefully acknowledge the help of their colleagues in this work. The guidance and assistance of I. M. Ross, J. M. Early, and J. M. Goldey is especially appreciated.

H. C. THEURER
J. J. KLEIMACK
H. H. LOAR
H. CHRISTENSEN
Bell Telephone Labs.
Murray Hill, N. J.

Use of the Hydrogen Line to Measure Vehicular Velocity*

The purpose of this correspondence is to present some of the considerations leading to the development of a device to measure the velocity of a vehicle by means of the Doppler shift in the stellar spectrum.

In 1947, the first laboratory measurements of the 21-cm hydrogen line in radio astronomy were made.[1] In 1955, the "red shift" of a distant radio source was detected by observing the 1420-mc absorption line Doppler shifted to 1340 mc.[2] To the present, sufficient data have been gathered on celestial radio sources so as to make it practical to employ the Doppler shift of their absorption spectra in the solution of navigation problems. Equipment is now being constructed to further study these sources for this special application. The celestial sources most highly regarded for their utility in navigation are Cassiopeia A, Taurus A and Sagittarius A. The closest of these (Taurus A) is 1100 parsecs from our planetary system, which is equivalent to approximately 3600 light years. These sources have several important physical characteristics in common. As discrete radio sources they each subtend an angle in the sky of approximately 6 minutes of arc. Their spectra may be observed both in emission and absorption. The absorption notch is quite sharp and is the basis for their utility in navigation. (It is a hydrogen cloud positioned between the observer and the radio source which causes the absorption feature to be formed.) For example, Cassiopeia A has a notch which is 25 kc wide at the half-power level. In emission, it is a line approximately 0.5 mc in width. This broadening is due to the turbulence of the hydrogen cloud whose subtended angle may be 10° of arc or more. The gross motion of the clouds represent radial velocities varying from −1 km/sec to 10 km/sec. This will Doppler shift the absorption notch 4735 cps per km/sec. The gross radial velocity of the absorbing medium may be regarded as constant over the period of an interplanetary voyage. The right ascensions of Cassiopeia A, Taurus A and Sagittarius A are 23 hours 21 minutes, 5 hours 31 minutes and 17 hours 43 minutes, respectively. Cassiopeia A and Taurus A may be found at declinations of 58° 32′ and 22° 00′ above the celestial equator, while Sagittarius is 28° 45′ below it.[3] This spacial distribution is favorable with regard to a determination of inertial velocity from three independent noncoplanar velocity measurements.

Of the three sources considered, Cassiopeia A has the greatest apparent intensity, and it is the only source which is continuously visible by an observer on earth at a latitude of +40°. Cassiopeia further lends itself to the navigation problem by having a fine absorption line approximately 200°K deep as measured with an antenna aperture of 75 feet. One may estimate the error in determining the center frequency of this fine absorption line with the use of the expression

$$\sigma_f = 2.94 \left(\frac{W}{T}\right)^{1/2} \times \frac{N}{S},$$

where

σ_f = the rms error in determining the center frequency of the notch;
W = spectrum bandwidth at the half-power level (25 kc);
T = the smoothing time (500 seconds);
N/S = noise-to-signal ratio (7);

$$\sigma_f = 2.94 \left(\frac{25 \times 10^3}{500}\right)^{1/2} \times 7$$

$$= 150 \text{ cps}.$$

This corresponds to a velocity of 70 mph.

The above equation is derived from relations given by Schultheiss *et al.*[4] for measuring the center frequency of a symmetrical power spectrum. The bandwidth is half power bandwidth for the narrow absorption line in the profile of Cassiopeia A. The time of integration, T, is taken as a period which is small compared to the duration of an interplanetary voyage. The N/S ratio is a function of the intensity of the source, size of the antenna and the noise figure of the receiver This uncertainty is attainable with a receiver whose noise figure is of the order of 7.5 db. With the use of a maser preamplifier, the noise figure will be considerably improved with a corresponding increase in the accuracy of measurement. For a comparison between celestial sources, it is indicated by a theoretical analysis that with a 30-foot antenna, a maser preamplifier, and a smoothing time of 21 seconds, σ_v would be 200 miles per hour, using Cassiopeia A as a source. The same system, using Taurus A as a source and a smoothing time of 26 seconds, gives a σ_v of 2000 miles per hour.

In order to obtain information pertinent to the design of an automatic hydrogen line tracker which will continuously measure the radial velocity of a vehicle with respect to a celestial source, a receiver-recording system is under construction. This will produce information on the statistical nature of the hydrogen line signal. The signal is "recorded live" on a wide-band magnetic tape recorder. A portion of the black body radiation continuum of the celestial source is also recorded. These two samples are 200 kc wide and approximately 1 mc apart. Since the continuum radiation has a constant power spectral density it is used as a reference signal in an AGC circuit to compensate for the non-flatness of the receiver-recorder system. The need for this becomes obvious when one realizes that with a receiver with a 7.5-db noise figure, the absorption notch in Cassiopeia A represents a narrow depression at most only 0.5 db below the power spectral density of the background noise. In addition to a live tape recording of the hydrogen spectrum, a pen-type recording of the profile of the notch is also made. It is expected that the basic information about these stellar spectra needed to design the frequency tracker will be derived from these recordings. The live recording will then be used as a "star simulator" during tracker tests.

Basically, the hydrogen line frequency tracker will be a 1420-mc receiver. The resonance feature of the received signal will be amplified by a low-noise RF amplifier such as a maser. This is mixed with a local oscillator signal f_{LO}. The intermediate frequency $f_v - f_{LO}$ is interpreted as a zero speed with respect to the local standard of rest. The velocity of the vehicle along the line of sight to the celestial source is given by[5]

$$V = \frac{f_v - f_{LO}}{1420.40576 \text{ mc}} C$$

where

C = velocity of light
f_v = measured center frequency of notch.

Two other velocity determinations are made with respect to the two other sources. The three velocity components are fed into a computer whose output is the inertial velocity of the vehicle. These data are compared with a stored velocity program for the voyaging vehicle, and the difference used to correct velocity components of the vehicle while in flight.

SEYMOUR FELDON
GPL Division
General Precision, Inc.
Pleasantville, N. Y.

* Received by the IRE, February 29, 1960.

[1] H. C. Van De Hulst, "Studies of the 21-cm Line and their Interpretation," International Astronomical Union Symp., Cambridge University Press, England, p. 3; 1957.

[2] F. T. Haddock, "Introduction to radio astronomy," PROC. IRE, vol. 46, pp. 3–12; January, 1958.

[3] J. P. Hagen, A. E. Lilley, and E. F. McClain, "Absorption of 21-cm radiation by interstellar hydrogen," *Astrophys. J.*, vol. 122, pp. 361–375; November, 1955.

[4] P. M. Schultheiss, C. A. Wogrin, and F. Zweig, "Short time frequency measurement of narrow-band random signals in the presence of wide-band noise," *J. Appl. Phys.*, vol. 25, pp. 1025–1036; August, 1954.

[5] Frequency 1420.40576 mc, cited by A. H. Barrett, "Spectral lines in radio astronomy," PROC. IRE, vol. 46, pp. 250–259; January, 1958. See second paragraph, p. 256.

Internal Field Emission and Low Temperature Thermionic Emission into Vacuum*

Mead has recently reported on tunnel-emission experiments using aluminum oxide sandwiched between two aluminum layers.[1] This note is to report independent work along similar lines by the writer.

The objective of the work is a cold cathode possessing the following desirable attributes:

1) Very high emission densities, for use in high-power beam-type microwave tubes.
2) Beams with low noise temperature for use in low-noise microwave tubes.
3) Instant cathode starting.
4) Long cathode life.

Barrier Material Considerations

It was decided almost at the outset that conventional insulating materials would not be the most suitable for the "tunnel" or barrier layer. There are two reasons, both having to do with the large forbidden gap

* Received by the IRE, May 31, 1960.

[1] C. A. Mead, "The tunnel-emission amplifier," PROC. IRE (Correspondence), vol. 48, pp. 359–361; March, 1960.

in insulators. For a given tunneling current density and barrier potential drop, the required barrier thickness is an inverse function of the barrier height; *i.e.*, the higher the barrier, the thinner the barrier has to be. (The barrier potential drop must be approximately equal to or greater than the work function of the surface film in order to obtain emission into the vacuum.) The uniformity and reproducibility problems of a thin film become increasingly difficult as the thickness of the film is decreased.

The second reason for deciding against conventional insulating materials is that of voltage breakdown. For a large forbidden gap and fixed barrier potential drop, the barrier thickness must be (relatively) small in order to achieve the desired tunneling current densities, as mentioned previously. The resulting high value of electric field is quite likely to cause destructive breakdown of the material. Mead reported destruction of his units at low currents.[1] This could be the result of one of two factors. First, the film thicknesses of his units could have been nonuniform. Thus some one very small area could have been producing essentially all of the emission, and attempts to increase the emission could have resulted in disruptive values of electric field over that small area. The other factor could have been the very intense values of electric field set up at the corners of his small evaporated aluminum squares, causing emission at these points and subsequent rupture upon increasing the applied potential.

At any rate, from uniformity, reproducibility, and dielectric strength considerations the writer decided essentially at the outset of his work to use a barrier material with a comparatively small forbidden gap, or in other words a semiconductor. The conductivity of the semiconductor is an important consideration, as it is desired that tunneling current should predominate over conduction current by a large factor. However, it should be recognized that bulk resistivities may be misleading when dealing with such thin films. For barrier films on the order of 50 to 500 Angstroms in intimate contact with metallic materials on both sides, the conductivity properties of the barrier material may be quite different from those of the bulk material. In effect, we are dealing with a surface phenomenon throughout the barrier, and surface states may be the important consideration rather than bulk properties.

Nevertheless, it was decided by the author that a semiconductor having high bulk resistivity would be the safest material to start with. Cuprous oxide was chosen for the initial experimental work because the calculated tunneling current, for the intended film thicknesses, greatly exceeds the conduction current calculated on the basis of bulk resistivity at room temperature.

Experimental Procedures and Results

The copper substrate was in the form of $\frac{1}{8}$ inch diameter rods. Only OFHC copper was employed, and the first step (after chemical cleaning of the surface) consisted of a vacuum-firing procedure to remove occluded gasses. The rods were then electrolytically etched in order to remove all microscopic high spots. The copper was then oxidized by several different methods, the most successful consisting of the formation first of cuprous chloride in a chloric solution and conversion at low temperature into cuprous oxide, according to the formulas:

$$Cu + Cl^- \rightarrow CuCl \quad (1)$$

$$4\,CuCl + 1/2\,O_2 \rightarrow Cu_2O + 2\,CuCl_2 \quad (2)$$

The cupric chloride product of the second reaction was dissolved out in warm water, leaving a fairly uniform and homogeneous thin film of cuprous oxide on the substrate.

The films were tested by point-contact techniques to display the current-voltage characteristics on an oscilloscope. The point-contact method has an important advantage over the evaporated film technique in that the uniformity of the coating can be subjected to direct test by probing different spots on the film. It has the obvious disadvantage, however, that the area of contact is not precisely known. Also, the contact pressure was found to be an important factor, larger pressures yielding larger tunneling currents. This is probably a result of a simple mechanical distortion of the lattice. At any rate, the pressure can be controlled in order to eliminate this variable. In addition, if the position of the Fermi level in the barrier material is known, the area of contact can be calculated, as can the film thickness, the voltage gradient, and the emission current density.

Fig. 1 shows a typical trace of the current-voltage characteristic of a point contact, taken directly from an oscilloscope. This curve would indeed appear to confirm the predominance of tunneling current over conduction current, at least for the current densities involved. If the electrical contact between the barrier layer and the substrate is presumed ohmic, then rectifying action should be in evidence for a nonohmic point contact on the cuprous oxide surface. There has been no such evidence in any of the experiments so far conducted. If the point contact on the surface is presumed ohmic, then the curve should possess a measurable slope at the origin. For all cases tested the slope is essentially zero at the origin, as in Fig. 1.

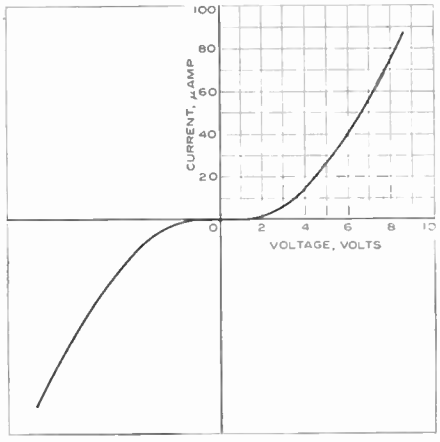

Fig. 1—Typical current-voltage tunneling characteristic of point contact on thin cuprous oxide film over a copper substrate.

Theoretical Considerations

It is believed that a good theoretical approximation to the situation being encountered can be obtained through application of the field-emission equation of Fowler and Nordheim.[2] It is only necessary to interpret the work function in the original equation as the barrier height of the semiconductor in the present application. The equation is rewritten here for convenience.

$$J = \frac{e}{2\pi h}\,\frac{\zeta^{1/2}}{(\zeta+\Phi)\Phi^{1/2}}\,E^2 \cdot \exp\left(-\frac{8}{3}\,\frac{\pi}{h}\,\sqrt{2m}\,\frac{\Phi^{3/2}}{E}\right) \quad (3)$$

where

J = the current density
e = the electronic charge
h = Planck's constant
ζ = the Fermi potential in the substrate
Φ = the barrier height of the semiconductor (the work function of the cold field emitter in the original usage of the equation)
E = the field strength in the semiconductor
m = the electronic mass.

The value of ζ for copper was calculated to be 7 ev from the relation

$$\zeta = \frac{h^2}{2m}\left(\frac{3n}{8\pi}\right)^{2/3} \quad (4)$$

where n is the number of free electrons per unit volume. The only unknown in (3) is then Φ, the barrier height in the semiconductor. For an assumed Φ of 0.9 volt (one-half the forbidden energy gap), (3) can be written

$$J = 2.17 \times 10^{-6} E^2 \exp\left(\frac{-57.9 \times 10^6}{E}\right). \quad (5)$$

Eq. (5) has been fitted to the experimental I-V curves of the type illustrated in Fig. 1 by matching at two arbitrary points on the curves. A comparison was then made between the experimental and theoretical curves. As shown in Fig. 2 for a typical case, the agreement is extremely close.

Typical calculated values for the film thickness and contact area from such comparisons are, respectively, 10 Angstroms

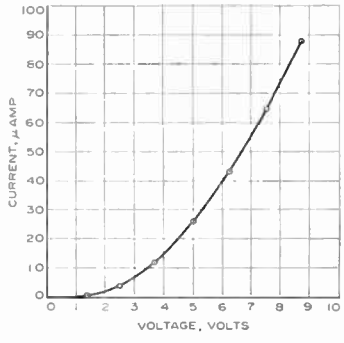

Fig. 2—Comparison between theoretical and experimental current-voltage tunneling characteristics of point contact on thin cuprous oxide film. The circles represent theoretical points plotted from (5).

[2] R. H. Fowler and L. Nordheim, "Electron emission in intense electric fields," *Proc. Roy. Soc.* (*London*) *A*, vol. 119, pp. 173–181; June, 1928.

and 2×10^{-14} cm². Peak calculated electric fields and current densities without dielectric rupture are typically 10^8 volts/cm and 10^{10} amp/cm². It is believed that the films are thicker than 10 Angstroms. If the Fermi level is actually closer to the conduction band than the assumed 0.9 volt, the calculated film thickness would be correspondingly larger. The calculated values of contact area would also be larger, and the electric fields and current densities would be correspondingly smaller.

A more desirable procedure would be an independent determination of the film thickness. This would permit an accurate evaluation of the barrier height in the semiconductor. This, in turn, would permit the evaluation of different methods of fabrication, as the Fermi level quite likely depends to a large degree on the method of preparation and the kind and concentration of impurities.

Temperature Considerations

The above measurements were all taken at room temperature. By taking measurements at different temperatures it may be possible to deduce the position of the Fermi level (and hence the barrier height) in the semiconductor film.

Temperature considerations can be expected to be important in the operation of the final finished cathode. For one thing, elevated temperatures would increase the intrinsic conductivity of the barrier layer to an intolerable level. But, more importantly, the transmission factor through the metallic surface film will certainly be a function of temperature. In fact, it may be necessary to refrigerate the cathode in order to secure sufficiently long mean free paths in the surface film.

Cold Thermionic Emission

The internal-field cathode could be operated in a space-charge-limited condition, as in the case of conventional thermionic emitters. In fact, when so operated, the internal field cathode is in every sense of the word a thermionic emitter, as only those electrons possessing sufficient thermal energy can surmount the potential barrier presented by the space-charge-formed virtual cathode and escape into the vacuum. This is true even if the cathode is refrigerated down to liquid helium temperatures. In effect, the internal field emission process produces a metallic emitting surface with an essentially zero or even negative work function, the value being controllable through the bias applied across the semiconductor film.

While ordinary high-field emitters have a comparatively high effective noise temperature[3] (owing to the absence of any virtual cathode), the internal field cathode operating under space-charge-limited conditions produces a velocity spread dependent upon the lattice temperature, just as in ordinary thermionic emitters. Therefore, a refrigerated internal field cathode should be capable of producing an electron stream in which current fluctuation noise predominates over velocity fluctuation noise. This is just the opposite of ordinary thermionic emitters. The possibilities for producing very low-noise traveling-wave tubes of otherwise conventional broad-band design are therefore quite attractive.

Conclusions

It is the author's hope that this note may contribute towards the achievement of a satisfactory internal field emitter. The potentialities offered by such a cathode appear to be rewarding enough to warrant a considerable amount of attention in the immediate future.

D. V. Geppert
Sylvania Electric Products Inc.
Mountain View, Calif.

[3] R. W. De Grasse and G. Wade, "Electron Beam Noisiness and Equivalent Thermal Temperature for High-Field Emission from a Low-Temperature Cathode," Electronics Labs., Stanford University, Stanford, Calif., Internal Memo.; March 27, 1956.

P-N Junctions Between Semiconductors Having Different Energy Gaps*

H. L. Armstrong[1] discussed the possible existence of junctions between two semiconductors of different energy gaps in 1958. He based the discussion on an earlier paper by Kroemer,[2] who had formulated a *p-n* junction in which the *p* side had a wider gap than the *n* side. Kroemer considered, in addition, the general case of an inhomogeneous semiconductor with a nonuniform bandwidth. In a germanium-silicon alloy, for instance, a change in the alloy composition might introduce a change in bandwidth in a spatial sense. Again, if the doping densities are different in two regions of a given semiconductor, the gradients of the band edges could be different for the conduction and the valence bands and the resulting quasi-electric fields could be unequal for electrons and holes.

The writer feels that these ideas can be further extended to include widely dissimilar semiconductors such as selenium and a semiconducting oxide, provided they are put together in such a manner as to form an effective junction. Reactive sputtering of a semiconducting oxide is believed to form such a junction with a suitable substrate material. An example is the junction known to exist in one type of selenium photovoltaic cell consisting of a selenium layer on which a thin layer of semiconducting cadmium oxide[3] is applied by reactive sputtering. These Se-CdO photocells, such as the Weston Type 5 Photronic® Cell, are now being produced and used in various applications. Earlier work on the photovoltaic effect in junctions between selenium and various metal oxides had been reported by Preston.[4] According to Preston, the limiting extent of the space-charge region is about 10^{-6} cm and the contact is an intimate one.

It is proposed that a junction of this type is an imperfect *p-n* junction between *p*-type selenium and the *n*-type oxide, such as represented in Fig. 1, rather than a metal semiconductor junction of the type generally described in connection with the earlier types of cells. The band gap in selenium is assumed to be 1.6 ev, as determined by Henkels[5] and Von F. Eckhart.[6] Acceptor levels are probably not more than 0.24 ev from the full band.[7]

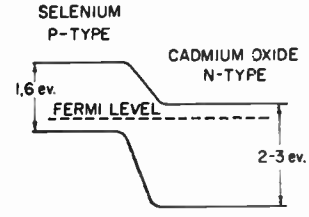

Fig. 1—The proposed Sd-CdO *p-n* junction.

The energy gap of CdO has not been determined accurately yet. An approximate estimate of 2 to 3 ev could be made on the basis of information available on ZnO. From the nature of the optical transmission through imperfect crystals, a rough value of 2 ev has been proposed.[8] Measurements made on sintered, compressed powder blocks of CdO[9] have yielded conductivities of the order of 100 ohm^{-1} cm^{-1} and carrier concentrations of the order of 10^{18}–10^{19} cm^{-3}. An earlier paper by Helwig[10] on reactively sputtered CdO films gave a conductivity approximately the same as the above value; no carrier concentrations were reported.

Detailed measurements were made by the author on the conductivity and Hall constant in reactively sputtered CdO films prepared in a manner similar to those used in the typical selenium photocell. These layers exhibit a negative Hall constant, yielding a carrier concentration of approximately 10^{19} cm^{-3}. The conductivity is about 100 ohm^{-1} cm^{-1} and increases with increasing temperature. Photovoltaic junctions with selenium were also produced using highly oxidized CdO layers of much lower conductivity. These samples are undoubtedly nondegenerate. The observed conductivity is, as in the case of many other non-

* Received by the IRE, March 14, 1960.

[1] H. L. Armstrong, "On junctions between semiconductors having different energy gaps," Proc. IRE, vol. 46, pp. 1307–1308; June, 1958.

[2] H. Kroemer, "Quasi-electric and quasi-magnetic fields in nonuniform semiconductors," *RCA Rev.*, vol. 18, pp. 332–342; September, 1957.

[3] T. K. Lakshmanan, "The Weston type 5 photronic cell," *Weston Engrg. Notes*, to be published.

[4] J. S. Preston, "Constitution and mechanism of the selenium rectifier photocell," *Proc. Roy. Soc. (London) A*, vol. 202, pp. 449–466; August, 1950.

[5] H. W. Henkels, "Model of Semiconducting Selenium," presented at AIEE Winter Mtg., New York, N. Y.; January, 1954.

[6] Von F. Eckhart, "Leitfähigkeits-Messungen an Hochgereinigtem Selen," *Ann. Physik*, vol. 17, pp. 84–93; February, 1956.

[7] K. W. Plessner, "Conductivity, Hall effect and thermo-electric power of selenium single crystals," *Proc. Phys. Soc. (London) B*, vol. 64, pp. 671–681; August, 1951.

[8] N. B. Hannay, "Semiconductors," Reinhold Publishing Co., New York, N. Y., p. 590; 1959.

[9] R. W. Wright and J. A. Bastin, "The characteristic temperature and effective electron mass for conduction processes in cadmium oxide," *Proc. Phys. Soc. (London) B*, vol. 71, pp. 109–116; January, 1958.

[10] G. Helwig, "Elektrische Leitfähigkeit und Struktur aufgestäubter Kadmiumoxydschichten," *Z. Physik*, vol. 132, pp. 621–642; August, 1952.

stoichiometric oxides,[11] due to the presence of oxygen deficiency or interstitial cadmium, or both.[12] By varying the sputtering conditions wide variations in the conductivity and carrier concentration can be produced.

In the proposed p-n junction between nondegenerate CdO and Se, Fig. 1, the energy gaps are assumed to be different and the quasielectric field for electron flow differs from that for hole flow. The general equations for current flow under dark conditions are, for such a junction,

$$J_h = e\mu_h pE^{(h)} - eD_h\nabla p$$
$$J_e = e\mu_e nE^{(e)} + eD_e\nabla n$$

where J is the current density, D the diffusion constant, μ the mobility and n and p the electron and hole densities, respectively. The subscripts or superscripts e and h refer, respectively, to electrons and holes.

It is interesting to note that Yamaguchi[12] had postulated that in the case of a blocking layer rectifier, the rectifying action existed at the junction between Se and CdSe and not at the CdSe-Cd junction. CdSe is well known to be n-type. More recently, Yashukova[13] has pointed out that a p-n junction may be supposed to exist between Se and CdSe. Furthermore, a simplified scheme with equal energy gaps on the p and n sides and with a barrier film in between has been given by Dietzel, Gorlich and Krohs[14] for a special type of selenium photovoltaic cell. The present scheme is considered to be an extension of these ideas.

Further work on the semiconducting properties of CdO is continuing. A more detailed examination of this type of p-n junction with unequal gaps is also being made.

T. K. Lakshmanan
Weston Div.
Daystrom, Inc.
Newark, N. J.

[11] E. J. W. Verwey and F. A. Kröger, "New views on oxidic semiconductors and zinc-sulphide phosphors," *Philips Tech. Rev.*, vol. 13, pp. 90–95; October, 1951.
[12] J. Yamaguchi, "On the blocking layer of selenium rectifier (II)," *J. Phys. Soc. Japan*, vol. 10, pp. 234–236; March, 1955.
[13] I. M. Yashukova, "Electrical Conductivity of Polycrystalline CdSe," *Soviet Phys.* (Solid-State), vol. 1, p. 349; March, 1959.
[14] G. Dietzel, P. Gorlich, and A. Krohs," Über Selenphotoelemente," in "Jenaer Jahrbuch," VEB Carl Zeiss, Jena, Ger., vol. 1, pp. 203–277; 1958.

An Optimal Discrete Stochastic Process Servomechanism*

In an article to be published elsewhere,[1] a complete optimal class of servos is derived which provides maximal smoothing in a certain novel sense for discrete stochastic processes. The present note represents an extension of Mills' theorem to indicate a particular member of the optimal class which, in addition to assuring maximal smoothing in Mills' sense, also provides quickest response and zero average error.

A brief review of Mills' theory is necessary in order to appreciate the import of of and constraint upon the present extension. Thus Mills considers a discrete servo-stochastic process defined to be a sequence of random variables of the form

$$P = (e_1, c_1, n_1, e_2, c_2, n_2, \cdots,) \tag{1}$$

where

e_t is interpreted as an "error" in an operation at the beginning of time period t,
c_t is a "correction" made in the operation at the beginning of period t, but with prior knowledge of e_t,
n_t is the "noise" entering the operation during period t.

The process P, in conjunction with a sequence of numbers representing the "initial conditions," is characterized by the following properties, for $t=0, 1, 2, \cdots$,

$$e_{t+1} = e_t + c_t + n_t \tag{2}$$
$$c_{t+1} = S(\cdots, n_{t-1}, e_t, c_t, n_t) \tag{3}$$
$$\text{Prob}\ (n_t \leq x) = N(x) \tag{4}$$

where S is an arbitrary function and N is an arbitrary distribution.

Eq. (2) represents a conservation of error in the operation (holding with probability 1); (3) specifies a "servo" or "decision policy" S (also holding with probability 1); and (4) describes the noise, which is taken to be identically and independently distributed period by period. The objective of Mills' paper is to determine that class of servos, that is, that class of functions, S, which are optimal in a certain sense. The sense in which they are optimal is related to an "uncertainty principle" for servo-stochastic processes, derived by Mills, namely, that for any servo

$$k_e \geq \frac{1}{2}\left(k_c + \frac{1}{k_c}\right), \tag{5}$$

or, in another form,

$$k_e k_c \geq \tfrac{1}{2}(1 + k_c^2) \geq \tfrac{1}{2}, \tag{6}$$

wherein k_e and k_c are respectively defined by

$$k_e = \sigma_e/\sigma_n, \qquad k_c = \sigma_c/\sigma_n, \tag{7}$$

the sigmas being variances, and it being assumed that $\sigma_n^2 > 0$. The ratios k_e and k_c, Mills calls the "error to noise ratio" and the "correction to noise ratio;" k_e gives a measure of "how well the servo is doing" and k_c gives a measure of "how hard the servo is working." Eqs. (5) and (6) demonstrate that both these ratios cannot simultaneously be decreased indefinitely by better servo design. Mills terms the relations (5) and (6) the "smoothing capacity" of servos in discrete servo-stochastic processes.

Mills limits his analysis to stable processes, that is, to those for which all first and second-order statistical moments approach definite limits in time, *e.g.*,

$$\bar{e} = \lim_{t\to\infty} \bar{e}_t, \qquad \bar{c} = \lim_{t\to\infty} \bar{c}_t, \qquad \bar{n} = \bar{n}_t,$$
$$\sigma_e^2 = \lim_{t\to\infty} \sigma_e^2(t), \qquad \text{etc.} \tag{8}$$

[where $\bar{e}_t = E(e_t)$, $\bar{c}_t = E(c_t)$, $\bar{n}_t = E(n_t)$, and E denotes the expectation or mean value].

Mills then formulates a complete optimal class of servos which achieves the equation form of the inequality of (5). These optimal servos turn out to be linear, namely, of the form

$$c_t = -\alpha(e_t - \beta) \tag{9}$$

where $0 < \alpha \leq 1$, and β is arbitrary.

As Mills states, "That so simple a class of policies is complete and optimal seems quite fortuitous considering the fact that they are in competition with all possible servos, nonlinear, discontinuous, or what have you." Eq. (9) is Mills' optimal class of servos; that is, (9) gives the form of the function S of (3) which is optimal in the sense that the uncertainty principle of (5) is minimized. Mills also demonstrates that the same class is also optimal for the case in which there are information time delays and/or servomechanical response times. Thus, with a composite time delay of T periods, the "uncertainty principle" of (5) is amended by squaring the expression and then adding the term $+T$ on the right-hand side, but the optimal class of servos given by (9) remains optimal without alteration.

The extension of Mills' theorem to include optimization with respect to response time and average error is easily gained as follows.

In the course of his derivation, Mills exhibits a formula for the limit average error,

$$\bar{e} = \frac{\bar{n}}{\alpha} + \beta. \tag{10}$$

Now the conditional expectation value of the error on the $t+1$ period, given the error on the previous period, is given by

$$\begin{aligned} E(e_{t+1}/e_t) &= E(e_t + c_t + n_t/e_t) \\ &= E(e_t(1-\alpha) + \alpha\beta + n_t/e_t) \\ &= (1-\alpha)e_t + \alpha\beta + \bar{n} \\ &= (1-\alpha)e_t + \alpha\bar{e}. \end{aligned} \tag{11}$$

In the evaluation of the conditional expectation, we have employed the expression for the optimal-smoothing servo class, given by (9). If in (11) we choose α to be equal to 1, then the expected error is no longer conditional, but is simply given by the average error independent of the previous history of the servo. Returning to (10), now with $\alpha = 1$, we see that minimal average error, namely 0 error, is gained by choosing the arbitrary constant β to be equal to the negative of the average noise. Thus letting $\alpha = 1$, and $\beta = -\bar{n}$, insertion in (9) yields

$$c_t = -(e_t + \bar{n}). \tag{12}$$

This simple expression represents the optimal servo which, providing maximal smoothing, assures quickest response, and zero average error. It is quickest in the sense that given some initial nonaverage error, the servo "assures" return to the mean error in the shortest number of periods possible, namely 1. Any other choice of α would lead to a servo which would approach the mean error value only in the limit.

The servo represented by (12) is the one which an engineer is first tempted to apply in any error correction servo system. It states that the correction to be applied is the negative of the error resulting from the previous step, plus the negative of the expected noise. Stated another way, if one has

* Received by the IRE, February 12, 1960.
[1] H. D. Mills, "Smoothing in discrete servo-stochastic processes," submitted for publication in the *J. Soc. Indus. and Appl. Mechanics.*

an error e_t, and one knows that the average noise is $\bar{n}$, then the "simple-minded" solution would be to make a correction given by the negative of the sum of the two errors. The extraordinary fact is that this "simple-minded" design is optimal, in that it provides maximum smoothing, quickest response, and zero average error.

GEORGE C. SPONSLER
Hoffman Electronics Corp.
Science Center
Santa Barbara, Calif.

On Stabilizing the Gain of Varactor Amplifiers*

A number of regenerative varactor amplifiers have been tested with a view to their use as low-noise preamplifiers in certain radioastronomical observations where a gain constancy of the order of one part in a thousand is required. This note is an account of experience with the stabilization of the so-called "degenerate" amplifier where $f_p = 2f_s$.

The power gain of a regenerative varactor amplifier is a sensitive function of the impedances presented to the varactor, and of the pump power level. For many situations, adequate impedance stability can be achieved by using rigid structures and firm connections, avoiding sliding contacts in the tuning systems, paying close attention to serving the cables and connectors, and using stable pump frequencies. Stabilizing the pump power level at the varactor requires equal care in the construction of the pump oscillator and the interconnecting circuits. But despite these precautions, the experimental amplifiers, using both fixed and self-bias, showed unacceptable gain variations which were traced to residual changes in the pump power level.

During the initial measurements on a 2000-mc degenerate amplifier using a germanium diode (Hughes type HPA 2810) and a low resistance bias circuit, it was noticed that the gain tended to become independent of the pump power level when the amplitude of the pump voltage was close to the value of the bias voltage. The degree of saturation observed depended upon the tuning of the signal and pump circuits. This behavior is illustrated by curves *a* and *b* of Fig. 1. With the adjustment of curve *b*, which placed the peak of the gain curve at a point where the net varactor dc current was zero (see Fig. 1, curve *c*), the gain remained constant to within ±1 per cent over a period of one hour. This saturation effect appears to be caused by a slight increase in the varactor losses and to the dependence of the mean varactor capacitance on the pump level, resulting in a change in both damping and tuning of the signal and pump circuits. No such tendency to saturate was observed with self-bias.

A considerable further improvement in gain stability was achieved by using the

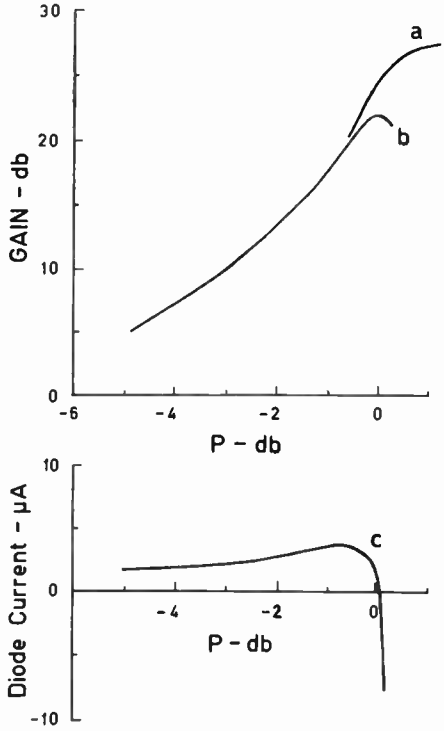

Fig. 1—Variation of insertion gain and dc varactor current as functions of the relative available pump power, *P*. Results for Hughes HPA2810 germanium varactor at 2000 mc with fixed bias of 2.7 volts.

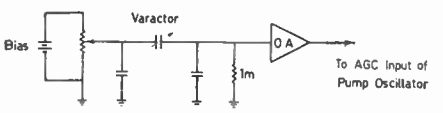

Fig. 2—DC circuit of pump stabilizer.

varactor dc current to control the pump level. The circuit of Fig. 2 was utilized to control the pump power so that operation was always at the crossover point "X" of curve *c* of Fig. 1.[1]

In Fig. 2, "O.A." is a high gain, chopper stabilized, dc operational amplifier with an equivalent input noise current less than a millimicroampere (Philbrick USA series units). Because of the steepness of the rectified varactor current characteristic, and the precautions discussed earlier, it has been possible to achieve an excellent gain stability. On the laboratory bench at gain settings of 20–25 db, the gain of a 400-mc amplifier was found to be more stable than that of the test receiver used, the measurements merely indicating that the instability was of the order of, or less than, one part in a thousand over periods of half an hour or more. Further, it has been possible to make precise measurements of excess noise, gain, and bandwidth, when operating at gains as high as 40 db. Thus it appears that gain fluctuations caused by pump variations are now relatively unimportant compared to those caused by impedance changes.

The stabilization scheme described above would appear to be susceptible to changes in the varactor currents caused by ambient temperature variations. In the laboratory no significant temperature sensitivity has been observed.

The rectified pump current will increase the noise generated in the amplifier beyond the value expected from the circuit and varactor losses. At 2400 mc and operating at the crossover point, the noise temperature has been observed to increase by about ten per cent from its minimum value for a *maximum rectified reverse current* of one μa.

This work has been carried out under the auspices of the Netherlands Foundation for Radio Astronomy, supported by the Netherlands Organization for Pure Research (Z.W.O.). One of the authors (Robinson) has been seconded from the Radiophysics Laboratory of C.S.I.R.O. (Australia).

B. J. ROBINSON
C. L. SEEGER
K. J. VAN DAMME
J. T. DE JAGER
The Leiden Observatory
Leiden, The Netherlands

A Conference on the Propagation of ELF Electromagnetic Waves*

On January 26, 1960, a conference was held at the Central Radio Propagation Laboratories (CRPL) in Boulder, Colo., which was devoted mainly to the subject of radiowave propagation of extremely low frequencies (ELF). The frequency range (less than about 3 kc) is well below those currently used in communications. Lightning discharges, however, produce considerable energy in this range, and the radiated fields have been used for studying the nature of lightning phenomena for many years at frequencies as low as 10 cps. Other natural sources of both a terrestrial and an extraterrestrial nature also radiate electromagnetic energy in this frequency range, but usually to a lesser extent than lightning.

Since ELF signals have been observed to propagate with very low attenuation, it has been suggested from time to time that they would be useful for communications on a world-wide scale. Furthermore, because of certain magneto-ionic phenomena, these waves may penetrate the ionosphere and enable communication with space vehicles. This is particularly so in the vicinity of 3 kc where a "window" in the ionosphere appears to exist. Another aspect of ELF waves is that the wavelength is extremely large (3000 km at 100 cps) and consequently, the signals may easily be diffracted around planetary objects. Furthermore, such signals penetrate with relatively small loss into conducting media such as rocks and soil. In fact, frequencies in this range have been used for many years in geophysical exploration.

The topics discussed at the conference were divided into two sessions. The first dealt with observed characteristics of natural ELF fields and was moderated by J. R. Wait. The second dealt with the theory of radiation and propagation of these waves and was moderated by A. D. Watt. A very

[1] This general method of stabilization has been used before in the design of ultra-stable conventional crystal mixers.

* Received by the IRE, May 13, 1960.

* Received by the IRE, February 23, 1960.

sketchy description of the individual presentations is presented here.

E. T. Pierce of Avco Corporation, Wilmington, Mass. gave an introductory paper on the nature of the waveforms of signals radiated from lightning discharges. He indicated that the characteristics of the "slow tail" portion of the waveform enabled electron densities and collision frequencies to be deduced for the lower edge of the ionosphere E region.

George Garland of the University of Alberta, Edmonton, Can., then presented a comprehensive paper on the nature of fluctuations of the earth's magnetic field. Particular attention was given to the basis of the magneto-telluric method of investigating the earth's crust. Essentially, the idea is to compare the tangential electric and magnetic field variations on the surface of the earth. The variation of the ratio of the frequency spectra of these fields is related to the conductivity of the earth's crust at depths of the order of kilometers.

W. Campbell of the University of Alaska, College, discussed the diurnal and seasonal variations of geomagnetic fluctuations. He concluded that for frequencies above about 2 cps the sources of the fields were primarily from lightning discharges, while below this frequency the field variations must be attributed to solar effects. Further papers on geomagnetic fluctuations were given by P. A. Goldberg of RAND Corporation, Santa Monica, Calif., and E. Maple of Air Force Cambridge Research Center, Cambridge, Mass. Both these authors confirmed the idea that magnetic energy in the audio-frequency range could be attributed almost solely to lightning discharges.

A. D. Watt and E. L. Maxwell of CRPL discussed the physical phenomena involved in cloud-to-ground lightning discharges, and the respective role of the static, induction, and radiation fields. The radiation field was shown to vary directly with frequency below about 6 kc, and observed spectral characteristics which depart from this law were satisfactorily explained.

A. G. Jean and W. L. Taylor of CRPL briefly described their experimental facilities for measuring the waveforms of atmospherics in this ELF range. The significant feature of the scheme is that simultaneous recordings are made of the same atmospheric at widely separated stations.

E. L. Tepley presented an extensive summary of the activities of the Institute of Geophysics at the University of California at Los Angeles. This included a statistical study of the characteristics of "atmospheric waveforms" using a large number of samples. Data on attenuation rates of ELF signals were also discussed. For example, at 100 cps, these are of the order of 1 db per 1000 km of path length.

In the first paper of the second session, J. R. Wait of CRPL gave a theoretical treatment of mode theory with special reference to ELF. The effect of earth curvature and the earth's magnetic field were included in the analysis. Particular attention was focused on the behavior of the electric and magnetic fields at distances from the source which were comparable to the wavelength. In the following paper, R. A. Helliwell of Stanford University, Stanford, Calif., mentioned certain peculiar characteristics of the whistler sonograms which indicate that whistlers sometimes contained appreciable energy at ELF.

W. L. Anderson of the University of New Mexico, Albuquerque, presented a theoretical discussion of the dispersion of electromagnetic pulses propagating in conducting media. Certain recommendations were made concerning the optimum pulse shape for signalling.

The transmission between two insulated loop antennas immersed in a conducting half-space was evaluated by H. A. Wheeler of Wheeler Laboratories, Great Neck, N. Y. He used a very straightforward method which made use of the reciprocity theorem and the known solution of the receiving antenna problem. In a sequel to this paper, L. Rawls of Developmental Engineering Company, Norwalk, Conn., discussed the engineering design of buried antennas. K. A. Norton of CRPL then emphasized the advantages of the system-loss concept in presenting radiation and propagation data at ELF.

R. K. Moore and R. H. Williams of the University of New Mexico, Albuquerque, outlined a theoretical treatment of the horizontal electric antenna immersed in a conducting half-space. Essentially, the problem is a generalization of the Sommerfeld problem of a dipole on the surface of the half-space. They also considered the impedance of the antenna, using an approximate method which has its roots in transmission line theory. C. H. Harrison, Jr. of Sandia Corporation, Albuquerque, N. M., then presented a full treatment of the finite cylindrical antenna immersed in a conducting medium of infinite extent. The King-Middleton method of iteration for antennas in air was modified for the case of dissipative media. This was followed by R. S. Macmillan of the University of Southern California, Los Angeles, who gave an account of investigations of power-line antennas. Essentially, the idea is to excite a section of power line which acts as a horizontal center-fed dipole. The pattern has a maximum looking straight up and thus is very suitable for ionospheric investigations.

Finally, G. V. Keller and F. Frischknecht of the U. S. Geological Survey, Denver, Colo., presented a paper on their electrical investigations of glaciers and ice sheets using audio frequencies. The energy was coupled to the medium by both electrodes and loops. Using such schemes, it was possible to outline the cross sections of the Athabaska glacier in Alberta, Can.

Papers from the conference will be published in early issues of the *Journal of Research* of the National Bureau of Standards, Section D (Radio Propagation). An edited transcript of the oral discussions following the papers is to be available.

A Note on Nomenclature

It is suggested by A. D. Watt and the author that the following designations be employed for these extra low frequencies.

VLF (very low frequency),	3 to 30 kc;
ELF (extremely low frequency),	1.0 to 3000 cps.

J. R. Wait
National Bureau of Standards
Boulder, Colo.

WWV and WWVH Standard Frequency and Time Transmissions*

The frequencies of the National Bureau of Standards radio stations WWV and WWVH are kept in agreement with respect to each other and have been maintained as constant as possible with respect to an improved United States Frequency Standard (USFS) since December 1, 1957.

The nominal broadcast frequencies should, for the purpose of highly accurate scientific measurements, or of establishing high uniformity among frequencies, or for removing unavoidable variations in the broadcast frequencies, be corrected to the value of the USFS, as indicated in the table below.

The characteristics of the USFS, and its relation to time scales such as ET and UT2, have been described in a previous issue,[1] to which the reader is referred for a complete discussion.

The WWV and WWVH time signals are also kept in agreement with each other. Also they are locked to the nominal frequency of the transmissions and consequently may depart continuously from UT2. Corrections are determined and published by the U. S. Naval Observatory. The broadcast signals are maintained in close agreement with UT2 by properly offsetting the broadcast frequency from the USFS at the beginning of each year when necessary. This new system was commenced on January 1, 1960. The last time adjustment was a retardation adjustment of 0.02 s on December 16, 1959.

WWV Frequency
With Respect to U. S. Frequency Standard

1960 June 1600 UT	Parts in 10^{10}†
1	−144
2	−144
3	−144
4	−144
5	−144
6	−145
7	−145
8	−146
9	−146
10	−146
11	−146
12	−146
13	−147
14	−147
15	−147
16	−146
17	−146
18	−146
19	−146
20	−147
21	−147
22	−147
23	−147
24	−147
25	−147
26	−147
27	−147
28	−146
29‡	−146
30	−148

† A minus sign indicates that the broadcast frequency was low.

‡ Method of averaging is such that an adjustment of frequency of the control oscillator appears on the day it is made. The frequency was decreased 3×10^{-10} on June 29.

National Bureau of Standards
Boulder, Colo.

* Received by the IRE, July 25, 1960.

[1] "United States National Standards of Time and Frequency," Proc. IRE, vol. 48, pp. 105–106; January, 1960.

Energy Fluxes from the Cyclotron Radiation Model of VLF Radio Emission*

Several authors[1,2] have suggested that certain natural audio-frequency electromagnetic background radiations, notably dawn chorus, are due to cyclotron radiation from protons incident on the earth's exosphere. The principal success of this theory is that with the Doppler and ionospheric dispersion effects taken into account, the theory nicely predicts the frequency *vs* time characteristics of the observed signals. The purpose of this note is to point out that the cyclotron theory, at least in its simple form, does not seem to account for the observed strength of the radiation. A crude calculation suffices to show a discrepancy.

We consider that the radiation comes from a spherical shell of thickness d centered around the earth at a mean altitude h above the earth's surface. The streams of incoming protons are described by a number density n and a particle velocity v. The expression for the radiated power passing through a horizontal unit area at the earth's surface involves the inverse-square spreading factor, the angular distribution and polarization of each elementary radiator, the magnetic field strength B, and the absorption and anisotropic propagation properties of the medium. This expression is difficult to evaluate. However, if we assume isotropic radiation from each volume element and phase coherence of all elementary radiators, some geometrical manipulations show that

$$P \approx nSd,$$

where P is the power incident on a horizontal unit area and S is the total power radiated by a charged particle moving (adiabatically) in a circular orbit.

The "enhanced" solar wind, characteristic of the active solar conditions under which dawn chorus is most frequently observed, may have a particle density of 10^4 to 10^5 protons per cm^3 and a particle velocity of 1500 km/sec. These parameters suggest that the particle flux will penetrate the geomagnetic field to a distance of about 1.5 earth radii.[3] Therefore, we postulate the radiating layer to be at an altitude of about 3500 km above the earth's surface. The effective layer thickness d can be estimated by computing the radial distance over which the magnetic field changes sufficiently to account for the observed bandwidth of the signal.[4] MacArthur[1] has shown that the true radiated frequency is inversely proportional to B. Then if ν is the radiated frequency, $\Delta\nu$ is the signal bandwidth, and ΔB the corresponding change in magnetic field, we have

$$\Delta B = B\left|\Delta\nu/\nu\right|.$$

If we represent the earth's field by a dipole of moment $p = 8\times10^{19}$ gauss-km^3, we may write $B = pr^{-3}(4-3\sin^2\theta)^{\frac{1}{2}}$. Then,

$$d \approx \Delta B\left(\frac{\partial B}{\partial r}\right)^{-1} = \frac{r}{3}\left(\frac{\Delta\nu}{\nu}\right).$$

The quantity $\Delta\nu/\nu$ does not exceed 0.2,[5] and we conclude that $d \approx 700$ km. The quantity S may be written in mks units as

$$S = \mu\frac{e^4B^2v^2}{6\pi cm_p^2}.$$

At an altitude of 3500 km and middle geomagnetic latitudes ($\theta \approx 45°$), $B = 0.12$ gauss. If we take $v = 1500$ km/sec, and note that in this part of the earth's exosphere the local velocity of light is about 1/100 the free space value,[2] we find $S \approx 2\times10^{-33}$ watts. Taking a particle density of 10^5 per cm^3, the energy flux density estimate becomes

$$P \approx 1.5\times10^{-16}\ \text{watts/m}^2.$$

Sferics, short electromagnetic pulses coming from lightning discharges, are by far the most energetic source of natural electromatic noise in the audio-frequency region. This sferic background level determines the ultimate detectability of signals from other sources. The sferic power spectrum shows a minimum in the neighborhood of 2 to 3 kc, and this minimum value will be used in making the following estimate of marginally detectable signal strengths. Although the sferic spectrum is highly variable, a reasonable estimate[6] for the mean field strength is $b \approx 10^{-9}$ gauss/cps. This value leads to a background energy flux density in a 500 cps bandwidth of about 1.5×10^{-8} watt/m^2. Let us assume that b has been overestimated by a factor of 10, and further assume that a continuous signal of 1/1000 the flux density of the background can just be detected. This minimum detectable energy flux density is then

$$P(\text{min}) \approx 1.5\times10^{-13}\ \text{watts/m}^2.$$

The dawn chorus fluxes observed must therefore equal or exceed this value. Hence it appears that the proton cyclotron radiation model fails by about a factor of 10^3 to account for the strength of the emissions.

In view of the crudity of the calculation, a factor of 10^3 is not conclusive. However, the isotropic radiating layer approximation probably overestimates the true situation in which focusing and absorption effects are included, and the minimum detectable signal flux has been estimated very conservatively. The basic difficulty with the cyclotron model is that cyclotron radiation is a very inefficient process for converting kinetic energy at audio frequencies. Also it is difficult to visualize how the necessary phase coherence can be obtained over a large volume of elementary radiators. The theory of Gallet,[7] in which the energy conversion process is similar to that in a traveling-wave tube, appears to offer the possibility of substantially better conversion efficiency. Furthermore, the necessary condition of Gallet's mechanism (that the particle velocities equal the local phase velocity of light) seems quite likely to be fulfilled at some point in the exosphere.

The author is indebted to Dr. J. W. MacArthur for a critical reading of the manuscript.

R. A. Santirocco
Stromberg-Carlson Division
of General Dynamics Corp.
Rochester, N. Y.

* Received by the IRE, February 18, 1960.

[1] J. W. MacArthur, "Theory of the very low-frequency radio emissions from the earth's exosphere," *Phys. Rev. Letters*, vol. 2, pp. 491–492; June 15, 1959.

[2] W. B. Murcray and J. H. Pope, "Doppler-shifted cyclotron frequency radiation from protons in the exosphere," *Phys. Rev. Letters*, vol. 4, pp. 5–6; January 1, 1960.

[3] E. N. Parker, "Auroral phenomena," Proc. IRE, vol. 47, pp. 239–244; February, 1959.

[4] We do not wish to imply that the magnetic field gradient is the only cause of broadening.

[5] See for example the frequency-time plots in footnotes 2 and 7.

[6] J. B. Wilcox and E. Maple, "Audio-Frequency Fluctuations of the Geomagnetic Field," U. S. Naval Ord. Lab. Navord Rept. 4009; July 9, 1957.

[7] R. M. Gallet, "The very low-frequency emissions generated in the earth's exosphere," Proc. IRE, vol. 47, pp. 211–231; February, 1959.

A Receiver for Observation of VLF Noise from the Outer Atmosphere*

Although high-frequency radio outbursts from the solar corona have been studied intensively over the past decade, it is only recently that much attention has been paid to the analogous radiations at kilocycle frequencies which are generated in the outer atmosphere of the earth, and there have been no reports of any extended series of observations which would compare with those made of solar radio emissions.

Nevertheless, observations of radio noise from the outer atmosphere provide a useful new technique for studying the processes responsible for auroras. It has been shown, for example, that charged particles traversing the plasma of the outer atmosphere will generate Cerenkov-like radiation at frequencies between about 1 kc and 1 mc.[1,2] As a result, it is likely that there is a steady background of radio noise in this frequency range because of the Van Allen particles, superimposed on which are much more intense bursts of noise caused by the passage of auroral particles through the atmosphere. Recent observations of the geographical pattern for illumination of a small region of the earth of radiation in the kilocycle band have suggested strongly that it is both patchy and sporadic.[2] It now seems likely that the study of the worldwide pattern will provide, for the first time, a map of the disturbed regions of the outer atmosphere which are the sources of auroral particles. It is therefore of considerable importance that observations be made at many places and to stimulate interest in such observations, a suitable receiver is described in this paper.

One of the principal reasons for the absence of previous observations of noise bursts at kilocycle frequencies has been the difficulty of recording them in the presence of the relatively much stronger interference from electric mains and from atmospherics

* Received by the IRE, March 4, 1969.

[1] G. R. A. Ellis, "Low frequency radio emission from aurorae," *J. Atmos. Terr. Phys.*, vol. 10, pp. 302–306; 1957.

[2] V. Ia. Eidman, "The radiation from an electron moving in a magnetoactive plasma," *J. Exptl. Theoret. Phys. (U.S.S.R.)*, vol. 34, pp. 131–138; January, 1958.
V. Ia. Eidman, "Soviet physics," *J. Exptl. Theoret. Phys. (U.S.S.R.)*, vol. 7, pp. 91–95; July, 1958.

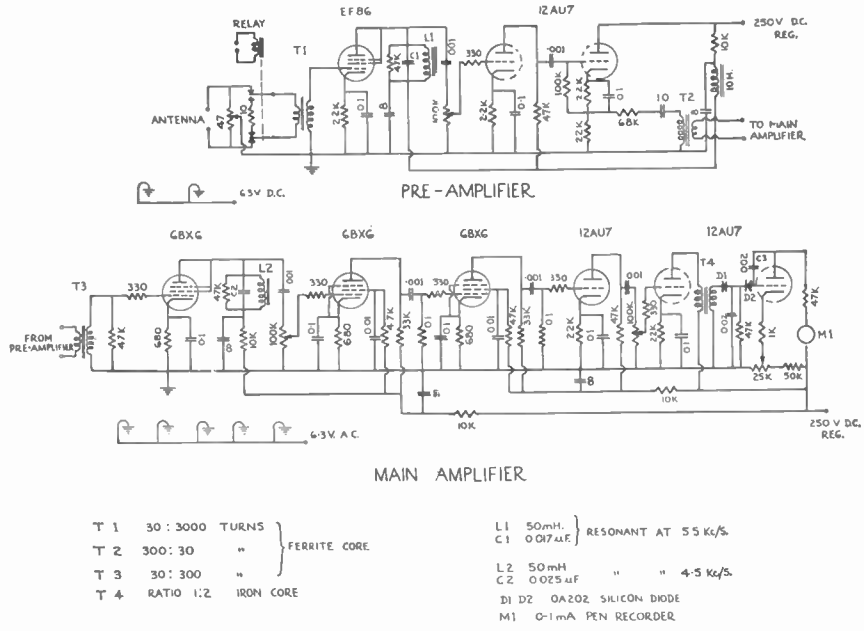

Fig. 1.

in the same frequency band. Although many attempts have been made at places remote from electrical supply systems the interference from atmospherics has still caused difficulties. Yet the wanted noise signal is usually bandwidth-limited white noise while the interference is impulsive, taking the form of intermittent short pulses, which last, for atmospherics, a fraction of a second, and, for mains, a few thousandths of a second recurring at half the mains period. Well-known techniques are available for improving signal-to-interference ratio in situations like this. Here a minimum reading recorder is used and has been found satisfactory. With this, discrimination against impulsive interference of the order of 30 db can be obtained without difficulty. This makes it possible to record easily noise bursts at 5 kc at geomagnetic latitudes greater than about 40°. This frequency has been chosen because it coincides both with a trough in the atmospherics spectrum and a peak in the VLF noise spectrum.

In its main details, the receiver follows practice standard for observations of whistling atmospherics.[3] The antenna is a four-turn vertical loop, 100 square meters in area and orientated in a north-south direction, which is connected to the preamplifier through a transformer with a turns ratio of 1:100. Because of the extremely small radiation resistance of the antenna, it is not feasible to match it to the input stage. To reduce mains interference, the preamplifier and antenna are 100 meters from the building housing the main amplifier and recording equipment. Signals in the frequency band from 4–6 kc are amplified in the main amplifier and, after rectification, are averaged in an RC circuit with a time constant of one millisecond. The dc output is then amplified further and applied to the minimum reading circuit (Fig. 1). When a positive-going pulse appears at the cathode or the detector D1, the impedance of diode D2 is very large and, together with the capacitor C3, presents a time constant of 30 seconds to the incoming signal. Negative-going pulses, on the other hand, cause the diode to conduct, lowering its impedance and giving a time constant of two milliseconds. The output of the minimum reading circuit is proportional to the average level of the continuous background noise, providing there are intervals of a few thousandths of a second in between the interfering impulses.

Receivers similar to this have been operated during the past twelve months at Camden (near Sydney), Hobart and Adelaide.[4] Apart from operating them away from the vicinity of electrical machinery, no special precautions have been taken to select noise-free sites. It has been found that the amplitude of the VLF noise increases with geomagnetic latitude, being about twice as great as Hobart [51° geomagnetic latitude as Camden (42°)]. The gain of the Camden receiver is normally set so that 0.65-μv input to the aerial terminals from a signal generator produces full scale deflection of the pen recorder at 5 kc. This corresponds to a radiation field strength of 0.36 $\mu v/m(c/s)^{-1/2}$. The recorded level of background noise interference is usually about 0.01 $\mu v/m^{-1}(c/s)^{-1/2}$, arising to double this at night when atmospherics become stronger The field strength of VLF noise bursts varies between 0.03 and 0.2 μv/m at Camden. The receiver sensitivity for signal equal to first-stage noise is 0.003 $\mu v/m^{-1}(c/s)^{-1/2}$.

One of the most important aspects of setting up the receiver is to ensure that strong impulsive signals from atmospherics are not limited unsymmetrically in the final amplifying stages. If this occurs, spurious low-frequency signals can be generated by the shift of bias levels. Adjusting the bias of the final stages will normally correct this condition.

G. R. A. Ellis
Upper Atmosphere Section
Commonwealth Sci. and
Industrial Res. Organization
Camden, N. S. W., Australia

[3] L. R. O. Storey, "An Equipment for Recording Whistlers Automatically," Defence Res. Telecommun. Est., Ontario, Can., Project Rept. No. 23-4-3; 1956.

[4] G. R. A. Ellis, "Low-frequency electromagnetic radiation associated with magnetic disturbances," *Planet. Space Sci.*, vol. 1, pp. 253–258; September, 1959.

An X-Band Parametric Amplifier Using a Silver-Bonded Diode*

The authors had previously reported that a silver-bonded germanium diode was suitable for a parametric amplifier diode, and that low-noise parametric amplifications were obtained by the use of these diodes at 4 and 6 kmc.[1,2] Recently, the authors have succeeded in getting the low-noise parametric amplification up to 11 kmc by utilizing the same type of diode as is assembled at the Electrical Communication Laboratory of the Nippon Telegraph and Telephone Public Corporation, Tokyo, Japan. This paper presents the results of such an amplifier.

The silver-bonded diode was constructed in the manner of the so-called "wafer type," that is to say, an *N*-type germanium piece was mounted at one broad side of a rectangular waveguide of a metal wafer, which was inserted transversely through the gap of the waveguide holder as shown in Fig. 1. A silver-gallium whisker of 100 microns in diameter inserted from the opposite side of the waveguide was in contact with the wafer at its tip. An electrical forming process was used by discharging current from a condenser through the contact point. The typical voltage-current characteristic of the diode is shown in Fig. 2. The barrier capacitance at breakdown voltage, the series resistance and the cut-off frequency of the diode are about 0.1 pF, 5 ohms and 300 kmc, respectively.

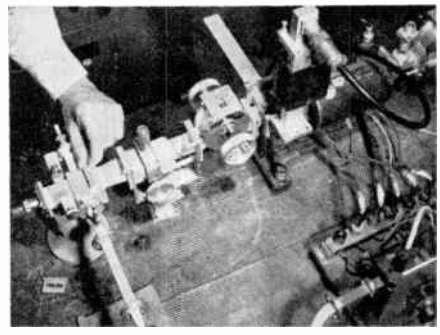

Fig. 1—Photograph of the amplifier.

* Received by the IRE, February 9, 1960.

[1] B. Oguchi, S. Kita, N. Inage and T. Okajima, "Microwave parametric amplifier by means of germanium diode," PROC. IRE, vol. 47, pp. 77–78; January, 1959.

[2] S. Kita, K. Sugiyama and T. Okajima, "Properties of silver bonded diode for parametric amplifier," ELECTRON DEVICES Meeting, Washington, D. C.; October 29–31, 1959.

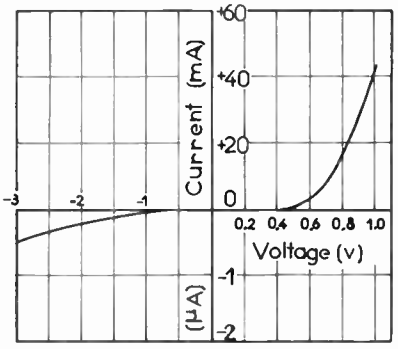

Fig. 2—Voltage-current characteristic of the silver-bonded diode.

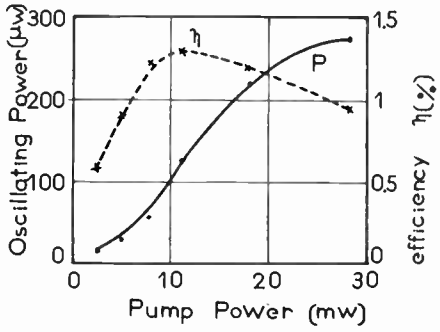

Fig. 3—Oscillation characteristics.

As the amplifier, a cross-type waveguide, a three-stub tuner of the K band and a slide-screw tuner of the X band were used. Two waveguides of the X and K bands were connected crosswise at both H planes.

The height of the X-band waveguide was tapered to the same height of the K-band waveguide. The diode was located near the cross point.

The pump power at a frequency of 23 kmc was supplied from a 2K33 klystron through a K-band isolator. An oscillation at one-half the pump frequency was produced by adjusting the three-stub tuner, the waveguide piston and the slide-screw tuner. The measured oscillating power vs pump power curve is shown in Fig. 3. The best efficiency was about 1.2 per cent at 10 mw pump power. The minimum required pump power for oscillation was about 1 mw.

As the slide-screw tuner was adjusted a little from the point of the oscillation, the oscillation stopped and the signal of almost one-half the pump frequency could be amplified at this condition for the nondegenerate-type amplification.

A typical amplification, bandwidth and noise figure vs bias voltage characteristics of the amplifier are shown in Fig. 4. In this case, the center frequency of the amplified signal is 11,440 mc, the pump frequency is 23,000 mc, and its power about 4 mw.

The noise figure was measured by using an X-band signal generator and a receiver. As the result, the minimum value of about 6.5 db was obtained for the single sideband operation. By increasing the pump power, the gain-band product of the amplifier increased, as shown in Fig. 5, and a gain of 15 db with a 50-mc bandwidth was produced at about 10 mw pump power.

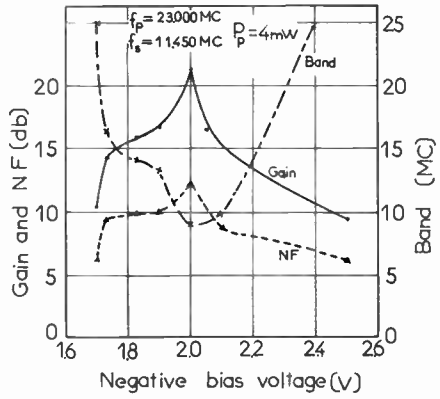

Fig. 4—The relation gain, bandwidth and noise figure vs bias voltage.

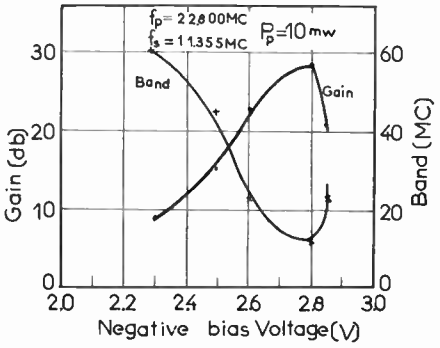

Fig. 5—The relation gain and bandwidth vs bias voltage.

The authors wish to express their gratitude to Dr. T. Fukami, T. Masuda and Dr. B. Oguchi for their interest and encouragement in the work.

S. Kita
F. Obata
Electrical Communication Lab.
Nippon Telegraph and
Telephone Public Corp.
Tokyo, Japan

Fourier Series Derivation*

Because the Fourier series is never *derived* (it is merely stated and sometimes proved), the following development by Laplace transform should be of interest. The transform of a periodic function $p(t)$ is well known to be

$$P(s) = (1 - \epsilon^{-Ts})^{-1} \int_0^T p(t)\epsilon^{-st}dt, \qquad (1)$$

where T = the period. Since $P(s)$ has the set of simple poles $s_n = j2\pi n/T$, $n = 0, \pm 1, \pm 2, \cdots$, it has[1] the partial fraction expansion

$$P(s) = \sum_{-\infty}^{\infty} c_n/(s - s_n) \qquad (2)$$

where

$$c_n = \lim_{s \to s_n} (s - s_n)P(s)$$
$$= T^{-1} \int_0^T p(t)\epsilon^{-j2\pi nt/T}dt.$$

Hence we obtain the standard exponential form of the series

$$p(t) = \sum_{-\infty}^{\infty} c_n \epsilon^{j2\pi nt/T} \qquad (3)$$

by inverting the expansion.

Christopher P. Gadsden
Dept. of Elec. Eng.
Tulane University
New Orleans, La.

Characteristic Impedance of a Slab Line*

A slab line in the form of a central cylindrical conductor between parallel planes is widely used as the slotted section in microwave measurement. Other applications of such a line are found in fields like the dee-stem transmission line inside the dee-chamber of a cyclotron. In these cases, the diameter of the central conductor may be a considerable fraction of the spacing between parallel planes. As such, a comparatively more general expression for the characteristic impedance of such a line is needed. Wholey and Eldred[1] using the transformation $w = \tan z$ derived an expression for the same. However, the expression turns out to be a complex one. A simpler yet reasonably accurate formula is, therefore, desirable. This is obtained in the following manner.

In the case of a central conductor of radius r and the spacing between parallel planes $2s$ we use the transformation $z_1 = \tan \pi z/4s$. This transforms the parallel planes in the z plane to a circle of unit radius in the z_1 plane and the circle of radius r in the z plane to an elliptical shape of semimajor axis $\tan \pi r/4s$ and semiminor axis $\tanh \pi r/4s$ in the z_1 plane. Both these axes are increasing functions of r, and consequently the eccentricity of the transformed ellipse increases comparatively much more slowly with r. This gives the clue that the results obtained for a coaxial transmission line with an elliptical inner conductor[2] may be used without much error up to a value of the diameter-to-spacing ratio as high as 0.75.

Using the transformation

$$\omega = A \ln \left(\frac{z}{k} + \sqrt{\left(\frac{z}{k}\right)^2 - 1} \right),$$

* Received by the IRE, December 17, 1959; revised manuscript received, February 5, 1960.

[1] A theorem justifying this type of expansion is proved in E. T. Copson, "Theory of Functions of a Complex Variable," Oxford University Press, pp. 144–145; 1935.

* Received by the IRE, January 19, 1960.

[1] W. B. Wholey and W. N. Eldred, "A new type of slotted line section," PROC. IRE, vol. 38, pp. 244–248; March, 1950.

[2] S. Mahapatra, "Coaxial transmission lines—effect of elliptical inner conductor on high frequency characteristics," *Elec. and Radio Engr.*, vol. 35, pp. 63–67; February, 1958.

the characteristic impedance of a coaxial transmission line with an elliptical inner conductor of semimajor axis a and semiminor axis b and an outer conductor of radius r is found[2] to be given by

$$Z_0 = 138 \log_{10} \frac{r + \sqrt{r^2 - (a^2 - b^2)}}{a + b} \text{ ohms.}$$

Hence in the case of a slab line with central cylindrical conductor of radius r between parallel planes of spacing $2s$, we get the characteristic impedance as

$$Z_0 = 138 \log_{10} \cdot \frac{1 + \sqrt{1 - (\tan^2 \alpha - \tanh^2 \alpha)}}{\tan \alpha + \tanh \alpha} \text{ ohms,}$$

where

$$\alpha = \frac{\pi r}{4s}.$$

A plot of characteristic impedance Z_0 vs diameter-to-spacing ratio (*i.e.*, r/s) is shown in Fig. 1. It may be noted that this concise formula gives reasonably better approximation up to a value of diameter-to-spacing ratio as high as 0.75. Thus for the values of r/s equal to 0.75, 0.7 and 0.6, the error is found to be about 5, 2.5 and 1 per cent, respectively, and for r/s less than 0.6, the error is negligible. However, the error will sharply increase for values of r/s greater than 0.75.

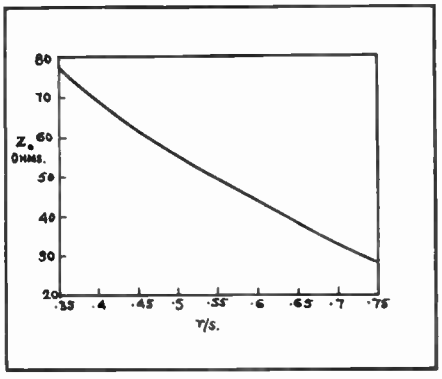

Fig. 1—Characteristic impedance vs diameter-to-spacing ratio.

We note that for values of r/s less than 0.35, we may use, without any appreciable error, the reduced formula,

$$Z_0 = 138 \log_{10} \frac{4s}{\pi r}$$

obtained by Frankel.[3] Knowing the characteristic impedance, we may calculate other parameters of the line.[2]

S. Mahapatra
Elec. Engrg. Dept.
Indian Inst. of Tech.
Powai, Bombay, India

[3] S. Frankel, "Characteristic impedance of parallel wires in rectangular troughs," Proc. IRE, vol. 30, pp. 182–190; April, 1942.

Generating Functions and the Summation of Infinite Series*

A problem often encountered in solving eigenvalue problems is to sum an infinite series of the form

$$\sum_{n=0}^{\infty} a_n \cdot b_n \cdots g_n \cdots \qquad n = 0, 1, 2. \quad (1)$$

An expedient method for manipulating or summing such series is provided by generating functions. Given the generating function

$$G(y) = \sum_{n=0}^{\infty} g_n y^n, \quad (2)$$

then $G(1)$ is the sum of the g_n series, whenever the g_n series converges.

Given the known generating function (2), one can obtain the generating function

$$F(y) = \sum_{n=0}^{\infty} f_n g_n y^n \quad (3)$$

if f_n is a rational polynomial in n. The poles of f_n must be rational or zero. The composition (3) is initiated through the partial fraction expansion of f_n; hence

$$F(y) = \sum_{n=0}^{\infty} \frac{a_0 n^r + a_1 n^{r-1} + \cdots + a_r}{b_0 n^q + b_1 n^{q-1} + \cdots + b_q} g_n y^n$$

$$F(y) = A_m \sum_{n=0}^{\infty} n^m g_n y^n + \cdots + A_0 \sum_{n=0}^{\infty} g_n y^n + \cdots + B_{k-1} \sum_{n=0}^{\infty} \frac{n^{k-1}}{(n+p)^k} g_n y^n + \cdots + B_0 \sum_{n=0}^{\infty} \frac{1}{(n+p)} g_n y^n \quad (4)$$

where p designates the poles; a, b, A and B have positive or negative values and are rational or zero; and k, m, q, and r are integers. The composition is completed by modification of the exponent of the y^n term in (2) so that differentiation or integration with respect to y will yield the desired partial fraction terms of (4).

Let

$$D[G(y)] = \frac{d}{dy} G(y),$$

$$D^{-1}[G(y)] = \int G(y) dy;$$

then, for example,

$$\sum_{n=0}^{\infty} n g_n y^n = yD[G(y)] - C(y^{-s}),$$

$$\sum_{n=0}^{\infty} n^2 g_n y^n = yDyD[G(y)] - C(y^{-s}),$$

$$\sum_{n=0}^{\infty} \frac{g_n y^n}{(n - 1/2)} = y^{1/2} D[y^{-3/2} G(y)] - C(y^{-s}),$$

$$\sum_{n=0}^{\infty} \frac{n}{(n+1)^2} g_n y^n = y^{-1} D^{-1} y^{-1} D^{-1} y^2 D[G(y)] - C(y^{-s}).$$

The $C(y^{-s})$ terms, where $s \geq 0$ and an integer, must be provided in some instances to correct for terms introduced by the operations on $G(y)$ that are not contained in the series expansion of the desired generating function. The number of correction terms cannot exceed the number of operations on $G(y)$. The expression $F(y)$ can then be acquired by summation of the generating functions derived for the expanded terms of (4).

Given (3), a generating function

$$H(y) = \sum_{n=0}^{\infty} f_n g_n h_n y^n \quad (5)$$

can be obtained (f_n need not be present) if h_n is of the form $(u)^n$, where u is any general function but not a function of n. It is evident that

$$H(y) = G(uy) = \sum_{n=0}^{\infty} g_n (uy)^n. \quad (6)$$

A good example of (6) is provided by

$$\sum_{n=0}^{\infty} (i)^n \cos\left[\frac{\pi}{2} n\right] g_n y^n = \tfrac{1}{2}[F(-y) + F(y)].$$

The two procedures just outlined appear rather limited in scope, but can be used to great utility if one expands the factors of (1) into their respective Taylor series. This technique can be demonstrated in the summation of a series of spherical Bessel functions $j_n(x)$ which have the following expansion:

$$\sum_{n=0}^{\infty} j_n(x) = \sum_{n=0}^{\infty} \cdot \left[\sum_{k=0}^{\infty} (-1)^{(n+k)} \frac{2^n k! x^{(2k-n)}}{(2k+1)!(k-n)!}\right]. \quad (7)$$

For large values of the argument x the series (7) is very slowly convergent.[1] The Taylor series expansion of the $j_n(x)$ terms now has made it possible to sum (7) over n to obtain

$$\sum_{n=0}^{\infty} j_n(x) = \sum_{k=0}^{\infty} \frac{x^k}{(2k+1)!} \left(\sin \frac{\pi}{2} k + \cos \frac{\pi}{2} k\right)$$

which is a form from which the generating function can be found using the procedures of this correspondence. Since

$$y^{-1/2} D^{-1}[\tfrac{1}{2} y^{-1/2} (e^{xy})] = \sum_{k=0}^{\infty} \frac{x^k}{(2k+1)!} y^k,$$

(7) has the generating function

$$y^{-1/2} D^{-1}[y^{-1/2} (\sin xy - \cos xy)]$$

which upon integration yields for $y = 1$

$$\sum_{n=0}^{\infty} j_n(x) = \frac{\sin x - \cos x}{2x} \cdot \left[1 + 2 \sum_{m=1}^{\infty} \frac{(2m-1)!}{(2m-2)!} (2x)^{-m} \cdot \left(\sin \frac{\pi}{2} m + \cos \frac{\pi}{2} m\right)\right]. \quad (8)$$

When (7) is slowly convergent the right side of (8) is rapidly convergent and vice versa.

The procedures described in this correspondence are certainly not new, but when employed in a systematic manner they can be used to reduce complex series of which the following is an example:

$$ix(\sin\theta) e^{ix \cos\theta} = \sum_{n=0}^{\infty} (i)^n \left[\frac{2n+1}{n(n+1)}\right] P_n'(\cos\theta) j_n(x) \quad (9)$$

[1] H. Feshbach and P. Morse, "Methods of Theoretical Physics," McGraw-Hill Book Co., Inc., New York, N. Y., pp. 1465–1468; 1953.

* Received by the IRE, February 12, 1960.

involving the spherical Bessel function and the associated Legendre polynomial P_n' (cos θ). Relationships such as (9) are often encountered when one seeks solutions to the wave equation in spherical coordinates.

T. H. VEA
Advanced Applications Section
Western Development Laboratories
Philco Corporation
Palo Alto, Calif.

Depth of Penetration as a Measure of Reflectivity of Thin Conductive Films*

The depth of penetration is a measure of the rate at which a wave is attenuated as it progresses in a conducting medium. In the case of very thin metallic films (surrounded on both sides by free space), where the thickness is much less than the depth of penetration, it is conceivable that more of the incident energy is transmitted through the film as it is made thinner. Thus it is desirable to determine the actual decrease in reflectivity as the film thickness is decreased. The investigation yields a multiplicative factor which, when applied to the depth of penetration, is a measure of the required thickness of the film for reflection of a normally incident wave.

A wave normally incident on a thin homogeneous conductive film suspended in free space is considered (Fig. 1). The voltage reflection coefficient is

$$\rho = \frac{Z_{in} - Z_0}{Z_{in} + Z_0} \tag{1}$$

where

Z_{in} = input impedance at the point of incidence,
Z_0 = intrinsic impedance of free space.

$$\rho = \frac{Z_{in} - 377}{Z_{in} + 377}. \tag{2}$$

The input impedance is determined by reflecting the termination impedance Z_R a distance equal to the film thickness l. Thus,

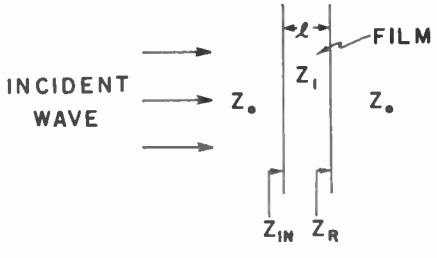

Fig. 1.

$$Z_{in} = \frac{Z_R + Z_1 \tanh \gamma_1 l}{1 + \frac{Z_R}{Z_1} \tanh \gamma_1 l} \tag{3}$$

where

$Z_R = Z_0 = 377$ ohms,
Z_1 = intrinsic impedance of the film,
γ_1 = propagation constant of the film $= \sqrt{j\omega\mu_1\sigma_1}$,
μ_1 = magnetic permittivity of the film (permeability),
ϵ_1 = electric permittivity of the film,
σ_1 = conductivity of the film.

For

$$|\gamma_1| l \leq 0.05,$$

$$Z_{in} = \frac{Z_R + Z_1 \gamma_1 l}{1 + \frac{Z_R}{Z_1} \gamma_1 l}.$$

Since Z_1 is always much less than Z_R for good conductors,

$$\left(\frac{\sigma_1}{\omega\epsilon_1} \gg 1\right);$$

however,

$$Z_{in} = \frac{Z_R}{1 + \frac{Z_R}{|Z_1|} |\gamma_1| l}. \tag{4}$$

Therefore, Z_{in} and ρ are always real.

A reflection coefficient of $\rho = -0.90$ is arbitrarily chosen as the limiting value for reflection; *i.e.*, to satisfy the condition for reflection it is required that the reflectivity be greater than 90 per cent. Hence, the thickness corresponding to a reflectivity of 90 per cent is referred to as the minimum required thickness for reflection. From (2),

$$\rho' = -0.90 = \frac{Z_{in} - 377}{Z_{in} + 377}.$$

Therefore,

$$Z_{in} = 19.85\ \Omega.$$

Substituting the above value into (4),

$$19.85 = \frac{377}{1 + \frac{377}{|Z_1|} |\gamma_1| l'},$$

$$|\gamma_1| l' = 0.0478\ |Z_1|.$$

Note that, since $|\gamma_1| l$ must be less than, or equal to, 0.05 for $\tanh \gamma_1 l = \gamma_1 l$, $|Z_1|$ must be less than, or approximately equal to, unity.

$$l' = \frac{0.0478\ |Z_1|}{|\gamma_1|}. \tag{5}$$

Also,

$$|\gamma_1| = |\alpha_1 + j\beta_1| = \sqrt{2}\alpha_1 = \frac{\sqrt{2}}{\delta} \tag{6}$$

where

δ = depth of penetration of the film.

Substituting (6) into (5),

$$l' = 0.0338\ |Z_1|\ \delta. \tag{7}$$

Eq. (7) gives the required thickness of the film as a fraction of the depth of penetration for a reflectivity of -0.90. Thus, any thickness greater than l' yields a reflectivity of greater than 90 per cent. With an intrinsic impedance of unity, the minimum required thickness for 90 per cent reflection is only 3.38 per cent of the depth of penetration. Therefore, very thin conductive films with thicknesses in the order of a fraction of the depth of penetration may possess excellent reflective qualities.

Fig. 2 illustrates the manner in which the minimum required thickness l' (in terms of percentage of δ) varies linearly with the intrinsic impedance $|Z_1|$ of the film.

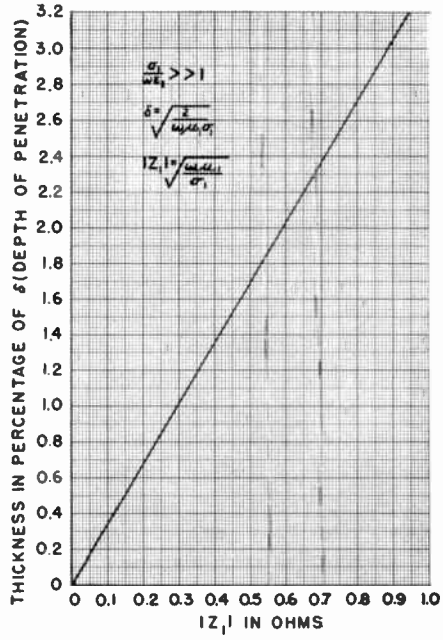

Fig. 2—Variation of minimum required thickness or conductive film with intrinsic impedance for 90 per cent reflectivity.

The actual required thickness for a reflectivity of 90 per cent is

$$l' = \frac{0.0478}{\sigma_1}. \tag{8}$$

Note that (8) is independent of frequency. Thus, the actual minimum required thickness is independent of the depth of penetration to the extent that the depth of penetration is a function of frequency; *i.e.*, for a specific material, the depth of penetration varies with the frequency, whereas the actual minimum required thickness remains constant. For this reason the depth of penetration alone cannot be used as a measure of the reflective properties of a thin conductive film.

It is important to remember that the entire analysis is valid only for good conductors with intrinsic impedances of unity or less.

* Received by the IRE, February 23, 1960.

$$\frac{\sigma_1}{\omega\epsilon_1} \gg 1. \tag{9}$$

$$|Z_1| \leqq 1. \tag{10}$$

The variation of reflection coefficient with film thickness for aluminum at 900 mc is illustrated in Fig. 3. Note that even with a thickness of only 20 Å, the reflectivity is greater than 80 per cent. The conductivity is assumed to be constant at 1.1×10^7 mhos/m. Similar curves may be drawn for frequencies other than 900 mc. For frequencies greater or less than 900 mc, the curves should lie below and above the 900-mc curve, respectively. The lower abscissa, however, is valid only for 900 mc.

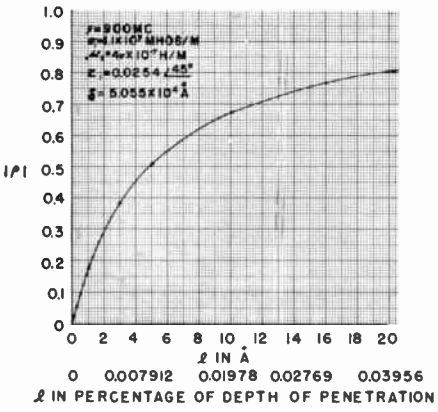

Fig. 3—Reflectivity vs film thickness for aluminum.

Extension of the curve in Fig. 3 to a thickness of 350 Å yields a reflectivity of 98.8 per cent. With this thickness and a frequency of 2000 mc instead of 900 mc, the film still exhibits excellent conductive properties with an intrinsic impedance of less than 0.04 Ω. Thus, according to (8), the coefficient of reflection is still equal to that obtained at 900 mc. For a reflectivity of 98.8 per cent, however, the constant coefficient in (8) and the condition of (10) are different. At all frequencies below 900 mc, the film appears to be, to a greater extent, an excellent conductor, whose intrinsic impedance decreases with decreasing frequency. Thus, the film has a reflectivity of 98.8 per cent for all frequencies below 900 mc. In the case of a sphere with such an aluminum film, then, the lower frequency limit is dependent on the diameter of the sphere.

In all cases satisfying (9) and (10) it is concluded that the minimum required thickness for reflection is a maximum of only 3.38 per cent of the depth of penetration, the percentage decreasing linearly as the intrinsic impedance of the film decreases. The multiplicative factor to be applied to the depth of penetration to obtain the minimum required thickness for a reflectivity of 90 per cent is $0.0338\,|Z_1|$.

F. T. Koide
Collins Radio Co.
Cedar Rapids, Iowa

The Optimum Detection of Analog-Type Digital Data*

An ever-increasing number of communication systems are concerned with the transmission of data. Conventionally, the criterion of good transmission is taken as the ability of the receiver to reproduce the transmitted data as faithfully as possible *i.e.*, that errors be held to a minimum. However, the data transmitted over the communication channel are seldom in their original form. The data may, for example, be the binary representations of an alphabet of numbers which are a code for the English alphabet, as in teletype. On the other hand, the data may be the binary representations of an alphabet of numbers which are a code for the quantized amplitudes of an analog quantity, as in PCM or telemetry.

It is apparent that the effects of errors are different in the two cases cited. The data stream for teletype can be termed "discrete-type" digital data to emphasize that the ultimate output must be discrete; specifically, a letter of the English alphabet must be selected. If the selection is made incorrectly, it is significant only that an error is committed—not what the erroneous selection is. In such a case, minimizing the probability of error is obviously the desirable criterion.

If the receiver output is to be a reproduction of an analog quantity, however, the fidelity with which it can be reconstructed from the imperfectly received stream of "analog-type" digital data becomes the important consideration. Errors committed at the detector are not of interest in themselves, but by virtue of the error magnitudes they reflect into the output.

Minimization of the mean-square error between the original and reconstructed signals is a reasonable criterion to apply to the reception of analog signals. It has the desirable property of penalizing large errors and also has the undeniable advantage of being mathematically tractable in many cases. Applied to speech, it seems a natural criterion since the net effect of reconstruction errors closely resembles that of noise which is usually measured by its mean-square value.

Previous work by the author[1] led to an energy redistribution for the pulses within a PCM code group (to be applied at the transmitter) which minimizes the mean-square error in the receiver output. This reduces the error probabilities for those pulses which contribute heavily to the output at the expense of the less important pulses which add fine detail. Though the error rate at the detector is thereby increased, the output is nevertheless a more faithful reproduction of the original signal.

The mean-square-error criterion can also be used to optimize receiver design by yielding new detector characteristics. The conventional detector for data reception is a decision device yielding one of two distinct outputs at specified intervals. If the final output is to be a sample of an analog signal, then each group of several pulses at the detector will denote (by their polarity, presence-or-absence, etc.) the appropriate coefficients to apply to the binary representation of a particular sample value. Thus, a group of k pulses yields coefficients α_n to permit evaluating the series

$$A = \sum_{n=1}^{k} \alpha_n 2^{n-1}, \qquad \alpha_n = \{0, 1\} \tag{1}$$

where A is the desired sample value.

Consider a binary symmetric channel in which pulses of amplitude $\pm a$ occur periodically in the presence of additive Gaussian noise having unity variance. The conventional detector samples the pulse stream at the appropriate times and makes its decision as to whether the α_n in (1) is a 0 or a 1 according to whether the sample value is negative or positive, respectively. However, the sample value is not intrinsically a discrete quantity. After reconstruction, it will be filtered together with the adjacent sample values to yield a smooth, continuous function of time. Therefore, it is not necessary that α_n be an integer. It is shown in the following that there is a detector characteristic which will yield values for α_n selected from the continuum such that the mean-square error is minimized (though the resulting improvement is rather modest).

The probability densities for the binary symmetric channel are illustrated in Fig. 1.

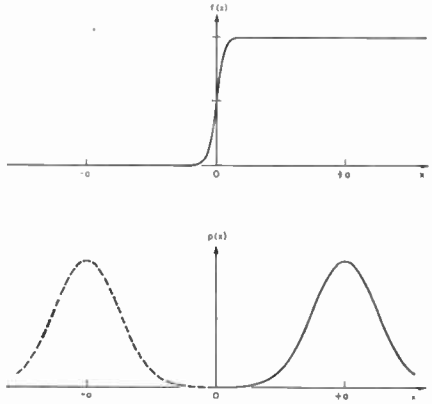

Fig. 1—Probability densities and detector characteristic for the binary symmetric channel, ($a=4$).

Let

$$p(x) = \frac{1}{\sqrt{2\pi}} e^{-x^2/2} \tag{2}$$

denote the density function for the noise. If the transmitted pulse is "positive," its density function is $p(x-a)$ when received in the presence of additive Gaussian noise at a signal-to-noise ratio a^2. Similarly, a "negative" pulse yields a density function $p(x+a)$.

Let $f(x)$ denote the desired detector characteristic. If a positive pulse is to signify the coefficient 1, then receiving it at an amplitude in the interval $(x, x+dx)$ causes an error $1-f(x)$ with probability $p(x-a)dx$. A negative pulse, signifying the coefficient 0,

* Received by the IRE, February 15, 1960.
[1] E. Bedrosian, "Weighted PCM," IRE Trans. on Information Theory, vol. IT-4, pp. 45–49; March, 1958.

causes an error $f(x)$ with probability $p(x+a)dx$. For the symmetric channel these events occur with equal probability so the mean-square error can be written

$$\overline{\epsilon^2} = \frac{1}{2}\int_{-\infty}^{\infty}[1-f(x)]^2 p(x-a)dx + \frac{1}{2}\int_{-\infty}^{\infty} f^2(x)p(x+a)dx. \quad (3)$$

Minimizing with respect to $f(x)$ is accomplished by setting

$$\frac{\partial\overline{\epsilon^2}}{\partial f} = -[1-f(x)]p(x-a) + f(x)p(x+a) = 0,$$

so that

$$f(x) = \frac{p(x-a)}{p(x-a)+p(x+a)} = \frac{1}{1-e^{-2ax}} = \frac{1}{2}+\frac{1}{2}\tanh ax \quad (4)$$

which is plotted in Fig. 1 for $a=4$. It is seen to be symmetrical about $f(0)=\frac{1}{2}$ and to tend monotonically to the exact coefficients, 0 and 1, as asymptotes. For large values of a, *i.e.*, high signal-to-noise ratios, it approaches the characteristic of the conventional detector.

The mean-square error can be evaluated by substituting (4) in (3), giving

$$\overline{\epsilon^2} = \frac{1}{2}\int_{-\infty}^{\infty}\frac{p(x+a)p(x-a)}{p(x+a)+p(x-a)}dx = \frac{1}{4}\frac{e^{-a^2/2}}{\sqrt{2\pi}}\int_{-\infty}^{\infty} e^{-x^2/2}\operatorname{sech} axdx. \quad (5)$$

Expanding the exponential in a Maclaurin's series and noting that[2]

$$\int_0^{\infty}\frac{x^{2n}}{\cosh ax}dx = E_n\left(\frac{\pi}{2a}\right)^{2n+1}, \quad a>0,\ n=0,1,2,\cdots, \quad (6)$$

where E_n is the Euler number: $E_0=E_1=1$, $E_2=5$, $E_3=61$, $\cdots$, yields

$$\overline{\epsilon^2} \approx \frac{\pi}{4}\frac{e^{-a^2/2}}{\sqrt{2\pi}a}\left[1-\frac{\pi^2}{8a^2}+\cdots\right]. \quad (7)$$

For the conventional detector,

$$f(x) = \begin{cases}0, & x<0,\\ 1, & x>0,\end{cases} \quad (8)$$

so the mean-square error of (3) becomes

$$\overline{\epsilon^2} = \frac{1}{2}\int_{-\infty}^{0}p(x-a)dx+\frac{1}{2}\int_0^{\infty}p(x+a)dx = \int_a^{\infty}p(x)dx \approx \frac{e^{-a^2/2}}{\sqrt{2\pi}a}\left[1-\frac{1}{a^2}+\cdots\right]. \quad (9)$$

Comparing (7) and (9) indicates that the optimum detector decreases the mean-square error in the reconstructed output by a factor of almost exactly $\pi/4$ (about 1 db) for all practical values of a. Of course, an improvement of this magnitude is not of much practical significance since the system with a conventional detector can achieve the same improvement by increasing the pulse amplitude by a factor of 1.025 (for $a=3$) which requires an increase of only 0.2 db in transmitted power. Nevertheless, it is interesting to observe that an improvement is possible and that the optimum detector characteristic resembles the sort of "nonideal" detector characteristic invariably obtained when practical diodes are used.

EDWARD BEDROSIAN
The RAND Corporation
Santa Monica, Calif.

[2] W. Grobner and N. Hofreiter, "Integral Tafel, Zweiter Teil, Bestimmte Integrale," Springer-Verlag, Vienna, Austria, No. 352.1a, p. 163; 1950.

On Network Synthesis with Negative Resistance*

Since the advent of the Esaki diode, there has been an increasing interest in the inclusion of the negative resistance as a basic building block in network theory. The inclusion of this element gives rise to a more general class of function that may be realized as driving point and transfer-impedances. A synthesis procedure will be outlined that enables the synthesis of arbitrary real coefficient, rational functions as driving point or transfer impedances utilizing the following elements: positive resistors, inductors, capacitors, and two-negative resistors. The procedure, in each case, results in networks that are realizable with lossy elements arranged in Foster forms.

Driving Point Impedance Synthesis

Any $Z(s)$ of the form,

$$Z(s) = \frac{N(s)}{D(s)} \quad (1)$$

where N and D are polynomials of arbitrary degree with real coefficients, may be written as

$$Z(s) = Q(s)\frac{\left[\frac{N(s)}{Q(s)}\right]}{D(s)} \quad (2)$$

where

$$Q(s) = \prod_{i=1}^{n}(s+a_i);\ a_i \text{ real}, \quad 0<a_1<a_2<a_3\cdots,$$

and n is one greater than the degree of N or D, whichever is larger.

Utilizing the technique demonstrated by Kinariwala,[1] (2) may be expanded as

$$Z(s) = \frac{Q}{D}\left[\frac{N_1}{D_1}-\frac{N_2}{D_2}\right] = \frac{D_2N_1}{D}-\frac{D_1N_2}{D}. \quad (3)$$

where

$$\frac{N_1}{D_1} \text{ and } \frac{N_2}{D_2}$$

are both RC r.p. functions. Since $Q=D_1D_2$, D_2N_1 and D_1N_2 are strict RC Hurwitz Polynomials[2] of degree $n-1$. Now defining

$$Z(s) = \frac{1}{Y_1}+\frac{1}{Y_2}, \quad (4)$$

we can identify

$$Y_1 = \frac{D}{D_2N_1}. \quad (5)$$

and

$$Y_2 = \frac{-D}{D_1N_2}. \quad (6)$$

The degrees of the denominators of Y_1 and Y_2 (which are strict RC Hurwitz polynomials) are equal to or greater than D. A simple extension of the above technique will enable the final synthesis.

Theorem: Any rational function $Y(s)$, whose denominator is a strict RC Hurwitz polynomial and of degree greater than or equal to the numerator, may be expanded into the sum of an RL Foster form, an RC Foster form, and one negative constant.

Proof:

$$Y(s) = \frac{N}{\prod_{u=1}^{m}(s+b_u)} = \sum_{k=1}^{m_1}\frac{|d_k|}{s+b_k}-\sum_{i=1}^{m_2}\frac{|e_i|}{s+b_i} = \sum_{k=1}^{m_1}\frac{|d_k|}{s+b_k}+\sum_{i=1}^{m_2}\frac{s\left|\frac{e_i}{b_i}\right|}{s+b_i}-\sum_{i=1}^{m_2}\left|\frac{e_i}{b_i}\right|$$

where

$$m_1+m_2=m.$$

Thus

$$Y(s) = Y_1(s)+Y_2(s)-R,$$

where

$$Y_1(s) = \sum_{k=1}^{m_1}\frac{|d_k|}{s+b_k} \quad \text{(an RL foster form)},$$

and

$$Y_2(s) = \sum_{i=1}^{m_2}\frac{s\left|\frac{e_i}{b_i}\right|}{s+b_i} \quad \text{(an RC Foster form)},$$

$$-R = \sum_{i=1}^{m_2}\left|\frac{e_i}{b_i}\right| \quad \text{(one negative resistor)}.$$

Therefore, (5) and (6) may be expanded as:

$$Y_1 = Y_3+Y_4-R_1 \quad (7)$$

$$Y_2 = Y_5+Y_6-R_2, \quad (8)$$

where Y_3 and Y_5 are RL Foster forms, and Y_4 and Y_6 are RC Foster forms. The network corresponding to (4), (7), and (8) is shown in Fig. 1.

Note that since the number of reactive elements or positive resistors in both the Y_1 and Y_2 realizations is equal to the degree of N or D (whichever is greater), the total quantity of each is at most twice this number.

Transfer Impedance Synthesis

The network shown in Fig. 2 yields an open-circuit voltage ratio which may be ex-

* Received by the IRE, March 24, 1960.

[1] B. K. Kinariwala, "Synthesis of active RC networks," *Bell Sys. Tech. J.*, vol. 38, p. 1302; September, 1959.

[2] Polynomials with simple negative real roots none of which are zero.

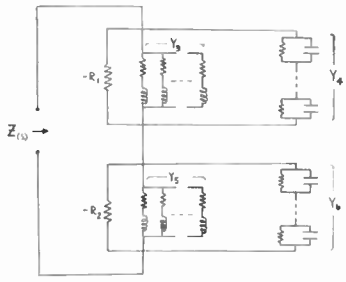

Fig. 1.

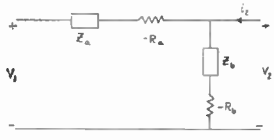

Fig. 2.

pressed as

$$\left.\frac{v_2(s)}{v_1(s)}\right|_{i_2=0} = \frac{Z_b - R_b}{Z_b - R_b + Z_a - R_a}$$

$$= \frac{1}{1 + \dfrac{Z_a - R_a}{Z_b - R_b}}. \tag{9}$$

The prescribed transfer impedance, however, may be written as

$$\left.\frac{v_2(s)}{v_1(s)}\right|_{i_2=0} = \frac{N(s)}{D(s)} = \left[\frac{1}{1 + \dfrac{D - N}{N}}\right] \tag{10}$$

where N and D are polynomials of any degree with real coefficients. From (9) and (10) the following identification is made

$$\frac{Z_a - R_a}{Z_b - R_b} = \frac{D - N}{N}, \tag{11}$$

which may also be expressed as

$$\frac{Z_a - R_a}{Z_b - R_b} = \frac{\dfrac{D - N}{Q}}{\dfrac{N}{Q}}, \tag{12}$$

with

$$Q(s) = \prod_{i=1}^{m} (s + a_i)^3$$

where m is equal to the degree of D or N, whichever is larger. Utilizing the previous theorem the right side of (12) can be expanded as

$$\frac{\dfrac{D - N}{Q}}{\dfrac{N}{Q}} = \frac{Z_1 + Z_2 - R_1}{Z_3 + Z_4 - R_2}, \tag{13}$$

where Z_1 and Z_3 are RL Foster forms, Z_2 and Z_4 RC Foster forms. Thus according to (12), we may make the identification

$$Z_a = Z_1 + Z_2$$
$$Z_b = Z_3 + Z_4$$
$$-R_a = -R_1$$
$$-R_b = -R_2,$$

[3] Where $Q(s)$ is subject to the same restrictions as in the previous case.

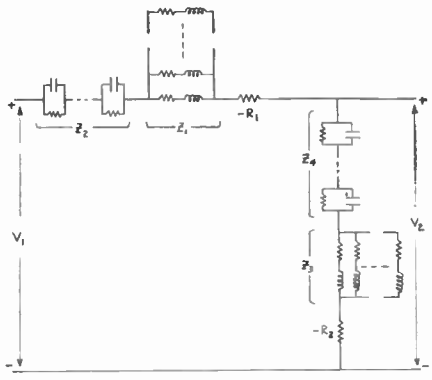

Fig. 3.

and the network of Fig. 2 becomes that shown in Fig. 3.

Note that the total number of reactive elements or positive resistors is equal to or less than twice the degree of N or D, whichever is larger.

It is anticipated that a more complete paper will be submitted at a later date.

F. T. Boesch
M. R. Wohlers
Dept. of Elec. Engrg.
Polytechnic Inst. of Brooklyn
Brooklyn 1, N. Y.

Electromagnetic Energy in a Dispersive Medium*

The energy density of the electromagnetic field in a dispersive medium was recently discussed by Hosono and Ohira.[1] It should be noted that their results had already been given by Levin[2] and derived still earlier by Rytov in references quoted by Levin.

It is of interest that the dispersive forms of the energy are also those required for the mean thermal fluctuation energy of the electric (or magnetic) fields in a CR (or LR) circuit to comply with the equipartition principle. Consider such a circuit, in which R is made very large compared with loss resistance of the capacitor (or inductor), which inevitably occurs when the permittivity (or permeability) is dispersive by virtue of the Kramers-Kronig relations. Then the mean energy of the electric field in the capacitor is given by

$$\int_0^\infty \frac{4kTR}{1 + (\omega CR)^2} \cdot \frac{1}{2} \frac{d}{d\omega}(\omega C) \cdot df = \frac{1}{2} kT$$

and similarly the mean energy of the magnetic field in the inductor is

$$\int_0^\infty \frac{4kTR}{\omega^2 L^2 + R^2} \cdot \frac{1}{2} \frac{d}{d\omega}(\omega L) \cdot df = \frac{1}{2} kT.$$

It may readily be shown that these results are independent of the geometry of the capacitor or inductor.

R. E. Burgess
Dept. of Physics
University of British Columbia
Vancouver, Canada

* Received by the IRE, March 10, 1960.

[1] T. Hosono and T. Ohira, "The electromagnetic energy stored in a dispersive medium," Proc. IRE, vol. 48, pp. 247–248; February, 1960.

[2] M. L. Levin, "An elementary derivation of the formula for the electromagnetic energy in a dispersive medium," *J. Exper. and Theoret. Phys.*, vol. 29, p. 252; August, 1955. Also in *Soviet Phys. JETP*, vol. 2, pp. 168–169; February, 1956.

Determination of Satellite Orbits from Radar Data*

The present paper is a report on an investigation of methods for the determination of satellite orbits from radar data. Of particular interest are problems which require the rapid calculation of the orbit elements from a limited amount of data. In some cases the available information may be restricted to the data obtained from a single pass, over a period of 2 to 4 minutes, as the satellite goes by the observing station. The solution to this computing problem requires methods which are rather different from those developed previously for the calculation of satellite orbits from observations extending over several revolutions of the satellite.

The following section describes in some detail a method which has been found to offer a good combination of speed and accuracy. It requires between 10 and 20 seconds for a rough determination, yielding orbit elements in this time with a precision of 0.001 in eccentricity and 0.05 minutes in period. This degree of accuracy is sufficient to determine whether the satellite is in orbit. The program then proceeds automatically with a correction routine which operates on the preliminary orbit elements to yield a more accurate prediction of the position of the satellite at later points along the orbit. The precision of the corrected predictions is 500 yards or better, which is sufficient for the purpose of acquisition by other radars at later points along the orbit. This correction routine requires an additional 40 seconds of computer time.

Procedure

The procedure chosen as optimum involves the following steps:

Orbit Inclination

A plane is passed through the center of the earth and through all the points along the radar track. The inclination of the plane and the position of the line of nodes are adjusted to the full set of data by a least-squares calculation. The plane of the orbit is now determined.

Orbit Elements in the Plane

The three orbit elements in the plane must still be determined after the plane of the orbit has been fixed. These may be taken

* Received by the IRE, March 18, 1960.

as the period, perigee altitude, and argument of perigee. They can be computed from any three items of information along the track. We have found it most accurate to choose 2 points on the track and the time between them as our three fundamental items. The procedure for the calculation of the orbit elements depends in an essential way on the dynamics of the satellite motion, and may be called the *dynamical* method. It is also known as the method of Gauss and Olbers.

Full use is made of the data by dividing the track into halves, and pairing the points in the first half with those in the second half through 3 data points along the track, again with the center of the earth as focus; this method does not make use of the dynamical equations of the satellite motion, and was investigated because the basic equations are exceedingly simple; however, it was found to be considerably less acurate than the dynamical or Gauss-Olbers procedure; 2) a least-squares adjustment of the orbit elements in place of the average; the results obtained by the least-squares method are inferior to the direct average in accuracy for short arcs (less than 4 minutes).

Table I presents a comparison of the results obtained from these methods.

TABLE I

ERRORS IN ORBIT ELEMENTS FOR EQUALLY SPACED POINTS ALONG AN ARC

	Gauss-Olbers (4-minute arc)	Geometric (4-minute arc)	Least-Squares Geometric (6½-minute arc)
Period (minutes)	0.004	0.06	0.09
Argument Perigee (degrees)	0.02	0.3	0.4
Perigree Altitude (miles)	0.3	0.8	2.3

in chronological order. The final orbit elements are obtained by taking an average of the individual results. A least-squares method is usually used instead, but we have found that the least-squares procedure does not, in fact, offer any advantage over the method of simple averages. The orbit elements obtained in this way are printed out as immediate results.

Differential Correction of the Orbit Elements

In the third step of the computation the slant ranges are used for a further improvement. The slant ranges are the most accurate elements of the radar data, and it is necessary to devote special attention to them at the end of the computing procedure in order to extract the greatest orbital precision from the tracking data. The adjustment of the orbit elements to the slant ranges is carried out by conventional differential correction routines.

A special procedure is used for orbits of an eccentricity less than 0.01. In this procedure a circular orbit is assumed as the first approximation to the results. The effects of the ellipticity are added as a small correction to the circular orbit. The program for the low-eccentricity calculation is extremely simple and requires an additional computing time of only 5 seconds if the supplementary procedure is incorporated into the main program described above. The accuracy of the supplementary method is the same as that given in the main procedure. In the actual computing operation the results of both procedures can be printed out in parallel, and the appropriate set of answers chosen by inspection of the computed eccentricity, or the choice can be made internally in the program, and a single answer printed out.

Other Possibilities for a Short Program

Other methods for the rapid determination of the orbit elements have been investigated, including: 1) a purely geometrical procedure in which an ellipse is passed

Accuracy

The errors in the computation of the orbit elements are listed below for the typical case of a radar pass lasting two minutes (these results constitute the average over 20 data points, selected in two groups of 10 points each at one second intervals at the beginning and end of the radar track):

0.004	minutes in period.
0.200	miles in perigee height.
0.15	degrees in perigee argument.
0.001	degrees in angle of inclination.

The above errors in orbit elements will produce the following uncertainties in the position of the satellite after ⅓ of a revolution:

300	yards along the track.
300	yards normal to the track in the orbit plane.
150	yards normal to the orbit plane.

The major portion of the uncertainty in position perpendicular to the track comes from the error in period (from which the mean radius is computed); the error in eccentricity contributes only an uncertainty of 0.04 mile in this direction.

Computing Rime

One minute of IBM 704 time is required for the determination of the orbit elements from one radar pass including 20 data points. By eliminating the differential correction routine, the computing time can be reduced to between 10 and 20 seconds, at the sacrifice of a factor of 10 in the accuracy of the orbit determination. In this latter case, the errors are approximately 5 miles in positional uncertainty, or 0.001 in eccentricity and 0.05 minutes in period. These errors are too great for the abbreviated determination to be useful in the acquisition of the orbit by other radars, but they are adequate to provide a decision as to whether the satellite is in orbit.

I. Harris
W. F. Cahill
Theoretical Div.
Goddard Space Flight Center
NASA
Washington, D. C.

A Traveling Wave Harmonic Generator*

In conventional harmonic generators the supply of harmonic power to the load is periodic at the fundamental frequency. This means that, as well as the wanted harmonic, unwanted harmonics are also generated. If the supply of power to the load could be arranged to be periodic at the harmonic frequency then this disadvantage could be overcome. Fig. 1 shows a device in which this is achieved. Power at the fundamental frequency F is fed to the input of a propagating structure that has n diodes connected to it as shown. Arrangements to supply dc bias to the diodes must be included. As the fundamental wave travels down the structure the diodes conduct in turn and pass pulses to the load R_L. If the delay per section is chosen to be $\{1/nF\}$ seconds and the bias adjusted so that only one diode is conducting at any time then the principal component of the voltage across R_L will be at a frequency of nF.

In traveling down the line the fundamental wave will be attenuated due to dissipation in the line and power fed to R_L. This can be compensated to a certain extent by progressively reducing the dc bias on the diodes.

If the device is made using distributed elements then it may not be convenient to connect all the diodes together to one point. In this case the diodes may be connected to a second propagating structure at distances equal to an integral number of wavelengths at the harmonic frequency.

If a circulator is available then the power that would otherwise be last in R_T can be conserved by connecting the output of the line back into the circulator as shown in Fig. 2.

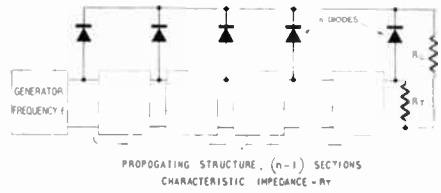

Fig. 1.

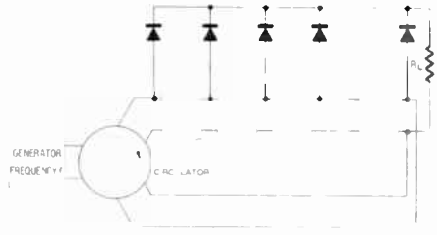

Fig. 2.

D. L. Hedderly
British Telecommunications Res., Ltd
Taplow Court, Berks., Eng

* Received by the IRE, March 29, 1960.

A Realization Theorem for Biquadratic Minimum Driving-Point Functions*

Kim[1] has introduced a method of synthesis for biquadratic minimum impedance functions in the form of an unbalanced bridge containing five elements. According to this method the network topology is first assumed, after which the driving-point impedance function is derived in terms of the branch elements and compared to the impedance function to be realized. The method always necessitates the augmentation of the impedance function with surplus factors. In a later publication, Van Valkenburg[2] stated the necessary conditions on the coefficients of biquadratic minimum impedance functions to be realizable in two special bridge forms with only five elements, but no derivation or proof was given. This letter not only presents a useful theorem for the synthesis of biquadratic minimum driving-point functions, but also gives a more general method of synthesis which leads directly to the results given by Kim and Van Valkenburg.

We begin with the positive real biquadratic impedance function

$$Z(s) = K\frac{s^2 + a_1 s + a_0}{s^2 + b_1 s + b_0}. \tag{1}$$

This function will be minimum, that is $Z(j\omega_1)=0\pm jX(\omega_1)$ at one ω_1 with $X(\omega_1)\neq 0$, only if

$$(\sqrt{a_0} - \sqrt{b_0})^2 = a_1 b_1. \tag{2}$$

The function (1) can be represented as the driving-point impedance to an RL two-port network terminated in a single capacitance. Such a representation is shown schematically in Fig. 1(a). A driving-point impedance function $Z(s)$ is related to the terminating capacitance and the open-circuit impedance

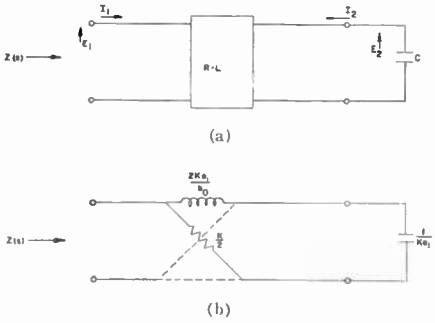

Fig. 1.

parameters of a two-port by the relation

$$Z(s) = z_{11}\frac{1 + sC\dfrac{1}{y_{22}}}{1 + sC(z_{22})}. \tag{3}$$

We now seek to express (1) in the form of (3). This is done by writing the former as

$$Z(s) = K\frac{a_1 s + a_0}{b_0}\,\frac{1 + sc\dfrac{s}{(a_1 s + a_0)C}}{1 + sc\dfrac{s + b_1}{b_0 C}}, \tag{4}$$

from which we make the identifications

$$z_{11} = K\frac{a_1 s + a_0}{b_0}, \quad z_{22} = \frac{s + b_1}{b_0 C}, \quad y_{22} = \frac{(a_1 s + a_0)C}{s}. \tag{5}$$

Eqs. (5) define a set of positive real RL driving-point functions. We have still to find a rational function representation of z_{12}. Recall that

$$z_{12}^2 = z_{11}\left(z_{22} - \frac{1}{y_{22}}\right). \tag{6}$$

Hence from (5) and (6) we have

$$z_{12} = \sqrt{\frac{a_1 s^2 + (a_1 b_1 + a_0 - b_0)s + a_0 b_1}{b_0^2/CK}}. \tag{7}$$

The quantity under the radical of (7) is always a perfect square, as comparison with (2) verifies, and so the open-circuit transfer impedance function reduces to

$$z_{12} = \frac{S + \dfrac{a_1 b_1 + a_0 - b_0}{2a_1}}{b_0\sqrt{C/a_1 K}}. \tag{8}$$

It can be easily verified that the residue and real-part conditions are always satisfied with the equal sign. Hence the poles are compact. This, plus the positive real character of the two RL driving-point impedances of (5), assures us that z_{11}, z_{22}, and z_{12} represent a physically realizable RL two-port network. This constitutes sufficient proof for establishment of the following theorem.

> Theorem: Any biquadratic minimum driving-point impedance function can be realized as the input to an RL two-port network terminated in a single capacitance.

Although a realization of $Z(s)$ is always possible according to the theorem, it is not impossible to say that no inductive coupling is necessary, or that the realization will yield a minimum number of elements. For obvious reasons, however, we seek those realizations which involve no inductive coupling. This means that the Fialkow-Gerst conditions must be satisfied. For this simple case we find, because of the compact nature of the poles, that this is possible only if the corresponding residues of the poles of z_{11}, z_{22}, z_{12} are equal. This implies that $z_{11}=z_{22}$, and so an additional restriction is imposed on the coefficients of $Z(s)$ in the form

$$\frac{a_0}{b_0} = 1/4. \tag{9}$$

The open-circuit impedance parameters of the two-port finally reduce to

$$z_{11} = z_{22} = K\frac{a_1 s + a_0}{b_0}, \quad z_{12} = K\frac{a_1 s - a_0}{b_0}, \tag{10}$$

which we recognize to be realizable in the form of a symmetrical lattice containing two reactive and two resistive elements. The network which realizes (1) is shown in Fig. 1(b).

The case treated above suggests the possibility of representing the function $z(s)$ as the input to an RC two-port network terminated in a single inductance. However, since the necessary and sufficient conditions for the realization of the complete impedance matrix as an RC two-port are still unknown, we cannot hope to achieve results as general as before. For this representation, shown schematically in Fig. 2(a), (3) is modified to give

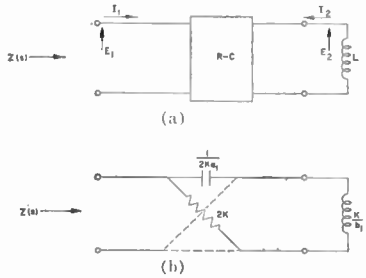

Fig. 2.

$$Z(s) = K\frac{s + a_1}{s}\,\frac{1 + \dfrac{1}{sL}\dfrac{a_0 L}{s + a_1}}{1 + \dfrac{1}{sL}\dfrac{(b_1 s + b_0)L}{s}}, \tag{11}$$

from which we find

$$z_{11} = K\frac{s + a_1}{s}, \quad z_{22} = \frac{(b_1 s + b_0)L}{s}, \quad y_{22} = \frac{s + a_1}{a_0 L}. \tag{12}$$

From (2), (6), and (12) we compute the open-circuit transfer function to be

$$z_{12} = \frac{s + \dfrac{b_0 + a_1 b_1 - a_0}{2b_1}}{(1/\sqrt{b_1 KL})S}. \tag{13}$$

Since the coefficients are always positive, the two open-circuit impedances of (12) represent positive real RC driving-point functions. Also, a check of the residue and real-part conditions again shows that they are satisfied with the equality sign. Because of the compact nature of the poles the only way we can possibly obtain a realization of $Z(s)$ as the input to an RC two-port terminated in a single inductor is for the corresponding residues of the poles of z_{11}, z_{22}, and z_{12} to be equal, in which case the Fialkow-Gerst conditions are automatically satisfied. Again $z_{11}=z_{22}$ so that the resulting restriction on the coefficients of $Z(s)$ will be

$$a_0/b_0 = 4. \tag{14}$$

The open-circuit impedances of the two-port now become

$$z_{11} = z_{22} = K\frac{s + a_1}{s}, \quad z_{12} = K\frac{s - a_1}{s}, \tag{15}$$

which are realizable as a symmetrical lattice. The complete network is shown in Fig. 2(b).

The method of synthesis of biquadratic minimum functions presented here has yielded directly the two networks of Figs. 1(b) and 2(b), both of which contain a mini-

* Received by the IRE, March 7, 1960.

[1] W. H. Kim, "A New Method of Driving-Point Function Synthesis," Electrical Engineering Research Lab., Rept. No. 1, Contract DA-11-022-ORD-1983, University of Illinois, Urbana; April 1, 1956.

[2] M. E. Van Valkenburg, "Special case of a bridge equivalent of Brune networks," PROC. IRE, vol. 44, p. 1621; November, 1956.

mum number of elements. No prior assumption was made as to their topological form, nor was any augmentation of the impedance function with surplus factors required as in Kim's method. Furthermore, the nature of the reactance $X(\omega)$ at the frequency ω_1 is of no consequence with the method presented here, and so need not be considered. In addition, (9) and (14), which are a direct consequence of the method of realization, are precisely those conditions on the coefficients of $Z(s)$ stated earlier by Van Valkenburg.

K. B. Irani
C. P. Womack
Dept. of Elect. Engrg.
University of Kansas
Lawrence, Kans.

Transformation of Impedances Having a Negative Real Part and the Stability of Negative Resistance Devices*

I. Transformation of Impedance

If a circuit element possessing a negative real part terminates one end of a transmission line, the magnitude of the reflection coefficient will, in general, be greater than unity. At first glance, it would appear that the standard transmission line calculator (Smith Chart[1]) would have to be expanded beyond $\rho=1$ (ρ is the reflection coefficient) in order that it can be used for finding the values of transformed impedances (admittances). However, as will be shown below, the present Smith Chart can be used if the radius sector is interpreted as the reciprocal of the reflection coefficient.

Basically, as is well known, the Smith Chart is the plot of the real and imaginary parts of the function.

$$\frac{1+\rho e^{2j\theta}}{1-\rho e^{2j\theta}}$$

in the plane where ρ and θ are polar co-ordinates; ρ is the reflection coefficient and θ is the electrical phase angle. A method for transforming impedances with a negative real part can be obtained by use of the following identity:

$$\frac{1+\rho e^{2j\theta}}{1-\rho e^{2j\theta}} = -\frac{1+\dfrac{1}{\rho}e^{-2j\theta}}{1-\dfrac{1}{\rho}e^{-2j\theta}} \qquad (1)$$

and its equivalent

$$\frac{Z}{Z_0} = -\left\{\frac{-Z_L + jZ_0\tan(-\theta)}{Z_0 + j(-Z_L)\tan(-\theta)}\right\} \qquad (2)$$

where

Z_0 = characteristic impedance of line
Z_2 = terminating impedance
Z = transformed impedance.

The procedure for transforming the impedance

$$Z_L = -R + jX,$$

through the electrical angle θ along a line of characteristic impedance using the Smith Chart, is as follows:

1) Normalize the impedance and form its negative:
$$+\frac{R}{Z_0} - j\frac{X}{Z_0}.$$
2) Plot this point on the Smith Chart.
3) Use the Smith Chart in the usual fashion except that the angular direction is opposite; *i.e.*, go "toward load" when physically the transformation is "toward generator" and conversely.
4) Take the negative of the reading on the Chart and multiply by Z_0 for the final result.
5) The reflection coefficient is the reciprocal of that given on the Chart.
6) The standing wave ratio is the negative of that on the Chart.
7) Use a similar procedure for transforming admittances.

In the case that the line has a loss per unit length given by the real part of the complex propagation factor γ, where

$$\gamma l = \alpha l + j\beta l \equiv \alpha l + j\theta, \qquad (3)$$

we must use a procedure similar to that used for ordinary impedances except to spiral outward instead of inward. This corresponds to replacing

$$\frac{1}{|\rho|} \text{ by } \frac{1}{|\rho|e^{-2\alpha l}} = \frac{e^{2\alpha l}}{|\rho|}.$$

If

$$\alpha l', \qquad 0 \le \beta l' \le \beta l \equiv \theta$$

is such that the rim of the Chart may be reached, we then have a transition from negative to positive input resistance. This, of course, corresponds to the physical situation, in that energy production by the active element is balanced by energy loss in the line.

II. Stability of Negative Resistance Devices

In low frequency series-fed circuits employing devices which possess negative resistance and series reactive elements, the condition for stability against oscillation is that the positive resistance (sink of energy) must exceed the negative resistance (source of energy). If the positive and negative resistances are separated by a finite length of transmission line, this condition is not sufficient, since the positive resistance may only lightly load the negative resistance device.

For the remainder of this section, we shall consider the shunt-fed circuit shown in Fig. 1. It consists of a contact current generator whose equivalent admittance is Y_+, connected to a transmission of characteristic admittance Y_0 and length L. The line is terminated in an admittance Y_- which has a negative real part. The condition for stable oscillations is that

$$Y_+ = -Y_-' \qquad (4)$$

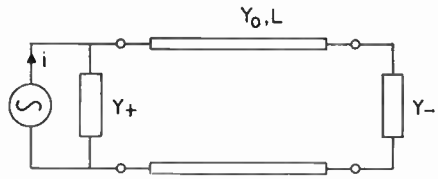

Fig. 1.

where

$$-Y_-' = \frac{(-Y_-) + jY_0\tan(-\theta)}{Y_0 + j(-Y_-)\tan(-\theta)};\ \theta = \beta L. \qquad (5)$$

Note that the value of Y_-' as a function of frequency (through θ) is given by the locus of points on the Smith Chart corresponding to the transformation given in section I for different values of θ. If the frequency band considered is sufficiently large, the curve will have to be continued on separate sheets). Similarly the values of Y_+/Y_0 as a function of frequency can be plotted on the Chart; a necessary condition for stability is that the two curves do not intersect. However, this condition is not sufficient, for two reasons:

1) It does not rule out the possibility of growing oscillations.
2) Because of nonlinearities, the absolute value of the real part of Y_- may range from zero to a maximum value (for example, a tunnel diode).

We can take the second factor into account by considering the locus to consist of the entire region bounded on the outside by the sum of the Chart ($|\rho|=1$), and on the inside by the locus determined from $|RlY_-|$ having its maximum value. The sufficient condition for stable amplification is then that the locus Y_+/Y_0 does not enter into this region.

The criterion conforms to the usual criteria for stable operation. First, for vanishingly-small θ it is assumed that:

$$|RlY_+| > |RlY_-| \qquad (6)$$

which is the condition for stable operation when the positive and negative conductances are located at points of equivalent electrical phase. Secondly, at any frequency, it implies that

$$|\rho_+| < \frac{1}{|\rho_-|}, \quad |\rho_+\rho_-| < 1$$

(cf. section I, Procedure, step 5) (7)

where $\rho_\pm$ are the reflection coefficients for the line terminated in $Y_\pm$. This condition[2] also insures that the Laplace transform of the current and voltage, at any point on the line, has no poles in the half-plane.

$$Rls = Rl(\sigma + j\omega) \ge 0$$

where s is the complex frequency variable.

Bernard Rosen
RCA
Surface Communication Lab.
75 Varick St.
New York, N. Y

* Received by the IRE, February 17, 1960.

[1] H. P. Smith, "Transmission line calculator," *Electronics*, pp. 29–31; January, 1939.

[2] E. Weber, "Linear Transient Analysis," John Wiley and Sons, Inc., New York, N. Y., vol. 2, pp 285–286; 1956.

Relativity: Blessing or Blindfold?*

The latest attempt to measure an ether drift (with the ammonia maser) gave the expected zero drift but with a much improved accuracy.[1] For some time the preferred interpretation of a null ether drift has been confirmation of the special theory of relativity and rejection of an ether. However, a second interpretation, based on the Fitzgerald-Lorentz contraction theory, also explains the null result but allows an ether. The special theory was originally preferred because of the *ad hoc* nature of the Fitzgerald-Lorentz theory. This *ad hoc* stigma has since been removed by Ives' classical derivation of the Lorentz transformations.[2] Furthermore, Ives has extended the Fitzgerald-Lorentz theory to explain the three famous tests of general relativity: the advance of the perihelion of Mercury[3] and the bending and frequency shift of light in a gravitational field.[4] Thus, a theoretical superiority of the relativistic interpretation is now questionable.

There is a major physical difference between the two theories: The special theory requires that the measured one-way velocity of light in a vacuum, c, be constant, while the Fitzgerald-Lorentz theory requires only that the measured average velocity of an out-and-back light signal be constant and equal to c. This difference has not yet been put to a proper test. All experiments to date, including the maser experiment,[1] give the average velocity of a two-way light signal, or the equivalent. A variation in the one-way velocity of light with direction in space (in the absence of a significant gravitational field) is *prima-facie* evidence for the existence of an ether.

Resolution of the ether problem is requisite for our efforts to fathom the hypostasis of matter and radiation. The present abundance of electrical particles has been compared to the enigmatic profusion of chemical elements before the discovery of the electron, and is considered to herald the discovery of a subelectrical form of matter. Is this subelectrical matter the constituent of a ubiquitous ether which forms an invisible sea in which the electrical particles (and radiation) exist; or is this subelectrical matter confined only to the electrical particles (and quanta)? Resolution of the ether question can be of considerable heuristic value here. Continued emphasis on the special theory detracts from the need for a crucial experiment.

Maxwell[5] was the first to propose a one-way measurement from observations of astronomical objects. Much later Bottlinger[6] suggested this as a test of relativity. Courvoisier,[7] following his suggestion, found, from the 1908–26 eclipse observations of Jovian satellites, an ecliptic component of the sun's motion through an ether of 715 ±95 km/sec directed at an angle of 132° ±6°. However, this result is not very convincing because the observed variation, which is somewhat less than the probable error in the eclipse observations, can also result from some flaw in the complicated and incomplete gravitational theory of the Jovian system.

An independent evaluation of the timing error due to the motion of the earth alone should overcome this objection of gravitational theory. In Fig. 1 the heliocentric longitudes of a planet, the earth and the light ray are respectively θ, ϕ, and ψ, with respect to the direction of the First Point of Aries, Υ. It is assumed that the component of the sun's motion through an ether in the ecliptic plane is w at angle α, $w \ll c$, and the paths of the earth and planet are coplanar.

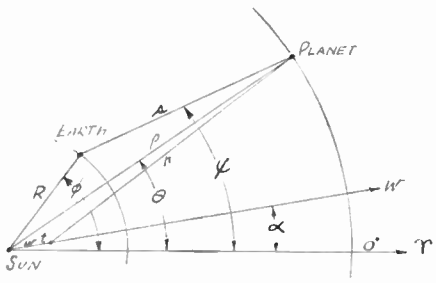

Fig. 1—Relation of sun, earth and planet.

Terms above the first order are neglected. Lorentzian variations in length, time, and mass therefore do not apply. During the time $t = \rho/c$ required for reflected light to return to the sun, the sun moves a distance wt in the ether. For a heliocentric observer, the error in determining the planet's position (calculated minus observed time) is

$$\Delta t_h = \rho/c - r/c = \rho(w/c^2)\cos(\theta - \alpha) \quad (1)$$

since, from the geometry

$$r = [(\rho\cos(\theta-\alpha) - wt)^2 + \rho^2\sin^2(\theta-\alpha)]^{1/2} \cong \rho - \rho(w/c)\cos(\theta-\alpha). \quad (2)$$

Similarly, with respect to a geocentric observer, the earth moves a distance wt in the calculated time s/c, to give a time error of

$$\Delta t_g = \pm\, s(w/c^2)\cos(\psi - \alpha) \quad (3)$$

where the plus and minus signs apply for outer and inner planets respectively. The two timing errors, (1) and (3), differ because the positions of the earth and sun do not coincide. The difference, which is the timing error due to the path of the earth, is

$$\Delta t_e \equiv \Delta t_g - \Delta t_h = -R(w/c^2)\cos(\phi - \alpha) \quad (4)$$

since $R\cos(\phi-\alpha) \pm s\cos(\psi-\alpha) = \rho\cos(\theta-\alpha)$, where the plus and minus signs apply as above. The result is independent of the observed object provided the object is not an earth satellite.

The timing error Δt_e should exist simultaneously with Δt_h and Δt_g in the residuals from calculated and observed times of astronomical observations. The relative error $\Delta t_e/R$ should then be equal in amplitude and opposite in phase to $\Delta t_h/\rho$ and for outer planets $\Delta t_g/s$. It would be difficult to explain how classical gravitational theory, *without specifying an anisotropy of space*, could introduce into two unrelated motions, such as those of the earth and a planet, a common periodic error referenced to some arbitrary direction in space. Courvoisier approximated the heliocentric error (1), but did not evaluate the independent timing error due to the earth. Analysis of a sufficient number of residuals of past astronomical observations with modern computers should permit an unambiguous check for a variation in the one-way velocity of light.

Because of the paucity of suitable astronomical objects substantially outside the ecliptic plane, past observations can only yield the ecliptic component of the sun's motion through an ether. Hence, experiments with artificial satellites are desirable to explore the direction normal to the ecliptic plane. For an earth satellite, the derivation of the timing error is the same as for (1). This may be rewritten for a satellite as

$$\Delta t_s = S(v/c^2)\cos\gamma \quad (5)$$

where S is the distance between observer and satellite, v is the velocity of the observer through the ether, and γ is the angle between S and v. A stable oscillator in a satellite may be used to seek this timing error. In any transmission between satellite and earth, the time Δt_s introduces a variable advance or delay which appears to the observer as a phase-modulated signal. The phase advance in cycles due to the time variation is $f\Delta t_s$ where f is the oscillator frequency. The time derivative of this gives the corresponding frequency shift. Substituting (5), differentiating, and solving for the relative frequency shift results in

$$\frac{\Delta f}{f} = \frac{v}{c^2}\left[(dS/dt)\cos\gamma - S(d\gamma/dt)\sin\gamma\right]. \quad (6)$$

The maximum values of dS/dt and $Sd\gamma/dt$ are of the order of the satellite's orbital velocity. Optimum sensitivities are thus obtained with low-altitude satellites and the expression in the brackets then has a maximum value of the order of 10 km/sec. Satellite transmission frequencies have been measured[8] to 1 part in 10^8, and should therefore permit the detection of an ether drift of the order of 100 km/sec. However, the frequency shift in (6) must compete with the Doppler shift and other sources of frequency variation, such as drift. Since the Doppler shift is of the order of the orbital velocity divided by c for most of the path of a low-altitude satellite, the maximum shift in (6) is v/c times smaller. Nevertheless, re-examination of a sufficiently

* Received by the IRE, March 17, 1960.

[1] J. P. Cedarholm and C. H. Townes, "A new experimental test of special relativity," *Nature*, vol. 184, pp. 1350–1351; October 31, 1959.

[2] H. E. Ives, "Derivation of the Lorentz transformations," *Phil. Mag.*, vol. 36, pp. 392–403; June, 1945.

[3] H. E. Ives, "The behavior of an interferometer in a gravitational field, II. Application to a planetary orbit," *J. Opt. Soc. Am.*, vol. 38, pp. 413–416; April, 1948.

[4] H. E. Ives, "The behavior of an interferometer in a gravitational field," *J. Opt. Soc. Am.*, vol. 29, pp. 183–187; May, 1939.

[5] J. C. Maxwell, "Ether," *Enc. Brit.*, 9th ed., vol. 8; 1878.
W. D. Niven, Ed., "The Scientific Papers of James Clerk Maxwell," Dover Publications, Inc., New York, N. Y., vol. 2, p. 763; 1890.
Anonymous, "Clerk Maxwell and the Michelson experiment," *Nature*, vol. 125, p. 566; April, 1930.

[6] K. F. Bottlinger, "Über eine astronomische Prüfungsmöglichkeit des Relativitätsprinzips," *Astronomische Nachrichten*, Band 211, No. 5051, columns 239–240; 1920.

[7] L. Courvoisier, "Ableitung der 'absoluten' Erdbewegung aus beobachteten Längen der Jupiter-Satelliten," *Astronomische Nachrichten*, band 239, nr. 5715, columns 33–38; 1930.

[8] M. Bernstein, G. H. Gougoulis, O. P. Layden, W. T. Scott, and H. D. Tanzman, "Satellite Doppler measurements," PROC. IRE, vol. 46, pp. 782–783; April, 1958.

large body of existing data may permit detection of an ether drift, or the establishment of an upper limit for one.

Use of an atomic clock should improve accuracy by increasing frequency resolution and oscillator stability. The improvement may be sufficient to give significant results with widely separated earth-bound clocks by simultaneous frequency measurements of the same radio transmission. Such comparisons are now being made in this country and in England for other purposes.[9]

A direct measurement of a variation in transmission time, such as the timing error in (5), may be made as suggested elsewhere[10] by precisely keying an oscillator in time. Measurement of the keyed periods by the observer is independent of frequency variations due to Doppler shift, drift, or other causes. With an atomic clock having a stability of 1 part in 10^{10} per day, a total variation in the keyed periods of ± 8.64 μs per day is detectable. A satellite with a period of one day hovers at an altitude of about 36,000 km. For an observer directly underneath, the minimum detectable ether drift in the plane of the satellite's orbit is, from (5), 21.6 km/sec. Sensitivity may be increased by increasing the satellite's distance provided the clock stability can be maintained over the longer orbital period. The ecliptic component timing error may be differentiated from the parameters of the satellite's orbit because the component's phase varies 360° per year. A more direct comparison is obtained by simultaneously measuring the satellite's distance S with an out-and-back radio signal by using the satellite as a beacon.

Regardless of the question of an ether, it is of scientific interest to measure the one-way velocity of light with at least the same precision as the measured average of a two-way signal. The apparent neglect of the one-way measurement, despite the means at hand and the current preparations for related experiments which are more elaborate and advanced, attests to the almost universal, but premature, acceptance of the second postulate of the special theory of relativity.

MARTIN RUDERFER
Dimensions, Inc.
Brooklyn 4, N. Y.

[9] L. V. Essen, J. V. L. Parry, and J. A. Pierce, "Comparison of caesium resonators by transatlantic radio transmission," *Nature*, vol. 180, pp. 526–528; September 14, 1957.
[10] J. T. Anderson, "Determination of the orbit of an artificial satellite," PROC. IRE, vol. 47, pp. 1658–1659; September, 1959.

Microwave Detection and Harmonic Generation by Langmuir-Type Probes in Plasmas*

The demodulation of microwave signals ($f \sim 10{,}000$ mc), when they are impressed upon a Langmuir-type metallic probe in contact with an ionized gaseous medium, has been examined. The plasma was that which forms in the negative glow region of a cold-cathode dc discharge established in helium or neon at pressures ~1–10 mm Hg. The metallic probe was generally a 0.5-cm length of 1.0-mil tungsten wire and was the extension of the center conductor of a coaxial microwave cable (TEM mode). A change in the "continuous" probe current, as the amplitude of the microwave electric potential varied, indicated demodulation.

The nonlinear volt-ampere characteristic of a probe immersed in a plasma is well known and would predict a rectification effect for alternating voltages similar to that observed for the point contact semiconductor diode. This effect has been proposed since at least 1916[1] for the demodulation of low-frequency electrical waves. The present interest stems from recent measurements[2] of the electron temperature in the negative glow plasma established in helium, which indicates quite a low temperature, ~400°K, approaching that of the gas, 300°K. A low effective temperature for the charge carriers (for our case electrons) will lead to a sharp "knee" in the volt-ampere characteristics of the metallic probe. This effect is clearly shown in Fig. 1. Here, the oscilloscopic presentation of probe current, while the probe voltage is swept at a low audio rate, is compared with the current flowing in a conventional 1N23B crystal diode treated in similar fashion. Note that both curves have sharp and similar knees which would predict equivalent sensitivity for demodulation of radio-frequency waves, provided that each curve retained its shape and significance at the higher frequencies.

In one of several arrangements it was possible to impress a pulsed microwave signal (9375 mc with 4-μsec pulse duration) alternately on the metallic probe or on the plasma medium surrounding the probe. Fig. 2 shows the resulting demodulated pulses. The crystal detected pulse is displayed in Fig. 2(c) for purposes of comparison. Fig. 2(a), with microwave energy present only in the plasma, shows a relatively slow response with time constant ~ one microsecond. The essential details of this response may be explained by an alteration of the temperature of the plasma electrons while absorbing microwave energy,[3] and an accompanying change in plasma space potential. When the microwave is impressed on the probe an additional response is noted in Fig. 2(b) at the time of application and removal of the pulse. The rapidity of this response is limited only by the oscilloscope and circuitry.

Of particular interest is the sensitivity of the gaseous discharge detector in comparison with a conventional 1N23B crystal diode. When both types of detectors were tuned for optimum output in equivalent mounts and for incident microwave power

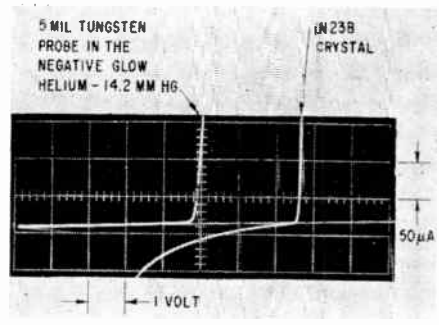

Fig. 1—Comparison of metallic probe and semiconductor diode volt-ampere characteristics with voltage swept at a low audio frequency.

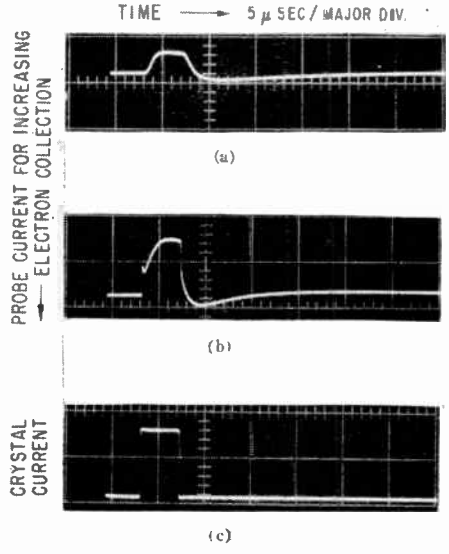

Fig. 2—Video response of Langmuir-type probes immersed in a negative glow plasma established in helium at a pressure of 5 mm Hg.

≈0.1 milliwatt, the crystal detector required approximately 3 db less power for equal response. The minimum detectable signal or noise level of the discharge detector was not examined in these tests. When the cold-cathode discharge plasma was established in neon instead of helium, the discharge detector was approximately 13 db inferior to the crystal.

The magnitude of the fast response, described above, was examined as a function of the incident microwave power. In all cases, the response of the discharge detector for low microwave powers, ≥ 10 mw, followed closely the square law expected from a semiconductor diode.

The above effects suggest a form of rectification between the metallic probe and the plasma wherein the nonlinearity of the device is active for each cycle of alternation of the incident microwave. The generation of waves harmonic in frequency to the incident microwave is immediately suggested. In an appropriately arranged K-band crystal detector mount tuned to 18,750 mc, an almost square pulse of microwave energy having rapid rise and fall was detected, which coincided in time with an incident microwave pulse at 9375 mc to the discharge detector. However, this frequency multiplier was found inferior to a semiconductor diode, 1N23B, by about 16 db in the ability to generate second harmonic energy. A neon-

* Received by the IRE March 30, 1960.

[1] P. C. Hewitt, "Method of, and Apparatus for, Translating Electrical Variations," U. S. Pat. No. 1,144,596; June 29, 1915.
[2] J. M. Anderson, "Ultimate and secondary electron energies with a negative glow of a cold-cathode discharge in helium," to be published in the *J. Appl. Phys.*; March, 1960.
[3] J. M. Anderson and L. Goldstein, "Interaction of electromagnetic waves of radio-frequency in isothermal plasmas," *Phys. Rev.*, vol. 100, pp. 1037–1046; November, 1960.

filled discharge detector was 17 db inferior to the crystal under similar circumstances. In these second-harmonic measurements, circumstances occasioned a hollow-cathode type of discharge as the only form employed. Later, electrons in this discharge type were found to have a characteristically high temperature, ~1000°K. Most probably, a discharge detector having a plane cathode, as used in the work associated with Figs. 1 and 2, would show a greater efficiency for harmonic generation, but such was not reexamined.

It may be mentioned that a portion of the experimental results reported by M. Uenohara, *et al.*,[4] and by J. R. Baird and P. D. Coleman[5] might possibly be explained on the basis of that given for the above experiments, since metallic electrodes were present in their discharge tubes. However, the above described detector is presumably dissimilar to one of current interest described by Udelson and by Gould,[6] wherein the dc discharge current sustaining the cold-cathode discharge is altered when microwave energy is incident on one or more plasma regions of the discharge.

J. M. Anderson
General Electric Res. Lab.
P. O. Box, 1088
Schenectady, N. Y.

[4] M. Uenohara, M. Uenohara, T. Masutani, and K. Inada, "A new high-power frequency multiplier," Proc. IRE, vol. 45, pp. 1419–1420; October, 1957.
[5] J. R. Baird and P. D. Coleman, "Millimeter waves," Polytechnic Institute of Brooklyn, N. Y., Microwave Res. Inst., *Symposia Series*, vol. 9, pp. 289–300; March, 1959.
[6] B. J. Udelson, "Effect of microwave signals incident upon different regions of a dc hydrogen glow discharge," *J. Appl. Phys.*, vol. 28, pp. 380–381; March, 1959. L. Gould, U. S. Army Signal Corps, Engrg. Labs., Fort Monmouth, N. J., Signal Corps Task No. 3238, Tech. Memo No. M-1836; October 31, 1956.

A New Use of the Junction Transistor as a Pulse-Width Modulator*

Price's paper[1] reports that transistors can be used as a pulse-width modulator in a saturation region, utilizing the minority carrier storage effect. That technique is described with a "selected point-contact transistor" whose current gain, alpha, is larger than five. The collector potential is modulated, using a common base configuration.

This paper describes a new method of pulse-width modulation which modulates the base pulse current in a common emitter configuration. This new method is more suited to junction transistors. It is expected, therefore, that a more applicable and practical method of modulation with good linearity and effectiveness will be obtained.

If enough input pulse current is supplied to saturate the transistor, each output pulse maintains a constant amplitude during the storage time, due to the fact that the collector load resistance and collector bias supply voltage are fixed.

When the input current is modulated by audio frequencies at the base of the transistor in saturation region, only the width of output pulses varies in accordance with the input modulation signal. Thus the pulse amplitude modulation at the input is transformed to the pulse-width (or phase) modulation at the output automatically.

A simplified circuit for this method is shown in Fig. 1. The modulated input and output voltage waveforms are shown in Fig. 2, where the pulse-width is 10 microseconds, repetition frequency is 10 kilocycles, R_C is 4.7 kilohms and E_C is 6 volts. In Fig. 3, the demodulated sine wave with a frequency of 100 cycles is illustrated. The distortion factor of the wave is about 5.5 per cent. Using a proper circuit, it was found that, according to the oscillographic observation, the distortion factor of the sine waves up to 10 kilocycles is almost the same as that of the wave at 100 cycles.

Triggering a flip-flop by the differentiated impulse of the output modulated pulse, as shown in Fig. 4, the distortion factor of the system will become less than 5 per cent.

This method also serves as a simple pulse-delaying circuit adaptable to various pulse and logic circuits.

Plans are being made for estimating the signal-to-noise ratio and limit of modulation factor at any given circuit and frequency conditions.

The author is grateful to Dr. H. Kuroda and Dr. T. Nakano for their valuable discussions.

I. Tagoshima
Tech. Res. Lab.
Japan Broadcasting Corp.
Kinuta, Setegaya, Tokyo, Japan

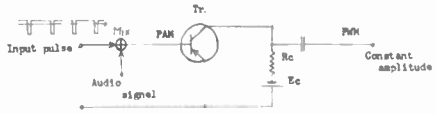

Fig. 1—Simplified PWM circuit.

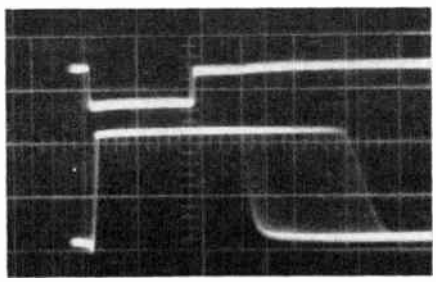

Fig. 2—Modulated pulse waves. Input voltage, PAM (upper) and output voltage, PWM (lower) of this method, using a low frequency junction transistor. Input alloy width is 00 μsec.

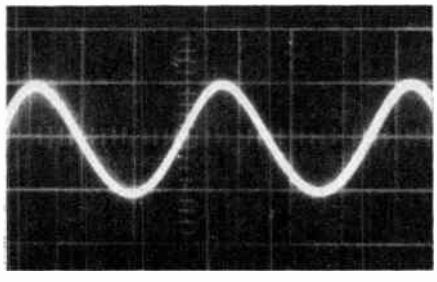

Fig. 3—Demodulated sine wave (100 cycles).

Fig. 4—Block diagram of a pulse readjusting circuit.

* Received by the IRE, March 28, 1960.
[1] J. C. Price, "A conductivity storage transistor pulse width modulator," *Elec. Engrg.*, vol. 30, pp. 88–90; February, 1958.

On the Uniqueness Theorem for Electromagnetic Fields*

The following proof of the uniqueness theorem of the solution of boundary value problems in electromagnetic field theory will be based on the general ideas of uniqueness theorem proof given by Stratton.[1] However, this proof will be original in a way, as it will consider also the case of resonant modes and mixed boundary conditions in the steady-state case, which were not considered by Stratton.

Let V be a region of space bounded by a closed surface S. It will be assumed that V is an isotropic medium with the scalar paramaters μ, ϵ, σ as arbitrary functions of position. Let $(\overline{E}_1; \overline{H}_1)$ and $(\overline{E}_2; \overline{H}_2)$ be two solutions of the field equations with harmonic time variation $e^{-i\omega t}$. Assuming linearity of the field equations, the difference field $\overline{E}=\overline{E}_1-\overline{E}_2$ and $\overline{H}=\overline{H}_1-\overline{H}_2$ is also a solution of the boundary value problem. Let us assume that the sources lie entirely outside the region V.

From Maxwell's equations with harmonic time variation one can get the following relation for the complex Poynting vector:[1]

$$\nabla\cdot(\overline{E}\times\overline{H}^*) = -\sigma\overline{E}\cdot\overline{E}^* + i2\omega\left(\frac{\mu}{2}\overline{H}\cdot\overline{H}^* - \frac{\epsilon}{2}\overline{E}\cdot\overline{E}^*\right). \quad (1)$$

Taking the volume integral on both sides of (1), and separating into real and imaginary pairs we get:

$$\mathrm{Re}\oiint_S(\overline{E}\times\overline{H}^*)\cdot\bar{n}dS = -\int_V\sigma E^2dV \quad (2a)$$

$$\mathrm{Im}\oiint_S(\overline{E}\times\overline{H}^*)\cdot\bar{n}dS = 2\omega\int_V\left(\frac{\mu}{2}H^2-\frac{\epsilon}{2}E^2\right)dV. \quad (2b)$$

If we prescribe $\bar{n}\times\overline{E}_1=\bar{n}\times\overline{E}_2$ *or* $\bar{n}\times\overline{H}_1=\bar{n}\times\overline{H}_2$ on the surface S, the left-hand side integrals in (2) will vanish since

$$(\overline{E}\times\overline{H}^*)\cdot\bar{n} = (\bar{n}\times\overline{E})\cdot\overline{H}^* = -(\bar{n}\times\overline{H}^*)\cdot\overline{E}, \quad (3)$$

* Received by the IRE, March 7, 1960.
[1] J. A. Stratton, "Electromagnetic Theory," McGraw-Hill Book Co., Inc., New York, N. Y., pp. 137, 486–488; 1941.

and $\overline{E}=\overline{E}_1-\overline{E}_2$, and $\overline{H}=\overline{H}_1-\overline{H}_2$. The integrals on the left-hand side of (2) will also vanish in the mixed boundary conditions case in which $\bar{n}\times\overline{E}_1=\bar{n}\times\overline{E}_2$ is prescribed over *part* of the closed surface S and $\bar{n}\times\overline{H}_1=\bar{n}\times\overline{H}_2$ is prescribed over the *rest* of the surface S. Therefore (2) will become

$$\int_V \sigma E^2 dV = 0, \tag{4a}$$

$$\int_V \frac{\mu}{2} H^2 dV = \int_V \frac{\epsilon}{2} E^2 dV. \tag{4b}$$

We must distinguish between two different cases in (4). a) $\sigma\neq 0$. The medium has losses. In this case we see from (4a) that since $\sigma>0$, we will have to have throughout the volume V, $\overline{E}=\overline{E}_1-\overline{E}_2=0$. Using this in (4b) we also get $\overline{H}=\overline{H}_1-\overline{H}_2=0$ throughout the volume V. Therefore, in those cases the two solutions will be identical. b) $\sigma=0$. The medium does not have any losses. In this case (4a) becomes an identity and only (4b) is left. From this equation we see that the differences $\overline{E}_1=\overline{E}_1-\overline{E}_2$ and $\overline{H}=\overline{H}_1-\overline{H}_2$ do not have to be identically zero throughout the volume V. The only requirement in (4b) by itself is that the total average electric energy of the difference field will be equal to the total average magnetic energy of the difference field; in other words it is required that the difference electromagnetic field between the two solutions will be a resonant mode. Only in cases where we do not have any resonant modes will we get a unique solution. One such case is the case of an unbounded region with radiation conditions prescribed at infinity.[2]

Let us summarize the uniqueness theorem:

> A harmonic time-varying electromagnetic field is uniquely determined within a *lossy* bounded region V, by prescribing *one* of the following on the surrounding surface S:
>
> 1) the tangential component of the electric vector.
> 2) the tangential component of the magnetic vector,
> 3) the tangential component of the electric vector over part of the surface S, and the tangential component of the magnetic vector over the rest of the surface S.

In case of a *lossless* bounded region V, the electromagnetic field will *not* be uniquely determined by the above, since by adding any number of resonant modes to a solution, a new solution will be found.

In case of an *unbounded* region V, with radiation conditions at infinity, any one of the above will determine a unique solution.

H. Unz
Elect. Engrg. Dept.
University of Kansas
Lawrence, Kans.

[2] W. K. Saunders, *Proc. Natl. Acad. Sciences*, vol. 38, pp. 342–348; April, 1952.

J-Band Strip-Line *Y* Circulator*

A strip-line Y circulator has been realized with successful results in the L-band case.[1,2]

The lower the operating frequency of the circulator is, the more difficult the realization of the circulator becomes, because of the lowering of the figure of merit which comes from the characteristics of both polycrystalline YIG and the strip-line. The triplate strip-line Y circulators in the lower bands of the UHF region have been tested in order to find out their practical lowest operating frequency, and good results have been obtained even in the J-band (from 350 mc to 530 mc), which is reported later in this letter. It has also been ascertained that the practical lowest limit of the operating frequency of the circulator is expected to be at some frequency band in the VHF region.

According to the experimental results of the circulator made up for the several bands in the UHF region, the figures of merit (the backward transmission loss in decibels upon the forward transmission loss in decibels), the necessary applied magnetic fields by Alnico magnets, and the sizes of the devices (in which three type n connectors, three coaxial line-strip line junctions, three Alnico magnets, and two adjustable pole pieces are included), are given in Fig. 1 against the operating free-space wavelength respectively. In the case of the circulator made up to 360-mc use in the J-band they are about 100, about 1250 oersteds, $6\frac{3}{4}$ inches in diameter (2 inches in height), respectively.

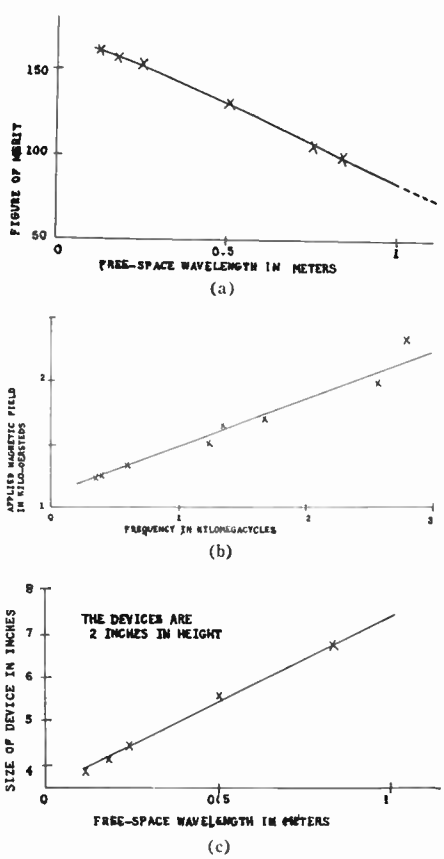

Fig. 1.

When a wave of frequency 360 mc enters, for example, through arm 1 from a matched generator, it comes out from arms 2 and 3 terminated by matched detectors. Transmission losses are shown against the applied dc magnetic field in Fig. 2. When the external dc magnetic field corresponding to point A (about 1250 oersteds) in this figure is applied, the clockwise circulator is completed in this case. In practice, three Alnico magnets, having a magnetic field corresponding to the point A, are set to the strip-line Y junction. The frequency characteristics of the circulator are shown in Fig. 3.

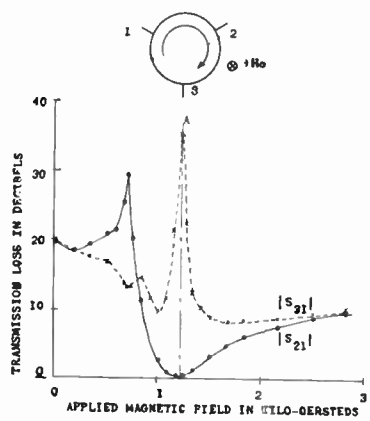

Fig. 2.

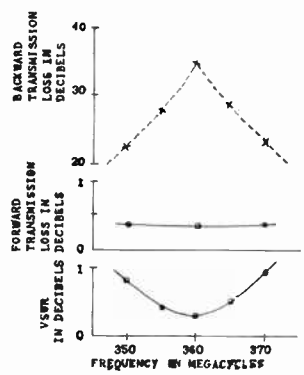

Fig. 3.

These data are obtained for the circulator with type n coaxial connectors. Typical performance is within 0.4-db insertion loss over 20-db isolation with VSWR less than 1 db over 7 per cent bandwidth of the center frequency in J-band, and is 0.3$_5$ to 34.8 db with VSWR 0.3 db at the center of the band. We can expect to get better characteristics when the strip-line circulator is used without the coaxial connectors and the coaxial strip-line junctions. The same type of circulator can be made in the case of the other types of strip-line. Also, a microwave switch can be easily made by the modulation of the external magnetic field.

S. Yoshida
Matsuda Res. Lab.
Tokyo Shibaura Electric Co., Ltd.
Kawasaki, Kanagawa, Japan

* Received by the IRE, March 29, 1960.

[1] L. Davis, Jr., U. Milano, and J. Saunders, "A strip-line L-band compact circulator," PROC. IRE, vol. 48, pp. 115–116; January, 1960.

[2] S. Yoshida, "Strip-line Y circulator," PROC. IRE, vol. 48, pp. 1337–1338; July, 1960.

Interaction of Two Microwave Signals in a Ferroelectric Material*

A conventional degenerate mode parametric amplifier was used as a research tool to study the ferroelectric interaction with two microwave signals. Certain interesting results were obtained, namely, that there was an exchange of energy from the pump frequency to the signal frequency in the ferroelectric material via an idler frequency. Results are shown in Table I.

There was too much loss in the system at 1200 mc and 820 mc to obtain any gain; in fact, the insertion loss of the microwave circuit with material used was 7.5 db. Removing the pump frequency removes the idler and also lowers the amplitude of the signal frequency. The operation is very similar to a parametric amplifier with a low-cutoff frequency or lossy varactor.

TABLE I

f_s	f_p	Relative Amplitude of the Idler to the Signal Frequency	Pump Power
2600 mc	5200 mc	−31 db	1 watt
1200 mc	2400 mc	−6 db	120 mw
820 mc	1640 mc	−6 db	150 mw

The ferroelectric material was Barium Titanate of the polycrystalline type, Aerovox Body 90, operating at room temperature below its Curie point. A small chip, 0.005 inch thickness and 0.010 inch on a side, was used in a modified microwave crystal holder. The capacity of the sample was 2.2 $\mu\mu$f.

It does appear that the permittivity of the material can be varied at a microwave frequency rate; hence, the material becomes a variable capacity, thus making possible the basic element for a ferroelectric parametric amplifier.

The author wishes to acknowledge the stimulating discussions with Dr. H. Diamond and T. H. Butler of the University of Michigan.

IRVING GOLDSTEIN, MANAGER
Solid-State Physics Branch
Raytheon Missile Systems Div.
Bedford, Mass

* Received by the IRE, April 11, 1960.

Contributors

Bruce B. Barrow (S'52–M'56–SM'59) was born on April 12, 1929, in Danville, Pa. He attended the Carnegie Institute of Technology, Pittsburgh, Pa., on a George Westinghouse Scholarship, and received the B.S.E.E. and M.S.E.E. degrees in 1950. He was awarded a Tau Beta Pi Fellowship for graduate study at the Massachusetts Institute of Technology, Cambridge, where he also taught in the Department of Electrical Engineering and worked on the staff of the Servomechanisms Laboratory. During this time, he was awarded a Fulbright Scholarship for a year of study at the Delft Institute of Technology in The Netherlands. In his last years at M.I.T. he worked in the Nuclear Instrumentation Group under the direction of Prof. T. S. Gray, and in 1955 he received the E.E. degree. His thesis was concerned with nuclear reactor instrumentation, and he has consulted for the General Electric Company in this field.

B. B. BARROW

In 1955, he joined Hermes Electronics Co., Cambridge, Mass., where he worked mainly on problems concerned with various communications systems, including the ACE High network now being constructed in Europe for SHAPE. Since 1958, he has been on leave with the SHAPE Air Defense Technical Center, The Hague, where he is studying improved methods of transmitting digital data over fading radio paths.

Mr. Barrow is a member of the Nederlands Radiogenootschap, Sigma Xi, and Tau Beta Pi.

Robert L. Carbrey (M'45) was born in Denver, Colo., on April 23, 1917. He received the B.S.E.E. degree with honors from the University of Colorado, Boulder, in 1940.

R. L. CARBREY

He joined the Bell Telephone Laboratories' outside plant department in 1940, where he engaged in work on coaxial and toll telephone cables. During World War II, he transferred to the radio research department where he worked on radar and pulse position modulation receivers, as well as single-sideband receivers. Since his transfer to the transmission research department at Murray Hill, N. J., in 1944, he has been engaged in work on a variety of pulse code modulation terminals and repeaters, except for an interval, during which time he worked on the design of time separation multiplexed speech interpolation systems.

Mr. Carbrey is a member of Tau Beta Pi and Eta Kappa Nu.

❖

Martin L. Cohen (M'60) was born in New York, N. Y., on May 20, 1929. He received the B.E.E. degree from Cornell University, Ithaca, N. Y., in 1952.

From 1952 to 1956, he worked for Raytheon Manufacturing Company, Newton, Mass., on the development of nonmicrophonic vacuum tubes and test equipment for microwave tubes. Before joining Arthur D. Little, Inc., Cambridge, Mass., in 1957 as a member of the Advanced Research Division, he studied applied mathematics and switching theory at Harvard University, Cambridge. His work at Arthur D. Little has been in the experimental development of superconductive computer elements, which has included research with the wire-wound cryotron and on the properties of vacuum-deposited superconductive films

M. L. COHEN

❖

Sid Deutsch (A'46–M'55) was born in New York, N. Y., on September 19, 1918. He received the B.E.E. degree in 1941 from Cooper Union, New York, N. Y., and the M.E.E. and D.E.E. degrees in 1947 and 1955 from the Polytechnic Institute of Brooklyn, Brooklyn, N. Y.

S. DEUTSCH

From 1935 to 1944, he was an electric motor technician and designer of electromechanical equipment and then served with the U. S. Navy until 1946. He was an electronics engineer from 1950 to 1954 at the Polytechnic Research and Development Company, Brooklyn, N. Y., and then joined

the Microwave Research Institute of the Polytechnic Institute of Brooklyn. At present, he is a consultant for the Budd Lewyt Electronics Company, Long Island City, N. Y.

Since 1943, he has also been teaching. He was a physics instructor at Hunter College, New York, N. Y. during 1943–1944, and was a radio and television instructor from 1946 to 1950. He taught at the College of the City of New York from 1955 to 1957, and since 1951 he has also taught at the Polytechnic Institute of Brooklyn, Brooklyn, N. Y., where he is now an associate professor of electrical engineering.

Dr. Deutsch is a member of Sigma Xi, Tau Beta Pi, and Eta Kappa Nu.

❖

A. Francis Dietrich was born in New York, N. Y., on November 24, 1909.

He joined the Bell Telephone Laboratories at Deal, N. J., in 1942. During 1942–1943, he worked on high-power radar transmitters. Since then, he has been engaged in experimental studies of broad-band microwave systems and terminal equipment. During the past ten years, he has specialized in high-speed millimicrosecond pulse techniques, including time separation return loss measuring sets and error-counting equipment for evaluating the performance of PCM microwave regenerative repeaters in the hundred-megabit range.

A. F. DIETRICH

❖

William M. Goodall (A'29–M'37–SM'43–F'51) was born on September 7, 1907 in Washington, D. C. He received the B.Sc. degree from the California Institute of Technology, Pasadena, in 1928. He joined the technical staff of the Bell Telephone Laboratories in 1928. He was located at Deal, N. J. until 1951, when he was transferred to Holmdel.

W. M. GOODALL

His early work included scale-model antenna studies of long-wave antennas, experimental ionosphere studies, and early radio-relay studies. During World War II, he worked on high-power pulse modulators for radar and PPM.

Later work included experimental PCM and broad-band microwave FM terminals, experimental studies of broad-band microwave PAM systems and broad-band microwave regenerative repeaters. More recently, he has been engaged in the field of high-speed short pulses including high resolution electrical stroboscopes.

Jack C. Greene was born in New York, N. Y., on May 11, 1928. He received the B.E.E. and M.E.E. degrees in 1947 and 1950, respectively, from the Polytechnic Institute of Brooklyn, Brooklyn, N. Y.

J. C. GREENE

From 1947 to 1948, he designed digital computers and magnetic data-storage devices for the Teleregister Corporation, New York, N. Y. In 1948, he joined Airborne Instruments Laboratory, Melville, N. Y., where he performed research and development work on microwave countermeasure receivers, display and data handling devices, and novel uses of traveling-wave tubes until 1953. From 1953 to 1955, he served in the U. S. Army Signal Corps, where he was assigned to the Countermeasures Division of Evans Signal Laboratory, Belmar, N. J. In 1955, he rejoined Airborne Instruments Laboratory, and is presently a section head in the Department of Applied Electronics. He is currently concerned with radio astronomy receiver design, the development of solid-state devices for receiving systems, and theoretical studies in the countermeasures and low-noise receiving systems fields.

Mr. Greene is a member of Tau Beta Pi and Eta Kappa Nu.

❖

Ralph E. Hiatt (M'47–SM'58) was born on April 12, 1910 in Portland, Ind. He received the B.A. degree in physics from Indiana Central College, Indianapolis, in 1932 and the M.A. degree in physics from Indiana University, Bloomington, in 1939. He later took several graduate courses in mathematics at Boston University, Boston, Mass. He taught mathematics and science in Indiana public schools until 1942. From 1942 until 1945 he was employed by the Radiation Laboratory of Massachusetts Institute of Technology, Cambridge. As a staff member in the Radiation Laboratory Antenna Group, he worked on microwave radar antennas; he organized the Ipswich Antenna Test Station and was Chief of this installation in 1944 and 1945.

R. E. HIATT

He joined the Air Force Cambridge Research Center in 1945 and was Chief of the Ground Antenna Section until 1956. From 1956 until 1958, he was Chief of the Antenna Laboratory (later the Electromagnetic Radiation Laboratory).

In 1958, he joined the Radiation Laboratory of The University of Michigan, Ann Arbor, as associate head of the laboratory. He organized and now heads an experimental group in the Radiation Laboratory. He is currently engaged in work on radar scattering, in antenna research, and in experimental plasma studies.

Mr. Hiatt is a member of the American Physical Society and of Sigma Xi.

❖

William M. Kaufman (S'53–A'54–M'59) was born in Pittsburgh, Pa., on Dec. 31, 1931. He received the B.S.E.E. and M.S.E.E. degrees from Carnegie Institute of Technology, Pittsburgh, in 1953, and the Ph.D. degree in electrical engineering from the same institution in 1955.

W. M. KAUFMAN

In 1955 he joined the Semiconductor Department of the Westinghouse Electric Corporation, Youngwood, Pa., where he was engaged in performance evaluation and electrical ratings of semiconductor devices. Since 1957 he has been with the Westinghouse Research Laboratories, Pittsburgh, investigating digital system design and switching circuits. From 1956 through 1959, he was also a part-time faculty member of Carnegie Institute of Technology. He is currently a supervisory engineer responsible for studies in distributed circuitry and molecular electronics.

Dr. Kaufman is a member of Tau Beta Pi, Eta Kappa Nu, and Phi Kappa Phi, and an associate member of the AIEE. He has five patents pending in the fields of digital circuits and distributed circuitry.

❖

Norman H. Meyers (S'54–SM'59) was born in Buffalo, N. Y., on February 11, 1931. He received the B.E.E. degree from Rensselaer Polytechnic Institute, Troy, N. Y., in 1952; and the M.S. and D.Sc. degrees, also in electrical engineering, in 1954 and 1957, respectively, from the Massachusetts Institute of Technology, Cambridge.

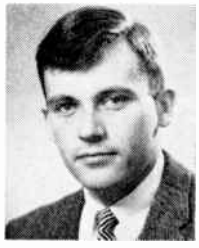

N. H. MEYERS

He remained at M.I.T. as an assistant professor of electrical engineering, from June, 1957 to June, 1958, during which time he also did research in the classical electrodynamics of moving media. Since that time, he has been on the staff of the research laboratory of the International Business Machines Corporation, in Poughkeepsie, N.Y. At IBM, he has been engaged in research and development of high-speed thin-film superconducting circuitry.

Dr. Meyers is a member of Tau Beta Pi, Eta Kappa Nu, Sigma Xi, and the Scientific Research Society of America.

Eugene W. Sard (A'49–M'55) was born in Brooklyn, New York, on December 21, 1923. He received the B.S.E.E. and M.S.E.E. degrees in 1944 and 1948, respectively, from the Massachusetts Institute of Technology, Cambridge.

E. W. Sard

From 1944 to 1946, he served in the USNR as a radar officer. From 1946 to 1948, he was a research assistant in the Center of Analysis and the Servomechanisms Laboratory of M.I.T., working on digital computers. Since 1948, he has been with Airborne Instruments Laboratory, Melville, N. Y., working at first in the Radar Department and more recently in the Applied Electronics Department, where he serves as a department consultant. For the past three years he has been working on the application of semiconductor diodes to various fields including fast switching, harmonic and subharmonic generation, and low-noise amplification. In the course of this work, he has made some fundamental theoretical contributions to the state of the art in these fields. Most recently he has been concerned with the analysis and implementation of tunnel diode amplifiers with very large bandwidths.

Mr. Sard is a member of Sigma Xi.

❖

Keeve M. Siegel (SM'57) was born in New York, N. Y. on January 9, 1923. He received the B.S. and M.S. degrees in physics from Rensselaer Polytechnic Institute, Troy, N. Y. in 1948 and 1950.

K. M. Siegel

He has been with The University of Michigan, Ann Arbor, since 1948, first as a research associate, then as a research engineer. He became head of the Upper Atmosphere Physics Section in 1949 and head of the Theory and Analysis Department in 1952. In 1957 he became head of the Radiation Laboratory. In 1957 he was appointed professor of Electrical Engineering. His work at The University of Michigan has been in the fields of electromagnetic theory (*e.g.*, scattering and diffraction), high-altitude research and work in thermodynamics and hydrodynamics (*e.g.*, incompressible ideal subsonic flow), and passage of plane waves of sound in air.

Professor Siegel is a member of the American Physical Society, American Institute of Physics, American Mathematical Society, and Sigma Xi. He is an Associate Fellow of the Institute of Aeronautical Sciences, a member of the USAF Scientific Advisory Board, and consultant to the Advanced Research Projects Agency and several major corporations. He is a member of the Editorial Boards of the *Journal of Research of the National Bureau of Standards* and the *Journal of Mathematical Physics*. He is a member of Commission VI of URSI. He is listed in *Who's Who in America*, *American Men of Science*, *Who's Who in World Aviation*, and *World Directory of Mathematicians*.

❖

Albert E. Slade was born in San Antonio, Tex., on September 14, 1923. He received the B.S. degree from the University of Maryland, College Park, in 1950, and then joined the National Security Agency, Washington, D. C., where he did research primarily in transistor circuits.

A. E. Slade

He joined Arthur D. Little, Inc., Cambridge, Mass., in 1956 as head of the Cryotron Research Program. His work at Arthur D. Little has been on research and development of superconductive computer components including vacuum evaporation of superconducting metals, design of circuits, and evaluation of devices.

❖

C. Russell Smallman was born in Quincy, Mass., on May 23, 1925. He received the B.S. degree in chemical engineering from Northeastern University, Boston, Mass., in 1947.

In 1947, he joined the staff of Arthur D. Little, Inc., Cambridge, Mass., where he has been active in infrared spectroscopic instrumentation and in electronic and electromechanical device development for meteorological research.

He has been associated with the cryotron project since its inception in 1955 by Dudley A. Buck and, as a member of the Advanced Research Division, has been active in the design of apparatus for vacuum deposition of superconductive circuits and in development of methods of fabrication and evaluation of superconductive circuits and devices.

C. R. Smallman

❖

Herschel Weil was born in Rochester, N. Y., on July 26, 1921. He received the B.S. degree in optics from the University of Rochester in 1943, and the M.S. and Ph.D. degrees in applied mathematics in 1945 and 1948, respectively, from Brown University, Providence, R. I.

H. Weil

During 1943–1944, he was employed as an optical engineer with the Bausch and Lomb Optical Company, Rochester. During 1946–1948, he was a research associate at Brown University working on theoretical problems in fluid mechanics. From 1948 to 1952, he was with the General Electric Company's General Engineering Laboratory, Schenectady, N. Y., where he worked on mathematical aspects of various engineering problems, becoming interested primarily in radar countermeasures work.

In 1952, he joined the staff of The University of Michigan Research Institute, Ann Arbor, where he has been mainly concerned with problems in electromagnetic theory with application to radar cross section computation. In February, 1960, he joined the faculty of the University of Michigan Electrical Engineering Department as an associate professor. He has continued his association with the UMRI through the Radiation Laboratory of The University.

Dr. Weil is a member of the American Mathematical Society, The Society for Industrial and Applied Mathematics, and Sigma Xi.

Books

Electrical Engineering Science, by Preston R. Clement and Walter C. Johnson

Published (1960) by McGraw-Hill Book Co., 330 West 42 St., N. Y. 26, N. Y. 574 pages+10 index pages+xiii pages+3 appendix pages+problems following each chapter. Illus. 6¼×9¼. $9.50.

In the preface the authors state that this book is intended as an introduction to electrical engineering as an applied science, and it seems to this writer that this has been accomplished most excellently. Since such a course is normally a part of the sophomore year, many colleges will have to "beef-up" their students' mathematical background if they wish to use this book, as differential and integral calculus is used freely, and frequent use is made of differential equations. On the other hand, while not suggested by the authors, it seems to this writer that the book might perhaps even better be used as a junior course following the usual sophomore "Elements of Electrical Engineering" and serve effectively to drive home the scientific basis for electrical engineering, a point that seems to be missed by far too many of today's graduates.

As a foundation for training in electronics, this book is particularly excellent, as its methods of presentation are very well thought out and the relationship of the widely diverse electronic concepts are well emphasized. This writer was particularly pleased with the methods used to introduce circuit and network theories and the extent to which these subjects are covered, but was a bit disappointed with the brief coverage of semiconductors. The usual introductory subjects of Electrical Forces and Fields, Magnetism and Electrodynamics, Principles of Energy Commission, and Measurements of Electrical Quantities are well and adequately handled. Fourier analysis is particularly well done.

The authors are to be especially congratulated for their excellent choice of problems, both as to quantity and quality. These vary from the quite simple to ones that will present great difficulties for a high percentage of electrical engineering graduates. In all cases, the problems require a carefully reasoned out approach and give the instructor an excellent means of measuring the students' thinking ability.

While the book is intended primarily as a college text, this writer believes that most electronics graduates of a dozen years or more will find a careful perusal of its contents well worthwhile.

CONAN A. PRIEST
314 Hulburt Rd.
Syracuse 3, N. Y.

The Dynamic Behavior of Thermoelectric Devices, by Paul E. Gray

Published (1960) by The Technology Press, Mass. Inst. of Tech., and John Wiley and Sons, Inc., 440 Fourth Ave., New York 16, N. Y. 106 pages+2 index pages+vii pages+1 bibliography page+26 appendix pages. Illus. 6¼×9¼. $3.50.

This book is an attempt to analyze the small-signal dynamic behavior of thermoelectric devices, specifically heat pumps and generators. This is a field which has not been explored previously and is of potential importance for the control aspects of thermoelectric devices. Specifically, the physical system and the mathematical model is considered, followed by small signal analyses for both the heat pump and the generator. Experimental work designed to test the heat pump model is described and the adequacy of the model is discussed. The last chapter preceding the brief conclusion treats the modification of the analysis to include a temperature-dependent resistivity.

The work described is definitely of value to the worker interested in the details of thermoelectric device behavior. Unfortunately, the field is not sufficiently advanced for most workers to be concerned with the details of transient behavior or control; to date, relatively brute-force empirical techniques have been adequate for his requirements while excusing him from the labor involved in the more elegant considerations. Also, unfortunately, this treatment suffers the fate of most attempts at detailed, theoretical studies in this field; that is, the more general functions derived turn out to be "sufficiently complicated to defy interpretation," and require highly restrictive assumptions to make them tractable. In spite of this, Dr. Gray's work shows, in this reviewer's opinion, sufficiently satisfactory agreement with experiment to induce a reasonable faith in its basic validity.

It would be unkind not to cite the publishers for their effort in making available to interested scientists a work of this nature —one too long for any journal article, but of insufficient scope and completeness for a finished book.

F. E. JAUMOT, JR.
Delco Radio Div., GMC
Kokomo, Ind.

Masers, by Gordon Troup

Published (1959) by John Wiley and Sons, Inc., 440 Fourth Ave., N. Y. 16, N. Y. 148 pages+4 index pages+x pages+4 bibliography pages+12 appendix pages. Illus. 4¼×6¼. $2.75.

This small book, another of Methuen's Monographs on Physical Subjects, is an introductory text to the subject of Microwave Amplification by Stimulated Emission of Radiation. Both gaseous (beam) masers and solid-state masers are discussed in quantum-mechanical terms. The book is the outgrowth of a dissertation written by the author.

After an introduction to the general subject, the approaches to stimulated and spontaneous emission from both thermodynamics and quantum mechanics are explained. The expressions for the power emitted by a gaseous and a paramagnetic molecule are then calculated, and the various factors affecting the emission process are discussed. Excitation methods for two-level and three-level masers are covered, but four-level excitation schemes are not discussed.

In the chapter on Amplifier Systems, the gain, bandwidth, and noise factor of a traveling-wave maser, and one-port and two-port cavity masers, are derived from fundamental considerations. The concept of magnetic Q is introduced in connection with cavity masers, but is not exploited elsewhere in the book. The conditions for oscillation, emitted power and frequency of oscillation of the ammonia beam maser oscillator are analyzed. In a chapter entitled "Experimental Work," the published designs of several ammonia beam masers and solid-state masers are discussed. The book covers the published literature to approximately the end of 1958.

The field of masers straddles several areas of physics and electronics, and the author faced a difficult choice on what to include in this small volume. He has chosen to concentrate on the quantum-mechanical fundamentals. Hence, this book can be recommended, and will be of primary interest to those interested in the physics of molecular amplifiers.

FRANK R. ARAMS
Airborne Instruments Lab.
Div. of Cutler-Hammer, Inc.
Melville, L. I., N. Y.

NAB Engineering Handbook, Fifth Edition, A. Prose Walker, Ed.

Published (1960) by McGraw-Hill Book Co., 330 West 42 St., N. Y. 36, N. Y. 1666 pages+35 index pages+xxv pages. Illus. 9¼×6¼. $27.50.

This Handbook was written for broadcast engineers and technicians. However, it will be highly educational to nontechnical persons wishing to increase their knowledge of the technology of broadcasting. Earlier editions of this Handbook were published in 1935, 1938, 1946 and 1949, consisting of loose leaf volumes utilizing offset printing. They highlighted various aspects of broadcast engineering which were of immediate need without attempting to deal with the entire system. The new edition, the first to utilize the letter press textbook format, covers the whole field of broadcast technology. It is a carefully edited compilation of a tremendous store of reference material and technical information much of which previously had been treated inadequately or so scattered through the literature that its use was limited. Forty-nine individual engineering authors, each an authority in his field and identified with broadcasting network or station operation or engineering, the design of apparatus or facilities, engineering consultation, the Bell Telephone System, the U. S. Information Agency or the Federal Communications Commission cooperated with the NAB engineering staff over a period of three and one-half years to produce a comprehensive work.

The book presents a logical treatment of the entire AM-FM-TV broadcasting system, including radio relaying, FCC rules, regula-

tions and standards, design, construction practices, cost estimating, industry standards, measuring systems and methods, network distribution, signal analysis, color fundamentals and the color TV system, remote pickup equipment and practices, auxiliary and supplementary services, new techniques and devices including semiconductors, FM multiplexing, compatible single sideband transmission, UHF television translators, remote control of broadcast stations, automatic logging and control of broadcast systems and the Conelrad system.

430 pages are devoted to the reproduction of pertinent FCC and industry standards, rules, regulations and related information. 300 pages are devoted to the planning, design, construction, performance and maintenance of antennas and towers, and wave propagation. 167 pages deal with network transmission facilities, microwave systems engineering and performance, and television signal analysis. 195 pages are devoted to the planning and construction of studio facilities, cost estimating, television lighting systems, audio and video effects, and magnetic recording of sound and pictures on tape and disks. The 261 pages on new techniques and devices which are contributing significant new trends, improvements and economies in the broadcasting industry constitute one of the valuable additions to this Handbook.

Any broadcast engineer or technician interested in broadening his knowledge, keeping abreast in his field and having at hand a comprehensive reference volume and guide will find this new Handbook an almost indispensable addition to his library.

RAYMOND F. GUY
National Broadcasting Co.
New York, N. Y.

Electromagnetic Theory and Engineering Applications, by John B. Walsh

Published (1960) by The Ronald Press Co., 15 E. 26 St., N. Y. 10, N. Y. 258 pages+4 index pages+21 appendix pages+x pages. Illus. 6¼×9¼. $8.50.

The book is an intermediate level text which combines some aspects of the physics of electromagnetic fields with engineering applications. It should be regarded as a textbook and its pedagogical value depends, of course, on the orientation of the course and its instructor. The nine chapters cover topics of Vector Analysis, Electrostatics, Magnetostatics, Maxwell's Equations, Plane Waves, Energy Flow and Guided Waves, Relation Between Field and Circuit Equations, and Transmission Lines. A set of appendices deals with mathematical matters and special problems which would be distracting if they were in the main body of the text.

The attempt to relate the formal aspects of the subject to physical pictures and basic concepts is a commendable feature. The author is necessarily limited to a cursory treatment of such matters by the requirement of covering "field theory for electrical engineers." One can hardly expect a student to really understand dielectric polarization or magnetic domain theory on the basis of such once-over-lightly presentations, and it is certain that the author does not suffer from misconceptions as to the effectiveness of his treatment. But enough is said to stimulate the live student, whet his appetite, and give him something more to think about than sets of equations.

The discussions of energy relations in fields follow conventional lines of development, which means that assumptions underlying their derivation and the limitations on the interpretation of the energy density functions are not stated and stressed explicitly enough.

The author very carefully develops the properties of complex vectors, distinguishing the phasor aspect from the spatial directional aspect of a harmonically time-varying electric field. Unfortunately, he does not proceed to discuss complex permittivity and permeability and show that even in an isotropic medium the vectors D and E, and B and H, are not necessarily colinear as they are in the case of static fields. His subsequent treatment of the Poynting vector and energy flow falls short by not dealing with complex constitutive parameters and their significance in representing energy exchange and dissipation in lossy media.

The exercises take the form of problems and questions, pertaining to interpretation of the results, which are certainly provocative. This is an excellent pedagogical device. A student will find the book a useful starting point for a course of study of the field of electricity and magnetism and its applications and, if he falls for the bait laid out for him and uses the library, he will fare very well.

SAMUEL SILVER
Space Sciences Lab.
Leuschner Observatory
Univ. of Calif.
Berkeley 4, Calif.

Quantum Electronics, Charles H. Towne, Ed.

Published (1960) by Columbia University Press, 2960 Broadway, N. Y. 27, N. Y. 602 pages+xviii pages+5 pages list of participants. Illus. 6¼×9¼. $15.00.

This volume contains the proceedings of the Conference on Quantum Electronics—Resonance Phenomena, which was held at High View, N. Y. in mid-September, 1959 under the auspices of the Office of Naval Research. This conference had a truly international flavor, being attended by about 160 scientists from at least ten countries, including Israel, Japan, and Russia.

The purpose of this gathering was to exchange and consolidate information bearing on atomic, molecular, and nuclear resonance phenomena, particularly those which involve quantum effects of various sorts. Among the many topics included were various types of masers, optical pumping and related effects, atomic frequency standards and clocks, noise in quantum-mechanical amplifiers, generation and detection of electromagnetic energy by atomic or molecular phenomena, and ferromagnetic, paramagnetic, and cyclotron resonance phenomena.

Since an excellent summary of this conference has recently been published by Irving Rowe of the Office of Naval Research (*Physics Today*, vol. 13, pp. 29–34; March, 1960), there is no need to attempt a further summary here. It is sufficient to say that the conference proved to be extremely fruitful to all concerned.

The present volume contains the texts of most of the papers that were presented, together with the discussions which followed these papers. Many of the papers, and probably the most valuable ones, are those which attempt to summarize the present state of our knowledge in various fields. Not surprisingly, these were found to be the most readable. There are also many original contributions, some of these apparently prepared expressly for this conference. These are also likely to be highly appreciated by the readers of this volume. Some of the papers are highly specialized; these should appeal most to readers seeking specific information rather than a general point of view. A number of papers are represented only by abstracts; even those are usually accompanied by a record of the ensuing discussion.

Because this volume brings together a wealth of up-to-date and authoritative information on a highly active subject, and also because this volume appears in print only six months after the conference, when the subject matter is still fresh and timely, it should receive a hearty welcome by the scientific community. At least a third of the content should appea to a very wide readership, while the remainder should prove most useful to specialists. The Office of Naval Research, the editor, Professor Charles H. Townes of Columbia University, and the assembly of contributors deserve our thanks for bringing this volume to fruition.

FRANK HERMAN
RCA Labs.
Princeton, N. J.

Transistor Circuit Analysis and Design, by Franklin C. Fitchen

Published (1960) by D. Van Nostrand Co., Inc., 120 Alexander St., Princeton, N. J. 324 pages+6 index pages+xi pages+bibliography by chapters+24 appendix pages. Illus. 6¼×9¼. $9.00.

This book is one of the Van Nostrand Series in Electronics and Communications edited by Prof. H. J. Reich. It was written as a one-semester textbook for E.E. junior or senior students. The development is elementary with only a working knowledge of dc and ac fundamentals being required. The subject treatment makes this book primarily suitable for engineers with a passing interest in transistors and particularly for those interested in usual circuit applications. The summary and extensive problems associated with each chapter should make it possible for practicing electronic engineers to use this as a self-study text. Chapter references are used frequently to direct the reader to more advanced treatments.

L. J. GIACOLETTO
Scientific Lab.
Ford Motor Co.
Dearborn, Mich.

Theory of Inertial Guidance, by Connie L. McClure

Published (1960) by Prentice-Hall, Inc., 70 Fifth Ave., N. Y. 11, N. Y. 302 pages+4 index pages+xi pages+3 bibliography pages+29 appendix pages. Illus. 6½×9¼. $12.00.

This is the first text on this subject to find its way into the reviewer's hands, although at least one other will be available August 1, 1960.

Mr. McClure's book provides, in one convenient source, the theoretical foundation of the subject. Presupposing a knowledge of undergraduate engineering mathematics and mechanics, it will be of interest primarily to students taking a formal course in the subject. In addition, it will be useful to two classes of active practitioners of inertial guidance—the younger man on the staff who has not had the benefit of a specialized course in the subject, and the experienced component designer who would like to fortify his understanding of how his component fits into the system as a whole.

The subject matter is confined almost exclusively to theory, with just enough introduction to practical instruments to render the subject plausible. The topics covered include the related mathematics (vectors, coordinate transformations, Coriolis' Law), three-dimensional kinematics, the elements of rigid body mechanics, and classical gyro theory, all of which form the background of the subject. The author then describes the use of gimbal systems and gyros for base-motion isolation, the single-axis Schuler-tuned vertical indicator, the single-axis velocity-damped vertial indicator, and then finally, the complete three-dimensional system, including the effects of ellipticity, variable altitude, and the choice of azimuth control law. There is a very brief discussion of error studies, both analytical and simulated.

The literary style is vigorous; the arrangement is orderly. The progression from one topic to the next is logical, and the most advanced sections build on that which precedes. Derivations are generally neat, but there are a few isolated sections which would benefit from revision (*e.g.*, sections 7.3, 10.4, and 10.5). Neither the historical development of the gyrocompass, nor the search to find a pendulum capable of tracking the vertical, the commonly-used approaches to the subject, are used here. Rather, the approach is mathematical in nature, based on a solution of the dynamic and kinematic problem of movement over the surface of a three-dimensional body. This in itself is fine, for, assuming that the student will eventually meet the pendulum concept in other readings, breadth of understanding is fostered by the assimilation and fusion of several points of view. The author does his thinking in terms of classical differential equations. It would seem that a more direct appeal to physical intuition through the use of vectors (which appears only incidentally) would make the presentation clearer.

Contrary to claims made on the dust jacket, this book does not treat "every aspect" of the subject. For example, it does not cover ballistic missile or space vehicle guidance. The computer design and the size, weight, and accuracy of other physical equipment are scarcely mentioned. A beginning student who might want to see at least one picture of a real gyro or a real platform will not find it in this book. Other important problems such as alignment techniques, "gyrocompassing," and the instability of the altitude channel are omitted.

Finally, the text does not contain practice problems. The author would do a service to himself and to the users of his book if he were to prepare a set of problems to be issued as a companion document. Problems are absolutely essential if the student is to assimilate the book's methods for later application to his own problem situations.

DR. ALAN M. SCHNEIDER
Missile Electronics and Controls Div.
RCA
Burlington, Mass.

Scanning the Transactions

Antenna arrays are usually thought of as having equal spacings between elements. It now appears that this is not necessary. A recent study of steerable broadband antenna array designs gives some rather surprising evidence that unequally-spaced arrays are apt to require fewer elements and have smaller sidelobes. In fact, one spacing arrangement was found to require only 21 elements as compared to 78 for an equally-spaced array of similar beamwidth. Although unequally-spaced arrays have not been explored in great detail yet, it is evident that they offer interesting possibilities for further investigation. (D. D. King, *et al.*, "Unequally-spaced, broad-band antenna arrays," IRE TRANS. ON ANTENNAS AND PROPAGATION, July, 1960.)

The interaction of sound and electromagnetic waves, though by no means a new subject to physicists, has not been discussed before in an IRE publication as far as can be recalled. It is then perhaps worthy of note that the subject has now arisen in two TRANSACTIONS at the same time. In one paper, investigators were interested in the reflection of radio waves as they are propagated through acoustically disturbed air. The reflections arise because sound waves cause variations in the index of refraction of air. In another paper, investigators were interested in the manner in which a narrow beam of light is diffracted when it passes through an ultrasonic wave, again due to sound-produced variations in the index of refraction of air. The latter phenomenon, incidentally, provides a way of optically measuring ultrasound intensity and of ultrasonically triggering a stroboscope. (B. L. Jones and P. C. Patton, "Solution of a reflection problem by means of a transmission line analogy," IRE TRANS. ON ANTENNAS AND PROPAGATION, July, 1960; H. L. Zankel and E. A. Hiedemann, "Diffraction of a narrow beam of light by ultrasonic waves," IRE TRANS. ON ULTRASONICS ENGINEERING, June, 1960.)

The search for factors that influence creativity has become increasingly intense and widespread during the last two decades of rapid scientific and technological progress. The processes which facilitate the production of new knowledge are now a matter of vital interest to scientists and technical managers as well as to social researchers. In an effort to shed more light on scientific productivity, a study was recently conducted among 57 academic researchers on the faculty of a mid-western university to determine whether a correlation exists between the productivity of a researcher and his behavioral standards. Their attitudes were examined with respect to freedom in research, impartiality, suspension of judgment until sufficient evidence is at hand, absence of bias, diffusion of information, and group loyalty. Against this, their creativity was measured by rate of publication by judgment of their associates. The results showed no significant correlation of factors, thus leading to the conclusion that the classical morality of science is not associated to any important degree with productive research. (S. S. West, "The ideology of academic scientists," IRE TRANS. ON ENGINEERING MANAGEMENT, June, 1960.)

Abstracts of IRE Transactions

The following issues of TRANSACTIONS have recently been published, and are now available from the Institute of Radio Engineers, Inc., 1 East 79th Street, New York 21, N. Y. at the following prices. The contents of each issue and, where available, abstracts of technical papers are given below.

Sponsoring Group	Publication	Group Members	IRE Members	Non-Members*
Antennas and Propagation	AP-8, No. 4	$1.90	$2.85	$5.70
Audio	AU-8, No. 3	.85	1.30	2.55
Automatic Control	AC-5, No. 2	1.80	2.70	5.40
Circuit Theory	CT-6, No. 2	1.75	2.60	5.25
Component Parts	CP-7, No. 2	1.25	1.90	3.75
Engineering Management	EM-7, No. 2	.85	1.30	2.55
Radio Frequency Interference	RFI-1, No. 2	.65	1.00	1.95
Space Electronics and Telemetry	SET-6, No. 2	.75	1.10	2.25
Ultrasonics Engineering	UE-7, No. 2	2.70	4.05	8.10
Vehicular Communications	VC-9, No. 1	1.30	1.95	3.90

* Libraries and colleges may purchase copies at IRE Member rates.

Antennas and Propagation

VOL. AP-8, NO. 4, JULY, 1960

Coupled Leaky Waveguides II: Two Parallel Slits in a Cylinder—S. Nishida (p. 354)

Theoretical expressions are derived for the effects of mutual coupling between two parallel leaky wave antennas which consists of slitted rectangular waveguides located in a cylinder. The expressions derived are presented in terms of the results for the mutual coupling of the same antennas but located in an infinite plane, with additional terms due to the curvature of the cylinder. The graphical presentation of the numerical attenuation constants for the cylindrical case are compared with those for the infinite plane.

Mutual Coupling Effects in Large Antenna Arrays II: Compensation Effects—S. Edelberg and A. A. Oliner (p. 360)

Mutual coupling effects in a large array cause a variation in the input impedance as a function of scan angle. This variation can be reduced considerably by the use of a compensating structure which appropriately modifies the environment of the array. A two-dimensional dipole array is treated as a typical example, and its input impedance is calculated by means of a unit cell equivalent network as a function of scan angle for different environmental situations. Reasonably constant performance up to scan angles of $\pm 60°$ is obtained on use of a periodic baffle compensation structure.

Paraboloidal Reflector Patterns for Off-Axis Feed—S. S. Sandler (p. 368)

The problem of predicting the radiation pattern for an asymmetrically illuminated paraboloid is covered in some detail. The current distribution method is given in a final form suitable for machine computation. An approximate analytical solution using scalar diffraction methods is compared with the experimental results and the machine solution.

Unequally-Spaced, Broad-Band Antenna Arrays—D. D. King, R. F. Packard, and R. K. Thomas (p. 380)

Requirements for a broad-band, steerable linear antenna array are given. The limitations due to grating lobes of an equally-spaced array are discussed. Results are given of the study of several different unequally-spaced arrays which have two advantages:

1) fewer elements for comparable beamwidth;
2) grating lobes and minor lobes replaced by sidelobes of unequal amplitude which are all less than the main beam.

A scheme for controlling the cosine arguments in the radiation pattern formula is given which has resulted in one of the best patterns of this study of unequally-spaced arrays. The universal pattern factor was computed for an array having a set of spacings determined by this scheme. This array is capable of steering a beam $\pm 90°$ over a 2-to-1 frequency band with no sidelobe above -5 db. It uses 21 elements, compared to 78 for an equally-spaced array of similar beamwidth.

The results obtained indicate that further study of the controlled cosine method and unequal spacing in general should result in better pattern characteristics.

Resonant Slots with Independent Control of Amplitude and Phase—Bernard J. Maxum (p. 384)

The design of slot arrays requiring nonuniform phase distributions, such as those having shaped beam radiation patterns, are facilitated by the development of slots having independent amplitude and phase control. A "complex" slot (which is inclined and displaced) on the broad wall of a rectangular waveguide makes it possible to control the coupling characteristics over a range in phase from zero to 2π and over a range in magnitude from zero to unity. The "voltage" across the slot as a function of its orientation is found and is related to the coupling parameters used in common array design. An experimental procedure for independently verifying the amplitude and phase characteristics is described. A typical complex slot array design is made and radiation patterns are included demonstrating the accuracy and usefulness of the design procedure.

Mutual Coupling of Shunt Slots—A. F. Kay and A. J. Simmons (p. 389)

Stevenson's method of analysis is extended to the case of a pair of shunt slots in the broad face of rectangular waveguide. The voltages in the slots are calculated including the effect of mutual coupling. Formulas suitable for calculation of mutual coupling are presented and the results of calculations for certain cases of overlapping quarter-wave spaced slots and nonoverlapping half-wave spaced slots are presented.

Measurement of the scattering matrix of the slot pairs inside the waveguide and the radiation patterns external to the waveguide for the overlapping case tend to confirm the results of the theory.

Calculations of the effect of mutual coupling on the patterns of three half-wave-spaced slot arrays indicate that mutual coupling is usually negligible for this type of slot.

A Wide-Band Transverse-Slot Flush-Mounted Array—E. M. T. Jones and J. K. Shimizu (p. 401)

This paper describes the design analysis and measured performance of an antenna composed of an H-plane array of parallel waveguides having quarter-wavelength-thick transverse slots extending completely across the array. Each relatively wide nonresonant slot in this array radiates only a small amount of power, and the dimensions of the slots are relatively uncritical. The radiated H field from this antenna lies parallel to the transverse slots. The cosine of the angle between the direction of maximum radiation and the plane of the antenna is equal to the velocity of light divided by the phase velocity of propagation along the array.

An experimental antenna was built with a radiating aperture 9 inches wide and 20 inches long. The antenna was fed from a hog horn which yielded an approximately sinusoidal H-plane illumination over the 9-inch aperture width. The power coupled from the transverse slots was varied along the 20-inch length of the aperture to achieve a Taylor aperture distribution with -25-db E-plane sidelobes. At the design frequency of 11 kmc, the E-plane and H-plane beamwidths were 5.4° and 7.3°, while the E-plane and H-plane first-sidelobe levels were -24.7 db and -24.2 db, respectively, in close agreement with theoretical expectations. The direction of maximum radiation was within 0.35° of the design value at 11 kmc. Good radiation patterns were obtained with the antenna from 7.0 kmc, which is slightly above the cutoff frequency of the guides, to 11.4 kmc, which is slightly below the frequency at which spurious lobes are generated by the widely-spaced slots.

Relation Between a Class of Two-Dimensional and Three-Dimensional Diffraction Problems—L. B. Felsen and S. N. Karp (p. 407)

By means of a certain transformation, a relationship is demonstrated between a class of two-dimensional and three-dimensional scalar or electromagnetic diffraction problems. The basic three-dimensional configuration consists of a perfectly reflecting half plane excited by a ring source centered about the edge and having a variation $\exp(\pm i\phi/2)$, where ϕ is the

azimuthal variable; in addition, a perfectly reflecting rotationally symmetric obstacle whose surface is defined by $f(\rho, z) = 0$ (ρ, z are cylindrical coordinates) may be superposed about the edge (z axis). This problem is shown to be simply related to the two-dimensional problem for the line source excited configuration $f(y, z) = 0$, where y and z are Cartesian coordinates. Various special obstacle configurations are treated in detail.

Forward Scatter from Rain—L. H. Doherty and S. A. Stone (p. 414)

The forward scatter of radio waves from rain has been observed over a 90-mile, 2720-mc path. The observations support the assumption of omnidirectional scattering from rain. On this link rain scatter may exceed the normal tropospheric scatter signal by 15 db. This latter signal may itself be increased by the presence of thunderstorms in the vicinity. Signal level distribution during rain and no-rain conditions are presented.

Among the effects of rain on a tropospheric scatter link are the increased fading rate and decreased bandwidth. The fading rate may increase by a factor of ten or more, and pulse-to-pulse fluctuations have been observed at a pulse repetition frequency of 600 pulses per second. Evidence for a decreased bandwidth is presented in the form of pulse photographs. The 1.5-μsec pulse is commonly broadened to 3 or 4 μsec and on occasions to lengths in excess of 20 μsec.

Solution of a Reflection Problem by Means of a Transmission Line Analogy—B. L. Jones and P. C. Patton (p. 418)

Through the use of a transmission line analogy, a problem related to the reflection of electromagnetic energy from a periodic acoustic disturbance is solved. This solution agrees well with a numerical solution of a wave equation of the Mathieu form, which has been derived from a different model of the same problem. Subsequent experimental research has given results in good agreement with the theoretical solutions.

Experimental Swept-Frequency Tropospheric Scatter Link—W. E. Landauer (p. 423)

An experimental swept-frequency tropospheric scatter link, with a path length of 194 miles, has been established in France between Cholet and Corbeville. The transmitter (designed by Compagnie Générale de Télégraphie Sans Fil) sweeps in a nearly linear manner from 3100 to 3600 mc and back to 3100 mc at about 10 cps. The average transmitted power is 250 watts. The receiver and data display (designed by Airborne Instruments Laboratory) sweep in synchronism with the transmitter. The synchronizing signal is derived from the carrier frequency of a broadcast station (Paris-Inter). The receiver is designed to track swept signal amplitudes down to about 4 db above noise level, and after severe fades, to reacquire signals larger than 6 db above noise level in about 1 to 2 milliseconds. Received signal amplitude is presented as a simultaneous function of frequency and time.

Preliminary data obtained from the link indicate that privileged transmission frequencies exist at all times in this band at which the transmission level is about 10 db above median. The preliminary data gathered from the link are described, as well as general design features of the system.

Energy Density in Continuous Electromagnetic Media—A. Tonning (p. 428)

After a discussion of various types of linear electromagnetic media, a general expression for the energy density for a lossless medium is derived by evaluation of the total influx of energy to a volume element. The result reduces to the commonly used expression only if the medium is nondispersive. The physical significance of the extra energy term resulting from the dispersion is discussed, and a general expression for the stored energy of an electric network is given.

Audio

Vol. AU-8, No. 3, May–June, 1960

Room Acoustics and Sound System Design—David L. Klepper (p. 77)

At the present time, there are in operation a large number of sound amplification systems installed mainly for the purpose of speech reinforcement. Many of the existing systems appear to have been installed without regard for the acoustical requirements for high speech intelligibility, and the phrase "public-address system" has become almost an anathema to sensitive listeners.

Bolt Beranek and Newman, Inc. has become involved in the design of sound amplification systems in conjunction with other aspects of architectural acoustics. A number of principles have been developed as guides for the design of speech reinforcement amplification systems that provide a high degree of intelligibility and naturalness. These principles will be discussed and illustrated by the designs of several typical speech reinforcement systems, including those installed in a large exhibition hall, a reverberant church, a stockholders' meeting room, and an auditorium designed for maximum "natural" reinforcement by proper acoustical design.

Time Compensation for Speed of Talking in Speech Recognition Machines—H. F. Olson and H. Belar (p. 87)

A simplified version, but nevertheless complete system, of a phonetic typewriter which types in response to words spoken into a microphone has been described. One of the many extensions of the original system is a means for compensating for the effects of the speed of talking. Instead of transferring information into the spectral memory in fixed-time increments, as was done in the original machine, the transformation of information is determined from a correlation with significant changes in the speech spectrum with respect to time. In the improved machine, coincidence detectors compare the current with the preceding speech spectrum. No information is fed into the spectral memory until a significant change has been detected in the speech spectrum. The system provides an automatic time compensator for variations in the speed of talking in a speech recognition machine.

Experiments and Experiences in Stereo—Paul W. Klipsch (p. 91)

A considerable number of observations as well as formal experiments in High Fidelity Stereo sound are reported. Three channel stereo with corner flanking speakers has been shown to achieve accuracy in both tonality and geometry. A large center speaker with small outriggers is observed to lack both tonality and geometry. A center speaker in the corner with wall outriggers is observed to produce a deeply curved stereo geometry. Limiting speakers to a bass range down to 300 cycles may preserve geometry, but not tonality.

Overly large bass speakers lead to a spatial and delay separation of bass and treble events. There is an optimum bass speaker size.

Wide spacing of speakers offers improved accuracy of stereo geometry. The array cannot normally exceed the speaker spacing, but because of the focusing effect of the center channel, it may be much narrower than the speaker spacing.

Numerous minor observations of radiation angle and polar response point up the desirability of corner speaker placement.

Large speakers may be placed at low or high level, but the dynamic range of small speakers is limited.

Corner speaker placement affects apparent room size and may be advantageously employed to improve the reverberation effects.

Wide Stage Stereo demonstrations using speaker spacing up to 50 feet or more are compared to home applications with 15-foot spacing.

High Fidelity Stereo is both high fidelity and stereo, and entails meeting the requirements of both.

A Resonance-Vocoder and Baseband Complement: A Hybrid System for Speech Transmission—James L. Flanagan (p. 95)

The production and perception of speech are characterized by certain constraints. The efficiency with which speech information can be communicated is considerably dependent upon how successfully these constraints can be incorporated into the transmission apparatus.

This paper undertakes to review some of these relations and to indicate their relevance to communication. It attempts to point out the extent to which vocal and auditory constraints are applied in existing speech compression systems such as the Vocoder and the resonance-Vocoder. The theory underlying the latter suggests savings in channel capacity greater than tenfold. To date, however, only moderate success has been achieved in transmitting speech of acceptable intelligibility and quality over such systems.

The last part of the paper describes a transmission scheme which is part conventional and part resonance-Vocoder. Through this compromise, some of the band-saving features of the latter can be retained, while its intelligibility and quality can be improved upon. The hybrid system occupies a total bandwidth of approximately 600 cps and requires a signal-to-noise ratio comparable to that of conventional voice channels. Articulation tests performed on the system yield mean scores ranging from 74 to 84 per cent for monosyllabic words.

Automatic Control

Vol. AC-5, No. 2, June, 1960

Accuracy Requirements of Nonlinear Compensation for Backlash—Donald Schulkind (p. 79)

Recent advances in the analysis of nonlinear control systems have given rise to a more logical and systematic approach to the elimination of the detrimental effects of inherent nonlinearities. The describing function technique is used in this paper to analyze two typical servos. The servos are shown to exhibit a stable limit cycle and are stabilized by linear

and nonlinear techniques. The nonlinear technique involves the insertion of an additional nonlinear feedback element which feeds back a distorted signal opposite in phase to the original distorted feedback signal. In particular, a method is developed in this paper for determining the accuracy required in the construction of a practical nonlinear compensating element.

Specification of the Linear Feedback System Sensitivity Function—William M. Mazer (p. 85)

This paper examines the problem of designing a linear feedback system so that its response to a specified input is relatively insensitive to slow changes in system parameters. Classical feedback design techniques involve the specification of the system sensitivity function on the basis only of the forced response to a given input. A new performance criterion has been derived, in which the mean square variation of the system response is minimized. This specification of the sensitivity function results in control over the variation of both the characteristic and forced responses with system changes. The approach is based upon the assumption of a differential change in the variable system parameter, but yields workable results for large changes. It employs mathematical techniques which have been well developed for other applications in network design. The stability problem associated with high loop gains is considerably reduced when the sensitivity function is specified on the basis of this criterion.

Synthesis of Linear, Multivariable Feedback Control Systems—Isaac M. Horowitz (p. 94)

A multivariable controlled process or plant is one in which there are n independent inputs and m outputs with $n>1$ and $m\leq n$. A control problem may exist for one or two principal reasons. 1) The plant parameters may vary or they may be only vaguely known, and the system response sensitivity to the parameter variation is to be reduced. 2) The system response to disturbances is to be reduced. A synthesis procedure for attaining these objectives and simultaneously realizing a desired set of system transmission functions is developed in this paper. The role of system configuration is considered. Design is broken up into two separate regions. In the significant system-response frequency region, there is straightforward synthesis in attaining the design objectives. In the higher frequency range, the loop transmission must be shaped so that the system is stable. The latter problem is considerably more difficult when there are substantial plant parameter variations. Some procedures are illustrated by two detailed examples ($n=m=2$ in one example, and $n=3$, $m=2$ in the second) in which there are large plant parameter variations.

Automatic Control of Three-Dimensional Vector Quantities—Part 3—A. S. Lange (p. 106)

This is the final part of a three-part paper on the application of vector techniques to automatic control systems whose input, output, and disturbance quantities may be characterized by three-dimensional vectors. In Parts 1 and 2, position and angular velocity vectors were introduced to demonstrate the solution of coordinate conversion and geometric stabilization problems, respectively. In brief, the subject of Part 3 is Newton's Second Law, with the application of the previously defined vector algebra to problems in kinetics. In particular, the behavior of "Newtonian sensors" such as gyroscopes and accelerometers is considered in detail, in order to develop the basic equations which describe the dynamic performance of these devices, determine the errors associated with their usage, and demonstrate the application of the vector algebra to more complex systems.

Statistical Evaluation of Digital-Analog Systems for Finite Operating Time—R. B. Northrop and G. W. Johnson (p. 118)

A frequency-domain mathematical model for comparing the performance of a linear sampled-data channel to a linear continuous channel is developed. The model assumes a suddenly applied stationary random input (input identically zero before the local time origin).

The model allows an explicit algebraic definition of ensemble mean-squared error, after a finite operating time, by application of residue theory. The ideal or comparison channel need not be realizable.

The quasi-stationary characteristics of the excitation are accounted for by including a starting switch as a variable parameter within the appropriate system weighting functions.

The technique developed in this paper is utilized to evaluate the ensemble mean-squared error due to processing a vehicle velocity estimate (as might be supplied by an integrating accelerometer) in a digital computer. The velocity estimate is used to calculate a numerical value of present vehicle position. This problem is of fundamental importance in present-day pure inertial, pure Doppler, or inertial-Doppler navigation systems. The effect of quantization, inherent in the process of analog-to-digital conversion, may be included in this evaluation.

It is shown that for cases where system inputs can be approximated by narrow-band, first-order, Markoff-type power spectra, the practical engineering use of the simplest digital integration program (rectangular) or the simplest hold (box-car) is well justified. The examples illustrate the mathematical techniques necessary to compute the ensemble mean-squared error, and illustrate how several simplifying assumptions may be used.

A Mathematical Representation of Hydraulic Servomechanisms—J. J. Rodden (p. 129)

This paper gives a basic representation of a high performance hydraulic servo actuator. The discussion gives a means of calculating the servo gain and rate limit characteristics as functions of the design parameters. Assumptions are discussed that would allow simplification of the equations for their application with computing equipment. Representation of the supply accumulator and pump is included. The effects of equipment nonlinearities can be incorporated into the basic model with appropriate modification of the computer program.

The work of this paper has been applied to the design and analysis of missile flight control systems where the rate limit characteristic of the actuator is significant to dynamic performance.

A General Method for Deriving the Describing Functions for a Certain Class of Nonlinearities—Rangasami Sridhar (p. 135)

Since Goldfarb's original work on describing functions, a considerable number of papers have been published in which the describing functions of particular nonlinearities have been derived. It appears, however, that little effort has been made to classify the nonlinearities. Since the describing function method is one of the more powerful methods available at present to analyze nonlinear feedback systems, it appears desirable to collect the expressions for the describing functions of a few different types of nonlinearities in one paper.

It is the purpose of this paper to derive the describing functions of two general types of nonlinearities and show how the describing functions of many other practical types of nonlinearities for which the describing function analysis is valid naturally follow.

Soviet Literature on Control Systems—P. L. Simmons and H. A. Pappo (p. 142)

Most of the better known articles from Soviet literature on the subject of control systems published between January, 1953 and March, 1959 are cited. Emphasis is on the theoretical aspects of control systems.

The items are arranged alphabetically according to author, with no attempt at classification. The first section includes all topics and the second section lists only articles which have English translations. Annotations are given only for articles which the bibliographer has examined.

The introduction mentions some of the existing bibliographies in the field and discusses possible schemes for classifying bibliographic references to control systems.

Circuit Theory

Vol. CT-6, No. 2, June, 1960

Component Parts

Vol. CP-7, No. 2, June, 1960

The techniques used in producing thin-film circuits are discussed. Conductive, resistive and

insulating films are evaporated separately onto glass substrates to form resistors, capacitors and interconnections. Active elements, transistors and diodes are mounted in holes drilled through the substrates. Studies aimed at developing thin-film active elements are discussed briefly. Several possible methods of interconnection are presented.

Precise LC Comb Filters, Packaged for Reliability—D. M. Lisbin (p. 44)

The engineering, packaging, and testing controls necessary to produce reliable, precise LC comb filters which are critical components in today's advanced military electronics systems, are often completely overlooked or inadequately stressed.

It is common practice for engineers to consider the filter as a "black box" to be accepted as soon as the electrical requirements have been met. Then, there usually follows a crash program of makeshift "fixes" in order that the unit in final form may reliably meet the rigid environments encountered in Military Systems.

This paper describes the design of a 60-filter comb, which is the critical front end of Doppler radar systems, and presents solutions to packaging problems encountered in its design, and the test controls devised to produce 60 precise LC filters with critical interrelated electrical specifications. The mechanical evolution of the design will be described.

In summation, LC comb filters can be designed stressing repairability, good shop practice, and precision electrical characteristics, as well as environmental reliability.

Transient Response of Variable Capacitance Diodes—D. Schulz (p. 49)

A solution for the transient response of a reverse biased semiconductor diode to a step function (voltage) may be found by considering the junction essentially a voltage variable capacitance. The assumptions from which the analysis is made are given and found to be applicable in a wide variety of cases. Specific solutions are obtained for abrupt and linearly graded junctions, and experimental evidence is presented which is in good agreement with the derived equations.

Cable Reliability in Ground Guided Missile Systems—J. Spergel and E. F. Godwin (p. 54)

The increasing demand by equipment and system design engineers for greater operational and functional reliability of components has dictated the need for greater understanding and improvement of individual supporting parts. The present trend, in order to obtain reliable systems, is to devote maximum effort to perfecting or developing highly reliable equipments without commensurate effort to the necessary supporting interconnecting network required to integrate the various components into a complex system. This approach to system design is extremely risky and usually costly.

Realizing the inefficiencies and risk to this approach, a joint Signal Ordnance Corps program under Contracts DA36-039, SC-73056 and SC-78175 was initiated with RCA Service Company, Alexandria, Va. to survey and evaluate all external cables and connectors associated with several guided missile systems. During the evaluation phase, it became apparent that a consolidated and functionalized approach to cable design was necessary to obtain the required reliability, especially when dealing with a large and complex system such as the Nike Hercules, which has approximately 150 cable runs, consisting of approximately 13 miles of cables, weighing approximately 13 tons, and over 300 connectors. This paper will discuss the effect of conductor grouping on the inherent cable reliability, signal compatability and operational system reliability. Approaches which will permit the design of optimum and efficient external interconnecting networks for systems application are suggested.

Temperature Distribution in Materials with Positive Temperature Coefficients of Electrical Conductivity When Heated by Eddy Currents—W. W. Buchman (p. 60)

Steady-state digital and analytical solutions are given for the temperature distribution in slabs and cylinders of materials heated by varying magnetic fields. The materials are assumed to have a positive temperature coefficient of electrical conductivity of the type associated with semiconductors. The stability of the temperature distribution is investigated. It is shown that the solutions can be either stable or unstable, depending upon the size of the sample. Some of the practical significance of such heating is discussed in relation to the design of high-power wide-band transformers.

Contributors (p. 66)

Engineering Management

VOL. EM-7, NO. 2, JUNE, 1960

About This Issue—The Editor (p. 43)

Phasing and Utilization of Engineering Personnel—G. L. Wagner, J. H. Redding, and F. B. Brown (p. 45)

A model is presented which permits an analysis of management policy relative to the utilization of engineering manpower. The model is derived by considering the flow of engineering personnel through an organization and the cost attributable to the flow. Analysis of the model indicates that costs will be minimized where engineering policies allow a smooth flow of manpower through the organization. Relative to the cost considered, smooth flow can most readily be achieved by a rather unorthodox organizational structure—the inverted pyramid. Since other costs normally prevent the use of inverted pyramids, another method of approaching the smooth flow idea is explored, in particular, the tactic of varying the time that engineers spend in grade.

The Ideology of Academic Scientists—S. S. West (p. 54)

The moral values associated with scientific research were studied by means of interviews with 57 academic researchers of faculty status. The areas examined were freedom in research, impartiality, suspension of judgment until sufficient evidence is at hand, absence of bias, diffusion of information, and group loyalty. Two dimensions of creativity were measured in the respondents: rate of publication and strength of motivation toward research as judged by peers. Neither of these measures was significantly related to acceptance of the classical position in any of the six areas of value. It is concluded that the classical morality of science is not associated to any important degree with productive research.

Measuring the Effectiveness of Technical Proposals and Marketing Effort in Military Electronics—William J. Stolze (p. 62)

A study was made of the bidding experience of Stromberg-Carlson in the military electronics field over the past six years. The methods of analysis and presentation are reviewed. A model of a military marketing organization is developed which can be used to measure the effectiveness of the various components of the marketing effort on a long-term basis.

Another Look at Team Contracting—J. J. Bialik (p. 67)

Previous discussions concerning group contracting have been presented from a group leader viewpoint. The need was felt to view the group contracting arrangements from the associate contractor viewpoint. The experiences gained by over two and one-half years association in a group contract arrangement as an associate contractor are described. Areas of concern not normally encountered in a conventional contracting arrangement are described for prospective group contracting participants.

Standards for Measuring the Effectiveness of Technical Library Performance—R. E. Maizell (p. 69)

Current criteria for the evaluations of technical library performance are examined. Data are lacking for establishing standards based on what the better libraries are doing. Guides are presented for evaluating the quality of book and journal collections, the adequacy of reference service, the library's effectiveness in meeting requests, and the impact of a technical library on its associated research laboratory.

The Systems Approach: Can Engineers Use the Scientific Method?—Albert E. Hickey, Jr. (p. 72)

Currently, the "systems approach" is more an attitude than a plan of action. The method and concepts of science can help this field achieve the latter status. A system is defined, and current practice in systems engineering is described. The methods of science are described and suggested as a guide for the systems approach. Some of the tools and concepts used in systems work are described.

Radio Frequency Interference

VOL. RFI-1, NO. 2, MAY, 1960

Editorial—O. P. Schreiber (p. 1)

New Line Impedance Stabilization Networks for Conducted Radio Interference Measurements up to 100 Megacycles—K. Oishi (p. 2)

Two line impedance stabilization networks—a single unit and a dual unit—for the measurement of conducted radio interference have been redesigned from the present line impedance stabilization network to yield a smooth repeatable response up to 100 megacycles.

Avenues for Improvement in the Design and Calibration of VHF-UHF Noise and Field Strength Meters—Willmar K. Roberts (p. 6)

Increased accuracy of measurement of VHF-UHF field strength may be obtained by improving the impedance match of the antenna-balun assembly and by taking into account the measured gain of the antenna system, rather than by relying on the assumption that the antenna performance approximates that of the idealized half-wave dipole. The latter assumption appears to be the basis of present practice. Although the standard field method of calibration is theoretically available as an over-all calibration procedure, the present types of instruments depart from ideal in a manner so complex with respect to frequency that it becomes a prohibitive task to make detailed periodic calibrations by the standard field method, aside from the difficulties in the technique of the standard field method itself.

A simple form of the reciprocity method is shown for measurement of the effective gain of the antenna-balun assembly under essentially free-space conditions. It is argued that the calibration of field strength meters should be carried out under conditions equivalent to free space.

A General Technique for Interference Filtering—W. A. Stirrat (p. 12)

With one exception, the radiation and leakage from a signal generator can be held below specified limits. Exception exists in the loop consisting of the signal generator power cord, the power main, the ground connection of the signal generator, and the signal generator itself. Signals passing through the line filter are resonated in this loop and these signals can only be reduced by mismatch or by reduction of the maximum power available. Since the nature of the loop is unpredictable, a mismatch that will hold in every case cannot be provided. A limit on the maximum power available holds in every case. This maximum available power theoretically can be measured and the limit which it should not exceed can readily be found. The load drawing maximum power from a three terminal network is found and the theory of measuring this maximum available power is developed herein. Also indicated are how a limit can be set on maximum available power and how a simple LC filter fails to provide reliable mismatch.

Correspondence (p. 18)

Space Electronics and Telemetry

Vol. SET-6, No. 2, June, 1960

A Device for Automatically Tracking the Roll Position of a Missile—Richard W. Lowrie (p. 67)

Many short range missiles are guided in angle or range by optical means. Since these missiles are usually caused to roll in flight for stability reasons, some type of roll position reference device is necessary. The only type of roll reference device in use is a gyro, although various horizon scanners, Doppler, and optical methods have been considered.

This paper describes an optical method of roll reference which utilizes the relative positions of two flares of different color attached to the rear of the missile. Since the roll position is known at the launch point, commands to the missile are commutated at the launch point rather than in the missile as is necessary when a gyro or other missile-borne roll reference device is used. Thus, the roll tracker removes from the missile two subsystems (gyro and commutator) while adding two components (two colored flares).

A Six-Channel High-Frequency Telemetry System—T. C. R. S. Fowler (p. 69)

A frequency-multiplex FM-AM system is described which provides six continuous channels via which waveforms with frequency components in the approximate band 10 cps to 10 kc may be simultaneously telemetered; extension of the frequency coverage to include the band 0–10 cps is achieved by the use of commutated reference levels. A radio frequency in the 465-mcs band and subcarrier frequencies between 250 and 500 kc are used. A short historical introduction is followed by description of the system and of units of the flight and ground equipment, and details of operational results. Future uses of the system are discussed and methods of increasing the useful range are suggested.

The Case of FM-AM vs FM-FM Telemetry—Lawrence L. Rauch (p. 81)

The future role of frequency-division multiplex telemetry is discussed and related to the sampled data problem of time-division multiplex telemetry. It is concluded that the frequency-division method will continue to have important applications, and the question is raised regarding what is a desirable frequency-division system on which to standardize in the future. An examination of the shortcomings of the FM-FM system and the electronics state of the art leads to the proposal of an FM-AM system to replace the FM-FM system. The AM radio link would be of synchronous type, without threshold, so that the FM-AM system is properly viewed as an FM system with frequency conversion. This has important advantages in spectrum utilization, receiving station design, and data reduction.

The Effect of Different Types of Video Filters on PDM-FM and PCM-FM Radio Telemetry—M. H. Nichols and A. T. Bublitz (p. 85)

The effects of two limiting types of video filters (namely the ideal low-pass vertical cutoff herein called the ILPF and the Gaussian) on the performance of PDM-FM are compared. It is found that minimum allowable pulse height controls the minimum allowed bandwidth with the Gaussian filter and if crosstalk suppression of 50 to 60 db is required, crosstalk controls the minimum allowed bandwidth of the ILPF. In PCM-FM using the sampling video detector, the critical effect is the overlapping of pulses at sampling time; using the integrading detector, the critical effect is the difference in area under the pulse with adjacent pulses not present and the area with no pulse present but the two adjacent pulses present. In general, the results of the theory agree well with experimental results of Aeronutronic and aid in their interpretation.

Ultrasonics Engineering

Vol. UE-7, No. 2, June, 1960

Ultrasonic Delay Lines Using Shear Modes in Strips—A. H. Meitzler (p. 35)

A new type of ultrasonic delay line is described in which piezoelectric, thickness-shear mode transducers are used to generate elastic shear wave motions in a delay medium having the form of a strip. By suitably arranging the transducers and delay medium, it is possible to obtain either dispersive or nondispersive propagation characteristics. An analysis of the elastic wave motion in the strip is given and formulas useful in the design and application of strip delay lines are derived. Results are given for the performance of experimental models operating in both dispersive and nondispersive conditions of pulse propagation.

Wire-Type Dispersive Ultrasonic Delay Lines—John E. May, Jr. (p. 44)

Ultrasonic delay lines are described which utilize the dispersion of longitudinal waves in cylindrical wires to provide a delay which is variable with frequency. Existence of an inflection point in the delay-vs-frequency characteristic for the first longitudinal mode allows the delay characteristics to be either approximately linear or to have positive or negative curvature. By operating below the cutoff frequency for the second longitudinal mode, the unwanted responses are limited mainly to flexural modes. Various designs are described which operate in different regions of the delay-vs-frequency characteristic. One model is described which departs by ± 7.5 microseconds from a linear delay slope of 1710 microseconds per megacycle over a 14 per cent band centered near 1.5 megacycles.

Dispersive Ultrasonic Delay Lines Using the First Longitudinal Mode in a Strip—T. R. Meeker (p. 53)

The existence of a dispersive longitudinal mode of propagation of elastic waves in a narrow strip is demonstrated experimentally. This mode corresponds closely to that predicted theoretically for the infinite plate with stress free surfaces.

Experimental delay lines using the first longitudinal mode in an aluminum alloy strip have been made. For a midband frequency of about 2 megacycles and a midband delay of about 1 millisecond, these delay lines have typical insertion losses of 15 db, typical discrimination to unwanted responses of 40 db over a 10 per cent band, delay changes of about 40 per cent of midband delay for frequency changes of about 15 per cent of midband frequency, and departures from linearity in the dependence of delay on frequency of about 1.2 per cent of midband delay for a frequency range of 15 per cent of the midband frequency.

The calculations used in the design of these lines are illustrated by a detailed example.

A Compact Electromechanical Band-Pass Filter for Frequencies Below 20 Kilocycles—W. P. Mason and R. N. Thurston (p. 59)

The filter structure, which can be milled or stamped from a single sheet of metal, consists of several bars parallel to each other, coupled at their midpoints by short torsionally vibrating shafts which are aligned at right angles to the bars. The torsional vibration of the couplers excites antisymmetric flexural vibration in the bars. The pass band is associated with the frequency of flexural resonance of the bars.

A composite piezoelectric (or electrostrictive) transducer for this filter also vibrates in antisymmetric flexure, the torsional drive resulting from the rotation of the central portion.

The theoretical capabilities of this arrangement are discussed and a test of the transducers is described.

Diffraction of a Narrow Beam of Light by Ultrasonic Waves—K. L. Zankel and E. A. Hiedemann (p. 71)

A light beam which is much narrower than one ultrasonic wavelength and which passes through the ultrasonic wave is deflected periodically. This causes broadening of an image formed by the light. The effects of the slit limiting the size of the light beam are included in an explanation of this phenomenon for progressive ultrasonic waves. The expressions are derived for the usual experimental conditions; they can be adapted to ultrasonic intensity measurements and ultrasonic stroboscopic investigations.

An Analytic Study of the Vibrating Free Disk—R. N. House, Jr. and J. Kritz (p. 76)

A piezoelectrically driven free disk vibrating in the first symmetrical mode has been shown to possess advantageous properties as a sonic source. Proper transducer design requires an evaluation of the disk's properties together with a development of the equivalent circuit. An expression for the deflection surface is presented which satisfies the necessary boundary conditions for a vibrating free circular plate. The potential and kinetic energies are derived which in turn lead to expressions for the equivalent stiffness and mass respectively. Expressions for the radiation impedance are developed using equivalent piston concepts. A derivation of the electromechanical transformer is given, together with an evaluation of the constants for quartz. The equivalent circuit, referred to center displacement, is constructed and the results are then compared with experimental data.

A Method for Improving Trace Brightness in Pulse Reflection Oscilloscope Displays—A. Lutsch (p. 85)

For several pulse reflection methods a low repetition frequency for the transmitter pulse must be chosen because multireflections and other groups of undesired pulses follow the wanted pattern. The brightness of the oscilloscope trace is improved if the repetition frequency is increased and frequency modulated. While the "desired" pattern is synchronized for the eye of an operator, the unwanted multireflections are rapidly moved across the oscilloscope screen.

Contributors (p. 88)

Vehicular Communications

VOL. VC-9, NO. 1, MAY, 1960

Impulse Noise Reduction Circuit for Communication Receivers—W. F. Chow (p. 1)

In this paper a comparatively simple scheme of reducing the impulse noise is suggested. This system consists of a gating signal generator and a balanced gate. It functions as follows: the impulse noise in the antenna triggers the gating signal generator. This generator produces a gating signal which in turn controls a balance gate. The function of the gate is to block the transmission during the gating period. Both the principle and the circuits of this impulse noise reduction scheme are described. Experimental results give the improvement of signal-to-noise ratio at the audio output ranging from 14 to 18 db.

A New Concept in the Reliability Evaluation of Vehicular Radio—Frederick L. Hilton (p. 10)

This paper describes automatic equipment developed to conduct temperature tests of two-way vehicular radio. The automatic test unit reported below controls the temperature chamber, maintains input voltages at proper EIA specified levels, turns test specimens on and off, measures the operational performance parameters of transmitters and receivers at each of the selected temperature conditions and prints the data. Four units can be tested at a time and these may be any combination of standard frequency bands, carrier or continuous tone coded squelch, and wide band or split channel.

The New Trend in Minified Communications Equipment—J. W. Knoll (p. 25)

This paper presents a brief description of the Micro-Module building-block and the current program status in terms of both up-to-date hardware accomplishments and future consideration, particularly in the area of miniaturized communications equipment. The advantages offered by the revolutionary Micro-Module are reviewed and illustrated with reference to size reduction and packaging design potential in the following:

(1) AN/PRC 36 Combat Helmet Radio Set
(2) AN/URC-11 Personal Rescue Receiver-Transmitter
(3) AN/PRC-25 Portable Radio Set
(4) IIF Single Sideband Receiver
(5) Non-Military and Commercial Communication Equipment

The Application of Semiconductors in a 860 MC Radio Receiver—L. G. Schimpf (p. 33)

An all solid state, FM radio receiver operating at 860 mc is described. The active elements used are transistors and variable reactance diodes. The receiver is of the double conversion type with IF frequencies at 63 and 10.7 mc.

The first local oscillator chain uses four stages to generate a signal at 923 mc. The crystal controlled oscillator and two frequency doublers use diffused base transistors. The output of the second doubler, at a frequency of approximately 300 mc, is then tripled in a circuit employing a varactor diode in order to obtain the desired local oscillator signal.

The receiver has a 6 db bandwidth of 30 kc. If the output is equalized for a phase modulated signal, 10 db of noise quieting is obtained with a 0.8 microvolt input signal.

A Hybrid Mobile Two-Way Radio—R. A. Beers, Jr. (p. 38)

Maximum effective use is made of transistors and tubes to achieve a mobile unit with superior performance characteristics and considerably improved reliability without, at the same time, appreciably increasing the cost of the radio equipment. No aspects of performance have been compromised to accommodate the use of transistors.

A rather unique mechanical design achieves a high degree of heat transfer from the interior of the mobile unit to the surrounding outside air. Both maintenance and production have been simplified by judicious use of "Circuit View" printed wiring in the more complex portions of the equipment. In addition, all critical adjustments have been designed out to further simplify routine maintenance adjustments. Maintenance may be performed using conventional test equipment and techniques.

Coordinated Broadband Mobile Telephone System—W. D. Lewis (p. 43)

The philosophy and broad outline of a coordinated broadband mobile telephone system are discussed. This system would be able to provide mobile telephone service of better quality than at present to many times the present number of customers. This could be made possible by means of an integrated switching and transmission design based upon a broad block of frequencies. All mobile units would be controlled over a data channel from a digital common control system at central.

The research, development, and production programs required to bring such a system into being would take a number of years, possibly as many as ten. Technical feasibility seems reasonably certain. To achieve economic feasibility might require a substantial effort. Realization of the system would have to be gradual and would require the cooperation of radio manufacturers, airplane and automobile manufacturers, and telephone companies.

Multi-Area Mobile Telephone System—H. J. Schulte, Jr. and W. A. Cornell (p. 49)

A research study directed toward a broadband, coordinated, mobile telephone system is reported. In particular, a system using many fixed transmitter-receiver installations is proposed. Such an arrangement has three principal advantages: (1) economy in spectrum usage, (2) relaxation of interference requirements in the fixed and mobile equipment, and (3) reduction of transmitter power. In order to gain these advantages, it is necessary to provide an interconnection facility for these many remote stations. Considerable use must also be made of modern high speed switching and common control techniques.

Precision Carrier Frequency Control and Modulation Phase Equalization of Base Transmitters in a Mobile Radio System—D. S. Dewire and E. A. Steere (p. 54)

Distortion-free reception by mobile units of base transmissions is essential in multiple base station mobile radio systems, where adjacent stations are operated simultaneously and modulated with the same intelligence. Phasing and heterodyne distortion factors in overlap coverage areas must be minimized. After many months of laboratory and field testing, a satisfactory solution has been developed and applied to a system using wire lines for base station and control point interconnection. This method provides precision control of carrier frequencies, and phase equalization of modulation by building out the wire lines so that transit times are equal. After two years of operation, this method has proven to assure satisfactory distortion-free reception.

Comparison of Wideband and Narrowband Mobile Circuits at 150 Megacycles—H. W. Nylund (p. 69)

This paper gives results of laboratory tests made to evaluate the relative transmission performances of wideband and narrowband mobile radio telephone circuits in the 150 mc band. It was found that the effects of changing from wideband to narrowband operation are dependent upon RF impulse noise, frequency errors and RF signal levels. Under ideal conditions the change to narrowband may improve circuit performance; but where impulse noise interference is severe, circuit performance will be seriously degraded unless rather large compensating changes can be made in such factors as RF signal power or average modulating levels.

A Transmission Line and Radiating System Measurement—W. F. Biggerstaff (p. 75)

One of the major problems in mobile system maintenance is adequate evaluation of the transmission line and antenna performance. This paper describes a practical method of technique for making line loss and antenna match measurements to assure proper installation and continued satisfactory performance. Certain innovations have been incorporated in the process which are calculated to provide the maximum information with a minimum effort.

The procedure consists essentially of making two transmission line input admittance measurements at widely differing frequencies. The results are plotted on a simplified version of the Smith Chart in a manner that yields transmission line loss and antenna match. These two properties adequately evaluate the transmission system for maintenance purposes.

Both measurements are made at the input end of the transmission line without altering or disturbing the antenna or load end of the line. This is important where tall towers are involved or the antenna is otherwise not readily accessible. Accuracies are more than adequate for service purposes and the results are consistent under a wide variety of conditions. A simple technique for determining the distance in feet to a fault such as a break or short circuit is also described.

An Omnidirectional Medium Gain 460 MC Base Station Antenna Using Simplified Suppressors—J. S. Brown (p. 80)

The use of suppressors to provide a collinear array that has a single feed point has been described. The suppressor design reported was one that provided optimum performance. During the course of the development program, several other types of suppressors were investigated. One type, although slightly inferior in performance to that described, is very attractive because of its simplicity. While it is not satisfactory for use in high gain (10 db) antennas, it is suitable for use in medium gain (4–6 db) antennas, and offers interesting cost reduction possibilities. The design and performance of a 6 db antenna for use in the 450–470 mc band is described.

Strictly Personal—George M. Dewire (p. 86)

Developments in miniaturization in radio design have been aimed for years at personalizing the equipment. The design parameters are affected by not only technical accuracy but also somewhat offset by personal likes and dislikes of the user. This paper describes a personal receiver in terms of development to achieve personal compatibility.

Mobile Interference Symposium—J. F. Chappell, W. A. Shipman, K. E. H. Backman, and B. H. Short (p. 91)

Abstracts and References

Compiled by the Radio Research Organization of the Department of Scientific and Industrial Research, London, England, and Published by Arrangement with that Department and *Electronic Technology* (incorporating *Wireless Engineer* and *Electronic and Radio Engineer*) London, England.

NOTE: The Institute of Radio Engineers does not have available copies of the publications mentioned in these pages, nor does it have reprints of the articles abstracted. Correspondence regarding these articles and requests for their procurement should be addressed to the individual publications, not to the IRE.

The number in heavy type at the upper left of each Abstract is its Universal Decimal Classification number. The number in heavy type at the top right is the serial number of the Abstract. DC numbers marked with a dagger (†) must be regarded as provisional.

UDC NUMBERS

Certain changes and extensions in UDC numbers, as published in PE Notes up to and including PE 666, will be introduced in this and subsequent issues. The main changes are:

Artificial satellites:	551.507.362.2	(PE 657)
Semiconductor devices:	621.382	(PE 657)
Velocity-control tubes, klystrons, etc.:	621.385.6	(PE 634)
Quality of received signal, propagation conditions, etc.:	621.391.8	(PE 651)
Color television:	621.397.132	(PE 650)

The "Extensions and Corrections to the UDC," Ser. 3, No. 6, August, 1959, contains details of PE Notes 598–658. This and other UDC publications, including individual PE Notes, are obtainable from The International Federation for Documentation, Willem Witsenplein 6, The Hague, Netherlands, or from The British Standards Institution, 2 Park Street, London, W.1., England.

ACOUSTICS AND AUDIO FREQUENCIES

534.2 2579
The Propagation of Sound in Lossy Media with Complex Shear and Compression Moduli—O. Weis. (*Acustica*, vol. 9, pp. 387–398; 1959. In German.)

A list of organizations which have available English translations of Russian journals in the electronics and allied fields appears at the end of the Abstracts and References section.

The Index to the Abstracts and References published in the PROC. IRE from February, 1959 through January, 1960 is published by the PROC. IRE, June, 1960, Part II. It is also published by *Electronic Technology* (incorporating *Wireless Engineer* and *Electronic and Radio Engineer*) and included in the April, 1960 issue of that Journal. Included with the Index is a selected list of journals scanned for abstracting with publishers' addresses.

534.23 2580
Sound Radiation from Plates with Point Excitation—M. Heckl. (*Acustica*, vol. 9, pp. 371–380; 1959. In German.) The finite radiation from an infinitely large plate with point excitation of damped flexural vibrations is calculated for flexural wavelengths smaller than the wavelength in air. Formulas are also obtained for finite plates and are checked by experiment.

534.23 2581
Sound Field of a Rectangular Piston—A. Freedman. (*J. Acoust. Soc. Amer.*, vol. 32, pp. 197–209; February, 1960.) The amplitude and phase pressure in the sound field are examined theoretically for ranges down to about a piston length. Laws of variation of this field are deduced, and the near field is compared with that of a circular piston.

534.232:534.38 2582
Designing Transducers for Sonar Systems—G. Rand. (*Electronics*, vol. 33, pp. 62–65; February 26, 1950.) Design charts and equivalent circuits are given for ADP crystal transducers.

534.24–14:534.88 2583
Reflection of Sound from Coastal Bottoms—K. V. Mackenzie. (*J. Acoust. Soc. Amer.*, vol. 32, pp. 221–231; February, 1960.) The theory for plane waves incident on a flat and uniform fluid bottom is discussed. A modification to Rayleigh's formula for reflection losses gives good agreement with experimental data.

534.26 2584
Scattering of a Plane Longitudinal Wave by a Spherical Fluid Obstacle in an Elastic Medium—N. G. Einspruch and R. Truell. (*J. Acoust. Soc. Amer.*, vol. 32, pp. 214–220; February, 1960.)

534.283–8:538.6 2585
Magnetic-Field Dependence of the Ultrasonic Attenuation in Metals—M. H. Cohen, M. J. Harrison and W. A. Harrison. (*Phys. Rev.*, vol. 117, pp. 937–952; February 15, 1960.) A self-consistent, semiclassical treatment of the attenuation of a sound wave by a free-electron gas in a positive background which supports the sound wave, with particular reference to the magnetic-field dependence of the propagation.

534.422:534.15 2586
High-Intensity Swept-Frequency Acoustic Test Equipment for the 1 to 60 kc/s Range—D. J. Birchall. (*Elec. Engrg.*, vol. 32, pp. 202–208; April, 1960.) Details are given of a siren source and a selective amplifier measuring channel which are locked to a reference frequency by means of thermistor control elements.

534.6:621.395.61 2587
The Determination of the Pressure Sensitivity of Microphones—H. G. Diestel. (*Acustica*, vol. 9, pp. 398–402; 1959. In German.) An experimental arrangement for determining the acoustic impedance of microphones over a wide frequency range is given. The calculation of the pressure sensitivity using a reciprocity method and the calibration of microphones in an air-filled coupler in the frequency range 30–15,000 cps are also discussed.

534.61–8 2588
Ultrasonic Attenuation Unit and its Use in Measuring Attenuation in Alkali Halides—B. Chick, G. Anderson and R. Truell. (*J. Acoust. Soc. Amer.*, vol. 32, pp. 186–193; February, 1960.) Attenuation and velocity are determined by measuring the amplitude decay and time interval of pulses reflected between parallel faces of the specimen. Details are given of the RF pulse generator, superheterodyne receiver, experimental-waveform generator, and delay, sweep and synchronization circuits for operation in the range 5–200 mc.

534.641:621.395.92 2589
The 2-ml Coupler and the High-Frequency Performance of Hearing Aids—H. C. van Eysbergen and J. J. Groen. (*Acustica*, vol. 9, pp. 381–386; 1959.) To avoid the sharp drop in response above 3 kc observed in measurements made with a 2-ml coupler, it is proposed to use a coupler with an air volume 0.5 ml in recording the frequency characteristic of hearing aids.

534.79 2590
Differences of Loudness in a Plane Wave and in a Diffuse Sound Field—W. Kuhl and W. Westphal. (*Acustica*, vol. 9, pp. 407–408; 1959. In German.) The results of subjective measurements of level differences are discussed with reference to loudness curves obtained by other authors. [See 1844 of 1960 (Jahn).]

534.84 2591
Room Acoustics Investigations with New Methods of Measurement in the Liederhalle Stuttgart—W. Junius. (*Acustica*, vol. 9, pp. 289–303; 1959. In German.) Sound distribution and reverberation are measured in a large concert hall using new techniques with microphones of spherical or highly directional response characteristics located at various points in the hall.

534.844.1 2592
Sound Energy Integrator with an Electrostatic Squaring Device—J. P. A. Lochner and P. Meffert. (*J. Acoust. Soc. Amer.*, vol. 32, pp. 267–273; February, 1960.) The instrument, developed for the analysis of reflection patterns in auditoriums, can integrate sound energy over predetermined short periods at any given interval after the direct sound.

534.845 2593
The Sound Absorption of Single Resonators for a Linear Arrangement in an Infinitely Large Wall and in a Closed Room—W. Wöhle. (*Hochfrequenz.*, vol. 68, pp. 7–14; May, 1959.) Interaction effects of the resonators are calculated and compared with results of measurements in a model chamber. (See also 1852 of 1960.)

534.846 2594
Acoustical Design and Performance of the Stratford (Ontario) Festival Theatre—R. H. Tanner. (*J. Acoust. Soc. Amer.*, vol. 32, pp. 232–234; February, 1960.)

534.846.6 2595
Models as an Aid in the Acoustical Design of Auditoria—A. K. Connor. (*Acustica*, vol. 9, pp. 403–407; 1959.) A review of experimental work on acoustic models indicates that they are of little direct value in auditorium design; their application is limited to investigations of specific physical problems.

621.395.623.54:534.833 2596
Variation in Ear Protector Attenuation as Measured by Different Methods—L. Weinreb and M. L. Touger. (*J. Acoust. Soc. Amer.*, vol. 32, pp. 245–249; February, 1960.) Results indicate that threshold shift measurements yield higher values of attenuation than either the loudness balance or the microphone method.

621.395.623.64 2597
The Determination of the Free-Field Response of Headphones—P. Bocker and H. Mrass. (*Acustica*, vol. 9, pp. 340–344; 1959. In German.) Two subjective methods, monaural and binaural, are used to test the response of an electrodynamic receiver in the frequency range 80–4000 cps. The monaural method may give unreliable results at low frequencies.

621.395.625.3 2598
The Influence of Magnetic Tape on the Field of a Recording Head—E. Della Torre. (*RCA Rev.*, vol. 21, pp. 45–52; March, 1960.) Expressions are derived for the potential in the tape and between the tape and the head, and curves are given for the variation of field with tape coating thickness and distance from the head.

621.395.625.3 2599
The Agfa Balancing Tape, an Aid to the Exact Adjustment of High-Frequency Balance in Magnetic Tape Recorders—F. Krones. (*Elektron. Rundschau*, vol. 13, pp. 181–184, 186; May, 1959.) The causes of the audibility of tape joints are discussed. Their effect can be reduced to a minimum with the aid of the test tape described in which the magnetic layer is given a periodic pattern. Other applications of the tape are mentioned.

621.395.625.3:538.221 2600
Determination of the Recording Performance of a Tape from its Magnetic Properties—E. D. Daniel and I. Levine. (*J. Acoust. Soc. Amer.*, vol. 32, pp. 258–267; February, 1960.) The recording performance of a tape with HF biasing is analyzed in terms of its anhysteretic properties (2466 of 1960) and results are compared with absolute measurements. Satisfactory agreement is obtained when the theory is corrected to take account of a loss in sensitivity attributed to a self-demagnetization effect during recording.

ANTENNAS AND TRANSMISSION LINES

621.315.212:539.12.04 2601
Gamma-Ray-Induced Conductivity in Polyethylene Coaxial Cable—K. Yahagi and A. Danno. (*J. Appl. Phys.*, vol. 31, p. 734; April, 1960.) A value of $\Delta = 0.68$ in the relation $I \propto R^{\Delta}$ where I is current and R the dose rate was obtained experimentally for dose rates up to 1.4×10^6 r/h.

621.372.2 2602
The Characteristic Impedance and Phase Velocity of a Shielded Helical Transmission Line—H. S. Kirschbaum. (*Commun. and Electronics*, no. 44, pp. 444–450; September, 1959.) Expressions for the characteristic impedance and phase velocity of a shielded line with an associated dielectric are developed from capacitance and inductance parameters. Experimental values for lines of length $\leq \lambda/4$ are in good agreement with calculations.

621.372.2:621.318.134:537.226 2603
Design Calculations for V.H.F. Ferrite Circulators—Y. Boyet, S. Weisbaum and I. Gerst. (IRE TRANS. ON MICROWAVE THEORY AND TECHNIQUES, vol. MTT-7, pp. 475–476; October, 1959.) Operating conditions of a coaxial ferrite phase shifter for 2 kmc [2963 of 1958 (Button)] have been scaled down for the 400–440-mc band. Design parameters are given.

621.372.8:537.226 2604
Experimental Determination of Wavelength in Dielectric-Filled Periodic Structures—E. Weissberg. (IRE TRANS. ON MICROWAVE THEORY AND TECHNIQUES, vol. MTT-7, pp. 480–481; October, 1959.) Determination of the elements of the scattering matrix [14 of 1954 (Deschamps)] avoids the errors incurred in the probe technique.

621.372.8.049 2605
Mechanical Design and Manufacture of Microwave Structures—A. F. Harvey. (IRE TRANS. ON MICROWAVE THEORY AND TECHNIQUES, vol. MTT-7, pp. 402–422; October, 1959. Abstract, PROC. IRE, vol. 48, p. 272; February, 1960.)

621.372.83 2606
Analytical Asymmetry Parameters for Symmetrical Waveguide Junctions—M. Cohen and W. K. Kahn. (IRE TRANS. ON MICROWAVE THEORY AND TECHNIQUES, vol. MTT-7, pp. 430–441; October, 1959. Abstract, PROC. IRE, vol. 48, p. 262; February, 1960.)

621.372.832 2607
A Method for Accurate Design of a Broad-Band Multibranch Waveguide Coupler—K. G. Patterson. IRE TRANS. ON MICROWAVE THEORY AND TECHNIQUES, vol. MTT-7, pp. 466–473; October, 1959. Abstract, PROC. IRE, vol. 48, p. 273; February, 1960.)

621.372.832.8 2608
Ferrite Phase-Shifter for Wide-Band Circulators—M. Vadnjal and A. Fiorini. (*Note Recensioni Notiz.*, vol. 8, pp. 305–313; May/June, 1959.) A nonreciprocal phase shifter for rectangular waveguide operating in the range 3.9–4.4 kmc is described.

621.372.85 2609
Orthogonality Relationships for Waveguides and Cavities with Inhomogeneous Anisotropic Media—A. T. Villeneuve. (IRE TRANS. ON MICROWAVE THEORY AND TECHNIQUES, vol. MTT-7, pp. 441–446; October, 1959. Abstract, PROC. IRE, vol. 48, p. 272; February, 1960.)

621.372.852.011.2 2610
Interaction-Impedance Measurements by Propagation-Constant Perturbation—P. R. McIsaac and C. C. Wang. (PROC. IRE, vol. 48, pp. 904–911; May, 1960.) General relations are developed for the perturbation produced by a rod inserted in a lossy nonreciprocal periodic waveguide parallel to the axis; these are applied to the determination of the interaction impedance.

621.372.852.1 2611
High-Power Microwave Rejection Filters Using Higher-Order Modes—J. H. Vogelman. (IRE TRANS. ON MICROWAVE THEORY AND TECHNIQUES, vol. MTT-7, pp. 461–465; October, 1959. Abstract, PROC. IRE, vol. 48, pp. 272–273; February, 1960.)

621.372.852.2:621.382.23 2612
Electronically Variable Phase Shifters Utilizing Variable-Capacitance Diodes—R. H. Hardin, E. J. Downey and J. Munushian. (PROC. IRE, vol. 48, pp. 944–945; May, 1960.) A phase shift $< 180°$ was obtained at 1 kmc for 1.2 db insertion loss.

621.372.852.21 2613
Note on Band Transmission in Multilayer Dielectric Filters—S. C. B. Gascoigne. (*Aust. J. Phys.*, vol. 12, pp. 296–298; September, 1959.) The filter action of an infinite medium is calculated by an adaption of the Kronig-Penney model for metal lattices.

621.372.852.3 2614
Mismatch Errors in Cascade-Connected Variable Attenuators—G. E. Schafer and A. Y. Rumfelt. (IRE TRANS. ON MICROWAVE THEORY AND TECHNIQUES, vol. MTT-7, pp. 447–453; October, 1959. Abstract, PROC. IRE, vol. 48, p. 272; February, 1960.)

621.396.67.095.1 2615
Generating a Rotating Polarization—P. J. Allen. (PROC. IRE, vol. 48, p. 941; May, 1960.) Outlines a method demonstrating how the rotation can be produced by a two-port circularly polarized antenna and two sources at different frequencies.

621.396.674.1 2616
Corner-Driven Coupled Square-Loop Antennas—S. Prasad. (*Canad. J. Phys.*, vol. 37, pp. 1407–1417; December, 1959.) The self-impedance and mutual impedance of two or more loops are derived when these are identical and stacked symmetrically with uniform spacing.

621.396.677.43 2617
Improved Antennas of the Rhombic Class—E. A. Laport and A. C. Veldhuis. (*RCA Rev.*, vol. 21, pp. 117–123; March, 1960.) Multiple rhombic antennas can give improved sidelobe suppression compared with the conventional rhombic. The results of tests on transatlantic transmissions are given.

621.396.677.45 2618
Improving the Helical Beam Antenna—A. G. Holtum, Jr. (*Electronics*, vol. 33, pp. 99–101; April, 1960.) Results of measurements made at 240 mc on a bifilar helix, compared with those for a single helix, show an improved directivity with a reduction in the sidelobe structure.

621.396.677.833.1 2619
Paraboloidal Reflector Aerial with a Helical Feed—H. E. Green. (PROC. IRE (*Australia*), vol. 21, pp. 71–83; February, 1960.) Design procedures are described and theoretical results are compared with those obtained experimentally at a frequency of 465 mc.

621.396.677.833.1 2620
Theoretical and Experimental Study of Wide-Band Paraboloid Antenna with Central-Reflector Feed—P. Foldes and S. G. Komlos. (*RCA Rev.*, vol. 21, pp. 94–116; March, 1960.) The theory and measurements of a circularly symmetrical high-gain paraboloidal antenna with a central reflector are summarized. The radiation pattern can be calculated by geometrical optics, but the impedance behavior is best found experimentally.

AUTOMATIC COMPUTERS

681.142 2621
Analogue Division Circuit—W. McMurray. (*Commun. and Electronics*, no. 45, pp. 606–612; November, 1959.) The circuit contains only magnetic cores and windings, and is suitable for use under severe environmental conditions. A detailed analysis is given.

681.142:621.318.4 2622
All-Transistor Magnetic-Core Memories—B. T. Goda, W. R. Johnston, S. Markowitz, M. Rosenberg and R. Stuart-Williams. (*Commun. and Electronics*, no. 45, pp. 666–673; November, 1959.) The properties of special small ferrite cores developed for use in high-speed transistor-drive storage systems are discussed.

681.142:621.395.625.3:621.318.57 2623
High-Speed Track Selection for a Magnetic Drum Store—A. D. Booth. (*Elec. Engrg.*, vol. 32, pp. 209–211; April, 1960.) A survey of mechanical and electronic relay switching systems is given and the advantages of transistor switch are discussed. A low-noise symmetrical transistor switch producing surges of less than 12 μsec duration is described.

CIRCUITS AND CIRCUIT ELEMENTS

621.3.011.3:621.385.5 2624
High-Q Inductance Simulation—J. E. Fulenwider. (PROC. IRE, vol. 48, pp. 954–955; May, 1960). Describes a circuit which eliminates the resistance component in a pentode reactance tube, giving a simulated inductance of infinite Q.

621.397.6:621.3.049.75 2625
The Application of Printed Wiring to Development and Small Batch Production with Particular Reference to Television Equipment—Davies. (See 2914.)

621.314.2.012.8 2626
An Equivalent Circuit for Transformers in which Nonlinear Effects are Present—H. W. Lord. (*Commun. and Electronics*, no. 45, pp. 580–586; November, 1959. Discussion.) Inductive parameters of a transformer are better represented by the H-type than by the T-type equivalent circuit.

621.318.435 2627
Analysis of Series-Connected Saturable Reactor with Capacitive Loading and Finite Control Resistance by Use of Difference Equations—H. C. Bourne and J. T. Salihi. (*Commun. and Electronics*, no. 45, pp. 461–471; November, 1959.)

621.318.435 2628
Observation of Transients in the Series-Connected Saturable Reactor with High-Impedance Control Source—H. L. Goldstein. (*Commun. and Electronics*, no. 45, pp. 521–526; November, 1959.) Details are given of apparatus for observing the effects of transients introduced into a reactor operating in the proportional mode.

621.319.4 2629
The Diffusion of Moisture in Electrical Capacitors and their Insulation Resistance—H. Veith. (*Frequenz*, vol. 13, pp. 142–147, 171–175; May/June, 1959.) The laws of moisture diffusion are derived mathematically and investigated experimentally on paper capacitors. The effect of moisture on the insulation resistance of the dielectric is calculated and comparison is made with measurements on plastic-covered capacitors stored under conditions of high humidity.

621.372.012 2630
The Optimum Formula for the Gain of a Flow Graph or a Simple Derivation of Coates' Formula—C. A. Desoer. (PROC. IRE, vol. 48, pp. 883–889; May, 1960.) An independent derivation of Coates' formula based on determinants is given. The difference between Mason's and Coates' flow graphs is discussed, and it is shown how one is obtained from the other.

621.372.4:621.318.4 2631
The Use of Iterated Laplace Transformations in the Solution of Combined Circuit-Field Problems—J. H. Mulligan, Jr. (*Commun. and Electronics*, no. 45, pp. 506–511; November, 1959.)

621.372.41 2632
The Characteristics of Different Types of Coupling of Two Coupled Undamped Electrical Oscillating Systems without an Impressed Voltage—D. Švarc. (*Arch. Elektrotech.*, vol. 44, pp. 234–250; 1959.) The effect of various types of coupling on the parameters of oscillatory circuits are considered.

621.372.44 2633
Statistical Spectral Output of Power-Law Nonlinearity—O. J. M. Smith. (*Commun. and Electronics*, no. 45, pp. 535–543; November, 1959.) Methods are given for calculating the output power and the error power for nonlinearities which can be described by power series for Gaussian and for certain other special kinds of input signals.

621.372.44 2634
Spectral Output of Piecewise-Linear Nonlinearity—O. J. M. Smith. (*Commun. and Electronics*, no. 45, pp. 543–549; November, 1959.) The transference or effective gain of a piecewise-linear component is derived.

621.372.5 2635
Topological Evaluation of Network Functions—W. H. Kim. (*J. Franklin Inst.*, vol. 267, pp. 283–293; April, 1959). The results are given of an investigation of various combinations of linear passive quadripoles by means of topological identities.

621.372.5 2636
The Analogy between the Weissfloch Transformer and the Ideal Attenuator (Reflection Coefficient Transformer) and an Extension to Include the General Lossy Two-Port—D. J. R. Stock and L. J. Kaplan. (TRANS. ON MICROWAVE THEORY AND TECHNIQUES, vol. MTT-7, pp. 473–474; October, 1959.)

621.372.512 2637
Matching and Bandwidths—H. Pecher. (*Frequenz*, vol. 13, pp. 161–166; June, 1959.) Formulas and curves are given for the bandwidth of different arrangements for input and output matching of single-stage and band-pass filters.

621.372.54 2638
The Structure of the Iterative Matrix of Reactance Quadripoles with a Given Derived Circuit or a Given Characteristic Function—G. Götz. (*Frequenz*, vol. 13, pp. 166–171; June, 1959.) The relations between the structure of the characteristic function, the iterative matrix and the derived circuit or canonical ladder network are established and the results are tabulated.

621.372.543 2639
Nomenclature of Band Filters and of Band-Filter Design—K. L. Eisele. (*Elektron. Rundschau*, vol. 13, pp. 169–175; May, 1959.) The principal design formulas and symbols and definitions of filter characteristics are summarized in tabular form.

621.372.6 2640
Solution to the Realizability Problem for Irredundant Boolean Branch Networks—L. Lofgren. (*J. Franklin Inst.*, vol. 268, pp. 352–377; November, 1959.) This type of network is defined for the 2-terminal and the n-terminal case and a general solution is given for the existence and realizability problem.

621.372.6 2641
Basic Concepts of the Multidimensional Space Filters—G. Kron. (*Commun. and Electronics*, no. 45, pp. 554–561; November, 1959.) The establishment of the basic tensors of a space filter is illustrated by means of a tetrahedron.

621.372.6 2642
Single-Control-Element Wien Bridge—E. R. Wigan. (*Electronic Technologist*, vol. 37, pp. 223–231; June, 1960.) The theory of operation of two modified forms of the Wien bridge is described. The network may be controlled by a single variable L, C or R and has applications as a frequency bridge, oscillator or selective amplifier.

621.372.6:621.316.727 2643
A Wide-Band Phase Shifter—A. A. Ahmed. (PROC. IRE, vol. 48, p. 945; May, 1960.) A method is described for obtaining a phase shift of exactly 90° over a bandwidth determined by the characteristics of the filter used.

621.372.632:621.382.23 2644
Low-Noise Tunnel-Diode Down-Convertor having Conversion Gain—K. K. N. Chang, G. H. Heilmeier and H. J. Prager. (PROC. IRE, vol. 48, pp. 854–858; May, 1960.) The nonlinearity of the negative-resistance characteristic of the tunnel diode can be used for frequency conversion. GaAs diodes given a conversion power gain of 22 db with a noise figure <30 db.

621.373.029.3 2645
Simple Amplitude-Stabilized Twin-T Audio Oscillator—C. Dean. (*Rev. Sci. Instr.*, vol. 31, pp. 213–214; February, 1960.) The stabilization is achieved by a clipping feedback loop.

621.373.1.029.422 2646
Electromechanical Low-Frequency Oscillator—E. W. Dickson. (*J. Sci. Instr.*, vol. 37, p. 149; April, 1960.) The sinusoidal linear movement of a slider is converted to a sinusoidal angular motion of a rotary potentiometer contact arm to provide electrical oscillations from 0.001–0.1 cps with amplitude distortion <1 per cent.

621.373.421–52:538.569.4 2647
Frequency Control of an Oscillator by Nuclear Magnetic Resonance—R. V. Pound and R. Freeman. (*Rev. Sci. Instr.*, vol. 31, pp. 96–102; February, 1960.) A description of a simple superregenerative oscillator that produces a coherent signal at the magnetic resonance frequency of a sample in its coil.

621.373.431.1 2648
Design Problems of Multivibrators—G. Kosel. (*Elektron. Rundschau*, vol. 13, pp. 165–168; May, 1959.) Design calculations for free-running, and for cathode-coupled and anode-coupled monostable multi-vibrator circuits are discussed.

621.373.431.2 2649
Blocking-Oscillator Circuit for Very Short Pulses of High Repetition Frequency—H. Hertwig. (*Elektron. Rundschau*, vol. 13, pp. 176–177; May, 1959). The design of a double-triode circuit is given which is capable of generating pulses of 45 mμsec base width at a free-running repetition frequency of 400 kc.

621.373.44:621.396.96 2650
Some Recent Improvements in Low-Power Pulse Generators—R. P. F. Lauder and P. A. James. (*J. Brit. IRE*, vol. 20, pp. 253–263; April, 1960.) Three miniature-thyratron circuits used as submodulators for radar transmitters are described. High-stability free-running and triggered versions are discussed with methods of overcoming duty-ratio limitations of the tubes used.

621.374.4:621.385.623 2651
Theory of a Fast-Switching Electron-Beam Frequency Divider—Kroll and Palócz. (See 2953.)

621.374.4:621.387 2652
Coherence and Bandwidth of a Gas-Discharge Harmonic Generator—N. R. Bierrum, D. Walsh and J. C. Vokes. (*Nature*, vol. 186, p. 626; May 21, 1960.) Coherent narrow-band signals at 8 mm λ have been obtained using Ne-filled discharge tubes pulsed by a 2-kw X-band klystron.

621.374.5:621.318.4 2653
Long Time Delays from a Single Magnetic Storage Core—C. E. Hardies. (*Commun. and Electronics*, pp. 457–461; November, 1959.) Time delays up to several minutes can be accurately achieved using an asymmetrical bidirectional core voltage. The delay may be controlled by a dc voltage or current change or by a change of resistance.

621.374.5:621.382.3 2654
Analysis and Design of a Transistor Linear-Delay Circuit—R. P. Nanavati. (*Commun. and Electronics*, pp. 577–580; November, 1959.) An analysis of the emitter-coupled linear-delay circuit is given. Maximum-to-minimum output pulse-width ratios of several hundred have been obtained.

621.375.13.018.75 2655
The Anode-Cathode Follower—C. H. Vincent and D. Kaine. (*Electronic Engrg.*, vol. 32, pp. 242–244; April, 1960.) A two-stage circuit of near-unity gain which inverts negative pulses is described. The unit is designed to transmit pulses of up to 50-v amplitude into a 100-Ω load.

621.375.3 2656
Analysis of Magnetic Amplifiers without Diodes—P. R. Johannessen. (*Commun. and Electronics*, no. 45, pp. 471–485; November, 1959.) A general method of magnetic-amplifier analysis is developed.

621.375.3 2657
Analysis of Magnetic Amplifier with Diodes—P. R. Johannessen. (*Commun. and Electronics*, no. 45, pp. 485–504; November, 1959.) An analysis restricted to amplifiers terminated in a resistive load and to voltage waveforms typical of such amplifiers.

621.375.3 2658
Graphical Evaluation of Magnetic Amplifier Performance Based on Constant-Voltage Reset Test—D. Nitzan. (*Commun. and Electronics*, no. 45, pp. 691–697; November, 1959. Discussion.) Core characteristics for various reset fluxes are determined experimentally, leading to a graphical evaluation of the performance of a 2-core self-saturating magnetic amplifier.

621.375.3 2659
Capacitively Coupled Magnetic Amplifiers—H. W. Collins. (*Commun. and Electronics*, no. 45, pp. 707–712; November, 1959.) The amplifier described operates at a high carrier frequency with capacitive coupling of the signal to the load. This technique realizes the advantages of true ac amplification. An experimental 3-stage amplifier is described.

621.375.3:621.318.435 2660
The Winding Capacitances in Magnetic Amplifiers—I. Johansen. (*Commun. and Electronics*, no. 45, pp. 702–707; November, 1959.) The distributed winding capacitance can be replaced by a lumped capacitance, for which an empirical formula is found.

621.375.4 2661
Calculations and Measurements for the Optimum Design of Low-Noise Transistor Amplfiers—K. Spindler. (*Nachrichtentech. Z.*, vol. 12, pp. 250–256; May, 1959.) The conditions for making the transistor noise factor a minimum are calculated for white noise. Equations are given for the most favorable combination of source impedance and emitter current. Measurements were made of these optimum values as a function of various transistor parameters and of temperature in the range $-90°$ to $+70°$C, and the resulting curves are given.

621.375.4 2662
Transistor Amplifier has 100-Megacycle Bandwidth—J. C. de Broekert and R. M. Scarlett. (*Electronics*, vol. 33, pp. 73–75; April 15, 1960.) Five stages with shunt feedback produce an over-all gain of 50 db ± 2 db from 8 kc to 130 mc.

621.375.432 2663
Analysis of the Split-Load State (Transistorized)—H. Pfyffer. (*Electronic Engrg.*, vol. 32, pp. 231–235; April, 1960.) Expressions are derived for the current and voltage gain, output impedance, and output return loss of a single-stage negative-feedback circuit. Results are incorporated in an analysis of a three-stage feedback amplifier with split-load output.

621.375.434 2664
Contribution on the Stabilization of the Operating Point of Transistors—K. Emden. (*Arch. elekt. Übertragung*, vol. 13, pp. 219–220; May, 1959.) Direct-current positive and negative feedback over two or more stages in earthed-emitter transistor amplifiers provides effective stabilization against temperature variations and differences in transistor characteristics.

621.375.9:538.569.4 2665
The Optimum Line Width for the Transition used in a Reflection Cavity Maser Amplifier—G. J. Troup. (*Aust. J. Phys.*, vol. 12, pp. 218–221; September, 1959.) The line width of the amplifying transition in a reflection cavity maser is shown to have an optimum value, which will give maximum amplification bandwidth at a fixed gain. Difficulties associated with achieving the optimum line width in practice for the paramagnetic maser are briefly discussed.

621.375.9:538.569.4 2666
Relaxation Time and Multiple Pumping Effects in Masers—A. Szabo. (*Canad. J. Phys.*, vol. 37, pp. 1557–1561; December, 1959.) Optimization of relaxation times combined with multiple pumping cannot by itself extend the operation of masers past the liquid-nitrogen range without degrading the performance below that now attainable at liquid-helium temperatures with three-level masers.

621.375.9:538.569.4 2667
Packaged Tunable L-Band Maser System—F. R. Arams and S. Okwit. (PROC. IRE, vol. 48, pp. 866–874; May, 1960.) A maser, tunable from 850 to 2000 mc with a voltage-gain × bandwidth product of 37.5 mc at 1.5°K, is combined with an L-band circulator and auxiliary equipment, into an operational unit. The circulator operates over a 200-mc range with insertion loss 0.3 db.

621.375.9:538.569.4 2668
Spontaneous Emission from an Inverted Spin System—A. Yariv. (*J. Appl. Phys.*, vol. 31, pp. 740–741; April, 1960.) A summary of results of calculation made in an attempt to explain the origin of the observed modulation effects in two-level masers.

621.375.9:538.569.4.029.65 2669
C.W. Millimetre-Wave Maser Using Fe^{3+} in TiO_2—S. Foner and L. R. Momo. (*J. Appl. Phys.*, vol. 31, pp. 742–743; April, 1960.) Characteristics are summarized and some useful properties of the paramagnetic material are described. Results indicate that the material will be useful far beyond the frequency range investigated, 26–39 kmc.

621.375.9:621.372.44 2670
Some Notes on the History of Parametric Transducers—W. W. Mumford. (PROC. IRE, vol. 48, pp. 848–853; May, 1960.) 200 references.

621.375.9:621.372.44 2671
A Ferromagnetic Amplifier Using Longitudinal Pumping—R. T. Denton. (PROC. IRE, vol. 48, pp. 937–938; May, 1960.) Describes early experimental results indicating a 25-db gain at 4 kmc with an X-band pump power <1 w.

621.375.9:621.372.44 2672
Parametric Phase-Distortionless L-Band Limiter—A. D. Sutherland and D. E. Countiss. (PROC. IRE, vol. 48, pp. 938–939; May, 1960.) 30-db dynamic limiting is observed at a pump frequency of 1 kmc using a 3-cavity varactor arrangement. Phase distortion is less than $\pm 2°$ over a 16-db range of limiting.

621.375.9:621.372.44:621.372.2 2673
The Diode-Loaded Helix as a Microwave Amplifier—G. Conrad, K. K. N. Chang and R. Hughes. (PROC. IRE, vol. 48, pp. 939–940; May, 1960.) Two alloy-diffused Ge diodes mounted between turns of the helix lead to a net power gain of 26 db at 2800 mc, a noise factor of 5–7 db, and a bandwidth of 30 mc. The low bandwidth is attributed to the loading introduced by the diodes. [See also 1167 of 1960 (Heilmeier).]

621.376.2 2674
Application of the Sampling Function to Circuit Analysis of Modulators and Demodulators Using Diodes—A. Feller. (*RCA Rev.*, vol. 21, pp. 130–141; March, 1960.) Takes into account the forward and reverse resistance of the diodes.

621.376.239:621.385.6 2675
A Broad-Band Cyclotron-Resonance R.F. Detector Tube—F. M. Turner. (PROC. IRE, vol. 48, pp. 890–897; May, 1960.) Operation is based on the cyclotron resonance of an electron beam in a static magnetic and RF electric field. In the pencil-beam tube described, spiralling electrons are detected by a honeycomb-mesh grid; the current intercepted by the grid is greatest at resonance and is proportional to the RF signal power. Mechanical details and operating conditions are given. A simplified energy-transfer analysis enables the electrical characteristics to be predicted.

GENERAL PHYSICS

53.081.6 2676

Universal Units of Magnetism, Mechanics and Temperature—A. T. Gresky. (*J. Franklin Inst.*, vol. 268, pp. 388–400; November, 1959.) Suggested practical values for universal units are: magnetic intensity $M=1.84253$G; mass $m=217.699$g; length $r=1.61562$ cm; time $t=0.538912$ sec.; temperature $°T=0.0708681°$K. (See also 1172 of 1960.)

535.62 2677

Some New Aspects of Colour Perception—M. M. Woolfson. (*IBM J. Res. Dev.*, vol. 3, pp. 313–325; October, 1959.) Computed theoretical figures, based on mathematical analysis, are shown to be in good agreement with empirical results of Land (see 3629 of 1959). An explanation is given in terms of classical color perception theories in conjunction with the experimental psychological phenomenon of color transformation.

537.29:537.56:621.385.833 2678

Efficiency of Field Ionization at a Metal Surface—H. Fiedeldey and D. Fourie. (*Phys. Rev.*, vol. 117, pp. 924–928; February 15, 1960.) Theoretical analysis of the dependence of the field ion current on various parameters.

537.311.1 2679

Variational Principle for Transport Phenomena—G. E. Tauber. (*J. Franklin Inst.*, vol. 268, pp. 175–221; September, 1959.) The variational principle for interband scattering is derived and generalized by the introduction of an external magnetic field and lattice vibrations.

537.312.62 2680

Quasi-Particles and Gauge Invariance in the Theory of Superconductivity—Y. Nambu. (*Phys. Rev.*, vol. 117, pp. 648–663; February, 1960.)

537.312.8 2681

Theory of Electrical Conduction in High Magnetic Fields—P. N. Argyres and L. M. Roth. (*J. Phys. Chem. Solids*, vol. 12, pp. 89–96; December, 1959.)

537.52 2682

The Rôle of Space Charge in Gas Break-Through between Equal Parallel Plane Electrodes below the Paschen *PD* Minimum—H. Ritow. (*J. Electronics Control*, vol. 7, pp. 423–438; November, 1959.) The Paschen characteristics for discharges is discussed in detail and some explanations are found with the help of the field-emission theory.

537.525 2683

Similitude and Anode Material Effects in H_2 and D_2 Discharges below the Critical Pressure—G. W. McClure. (*J. Electronics Control*, vol. 7, pp. 439–447; November, 1959.) The breakdown potentials of H_2 and D_2 gases were determined below the critical pressure in two similarly shaped discharge tubes of different size. With stainless steel anodes and cathodes both gases obeyed Paschen's Law. When the anodes were made of Pb or Al some deviations were observed, possibly resulting from deposition of anode material on the cathode.

537.525.5:621.391.822 2684

Microwave Noise from Low-Pressure Arcs—R. M. Hill and S. K. Ichiki. (*J. Appl. Phys.*, vol. 31, p. 735; April, 1960.) Experimental data indicate that the ignition of an arc discharge is accompanied by considerable microwave noise.

537.533 2685

Solutions of the Equations of Space-Charge Flow for Radial Flow between Concentric Spherical Electrodes—I. Itzkan. (*J. Appl. Phys.*, vol. 31, pp. 652–655; April, 1960.) The solutions are formulated so that arbitrary initial conditions may be introduced. By this means a variety of physical problems can be solved with the aid of a table of Airy functions.

537.533:621.385.6 2686

Some Solutions to the Equations of Steady Space-Charge Flow in Magnetic Fields—P. T. Kirstein. (*J. Electronics Control*, vol. 7, pp. 417–422; November, 1959.) Earlier analysis [764 of 1959 (Kirstein and Kino)] is extended to include the case of magnetic-field components perpendicular to the cahode. Sets of solutions are given for the flow from conical and cylindrical cathodes for a broad class of magnetic-field configurations.

537.533.08 2687

The Possibility of Electron Total-Energy-Distribution Analysis in a Quasi-Spherical Capacitor—D. A. Ganichev and K. G. Umkin. (*Fiz. Tverdogo Tela*, vol. 1, pp. 648–653; April, 1959.) The energy distribution of electrons emitted at various angles from a plane disk-shaped target at the center of a spherical collector is determined from an analysis of electron trajectories. The discrepancy between these results and those for a spherical capacitor does not exceed 1 per cent. The provision of an aperture in the collector for an electron gun results in a 5 per cent error.

537.533.73 2688

The Formulation of Electron Difffraction by Means of a Scattering Matrix and its Practical Applicability—H. Niehrs. (*Z. Naturforsch.*, vol. 14a, pp. 504–511; May/June, 1959.) Electron diffraction by a crystal plate is treated by dynamic diffraction theory.

537.533.73 2689

Apparatus for Direct Observation of Low-Energy Electron Diffraction Patterns—E. J. Scheibner, L. H. Germer and C. D. Hartman. (*Rev. Sci. Instr.*, vol. 31, pp. 112–114; February, 1960.) The equipment, designed for high vacuum, gives the diffraction pattern on a fluorescent screen.

537.533.79:538.221 2690

On the Magnetic Perturbation of an Electron Beam—S. Yamaguchi. (*Indian J. Phys.*, vol. 33, pp. 547–549; December, 1959.) (See 3636 of 1959.)

537.56 2691

A New Method for Measuring the Attachment of Slow Electrons in Gases—L. G. H. Huxley, R. W. Crompton and C. H. Bagot. (*Aust. J. Phys.*, vol. 12, pp. 303–308; September, 1959.) Simultaneous measurements of attachment coefficient and the ratio of drift velocity to diffusion coefficient are reported.

537.56 2692

Measurement of Plasma Temperature and Electron Density—K. Murakawa and S. Hashimoto. (*J. Phys. Soc. Japan*, vol. 14, p. 1824; December, 1959.) The value of electron density deduced earlier (451 of 1960) is twice the true value.

538.56:537.56 2693

Microwave Investigation of Plasma in Shock Tube—M. Takeyama, S. Hamamura and T. Oda. (*J. Phys. Soc. Japan*, vol. 14, pp. 1637–1638; November, 1959.) Experimental details and results obtained at 3.4 cm λ are given.

538.566:535.42 2694

On the Diffraction of Electromagnetic Pulses by Curved Conducting Surfaces—J. R. Wait and A. M. Conda. (*Canad. J. Phys.*, vol. 37, pp. 1384–1396; December, 1959.) "Starting with the known steady-state solutions for diffraction by a perfectly conducting convex surface, the corresponding transient responses are derived using Fourier-Laplace inversion. Explicit results are given for an incident wave which varies with time as a step function."

538.566:535.43 2695

Total Electromagnetic Cross-Sections of Imperfectly Conducting Cylinders—E. S. Cassedy and J. Fainberg. (*J. Appl. Phys.*, vol. 31, pp. 739–740; April, 1960.) Experimental and theoretical results are discussed for the case of scattering from cylinders with length comparable to and with diameter small compared with the wavelength of illumination.

538.566:539.23 2696

Use of Chebychev Polynomials in Thin-Film Computations—K. D. Mielenz. (*J. Res. Nat. Bur. Stand.*, vol. 63A, pp. 297–300; November/December, 1959.) "From Herpin's expression from the mth power of a multilayer matrix (3865 of 1947), very simple closed formulas are derived for the matrices and optical constants of any multilayer with a periodic structure."

538.569.4:535.853 2697

High-Resolution N.M.R. Spectrometer with the Radio Frequency Controlled by the Magnetic Field—R. Freeman and R. V. Pound. (*Rev. Sci. Instr.*, vol. 31, pp. 103–106; February, 1960.) A spectrometer for observing proton magnetic resonance at 30 mc.

538.569.4:535.853 2698

Precision Zeeman-Modulation Microwave Spectrometer—R. W. Zimmerer. (*Rev. Sci. Instr.*, vol. 31, pp. 106–111; February, 1960.) A spectrometer is described for measuring the rotational fine structure of oxygen at frequencies between 50 and 65 kmc.

538.569.4.029.64.65:546.217 2699

Anomalies in the Absorption of Radio Waves by Atmospheric Gases—A. W. Straiton and C. W. Tolbert. (Proc. IRE, vol. 48, pp. 898–903; May, 1960.) Reasonable agreement is shown between the losses predicted by Van Vleck (3098 and 3100 of 1947) and recent measurements for oxygen, but for water vapor the measured loss is greater. Reasons for the discrepancy are discussed.

539.12 2700

Remarks on the Mass, Energy and Momentum of Photons, Electrons and other Elementary Particles—J. Picht. [*Optik* (*Stuttgart*), vol. 16, pp. 257–275; May, 1959.] Relations between the corpuscular velocity of a particle and the phase velocity of the corresponding wave are considered, and the theoretical equivalence of particle and wave are discussed with reference to a possible experimental verification of the particle concept.

GEOPHYSICAL AND EXTRATERRESTRIAL PHENOMENA

523.164.3 2701

A Note on the Polar Apsorption Event of 11–18 May 1959—K. W. Eriksen, O. Holt and B. Landmark. (*J. Atmos. Terr. Phys.*, vol. 18, pp. 78–81; April, 1960.) Galactic noise measurements at five stations showed an increase in absorption lasting up to 36 h. Possible solar control mechanisms are discussed.

523.164.3:523.75 2702

Extraordinary Noise Distrubances Following a Mögel-Dellinger Effect—H. A. Hess and K. Rawer. (*Geofis. pura e appl.*, vol. 45, pp. 175–178; January–April, 1960. In German.) During the large solar eruption of March 29, 1960 an initial decrease of cosmic noise intensity ob-

served was followed by a high-intensity noise burst lasting several hours.

523.164.32:523.165 2703
A Relation between Solar Radio Emission and Polar-Cap Absorption of Cosmic Noise—M. R. Kundu and F. T. Haddock. (*Nature*, vol. 186, pp. 610–612; May 21, 1960.) A statistical study has been made of the relation. It appears that the polar-cap absorption events are closely associated with the occurrence of wide-band cm-wave outbursts or type IV events and their duration is related to the presence on the sun of "active regions" of noise storms. [See also 842 of 1960 (Thompson and Maxwell).]

523.164.32:523.75 2704
Radio Astronomical Measurements of the Sun with Particular Regard to the Phenomena during Chromospheric Eruptions—O. Hachenberg. (*Naturwiss.*, vol. 46, pp. 295–303; May, 1959.) Survey of the measurements of solar RF emission in relation to various types of solar disturbance. 17 references.

523.164.4 2705
A Shell Source of Radio Emission—P. R. R. Leslie. (*Observatory*, vol. 80, pp. 23–26; February, 1960.) Report of observations made with the 178-mc interferometer at the Mullard Radio Astronomy Observatory, Cambridge, Eng.

523.164.4 2706
The Eta Carinae Nebula and Centaurus A near 1400 Mc/s: Part 1—Observations—J. V. Hindman and C. M. Wade. (*Aust. J. Phys.*, vol. 12, pp. 258–269; September, 1959.) Continuum measurements made with a modified 21-cm receiver and a 36-ft-diameter antenna show Centaurus A to cover 7° in declination and 3° in R.A. at 1400 mc. Flux densities and contour diagrams are given.

523.164.43 2707
A 21-cm Survey of the Southern Milky Way—F. J. Kerr, J. V. Hindman and C. S. Gum. (*Aust. J. Phys.*, vol. 12, pp. 270–292; September, 1959.) A report of measurements made using a beamwidth of 1.4° and bandwidth 40 kc. Contour diagrams show the radiation intensity along 41 measured tracks.

523.165 2708
Elementary Particles in Cosmic Radiation—E. Schopper. (*Naturwiss.*, vol. 46, pp. 290–295; May, 1959.) Review of present state of knowledge and measurement techniques.

523.165 2709
Cosmic-Radiation Intensity Decreases observed at the Earth and in the Nearby Planetary Medium—C. Y. Fan, P. Meyer and J. A. Simpson. (*Phys. Rev. Lett.*, vol. 4, pp. 421–423; April 15, 1960.) Measurements made simultaneously at 7.5 earth radii, at balloon altitudes and on the earth's surface at the time of a large Forbush decrease show the same magnitude of decrease of primary cosmic radiation. These results do not therefore agree with hypotheses which invoke the presence of the earth and the geomagnetic field to account for the Forbush decrease.

523.165 2710
Maximum Total Energy of the Van Allen Radiation Belt—A. J. Dessler and E. H. Vestine. (*J. Geophys. Res.*, vol. 65, pp. 1069–1071; March, 1960.) The results of the spherical harmonic analysis of the geomagnetic field show an upper limit for the energy that can be stored in the Van Allen radiation belt.

523.165:550.385:551.507.362.2 2711
Distribution of Trapped Radiation in the Geomagnetic Field—S. Yoshida, G. H. Ludwig and J. A. Van Allen. (*J. Geophys. Res.*, vol. 65, pp. 807–813; March, 1960.) An examination of the altitude dependence (360–2090 km) of trapped radiation from Explorer I measurements shows that the radiation-intensity data in the vicinity of the magnetic equator can be well represented by the scalar intensity B of the real geomagnetic field. The value of B at the lower boundary of the inner zone increases with magnetic dip latitude.

523.165:550.385.4:551.507.362.2 2712
Magnetic Storms and the Van Allen Radiation Belts—Observations from Satellite 1958 ε (Explorer IV)—P. Rothwell and C. E. McIlwain. (*J. Geophys. Res.*, vol. 65, pp. 799–806; March, 1960.) A marked decrease in intensity of particles in the outer belt was observed during magnetic storms. It is suggested that this is due to atmospheric heating and expansion at fairly high latitudes. The absence of intensity changes in the inner belt is consistent with a cosmic-ray albedo neutron origin of inner-zone protons.

523.3:621.396.96 2713
Radio-Frequency Scattering from the Surface of the Moon—R. L. Leadabrand, R. B. Dyce, A. Fredriksen, R. I. Presnell and J. C. Schlobohm. (PROC. IRE, vol. 48, pp. 932–933; May, 1960.) Sensitive radars show the presence at 400 mc of a scattered component in addition to the quasi-specular "high-light" from the moon center.

523.3:621.396.96 2714
Measurements of Lunar Reflectivity using the Millstone Radar—G. H. Pettengill. (PROC. IRE, vol. 48, pp. 933–934; May, 1960.) Highly stable coherent-pulse measurements made at 440 mc enable range/Doppler-frequency contours to be plotted for the rotating moon. A precision of 2 parts in 10^5 for the observed Doppler frequency has been obtained. A number of measurements are described; substantial echoes are observed out to the lunar limbs.

523.3:621.396.96 2715
Lunar Echoes Received on Spaced Receivers at 106.1 mc—R. B. Dyce and R. A. Hill. (PROC. IRE, vol. 48, pp. 934–935; May, 1960.) Results obtained imply that a minimum diversity distance of about 1 km on the earth's surface is adequate to achieve diversity reception for communications via the moon.

523.7:621.396.969 2716
Radar Echoes from the Sun—V. R. Eshleman, R. C. Barthle and P. B. Gallagher. (*Science*, vol. 131, pp. 329–332; February 5, 1960.) Details are given of tests made in April, 1959 using a 40-kw transmitter operating at about 25.6 mc with an antenna system consisting of four rhombics in broadside array covering a rectangular area 800×725 ft. Data were analyzed by computer; cross-correlation curves are reproduced and discussed.

523.75:551.594.6 2717
Solar Limb Surges accompanied by X-Ray Emission—J. Kleczek and L. Křivský. (*Nature*, vol. 186, pp. 1035–1036; June 25, 1960.) Simultaneous observations of Hα radiation and recordings of atmospherics at 27 kc indicate a pronounced coincidence in time of sudden enhancements of atmospherics with surge appearances. The sudden enhancements could be interpreted as X radiation emitted by an adjacent region of the solar corona.

550.3:551.510.535:519.272 2718
Correlation in Geophysics—K. Rawer. (*Geofis. pura e appl.*, vol. 43, pp. 218–226; May–August, 1959. In English.) The advantages of using a correlation number based on a counting process are discussed in comparison with the limitations inherent in the use of a correlation coefficient. Examples are given of the correlation of ionospheric data.

550.38 2719
Earth's Main Magnetic Field to 152 Kilometres above Fort Churchill—J. M. Conley. (*J. Geophys. Res.*, vol. 65, pp. 1074–1075; March, 1960.) A report on rocket flight measurements under magnetically quiet conditions in the daytime.

551.507.362 2720
Rockets and Satellites in the Service of Geophysics—E. Stuhlinger. (*Naturwiss.*, vol. 46, pp. 303–309; May, 1959.) A review of measurements made by artificial satellites with an outline of future plans.

551.507.362:061.3 2721
Space Science—R. L. F. Boyd. (*Nature*, vol. 186, pp. 749–751; June 4, 1960.) A report of the International Space Science Symposium held in Nice, France, January 11–15, 1960, reviewing in particular the results of earth-satellite and lunar-probe measurements.

551.507.362.2 2722
Magnetic Damping of Rotation of the Vanguard I Satellite—L. LaPaz and R. H. Wilson, Jr. (*Science*, vol. 131, pp. 355–357; February 5, 1960.) Comment on an error in calculations given in 1592 of 1960 and author's reply.

551.507.362.2 2723
Density of the Upper Atmosphere and its Dependence on the Sun, as revealed by Satellite Orbits—D. G. King-Hele and D. M. C. Walker. (*Nature*, vol. 186, pp. 928–931; June 18, 1960.) An extension of earlier work (1997 of 1960).

551.507.362.2 2724
Triangulation—a Precise Method for Satellite Tracking—P. G. Kirmser and I. Wakabayashi. (*J. Franklin Inst.*, vol. 268, pp. 337–351; November, 1959.) The theory of triangulation is described and applied to a photographic system.

551.507.362.2 2725
Determination of Corrections to Mark II Minitrack Station Coordinates from Artificial-Satellite Observations—W. D. Kahn. (*J. Geophys. Res.*, vol. 65, pp. 845–849; March, 1960.) Corrections may be deduced from a comparison of radio observations with the predicted orbit.

551.507.362.2 2726
Radio Observations during the Decay Period of the Soviet Satellite 58-Delta Two [1958 δ2]—H. A. Hess. (*Geofis. pura e appl.*, vol. 45, pp. 62–64; January–April, 1960. In English.) Measurements made at Breisach, West Germany, on Sputnik III during the period March 14–April 6, 1960 show irregularities in the period of revolution.

551.507.362.2 2727
Faraday Effect in the Transmissions from Fast-Spinning Satellites—R. S. Roger and J. H. Thomson. (*Nature*, vol. 186, pp. 622–623; May 21, 1960.) A note on signal-strength variations for the case of a satellite rotation period small compared to the Faraday fading period.

551.507.362.2:551.510.535 2728
Scintillations of the 20-Mc/s Signal from the Earth Satellite 1958 δII—J. Frihagen and J. Trøim. (*J. Atmos. Terr. Phys.*, vol. 18, pp. 75–78; April, 1960.) Information on the structure and movements of ionospheric irregularities has been obtained by studying fading patterns on spaced receivers.

551.507.362.2:551.510.535 2729
Electron Density Measurements in the Upper Ionosphere using the Faraday Rotation of Radio Signals from Artificial Satellites—D. M. A. Wilson. (*Nature*, vol. 186, pp. 623–624; May 21, 1960.) Agreement between observations and the calculated Faraday-rotation curve is improved when account is taken of horizontal variations of the ionosphere estimated from hourly ionograms.

551.507.362.2:621.317.444:538.569.4 2730
The Vector-Field Proton Magnetometer for I.G.Y. Satellite Ground Stations—I. R. Shapiro, J. D. Stolarik and J. P. Heppner. (*J. Geophys. Res.*, vol. 65, pp. 913–920; March, 1960.) Vector magnetic field measurements of high accuracy can be obtained by applying homogeneous bias fields to a proton precessional magnetometer.

551.507.362.2:621.382.3 2731
Radiation Damage and Transistor Life in Satellites—Denney and Pomeroy. (See 2932.)

551.510.535 2732
Artificial Electron Clouds: Part 4—J. Pressman, F. F. Marmo and L. M. Aschenbrand. (*Planet. Space Sci.*, vol. 2, pp. 17–25; October, 1959.) Report of radio-radar and optical observations of an electron cloud created by the night-time release of cesium at 101 km from a Nike-Cajun rocket. An analysis of experimental data indicates that the electrons observed can reasonably be ascribed to thermal ionization. [See pt. 3: 2366 of 1960 (Marmo, *et al.*).]

551.510.535 2733
A Theory of Electrostatic Fields in the Ionosphere at Nonpolar Geomagnetic Latitudes—D. T. Farley, Jr. (*J. Geophys. Res.*, vol. 65, pp. 869–877; March, 1960.) Electrostatic coupling between the dynamo and F regions, and between magnetically conjugate parts of the regions themselves, the electric source field produced by winds in the dynamo region, and the possibility of significant electron-density variations in the F region due to electrostatic fields are examined.

551.510.535 2734
Development of the Maximum Electron Density of the E Layer at Leopoldville-Binza—P. Herrinck and J. Goris. (*Geofis. pura e appl.*, vol. 45, pp. 153–166; January–April, 1960. In French.) E-layer data obtained during the period February, 1952—December, 1958, are analyzed. The diurnal variation of maximum electron density conforms closely to Chapman's law.

551.510.535 2735
Sporadic-E as Observed by Back-Scatter Techniques in United Kingdom—E. D. R. Shearman and J. Harwood. (*J. Atmos. Terr. Phys.*, vol. 18, pp. 29–42; April, 1960.) Using a rotating-antenna back-scatter sounder during the IGY diurnal, seasonal and grographical E_s characteristics have been obtained. On particular occasions the movement of E_s clouds has been tracked and their size and ionization determined.

551.510.535 2736
Peculiarities of the Ionosphere in the Far East: a Report on I.G.Y. Observations of Sporadic E- and F-Region Scatter—E. K. Smith, Jr., and J. W. Finney. (*J. Geophys. Res.*, vol. 65, pp. 885–892; March, 1960.) Oblique-incidence observations at 50 mc show that for any given transmission loss sporadic E is three to five times more prevalent in the Far East than in the Caribbean.

551.510.535 2737
Height and Thickness Parameters for Region F of the Ionosphere—E. R. Schmerling. (*J. Geophys. Res.*, vol. 65, pp. 1072–1073; March, 1960.) More useful parameters may be obtained by replacing measurements of h_m by measurements of heights at fixed submultiples of the maximum density.

551.510.535 2738
Theoretical World Curves of Maximum Ion Density in a Quiet F Region—J. E. C. Gliddon and P. C. Kendall. (*J. Atmos. Terr. Phys.*, vol. 18, pp. 48–60; April, 1960.) The curves, plotted in terms of latitude and local time for solstice and equinox conditions, are generally the same as those measured practically. The analysis shows that diffusion plays a significant part in controlling F_2 ionization.

551.510.535 2739
Asymmetry between the F_2 Region of the Ionosphere in the Northern and Southern Hemispheres—R. G. Rastogi. (*J. Geophys. Res.*, vol. 65, pp. 857–868; March, 1960.) An explanation is sought of the asymmetry in the seasonal variations of the critical frequency of the F_2 layer at high-latitude stations in the northern and southern hemispheres during years of minimum sunspot number. An extensive survey suggests that horizontal wind systems in the F_2 region may be the cause.

551.510.535 2740
Spread-F in Baguio through Half a Solar Cycle—V. Marasigan. (*J. Atmos. Terr. Phys.*, vol. 18, pp. 43–47; April, 1960.) A statistical survey over 6 years shows that the occurrence of spread-F is associated with periods of downward movement of ionization. The seasonal and diurnal variation of occurrence is also markedly different between periods of high and low solar activity.

551.510.535 2741
Critical Remarks on the Description of the Ionization in the Ionospheric E layer—R. Eyfrig. (*Geofis. pura e appl.*, vol. 45, pp. 179–184; In German.) Changes from nominal value in the exponent of the $\cos^{\frac{1}{2}}\chi$ law of E-layer ionization are discussed; these are necessitated by the difference between seasonal and daily variation of E-layer noon values. Harnischmacher's empirical formula for this exponent (1682 of 1950) is not confirmed by an analysis of data for 1952–1959. The derivation of a world-wide E-layer character figure from data obtained at one locality [1580 of 1960 (Minnis and Bazzard)] is considered impossible in view of geographic differences in ionization characteristics.

551.510.535:523.745 2742
Some Abnormalities in the Variations of F_2-Layer Critical Frequency during the Period of High Solar Activity of Solar Cycle 8–19—C. M. Huang. (*J. Geophys. Res.*, vol. 65, pp 897–906; March, 1960.) The values of foF_2 at Taipei become independent of sunspot numbers at high solar activity. This saturation effect is related to other abnormalities in the variations of foF_2 at this station.

551.510.535:523.75 2743
The Ionosphere and Solar Activity—N. C. Gerson. (*Geofis. pura e appl.*, vol. 45, pp. 117–122; January–April, 1960. In English.) "The correlation between monthly median critical frequencies and solar activity was determined for Washington, D. C. Results were compared with those from a similar study made for six Arctic stations. For noon data (E, F_2 and F_2 layers), a greater value of f_c (at zero sunspot number) and a slightly greater slope were obtained for Washington than for the Arctic locations. The influence of increased solar activity on the behaviour of the midnight ionosphere is discussed."

551.510.535:523.78 2744
The "Valley Effect" in the Interpretation of Ionospheric Eclipse Records—J. A. Gledhill and A. D. M. Walker. (*J. Atmos. Terr. Phys.*, vol. 18, pp. 61–64; April, 1960.) The spurious maxima in electron-density curves at fixed heights can be explained by the presence of a valley between the F_1 and F_2 layers.

551.510.535:523.78 2745
Effect of Annular Solar Eclipse of 19th April 1958 (at Sunrise) on the F_2 Layer of the Ionosphere—S. K. Mitra and B. C. N. Rao. (*Indian J. Phys.*, vol. 33, pp. 540–545; December, 1959.) Results are given of observations made at three stations in South India. A marked decrease in ionization density with the progress of the eclipse was observed.

551.510.535:550.38 2746
A Theory of the Origin and Geomagnetic Control of Two Types of High-Latitude E_s—J. E. Shaw. (*Planet. Space Sci.*, vol. 2, pp. 56–59; October, 1959.) The auroral belt type of E_s [1561 of 1959 (Penndorf and Coroniti)] may be caused by electrons from a region of trapped particles, indicated by the extent of a night-time peak in *f*-type E_s. Thule-type E_s may be caused by an influx of electrons approaching from the direction of the sun at geomagnetic noon.

551.510.535:550.38:552.594.5 2747
Outline of a Theory of Magnetic Separation of Auroral Particles and the Origin of the S_D Field—J. E. Shaw. (*Planet. Space Sci.*, vol. 2, pp. 49–55; October, 1959.) Diurnal variations of sporadic-E ionization at Macquarie Island (geomagnetic latitude 61.1°S) are identified with magnetic separation of incoming protons and electrons. Associated visual auroras are discussed.

551.510.535:550.385 2748
Geomagnetic and Current Control of E-Region Absorption—J. E. Shaw. (*Planet. Space Sci.*, vol. 2, pp. 1–9; October, 1959.) Observations of f_{min} at 18 ionospheric stations show that the ratio f_{min}/f_0E is related to the S_q current intensity and the latitude of the station.

551.510.535:550.385.4 2749
Magnetic Storm Effects on the F Region of the Ionosphere—Y. V. Somayajulu. (*J. Geophys. Res.*, vol. 65, pp. 893–895; March, 1960.) A preliminary report on the results of a true-height analysis carried out for Washington, D. C., during three severe SC-type magnetic storms.

551.510.535:551.594 2750
Ionospheric Thermal Radiation at Radio Frequencies in the Auroral Zone—R. L. Dowden. (*J. Atmos. Terr. Phys.*, vol. 18, pp. 8–19; April, 1960.) The temperature of the lower ionosphere is estimated for observations of radio noise at 2 mc. Temperature range and seasonal variation of temperature are the same as for temperature latitudes.

551.510.535(99) 2751
An Unusual Ionospheric Disturbance in the Antarctic on 30 June to 1 July 1957—V. A. W. Harrison. (*J. Atmos. Terr. Phys.*, vol. 18, pp. 72–75; April, 1960.) Unusually high f_0F_2 values were obtained for 12 hours at two ionospheric observatories during a magnetic storm.

551.594.5:621.396.677.833 2752
Auroral Research at the Hillhead Experimental Station.—(*RSGB Bull.*, vol. 35, p. 548; June, 1960.) General information is given about the 142-ft. paraboloid installed at Hillhead, Scotland, to study the effects of aurora on the propagation of radio waves.

551.594.6 2753
A Theory of Trapping of Whistlers in Field-Aligned Columns of Enhanced Ionization—R. L. Smith, R. A. Helliwell and I. W. Yabroff. (*J. Geophys. Res.*, vol. 65, pp. 815–823; March, 1960.) Using ray theory it is shown that the condition for whistler propagation in ducts depends on the ratio of the electron density in the column to that of the background. The theory explains part of the variation of whistler rate with latitude.

551.594.6:550.385.4 2754
Directional Observations of 5-kc/s Radiation from the Earth's Outer Atmosphere—G. R. A. Ellis. (*J. Geophys. Res.*, vol. 65, pp. 839–843; March, 1960.) An account is given of the estimation of the position and size of sources of LF noise bursts associated with geomagnetic disturbances.

551.594.6:551.594.221 2755
H.F. Noise Radiators in Ground Flashes of Tropical Lightning—S. V. C. Aiya. (PROC. IRE, vol. 48, pp. 955–956; May, 1960.) A detailed analysis of HF noise sources in tropical ground flashes.

551.594.6:621.391.812.6.029.4 2756
V.L.F. Phase Characteristics deduced from Atmospheric Waveforms—Jean. Taylor and Wait. (See 2881.)

LOCATION AND AIDS TO NAVIGATION

621.396.932 2757
Radio Aids to Hydrography—C. Powell. (*Wireless World*, vol. 66, pp. 351–358; July, 1960.) A general description of the Decca two-range position-fixing system incorporating a low-ambiguity ('Lambda') method of lane identification.

621.396.96 2758
The Spectrum of X-Band Radiation Back-Scattered from the Sea Surface—B. L. Hicks, N. Knable, J. J. Kovaly, G. S. Newell, J. P. Ruina and C. W. Sherwin. (*J. Geophys. Res.*, vol. 65, pp. 825–837; March, 1960.) The power spectra of more than 200 samples of sea back-scatter were obtained using a coherent radar. The spectral widths are related to certain sea-state parameters, and the effect of wave and whitecap velocities, radar depression angle, and wind direction is discussed.

621.396.965.81:551.507.362.2 2759
Tracking Radar for Tiros Weather Satellite—H. E. O'Kelley. (*Electronics*, vol. 33, pp. 57–60; April 15, 1960.) A 60-ft. parabolic reflector with circularly polarized feed for frequencies in the range 100–300 mc is described. Conical scanning is effected by a rotating lens.

621.396.969.3 2760
Portable Radar traces Battlefield Deployment—J. Scott, D. Randise and R. P. Lukacovic. (*Electronics*, vol. 33, pp. 67–70; March 18, 1960.) A 50-lb Doppler X-band radar, with ranging and AFC circuits uses transistors in nearly all stages. It can detect and accurately locate men and vehicles.

621.396.969.35 2761
New Missile-Warning Radar Site—(*Electronics*, vol. 33, p. 47; March 18, 1960.) A description of the tracking radar at Fylingside Moor, Yorkshire.

MATERIALS AND SUBSIDIARY TECHNIQUES

535.215 2762
Induction Effects in Photoconductive Single Crystals—W. Thielemann and K. Kreher. (*Z. Naturforsch.*, vol. 14a, pp. 687–688; July, 1959.) Report on measurements of induced charges, their variation with time, and the simultaneous changes of photoconductivity in single-crystal CdS and ZnS specimens. [See also 2396 of 1960 (Thielemann).]

535.215 2763
Electrical Properties of Alkali Antimonides—S. Imamura. (*J. Phys. Soc. Japan*, vol. 14, pp. 1491–1496; November, 1959.) Measurements are made of the changes of electrical properties during preparation, and their subsequent variation with temperature. Results elucidate the unusual variation of semiconductor type observed among these compounds.

535.215 2764
Photoelectrical Properties of Alkali Antimonides—S. Imamura. (*J. Phys. Soc. Japan*, vol. 14, pp. 1497–1505.) The correlation of photoemission and photoconduction properties with impurity states is investigated and energy-band models for cubic and hexagonal crystal structures are derived.

535.215:535.376 2765
Luminescence and Conductivity Induced by Field Ionization of Traps—R. R. Haering. (*Canad. J. Phys.*, vol. 37, pp. 1374–1379; December, 1959.) If the electric field increases linearly with time the conductivity and luminescence brightness display a sharp maximum. It is shown theoretically how this maximum may be used to determine the trap energy.

535.215:546.48'221+[546.817'221 2766
Effects of the Surface State of PbS and CdS on the Contact Potential Difference—L. P. Strakhov. (*Fiz. Tverdogo Tela*, vol. 1, pp. 583–588; April, 1959.) Experimental investigation of the effect of heat treatment, irradiation and an applied magnetic field on the contact potential difference of single crystals and thin films.

535.215:546.48'221 2767
Fluctuations in CdS due to Shallow Traps—J. J. Brophy and R. J. Robinson. (*Phys. Rev.*, vol. 117, pp. 738–739; February 1, 1960.) The observed current noise in single-crystal CdS is quantitatively explained by application of the generation-recombination theorem to retrapping effects. Characteristics of the trapping levels involved are deduced.

535.215:546.48'221 2768
The Effect of Surface Treatment on some Characteristics of the Photoconductivity of CdS Single Crystals—E. A. Sal'kov, G. A. Fedorus and M. K. Sheĭnkman. (*Fiz. Tverdogo Tela.*, vol. 1, pp. 579–582; April, 1959.)

535.215:546.561–31 2769
Photoconductivity of Cuprous Oxide in Relation to its Other Semiconducting Properties—F. L. Weichman. (*Phys. Rev.*, vol. 117, pp. 998–1002; February 15, 1960.) At least two of the three known peaks in the photoconductivity wavelength curve are found to be strongly dependent on the oxygen content of the material. The results are consistent with the high-temperature actuation energy of the process, and with changes of band gap with temperature.

535.37:546.47'221 2770
Photoelectromotive Forces in Phosphors—P. Brauer. (*Z. Naturforsch*, vol. 14a, pp. 556–559; May/June, 1959.) Discussion of photoelectric measurements on ZnS phosphors and their interpretation with regard to the direction of the displacement current and the polarity of the released carriers.

535.376 2771
Decay Properties of ZnS(Ag) Phosphors—T. Asada, M. Masuda, M. Okumura and J. Okuma. (*J. Phys. Soc. Japan*, vol. 14, pp. 1766–1770; December, 1959.)

537.227 2772
Ageing Process in Triglycine Sulphate—J. Stankowska and J. Stankowski—(*Proc. Phys. Soc.*, vol. 75, pp. 455–456; March 1, 1960.)

537.227:546.431'824–31 2773
Dielectric Properties of Mixed Crystals of Barium-Strontium Titanate—S. Kisaka, S. Ikegami and H. Sasaki. (*J. Phys. Soc. Japan*, vol. 14, pp. 1680–1685; December, 1959.) Results are given of dielectric measurements on mixed crystals with varying Sr content up to 10 mole per cent.

537.227:546.431'824–31 2774
Effect of Hydrostatic Pressure on the Dielectric Properties of $BaTiO_3$—J. Klimowski and J. Pietrzak. (*Proc. Phys. Soc.*, vol. 75, pp. 456–459; March 1, 1960.)

537.227:546.431'824–31 2775
The Effect of Pressure on the Electric Properties of Barium Titanate in Weak Fields—Ya. M. Ksendzov and B. A. Rotenberg. (*Fiz. Tverdogo Tela.*, vol. 1, pp. 637–642; April, 1959.)

537.227:546.431'824–31 2776
Optical Studies on the Effect of Electric Fields on the Transitions of Barium Titanate—K. Kawabe. (*J. Phys. Soc. Japan*, vol. 14, pp. 1755–1765; December, 1959.)

537.227:546.431'824–31 2777
Motion of 180° Domain Walls in Metal Electroded Barium Titanite Crystals as a Function of Electric Field and Sample Thickness—R. C. Miller and A. Savage. (*J. Appl. Phys.*, vol. 31, pp. 662–669; April, 1960.) The wall velocity was measured over several decades of velocity and found to be $v_\infty \exp(-\delta/E)$ where E is the electric field and δ and v_∞ are v_∞ constants. The results are discussed.

537.227:546.431'824–31 2778
Stability of the Piezoelectric Effect in Compressed Barium Titanate—M. M. Kitaĭgorodskiĭ. (*Fiz. Tverdogo Tela*, vol. 1, pp. 628–629; April, 1959.) A long-term stability is observed. [See 444 of 1955 (Kogan and Kitaĭgorodskiĭ).]

537.228.1:549.514.51 2779
Internal Friction in Synthetic Quartz—C. S. Brown. (*Proc. Phys. Soc.*, vol. 75, pp. 459–460; March 1, 1960.) The Q-factor of synthetic quartz crystals is found to approach that of natural crystals when the growth rate is below 0.15 mm/day.

537.311.31 2780
The Electrical Conductivity of Copper with Particular Regard to the Anisotropy of the Lattice Vibration Spectrum—H. Bross. (*Z. Naturforsch*, vol. 14a, pp. 560–580; May/June, 1959.)

537.311.33 2781
Statistical Theory of Electrical Conductivity of Semiconductors: Part 3—M. I. Klinger. (*Fiz. Tverdogo Tela*, vol. 1, pp. 1385–1392; September, 1959.) Mathematical treatment of semiconductor theory taking account of electron transitions from the conduction band to impurity levels and the converse, as a result of inelastic collisions with phonons. For earlier work see 1269 and 2291 of 1960.

537.311.33 2782
Rules for Prediction of Semiconductivity in Inorganic Crystal Lattices—J. P. Suthet. (*J. Phys. Chem. Solids*, vol. 12, pp. 74–88; December, 1959. In French.) Rules and bonding schemes are studied. 89 references.

537.311.33 2783
The Theory of the Mobility of Electrons in Semiconductors—I. I. Boĭko. (*Fiz. Tverdogo Tela*, vol. 1, pp. 574–578; April, 1959.) Mathematical analysis, using the Born approximation, of the scattering of electrons by Coulomb centers in an anisotropic medium. The calculated mobilities are approximately twice as high as experimental values, indicating additional scattering factors.

537.311.33 2784
Theory of the Trapping Mechanism in Semiconductors—W. Heywang and M. Zerbst. (*Z. Naturforsch*, vol. 14a, pp. 641–645; July, 1959.) The influence of traps on the photoconductivity of semiconductors is investigated for stationary and nonstationary excitation conditions.

537.311.33 2785
Location of *p-n* and *l-h* Junctions in Semiconductors—P. A. Iles and P. J. Coppen. (*Brit. J. Appl. Phys.*, vol. 11, pp. 177–184; May, 1960.) Properties of *p-n* and *l-h* junctions [see 489 of 1957 (Arthur, *et al.*)] are discussed and methods of location particularly applicable to Ge and Si are summarized. 77 references.

537.311.33 2786
Effect of External Illumination on Carrier Lifetime in Semiconductors—J. Okada. (*J. Phys. Soc. Japan*, vol. 14, pp. 1550–1557; November, 1959.) Carrier lifetime is discussed for nondegenerate semiconductors illuminated by light both in the fundamental absorption band and of a longer wavelength. Recombination equations for many recombination-center levels are formulated giving exact steady-state and transient solutions for specific cases.

537.311.33 2787
Optical Absorption by Free Carriers in a Semiconductor Containing a Dispersed Colloidal Phase—B. R. Gossick. (*J. Appl. Phys.*, vol. 31, pp. 648–649; April, 1960.) A treatment is given taking into account the dipolar diffusion of minority carriers about the particles.

537.311.33 2788
Effect of the Space Charge of Moving Carriers on the Electrical Breakdown of a Strongly Asymmetric *p-n* Junction—A. I. Uvarov. (*Fiz. Tverdogo Tela*, vol. 1, pp. 1457–1459; September, 1959.)

537.311.33:535.215 2789
Relaxation Characteristics of Semiconductor Photoresistors and Photoelements—F. A. Gisina. (*Fiz. Tverdogo Tela*, vol. 1, pp. 1434–1440; September, 1959.) The variations of photoconductivity and photodiffusion EMF of Ge-type semiconductors as a function of time are determined by application of operational methods to the solution of the diffusion equation.

537.311.33:537.29 2790
Application of the Magnetoconcentration Effect for Investigation of Semiconductor Surfaces—V. P. Zhuze, G. E. Pikus and O. V. Sorokin. (*Fiz, Tverdogo Tela*, vol. 1, pp. 1420–1430; September, 1959.) A method reported earlier (500 of 1959) for measuring surface recombination velocity s, was based on the relation of the resistance of a thin specimen in a magnetic field to the difference in the value of s for the two faces. This method has been adapted for measuring changes in s under the influence of an external electric field. Data obtained by this method on the position and density of fast surface states in n- and p-type Ge are discussed.

537.311.33:583.63 2791
Magnetoresistance Effect in Anisotropic Semiconductors—L. Rothkirch. (*Z. Naturforsch*, vol. 14a, pp. 683–684; July, 1959.) The dependence of the magnetoresistance effect in elongated semiconductor crystals on the orientation of the magnetic field is investigated theoretically.

537.311.33:538.63 2792
A New Longitudinal Magnetoconcentration Effect and its Use in Determining the Ratio of the Densities of Heavy and Light Holes—S. M. Ryvkin, Yu. L. Ivanov, A. A. Grinberg, S. R. Novikov and N. D. Potekhina. (*Fiz. Tverdogo Tela*, vol. 1, pp. 1372–1375; September, 1959.) An experimental arrangement for measuring the increase in carrier density in a longitudinal magnetic field is outlined and results of measurements on p- and n-type Ge are plotted. A theoretical density ratio of 57 fits the experimental data for n-type Ge.

537.311.33:538.632 2793
Influence of a High-Frequency Alternating Magnetic Field on the Hall Effect in Semiconductors with High Conductivity—F. Kuhrt, H. J. Lippmann and K. Wiehl. (*Naturwiss*, vol. 46, pp. 351–352; May, 1959.) Preliminary note on theoretical investigations, and on experimental measurements of the Hall effect in InAs in an alternating magnetic field in the frequency range 0.1–1.5 mc.

537.311.33:546.24 2794
Recombination and Trapping in Tellurium—J. S. Blakemore, J. D. Heaps, K. C. Nomura and L. P. Beardsley. (*Phys. Rev.*, vol. 117, pp. 687–688; February 1, 1960.) Discussion of lifetime measurements by a photoconductive-decay method, at temperatures from 100° to 300°K.

537.311.33:546.26-1 2795
Intrinsic Recombination Radiation in Diamond—J. C. Mals and J. R. Prior. (*Nature*, vol. 186, pp. 1037–1038; June 25, 1960.)

537.311.33:[546.28+546.289 2796
Improvements on the Pedestal Method of Growing Silicon and Germanium Crystals—W. C. Dash. (*J. Appl. Phys.*, vol. 31, pp. 736–737; April, 1960.) A tapered pedestal permits the growth of large dislocation-free crystals. (See also 2785 of 1958).

537.311.33:546.28 2797
Precipitation in Silicon Crystals Containing Aluminium—R. Bullough, R. C. Newman, J. Wakefield and J. B. Willis. (*J. Appl. Phys.*, vol. 31, pp. 707–714; April, 1960.)

537.311.33:546.28 2798
Experimental Investigations of Traps in Silicon—M. Zerbst and W. Heywang. (*Z. Naturforsch*, vol. 14, pp. 645–649; July, 1959.) The effect of traps on the decay of photoconductivity is measured in high-purity Si and results are related to theoretical investigations. (See 2784 of 1960.)

537.311.33:546.28 2799
Infrared Radiation from Silicon Grown Junction—I. Uchida. (*J. Phys. Soc. Japan*, vol. 14, p. 1831; December, 1959.) Measurements have been made on a sample resistivity 0.08Ωcm in the region doped with B, and 2.4Ωcm in the region doped with Sb. The diffusion length of the radiative carriers is calculated to be approximately 300 μ and the lifetime of holes in the n region 77 μsec.

537.311.33:546.289 2800
Measurements of Drift Mobility, Electrical Resistance and Lifetime of Minority Charge Carriers in *n*- and *p*-Type Germanium under High Hydrostatic Pressure—G. Landwehr. (*Z. Naturforsch*, vol. 14a, pp. 520–531; May/June, 1959.) Measurements were made at pressures up to 1400 kp/cm² using pulse methods.

537.311.33:546.289 2801
Properties of Cleaned Germanium Surfaces—R. Forman. (*Phys. Rev.*, vol. 117, pp. 698–704; February 1, 1960.) Field-effect and conductivity measurements show that a (100) surface is more highly p-type than a (111) surface, and these results are interpolated qualitatively by an atomistic model.

537.311.33:546.289 2802
Origin of the "First-Order Structure" of CP4-Etched Ge Surfaces—G. Bonfiglioli, A. Ferro and A. Mojoni. (*J. Appl. Phys.*, vol. 31, pp. 684–687; April, 1960.) Examination of micrographs indicates that the "first-order structure" originates from dislocation etch pits which have stopped growing.

537.311.33:546.289 2803
Hot Electron in *n*-Type Germanium—Y. Yamashita and K. Inoue. (*J. Phys. Chem. Solids*, vol. 12, pp. 1–21; December, 1959.) The nonohmic current in a many-valley semiconductor has been investigated by considering scattering by acoustic and optical modes of vibrations and intervalley scatterings. The intensity of these interactions has been determined from observed data for the temperperature-dependence of the ohmic current, and the acoustic-electric effect. The theoretical result for the drift velocity is in good quantitative agreement with the observations of Gunn (3326 of 1953) and of Ryder (3782 of 1956) over a wide range of the applied field. The anisotropy in the hot-electron current obxerved by Sasaki, *et al.*, (3883 of 1958) is also discussed.

537.311.33:546.289 2804
Properties of Oxygen in Germanium—J. Bloem, C. Haas and P. Penning. (*J. Phys. Chem. Solids.*, vol. 12, pp. 22–27; December, 1959.) The observed properties are described and compared with those of oxygen in Si.

537.311.33:546.289 2805
Possible Evidence for the Light-Induced Plasticity in Germanium—M. Kikuchi. (*J. Phys. Soc. Japan*, vol. 14, p. 1642; November, 1959.

537.311.33:546.289 2806
Investigations on *p-n* Junctions in Germanium with Differing Densities of Recombination Centres—H. Dorendorf. (*Z. angew. Phys.*, vol. 11, pp. 162–164; May, 1959.) Lifetime, reverse current and photocurrent as a function of recombination-center concentration were measured on Ni-doped p-n junctions in Ge. The results obtained are compared with those concerning transient behavior calculated using the equations derived by Clarke (484 of 1958).

537.311.33:546.289 2807
The Elastic Constants of Germanium under Hydrostatic Pressure up to 12000 kp/cm²—J. Koppelmann and G. Landwehr. (*Z. angew. Phys.*, vol. 11, pp. 164–167; May, 1959.) The elastic constants are calculated from the results of measurements of ultrasonic velocity in single-crystal Ge. (See 2800 of 1960.)

537.311.33:546.289 2808
The Dependence of the Lifetime of Electrons and Holes in Germanium on their Concentrations—V. G. Alekseeva, I. V. Karpova and S. G. Kalashnikov. (*Fiz. Tverdogo Tela*, vol. 1, pp. 529–534; April, 1959.) Report of experiments on P and B as doping elements.

537.311.33.546.289 2809
The Effect of Temperature on the Rate of Recombination of Electrons and Holes at Copper Atoms in Germanium—N. G. Zhadnova, S. G. Kalashnikov and A. I. Morozov. (*Fiz. Tverdogo Tela*, vol. 1, pp. 535–544; April, 1959.)

537.311.33:546.289 2810
Recombination of Electrons and Holes at Nickel Atoms in Germanium—S. G. Kalashnikov and K. P. Tissen. (*Fiz. Tverdogo Tela*, vol. 1, pp. 545–552; April, 1959.)

537.311.33:546.289 2811
Restoration of the Parameters of Germanium Subjected to Thermal Treatment by Annealing in Vapours of Antimony and Arsenic—N. I. Chetverkiov. (*Fiz. Tverdogo Tela*, vol. 1, pp. 553–555; April, 1959.)

537.311.33:546.289 2812
Investigation of the State of Silver and Gold Local Levels in Germanium—K. D. Glinchuk, E. G. Miselyuk and N. N. Fortunatova. (*Fiz. Tverdogo Tela*, vol. 1, pp. 1345–1350; September, 1959.) Local levels of Ag were "deactivated" by annealing at 400°–600°C, resulting in a change in the temperature of the majority-carrier density and a sharp rise in minority-carrier lifetime. Local levels of Au were practically unaffected.

537.311.33:546.289 2813
Investigation of the Interaction of Holes in *p*-Type Germanium with Acoustic-Mode Vibrations—I. V. Mochan, Yu. N. Obraztsov and T. V. Smirnova. (*Fiz. Tverdogo Tela*, vol. 1, pp. 1351–1359; September, 1959.) An investigation of the temperature dependence of the phonon component of the thermal EMF and its variation in a magnetic field. The temperature dependence of the hole free-path time corresponding to single-phonon scattering in *p*-type Ge approximates to the theoretical value $T^{-3/2}$. The observed temperature dependence of hole mobility indicates the considerable effect of some other scattering mechanism.

537.311.33:546.289 2814
On the Nature of Surface Recombination Centres in Germanium—A. V. Rzhanov, Yu. F. Novototskil-Vlasov and I. G. Neizvestnyil. (*Fiz. Tverdogo Tela*, vol. 1, pp. 1471–1474; September, 1959.) Discussion of the dependence of the maximum surface recombination velocity on the temperature of heat treatment.

537.311.33:546.289 2815
Electrical Conductivity of Germanium at Low Temperatures—I. A. Kurova and S. G. Kalashnikov. (*Fiz. Tverdogo Tela*, vol. 1, pp. 1476–1479; September, 1959.) Results of resistivity, Hall-constant and magnetoresistance measurements on Ge-Sb alloys are shown. In high-resistance Ge with impurity concentration $\sim 10^{15}$ cm^{-3} or lower, weak conductivity in the conduction band is retained at low temperatures.

537.311.33:546.289:535.37 2816
Visible Light Emission from Germanium Diffused *p-n* Junction—M. Kikuchi and K. Tachikawa. (*J. Phys. Soc. Japan*, vol. 14, p. 1830; December, 1959.) Visible light emission was observed at the periphery of an oxygen-enriched *p-n* junction.

537.311.33:546.289:538.632 2817
Longitudinal Hall Effect—L. Grabner. (*Phys. Rev.*, vol. 117, pp. 689–697; February 1, 1960.) The "Hall field," defined as the electric field which is an odd function of the magnetic field, is split into the conventional transverse (TH) field and a longitudinal (LH) field. Some properties of the LH field contrast with those of the TH field. The LH field is investigated theoretically and experimentally for *n*-type Ge.

537.311.33:546.289:539.12.04 2818
Bulk Distribution of Lattice Defects in Germanium Crystals Irradiated by Fast Electrons—L. S. Smirnov and P. A. Glazunov. (*Fiz. Tverdogo Tela*, vol. 1, pp. 1376–1378; September, 1959.)

537.311.33:546.289:539.12.04 2819
Determination of the Number of Acceptor Levels of Defects Formed in Germanium by γ-Ray Irradiation—N. A. Vitovskii, T. V. Mashovets and S. M. Ryvkin. (*Fiz. Tverdogo Tela*, vol. 1, pp. 1381–1384; September, 1959.)

537.311.33:546.47–31 2820
Electrical Conductivity of ZnO-SiO_2 Mixtures—J. Dereń, J. Haber and T. Wilkowa. (*Naturwiss.*, vol. 46, pp. 350–351; May, 1959.) The temperature dependence of electrical conductivity of nonsintered Zno-SiO_2 mixtures was measured in the range 100°–700°C. The results obtained are compared with those for pure sintered ZnO, sintered ZnO+SiO_2, and pure SiO_2.

537.311.33:546.623'86 2821
Infrared Absorption in *n*-Type Aluminium Antimonide—W. J. Turner and W. E. Reese. (*Phys Rev.*, vol. 117, pp. 1003–1004; February 15, 1960.)

537.311.33:546.681'23'19 2822
The Question of Electrical Properties of Gallium Arsenoselenides—D. N. Nasledov and I. A. Feltin'sh. (*Fiz. Tverdogo Tela*, vol. 1, pp. 565–567; April, 1959.) Results of measurements of conductivity and thermo-EMF of different compositions are given.

537.311.33:546.682'19:538.63 2823
The Anomaly of the Hall Coefficient of Weakly *p*-Doped InAs—H. Rupprecht and H. Weiss. (*Z. Naturforsch*, vol. 14a, pp. 531–535; May/June, 1959.) Further investigations of the anomalous temperature characteristics of the Hall coefficient. [See also 3385 of 1959 (Rupprecht).] The anomaly is due to the formation of a thin *n*-type film on the material after mechanical surface treatment.

537.311.33:546.682'19'18 2824
Electron Mobility of Indium Arsenide Phosphide [$In(As_yP_{1-y})$]—H. Ehrenreich. (*J. Phys. Chem. Solids*, vol. 12, pp. 97–104; December, 1959.) Calculations of the mobility based on combined polar and impurity scattering agree within 30 per cent with the experimental results of Weiss. (*Z. Naturforsch*, vol. 11a, pp. 430–434; June, 1956.)

537.311.33:546.682'86 2825
Dislocation Etch Pits on the {111} and {$\bar{1}\bar{1}\bar{1}$} Surfaces of InSb—H. C. Gatos and M. C. Lavine. (*J. Appl. Phys.*, vol. 31, pp. 743–744; April, 1960.)

537.311.33:545.682'86 2826
Photomagnetic Effect in Single Crystals of *n*-Type Indium Antimonide—D. N. Nasledov and Yu. S. Smetannikova. (*Fiz. Tverdogo Tela*, vol. 1, pp. 556–558; April, 1959.) The variation of photo-EMF with magnetic field intensity in the range 300–20,000 oersteds is linear. An exponential increase in photo-EMF is observed with decreasing temperature.

537.311.33:546.682'86 2827
Electrical Properties of *p*-Type InSb at Low Temperatures—Lyan'Chzhi-chao and D. N. Nasledov. (*Fiz. Tverdogo Tela*, vol. 1, pp. 570–571; April, 1959.)

537.311.33:[546.817'241+546.873'241 2828
Investigation of the Scattering Mechanism of Carriers in some Semimetals—M. N. Vinogradova, O. A. Golikova, B. A. Efimova, V. A. Kutasov, T. S. Stavitskaya, L. S. Still'bans and L. M. Sysoeva. (*Fiz. Tverdogo Tela*, vol. 1, pp. 1333–1344; September, 1959.) Results of measurements relating to the thermoelectric properties of polycrystalline PbTe and Bi_2Te_3 samples are compared with theoretical characteristics.

537.311.33:[546.817'241+546.873'241 2829
Carrier Scattering Mechanism in some Solid Solutions based on Lead and Bismuth Tellurides—B. A. Efimova, T. S. Stavitskaya, L. S. Still'bans and L. M. Sysoeva. (*Fiz. Tverdogo Tela*, vol. 1, pp. 1325–1332; September, 1959.)

537.311.33:546.817'241 2830
Piezoresistive Effect in *p*-Type PbTe—L. E. Hollander and T. J. Diesel. (*J. Appl. Phys.*, vol. 31, pp. 692–693; April, 1960.) A large positive effect is observed. Measurements of longitudinal, transverse and hydrostatic piezoresistive coefficients indicate that the energy ellipsoids are most likely oriented in the [111] direction.

537.311.33:546.863'221 2831
Conductivity Fluctuations in a Solid and Liquid Antimony Sulphide System—M. I. Korntel'd and L. S. Sochava. (*Fiz. Tverdogo Tela*, vol. 1, pp. 1366–1369; September, 1959.)

537.311.22:546.873'241:539.23 2832
Vapour-Deposited Bismuth Telluride Films—W. Hänlein and K. G. Günther. (*Naturwiss.*, vol. 46, p. 319; May, 1959.) Bi_2Te_3 films are obtained by the "three-temperature method." [See 3349 of 1959 (Günther).]

537.311.33:621.317.3.029.6 2833
Measurement of the Electrical Parameters of a Semiconductor by means of U.H.F. Techniques—I. I. Gaskka and Yu. K. Pozhela. (*Fiz. Tverdogo Tela*, vol. 1, pp. 1431–1433; September, 1959.) Methods of measuring the lifetime, sign and drift velocity of minority carriers are outlined, based on the attenuation of EM waves by a semiconductor plate inserted in a waveguide.

537.311.33:621.317.3.029.6 2834
Measurement of Semiconductor Properties through Microwave Absorption—R. D. Larrabee. (*RCA Rev.*, vol. 21, pp. 124–129; March, 1960.) Minority-carrier lifetime can be measured without any direct electrical connections to the sample.

537.311.33:621.391.822 2835
Conductivity Fluctuation in Amorphous Semiconductors—M. I. Korntel'd and L. S. Sochava. (*Fiz. Tverdogo Tela*, vol. 1, pp. 1370–1371; September, 1959.) A note on noise measurements at 1400 cps on $Tl_2Te \cdot As_2Te_3$ and $Tl_2Se \cdot As_2Te_3$ in the temperature range −85° to 20°C. Current noise is unexpectedly low.

537.311.33:669.09 2836
Application of Vibrational Mixing to the Synthesis of Semiconductor Materials—A. S. Borshchevskil and D. N. Tret'yakov. (*Fiz. Tverdogo Tela*, vol. 1, pp. 1483–1485; September, 1959.)

537.533 2837
Investigations of Exo-electrons on Vapour-Deposited Metal Films and some Nonmetallic Surfaces—J. Wüstenhagen. (*Z. Naturforsch*, vol. 14a, pp. 634–641; July, 1959.) Measurements of exo-electron emission were made on Al films in vacuum and in the presence of oxygen and nitrogen at various pressures. The

emission was also measured on Ag-doped NaCl specimens subjected to X-ray and electron bombardment. (See also 3097 of 1957.)

537.533:537.311.31 2838
The Influence of the Individual Field Component on the Electron Emission of Metals—G. Ecker and K. G. Müller. (*Z. Naturforsch*, vol. 14a, pp. 511–520; May/June, 1959.) The field electron emission of metals under the influence of space charges is investigated, taking account of the field fluctuations on the surface due to the statistical distribution of charge carriers.

537.533:546.682 2839
Photoelectric Determination of the Electron Work Function of Indium—J. van Laar and J. J. Scheer. (*Philips Res. Repts.*, vol. 15, pp. 1–6; February, 1960.) "The photoelectric work function of evaporated indium films prepared in ultra-high vacuum is found to be 4.08 ± 0.01 ev."

537.533.8 2840
On the Yield and Energy Distribution of Secondary Positive Ions from Metal Surfaces—H. E. Stanton. (*J. Appl. Phys.*, vol. 31, pp. 678–683; April, 1960.) Measurements were made using a mass spectrometer with an energy analyzer.

538.221 2841
Ferromagnetic Anisotropy in Cubic Crystals—F. Keffer and T. Oguchi. (*Phys. Rev.*, vol. 117, pp. 718–725; February 1, 1960.) A re-evaluation of Van Vlech's second-order perturbation theory of dipole-type anisotropy in cubic ferromagnets.

538.221:539.23 2842
Anisotropy Induced by a Magnetic Field in Electrolytically Produced Nickel Films—O. Stemme and W. Andrä. (*Naturwiss.*, vol. 46, p. 352; May, 1959.) The anisotropy constant was measured by the torque method in Ni films of thickness $5\times10^{2}-1\times10^{4}$Å. [See also 2457 of 1960 (Andrä, *et al.*).]

538.221:539.23 2843
Millimicrosecond Magnetization Reversal in Thin Magnetic Films—W. Dietrich and W. E. Proebster. (*IBM J. Res. Dev.*, vol. 3, pp. 375–376; October, 1959.) Fast changes in both longitudinal and transverse flux components of permalloy film have been measured.

538.221:621.318.134 2844
Magnetic Properties of Polycrystalline Materials—D. M. Grimes, R. D. Harrington and A. L. Rasmussen. (*J. Phys. Chem. Solids*, vol. 12, pp. 28–40; December, 1959.) The variation of the magnetic Q with internal magnetization is discussed using both the domain-rotation and the domain-wall-motion models of magnetization change. Experimental results on four ferrites are given and the results examined. (See also Grimes, *J. Phys. Chem. Solids*, vol. 3, pp. 141–152; 1957.)

538.221:621.318.134 2845
Experimental and Theoretical Study of the Domain Configuration in Thin Layers of $BaFe_{12}O_{19}$—C. Kooy and U. Enz. (*Philips Res. Repts.*, vol. 15, pp. 7–29; February, 1960.) The domain configuration and the magnetization process in transparent single-crystal plates are studied by means of the optical Faraday effect.

538.221:621.318.134 2846
Ferromagnetic Crystalline Anisotropy of Fe-Mn Ferrite System—Z. Funatogawa, N. Miyata and S. Usami. (*J. Phys. Soc. Japan*, vol. 14, pp. 1583–1587; November, 1959.) Variations of magnetic crystalline anisotropy, g-value and line width for $Mn_xFe_{3-x}O_4$ are given for changes in composition and temperature. The results are difficult to explain on the basis of the one-ion model successful elsewhere.

538.221:621.318.134 2847
The Aging of Permeability in Manganese-Zinc Ferrite—S. Miyahara and T. Yamadaya. (*J. Phys. Soc. Japan*, vol. 14, p. 1635; November, 1959.) Results show that the decrease of permeability after sintering arises from disaccommodation and not from irreversible structural changes.

538.221:621.318.134:538.569.4 2848
Electron Spin Relaxation in Ferromagnetic Insulators—R. C. Fletcher, R. C. LeCraw and E. G. Spencer. (*Phys. Rev.*, vol. 117, pp. 955–963; February 15, 1960.) The rate of energy transfer between the uniform precession, the spin waves, and the lattice is used to develop a theory of the relaxation phenomena. Experimental data on Y-Fe garnet agree well with the theory and enable various pertinent relaxation times to be determined.

538.221:621.318.134:538.569.4 2849
Theory of Ferromagnetic Resonance in Rare-Earth Garnets: Part 3—Giant Anisotropy Anomalies—C. Kittel. (*Phys. Rev.*, vol. 117, pp. 681–687; February 1, 1960.) The giant sharp anisotropy anomalies in Y-Fe garnet are explained in terms of the crossovers or, most probably, near crossovers of the energy levels of the rare-earth ions in the combined crystal and exchange fields. Part 2. [See Pt. 2, 1722 of 1960 (de Gennes, *et al.*).]

538.221:621.318.134:621.318.4 2850
Data on Ferrite Materials when used as Rod Cores in Solenoidal Inductors and Transformers—A. J. Fuller. (*Electronic Engrg.*, vol. 32, pp. 236–237; April, 1960.) Charts are presented of Q-factor and core-insertion-factor variations over the frequency range 2 mc–80 mc.

538.221:621.395.625.3 2851
Determination of the Recording Performance of a Tape from its Magnetic Properties—Daniel and Levine. (See 2600.)

538.652 2852
Temperature Dependence of the Magnetostriction Constants in Iron and Silicon Iron—E. Tatsumoto and T. Okamoto. (*J. Phys. Soc. Japan*, vol. 14, pp. 1588–1594; November, 1959.)

MATHEMATICS

517.918 2853
Taylor-Cauchy Transforms for Analysis of a Class of Nonlinear Systems—Y. H. Ku, A. A. Wolf and J. H. Dietz. (PROC. IRE, vol. 48, pp. 912–922; May, 1960.) Nonlinear differential equations are transformed into algebraic equations which can be solved recursively.

517.918 2854
Laurent-Cauchy Transforms for Analysis of Linear Systems Described by Differential-Difference and Sum Equations—Y. H. Ku and A. A. Wolf. (PROC. IRE, vol. 48, pp. 923–931; May, 1960.) It is shown that Laurent-Cauchy transforms can be derived from Taylor-Cauchy transforms by a simple mapping and used in the analysis of discrete-continuous systems.

517.932 2855
An Improvement of the WKB Method in the Presence of Turning Points and the Asymptotic Solutions of a Class of Hill Equations—H. Moriguchi. (*J. Phys. Soc. Japan*, vol. 14, pp. 1771–1796; December, 1959.)

MEASUREMENTS AND TEST GEAR

529.786:621.3.018.41(083.74) 2856
Preliminary Flight Tests of an Atomic Clock in Preparation of Long-Range Clock Synchronization Experiments—F. H. Reder and G. M. R. Winkler. (*Nature*, vol. 186, pp. 592–593; May 21, 1960.) Two flight tests of the stability of an "atomichron" Cs-beam frequency standard were made by comparison with a similar ground-based unit via a microwave link. Results suggest that synchronization of remote clocks by means of a shuttle airoplane is entirely feasible.

621.3.018.41(083.74) 2857
The Broadcasting of Standard Frequencies of the Phys kalisch-Technische Bundesanstalt over the Transmitter DCF 77—U. Adelsberger. (*Nachrichtentech. Z.*, vol. 12, pp. 261–262; May, 1959.) Details are given of the program schedule covering transmission of the 77.5-kc carrier frequency with or without 200 and 400 cps modulation and time signals based on a Cs clock standard.

621.3.018.41(083.74)+529.786:538.569.4 2858
Frequency Shift in Ammonia Absorption Lines Other than (3.3)—K. Matsuura. (*J. Phys. Soc. Japan*, vol. 14, p. 1826; December, 1959.) Measurements have been made of the shift in resonance frequency with pressure for various lines at 30°C and 100°C. The shift coefficient, a decreases with increasing J, being very small at $J=K=5$ or 6 and finally going negative.

621.3.018.41(083.74):621.396.712 2859
WWV—the Frequency Standard—(*Wire Radio Commun.*, vol. 12, pp. 38–39, 58; December, 1959.) A general description of the standard-frequency transmission service provided by radio staions WWV and WWVH.

621.317.3:621.382.3:621.391.822 2860
The Measurement of Transistor Noise Figure—F. J. Hyde. (*Electronic Engrg.*, vol. 32, pp. 224–226; April, 1960.) Formulas are presented for the determination of the noise figure of a quadripole in terms of readily measurable admittance and voltage ratios. Standard noise-diode techniques are used and the effects of the coupling circuit and of the amplifier noise are considered.

621.317.335.3 2861
Improved Circuits for the Measurement of the Dielectric Constants of Gases—E. J. Gauss and T. S. Gilman. (*Rev. Sci. Instr.*, vol. 31, pp. 164–165; February, 1960.) "Chien's apparatus for the measurement of dielectric constants has been modified by the use of a Clapp oscillator. The measuring cell and the technique used to detect capacitance differences of about 10^{-3} pf are described."

621.317.335.3.029.6 2862
An Automatic Microwave Dielectrometer—W. F. Gabriel. (IRE TRANS. ON MICROWAVE THEORY AND TECHNIQUE, vol. MTT-7, p. 481; October, 1959.) The slotted-line technique is modified to give a direct reading of dielectric constant by replacing the slotted line with an automatic microwave impedance instrument indicating the magnitude and phase of the reflection coefficient.

621.317.343.2:621.372.2 2863
Measurement of Balanced Impedances in the Metre- and Decimetre-Wavelength Ranges—H. Fricke. (*Nachrichtentech. Z.*, vol. 12, pp. 233–238; May, 1959.) The use of tunable cavity resonators as balancing networks enables the measurement of balanced impedances to be carried out by means of unbalanced standing-wave indicators.

621.317.39:536.5:621.391.822 2864
A New Absolute Noise Thermometer at Low Temperatures—H. J. Fink. (*Canad. J. Phys.*, vol. 37, pp. 1397–1406; December, 1959.) If three resistors, which are kept at different temperatures, are arranged in form of a π network and if two of the thermal noise voltages appearing across the π network are multiplied together and averaged with respect to time, then under certain conditions the correlation between those voltages can be made zero. This condition is used to calculate the temperature of one noise source provided all the resistance values and the other temperatures are known.

621.317.444:538.569.4:551.507.362.2 2865
The Vector-Field Proton Magnetometer for I.G.Y. Satellite Ground Stations—Shapiro, Stolarik and Heppner. (See 2730.)

621.317.715:†621.383.292 2866
Tunable Galvanometer Amplifier—R. M. Huey and B. J. Lancaster. (*J. Sci. Instr.*, vol. 37, pp. 136–138; April, 1960.) Construction and performance details of an instrument using a photomultiplier tube are described. This provides a tuning range >2 octaves with resonant voltage gain $>10^4$ and Q-values ranging from 1.7 to 7.5.

621.317.73 2867
Automatic Q-Meter Peaking Circuit—F. M. Wanlass. (*Rev. Sci. Instr.*, vol. 31, pp. 199–201; February, 1960.) A circuit for rapid measurement of the Q-factor and capacitance of a low-loss sample is described.

621.317.733:539.23 2868
Instrument for Recording the Resistance during the Deposition of a Thin Film.—J. A. Bennett and T. P. Flanagan. (*J. Sci. Instr.*, vol. 37, pp. 143–144; April, 1960.) The unknown resistance forms one arm of a Wheatstone bridge circuit. Out-of-balance voltages control a relay and at balance a uniselector changes the reference resistance arm, giving instants at which selected fixed values are attained.

621.317.738:621.374.3 2869
Device for Measuring Small Capacitances—W. P. Davis, Jr. (*Rev. Sci. Instr.*, vol. 31, pp. 217–218; February, 1960.) Description of a simple measuring circuit using a counting-rate meter.

621.317.79:531.76:621.374.32 2870
Digitron—a Digital Time Analyzer for Microsecond Intervals—R. A. Swanson. (*Rev. Sci. Instr.*, vol. 31, pp. 149–154; February, 1960.) A system is described for measuring time intervals by counting pulses from a 10-mc ringing circuit. The drift in absolute time calibration is <0.1 per cent over several days.

621.317.79:621.397.74.001.4 2871
A Waveform Generator of Limited Spectrum—Giva. (See 2921.)

621.317.794:621.391.822 2872
Low-Frequency Noise Generator—D. A. Bell and A. M. Rosie. (*Electronic Technologist*, vol. 37, pp. 241–245; June, 1960.) The generator described provides a source of noise having a spectrum which is level within ± 1 db from zero frequency to 60 cps and a Gaussian probability distribution of amplitudes.

621.317.799:621.396.62 2873
A Nonlinearity Test Set for Broadcast Transmission Systems—E. A. Pavel and M. Bidlingmaier. (*Nachrichtentech. Z.*, vol. 12, pp. 243–249; May, 1959.) Equipment is described for the measurement of distortion in AF transmission circuits using a single-tone method at 60, 90, 533 and 800 cps, and a double-tone method at 4.2+6.8 kc and 5.6+7.2 kc.

OTHER APPLICATIONS OF RADIO AND ELECTRONICS

621.318.134:536.581.1 2874
The Use of the Curie Point of Ferrites for the Regulation of Temperature—H. Straubel. (*Z. angew. Phys.*, vol. 11, pp. 172–174; May, 1959.) The rapid change of permeability in Mn-Zn ferrites in the vicinity of the Curie point can be utilized for control purposes. The devices briefly described include a thermostat, a pyrometer, and flow-regulating mechanisms.

621.385.833 2875
Improvement of the Remote-Focus Cathode developed by Steigerwald by the Addison of a Further Electrode—F. W. Braucks. (*Optik (Stuttgart)*, vol. 16, pp. 304–312; May, 1959.) The improvements obtained by the addition of an auxiliary electrode to the focusing system are discussed in relation to the performance of the original system (936 of 1959.)

621.385.833 2876
The Electron-Optical Formation of Images by Orthogonal Systems using a New Model Field with Rigorously Defined Paraxial Paths—H. Dušek. (*Optik (Stuttgart)*, vol. 16, pp. 419–445; July, 1959.)

621.385.833 2877
Correction of Errors in Electron Stereomicroscopy—O. C. Wells. (*Brit. J. Appl. Phys.*, vol. 11, pp. 199–201; May, 1960.)

621.385.833 2878
A Simple Method of Interpreting Electron-Microscope Stereograms—G. Pohlmann and M. Ahrend. (*Optik (Stuttgart)*, vol. 16, pp. 461–471; August, 1959.)

621.385.833 2879
The Aberrations in Electron-Optical Diffraction Patterns—F. Lenz. (*Optik (Stuttgart)*, vol. 16, pp. 457–460; August, 1959.) The aberrations produced by axially symmetric lenses are calculated, and the effects of small deviations from axial symmetry are considered.

PROPAGATION OF WAVES

621.391.812 2880
Experimental Proof of Focusing at the Skip Distance by Back-Scatter Records—K. Bibl. (PROC. IRE, vol. 48, pp. 956–957; May, 1960.) An analysis of records showing focusing effects obtained on 16.65 mc over a period of six months.

621.391.812.6.029.4:551.594.6 2881
V.L.F. Phase Characteristics deduced from Atmospheric Waveforms—A. G. Jean, W. L. Taylor and J. R. Wait. (*J. Geophys. Res.*, vol. 65, pp. 907–912; March, 1960.) The dispersion curve derived from observations at four widely separated stations shows good agreement with that predicted by theory and indicates that the phase velocity is about 3 per cent greater than c and 4 kc and about 1 per cent greater at 8 kc.

621.391.812.62 2882
The Theory of Fading—H. Bremmer. (*Note Recensioni Notiz.*, vol. 8, pp. 257–268; May/June, 1959. In French.) The origin of fast fading in tropospheric scatter transmissions is discussed and expressions for the fading rate are derived.

621.391.812.62.029.53 2883
Propagation of Ground Waves across a Land/Sea Boundary—P. Venkateswarlu and R. Satyanarayana. (*Curr. Sci.*, vol. 28, p. 239; June, 1959.) The reception of a weak ground-wave signal on 447.9 m λ from a transmitter 1370 km distant is noted. This can be explained on the basis of Millington's theory of transmission across a land/sea boundary.

621.391.812.621:523.164.32 2884
The Refraction of dm Waves in the Troposphere—O. Hachenberg and R. Schachenmeier. (*Hochfrequenz.*, vol. 68, pp. 1–7; May, 1959.) Measurements of refraction angle of solar radio emission at the horizon over the sea were made at 20 cm λ using equipment described in 1013 of 1958 (Mollwo). Results are analyzed and related to radiosonde measurements of atmospheric refraction. Evidence of ducting has been obtained on some days.

621.391.812.624 2885
On the Question of Multiple Scattering in the Troposphere—D. S. Bugnolo. (*J. Geophys. Res.*, vol. 65, pp. 879–884; March, 1960.) A criterion of multiple scattering is developed which may check the reliability of single-scatter approximations and which indicates the importance of multiple-scattering effects in the microwave spectrum.

621.391.812.63 2886
Fading of Short-Wave Signals—V. L. Lokre. (*Curr. Sci.*, vol. 28, pp. 237–238; June, 1959.) A preliminary analysis of facing patterns recorded at Nagpur in the frequency range 4920–15120 kc.

621.391.812.63 2887
Twisted Ray Paths in the Ionosphere—C. B. Haselgrove and J. Haselgrove. (*Proc. Phys. Soc.*, vol. 75, pp. 357–363; March 1, 1960.) The Hamiltonian equations for a ray in an anisotropic medium are used to calculate ray paths in three dimensions using an electronic computer.

621.391.812.63 2888
Gyro Splitting of Ionospheric Echoes—G. R. A. Ellis. (*J. Atmos. Terr. Phys.*, vol. 18, pp. 20–28; April, 1960.) Highly retarded F-region echoes observed at frequencies just below the gyro-frequency may be explained if they are caused by the reflection of the X mode at the normal extraordinary-wave reflection level.

621.391.812.63 2889
Sudden Ionospheric Disturbances and the Propagation of Long Waves—A. Haubert. (*J. Atmos. Terr. Phys.*, vol. 18, pp. 71–72; April, 1960. In French.) There is a marked seasonal variation in the proportion of the number of enhancements of signal strength of 200-kc transmissions from Droitwich received at Rabat, to the number of fades. The enhancements show a maximum during summer months. (See also 643 of 1960.)

621.391.812.63 2890
Conditions for the Persistence of Purely Longitudinal or Purely Transverse Propagation—W. C. Hoffman. (*J. Atmos. Terr. Phys.*, vol. 18, pp. 1–7; April, 1960.) The forms of the refractive indexes required for purely longitudinal or transverse propagation are determined by integration of a simpler form of the Haselgrove equations for ray tracing in an inhomogeneous anisotropic medium.

621.391.812.63:523.78 2891
Propagation of Radio Waves Reflected from the Ionosphere during a Solar Eclipse—R. G. Rastogi. (*Geofis. pura e appl.*, vol. 45, pp. 123–152; January–April, 1960. In English.) Observations on radiowave propagation during solar eclipses are reviewed in chronological order. Measurements of vertical-incidence absorption and of propagation at oblique incidence made at various localities during different eclipses are discussed. A theory cov-

ering the changes of ionospheric absorption during an eclipse is given and used to explain some of the apparent discrepancies in the results of observations. 44 references.

621.391.814.029.64 2892

Surface-Wave Propagation over a Sand-Covered Conducting Plane—A. G. Mungall and D. Morris. (*Canad. J. Phys.*, vol. 37, pp. 1349–1356; December, 1959.) The velocity as a function of depth of sand has been investigated experimentally at 9 kmc using a phase comparison system. The application of the results to distance measuring techniques is discussed.

RECEPTION

621.376.23:621.391.822 2893

An Experimental Study of Detection in Nonstationary Noise—T. R. Williams and J. B. Thomas. (*Commun. and Electronics*, pp. 678–682; November, 1959.) A system simulating receiver outputs enables the effects of nonstationary noise on receiver performance to be studied experimentally.

621.391.822 2894

First- and Second-Order Distributions of a Sine Wave of Random Phase plus Gaussian Noise—R. Leipnik. (*Z. angew. Math. Phys.*, vol. 11, pp. 117–126; March 25, 1960. In English.) Calculation of the distributions using Rice's formula (2219 of 1948).

621.396.662.078 2895

Increasing the Dynamic Tracking Range of a Phase-Locked Loop—C. S. Weaver. (PROC. IRE, vol. 48, pp. 952–953; May, 1960.) This can be effected without adversely affecting the transient response or the effective noise bandwidth.

STATIONS AND COMMUNICATION SYSTEMS

621.391 2896

A Systematic Method for the Construction of Error-Correcting Group Codes—R. B. Banerji. (*Nature*, vol. 186, p. 627; May 21, 1960.)

621.394.3:621.371 2897

A Monitor for 7-Unit Synchronous Error-Correcting Systems for Use on Radio-Telegraph Circuits—R. P. Froom, F. J. Lee, C. G. Hilton and P. Mackrill. (*P. O. Elec. Engrg. J.*, vol. 53, pp. 1–8; April, 1960.) A unit designed to monitor telegraph circuits and count the character errors has been found satisfactory after a year's testing. Details of operation are given.

621.394.441:621.396.41 2898

Frequency-Modulated Voice-Frequency Telegraph Systems for Radio Telegraph Services—G. S. Hunt. (*P. O. Elec. Engrg. J.*, vol. 53, pp. 21–23; April, 1960.) The system was designed to overcome the deterioration in performance due to fluctuations in gain of transmission path. Speeds up to 260 bauds are possible.

621.396:523.1 2899

How can we detect Radio Transmissions from Distant Planetary Systems?—F. D. Drake. (*Sky & Telesc.*, vol. 19, pp. 140–143; January, 1960.) Brief description of the Project Ozma radiometer. The equipment operates near 1420 mc and is essentially a highly stable narrow-band superheterodyne receiver fed from two switched horns mounted at the focus of a parabola.

621.396:523.1 2900

Communications from Superior Galactic Communities—R. N. Bracewell. (*Nature*, vol. 186, pp. 670–671; May 28, 1960.) It is reasoned that a neighboring superior community is more likely to communicate with the earth via artificial satellites or probes than by direct radio communication. [See 320 of 1960 (Cocconi and Morrison).] This argument is developed and possible characteristics of the signals are discussed.

621.396.65 2901

A New High-Capacity Microwave Relay System—C. G. Arnold, V. E. Isaac, H. R. Mathwich, R. F. Privett and L. E. Thompson. (*Commun. and Electronics*, pp. 712–722; November, 1959.) By using new components and techniques, a high-capacity relay system has been developed for the 2-kmc band. It is suitable for varied commercial and military communication needs.

SUBSIDIARY APPARATUS

621–52 2902

A 'Z-Transform Describing Function' for On/Off-Type Sampled-Data Systems—B. C. Kuo. (PROC. IRE, vol. 48, pp. 941–942; May, 1960.) The derivation of the function for a sinusoidal error signal is fully described.

621–52 2903

A Note on the Steady-State Response of Linear Time-Invariant Systems to General Periodic Input—E. I. Jury. (PROC. IRE, vol. 48, pp. 942–944; May, 1960.)

621–526 2904

A Class of Optimum Control Systems—C. W. Merrian, III. (*J. Franklin Inst.*, vol. 267, pp. 267–281; April, 1959.) A class of opimum control systems is defined and investigated with special emphasis on time-domain concepts. This class is particularly suitable for feedback-control applications where adaptability to changing conditions is desired.

621.314.58 2905

Linear Circuits Regulate Solid-State Inverter—R. Wileman. (*Electronics*, vol. 33, pp. 61–63; April 15, 1960.) Circuits are described for the regulation of a 50-w transistorized dc/ac converter using a tuning-fork oscillator. The output of 115 v at 400 cps is regulated to within ± 0.2 per cent with 1 per cent harmonic distortion.

621.314.58:621.382.3 2906

A More Stable 3-Phase Transistor-Core Power Inverter—W. E. Jewett and P. L. Schmidt. (*Commun. and Electronics*, pp. 686–691; November, 1959.) A square-wave inverter for driving gyroscope motors is described, which could provide up to 1-kw continuous power.

621.316.9:621.311.62:621.382.3 2907

A Circuit for the Protection of a Stabilized Transistor Power Supply—H. Kemhadjian and A. F. Newell. (*Electronic Engrg.*, vol. 32, pp. 228–230; April, 1960.) Details are given of a transistorized protection circuit providing switch-off times $< 50\mu$sec and activated by currents below the full-load value.

TELEVISION AND PHOTOTELEGRAPHY

621.397.132:621.397.331.222 2908

Simultaneous Signal Separation in the Tricolour Vidicon—H. Borkan. (*RCA Rev.*, vol. 21, pp. 3–16; March, 1960.) The high capacity between adjacent color electrodes requires circuits to maintain adequate color separation and satisfactory signal per noise ratio. The system described involves low input impedance, feedback preamplifiers and "mixed-highs" circuitry.

621.397.2:621.391 2909

Investigations into Redundancy and Possible Bandwidth Compression in Television Transmission—K. Teer. (*Philips Res. Repts.*, vol. 14, pp. 501–556; December, 1959. Also vol. 15, pp. 30–95; February, 1960.) Three different aspects of redundancy are considered, 1) statistical, 2) physiological, and 3) psychological. Transmission systems with narrow bandwidths are described in which bandwidth compression is affected either by decreasing the frame frequency using a vidicon-type camera tube as a storage device, or by decreasing the information per frame, which may be realized by dot-interlace and subcarrier techniques. The application of these principles to color television is considered in the case of the NTSC system and a two-subcarrier system.

621.397.331.22 2910

Possibilities of Reducing After-Effects in Camera Tubes of the Vidicon Type—W. Heimann. (*Arch. elekt. Übertragung*, vol. 13, pp. 221–225; May, 1959.) Some of the inertia effects discussed in 2552 of 1956 may be due to semiconductor processes in the photoconductive storage element. Special forming treatment of the photoconductive layer can halve the inertia effects.

621.397.331.22 2911

Noise Limitations to Resolving Power in Electronic Imaging—J. W. Coltman and A. E. Anderson. (PROC. IRE, vol. 48, pp. 858–865; May, 1960.) Theory and experiment show that the masking effect of white noise depends only on the noise power per unit bandwidth; knowing the response of the system, the resolution limit can be predicted.

621.397.331.24 2912

Deflection Techniques for 110° Picture Tubes—B. Eastwood. (*J. Telev. Soc.*, vol. 9, pp. 185–196; January–March, 1960.)

621.397.6 2913

A Television Focus Indicator Unit—J. B. Potter. (*Electronic Engrg.*, vol. 32, pp. 240–241; April, 1960.) A description is given of equipment providing an objective quality criterion on the assumption that correct electrical and optical focus gives a relative maximum of the high-frequency content of the picture signal.

621.397.6:621.3.049.75 2914

The Application of Printed Wiring to Development and Small Batch Production with Particular Reference to Television Equipment—E. Davies. (*J. Brit. IRE*, vol. 20, pp. 265–279; April, 1960.) Details of production methods for incorporating printed circuits in television equipment are given. Standards, methods of circuit translation and production equipment are discussed.

621.397.62:621.3.049.75 2915

The Plated Circuit in the Large-Scale Production of Television Receivers—W. I. Flack. (*J. Brit. IRE*, vol. 20, pp. 283–289; April, 1960.) Etched-foil and plated circuits are compared and details of the latter are given in respect of the plating process, equipment for assembly and advantages over printed wiring.

621.397.62:621.3.049.75 2916

Printed-Circuit Production for a Television Tuner—P. C. Ganderton. (*J. Brit. IRE*, vol. 20, pp. 290–292; April, 1960.) Greater consistency of production of tuners with narrower spread of gain and improved frequency stability has been obtained with printed circuits.

621.397.62:621.382.333 2917

Designing TV Tuners with Mesa Transistors—H. F. Cooke. (*Electronics*, vol. 33, pp. 64–69; April 8, 1960.) Design procedure for RF amplifier, mixer and oscillator stages is de-

tailed. Noise performance is equal to that obtained using tubes.

621.397.62:621.396.662 2918
Transistorized Tuners for Portable Television—V. Mukai and P. V. Simpson. (*Electronics*, vol. 33, pp. 76–78; March 18, 1960.) Micro-alloy diffused-base transistors in a typical tuner give 18–19 db power gain at 210 mc with 12 db noise factor. Design details are given.

621.397.62.001.4 2919
A Television Line Selector—H. Wolt. (*Nachrichtentech. Z.*, vol. 12, pp. 239–242; May, 1959.) Circuit details are given of a selector unit for CRO representation of picture signal waveforms, and oscillograms obtained with the instrument are reproduced.

621.397.621 2920
Ringing in Horizontal-Deflection and High-Voltage Television Circuits—T. Murakami (*RCA Rev.*, vol. 21, pp. 17–44; March, 1960.) An analytical study and results of measurements, show that, by correct choice of circuit constants, ringing during the trace period can be eliminated at the source. Simplified design information is given.

621.397.74.001.4:621.317.79 2921
A Waveform Generator of Limited Spectrum—E. Giva. (*Note Recensioni Notiz.*, vol. 8, pp. 269–287; May/June, 1959.) The circuit described generates four different types of pulse and step waveform which can be superimposed on a television synchronizing waveform for testing long-distance television links.

621.397.743 2922
Experience with Long-Distance Television Fields used for Retransmission—W. L. Braun. (*Commun. and Electronics*, pp. 594–596; November, 1959.) A report of experience gained in the application of long-distance "diffraction" fields for broadcasting and television.

621.397.743:621.372.2 2923
Television Coverage of Mountain Valleys and Remote Localities by means of Single-Wire Transmission Line (Goubau Line)—J. Kornfeld. (*Radioschau*, vol. 9, pp. 416–418, 460–463; December, 1959.) The principle of the surface-wave transmission line and its application in extending the coverage of television transmitters in difficult terrain are discussed. Details are given of an experimental installation successfully operated in an Austrian mountain valley.

TUBES AND THERMIONICS

621.382.23 2924
The Dependence of the Reverse Current in a Germanium Diode on the Repetition Rate of Voltage Pulses—S. G. Shul'man. (*Fiz. Tverdogo Tela*, vol. 1, pp. 597–601; April, 1959.) Investigation of the influence of surface treatment of a *p-n* junction on the magnitude of the reverse current and the breakdown voltage.

621.382.23 2925
Solution of the Diffusion Equation of a Semiconductor Diode of Rotational Symmetry taking account of Volume and Surface Recombination by means of an Analogue Network, and Comparison with Measurements on Diodes—A. H. Frei and M. J. O. Strutt. (*Arch. elekt. Übertragung*, vol. 13, pp. 199–210; May, 1959.)

621.382.23 2926
Esaki Tunnelling—P. J. Price and J. M. Radcliffe. (*IBM J. Res. Dev.*, vol. 3, pp. 364–371; October, 1959.) Tunnelling probabilities are found for the "elastic" process of Esaki (1784 of 1958) and for the "phonon-assisted" processes. *I/V* characteristics are calculated.

621.382.23 2927
Tunel Diodes—G. N. Roberts. (*Electronic Technologist*, vol. 37, pp. 217–222; June, 1960.) The principle of operation and a number of applications of the tunnel diode are described.

621.382.23:621.372.44 2928
Effect of Minority Carriers on the Dynamic Characteristic of Parametric Diodes—I. Hefni. (*Electronic Engrg.*, vol. 32, pp. 226–227; April, 1960.) Investigations of *I/V* relations for large signal inputs at frequencies above 10 mc have shown a secondary breakdown and negative-resistance region.

621.382.23:621.372.632 2929
Noise Figure of Tunnel-Diode Mixer—D. I. Breitzer. (PROC. IRE, vol. 48, pp. 935–936; May, 1960.) Analysis leads to a best value of 8.3 db as a mixer and 5 db as a negative-resistance amplifier for a Ge Type-ZJ56 diode.

621.382.23:621.373.029.64 2930
A 3000-Mc/s Lumped-Parameter Oscillator using an Esaki Negative-Resistance Diode—R. F. Rutz. (*IBM J. Res. Dev.*, vol. 3, pp. 372–374; October, 1959.) The construction and some experimental measurements are described.

621.382.3 2931
The Thermal Stability of Transistors under Dynamic Conditions—F. Weitzsch. (*Arch. elekt. Übertragung*, vol. 13, pp. 185–198; May, 1959.) The general criteria governing thermal stability under dynamic conditions with sine-wave and pulse input are investigated and practical formulas and curves are derived. (See also 1713 of 1959.)

621.382.3:551.507.362.2 2932
Radiation Damage and Transistor Life in Satellites—J. M. Denney and D. Pomeroy. (PROC. IRE., vol. 48, pp. 950–952; May, 1960.) Curves of the estimated lifetime of Ge and Si semiconductors as a function of altitude in the equatorial (±25°) radiation belt are given. Heights between 1000 and 2000 miles are unsuitable for a semiconductor life of 1 year.

621.382.3:621.391.822:621.317.3 2933
The Measurement of Transistor Noise Figure—Hyde. (See 2860.)

621.382.3:621.396.665 2934
The Controlled Transistor—L. Steinke. *Nachrichtentech. Z.*, vol. 9, pp. 261–264; June 1959.) The gain control of transistors is investigated as a function of operating conditions, and the suitability of transistors for various gain-control circuits is considered.

621.382.3.012 2935
Four-Pole Locus Curves of the Transistor for Use in Circuit Design—H. Rohr. (*Nachrichtentech. Z.*, vol. 9, pp. 253–260; June, 1959.) The transistor is considered as a four-pole network and the circuits are given for the measurement of the parameters on which the locus curves are based. A graphical method of constructing the locus curves is described which yields results sufficiently accurate for design purposes.

621.382.323:621.373.5 2936
A High-Field-Effect Two-Terminal Oscillator—R. W. Lade and T. R. Schlax. (PROC. IRE, vol. 48, pp. 940–941; May, 1960.) Application of known theory to sinusoidal oscillators using readily available solid-state devices is outlined, and some measurements are described.

621.382.333 2937
Calculation of the Relaxation Characteristics of a *p-n-p-n-p-n* Combination—K. Leberwurst. (*Nachrichtentech. Z.*, vol. 9, pp. 246–253; June, 1959). Equivalent circuits are given and operating parameters calculated and measured for the different switching states of a two-transistor relaxation oscillator.

621.382.333 2938
An Electric Analogue of Heat Flow in Power Transisistors—J. Reese, W. W. Grannemann and J. R. Durant. (*Commun. and Electronics*, pp. 640–643; November, 1959.)

621.382.333 2939
Transistor with Base containing a Dispersed Colloidal Phase—B. R. Gossick. (*J. Appl. Phys.*, vol. 31, p. 745; April, 1960.) The manner in which the presence of colloidal particles in the base could simultaneously increase both gain and bandwidth is explained for a simple junction transistor.

621.382.333 2940
Negative Resistance in Transistors based on Transit-Time and Avalanche Effects—H. N. Statz and R. A. Pucel. (PROC. IRE, vol. 48, pp. 948–949; May, 1960.) It is shown theoretically that with specially designed transistors having small collector capacity and extrinics base resistance a negative-resistance effect is possible at microwave frequencies.

621.382.333:391.822 2941
Effect of External Base and Emitter Resistors on Noise Figure—J. W. Halligan. (PROC. IRE, vol. 48, pp. 936–937; May, 1960.) Analysis based on an equivalent circuit of a common-emitter amplifier neglecting only the excess noise in the transistor.

621.382.333.34:621.318.57 2942
Germanium *p-n-p-n* Thyratron—M. Klein and A. P. Kordalewski. (*IBM J. Res. Dev.*, vol. 3, pp. 377–379; October, 1959.) The design, construction and characteristics of the device are given.

621.383.032.217.2 2943
Bismuth-Silver-Caesium Photocathodes—A. A. Mostovskiĭ, O. B. Vorob'eva and K. A. Maĭskaya. (*Fiz. Tverdogo Tela*, vol. 1, pp. 643–647; April, 1959.) Experimental investigation of the properties of Bi-Ag-Cs photocathodes, with sensitivities up to 120 μA/lumen. The spectral sensitivity depends principally on the thickness of the evaporated layer of Bi and on the degree of oxygen sensitization.

†621.383.292 2944
Use of an Auxiliary Grid to Stabilize the Gain of a Photomultiplier—C. F. G. Delaney and A. J. Walton. (*Nature*, vol. 186, pp. 625–626; May 21, 1960.) The sensitivity of a photomultiplier to changes in supply voltage is reduced by means of feedback to an auxiliary grid with an appropriate dc bias between cathode and first dynode.

621.383.5 2945
Spectral Characteristics of GaAs Photocells—D. N. Nasledov and B. V. Tsarenkov. (*Fiz. Tverdogo Tela*, vol. 1, pp. 1467–1470; September, 1959.)

†621.383.53 2946
Cadmium Sulphide Field-Effect Phototransistor—R. R. Bockemuehl. (PROC. IRE, vol. 48, pp. 875–882; May, 1960.) Experimental investigation indicates that CdS gives a useful power gain and has certain advantages in phototransistor applications.

621.384.6 2947
Nonlinear Theory of a Velocity-Modulated Electron Beam with Finite Diameter—F.

Paschke. (*RCA Rev.*, vol. 21, pp. 53–74; March, 1960.) The conditions of bunching in the beam are considered with particular attention to the generation of harmonics. Two high-efficiency klystrons are proposed, one with a disk-loaded nonpropagating drift tube and the other with a third cavity tuned to the second harmonic.

621.385.032.213.13 2948
Investigation and Assessment of Oxide Cathodes by means of Test Valves—G. Landauer and W. Veith. (*Arch. elekt. Übertragung*, vol. 13, pp. 211–218; May, 1959.) A twin test tube is described which can be used for measurement of interface and bulk resistance in oxide cathodes under normal operating conditions. Some experimental results are given and differences in the effects of temperature and current activation are discussed.

621.385.032.213.13 2949
The Poisoning of Impregnated Cathodes—R. O. Jenkins and W. G. Trodden. (*J. Electronics Control*, vol. 7, pp. 393–415; November, 1959.) The poisoning of tungsten cathodes impregnated with Ba-Ca aluminate has been investigated experimentally. Oxygen, water vapor, carbon dioxide and air poison these cathodes if certain critical pressures are exceeded. The critical pressures are given and other effects are discussed.

621.385.3.011 2950
A General Relation among the Parameters of Multi-electrode Valves—B. Meltzer. (*J. Electronics Control*, vol. 7, p. 416; November, 1959.) A short theoretical treatment is given.

621.385.3.026.447 2951
Super-Power Electron Tube for U.H.F. Band—G. Flynn. (*Electronics*, vol. 33, pp. 70–72; April 8, 1960.) Details are given of a tube with a peak rating of 5 mw.

621.385.6:621.376.239 2952
A Broad-Band Cyclotron-Resonance R. F. Detector Tube—Turner. (See 2675.)

621.385.623:621.374.4 2953
Theory of a Fast-Switching Electron-Beam Frequency Divider—N. M. Kroll and I. Palócz. (*IBM J. Res. Dev.*, vol. 3, pp. 345–354; October, 1959.) The operation is analyzed in terms of velocity-modulation bunching theory. Two stable states of opposite phase exist; the time required to switch the device is discussed.

621.385.623.5 2954
Ferrite Tuning of Reflex Klystrons—P. E. V. Allin. (*J. Electronics Control*, vol. 7, pp. 377–392; November, 1959.) "Experimental results on the ferrite tuning of the reflex klystrons CV2164 and CV2346 are given and the relation between valve parameters and expected tuning ranges is discussed." See also *Proc. IEE*, vol. 105, pp. 978–984; 1958.

621.385.623.5:621.375.2.029.65 2955
Using Reflex Klystrons as Millimetre-Wave Amplifiers—K. Ishii. (*Electronics*, vol. 33, pp. 71–73; March 18, 1960.) A gain of 10 db is obtained with a reflex klystron as a regenerative amplifier at 60 kmc by adjustment of output impedance and electrode potentials.

621.385.633.24 2956
Noise Measurements on an M-Type Backward-Wave Amplifier—J. R. Anderson. (PROC. IRE, vol. 48, pp. 946–947; May, 1960.) Results of measurements of noise figure, signal-to-noise ratio and velocity spread are given for various operating conditions.

621.385.644 2957
A Frequency-Locked Grid-Controlled Magnetron—C. L. Cuccia. (*RCA Rev.*, vol. 21, pp. 75–93; March, 1960.) An 800-mc magnetron is described in which a frequency-locking signal can be introduced into the electron cloud. The output power can be varied from zero to several hundred watts without change of frequency.

621.385.832:536.5 2958
Techniques of Cathode Temperature Measurements as applied to Commercial Cathode-Ray Tubes—P. P. Coppola. (*Rev. Sci. Instr.*, vol. 31, pp. 137–143; February, 1960.) A review of the thermocouple, optical pyrometer, and retarding potential techniques for measuring cathode temperatures.

621.387 2959
Effects of Argon Content on the Characteristics of Glow-Discharge Tubes—F. A. Benson and P. M. Chalmers. (*Electronic Engrg.*, vol. 32, pp. 218–223; April, 1960.) Results are presented showing the variation of the striking and running voltages, the running-voltage/temperature curves, the initial drifts, and the impedance/frequency and noise characteristics of Ne- and He-filled tubes.

621.387:621.362 2960
Efficiency of the Plasma Thermocouple—H. W. Lewis and J. R. Reitz. (*J. Appl. Phys.*, vol. 31, pp. 723–727; April, 1960.) The efficiency is calculated where the plasma density is sufficient for the random current density to be large compared with the actual curernt density. (See also 1082 of 1960.)

MISCELLANEOUS

621.3:061.4 2961
Instruments, Electronics and Automation—(*Wireless World*, vol. 66, pp. 314–321; July, 1960.) Review of the IEA exhibition held in London, May 23–28, 1960.

Translations of Russian Technical Literature

Listed below is information on Russian technical literature in electronics and allied fields which is available in the U. S. in the English language. Further inquiries should be directed to the sources listed. In addition, general information on translation programs in the U. S. may be obtained from the Office of Science Information Service, National Science Foundation, Washington 25, D. C., and from the Office of Technical Services, U. S. Department of Commerce, Washington 25, D. C.

PUBLICATION	FREQUENCY	DESCRIPTION	SPONSOR	ORDER FROM:
Acoustics Journal (Akusticheskii Zhurnal)	Quarterly	Complete journal	National Science Foundation—AIP	American Institute of Physics 335 E. 45 St., New York 17, N. Y.
Automation and Remote Control (Avtomatika i Telemekhanika)	Monthly	Complete journal	National Science Foundation—MIT	Instrument Society of America 313 Sixth Ave., Pittsburgh 22, Pa.
	Monthly	Abstracts only		Office of Technical Services U. S. Dept. of Commerce Washington 25, D. C.
Journal of Abstracts, Electrical Engineering (Referativnyy Zhurnal: Electronika)	Monthly	Abstracts of Russian and non-Russian literature		Office of Technical Services U. S. Dept. of Commerce Washington 25, D. C.
Journal of Experimental and Theoretical Physics (Zhurnal Eksperimentalnoi i Teoreticheskoi Fiziki)	Monthly	Complete journal	National Science Foundation—AIP	American Institute of Physics 335 E. 45 St., New York 17, N. Y.
Journal of Technical Physics (Zhurnal Tekhnicheskoi Fiziki)	Monthly	Complete journal	National Science Foundation—AIP	American Institute of Physics 335 E. 45 St., New York 17, N. Y.
Proceedings of the USSR Academy of Sciences: Applied Physics Section (Doklady Akademii Nauk SSSR: Otdel Prikladnoi Fiziki)	Bimonthly	Complete journal		Consultants Bureau Inc. 227 W. 17 St., New York 22, N. Y.
Radio Engineering (Radiotekhnika)	Monthly	Complete journal	National Science Foundation—MIT	Pergamon Institute 122 E. 55 St., New York 22, N. Y.
	Monthly	Abstracts only		Office of Technical Services U. S. Dept. of Commerce Washington 25, D. C.
Radio Engineering and Electronics (Radiotekhnika i Elektronika)	Monthly	Complete journal	National Science Foundation—MIT	Pergamon Institute 122 E. 55 St., New York 22, N. Y.
	Monthly	Abstracts only		Office of Technical Services U. S. Dept. of Commerce Washington 25, D. C.
Solid State Physics (Fizika Tverdogo Tela)	Monthly	Complete journal	National Science Foundation—AIP	American Institute of Physics 335 E. 45 St., New York 17, N. Y.
Telecommunications (Elekprosviaz')	Monthly	Complete journal	National Science Foundation—MIT	Pergamon Institute 122 E. 55 St., New York 22, N. Y.
	Monthly	Abstracts only		Office of Technical Services U. S. Dept. of Commerce Washington 25, D. C.
Automation Express	10/year	A digest: abstracts, summaries, annotations of various journals		International Physical Index, Inc. 1909 Park Ave., New York 35, N. Y.
Electronics Express	10/year	A digest: abstracts, summaries, annotations of various journals		International Physical Index, Inc. 1909 Park Ave., New York 35, N. Y.
Physics Express	10/year	A digest: abstracts, summaries, annotations of various journals		International Physical Index, Inc. 1909 Park Ave., New York 35, N. Y.
Express Contents of Soviet Journals Currently being Translated into English	Monthly	Advance tables of contents of translated journals		Consultants Bureau, Inc. 227 W. 17 St., New York 22, N. Y.
Technical Translations	Twice a month	Central directory in the U. S. of translations available from all major sources in the U. S.	OTS and Special Libraries Assoc.	Superintendent of Documents U. S. Gov't Printing Office Washington 25, D. C.